MOLECULAR AND CELLULAR BIOLOGY OF PODOCYTES

EDITED BY: Hans Kristian Lorenzo and Mario Ollero
PUBLISHED IN: Frontiers in Cell and Developmental Biology

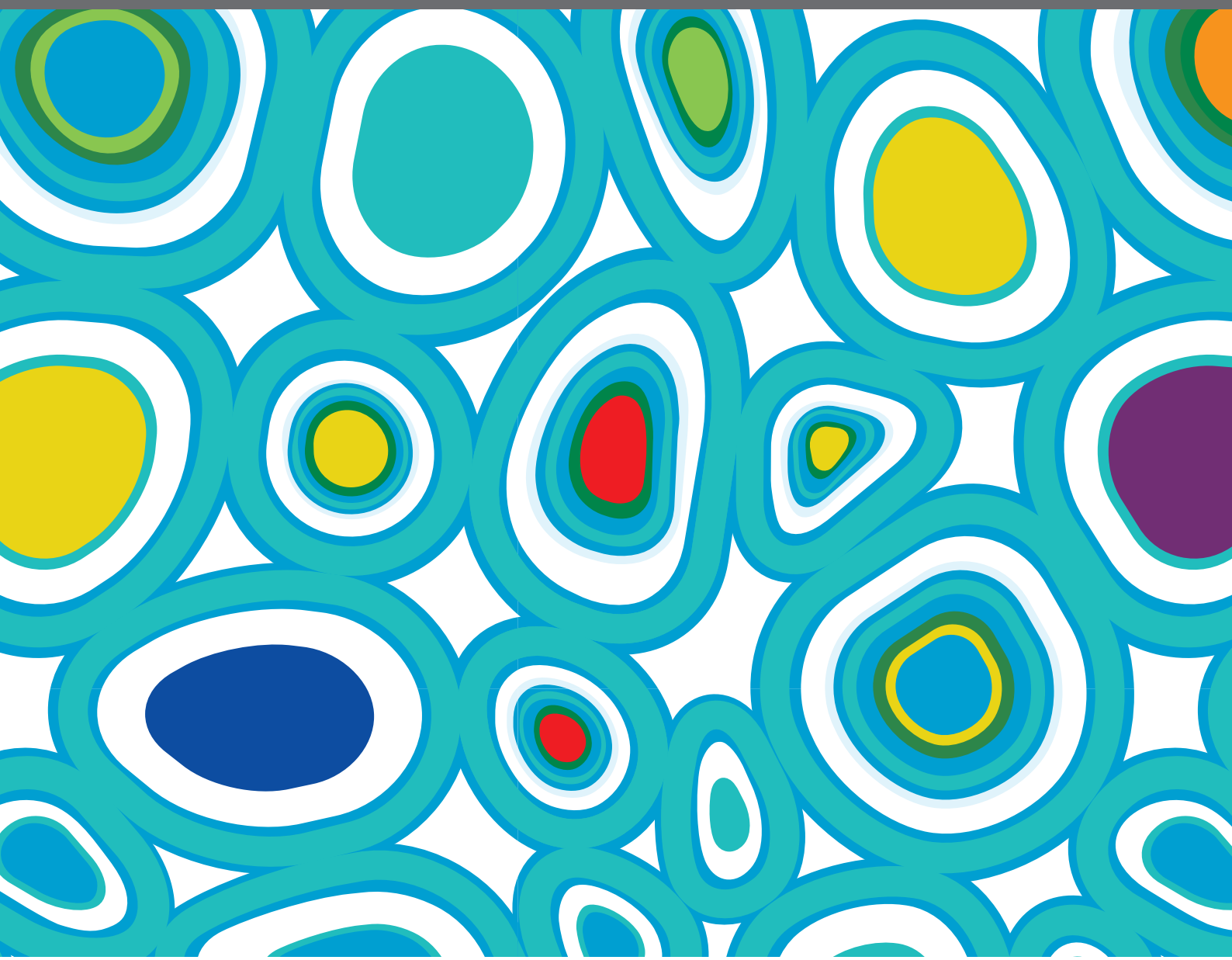

frontiers Research Topics

frontiers

ISSN 1664-8714
ISBN 978-2-83250-579-3
DOI 10.3389/978-2-83250-579-3

About Frontiers

Frontiers is more than just an open-access publisher of scholarly articles: it is a pioneering approach to the world of academia, radically improving the way scholarly research is managed. The grand vision of Frontiers is a world where all people have an equal opportunity to seek, share and generate knowledge. Frontiers provides immediate and permanent online open access to all its publications, but this alone is not enough to realize our grand goals.

Frontiers Journal Series

The Frontiers Journal Series is a multi-tier and interdisciplinary set of open-access, online journals, promising a paradigm shift from the current review, selection and dissemination processes in academic publishing. All Frontiers journals are driven by researchers for researchers; therefore, they constitute a service to the scholarly community. At the same time, the Frontiers Journal Series operates on a revolutionary invention, the tiered publishing system, initially addressing specific communities of scholars, and gradually climbing up to broader public understanding, thus serving the interests of the lay society, too.

Dedication to Quality

Each Frontiers article is a landmark of the highest quality, thanks to genuinely collaborative interactions between authors and review editors, who include some of the world's best academicians. Research must be certified by peers before entering a stream of knowledge that may eventually reach the public - and shape society; therefore, Frontiers only applies the most rigorous and unbiased reviews.
Frontiers revolutionizes research publishing by freely delivering the most outstanding research, evaluated with no bias from both the academic and social point of view. By applying the most advanced information technologies, Frontiers is catapulting scholarly publishing into a new generation.

What are Frontiers Research Topics?

Frontiers Research Topics are very popular trademarks of the Frontiers Journals Series: they are collections of at least ten articles, all centered on a particular subject. With their unique mix of varied contributions from Original Research to Review Articles, Frontiers Research Topics unify the most influential researchers, the latest key findings and historical advances in a hot research area! Find out more on how to host your own Frontiers Research Topic or contribute to one as an author by contacting the Frontiers Editorial Office: frontiersin.org/about/contact

MOLECULAR AND CELLULAR BIOLOGY OF PODOCYTES

Topic Editors:
Hans Kristian Lorenzo, Université Paris-Saclay, France
Mario Ollero, INSERM U955 Institut Mondor de Recherche Biomédicale (IMRB), France

Citation: Lorenzo, H. K., Ollero M., eds. (2022). Molecular and Cellular Biology of Podocytes. Lausanne: Frontiers Media SA. doi: 10.3389/978-2-83250-579-3

Table of Contents

frontiers | Frontiers in Cell and Developmental Biology

TYPE Editorial
PUBLISHED 10 October 2022
DOI 10.3389/fcell.2022.1037931

OPEN ACCESS

EDITED AND REVIEWED BY
You-Wen He,
Duke University, United States

*CORRESPONDENCE
Hans Kristian Lorenzo,
hans.lorenzo@universite-paris-saclay.fr

SPECIALTY SECTION
This article was submitted to Molecular and Cellular Reproduction, a section of the journal Frontiers in Cell and Developmental Biology

RECEIVED 06 September 2022
ACCEPTED 22 September 2022
PUBLISHED 10 October 2022

CITATION
Lorenzo HK and Ollero M (2022), Editorial: Molecular and Cellular Biology of podocytes.
Front. Cell Dev. Biol. 10:1037931.
doi: 10.3389/fcell.2022.1037931

Editorial: Molecular and Cellular Biology of podocytes

Hans Kristian Lorenzo[1]* and Mario Ollero[2]

[1]Faculté de Médecine, Université Paris-Saclay, Le Kremlin Bicêtre, France, [2]University Paris Est Creteil, INSERM, IMRB, Créteil, France

KEYWORDS

podocyte, glomerulopathy, proteinuria, chronic kindey diseases, cell death, cytosqueletton

Editorial on the Research Topic
Molecular and Cellular Biology of Podocytes

Podocytes are highly differentiated (post-mitotic) epithelial cells that are attached to the glomerular basement membrane. They are an essential part of the filtration barrier, preventing the loss of serum proteins into the urine. Because the function of podocytes constitutes the cornerstone of glomerular filtration, any alteration is likely to lead to proteinuria (nephrotic syndrome) and serious pathologies. Under normal circumstances podocytes are theoretically not replaceable and their behavior has been compared with that of neurons. Although the progressive loss of podocytes is a characteristic of healthy aging, it is particularly marked in the course of glomerular lesions (glomerulopathies). Stress response or morphological integrity are key points to establish a balance between normal and pathological states.

This Research Topic represents a snapshot of the current concerns of the nephrological community regarding this cell and its particular microenvironment. The contributions presented in this Research Topic point to several key aspects of podocyte physiology and their impact on renal function. Different points of view are considered such as 1) morphostructural features (cytoskeleton or slit diaphragm alterations), 2) mechanisms of stress response (death and loss, protection and adaptation) as well as 3) new methodological approaches for the study of these cells.

1) Structure-function relationship

Cytoskeleton integrity, always linked to morphology, is a key point in podocyte function. This is the main concern addressed by Liu et al. in their article. These authors present the WNK-OSR1/SPAK signaling pathway at the crossroads of cytoskeleton integrity, slit diaphragm function and glomerular capillary function. Another study conducted by Hamasaki et al. explores the role of dynamin 2 as a regulator of cytoskeleton function. For this purpose, the authors used a Dynamin-2 mutant (K562E) found in Charcot-Marie-Tooth disease, a sensory-motor neuropathy. This

mutant revealed a reduced affinity of the cytoskeleton for the lipid membrane and led to actin disorganization in podocytes.

Another key aspect of podocyte function is the maintenance of the integrity of the slit diaphragm, a unique structure in which nephrin and beta-integrin are considered the main gatekeepers. Maywald et al. addressed the study by combining *in vivo* Drosophila experiments with *in vitro* experiments in human podocytes. The authors demonstrated that Rap1 functions downstream of nephrin signaling to β-integrin at the slit diaphragm. Additionally, a discussion on the formation and maintenance of the slit diaphragm in a Drosophila model is addressed in the review by van de Leemput et al.

2) Stress response mechanisms

Podocyte injury in response to stress causes their detachment from the glomerular basement membrane, followed by proteinuria and progressive renal failure. A review on the state of the art of the lesions present in podocytopathies, with a provocative interpretation of their meaning is provided by Ravaglia et al. Within the cellular and molecular characteristics of podocyte alteration, mitochondrial destabilization is present in many forms of stress associated with the pathology. In the study by S. Liu et al. alterations in podocyte mitochondria such as mitochondrial function, mitophagy, and the role of mitochondria-associated membranes are examined. Another source of stress is viral infection, such as SARS-Cov-2. Kalejaiye et al. confirm that podocytes are one of the cellular targets and characterize BSG/CD147 and ACE2 as the receptors involved in the entry of this pathogen into iPSC-derived human podocytes.

An interesting point of podocyte biology is the understanding of the mechanisms of death, protection and adaptation of these cells in response to potentially deleterious stimuli. The different causes of podocyte death, detachment and loss is a topic reviewed by Yin et al. which includes the loss of viable podocytes in the urine or the "podocyte domino effect" as a mechanism of disease progression. Other papers have addressed these points in this Research Topic. Thus, Ristov et al. show the protective effect of small molecules, such as vitamin D3 and calcipotriol. Also, Chung et al. report the beneficial effects of curcumin on podocyte viability. These authors, using a high-glucose-induced injury model, demonstrate that the reactive oxygen species (ROS) produced under these conditions are diminished after curcumin treatment. Furthermore, curcumin treatment also restored the levels of RIPK3 and other necroptosis-associated proteins, revealing an interesting protective role. Again, Liu et al. examine the protective role of calcineurin inhibitors (immunosuppressants widely used in nephrology) and demonstrated their association with WNK kinase activity. Finally, a perspective article by Lavecchia et al. explores the potential of hypertrophy, at the crossroads of cell biology and biophysics, as an adaptive response to podocyte injury.

3) Experimental and methodological issues

Another key aspect of research on glomerulopathies is the need for robust experimental models (especially *in vitro*), so the study and characterization of the ones available and the development of new ones is crucial. Some of the articles in this Research Topic address this topic. Thus, thanks to the study by Bryant et al. we know that the administration of adriamycin, a widely accepted model of nephropathy, induces proteinuria depending on the genetic background of mice. In this study, the authors analyze in depth the impact of the C57B6 background, usually considered as resistant, and show the differences between two substrains, providing valuable information for *in vivo* assays. One of the major methodological problems consists of having *in vivo* access to podocytes in mammals. The use of Drosophila nephrocytes has recently been shown as an alternative model due to their similarity at the genetic, molecular and functional level to mammal podocytes. The challenges associated with *in vitro* study of the slit diaphragm using Drosophila nephrocytes is reviewed by van de Leemput et al. Another methodological problem is the weakness of podocytes in culture as a model to study new drugs and te difficulties to translate the results to the clinical level. This is due to the complex structure of the glomerular filtration barrier, which is barely represented by a simple podocyte culture. To overcome this problem, Ristov et al. propose an innovative assay to examine glomerular function. This is the so-called "GlomAssay", a semi-automated high-throughput screening method that allows the study of hundreds of compounds in combination with pathway analysis (transcriptomics and proteomics). Its robustness is demonstrated within the study on the protective role of vitamin D3 in podocytes discussed above.

Author contributions

HKL and MO contributed equally to manuscript revision, read, and approved the submitted version.

Conflict of interest

The authors declare that the research was conducted in the absence of any commercial or financial relationships that could be construed as a potential conflict of interest.

Publisher's note

frontiers in Cell and Developmental Biology

ORIGINAL RESEARCH
published: 02 February 2021
doi: 10.3389/fcell.2020.618898

Control of Podocyte and Glomerular Capillary Wall Structure and Elasticity by WNK1 Kinase

Zhenan Liu[1,2], Joonho Yoon[1,2], Chonlarat Wichaidit[3], Ankita B. Jaykumar[3], Hashem A. Dbouk[3], Addie E. Embry[1], Liping Liu[1], Joel M. Henderson[4], Audrey N. Chang[1,2], Melanie H. Cobb[3] and Richard Tyler Miller[1,2]**

[1] Department of Internal Medicine, Division of Nephrology, University of Texas Southwestern Medical Center, Dallas, TX, United States, [2] Medicine Service, VA North Texas Health Care System, Dallas, TX, United States, [3] Department of Pharmacology, University of Texas Southwestern Medical Center, Dallas, TX, United States, [4] Department of Pathology and Laboratory Medicine, Boston University School of Medicine, Boston, MA, United States

OPEN ACCESS

Edited by:
Greg B. Moorhead,
University of Calgary, Canada

Reviewed by:
Kirk Campbell,
Icahn School of Medicine at Mount Sinai, United States
Jérôme Boudeau,
UMR 5237 Centre de Recherche en Biologie Cellulaire de Montpellier (CRBM), France

***Correspondence:**
Richard Tyler Miller
Tyler.miller@utsouthwestern.edu
Melanie H. Cobb
Melanie.cobb@utsouthwestern.edu

Specialty section:
This article was submitted to Signaling, a section of the journal Frontiers in Cell and Developmental Biology

Received: 19 October 2020
Accepted: 31 December 2020
Published: 02 February 2021

Citation:
Liu Z, Yoon J, Wichaidit C, Jaykumar AB, Dbouk HA, Embry AE, Liu L, Henderson JM, Chang AN, Cobb MH and Miller RT (2021) Control of Podocyte and Glomerular Capillary Wall Structure and Elasticity by WNK1 Kinase. Front. Cell Dev. Biol. 8:618898. doi: 10.3389/fcell.2020.618898

Cytoskeletal structure and its regulation are essential for maintenance of the differentiated state of specific types of cells and their adaptation to physiologic and pathophysiologic conditions. Renal glomerular capillaries, composed of podocytes, endothelial cells, and the glomerular basement membrane, have distinct structural and biophysical properties and are the site of injury in many glomerular diseases. Calcineurin inhibitors, immunosuppressant drugs used for organ transplantation and auto-immune diseases, can protect podocytes and glomerular capillaries from injury by preserving podocyte cytoskeletal structure. These drugs cause complications including hypertension and hyperkalemia which are mediated by WNK (With No Lysine) kinases as well as vasculopathy with glomerulopathy. WNK kinases and their target kinases oxidative stress-responsive kinase 1 (OSR1) and SPS1-related proline/alanine-rich kinase (SPAK) have fundamental roles in angiogenesis and are activated by calcineurin inhibitors, but the actions of these agents on kidney vasculature, and glomerular capillaries are not fully understood. We investigated WNK1 expression in cultured podocytes and isolated mouse glomerular capillaries to determine if WNK1 contributes to calcineurin inhibitor-induced preservation of podocyte and glomerular structure. WNK1 and OSR1/SPAK are expressed in podocytes, and in a pattern similar to podocyte synaptopodin in glomerular capillaries. Calcineurin inhibitors increased active OSR1/SPAK in glomerular capillaries, the Young's modulus (E) of glomeruli, and the F/G actin ratio, effects all blocked by WNK inhibition. In glomeruli, WNK inhibition caused reduced and irregular synaptopodin-staining, abnormal capillary and foot process structures, and increased deformability. In cultured podocytes, FK506 activated OSR1/SPAK, increased lamellipodia, accelerated cell migration, and promoted traction force. These actions of FK506 were reduced by depletion of WNK1. Collectively, these results demonstrate the importance of WNK1 in regulation of the podocyte actin cytoskeleton, biophysical properties of glomerular capillaries, and slit diaphragm structure, all of which are essential to normal kidney function.

Keywords: glomerulus, podocyte, WNK1 kinase, elasticity, cytoskeleton

INTRODUCTION

Characteristics of the cell cytoskeleton are basic determinants of the structural and biophysical properties of cells and ultimately tissues. In the kidney, renal glomerular capillaries function at relatively high pulsatile pressures and filter blood to form the initial urine. They consist of fenestrated endothelial cells that participate in filtration, podocytes, or visceral epithelial cells that have several orders of branched processes, and a glomerular basement membrane (GBM) that is synthesized by both endothelial cells and podocytes. The primary and secondary processes of podocytes wrap around the capillaries. The terminal foot processes, the interdigitating final extensions of neighboring podocytes, anchor these cells to the GBM. These podocyte processes also provide structural and mechanical support to glomerular capillaries by opposing and accommodating hemodynamic force. The narrow gap, or filtration slit, between adjacent terminal foot processes is bridged by specialized tight junctions, known as slit diaphragms that constitute the final component of the filtration barrier. Glomerular disease is frequently associated with podocyte injury and actin cytoskeletal remodeling which disrupt interactions with neighboring podocytes and the GBM. This podocyte failure is characterized by foot process effacement, broadening and flattening of foot processes, and loss of slit diaphragms. The result is abnormal filtration function as well as disrupted podocyte and capillary wall mechanical properties, culminating in detachment of podocytes and their loss in the urine.

The With No Lysine (WNK) kinases are a family of serine-threonine kinases with the unusual location of a conserved lysine residue in the active site (Xu et al., 2000). These kinases have been studied most in their roles in epithelial transport because mutations in two of them, WNK1 and WNK4, are associated with renal transport phenotypes. The WNKs control vectorial transport in epithelial cells and cell volume in non-epithelial cells where they regulate cation-chloride cotransporters (Kochl et al., 2016; Shekarabi et al., 2017). WNKs are activated by hypotonic and hypertonic medium and osmotic shrinkage of cells. With an inhibitory Cl binding site in the active site of the kinase domain, WNKs function as Cl sensors (Zagorska et al., 2007; Piala et al., 2014; Chen et al., 2019). The adaptor KLHL3 binds WNKs to promote their degradation by Cullin3-mediated ubiquitination (Ohta et al., 2013; Cornelius et al., 2018). Many actions of WNK kinases are carried out by their substrates, the Sterile 20 Kinases, oxidative stress-responsive kinase 1 (OSR1) and its close homolog SPS1-related proline/alanine-rich kinase (SPAK).

With No Lysine 1 is ubiquitously expressed in non-renal and renal cells, including podocytes, while WNK4 is predominantly expressed in renal tubules (Shekarabi et al., 2017). WNK1 participates in fundamental biologic processes including angiogenesis, and mitosis (Xie et al., 2009, 2013; Tu et al., 2011; Gallolu Kankanamalage et al., 2016). WNK1 kinase is also involved in cell migration and adhesion where it controls cytoskeletal structure and migration-associated local cell volume fluctuations as demonstrated in endothelial cells, T cells, corneal epithelial cells and certain cancers, notably glioblastoma cells (Haas et al., 2011; Dbouk et al., 2014; Zhu et al., 2014; Kochl et al., 2016; Desjardins et al., 2019).

Tacrolimus (FK506) and cyclosporine A (CsA) are immunosuppressive drugs used following organ transplantation to prevent rejection and to treat autoimmune diseases. FK506 and CsA act by inhibiting the calcium and calmodulin-dependent phosphatase calcineurin. Among other substrates, calcineurin dephosphorylates KLHL3 leading to increased degradation of WNK1 and WNK4 (Ohta et al., 2013; Shekarabi et al., 2017; Ishizawa et al., 2019). As a consequence of increased WNK expression, FK506 and CsA cause increased activity of the WNK targets OSR1/SPAK explaining in part the volume-dependent hypertension and hyperkalemia seen with their use (Hoorn et al., 2011). Calcineurin inhibitors also have protective effects on podocytes in glomerular injury models, including preservation of cytoskeletal structure, and can improve the course of some human renal diseases (Meyrier, 2005; Charbit et al., 2007; Faul et al., 2008; Plank et al., 2008; Bensman and Niaudet, 2010; Li et al., 2015; Shen et al., 2016). However, use of these drugs can be limited by nephrotoxicity, characterized by vasculopathy, glomerular injury, tubular atrophy, interstitial fibrosis, hypertension, and hyperkalemia (Issa et al., 2013).

Despite the importance of WNK1 kinase signaling in vascular tissue, and the toxic and beneficial effects of calcineurin inhibitors in the kidney, the roles of WNK kinases in these processes are not fully understood. We studied the responses of isolated glomeruli and cultured podocytes to calcineurin inhibitors and WNK1 inhibition to investigate the contributions of WNK1 to the structural and mechanical properties of glomerular capillaries and podocytes.

EXPERIMENTAL PROCEDURES

Reagents

Antibodies recognizing the indicated proteins were from the following sources: WNK1 (Origene 06363PU-N), OSR1 was from MyBiosSource, and pOSR1(Ser325)/SPAK(Ser373) – Millipore-Sigma, anti-synaptopodin – Santa Cruz; β-actin – Sigma; Cortactin H222 Cell Signaling; FK506 and cyclosporin A – LC Laboratories, sorbitol – Sigma, and Jasplakinolide and Latrunculin B – Fisher; WNK463 – MedChemExpress. All fluorescent antibodies were purchased from Invitrogen.

Cell Culture and Lysis Conditions

Conditionally-immortalized mouse podocytes were cultured in RPMI 1640 with 10% FBS as previously described (Tandon et al., 2007). Cells proliferated at 33°C and differentiated at 37°C with addition of IFNγ. Confluent cells in RPMI 1640 without FBS were treated with 0.5 μM FK-506, 1 μM CsA, 0.5 M sorbitol, 0.5 M NaCl, and 0.5 to 20 μM WNK463 for the times shown, then lysed in 1× RIPA (Cell Signaling) with Halt phosphatase/protease inhibitor cocktail (Thermo) containing 1-3% NaF and Trisodium tetraoxovanadate. DMSO (final concentration 0.05% for added chemicals) was used as a control. A range of WNK463 concentrations (1 to 20 μM) were used to confirm minimal cytotoxicity (**Supplementary Figure 1**).

Reversibility of WNK463 treatments were evaluated by washout studies at the highest dose (**Supplementary Figure 2**).

Isolation of Mouse Glomeruli

To isolate glomeruli, kidneys were removed from mice, placed in iced buffer, decapsulated, and dissected on ice to isolate the cortices from the medullae. The cortices were minced with a razor blade and pushed through a screen (180 μm, W.S. Tyler Co, Cleveland, OH, United States) with a flexible metal spatula. The minced tissue was suspended in PBS with 5.5 mM glucose and 0.3 mM pyruvate (GIBCO), filtered through a 90 μm nylon mesh (Falcon) to remove vessels and large pieces of tissue. The filtrate was collected in a 45 μm mesh nylon filter (Falcon) and contained intact glomeruli with minimal contamination (<2%) by tubular cells (Schlondorff, 1990; Embry et al., 2016, 2018). Glomeruli were maintained in DMEM with 0.1% FBS at room temperature and treated with drugs (FK506 5 μm, CsA 10 μM, and WNK463 0.5–20 μM) as indicated for 2 h before elasticity measurements or confocal imaging.

Animal research was performed in accordance with the UT Southwestern Medical Center Animal IACUC guidelines. The research study protocol (number 2014–0078) was approved by the UT Southwestern Medical Center Animal IACUC (NIH OLAW Assurance Number A3472-01). UT Southwestern Medical Center is fully accredited by the American Association for the Assessment and Accreditation of Laboratory Care, International (AAALAC). Animals are housed and maintained in accordance with the applicable portions of the Animal Welfare Act and the Guide for the Care and Use of Laboratory Animals. Veterinary care is under the direction of a full-time veterinarian boarded by the American College of Laboratory Animal Medicine. Mice were sacrificed for experiments by first anesthetizing with Avertin and then euthanizing by cervical dislocation.

Measurement of Glomerular Elasticity

The elastic moduli of glomeruli isolated from 3–6 month old mice were measured using a microprobe indenter device (Levental et al., 2010; Embry et al., 2016, 2018). Briefly, a tensiometer probe (Kibron, Inc, Helsinki, Finland) with a 250 μm radius flat-bottom needle was mounted on a 3-D micromanipulator with 160 nm step size (Eppendorf, Inc) attached to a Leica inverted microscope. A glass slide containing a dilute sample of glomeruli was imaged by bright field illumination and the bottom of the probe was brought through the air-water interface until it was just above the surface of a single glomerulus of diameter approximately 60 μm. The probe was calibrated using the known surface tension of a pure water/air interface, and the stress applied to the probe as it was lowered onto the glomerulus was measured as a function of indentation depth. In principle, this deformation geometry is that of an infinite plane compressing a spherical object. The absolute values of elastic modulus can be calculated from appropriate models that require assumptions about the adherence of the glomerulus to the probe and the glass slide, whether the glomerular elasticity is modeled as a uniform sphere or an elastic shell, and other structural factors that confound calculation of the magnitude of elastic modulus from the force-indentation data alone. In all cases indentations were kept below 15 μm to avoid large strains that could damage the glomeruli. After the largest indentations, measurements were repeated at small strains to confirm that the deformations were recoverable.

Fractionation of F/G-Actin (Glomeruli)

Isolation of filamentous (F) and globular (G) actin was performed as previously described (Wyss et al., 2011; Embry et al., 2016). Briefly, glomeruli were treated with DMSO (0.05%), FK-506 (5 μM), Jasplakinolide (10 μM), or Latrunculin B (1 μM) for 2 h, then lysed in 20 mM Hepes pH = 7.4, 100 mM NaCl, 1 μM ATP, 1 mM $NaVO_4$, 50 mM NaF, 1% Triton X-100, and protease inhibitor mix as above. Lysates were passed 6 times through a 25-gage needle and then centrifuged at 100,000 × *g* in a TAL-100 rotor for 1 h at 4°C. The supernatant was removed for G-actin analysis, while the pellet containing F-actin was resuspended in 15 mM Hepes pH 7.5, 150 μM NaCl, 1% Triton X-100, 1% Na-deoxycholate, 0.1% SDS, 10 mM EDTA, 1 mM dithiothreitol, 1 mM $NaVO_4$, and protease inhibitor mix. Samples were mixed 1:1 with 2x Laemmli sample buffer, and proteins were separated on 10% acrylamide gels in SDS.

Fractionation of F/G Actin (Cultured Podocytes)

For cell fractionation of F/G-actin, Podocytes were grown to 80–90% confluence in culture medium containing 10% FBS, then changed to serum-free medium for 1 h. Cells were then treated with serum-free medium containing DMSO, FK506 (0.5 μM), Jasplakinolide (1 μM), or Latrunculin B (4 μM) for 3 h. Cells were lysed in F-actin stabilization buffer [G/F KIT Cat. #BK037 CYTOSKELETON, 50 mM PIPES pH 6.9, 50 mM NaCl, 5 mM MgCl2, 5 mM EGTA, 5% (v/v) Glycerol, 0.1% Non-idet P40, 0.1% Triton X-100, 0.1% Tween 20, 0.1% 2-mercapto-ethanol] at 37°C for 30 min. Lysate debris was pre-cleared by centrifugation at 350 × *g* for 5 min at room temperature, then separated into supernatant (S) and pellet (P) fractions by centrifugation at 100,000 × *g* at 37°C for 1 h. F-actin containing pellets were resolublized in 100 μl of F-actin depolymerization buffer (8 M Urea, 10% Glycerol, 20% SDS, 1 M DTT, and 1.5 M Tris pH6.8) on ice for 1 h, pipetting up and down several times every 15 min. Equivalent volumes of input, supernatant, and pellet fractions were analyzed by SDS-PAGE and western blot.

Three-Dimensional Collagen Matrix Contraction Assay

Methods for preparing cell-containing collagen matrices have been described previously (Liu et al., 2014; Embry et al., 2018). Briefly, collagen matrices containing cultured podocytes (2×10^5 cells/200 μL gel) were polymerized for 1 h at 37°C. The gels were released from their substrates to float in RPMI 1640 medium with or without FK506, WNK463, 10% FBS, or DMSO (control) for 4 h and then fixed with 4% paraformaldehyde/PBS. Images of collagen matrices were obtained with an Epson photo scanner. Gel area was analyzed

using ImageJ, and reduction in area was calculated as: original area (12 mm diameter circle) – area after treatment. Relative gel area reduction was normalized to the untreated (DMSO) control condition. Statistical analyses were performed using GraphPad Prism software.

WOUND-INDUCED CELL MIGRATION

Equal numbers of podocytes were seeded on collagen-coated six well plates. Confluent cell monolayers were washed and scratch wounds were created with a 1 ml pipette tip. Culture medium (10% FBS or serum-free) was replaced with medium containing DMSO, FK506 (0.5 μM), or FK506 (0.5 μM) + WNK463 (2 μM). Images were obtained immediately after wound creation and before cell migration. Plates were returned to the incubator and cells were allowed to migrate for 18 h, at which time repeat images were obtained.

IMMUNOFLUORESCENCE STAINING

Treated glomeruli were spun down at 5,000 *g* for 5 min, resuspended and fixed in 4% paraformaldehyde for 30 min, and then washed 3x in PBS. Washed glomeruli were resuspended in PBS, 100 μl pipetted onto a slide, and attached to a coverslip overnight at 4°C. The slide was rinsed in PBS to remove unattached glomeruli and further fixed with 4% paraformaldehyde for 1 h at room temperature. Attached and fixed glomeruli on coverslips were then washed 3x in PBS, blocked with SEA BLOCK Blocking Buffer (PIERCE) for 40 min, then permeabilized with 0.5% Triton X-100 in PBS for 10 min. Glomeruli on coverslips were then stained using standard procedures, and imaging was performed using a Zeiss LSM 880 confocal microscope.

MICROSCOPY AND IMAGE ANALYSIS

Confocal imaging was performed in the Cell Biology and Imaging Core in the O'Brien Kidney Research Core, on a Zeiss LSM880 with Airyscan laser scanning microscope equipped with Plan-Apochromat 10x/0.3 NA, 20x/0.8 NA, 25x/0.8 NA, and 63x /1.40 NA oil-immersion objective (ZEISS, Oberkochen, Germany). Fluorescence images were acquired using ZEN black 2.3 software with a 20x/0.8 NA or 63x/1.40 NA objective and Zeiss Immersion Oil 518F was used for the 63x/1.40 NA objective. Experiments were performed at constant room temperature. Images or regions of interest (ROIs) were further processed with ZEN 2.6 (blue edition) software.

IMAGE ANALYSIS

Podocytes were seeded at low density in 2 of 96 well imaging plates (BD Falcon 353219), treated with the following conditions: control, FK506, WNK463, and FK506 + WNK463 – with and without serum (FBS), and then stained with Hoechst, Rhodamine Phalloidin (542/565), and pOSR1/SPAK (Alexa 488) as detailed above. Images were taken (25 frames per well) using an INCell Analyzer 6000 (GE). CellProfiler was used to identify the nucleus and cell boundary from Hoechst and Phalloidin, respectively, (Kamentsky et al., 2011). Cell size and number of "touching" neighbors for all the cells were obtained. We utilized a MeasureObjectIntensity Distribution module to (1) equally divide each cell along its radius from the center of its nucleus to the membrane edge into 6 bins, (2) measure pOSR1/SPAK average intensities from all the bins in each cell. The average pOSR1/SPAK intensity of outer most bin, i.e., the 6th bin was then used to represent the cell membrane/peri-membrane area. Cells with poorly and under-segmented boundaries were excluded by setting a threshold of cell area/nuclear area ≤ 2. Furthermore, cells with two or more touching neighboring cells were excluded (Note: on average, about 30–40% of cells were excluded). Ruffling cells (cells with lamellipodia) usually have "high" pOSR1/SPAK intensities at the membrane regions. Cells with average intensity in the 6th bin equals or higher than 90th percentile were considered to be "ruffling." The range was carefully chosen by visual inspection. There were 12 replicate wells for each condition (from 2 plates) and roughly 100–150 cells per replicate well.

ELECTRON MICROSCOPY

Tissue samples were fixed with 2.5% (v/v) glutaraldehyde in 0.1 M sodium cacodylate buffer (pH7.4). After three rinses with 0.1 M sodium cacodylate buffer, samples were embedded in 3% agarose and sliced into small blocks (1 mm^3), rinsed with the same buffer three times and post-fixed with 1% osmium tetroxide and 0.8% potassium ferricyanide in 0.1 M sodium cacodylate buffer for one and a half hours at room temperature. Samples were rinsed with water and then block stained with 4% uranyl acetate in 50% ethanol for 2 h. They were then dehydrated with increasing concentration of ethanol, transitioned into propylene oxide, infiltrated with Embed-812 resin and polymerized in a 60°C oven overnight. Blocks were sectioned with a diamond knife (Diatome) on a Leica Ultracut 7 ultramicrotome (Leica Microsystems) and collected onto copper grids, post stained with 2% aqueous uranyl acetate and lead citrate. Images were acquired on a JEM-1400 Plus transmission electron microscope equipped with a LaB_6 source operated at 120 kV using an AMT-BioSprint 16 M CCD camera.

Statistical Analysis

Student *t* test and one-way analysis of variance were used to determine statistical significance.

RESULTS

WNK1 and OSR1/SPAK Are Expressed in Podocytes

Renal glomeruli are vascular structures responsible for producing the initial urinary filtrate. Glomerular podocytes are the cells that

support glomerular capillaries and form the filtration barrier. Because of the importance of WNK protein kinases in the kidney and the vasculature, we investigated the contributions of WNKs to glomerular structure and function. Single cell RNAseq data from the Humphreys laboratory at Washington University[1] shows that WNK1 mRNA is expressed at moderate levels in podocytes, mesangial cells and endothelial cells. Expression of mRNAs for WNK2, WNK3, and WNK4 is negligible or low in these cells, which suggests minimal contributions of these other family members to glomerular processes. Based on these data suggesting that WNK1 is the predominant WNK family member in glomeruli and podocytes, we examined expression of WNK1 in freshly isolated mouse glomeruli using confocal microscopy. WNK1 (**Figure 1A**) and its closely related substrate kinase OSR1 (**Figure 1B**) are expressed in a pattern similar to synaptopodin, a podocyte marker (**Figure 1A**). Synaptopodin (green) is located in capillary loops in the podocyte cytoplasm. WNK1 and OSR staining (magenta) are also observed in the cytoplasm of podocytes. The enlarged images below **Figures 1A,B** show capillary walls where overlap of synaptopodin (green) and WNK1 or OSR1 (magenta) is seen as white. Western blots of cultured mouse podocyte extracts show expression of WNK1 (**Figure 1C**). The specificity of the antibody used was confirmed by siRNA-mediated depletion of WNK1 from Hela cells.

Calcineurin Inhibitors Increase WNK Kinase Activity in Cultured Podocytes

To measure the effects of calcineurin inhibitors on WNK kinase activity in podocytes, cells were treated with 0.5 μM FK506, and WNK activity was measured as accumulation of pOSR1/SPAK (pSer 325) over time. As positive controls, WNK was activated with 0.5 M NaCl or 0.5 M sorbitol. The panWNK inhibitor WNK463 was used to demonstrate a requirement for WNK in OSR1/SPAK activation (**Figure 2**; Yamada et al., 2016a,b). WNK463 reduced phosphorylation of both SPAK and OSR1 below that of untreated podocytes indicating that OSR1/SPAK are partially activated by WNK prior to osmotic stimulation (**Figures 2A,B**). Both 0.5 M NaCl and 0.5 M sorbitol increased pOSR1/SPAK by nearly 2-fold within 20 min and phosphorylation was sustained for over 1 h (**Figure 2B**, brown tracing at top). FK506 also increased pOSR1/SPAK by 20 min (blue bars), with no additional accumulation by 80 min. Inhibition of WNK kinase activity with WNK463 reduced pOSR1/SPAK to half of their activity in untreated cells. We compared the effects of FK506 and CsA on podocyte pOSR1/SPAK and found, as expected, that both calcineurin inhibitors increase WNK activity as determined by increased pOSR1/SPAK sensitive to WNK463 (**Figure 2C**). The extent of pOSR1/SPAK accumulation at 60 min in CsA-treated podocytes was nearly identical to that in FK506-treated podocytes, and in both cases, pOSR1/SPAK was reduced to values below basal by 1 μ M WNK463.

[1]http://humphreyslab.com/SingleCell/

FK506 Increases Glomerular Elastic Modulus (E) by a WNK-Dependent Mechanism

To determine if calcineurin inhibitors affect glomerular elasticity through effects on WNK kinases, we isolated mouse glomeruli and used microindentation to measure Young's modulus (E) following treatment with FK506, CsA, or WNK463 (**Figure 3A**; Levental et al., 2010; Embry et al., 2018). The E of untreated glomeruli from 3–6 month-old mice was 2.0 kPa. FK506 increased E by 25%, to 2.5 kPa, and 2 μm WNK463 reduced E to 1.7 kPa. WNK463 blocked the FK506-induced stiffening of the glomeruli, reducing E to values comparable to controls. The effects of CsA on glomerular elasticity were comparable to those of FK506. WNK463 reduced E of glomerular capillaries in a dose-dependent manner from 2.1 (C) to 1.2 kPa over a dose range of 0.5 to 20 μm (**Figure 3B**). As was the case in cultured podocytes, FK506 increased pOSR1/SPAK approximately two-fold in isolated glomeruli at 30 and 90 min, and the effect was inhibited by WNK463 (**Figure 3C**). These results indicate that effects of FK506 on glomerular stiffening require WNK kinase activity. We assessed the effect of FK506 on the structure of the podocyte actin cytoskeleton by measuring the F/G actin ratio in glomeruli treated with FK506. For comparison latrunculin was used to depolymerize actin and jasplakinolide was used to increase actin polymerization (**Figure 3D**). FK506 increased the F/G actin ratio by 2.8-fold, consistent with the contribution of increased F-actin to the glomerular stiffening response to FK506 and CsA.

FK506-Increased F-Actin and Podocyte Traction Force Require WNK Kinase Activity

An intact podocyte actin cytoskeleton and non-muscle myosins are required for generation of traction force and are basic determinants of the elastic properties of glomerular capillary walls. To assess the effects of FK506 and WNK kinase activity on the ability of podocytes to generate traction force, we used a gel contraction assay which measures the ability of podocytes to bind and move a collagen-based matrix (**Figure 4**). Cultured podocytes were embedded in 3-D collagen gels, treated with FK506, and their ability to contract the gels was measured (Liu et al., 2014; Embry et al., 2018). FK506 caused a concentration-dependent increase in traction force by the embedded podocytes, as demonstrated by a progressive decrease in gel size (**Figure 4A**). This effect of FK506 was substantially reduced by WNK463 (**Figure 4B**). We measured the contribution of WNK activity to gel contraction by 10% serum, which is a strong stimulus for gel contraction (**Figure 4B**). Gel contraction by both agents was reduced by WNK463; however, higher concentrations of WNK463 were required for slightly less effective blockade of serum-induced gel contraction compared to FK506-induced contraction, suggesting that serum acts in part by a WNK-independent mechanism. Measurements of actin F/G ratios in podocytes after FK506 treatment showed that consistent with

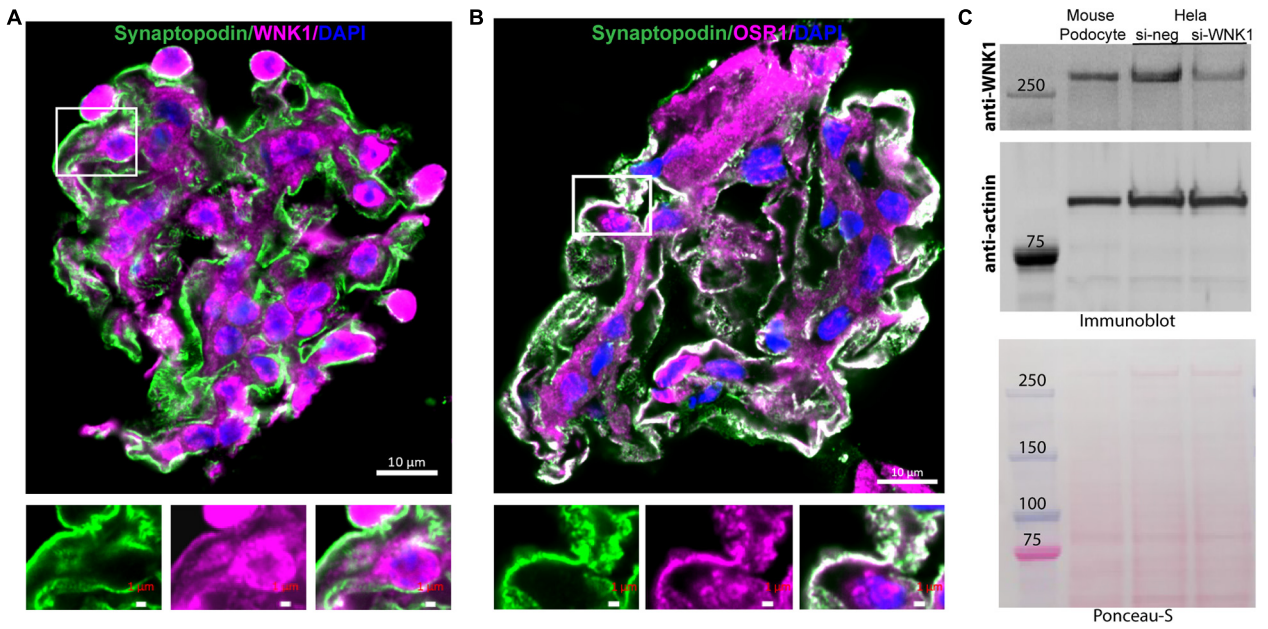

FIGURE 1 | WNK1 and OSR1 are expressed in glomerular podocytes. **(A)** Localization of WNK1 (magenta) and **(B)** OSR1 (magenta) with synaptopodin, a podocyte marker (green) in mouse glomeruli using confocal microscopy. A selected region of the merged double-stained image is enlarged to show overlap (white) of the kinases with synaptopodin below each panel. The images show that WNK1 and OSR1 overlap with synaptopodin indicating that all three proteins are expressed in the cytoplasm of glomerular podocytes. Scale bar in the mages of glomeruli is 10 µm, and in the magnified images is 1 µm. **(C)** Expression of WNK1 in cultured mouse podocytes and specificity of antibody for WNK1. Mouse podocyte cell lysates were separated on a 3–8% Tris-acetate gel and immunoblotted for WNK1. As cultured mouse podocytes are not easily transfected using standard methods, human Hela cells were transfected with siRNA toward WNK1 (si-WNK1) or scrambled control (si-neg), and lysates were used to demonstrate specificity of the antibody. Actinin was used as the immunoblot loading control, and the Ponceau-S stained membrane confirms even transfer of proteins. Molecular mass of protein standards is indicated. Relative to control, siWNK reduced WNK protein by 70 ± 8%.

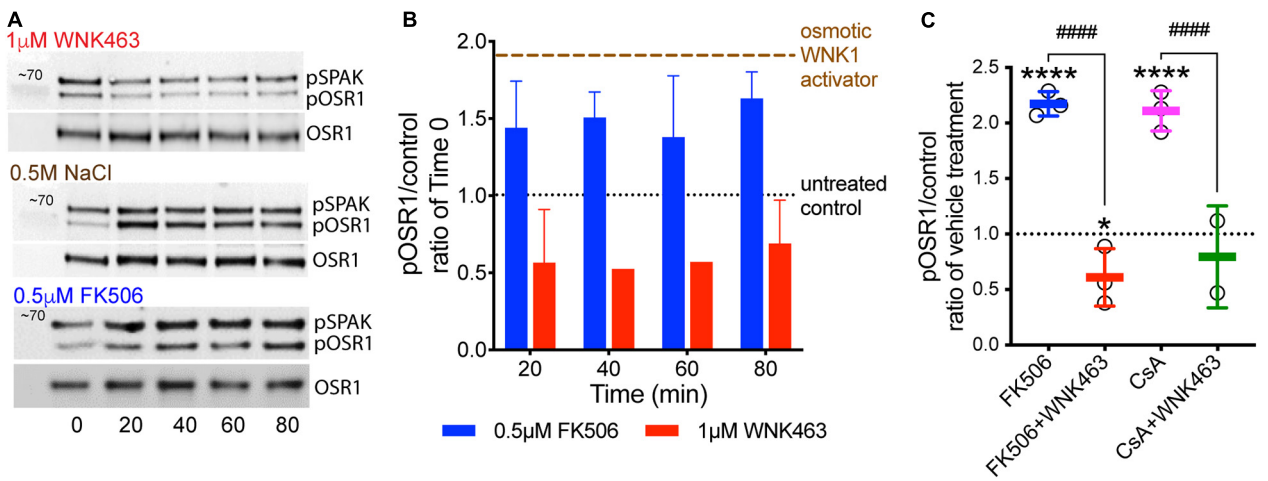

FIGURE 2 | Calcineurin inhibitor-induced increases in pOSR1/SPAK are inhibited by the WNK inhibitor WNK463. **(A)** Representative immunoblots of pOSR1/SPAK and total OSR1 as a loading control in podocyte lysates from cells treated with 1 µM WNK463, 0.5 M NaCl, or 0.5 µM FK506 at indicated times. **(B)** Time course of OSR1 phosphorylation in cultured podocytes in response to FK506 (blue), WNK463 (red) relative to basal phosphorylation at time 0 (black). Phosphorylated OSR1 in response to hypertonic extracellular conditions with added osmotic WNK activators, 0.5 M NaCl or 0.5 M sorbitol (brown tracing) are shown as positive control. The averaged pOSR1/SPAK values ± S.D. were: osmotic activators- 1.8 ± 0.3, $N = 10$; FK506- 1.6 ± 0.3, $N = 14$; and WNK463- 0.6 ± 0.3, $N = 9$. **(C)** Increased phosphorylation of OSR1/SPAK by FK506 (0.5 µM, blue) or cyclosporine A (1 µM, pink), is inhibited by WNK463 (1 µM) at 60 min with indicated treatments. The fold pOSR1/SPAK accumulation at 60 min in CsA-treated podocytes (1 µM) was nearly identical to that in FK506 treated podocytes (2.2 ± 0.11 for FK506 and 2.1 ± 0.25 for CsA), In both conditions pOSR1/SPAK was reduced by 1 µM WNK463 (FK506 0.62 ± 0.25, and CsA 0.79 ± 0.46). Relative amounts of pOSR1 increased by calcineurin inhibitors is significantly inhibited by WNK463. $^{*}p < 0.05$ vs control, $^{****}p < 0.001$ vs control, $^{\#\#\#\#}p < 0.001$ FK506 or CsA vs FK605 or CsA + WNK463 by ANOVA.

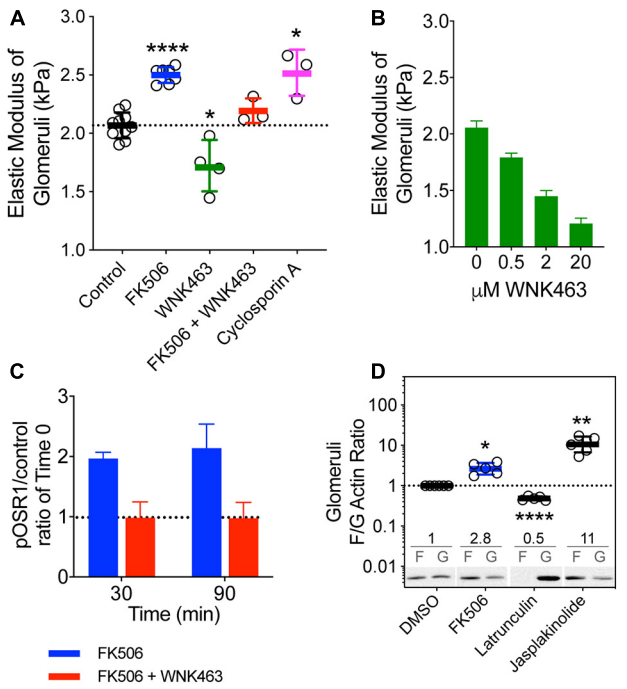

FIGURE 3 | Effects of calcineurin inhibition on the biophysical properties of mouse glomeruli. **(A)** Mouse kidney glomerular elastic modulus (E, Young's modulus) response to FK506 (5 μM), cyclosporine A (10 μM), and WNK463 (10 μM). FK506-induced increase in E is attenuated by WNK kinase inhibition with WNK463. The E of normal control glomeruli from 3–6 month-old mice is 2.01 ± 0.03 kPa. FK506 (0.5 μM) increased E to 2.50 ± 0.03 kPa. WNK463 (2 μM) decreased E to 1.7 ± 0.2 kPa. WNK463 blocked the FK506-induced stiffening of the glomeruli, reducing the value to 1.97 ± 0.03 kPa, indistinguishable from the control value of 2 kPa. CsA increased E to 2.52 ± 0.11 kPa. ****$p < 0.0001$ and *$p < 0.05$ by ANOVA. Mouse glomeruli were freshly isolated and incubated in equivalent volumes of DMSO (Control) FK506, CsA, or WNK463, for 2 h. Glomerular elasticity was measured by microindentation as described in the methods section. **(B)** Increasing doses of WNK463 caused progressive decreases in E. Average values (kPa) ± S.E. are as follows: Control- 2.1 ± 0.59, $N = 2$; 0.5 μM – 1.8 ± 0.4, $N = 6$; 2 μM – 1.5 ± 0.5, $N = 5$; 20 μM – 1.2 ± 0.5, $N = 5$. N refers to the number of glomeruli measured. **(C)** FK506 (0.5 μM) increases glomerular pOSR1/SPAK over basal control levels at 30 and 90 min and the response is inhibited by 10 μM WNK463. *$p < 0.05$, **$p < 0.01$, by ANOVA **(D)** Relative to vehicle control (DMSO), FK506 (0.5 μM, blue) increases glomerular F/G actin ratios by 2.8 ± 0.5-fold ($N = 6$), Latrunculin B (1 μM) 0.48 ± 0.05-fold ($N = 5$), and Jasplakinolide (10 μM) 11.4 ± 4.5-fold. Average F/G actin ratios are indicated above representative immunoblot images for each treatment. Values shown are mean ± SD.

enhanced traction force, the F/G actin ratio is increased 2.4-fold over that in control DMSO-treated podocytes (**Figure 4C**). To investigate the morphologic changes in podocytes and how they relate to gel contraction, podocytes in 3D matrices were imaged with phalloidin staining (**Figure 4D**). After FBS or FK506-induced gel contraction, extensions are fully retracted with wide, rounded processes, lamellipodia, in the majority of cells. In the gels treated with WNK463 that have reduced traction force, most cells in the 3D matrices have long extensions with a reduced number of the rounded processes seen in the retracted state (**Figure 4D**; Liu et al., 2014). **Supplementary Figure 3** shows higher magnification images of podocytes in gels with FK506, serum, and WNK463 treatment where the effects of the treatments on their structure are more clear. These profound differences in cell morphology after FK506- and serum-stimulated contraction, or with WNK kinase inhibition indicate that WNK activity contributes to actin-mediated cell adhesion, lamellipodium generation, and traction force generation in a collagen matrix.

WNK Activity Is Necessary for Maintenance of Lamellipodia at Cell Leading Edges

Because calcineurin inhibitors activate WNK and OSR1/SPAK, increase the elastic modulus of glomeruli, the fraction of F-actin, and the traction force of cultured podocytes in 3-D collagen gels, we investigated the effects of FK506 and WNK463 on the morphology and localization of pOSR1/SPAK in cultured podocytes. Brightfield images of cells (panels a, e) show enhanced contrast at membrane protrusions (arrows) that increased in response to FK506. FK506-stimulated membrane edge contrast was reduced by WNK463 (panel i). Confocal images of pOSR1/SPAK (panels b, f, j; green) show punctate cytoplasmic patterns with concentration at the edges of protrusions that is increased by FK506- and reduced in WNK463-treated cells. F-actin/phalloidin staining (panels c, g, k; red) shows a pattern of edge staining with cytoplasmic haziness in untreated cells. In FK506-treated cells, the cell edge staining is thicker and more intense. In the cells treated with FK506 and WNK463, the edge staining is markedly reduced. The merged views (panels d, h, l) show overlap (yellow areas) of pOSR1/SPAK and F-actin staining most easily seen in the high magnification insets. Comparison of the high magnification views of panels d (control) and h (FK506) shows an increase in the width and intensity of actin and pSPAK/OSR1 (yellow) staining indicating increased actin and pSPAK/OSR1 density at the cell edge in cells treated with FK506. Panel l, FK506 + WNK463, shows a marked reduction in the intensity and width of edge staining compared to control or FK506 alone. The effects of FK506 on lamellipodium formation were confirmed by imaging podocytes for cortactin, considered a marker for cortical actin found in lamellipodia, and F-actin (**Supplementary Figure 4**; Boguslavsky et al., 2007; Sun et al., 2013). An increase in lamellipodia in response to FK506 is readily appreciated as is the effect of WNK463 to reduce lamellipodia (best seen in the high magnification insets).

To quantify changes in pOSR1/SPAK and F-actin in the membrane-edge observed in **Figure 5A**, the cells were cultured in collagen coated 96 well plates. The average intensity of pOSR1/SPAK in the membrane region was used to determine the number of cells with "ruffles" (see experimental procedure). Under these conditions, FK506 significantly increased the number of cells with membrane ruffling by 136% compared to control, and WNK463 significantly decreased number of cells with ruffling to 60% compared to control. The extent and number of cells with membrane ruffling that were treated with FK506 and WNK463 was similar to that in control (87% of control) and significantly different from FK506 treatment alone

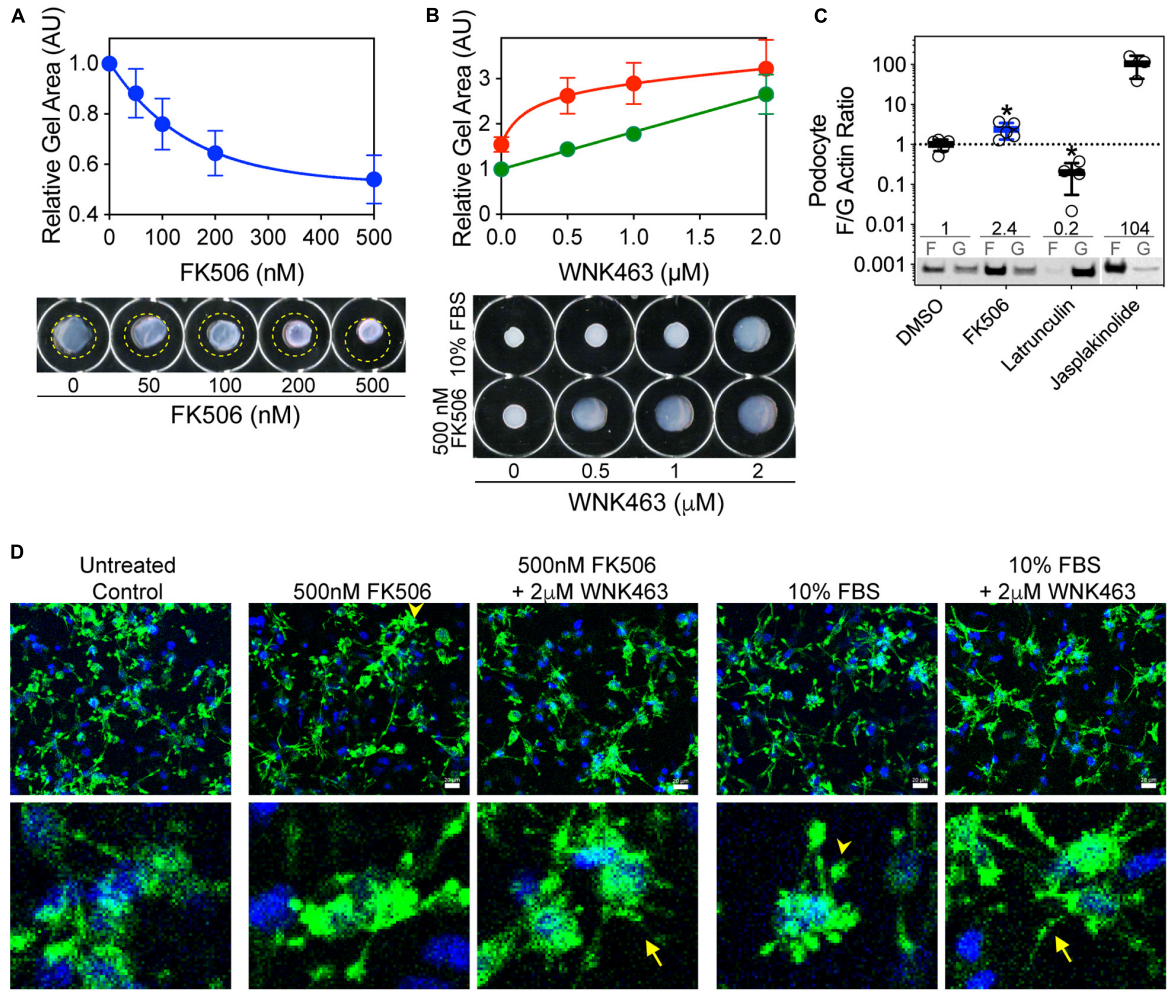

FIGURE 4 | FK506-induced podocyte traction force in floating 3D collagen matrix gels is inhibited by WNK463. **(A)** Effects of increasing concentrations of FK506 on podocyte traction force in 3D collagen matrix. Average gel area ± S.D. of three independent experiments performed in duplicate are shown. The relative areas ± S.D are: C, 1.00; 50 nm, 0.88 ± 0.09; 100 nm, 0.76 ± 0.10; 200 nm, 0.64 ± 0.09; and 500 nm, 0.54 ± 0.1. Representative images of floating collagen matrices are shown, with original matrix size indicated (yellow dotted line). **(B)** Attenuation of FK506- (red) or serum-induced (green) matrix contraction by WNK463. Representative images of floating collagen matrices are shown. **(C)** Podocyte F/G actin ratio is increased by FK506 treatment (0.5 μM) 2.4 ± 0.2-fold, 104 ± 50-fold by Jasplakinolide (1 μm), and decreased to 0.20 ± 14-fold of control by Latrunculin B (1 μm). Values shown are mean ± S.D. and are above representative immunoblots. **(D)** Podocytes in 3D collagen matrix at end of floating matrix contraction assay were fixed and stained for actin to visualize cell extensions. Untreated cells are shown as control. After treatment with 0.5 μM FK506 or 10% FBS, consistent with enhanced contraction measured by reduction in gel size, cells have retracted processes that are in close proximity to the cell bodies (arrowheads). When also treated with 2 μM WNK463, most cell processes remain extended (arrows) with diffuse staining throughout, consistent with decreased retraction force. Insets show higher magnification of cell structures under the five experimental conditions.

(**Figure 5B**). The effects of FK506 and WNK463 are confirmed in **Supplementary Figure 4** with cortactin and F-actin staining.

FK506 Increases, and WNK Inhibition Decreases Podocyte Migration

To provide an independent measurement of the functional consequences of increased cell process formation, we used wound healing assays to measure the effects of FK506 and WNK463 on podocyte migration (**Figure 6**). Images of podocytes immediately after a region of adherent cells was removed (upper row), were compared to images of the same area 18 h after no treatment (Control), FK506 (0.5 μm), or FK506 (0.5 μM) plus WNK463 (2 μM; lower row; **Figure 6A**). The percentage of the original wound area (outlined in yellow), covered by cells that migrated was quantified. The control cells migrated to cover 60% of the denuded area, FK506 treated cells covered 85% of the area, but the cells treated with FK506 + WNK463 covered only 30% of the area (**Figure 6B**).

Depletion of WNK1 Replicates the Effects of WNK463

Because WNK463 is a pan-WNK inhibitor, it cannot distinguish which or how many of the four WNKs mediate the effects we observe. Based on the single cell RNAseq data cited above, we

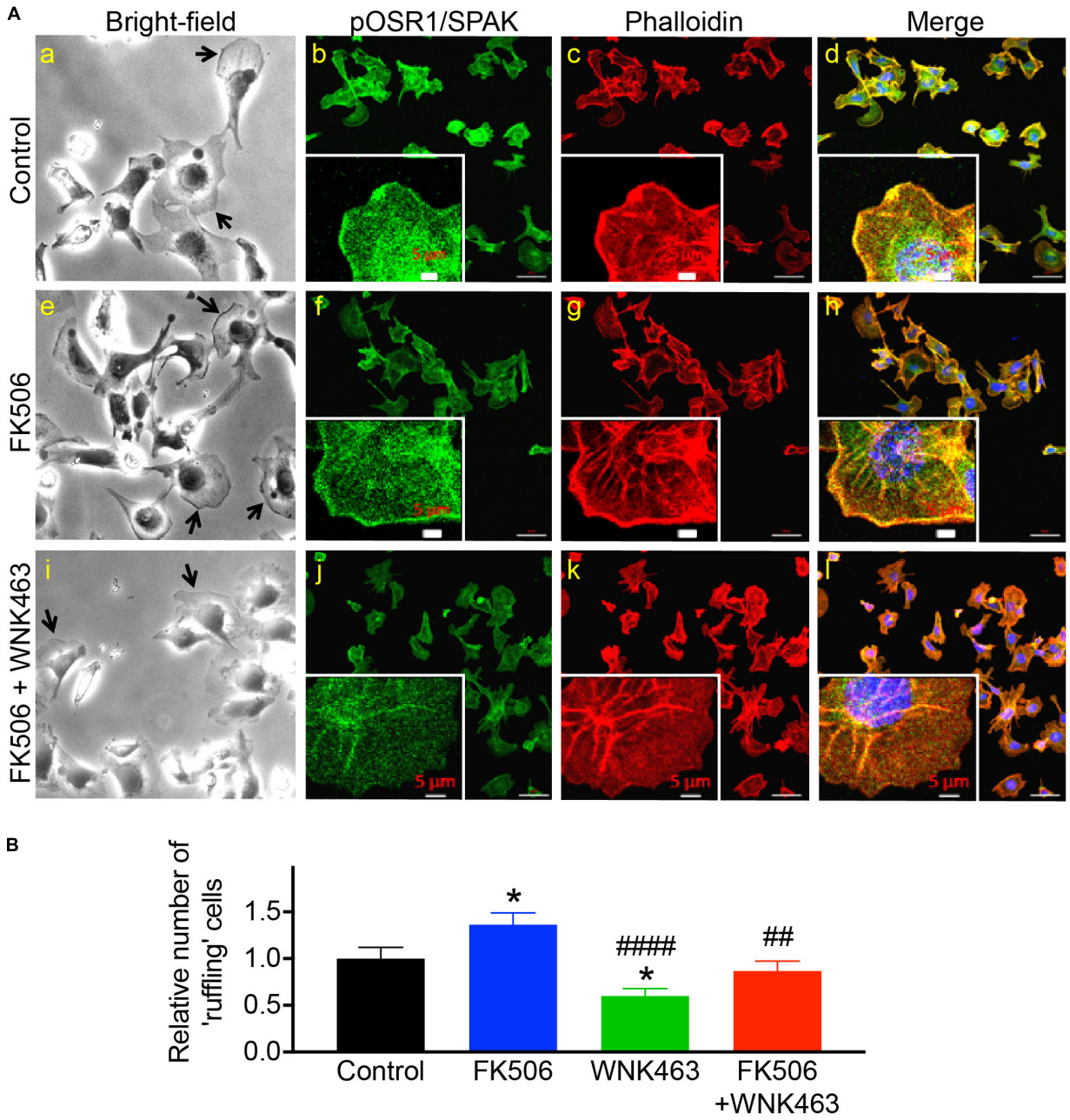

FIGURE 5 | Phospho-OSR1/SPAK co-localization with F-actin at edges of podocyte membrane protrusions is reduced with WNK kinase inhibition. **(A)** Bright-field image of podocytes in culture (panels a, e, i), and confocal microscopy of pOSR1/SPAK (green, panels b, f, j) and F-actin (red, phalloidin panels c, g, k), as indicated. Protruding edges of spread cells in culture are indicated with arrows in bright-field images. Cells treated with FK506 have darker edges in bright-field and confocal images, with visibly stronger co-localization of pOSR1/SPAK and actin (merged panels d, h, l). Localization to the membrane periphery is attenuated with WNK463. **(B)** Relative number of cells with protrusions or "ruffling" cells for control, FK506, WNK463, and FK506 + WNK463 (compared to control) in FBS-containing medium are shown. The values shown are average ± S.E.M from 12 replicate samples and are Control 1.0 ± 0.12, FK506 1.36 ± 0.12, WNK463 0.60 ± 0.08, and FK506 + WNK463, 0.869 ± 0.10; $^{*}p < 0.05$, compared to control, $^{\#\#}p < 0.05$, and $^{\#\#\#\#}p < 0.001$ compared to FK506 by ANOVA.

tested WNK1 as the most likely candidate. We depleted WNK1 in podocytes with siRNA achieving a 40–50% reduction in WNK1 protein compared to the control siRNA, that was accompanied by a proportional (∼50%) reduction in pOSR1/SPAK (**Figure 7A**). If WNK1 is the predominant WNK family member expressed and responsible for lamellipodium formation, cell migration, and cell spreading in cultured cells, the reduction in WNK1 should be accompanied by proportional reductions in these three cell behaviors. In the control (si-neg control) panel stained for WNK1, WNK1 is seen at the leading edges of two cells (arrows)

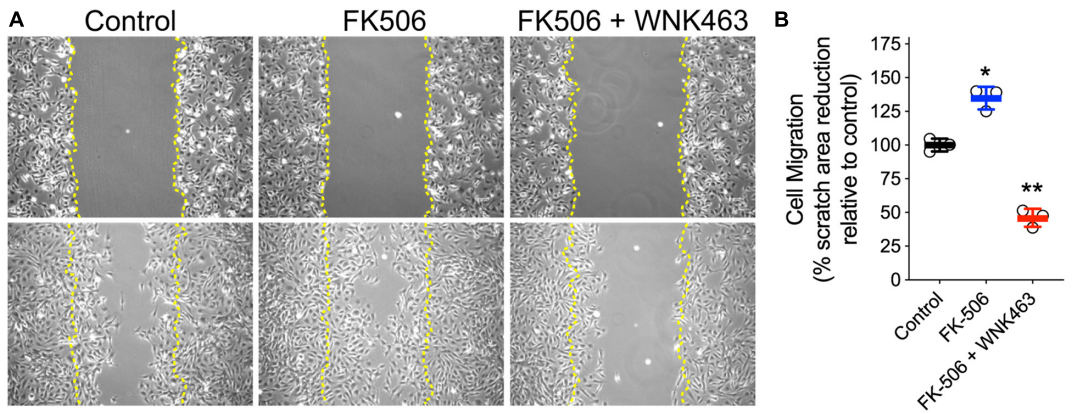

FIGURE 6 | Activation of cell migration by FK506 is attenuated by WNK463-inhibition of WNK kinases. **(A)** Representative images of podocytes at $T = 0$ (top row) and 18 h after indicated treatments (bottom row). Margins of wound from scratched monolayer are shown with yellow dotted lines. **(B)** Cell migration is calculated as percentage original wound area occupied by cells after 18 h in culture in indicated treatment conditions. Cell migration relative to control cells is shown. The control cells migrated to cover 63 ± 3% (Mean ± S.D.) of the denuded area, FK506 treated cells covered 85 ± 5% of the area, but the cells treated with FK506 + WNK463 covered only 29 ± 4% of the area. $N = 3$ independent experiments. $^{*}p < 0.05$ and $^{**}p < 0.01$ by ANOVA.

and F-actin is concentrated in the same areas (**Figure 7B**). Lamellipodium and WNK1 staining at the leading edges of podocytes were reduced in WNK1-depleted podocytes. The two cells on the right side of the si-WNK1 panel stained for WNK1 have irregular borders and less intense staining for WNK1 than the two spread cells on the left of the panel or the cells in the si-neg cont panel and do not have structures that resemble lamellipodia. These cells resemble the cells in **Supplementary Figures 1**, **2** that were treated with high concentrations of WNK463 and may have the greatest level of WNK1 depletion. The two cells on the left of this panel are spread but do not have structures consistent with lamellipodium formation and may have intermediate levels so WNK1. WNK1 siRNA reduced podocyte migration in the wound healing assay (**Figure 7C**), as well as the number of spreading cells and lamellipodium formation (**Figures 7D,E**), compared to that of cells transfected with the control siRNA. WNK1 depletion caused decreases in these WNK463-sensitive responses in proportion to the degree of WNK1 depletion. These results support the conclusion that WNK1 mediates much if not all of the effects of calcineurin inhibitors on cytoskeletal structures in podocytes.

WNK/OSR1/SPAK Activity Are Required for Structural Integrity of Glomeruli

In vivo cells function in a highly complex three-dimensional microenvironment, composed of multiple matrix proteins, direct contact and communication with other cells, and soluble factors. They cannot develop comparable cell morphology or structure within a less complex *in vitro* environment. Extending our biophysical measurements of glomerular stiffness and podocyte cell contraction and migration, we used confocal microscopy of freshly isolated glomeruli to determine if WNK kinase activity contributes to podocyte and glomerular capillary structure (**Figure 8**). Staining for synaptopodin (green), pOSR1/SPAK (magenta), and nuclei (blue, DAPI) in DMSO (vehicle control), or WNK463 treated glomeruli shows that inhibition of WNK activity caused dramatic structural changes in the podocytes, resulting in a fundamentally different appearance of glomeruli (**Figure 8A**). The DMSO-treated glomeruli have the expected structure and patterns of staining for synaptopodin and pOSR1/SPAK can be seen along capillary walls. In contrast, treatment with 2 μM WNK463 leads to dramatically reduced and irregular synaptopodin and pOSR1/SPAK staining (**Figure 8B**). Unlike the appearance in control cells, pOSR1/SPAK staining in capillary walls in a pattern that corresponds to synaptopodin staining is markedly reduced. These images suggest dramatic changes in cell structure and cell-matrix interactions with WNK inhibition.

In order to define the effects of FK506 and WNK643 on glomerular capillaries at the ultrastructural level, we used transmission electron microscopy of isolated glomeruli treated for 2 h with vehicle (DMSO), FK506 (0.5 μm), or WNK463 (2.0 μm) to analyze podocyte and foot process structure (Pisarek-Horowitz et al., 2020). Transmission electron microscopy showed that FK506 has a minimal effect on the structure, size, or organization of foot processes (**Figures 9A–C**). The foot processes are approximately 3 μm wide (0.28 Control, 0.26 FK506), and the slit diaphragm density was similar in the control and FK506-treated mice, 4–4.4 SD/μm GBM (**Figures 9B,C**). However, treatment with WNK463 resulted in wider and irregularly-sized foot processes, demonstrating early signs of podocyte injury (**Figure 9A**). In these samples, the foot processes were wider, approximately 0.5 μm on average (**Figure 9B**), and the slit diaphragm density was reduced by approximately 40% from 3.9 (control) to 2.4 slit diaphragms/μm GBM (**Figure 9C**).

DISCUSSION

The podocyte actin cytoskeleton is essential for the normal functions of podocytes including their interactions with

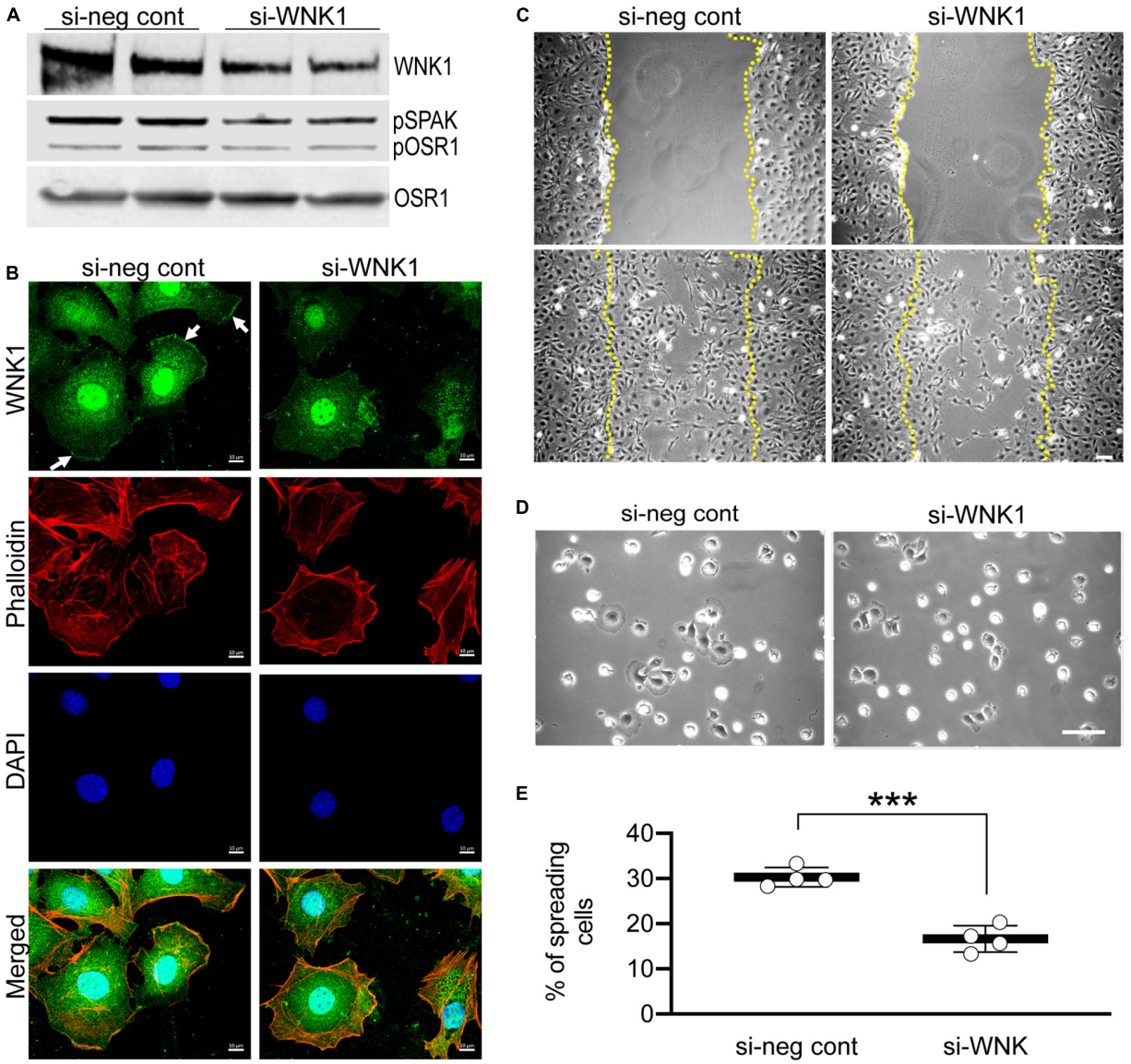

FIGURE 7 | siRNA-mediated depletion of WNK1 replicates the effects of WNK463. Podocytes were transfected with siRNA directed against WNK1 or non-specific control siRNA and studies were carried out 24 h later. **(A)** shows a representative paired experiment comparing the basal level of pOSR1/SPAK in cells transfected with non-specific negative control siRNA (si-neg cont) or the WNK1 targeted siRNA (si-WNK1), as indicated. **(B)** Podocytes transfected with si-neg cont or si-WNK1 were stained with WNK1 antibody (green, enlarged image), rhodamine phalloidin (red, smaller top panel), and DAPI (blue, smaller center panel). Merged (smaller lower panel) image is shown. WNK1 stained panel is enlarged to show localization at the lamellipodia in si-neg cont (arrows) that disappears with WNK1 protein knockdown with si-WNK1. Scale bar = 10 μm. **(C)** Representative images of podocytes transfected with si-neg cont or siWNK1 as indicated at $T = 0$ (upper row) and 22 h (lower row) after treatments. Margins of wound from scratched monolayer are shown with yellow dotted lines. Scale bar = 150 μm. **(D)** Representative images of podocyte cell spreading, captured 2 h after replating, post 48 h after transfection with si-neg cont or si-WNK1. Scale bar = 100 μm. **(E)** Quantification of% of spreading cells in si-neg cont and si-WNK1 transfected cells. The values for si-neg control are 30.3 ± 2.13 and for si-WNK1 are 16.6 ± 2.92, and represent average ± S.D. from 4 random fields of at least 250 cells; $^{***}p < 0.001$ by *t*-test.

matrix and neighboring podocytes. These matrix and cell-cell interactions determine the ability of podocytes to adhere to the glomerulus, as well as the mechanical properties of podocytes and glomerular capillaries. Following experimental injury and in renal disease, podocytes are lost from glomeruli at an increased rate leading to cycles of hypertrophy and further podocyte loss (Wiggins et al., 2005; Faul et al., 2008; Ding et al., 2017; Lemley, 2017; Nishizono et al., 2017; Schell and Huber, 2017).

In small clinical studies and collections of patient cases with kidney diseases including WT1 mutation-associated glomerular disease, membranous nephropathy, and Alport nephropathy, CsA or FK506 can improve the course of the kidney disease (Charbit et al., 2007; Waldman et al., 2007;

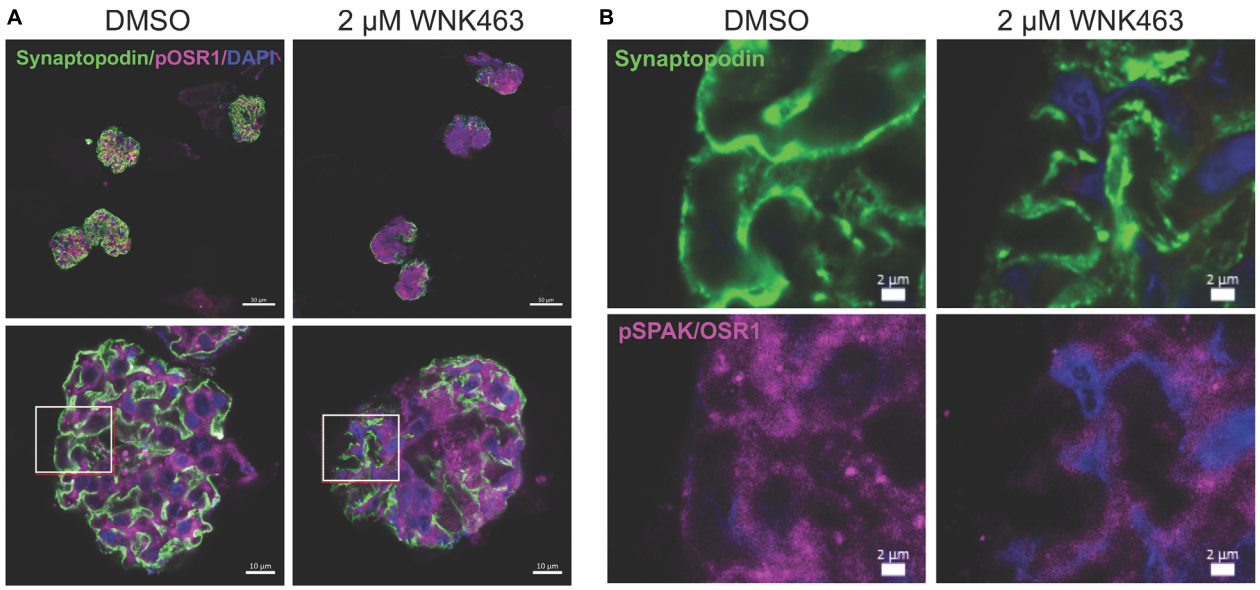

FIGURE 8 | WNK1 and OSR1/SPAK activity are required for normal glomerular capillary structure. Confocal microscopy of isolated mouse glomeruli treated with vehicle (DMSO) or WNK463 (2 μM) for 3 h. Glomeruli were stained for pOSR1/SPAK (magenta), synaptopodin (green), and DAPI (blue) for nuclei. **(A)** The top panels show four glomeruli at low magnification (50 μm scale bars), and the bottom panels show single glomeruli at high magnification (10 μm scale bars). Synaptopodin staining is reduced in the glomeruli treated with WNK463. Insets (white boxes) show the locations of the higher magnification images in **(B)** from the DMSO and WNK463-treated glomeruli (scale bars 2 μm) stained for synaptopdin (green, top), (pOSR1/SPAK magenta, bottom), or nuclei (DAPI, blue). The capillary wall pOSR1/SPAK and synaptopodin staining is even and distinct in the DMSO-treated capillary wall, but not the WNK463-treated capillary wall. In the insets representing the WNK463-treated glomerulus, capillary wall structure is disrupted with reduced intensity of pOSR1/SPAK staining and absence in regions of synaptopodin staining. The synaptopodin staining is irregular in contour and intensity.

Bensman and Niaudet, 2010; Chiba and Inoue, 2019). Alport nephropathy, for example, is caused by mutations in type IV collagen which forms the GBM; calcineurin inhibitor-based improvement in this disease occurs by mechanisms that appear to be independent of T-cell involvement (Charbit et al., 2007; Bensman and Niaudet, 2010). Consistent with effects observed in patients, calcineurin inhibitors preserve podocyte cytoskeletal structure and glomerular integrity in mouse experimental models following exposure to lipopolysaccharide, puromycin aminonucleoside, or protamine sulfate, also by mechanisms that are T cell-independent. Proposed mechanisms for preservation of podocyte structure include prevention of synaptopodin degradation, reduction in injury-induced WAVE1 [Wiscott-Aldrich Syndrome Protein (WASP)-family protein 1] expression, and inhibition of apoptosis (Faul et al., 2008; Vassiliadis et al., 2011; Li et al., 2015; Shen et al., 2016; Buvall et al., 2017). Because calcineurin inhibitors activate WNKs, we investigated the contribution of WNK regulation by calcineurin inhibitors to the calcineurin inhibitor-mediated improvement in glomerular podocyte function and glomerular structure.

Using a distinct set of assays for glomerular capillary and podocyte cell structure and function, we found evidence for a mechanism involving calcineurin, WNK kinases and OSR1/SPAK kinases that regulates podocyte cytoskeleton structure, foot process structure, and glomerular capillary wall structure and elasticity. Stabilization of podocytes on the GBM and glomeruli with increased capillary stiffness mediated by the calcineurin-WNK-OSR1/SPAK signaling pathway-stimulated increase in F-actin may contribute to protection of podocytes and glomeruli in some glomerular diseases and disease models where a component of glomerular injury is softening of glomeruli and podocytes (Wyss et al., 2011; Embry et al., 2016, 2018; Calizo et al., 2019; Ge et al., 2020). These discoveries in renal glomeruli may be applicable to other cells and tissues where WNKs may have a fundamental role in regulating cytoskeleton, cell, and tissue structure, and mechanical properties.

Several lines of evidence suggest that WNK1 is the primary mediator of these processes. The high degree of WNK463 specificity for WNK family members and involvement of OSR1/SPAK in these events clearly implicate WNK kinases as the integrators of these podocyte and glomerular capillary functions (Zhang et al., 2016; Yamada et al., 2016a,b). WNK1 is expressed ubiquitously and has a central role in numerous cell behaviors notably in endothelial cells where WNK1 knockdown has effects similar to those of WNK463 in podocytes and on glomerular cytoskeletal structure (Xie et al., 2009, 2013; Dbouk et al., 2014). We find that WNK1 protein is expressed in cultured podocytes and glomeruli in a pattern consistent with podocyte expression. Expression of the other WNK kinases in the glomerulus has not been unequivocally defined, but snRNAseq data from the Humphreys laboratory at Washington University (see text footnote 1) shows that WNK1 mRNA is the predominant form expressed in glomerular cells, particularly podocytes, suggesting minimal contributions of other family members.

With No Lysine 1 has been implicated in cytoskeletal structure and cell motility for more than 10 years but mechanistic

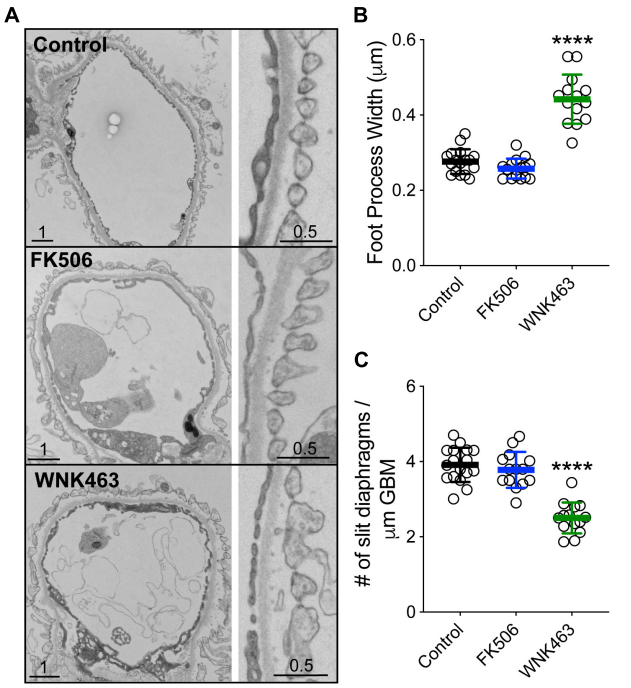

FIGURE 9 | WNK1 activity controls glomerular capillary and podocyte foot process structure. **(A)** Isolated mouse glomeruli were treated with DMSO (Control, top panel), FK506 (500 μM, middle panel), or WNK463 (2 μM bottom panel) for 2 h and fixed, **(B)** Summary of podocyte foot process width measurements. The foot processes are approximately μm wide [0.28 ± 0.04 μm (Control, $n = 17$) and 0.26 ± 0.06 μm FK506, $n = 17$]. Treatment with 2 mM WNK463 for 2 h resulted in wider and irregularly-sized foot processes **(B)**. In these samples, the foot processes are 0.478 ± 0.647 μm ($n = 15$). **(C)** Summary of slit diaphragm density measurements. The slit diaphragm density was similar in the control and FK506-treated mice, 3.91 ± 0.44 and 4.49 ± 1.05 SD/μm GBM, respectively. **(B)** Slit diaphragm density was reduced from 3.91 ± 0.44 (control) to 2.41 ± 0.5 (number SD/μm GBM) by WNK463 treatment. Isolated glomeruli were fixed in glutaraldehyde and cacodylate buffer, and processed as described in Methods. Images shown were obtained at 3,000×. In each condition, the widths of approximately 200 foot processes over approximately 200 μm of GBM were measured from at least six separate glomeruli. Values shown are mean ± SD. ****$p < 0.0001$ by ANOVA with multiple comparisons post-test against Control.

details have emerged only recently. WNK463 inhibits corneal wound healing and reduces filopodium formation in engineered corneas and cultured corneal epithelial cells where WNK1 is the predominant WNK isoform expressed (Desjardins et al., 2019). A pathway including WNK1, SPAK and NKCC1 mediates vascular tone and the pressor response to α_1 adrenergic agonists in WNK1$^{+/-}$ mice (Bergaya et al., 2012). Knockdown of WNK1 reduces cord formation and migration toward serum by human vein endothelial cells (Dbouk et al., 2014). In T lymphocytes, activation of WNK1 by the T-cell receptor or CCR7 decreases T-cell adhesion to LFA and increases migration, both by WNK1 kinase-dependent mechanisms. Stimulation of migration in T lymphocytes also requires activation of OSR1/SPAK and NKCC1 (SLC12A2), and is convergent with models that involve Cl flux-determination of cell volumes at the cell leading and training edges (Kochl et al., 2016). WNK1 and 3 and their regulation of OSR1/SPAK and NKCC1 are essential for glioblastoma cell migration (Haas et al., 2011; Zhu et al., 2014). This mechanism may be applicable to podocytes and glomeruli, where we identified WNK1 and OSR1/SPAK activity-dependent changes in cell membrane morphology and migration as well as capillary elasticity.

We found that calcineurin inhibitors increased OSR1/SPAK activity in cultured podocytes, in glomerular homogenates, and in capillary walls, and led to increased levels of F-actin, lamellipodium formation with increased cortical actin density, cell migration in monolayers, increased stress fibers, and podocyte traction force in 3-D collagen gels. All effects were sensitive to WNK inhibition. Additionally, in intact isolated glomeruli, a native 3-D structure with intact podocyte geometry and cell interactions, activation of WNK/OSR1/SPAK stiffens glomeruli. This response is at least partly attributable to increased cortical F-actin in podocytes, and may also reflect other alterations in cell structure, such as cell-cell adhesion, cell-matrix adhesion, and possibly cell volume (Kochl et al., 2016; Embry et al., 2016, 2018). Treatment of glomeruli with a WNK inhibitor resulted in loss of active OSR1/SPAK in capillary walls, progressive loss of synaptopodin staining, disruption of capillary wall structure, and softening of capillary walls. Transmission electron microscopy images of glomeruli after acute WNK inhibition *ex vivo*, shows widening of foot processes and a reduction in slit diaphragm density consistent with early podocyte injury. The findings that WNK463 causes specific structural changes in cultured podocytes (loss of lamellipodia, reduced cortical actin) that are reversible with drug removal, and that WNK kinase inhibition disrupts glomerular capillary structure with widening of foot processes and reduction in slit diaphragm density are evidence for specific WNK effects on cell and tissue structure in 2-D and 3-D environments, and not toxicity (**Supplementary Figures 3**, **4**).

Some studies in 2-D culture systems associate increased podocyte motility and lamellipodium formation with podocyte injury and glomerular pathology (Asanuma et al., 2006; Akilesh et al., 2011). We find that WNK1 contributes to increased podocyte motility and lamellipodium formation in 2-D culture systems in concert with increased F-actin formation. In 3-D systems, WNK1 activation is associated with increased podocyte contractility and increased stiffness of glomerular capillary walls, concurrent with increased F-actin formation. These effects are consistent with the protective effects of calcineurin inhibitors on podocytes and glomeruli in disease models and some human diseases where evidence exists for podocyte and capillary softening as part of the disease process (Wyss et al., 2011; Embry et al., 2016, 2018; Calizo et al., 2019; Ge et al., 2020).

In 2-D and 3-D environments, cell migration utilizes the same basic biochemical mechanisms including small GTPase-regulated actin cytoskeletal rearrangements, but the processes by which the cells move may differ (Asanuma et al., 2006; Akilesh et al., 2011; Paluch et al., 2016; Yamada and Sixt, 2019). In 2-D environments, cells migrate by extending lamellipodia or sometimes filopodia in the direction of travel, forming adhesions to matrix, and retracting the rear of the cell. In 3-D environments, where

cells are more confined, migration is thought to occur through "mesenchymal" or "ameboid" mechanisms, or a combination of the two (Paluch et al., 2016). Mesenchymal migration in 3-D is characterized by extension of lamellipodia or filopodia-like structures into the matrix, and establishment of adhesive contacts followed by retraction of the cell in the direction of migration, similar to migration in 2-D environments. Ameboid migration is characterized by extensive changes in cell shape without specific interactions with the matrix. The structures involved in ameboid motility are blebs, microscopic cytoplasm-filled bulges in the plasma membrane, and lobopodia, bleb-like protrusions at the leading edge driven by cytoskeleton-generated asymmetric hydrostatic pressure gradients within the cell. Lobopodia may result from changes in local cytoskeletal rearrangement and generalized or localized cell volume alterations (Paluch et al., 2016). Our results indicate that WNK1 signaling is important for migration and by implication regulated changes in cytoskeletal structure in both 2-D and 3-D environments.

In conclusion, we demonstrated that WNK1 and OSR1/SPAK are essential for maintenance of normal glomerular and podocyte architecture and biomechanical properties. WNK1 and its substrate kinases OSR1/SPAK are expressed in isolated glomeruli, glomerular podocytes, and cultured podocytes with similar cytoplasmic distributions. Our studies reveal that WNK1 and OSR1/SPAK kinases regulate actin structures and affect cell interactions with matrix and neighboring cells. We found that FK506 and CsA activate WNK1 and OSR1/SPAK in these cells and their activation causes an increase in F-actin that leads to increased stiffness of glomeruli and increased cell protrusions in cultured podocytes. These structural changes manifest as cell migration in 2D culture or collagen gel contraction in 3-D culture. Our work reveals new functions for WNK and OSR1/SPAK kinases, and suggests an important mechanism by which podocyte cytoskeletal structure and matrix interactions can be modified, and by which calcineurin inhibitors may protect podocytes and glomeruli from injury.

DATA AVAILABILITY STATEMENT

The raw data supporting the conclusions of this article will be made available by the authors, without undue reservation.

ETHICS STATEMENT

The animal study was reviewed and approved by UT Southwestern Medical Center Animal IACUC.

AUTHOR CONTRIBUTIONS

RTM, MHC, ZL, ANC, and CW: conceptualization and formal analysis. ZL, JY, AE, LL, HAD, and ABJ: investigation. ZL, JY, JMH, MHC, and RTM: methodology. RTM, ANC, JMH, MHC, and ZL: writing first draft, revisions, and editing. ANC, RTM, and MHC: supervision. RTM and MHC: funding Acquisition. All authors contributed to the article and approved the submitted version.

FUNDING

This work was supported by the National Institute of Health, (NIH RO1-DK083592, RTM; VA Merit Award BX004691, RTM; and R01 HL147661, MHC), the Welch Foundation (I1243, MHC), AHA postdoctoral fellowships (ABJ and HAD), the Charles and Jane Pak Foundation (RTM), and NIH 1S10OD021685-01A1 to Katherine Luby-Phelps (JEOL1400 Plus electron microscope).

ACKNOWLEDGMENTS

The authors thank members of the electron microscopy core, Anza Darehshouri and Robyn Roman, Svetlana Earnest, Dr. Michael Kalwat, members of the Cobb lab, Chou-Long Huang, Orson Moe, and Charles Pak for insightful discussions, Dr. Barbara Barylko for assistance with F/G-actin fractionation, and Dionne Ware for administrative assistance.

SUPPLEMENTARY MATERIAL

The Supplementary Material for this article can be found online at: https://www.frontiersin.org/articles/10.3389/fcell.2020.618898/full#supplementary-material

REFERENCES

Akilesh, S., Suleiman, H., Yu, H., Stander, M. C., Lavin, P., Gbadegesin, R., et al. (2011). Arhgap24 inactivates Rac1 in mouse podocytes, and a mutant form is associated with familial focal segmental glomerulosclerosis. *J. Clin. Invest.* 121, 4127–4137. doi: 10.1172/jci46458

Asanuma, K., Yanagida-Asanuma, E., Faul, C., Tomino, Y., Kim, K., and Mundel, P. (2006). Synaptopodin orchestrates actin organization and cell motility via regulation of RhoA signaling. *Nat. Cell Biol.* 8, 485–491. doi: 10.1038/ncb1400

Bensman, A., and Niaudet, P. (2010). Non-immunologic mechanisms of calcineurin inhibitors explain its antiproteinuric effects in genetic glomerulopathies. *Pediatr. Nephrol.* 25, 1197–1199. doi: 10.1007/s00467-010-1469-2

Bergaya, S., Vidal-Petiot, E., Jeunemaitre, X., and Hadchouel, J. (2012). Pathogenesis of pseudohypoaldosteronism type 2 by WNK1 mutations. *Curr. Opin. Nephrol. Hypertens.* 21, 39–45. doi: 10.1097/mnh.0b013e32834d2fde

Boguslavsky, S., Grosheva, I., Landau, E., Schtutman, E., Cohen, M., Arnold, K., et al. (2007). p120 catenin regulates lamellipodial dynamics and cell adhesion in cooperation with cortactin. *Proc. Natl. Acad. Sci. U.S.A.* 104, 10882–10887. doi: 10.1073/pnas.0702731104

Buvall, L., Wallentin, H., Sieber, J., Andreeva, S., Choi, H. Y., Mundel, P., et al. (2017). Synaptopodin is a coincidence detector of tyrosine versus Serine/Threonine Phosphorylation for the modulation of rho protein crosstalk in Podocytes. *J. Am. Soc. Nephrol.* 28, 837–851. doi: 10.1681/asn.2016040414

Calizo, R. C., Bhattacharya, S., Van Hasselt, J. G. C., Wei, C., Wong, J. S., Wiener, R. J., et al. (2019). Disruption of podocyte cytoskeletal biomechanics by dasatinib leads to nephrotoxicity. *Nat. Commun.* 10: 2061.

Charbit, M., Gubler, M. C., Dechaux, M., Gagnadoux, M. F., Grunfeld, J. P., and Niaudet, P. (2007). Cyclosporin therapy in patients with Alport syndrome. *Pediatr. Nephrol.* 22, 57–63. doi: 10.1007/s00467-006-0227-y

Chen, J. C., Lo, Y. F., Lin, Y. W., Lin, S. H., Huang, C. L., and Cheng, C. J. (2019). WNK4 kinase is a physiological intracellular chloride sensor. *Proc. Natl. Acad. Sci. U.S.A.* 116, 4502–4507. doi: 10.1073/pnas.1817220116

Chiba, Y., and Inoue, C. N. (2019). Once-daily low-dose cyclosporine a treatment with angiotensin blockade for long-term remission of nephropathy in frasier syndrome. *Tohoku J. Exp. Med.* 247, 35–40.

Cornelius, R. J., Si, J., Cuevas, C. A., Nelson, J. W., Gratreak, B. D. K., Pardi, R., et al. (2018). Renal COP9 signalosome deficiency alters CUL3-KLHL3-WNK signaling pathway. *J. Am. Soc. Nephrol.* 29, 2627–2640. doi: 10.1681/asn.2018030333

Dbouk, H. A., Weil, L. M., Perera, G. K., Dellinger, M. T., Pearson, G., Brekken, R. A., et al. (2014). Actions of the protein kinase WNK1 on endothelial cells are differentially mediated by its substrate kinases OSR1 and SPAK. *Proc. Natl. Acad. Sci. U.S.A.* 111, 15999–16004. doi: 10.1073/pnas.1419057111

Desjardins, P., Couture, C., Germain, L., and Guerin, S. L. (2019). Contribution of the WNK1 kinase to corneal wound healing using the tissue-engineered human cornea as an in vitro model. *J. Tissue Eng. Regen. Med.* 13, 1595–1608. doi: 10.1002/term.2912

Ding, F., Wickman, L., Wang, S. Q., Zhang, Y., Wang, F., Afshinnia, F., et al. (2017). Accelerated podocyte detachment and progressive podocyte loss from glomeruli with age in Alport Syndrome. *Kidney Int.* 92, 1515–1525. doi: 10.1016/j.kint.2017.05.017

Embry, A. E., Liu, Z., Henderson, J. M., Byfield, F. J., Liu, L., Yoon, J., et al. (2018). Similar biophysical abnormalities in glomeruli and podocytes from two distinct models. *J. Am. Soc. Nephrol.* 29, 1501–1512. doi: 10.1681/asn.2017050475

Embry, A. E., Mohammadi, H., Niu, X., Liu, L., Moe, B., Miller-Little, W. A., et al. (2016). Biochemical and cellular determinants of renal glomerular elasticity. *PLoS One* 11:e0167924. doi: 10.1371/journal.pone.0167924

Faul, C., Donnelly, M., Merscher-Gomez, S., Chang, Y. H., Franz, S., Delfgaauw, J., et al. (2008). The actin cytoskeleton of kidney podocytes is a direct target of the antiproteinuric effect of cyclosporine A. *Nat. Med.* 14, 931–938. doi: 10.1038/nm.1857

Gallolu Kankanamalage, S., Lee, A. Y., Wichaidit, C., Lorente-Rodriguez, A., Shah, A. M., Stippec, S., et al. (2016). Multistep regulation of autophagy by WNK1. *Proc. Natl. Acad. Sci. U.S.A.* 113, 14342–14347. doi: 10.1073/pnas.1617649113

Ge, X., Zhang, T., Yu, X., Muwonge, A. N., Anandakrishnan, N., Wong, N. J., et al. (2020). LIM-Nebulette reinforces Podocyte structural Integrity by linking Actin and Vimentin filaments. *J. Am. Soc. Nephrol.* 31, 2372–2391. doi: 10.1681/asn.2019121261

Haas, B. R., Cuddapah, V. A., Watkins, S., Rohn, K. J., Dy, T. E., and Sontheimer, H. (2011). With-No-Lysine Kinase 3 (WNK3) stimulates glioma invasion by regulating cell volume. *Am. J. Physiol. Cell Physiol.* 301, C1150–C1160.

Hoorn, E. J., Walsh, S. B., Mccormick, J. A., Furstenberg, A., Yang, C. L., Roeschel, T., et al. (2011). The calcineurin inhibitor tacrolimus activates the renal sodium chloride cotransporter to cause hypertension. *Nat. Med.* 17, 1304–1309. doi: 10.1038/nm.2497

Ishizawa, K., Wang, Q., Li, J., Yamazaki, O., Tamura, Y., Fujigaki, Y., et al. (2019). Calcineurin dephosphorylates Kelch-like 3, reversing phosphorylation by angiotensin II and regulating renal electrolyte handling. *Proc. Natl. Acad. Sci. U.S.A.* 116, 3155–3160. doi: 10.1073/pnas.1817281116

Issa, N., Kukla, A., and Ibrahim, H. N. (2013). Calcineurin inhibitor nephrotoxicity: a review and perspective of the evidence. *Am. J. Nephrol.* 37, 602–612. doi: 10.1159/000351648

Kamentsky, L., Jones, T. R., Fraser, A., Bray, M. A., Logan, D. J., Madden, K. L., et al. (2011). Improved structure, function and compatibility for CellProfiler: modular high-throughput image analysis software. *Bioinformatics* 27, 1179–1180. doi: 10.1093/bioinformatics/btr095

Kochl, R., Thelen, F., Vanes, L., Brazao, T. F., Fountain, K., Xie, J., et al. (2016). WNK1 kinase balances T cell adhesion versus migration in vivo. *Nat. Immunol.* 17, 1075–1083. doi: 10.1038/ni.3495

Lemley, K. V. (2017). Mechanical challenges to the glomerulus and podocyte loss: evolution of a paradigm. *Pflugers. Arch.* 469, 959–963. doi: 10.1007/s00424-017-2012-0

Levental, I., Levental, K. R., Klein, E. A., Assoian, R., Miller, R. T., Wells, R. G., et al. (2010). A simple indentation device for measuring micrometer-scale tissue stiffness. *J. Phys. Condens. Matter.* 22:191420.

Li, X., Ding, F., Wang, S., Li, B., and Ding, J. (2015). Cyclosporine A protects podocytes by regulating WAVE1 phosphorylation. *Sci. Rep.* 5:17694.

Liu, Z., Ho, C. H., and Grinnell, F. (2014). The different roles of myosin IIA and myosin IIB in contraction of 3D collagen matrices by human fibroblasts. *Exp. Cell Res.* 326, 295–306. doi: 10.1016/j.yexcr.2014.04.013

Meyrier, A. (2005). Treatment of focal segmental glomerulosclerosis. *Expert Opin. Pharmacother.* 6, 1539–1549.

Nishizono, R., Kikuchi, M., Wang, S. Q., Chowdhury, M., Nair, V., Hartman, J., et al. (2017). FSGS as an adaptive response to growth-induced Podocyte stress. *J. Am. Soc. Nephrol.* 28, 2931–2945. doi: 10.1681/asn.2017020174

Ohta, A., Schumacher, F. R., Mehellou, Y., Johnson, C., Knebel, A., Macartney, T. J., et al. (2013). The CUL3-KLHL3 E3 ligase complex mutated in Gordon's hypertension syndrome interacts with and ubiquitylates WNK isoforms: disease-causing mutations in KLHL3 and WNK4 disrupt interaction. *Biochem. J.* 451, 111–122. doi: 10.1042/bj20121903

Paluch, E. K., Aspalter, I. M., and Sixt, M. (2016). Focal adhesion-independent cell migration. *Annu. Rev. Cell Dev. Biol.* 32, 469–490.

Piala, A. T., Moon, T. M., Akella, R., He, H., Cobb, M. H., and Goldsmith, E. J. (2014). Chloride sensing by WNK1 involves inhibition of autophosphorylation. *Sci. Signal.* 7:ra41.

Pisarek-Horowitz, A., Fan, X., Kumar, S., Rasouly, H. M., Sharma, R., Chen, H., et al. (2020). Loss of roundabout guidance receptor 2 (Robo2) in Podocytes protects adult mice from glomerular injury by maintaining podocyte foot process structure. *Am. J. Pathol.* 190, 799–816.

Plank, C., Kalb, V., Hinks, B., Hildebrandt, F., Gefeller, O., and Rascher, W. (2008). Cyclosporin A is superior to cyclophosphamide in children with steroid-resistant nephrotic syndrome - a randomized controlled multicentre trial by the Arbeitsgemeinschaft fur Padiatriche Nephrologie. *Pediatr. Nephrol.* 23, 1483–1493.

Schell, C., and Huber, T. B. (2017). The evolving complexity of the Podocyte cytoskeleton. *J. Am. Soc. Nephrol.* 28, 3166–3174.

Schlondorff, D. (1990). Preparation and study of isolated glomeruli. *Methods Enzymol.* 191, 130–140.

Shekarabi, M., Zhang, J., Khanna, A. R., Ellison, D. H., Delpire, E., and Kahle, K. T. (2017). WNK kinase signaling in ion homeostasis and Human disease. *Cell Metab.* 25, 285–299.

Shen, X., Jiang, H., Ying, M., Xie, Z., Li, X., Wang, H., et al. (2016). Calcineurin inhibitors cyclosporin A and tacrolimus protect against podocyte injury induced by puromycin aminonucleoside in rodent models. *Sci. Rep.* 6:32087.

Sun, H., Schlondorff, J., Higgs, H. N., and Pollak, M. R. (2013). Inverted formin 2 regulates actin dynamics by antagonizing Rho/diaphanous-related formin signaling. *J. Am. Soc. Nephrol.* 24, 917–929.

Tandon, R., Levental, I., Huang, C., Byfield, F. J., Ziembicki, J., Schelling, J. R., et al. (2007). HIV infection changes glomerular podocyte cytoskeletal composition and results in distinct cellular mechanical properties. *Am. J. Physiol. Renal. Physiol.* 292, F701–F710.

Tu, S. W., Bugde, A., Luby-Phelps, K., and Cobb, M. H. (2011). WNK1 is required for mitosis and abscission. *Proc. Natl. Acad. Sci. U.S.A.* 108, 1385–1390.

Vassiliadis, J., Bracken, C., Matthews, D., O'brien, S., Schiavi, S., and Wawersik, S. (2011). Calcium mediates glomerular filtration through calcineurin and mTORC2/Akt signaling. *J. Am. Soc. Nephrol.* 22, 1453–1461.

Waldman, M., Crew, R. J., Valeri, A., Busch, J., Stokes, B., Markowitz, G., et al. (2007). Adult minimal-change disease: clinical characteristics, treatment, and outcomes. *Clin. J. Am. Soc. Nephrol.* 2, 445–453.

Wiggins, J. E., Goyal, M., Sanden, S. K., Wharram, B. L., Shedden, K. A., Misek, D. E., et al. (2005). Podocyte hypertrophy, "adaptation," and "decompensation" associated with glomerular enlargement and glomerulosclerosis in the aging rat: prevention with caloric restrictuion. *J. Am. Soc. Nephrol.* 16, 2953–2966.

Wyss, H. M., Henderson, J. M., Byfield, F. J., Bruggeman, L. A., Ding, Y., Huang, C., et al. (2011). Biophysical properties of normal and diseased renal glomeruli. *Am. J. Physiol.* 300, C397–C405.

Xie, J., Wu, T., Xu, K., Huang, I. K., Cleaver, O., and Huang, C. L. (2009). Endothelial-specific expression of WNK1 kinase is essential for angiogenesis and heart development in mice. *Am. J. Pathol.* 175, 1315–1327.

Xie, J., Yoon, J., Yang, S. S., Lin, S. H., and Huang, C. L. (2013). WNK1 protein kinase regulates embryonic cardiovascular development through the OSR1 signaling cascade. *J. Biol. Chem.* 288, 8566–8574.

Xu, B., English, J. M., Wilsbacher, J. L., Stippec, S., Goldsmith, E. J., and Cobb, M. H. (2000). WNK1, a novel mammalian serine/threonine protein kinase lacking the catalytic lysine in subdomain II. *J. Biol. Chem.* 275, 16795–16801.

Yamada, K., Park, H. M., Rigel, D. F., Dipetrillo, K., Whalen, E. J., Anisowicz, A., et al. (2016a). Small-molecule WNK inhibition regulates cardiovascular and renal function. *Nat. Chem. Biol.* 12, 896–898.

Yamada, K., Zhang, J. H., Xie, X., Reinhardt, J., Xie, A. Q., Lasala, D., et al. (2016b). Discovery and characterization of allosteric WNK Kinase inhibitors. *ACS Chem. Biol.* 11, 3338–3346.

Yamada, K. M., and Sixt, M. (2019). Mechanisms of 3D cell migration. *Nat. Rev. Mol. Cell Biol.* 20, 738–752.

Zagorska, A., Pozo-Guisado, E., Boudeau, J., Vitari, A. C., Rafiq, F. H., Thastrup, J., et al. (2007). Regulation of activity and localization of the WNK1 protein kinase by hyperosmotic stress. *J. Cell Biol.* 176, 89–100.

Zhang, J., Deng, X., and Kahle, K. T. (2016). Leveraging unique structural characteristics of WNK kinases to achieve therapeutic inhibition. *Sci. Signal.* 9:e3.

Zhu, W., Begum, G., Pointer, K., Clark, P. A., Yang, S. S., Lin, S. H., et al. (2014). WNK1-OSR1 kinase-mediated phospho-activation of Na+-K+-2Cl- cotransporter facilitates glioma migration. *Mol. Cancer* 13:31.

Conflict of Interest: The authors declare that the research was conducted in the absence of any commercial or financial relationships that could be construed as a potential conflict of interest.

frontiers in Cell and Developmental Biology

REVIEW
published: 22 November 2021
doi: 10.3389/fcell.2021.771931

Controversies in Podocyte Loss: Death or Detachment?

Lijun Yin[1], *Lu Yu*[1,2], *John Cijiang He*[3,4] *and Anqun Chen*[1]*

[1]Hunan Key Laboratory of Kidney Disease and Blood Purification, Department of Nephrology, Institute of Nephrology, The Second Xiangya Hospital at Central South University, Changsha, China, [2]Department of Health Sciences, Boston University College of Health and Rehabilitation Sciences: Sargent College, Boston University, Boston, MA, United States, [3]Division of Nephrology, Department of Medicine, Icahn School of Medicine at Mount Sinai, New York, NY, United States, [4]Renal Program, James J. Peters Veterans Affairs Medical Center at Bronx, New York, NY, United States

Glomerular podocytes are characterized by terminally differentiated epithelial cells with limited proliferating ability; thus, podocyte loss could not be fully compensated by podocyte regeneration. A large body of clinical studies collectively demonstrated that podocyte loss correlated with glomerular diseases progression. Both podocyte death and podocyte detachment lead to podocyte loss; however, which one is the main cause remains controversial. Up to date, multiple mechanisms are involved in podocyte death, including programmed apoptotic cell death (apoptosis and anoikis), programmed nonapoptotic cell death (autophagy, entosis, and podoptosis), immune-related cell death (pyroptosis), and other types of cell death (necroptosis and mitotic catastrophe-related cell death). Apoptosis is considered a common mechanism of podocyte loss; however, most of the data were generated *in vitro* and the evidence of *in vivo* podocyte apoptosis is limited. The isolation of podocytes in the urine and subsequent culture of urinary podocytes *in vitro* suggest that detachment of viable podocytes could be another important mechanism for podocyte loss. In this review, we summarize recent advances that address this controversial topic on the specific circumstances of podocyte loss.

Keywords: podocyte loss, cell death, detachment, apoptosis, autophagic cell death, mitotic catastrophe, anoikis, pyroptosis

OPEN ACCESS

Edited by:
Mario Ollero, INSERM U955 Institut Mondor de Recherche Biomédicale (IMRB), France

Reviewed by:
Igor Pottosin, University of Colima, Mexico
Guangrui Huang, Beijing University of Chinese Medicine, China

***Correspondence:**
Anqun Chen
anqunchen@csu.edu.cn

Specialty section:
This article was submitted to Cell Death and Survival, a section of the journal Frontiers in Cell and Developmental Biology

Received: *07 September 2021*
Accepted: *03 November 2021*
Published: *22 November 2021*

Citation:
Yin L, Yu L, He JC and Chen A (2021) Controversies in Podocyte Loss: Death or Detachment? Front. Cell Dev. Biol. 9:771931. doi: 10.3389/fcell.2021.771931

INTRODUCTION

Glomerular podocytes account for approximately 30% of glomerular cells in number, which constitute glomerular filtration barrier (GFB) together with endothelial cell and glomerular basement membrane (GBM) (Nishad et al., 2021). Podocyte is the last barrier of GFB (**Figure 1**), the injury of which is a key manifestation of glomerular diseases, including minimal change disease (MCD), focal segmental glomerulosclerosis (FSGS), and diabetic nephropathy. Podocytes are characterized by terminally differentiated epithelial cells with a limited capacity of proliferation; thus, podocyte loss cannot be fully compensated by regeneration from nearby healthy podocytes. One of the features of glomerulosclerosis is the continuous loss of podocytes, which correlates with the progression of glomerular diseases (Lemley et al., 2002). When the loss of podocytes per glomerulus is above 20%, glomerulosclerosis takes place. When the podocyte loss is more than 40%, reduced renal function occurs (Wharram et al., 2005). However, the underlying mechanism of this remains unclear.

Podocyte loss can be caused by either podocyte death or podocyte detachment; however, which one is the main cause remain controversial. The major pathways involved in podocyte death include

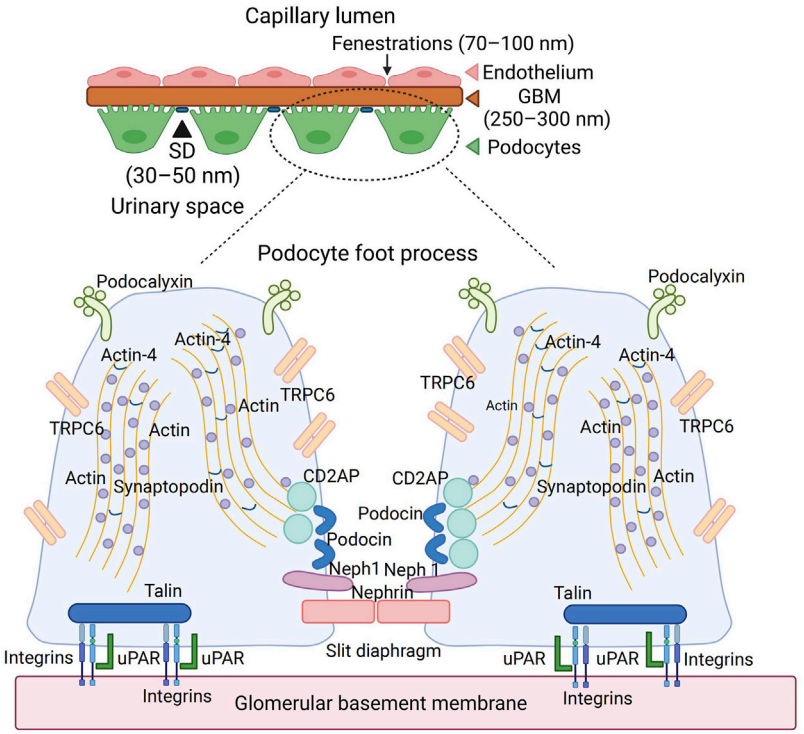

FIGURE 1 | The anatomy of glomerular basement membrane and podocyte. Podocyte is the last barrier of the glomerulus filtration membrane, which contains a slit diaphragm with 30–50 nm width. The abundant cytoskeleton proteins, such as actin and synaptopodin, maintain the normal shape of podocytes. The membrane proteins, such as podocalyxin, TRPC6, podocin, and nephrin, played an essential role in the podocyte function. Podocyte anchored into the GBM through integrins and uPAR interaction. TRPC6, transient receptor potential cation channel subfamily C member 6; GBM, glomerular basement membrane; uPAR, urokinase-type plasminogen activator receptor; CD2AP, CD2-associated protein.

programmed apoptotic cell death (apoptosis and anoikis), programmed nonapoptotic cell death (autophagy, entosis, and podoptosis), immune-related cell death (pyroptosis), and other types of cell death (necroptosis and mitotic catastrophe-related cell death) (Galluzzi et al., 2018). Apoptosis is a common mechanism of podocyte loss; however, most of the data were generated *in vitro* and the *in vivo* evidence of podocyte apoptosis is limited. The isolation of podocytes in the urine and subsequent culture of urinary podocytes *in vitro* suggest that detachment of viable podocytes could be another important mechanism for podocyte loss. In this review, we will summarize recent advances that address the mechanisms of podocytes loss.

THE ANATOMY AND PHYSIOLOGY OF PODOCYTE

Podocytes possess a complicated cellular structure, which consists of a cell body, a major process extending outwardly from their cell body, and a secondary process (foot process) surrounding the glomerular capillary loops. Major processes are restrained by microtubules and intermediate filaments, while foot processes are tethered by an actin-based cytoskeleton. Podocyte foot processes are connected by a functioning structure named slit diaphragm (SD), consisting of many proteins such as nephrin, Neph1, and podocin, which actively participate in podocyte signaling (**Figure 1**). Additionally, foot processes possess a thick coat (glycocalyx) with a negative charge facing the urinary space. Microtubules and intermediate filaments dominate within the cell body and the major processes, while longitudinally, bundles of microfilaments are encountered within the foot processes. Podocytes are coated by negatively charged podocalyxin, which repels each other electrostatically between the neighboring FP (Reiser and Altintas, 2016), contributing to the impairment of albumin filtration (Trimarchi, 2017) (**Figure 1**).

The cytoskeleton of podocytes and its interaction with GBM accounts for not only the attachment of the cells to the extracellular matrix but also the regulation of the capillary width, which is critical for determining the glomerular filtration rate (**Figure 1**). Many proteins of the cytoskeleton system (e.g., actin, α-actinin 4, and synaptopodin) are connected to the cytoplasmic membrane, playing roles in its relaxation and contraction, which regulate the width of the slit diaphragm and determine the size and rate of filtered molecules. Actin receives the information from CD2AP (CD2-associated protein), which translates the information from TRPC6 (Transient Receptor Potential Cation Channel Subfamily C Member 6) and from podocin, which is located in the foot process and forms part of the slit diaphragm. Podocytes are anchored to the glomerular basement membrane with anchoring proteins talin-1 and integrins. The interaction between actin,

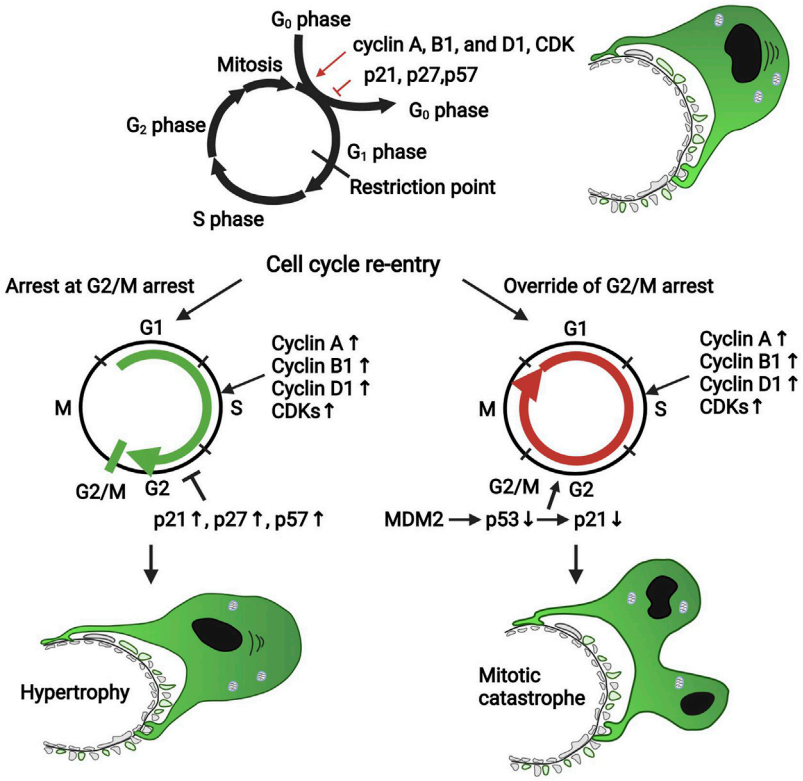

FIGURE 2 | The cell cycle of the podocyte in diseased condition. Cell cycle proteins such as cyclin A, cyclin B1, cyclin D1, and CDKs promote podocyte re-entry into the cell cycle; however, the CDK inhibitors such as p21, p27, and p57 block the cell cycle. Mature podocytes express negligible cyclin A, cyclin B1, cyclin D1, and CDKs but constitutively express p27, p57, and WT-1, which maintain the cell cycle quiescence. During podocyte injury, many pathogenic factors such as FGF and TGF-β upregulated the expression of cell cycle proteins favoring the proliferation to promote the podocyte to override the G1 restriction point; also, the CDK inhibitors were upregulated to keep the cells arrest in the G2/M phase. Under some conditions, podocytes could override the G2/M restriction by MDM2 through inhibiting p53-dependent cell cycle arrest. However, due to the incomplete formation of mitosis and cytokinesis, podocytes could not complete successful division; thus, a mitotic catastrophe of podocytes occurs. CDK, cyclin-dependent kinase; MDM2, murine double minute 2.

urokinase-type plasminogen activator receptor (uPAR), and integrins also determines the relaxation and contraction of podocytes (**Figure 1**). The SD proteins such as nephrin, Neph1, and podocin form a receptor complex; therefore, upon ligand binding, both nephrin and Neph1 become phosphorylated, recruiting adaptor molecules subsequently and coordinating junction formation and cytoskeleton dynamics (Moreno et al., 2008).

THE CELL CYCLE OF THE PODOCYTE IN DISEASED CONDITION

The cell cycle is a tightly regulated event that consists of four phases: G1 phase (ready for DNA synthesis), S phase (DNA replication), G2 phase (the gap between DNA synthesis and mitosis), and M phase (mitosis and cytokinesis). Cell enters a state of quiescence at the G0 phase. The cell's nucleus divides in the mitosis process, while the cell's cytoplasm divides in the cytokinesis process. A balance of cyclins and cyclin-dependent kinase (CDK) (e.g., cyclin A, cyclin B1, cyclin D1, and CDK2, 4, and 6) and CDK inhibitors (p21, p27, and p57) governs the cell cycle (**Figure 2**). Different types of cyclins bind to different CDK at each specific phase (Shankland and Wolf, 2000), while CDK inhibitors bind to and inactivate cyclin-CDK complexes. Mature podocytes remain quiescent by constitutively expressing p27, p57, and WT-1 in the mature glomeruli. WT-1 downregulates β-catenin/Wnt signaling, which directly activates cyclin D1, controlling podocyte proliferation (Grouls et al., 2012). MDM2 negatively regulates p53 tumor suppressor, functioning as an E3 ubiquitin ligase responsible for the ubiquitination and degradation of p53 or retaining p53 in the cytosol (Iwakuma and Lozano, 2003). Multiple stimuli during podocyte injury increased the secretion of many growth factors such as angiotensin II (ANG II), fibroblast growth factors (FGFs), growth hormone (GH), and transforming growth factor-β (TGF-β), which upregulate the expression levels of cyclin A, cyclin B1, cyclin D1, and CDKs to override the G1/S transition and to drive the cell re-entering the cell cycle (Srivastava et al., 2006; Grahammer and Huber, 2016; Sakairi et al., 2010). However, in most situations, the podocytes will arrest in the G2/M phase, the exact mechanism of which is not clear. It is reported that the CDK inhibitors (p21, p27, and p57) were also increased, which prevents the cell cycle from bypassing the G1 or G2/M restriction point (Hagen et al., 2016) (**Figure 2**). Under

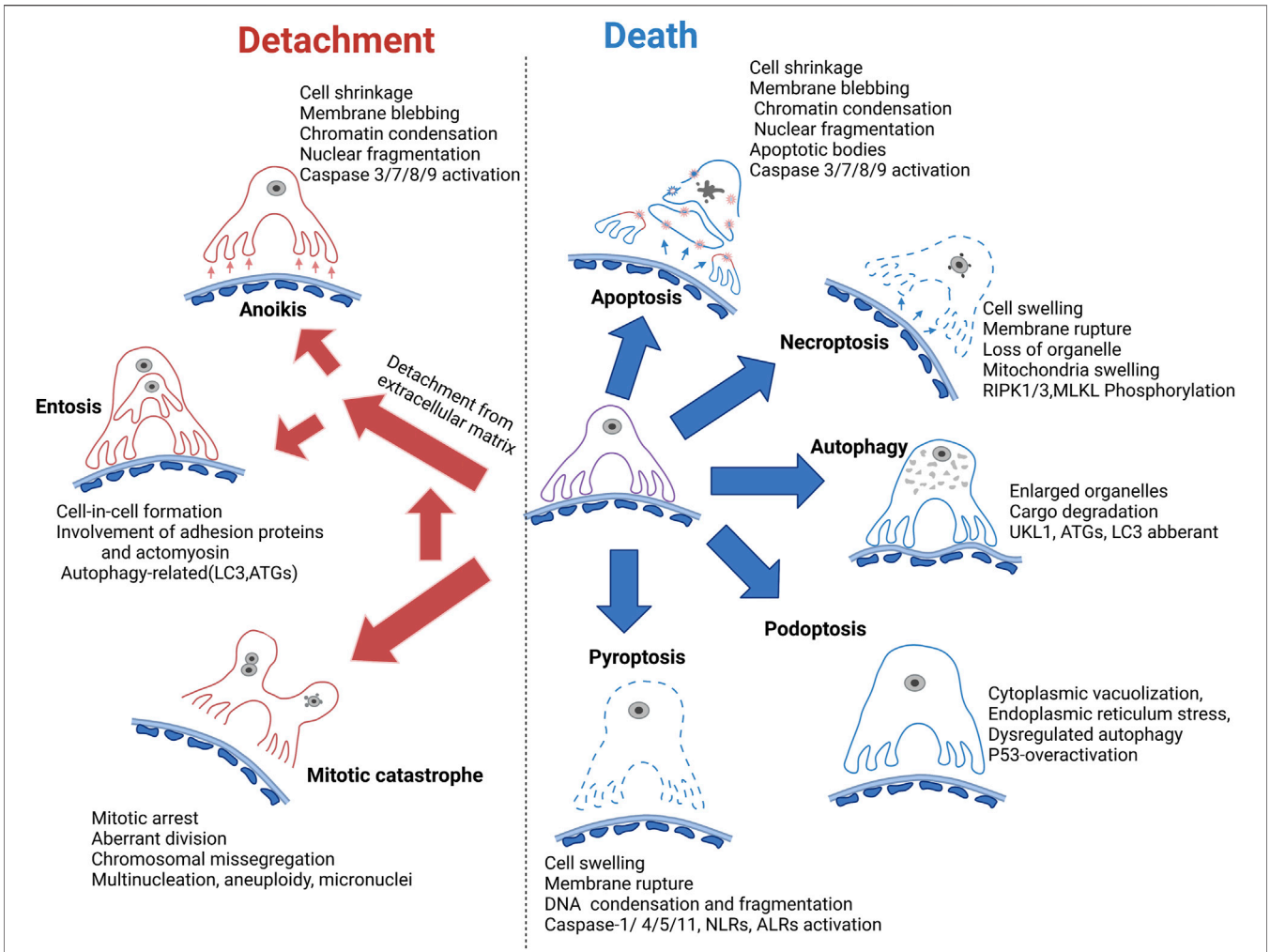

FIGURE 3 | Mechanism of podocyte loss. Apoptosis is previously considered the common form of podocyte death; however, the *in vivo* evidence is lacking. Autophagy dysregulation related cell death is generally accepted as a major mechanism of podocyte cell death. Necroptosis, podoptosis, and pyroptosis are also involved in podocyte death. Meanwhile, podocyte detachment and detachment-induced cell death such as anoikis and entosis remain the major mechanism of podocyte loss. Mitotic catastrophe could promote podocyte detachment from GBM. GBM, glomerular basement membrane. RIPK, receptor-interacting protein kinase 1; MLKL, mixed lineage kinase domain-like pseudokinase; UKL1, unc-51 like autophagy activating kinase 1; LC3, microtubule-associated protein light chain 3; ATGs, autophagy-related proteins; NLRs, NOD-like receptors; ALRs, AIM-2-like receptors.

some conditions, podocytes could bypass cell cycle G2/M arrest, entering mitosis by MDM2 through inactivating p53-mediated cell cycle arrest and subsequently decreasing p21 expression (Mulay et al., 2013). However, because of the incomplete formation of mitotic spindles and failure of cytokinesis due to the sophisticated anatomical structure and inadequate expression of Aurora kinase B, which is crucial for cytokinesis, aberrant mitosis (mitotic catastrophe) in podocytes takes place (Lasagni et al., 2013) (**Figure 2**).

MECHANISM OF PODOCYTE LOSS

Podocyte loss is a prerequisite for glomerulosclerosis; however, the underlying mechanism remains unclear. Podocyte death *in situ* on the glomerular basement membrane could result in cell detachment. Conversely, podocyte detachment leads to cell death. However, detachment of viable podocytes also occurs. In addition, we do not know whether podocytes detach because of their death or die because they lose their adhesion to GBM. Currently, in human kidney disease, podocytes injury was assessed mainly by the ultrastructural appearance of the secondary foot processes under transmission electron microscopy (EM), which are interdigitating and teethlike in normal condition but usually appear flat due to foot process effacement during podocyte injury. The assessment of podocyte death or detachment is not routinely performed in human renal biopsy specimens (Liapis et al., 2013).

There are numerous mechanisms for podocyte loss (**Figure 3**), including detachment related cell death (anoikis and entosis), programmed apoptotic cell death (apoptosis), programmed nonapoptotic cell death (e.g., autophagy and podoptosis),

immune-reactive cell death such as pyroptosis, and other types of cell death such as necroptosis and mitotic catastrophe-induced cell death. Each individual type of cell death is discussed separately.

PODOCYTE LOSS DUE TO CELL DEATH

Apoptosis

Apoptosis is the process of programmed cell death, the first sign of which is the condensation of the nuclear material, accompanied by cell shrinkage and the formation of many membrane-bound, ultra-structurally well-preserved fragments resulting from cell breakup (Westman et al., 2019; Yan et al., 2020). Both the extrinsic and intrinsic apoptotic pathway share the common executioner caspases, mainly caspase 3, and ultimately promote chromatin condensation, nuclear fragmentation, and formation of apoptotic bodies (Galluzzi et al., 2018). Usually, terminal deoxynucleotidyl transferase dUTP nick-end labeling (TUNEL) assay using live cell-impermeant staining in combination with annexin V conjugates and caspase assay such as cleaved caspase-3 was used to assess apoptosis (Yan et al., 2020).

Apoptosis has been previously considered as a common cause of podocyte loss because podocytes apoptosis was observed *in situ* in various experimental animal models such as diabetic nephropathy, progressive glomerular sclerosis, and transforming growth factor-β1 (TGF-β1) transgenic mice (Schiffer et al., 2001; Susztak and Böttinger, 2006; Jia et al., 2008). Nevertheless, the data favoring podocyte apoptosis have been generated mostly from *in vitro* studies, and evidence derived from *in vivo* experiments has been mainly based on tissue staining with cleaved caspase 3 or TUNEL (Schiffer et al., 2001; Ryu et al., 2011). It is known that detecting DNA fragmentation *in situ via* TUNEL as evidence of apoptosis has been challenged (Graslkraupp, 1995) because TUNEL detects different kinds of cell death such as necrosis and autolytic cell death. The presence of apoptotic bodies in podocytes by EM is the most reliable indicator of apoptosis; however, no detection of apoptotic bodies has been reported in human kidney biopsies by EM so far (Nagata, 2016). It is important to understand that the time course of apoptosis is very fast (Tharaux and Huber, 2012; Westman et al., 2019), irrespective of the initiating insult. Usually, phagocytes eliminate apoptotic bodies within hours (Matter, 1979); thus, the chance of observing the apoptotic cells is very low. Even if the phagocytosis is absent, apoptotic cells can detach rapidly or become secondary necrotic cells, which is difficult to distinguish from primary necrosis. Therefore, it is difficult to confirm the role of podocyte apoptosis in kidney disease (Liapis et al., 2013).

Autophagic Cell Death

Autophagic cell death (ACD) is a type of nonapoptotic cell death, which occurs in the absence of chromatin condensation but through a lysosome-dependent degradation pathway, accompanied by large-scale autophagic vacuolization of the cytoplasm (Galluzzi et al., 2018). The detection methods include measurement of autophagic activity (e.g., autophagic flux) and indirect analysis with autophagy-specific key molecules, such as UKL1 (unc-51 Like Autophagy Activating Kinase 1), LC3 (microtubule-associated protein light chain 3), and ATG (autophagy-related proteins) (Yan et al., 2020).

Autophagy is extraordinarily important in maintaining the homeostasis of terminally differentiated cells such as podocytes under physiological and stress conditions (Asanuma et al., 2003). Autophagy deficiency in podocytes results in the loss of cellular protein homeostasis and a dramatic acceleration of glomerular diseases (Hartleben et al., 2010). In diabetic patients and animal models with massive proteinuria, podocyte autophagy was observed to be insufficiently accompanied by podocyte loss (Yasuda-Yamahara et al., 2015). The transgenic mice with autophagy-specific deficiency in podocytes developed massive proteinuria and podocyte loss in a high-fat diet (HFD)-induced diabetic model, in which minimal proteinuria was often induced (Tagawa et al., 2016). Serum from diabetic patients and experimental rodents with massive proteinuria could cause autophagy insufficiency, lysosome dysfunction, and apoptosis of cultured podocytes (Yasuda-Yamahara et al., 2015). This indicates that autophagy impairment in podocytes under diabetic conditions plays an important role in the pathogenesis of podocyte loss and massive proteinuria in diabetic nephropathy (Yasuda-Yamahara et al., 2015; Tagawa et al., 2016). It has been shown that activation of autophagy suppresses podocyte apoptosis and glomerulopathy in the adriamycin-induce mice model; conversely, inhibition of autophagy promoted adriamycin-induced podocyte injury *in vitro* and *in vivo* (Yi et al., 2017). All of these findings suggest the dysregulated autophagy-related podocyte death both *in vivo* and *in vitro*.

mTOR (mammalian target of rapamycin) pathway is the best-characterized repressor of autophagy (Laplante and Sabatini, 2012). The mechanistic target of rapamycin complex 1 (MTORC1) is one of the multiprotein complexes of mTOR, inhibiting the autophagy process by phosphorylating ULK1 (Ganley et al., 2009). There are pieces of evidence showing that MTORC1 activation was strengthened in podocytes of individuals with progressive diabetic nephropathy, and abnormal MTORC1 activation recapitulated many diabetic kidney disease features in nondiabetic rodents such as loss of podocyte, thickening of the glomerular basement membrane, glomerular mesangial expansion, and proteinuria (Inoki et al., 2011). Rapamycin, the selective inhibitor of mTOR protein kinase, was proved to reduce podocyte apoptosis by inhibiting the mTOR/P70S6K/4EBP1 signaling pathway and activating podocyte autophagy in idiopathic membranous nephropathy (IMN) mice model (Wu et al., 2013). AGEs can promote the activation of mTOR in human podocytes and inhibit nuclear translocation of the transcription factor EB, downregulating the expression of autophagy-related genes, thereby inhibiting the formation of autophagosomes in the cell and simultaneously increasing the early and late apoptosis of podocytes.

Altogether, these data suggest that autophagy dysregulation related cell death could be a major pathway for podocyte death, particularly in diabetic kidney disease.

Necroptosis

Necroptosis is a regulated cell death that shows the same characteristics as necrosis in morphology (lysis of cell membrane) and is different from the apoptosis signal pathway in its mechanism. A variety of molecules such as RIPK1 (receptor-interacting protein kinase 1), RIPK3 (receptor-interacting protein kinase 3) and its substrate MLKL (mixed lineage kinase domain-like pseudokinase) participate in the regulation of cell necroptosis (Galluzzi et al., 2018). Western blot assay of the marker involved in the necroptosis pathway, mitochondrial potential analysis by fluorescent probes, and morphology observation by EM can be applied to the assessment of necroptosis (Yan et al., 2020).

The studies on podocyte necroptosis are rare. A few studies suggested that high glucose could induce necroptosis in podocytes, which is regulated by ubiquitin C-terminal hydrolase L1 (UCH-L1) *via* RIPK1/RIPK3 pathway, evidenced by western blot assay of necrosis pathway markers such as RIPK3 and MLKL and scanning EM (Xu et al., 2019). Sosna and co-workers showed that HtrA2/Omi (a serine protease previously implicated in programmed cell death) and ubiquitin C-terminal hydrolase L1 (UCH-L1) regulate TNF-induced necroptosis in podocytes using necroptosis specific inhibitors such as necrostatin-1 (Sosna et al., 2013). Recently, Guo and co-workers observed that the activation of RIPK3 and MLKL was observed in kidney podocytes from class IV human lupus nephritis and experimental animal models such as lupus-prone NZM2328 and MRL/lpr mice, as evidenced by staining of phosphorylated forms of RIP3 and MLKL in podocytes. Furthermore, GSK872 (a specific RIPK3 kinase inhibitor) treatment alleviates the disease activity of MRL/lpr mice (Guo et al., 2019). Thus, these limited studies suggest that podocyte necroptosis might occur in diseased kidneys.

Pyroptosis

Pyroptosis is an inflammatory form of programmed cell death regulating immunity response (Xiong et al., 2020). There are two pathways related to pyroptosis that have been identified: the canonical pathway mediated by caspase-1 and induced by inflammatory bodies such as NLRP3 (NLR family pyrin domain containing 3) and the noncanonical pathway mediated by caspase-4/5/11 and activated by lipopolysaccharide (LPS) (Yu et al., 2021; Zhang et al., 2021). The common consequence of the above two pathways is the cleavage of gasdermin-D (GSDMD) into N-terminal fragments of GSDMD (GSDMD-NT), which played an essential role in the pore formation through insertion into the cell membrane and subsequent cellular contents release such as IL-1β and IL-18 (Evavold et al., 2021; Yu et al., 2021).

The activation of NLRP3 inflammasomes could recruit caspase-1 *via* the adaptor protein of CARD-PYRIN (von Moltke et al., 2013) and induce pyroptosis subsequently. Murine podocytes expressed three essential components of the NLRP3 inflammasome complex (Zhang et al., 2012). NLRP3 inflammasome activation played an important in initiating obesity-associated podocyte injury (Boini et al., 2014) and promoting diabetic nephropathy development in the diabetic rodents (Shahzad et al., 2015). The expression levels of proteins involved in the pyroptosis pathway such as GSDMD-N, NLRP3, cleaved caspase-1, and IL-1β were considerably enhanced in the mouse models treated with a high-fat diet or streptozotocin and in the high glucose-treated podocytes (An et al., 2020; Li et al., 2020; Zhan et al., 2020). Activation of NLRP3 inflammasome could be induced by high glucose and blockade of its activation or inhibition of caspase-1 reduced the production of IL-1β and mitigated podocyte and glomerular injury in diabetic mouse models (Gao et al., 2014; Shahzad et al., 2015). In addition, NLRP3 inflammasomes are also activated in podocytes from patients with lupus nephritis and lupus-prone mice (Fu et al., 2017). The activation of NLRP3 inflammasome and caspase-1, as well as increased IL-1β production, also plays a crucial role in podocyte injury induced by hyper-homocysteinemia (hHcys) (Abais et al., 2014; Xia et al., 2014).

Recently, the evidence demonstrated that noncanonical pyroptosis-regulated cell death was also involved in the pathogenesis of diabetic nephropathy and disease progression. They showed that the expression levels of caspase-11 and GSDMD-N in podocytes were significantly increased, associated with the decreased expression level of podocyte-specific proteins such as nephrin and podocin, effacement of podocyte foot processes, expansion of glomerular matrix, and higher urinary albumin-to-creatinine ratio. These data suggest a role of pyroptosis in podocyte injury in diabetic nephropathy (Cheng et al., 2021). However, evidence of podocyte pyroptosis in human kidney disease is still lacking.

Podoptosis

Podoptosis is referred to as p53 overactivation-related cell death (Thomasova et al., 2015). It is known that the maintenance of p53 balance is crucial for podocyte survival; thus, many proteins enriched in podocytes such as WT-1 (Maheswaran et al., 1995), MDM2 (Mulay et al., 2013), and RARRES1 (Chen et al., 2020) interact with the p53 pathway. MDM2 could promote podocyte loss by overriding cell cycle G2/M restriction and entering mitosis through degradation of p53 or by retaining p53 in the cytosol (Mulay et al., 2013; Tang et al., 2017). It also prevents p53 overactivation-related cell death (Thomasova et al., 2015). Morphologically, podoptosis is characterized by massive cytoplasmic vacuolization and signs of endoplasmic reticulum stress. Mechanistically, the p53-overactivation-related cell death is p53 inhibitor-sensitive but pan-caspase inhibitor-insensitive, suggesting that it does not require caspase activation, and therefore this p53 overactivation-related cell death is not apoptosis. Moreover, podoptosis is not affected by specific inhibitors for pyroptosis, pyronecrosis, necroptosis, ferroptosis, and parthanatos. Thus, podoptosis, a p53 overactivation-related podocyte death, is a new form of cell death (Thomasova et al., 2015).

Detachment-Induced Podocyte Loss

Many studies confirmed the presence of viable urinary podocytes in human and experimental glomerular diseases (Vogelmann et al., 2003). These urine-derived podocytes from animal models and human subjects have been cultured and made into

immortalized cell lines (Petermann et al., 2003; Sakairi et al., 2010). Urinary podocytes from patients with active glomerular disease shared the same morphology and growth pattern with primary podocytes isolated from human kidneys. However, the cultured urinary podocytes from healthy control individuals showed very limited growth capability and underwent death much sooner than those of patients with glomerular disease. These results suggest that viable podocytes may detach from the glomerular tuft of diseased kidneys due to the local altered microenvironment instead of the defect of podocyte per se in patients, whereas urine podocytes in healthy individuals are most likely from the shedding of senescent cells.

There is very limited insight into the mechanisms that mediate the detachment of podocytes. Currently, podocyte detachment is thought to be caused by the increased mechanical shear forces and/or disruption of the cell-GBM adhesion (Kriz and Lemley, 2015). Glomerular hypertension and hyperfiltration increase the shear stresses on podocytes, promoting the detachment of podocytes (Benzing and Salant, 2021). Podocyte-GBM adhesion is modulated by several integrins and cytoskeletal protein such as αVβ3 or α3β1 integrin and talin-1 (Nagata, 2016), disruption of which causes podocyte detachment (Yu et al., 2013; Tian et al., 2014). It is reported that the significant decrease of α3β1 integrin at the basal plasma membrane of podocytes takes place as early as one month after the occurrence of hyperglycemia, at the time when the morphological changes of glomerular basement membrane are not yet established; thus, it might be an early event which promotes podocyte detachment before the onset of diabetic nephropathy (Regoli and Bendayan, 1997). Podocytes are especially susceptible to injury in many glomerular diseases, during which the cell shapes of podocytes change, including retraction and broadening of their foot processes. There are two opposite hypotheses for this observation: this could be an early sign of podocyte detachment or this could be a defense mechanism of podocytes against detachment from the GBM (Kriz and Lemley, 2015). On the one hand, podocyte effacement reduced the buttressing force of podocytes and the compressive force of the GBM, subsequently drastically increasing capillary pressure and local fluid flow at the barrier due to the decreased filtration area, thus leading to loss of podocytes through detachment because of enhanced transverse shear stress (Benzing and Salant, 2021). On the other hand, podocyte effacement closes the slits and could prevent podocytes from suffering from high flows and shear stresses (Kriz and Lemley, 2015).

Under high glucose conditions, podocytes undergo cell hypertrophy to compensate for podocyte loss (Hoshi et al., 2002). However, hypertrophy of podocytes could result in the alteration of structure that leads to the podocyte detachment from the GBM (Kriz et al., 2014). Complement activation in lupus nephritis can impede podocyte focal adhesions (Topham et al., 1999); meanwhile, exposure to the circulating factors in focal segmental glomerulosclerosis (FSGS) might dysregulate the actin cytoskeleton (Kemeny et al., 1995). The alteration of focal adhesions and actin cytoskeleton leads to podocyte detachment. Consistently, podocytes with CD2AP- deficiency are more susceptible to cell death induced by detachment than wild-type podocytes (Huber et al., 2003). mTORC1 activation in diabetic conditions may induce epithelial-mesenchymal transition-like phenotypic changes in podocytes, promoting podocyte detachment from GBM (Inoki et al., 2011). Altogether, these studies support the early occurrence of podocyte detachment as a major mechanism of podocyte loss.

Mitotic Catastrophe-Induced Podocyte Detachment

Mitotic catastrophe is a sequence of events resulting from aberrant mitosis caused by DNA damage or any other aberrations affecting the mitotic process (Galluzzi et al., 2018). Mitotic catastrophe is morphologically characterized by nuclear abnormalities, including multinucleation (aneuploidy), micronuclei, or irregularly shaped nuclei (Galluzzi et al., 2018). The cells suffering from mitotic catastrophe often undergo programmed cell death, such as intrinsic apoptosis.

Mature podocytes sustained cell cycle quiescence. Differentiated podocytes could re-enter the cell cycle in response to various stimuli; however, they cannot accomplish cytokinesis despite karyokinesis, thus resulting in mitotic catastrophe (Liapis et al., 2013). Recently, Hara and co-workers examined urinary podocytes, 53.5% of which were considered as mitotic catastrophe cells, with the character of abnormal shape, aneuploidy, mitotic spindles, and denucleation (Hara et al., 2019). They suggest that in diabetic patients, the majority of urinary podocytes show the character of mitotic catastrophe, not apoptosis. Mitotic catastrophe has been observed in a variety of nephropathies in which podocytes were extensively damaged, such as membranous nephropathy, focal segmental glomerulosclerosis (FSGS), diabetic kidney disease, and IgA nephropathy (Vakifahmetoglu et al., 2008; Liapis et al., 2013). Consistent with the urinary analysis, the detection of mitotic podocytes in human glomerular disease from IgA nephropathy, collapsing FSGS, and drug-induced minimal change disease were all observed in the urinary space away from the glomerular tuft (Liapis et al., 2013). Blockade of MDM2 (an inhibitor of p53-dependent cell cycle arrest) prevented podocytes from aberrant mitosis by inducing G2/M arrest and detachment of dying aneuploid podocytes in the adriamycin nephropathy mice model (Mulay et al., 2013), supporting the hypothesis that mitotic catastrophe plays important roles in podocyte detachment. The mitotic podocytes detach from the GBM mainly because of the inability of actin assembly to form mitotic spindle and support the cytoskeletal structure of foot processes at the same time (Lasagni et al., 2013). These shreds of evidence suggest that mitotic catastrophe plays an important role in podocyte detachment.

Detachment-Induced Podocyte Death

Currently, the detachment of epithelial cells from the extracellular matrix could trigger two kinds of cell death, anoikis and entosis. Anoikis is a kind of apoptosis induced by the loss of attachment to the extracellular matrix (ECM) or the neighboring cells, which could be regulated *via* both the intrinsic and extrinsic apoptotic pathways (Frisch and Francis, 1994; Cardone et al., 1997; Reginato et al., 2003). Gilmore and co-workers demonstrated

that cells lacking ECM attachment suffered from classical apoptosis eventually (Gilmore, 2005). However, the mechanism underlying the relationship between cell architecture alteration and apoptosis needs to be further explored. Overholtzer and co-workers found that detached epithelial cells from the extracellular matrix and subsequent loss of integrin signaling would trigger entosis, which is a nonapoptotic cell death pathway, during the process of which one cell invades or is engulfed by another cell (Overholtzer et al., 2007). However, there is no specific method to detect entosis currently. The detection of the typical cell-in-cell structure by fluorescence imaging and EM was applied to identify the cells with entosis (Yan et al., 2020). However, this has not been reported in human kidney disease.

Podocyte Shedding of Viable Cells in the Urine

Despite the above observations that favor the early and essential role of detachment in podocyte loss, there are two remaining issues regarding the urinary podocytes: 1) the identification of podocytes mainly relied on the podocalyxin-positive cells. Nevertheless, podocalyxin-positive cells are not necessarily podocytes since many other cells express podocalyxin, such as hematopoietic stem cells, vascular endothelial cells, platelets, and macrophages (Orikasa et al., 1996). 2) Though there is evidence that urinary podocytes can be cultured, these cells might be from other sources. For instance, podocyte progenitor cell populations such as CD133 and CD24 double-positive stem cells and the cells of renin lineage, identified as a FoxD1þ stromal progenitor (Nagata, 2016), might contribute to these observations. The co-expression of WT1 and α-smooth muscle actin or cytokeratin 8 might indicate this possibility, although co-expression of these markers could indicate less differentiated podocytes (Vogelmann et al., 2003).

Podocyte Domino Effect

The "podocyte domino effect" is recently identified as a novel mechanism of progressive podocyte loss (Mulay et al., 2013; Nagata, 2016). Podocyte damage due to primary insult can spread injury by inducing secondary damage to the remaining intact podocytes, even though the initial insult is very short-lived (Nagata, 2016). This was suggested by utilizing chimeric mice, in which only a subpopulation of podocytes expressed hCD25, the receptor for the immunotoxin LMB2. LMB2 injection to the chimeric mice initially causes the podocyte injury limited to the subpopulation of podocyte expressing hCD25; however, hCD25-negative podocytes developed injury as early as the four days after the LMB2 injection, evidenced by foot process effacement and decreased expression of podocyte markers such as nephrin, podocin, and podocalyxin (Matsusaka et al., 2011). The exact mechanism of this observation remains to be determined. However, this could be due to podocytes-podocytes crosstalk or podocytes-endothelial cells-podocytes crosstalk. When podocytes are injured, they secrete cytokines that could damage neighborhood podocytes or glomerular endothelial cells, which in turn affect other podocyte functions.

CONCLUSION

Podocyte number was correlated with the amount of proteinuria and extent of glomerulosclerosis. Due to its limited regeneration capacity, it is important to understand the underlying mechanism of podocyte loss, and therefore, we could develop effective measures to prevent their loss. Several common cell death pathways likely apply to podocyte loss in kidney diseases; however, podocytes may have unique pathways such as anoikis, podoptosis, and mitotic catastrophe. Podocytes may undergo cell death and detachment sequentially; however, the evidence of increased viable urinary podocytes in patients with glomerular disease supports that they may detach and stay alive. The dead podocytes are eliminated quickly by phagocytosis, so it is difficult to detect them *in vivo* and therefore may mask the fact that they are dead before detachment. Our understanding of the mechanisms of podocyte loss needs to be improved with more studies. Ultimately, we could develop effective measures to prevent podocyte loss as a therapy for glomerular disease.

AUTHOR CONTRIBUTIONS

LiY, LuY, JH, and AC drafted, edited, and revised the manuscript; LiY and LuY prepared the figures; LiY, LuY, JH, and AC approved the final version of the manuscript.

FUNDING

AC is supported by grants from the National Natural Science Foundation of China (No. 81800637) and Hunan Natural Science Outstanding Youth Fund Projects (No. 2021JJ10075).

REFERENCES

Abais, J. M., Xia, M., Li, G., Gehr, T. W. B., Boini, K. M., and Li, P.-L. (2014). Contribution of Endogenously Produced Reactive Oxygen Species to the Activation of Podocyte NLRP3 Inflammasomes in Hyperhomocysteinemia. *Free Radic. Biol. Med.* 67, 211–220. doi:10.1016/j.freeradbiomed.2013.10.009

An, X., Zhang, Y., Cao, Y., Chen, J., Qin, H., and Yang, L. (2020). Punicalagin Protects Diabetic Nephropathy by Inhibiting Pyroptosis Based on TXNIP/NLRP3 Pathway. *Nutrients* 12, 1516. doi:10.3390/nu12051516

Asanuma, K., Tanida, I., Shirato, I., Ueno, T., Takahara, H., Nishitani, T., et al. (2003). MAP-LC3, a Promising Autophagosomal Marker, Is Processed during the Differentiation and Recovery of Podocytes from PAN Nephrosis. *FASEB j.* 17, 1165–1167. doi:10.1096/fj.02-0580fje

Benzing, T., and Salant, D. (2021). Insights into Glomerular Filtration and Albuminuria. *N. Engl. J. Med.* 384, 1437–1446. doi:10.1056/NEJMra1808786

Boini, K. M., Xia, M., Abais, J. M., Li, G., Pitzer, A. L., Gehr, T. W. B., et al. (2014). Activation of Inflammasomes in Podocyte Injury of Mice on the High Fat Diet: Effects of ASC Gene Deletion and Silencing. *Biochim. Biophys. Acta (Bba) - Mol. Cel Res.* 1843, 836–845. doi:10.1016/j.bbamcr.2014.01.033

Cardone, M. H., Salvesen, G. S., Widmann, C., Johnson, G., and Frisch, S. M. (1997). The Regulation of Anoikis: MEKK-1 Activation Requires Cleavage by Caspases. *Cell* 90, 315–323. doi:10.1016/s0092-8674(00)80339-6

Chen, A., Feng, Y., Lai, H., Ju, W., Li, Z., Li, Y., et al. (2020). Soluble RARRES1 Induces Podocyte Apoptosis to Promote Glomerular Disease Progression. *J. Clin. Invest.* 130, 5523–5535. doi:10.1172/JCI140155

Cheng, Q., Pan, J., Zhou, Z. L., Yin, F., Xie, H. Y., Chen, P. P., et al. (2021). Caspase-11/4 and Gasdermin D-Mediated Pyroptosis Contributes to Podocyte Injury in Mouse Diabetic Nephropathy. *Acta Pharmacol. Sin* 42, 954–963. doi:10.1038/s41401-020-00525-z

Evavold, C. L., Hafner-Bratkovič, I., Devant, P., D'Andrea, J. M., Ngwa, E. M., Boršić, E., et al. (2021). Control of Gasdermin D Oligomerization and Pyroptosis by the Ragulator-Rag-mTORC1 Pathway. *Cell* 184, 4495–4511. doi:10.1016/j.cell.2021.06.028

Frisch, S., and Francis, H. (1994). Disruption of Epithelial Cell-Matrix Interactions Induces Apoptosis. *J. Cel Biol* 124, 619–626. doi:10.1083/jcb.124.4.619

Fu, R., Guo, C., Wang, S., Huang, Y., Jin, O., Hu, H., et al. (2017). Podocyte Activation of NLRP3 Inflammasomes Contributes to the Development of Proteinuria in Lupus Nephritis. *Arthritis Rheumatol.* 69, 1636–1646. doi:10.1002/art.40155

Galluzzi, L., Vitale, I., Aaronson, S. A., Abrams, J. M., Adam, D., Agostinis, P., et al. (2018). Molecular Mechanisms of Cell Death: Recommendations of the Nomenclature Committee on Cell Death 2018. *Cell Death Differ* 25, 486–541. doi:10.1038/s41418-017-0012-4

Ganley, I. G., Lam, D. H., Wang, J., Ding, X., Chen, S., and Jiang, X. (2009). ULK1·ATG13·FIP200 Complex Mediates mTOR Signaling and Is Essential for Autophagy. *J. Biol. Chem.* 284, 12297–12305. doi:10.1074/jbc.M900573200

Gao, P., Meng, X.-F., Su, H., He, F.-F., Chen, S., Tang, H., et al. (2014). Thioredoxin-interacting Protein Mediates NALP3 Inflammasome Activation in Podocytes during Diabetic Nephropathy. *Biochim. Biophys. Acta (Bba) - Mol. Cel Res.* 1843, 2448–2460. doi:10.1016/j.bbamcr.2014.07.001

Gilmore, A. P. (2005). Anoikis. *Cel Death Differ* 12 (Suppl. 2), 1473–1477. doi:10.1038/sj.cdd.4401723

Grahammer, F., and Huber, T. B. (2016). Aberrant Podocyte Cell Cycle in Glomerular Disease. *Cell Cycle* 15, 2237–2238. doi:10.1080/15384101.2016.1205413

Graslkraupp, B. (1995). *In Situ* detection of Fragmented DNA (Tunel Assay) Fails to Discriminate Among Apoptosis, Necrosis, and Autolytic Cell Death: A Cautionary Note*1. *Hepatology* 21, 1465–1468. doi:10.1002/hep.184021053410.1016/0270-9139(95)90071-3

Grouls, S., Iglesias, D. M., Wentzensen, N., Moeller, M. J., Bouchard, M., Kemler, R., et al. (2012). Lineage Specification of Parietal Epithelial Cells Requires β-Catenin/Wnt Signaling. *Jasn* 23, 63–72. doi:10.1681/ASN.2010121257

Guo, C., Fu, R., Zhou, M., Wang, S., Huang, Y., Hu, H., et al. (2019). Pathogenesis of Lupus Nephritis: RIP3 Dependent Necroptosis and NLRP3 Inflammasome Activation. *J. Autoimmun.* 103, 102286. doi:10.1016/j.jaut.2019.05.014

Hagen, M., Pfister, E., Kosel, A., Shankland, S., Pippin, J., Amann, K., et al. (2016). Cell Cycle Re-entry Sensitizes Podocytes to Injury Induced Death. *Cell Cycle* 15, 1929–1937. doi:10.1080/15384101.2016.1191710

Hara, M., Oohara, K., Dai, D.-F., and Liapis, H. (2019). Mitotic Catastrophe Causes Podocyte Loss in the Urine of Human Diabetics. *Am. J. Pathol.* 189, 248–257. doi:10.1016/j.ajpath.2018.10.016

Hartleben, B., Gödel, M., Meyer-Schwesinger, C., Liu, S., Ulrich, T., Köbler, S., et al. (2010). Autophagy Influences Glomerular Disease Susceptibility and Maintains Podocyte Homeostasis in Aging Mice. *J. Clin. Invest.* 120, 1084–1096. doi:10.1172/jci39492

Hoshi, S., Shu, Y., Yoshida, F., Inagaki, T., Sonoda, J., Watanabe, T., et al. (2002). Podocyte Injury Promotes Progressive Nephropathy in Zucker Diabetic Fatty Rats. *Lab. Invest.* 82, 25–35. doi:10.1038/labinvest.3780392

Huber, T. B., Hartleben, B., Kim, J., Schmidts, M., Schermer, B., Keil, A., et al. (2003). Nephrin and CD2AP Associate with Phosphoinositide 3-OH Kinase and Stimulate AKT-dependent Signaling. *Mol. Cel Biol* 23, 4917–4928. doi:10.1128/mcb.23.14.4917-4928.2003

Inoki, K., Mori, H., Wang, J., Suzuki, T., Hong, S., Yoshida, S., et al. (2011). mTORC1 Activation in Podocytes Is a Critical Step in the Development of Diabetic Nephropathy in Mice. *J. Clin. Invest.* 121, 2181–2196. doi:10.1172/jci44771

Iwakuma, T., and Lozano, G. (2003). MDM2, an Introduction. *Mol. Cancer Res.* 1, 993–1000.

Jia, J., Ding, G., Zhu, J., Chen, C., Liang, W., Franki, N., et al. (2008). Angiotensin II Infusion Induces Nephrin Expression Changes and Podocyte Apoptosis. *Am. J. Nephrol.* 28, 500–507. doi:10.1159/000113538

Kemeny, E., Mihatsch, M. J., Dürmüller, U., and Gudat, F. (1995). Podocytes Loose Their Adhesive Phenotype in Focal Segmental Glomerulosclerosis. *Clin. Nephrol.* 43, 71–83.

Kriz, W., Hã¤hnel, B., Hosser, H., Rã¶sener, S., and Waldherr, R. (2014). Structural Analysis of How Podocytes Detach from the Glomerular Basement Membrane under Hypertrophic Stress. *Front. Endocrinol.* 5, 207. doi:10.3389/fendo.2014.00207

Kriz, W., and Lemley, K. V. (2015). A Potential Role for Mechanical Forces in the Detachment of Podocytes and the Progression of CKD. *Jasn* 26, 258–269. doi:10.1681/ASN.2014030278

Laplante, M., and Sabatini, D. M. (2012). mTOR Signaling in Growth Control and Disease. *Cell* 149, 274–293. doi:10.1016/j.cell.2012.03.017

Lasagni, L., Lazzeri, E., J. Shankland, S., Anders, H.-J., and Romagnani, P. (2013). Podocyte Mitosis - a Catastrophe. *Curr. Mol. Med.* 13, 13–23. doi:10.2174/1566524011307010013102174/156652413804486250

Lemley, K. V., Lafayette, R. A., Safai, M., Derby, G., Blouch, K., Squarer, A., et al. (2002). Podocytopenia and Disease Severity in IgA Nephropathy. *Kidney Int.* 61, 1475–1485. doi:10.1046/j.1523-1755.2002.00269.x

Li, F., Chen, Y., Li, Y., Huang, M., and Zhao, W. (2020). Geniposide Alleviates Diabetic Nephropathy of Mice through AMPK/SIRT1/NF-κB Pathway. *Eur. J. Pharmacol.* 886, 173449. doi:10.1016/j.ejphar.2020.173449

Liapis, H., Romagnani, P., and Anders, H.-J. (2013). New Insights into the Pathology of Podocyte Loss. *Am. J. Pathol.* 183, 1364–1374. doi:10.1016/j.ajpath.2013.06.033

Maheswaran, S., Englert, C., Bennett, P., Heinrich, G., and Haber, D. A. (1995). The WT1 Gene Product Stabilizes P53 and Inhibits P53-Mediated Apoptosis. *Genes Dev.* 9, 2143–2156. doi:10.1101/gad.9.17.2143

Matsusaka, T., Sandgren, E., Shintani, A., Kon, V., Pastan, I., Fogo, A. B., et al. (2011). Podocyte Injury Damages Other Podocytes. *Jasn* 22, 1275–1285. doi:10.1681/asn.2010090963

Matter, A. (1979). Microcinematographic and Electron Microscopic Analysis of Target Cell Lysis Induced by Cytotoxic T Lymphocytes. *Immunology* 36, 179–190.

Moreno, J., Sanchez-Nino, M., Sanz, A., Lassila, M., Holthofer, H., Blanco-Colio, L., et al. (2008). A Slit in Podocyte Death. *Cmc* 15, 1645–1654. doi:10.2174/092986708784911542

Mulay, S. R., Thomasova, D., Ryu, M., Kulkarni, O. P., Migliorini, A., Bruns, H., et al. (2013). Podocyte Loss Involves MDM2-Driven Mitotic Catastrophe. *J. Pathol.* 230, 322–335. doi:10.1002/path.4193

Nagata, M. (2016). Podocyte Injury and its Consequences. *Kidney Int.* 89, 1221–1230. doi:10.1016/j.kint.2016.01.012

Nishad, R., Mukhi, D., Singh, A. K., Motrapu, M., Chintala, K., Tammineni, P., et al. (2021). Growth Hormone Induces Mitotic Catastrophe of Glomerular Podocytes and Contributes to Proteinuria. *Cell Death Dis* 12, 342. doi:10.1038/s41419-021-03643-6

Orikasa, M., Iwanaga, T., Takahashi-Iwanaga, H., Kozima, K., and Shimizu, F. (1996). Macrophagic Cells Outgrowth from normal Rat Glomerular Culture: Possible Metaplastic Change from Podocytes. *Lab. Invest.* 75, 719–733.

Overholtzer, M., Mailleux, A. A., Mouneimne, G., Normand, G., Schnitt, S. J., King, R. W., et al. (2007). A Nonapoptotic Cell Death Process, Entosis, that Occurs by Cell-In-Cell Invasion. *Cell* 131, 966–979. doi:10.1016/j.cell.2007.10.040

Petermann, A. T., Krofft, R., Blonski, M., Hiromura, K., Vaughn, M., Pichler, R., et al. (2003). Podocytes that Detach in Experimental Membranous Nephropathy Are viable11See Editorial by Mundel, P. 1529. *Kidney Int.* 64, 1222–1231. doi:10.1046/j.1523-1755.2003.00217.x

Reginato, M. J., Mills, K. R., Paulus, J. K., Lynch, D. K., Sgroi, D. C., Debnath, J., et al. (2003). Integrins and EGFR Coordinately Regulate the Pro-apoptotic Protein Bim to Prevent Anoikis. *Nat. Cel Biol* 5, 733–740. doi:10.1038/ncb1026

Regoli, M., and Bendayan, M. (1997). Alterations in the Expression of the a 3 B 1 Integrin in Certain Membrane Domains of the Glomerular Epithelial Cells (Podocytes) in Diabetes Mellitus. *Diabetologia* 40, 15–22. doi:10.1007/s001250050637

Reiser, J., and Altintas, M. M. (2016). Podocytes. *F1000Res* 5, 114. doi:10.12688/f1000research.7255.1

Ryu, M., Kulkarni, O. P., Radomska, E., Miosge, N., Gross, O., and Anders, H.-J. (2011). Bacterial CpG-DNA Accelerates Alport Glomerulosclerosis by Inducing an M1 Macrophage Phenotype and Tumor Necrosis Factor-α-Mediated Podocyte Loss. *Kidney Int.* 79, 189–198. doi:10.1038/ki.2010.373

Sakairi, T., Abe, Y., Kajiyama, H., Bartlett, L. D., Howard, L. V., Jat, P. S., et al. (2010). Conditionally Immortalized Human Podocyte Cell Lines Established from Urine. *Am. J. Physiology-Renal Physiol.* 298, F557–F567. doi:10.1152/ajprenal.00509.2009

Schiffer, M., Bitzer, M., Roberts, I. S. D., Kopp, J. B., ten Dijke, P., Mundel, P., et al. (2001). Apoptosis in Podocytes Induced by TGF-β and Smad7. *J. Clin. Invest.* 108, 807–816. doi:10.1172/jci1236710.1172/jci200112367

Shahzad, K., Bock, F., Dong, W., Wang, H., Kopf, S., Kohli, S., et al. (2015). Nlrp3-inflammasome Activation in Non-myeloid-derived Cells Aggravates Diabetic Nephropathy. *Kidney Int.* 87, 74–84. doi:10.1038/ki.2014.271

Shankland, S. J., and Wolf, G. (2000). Cell Cycle Regulatory Proteins in Renal Disease: Role in Hypertrophy, Proliferation, and Apoptosis. *Am. J. Physiology-Renal Physiol.* 278, F515–F529. doi:10.1152/ajprenal.2000.278.4.F515

Sosna, J., Voigt, S., Mathieu, S., Kabelitz, D., Trad, A., Janssen, O., et al. (2013). The Proteases HtrA2/Omi and UCH-L1 Regulate TNF-Induced Necroptosis. *Cell Commun Signal* 11, 76. doi:10.1186/1478-811x-11-76

Srivastava, T., Garola, R. E., and Singh, H. K. (2006). Cell-cycle Regulatory Proteins in the Podocyte in Collapsing Glomerulopathy in Children. *Kidney Int.* 70, 529–535. doi:10.1038/sj.ki.5001577

Susztak, K., and Böttinger, E. P. (2006). Diabetic Nephropathy: A Frontier for Personalized Medicine: Figure 1. *Jasn* 17, 361–367. doi:10.1681/ASN.2005101109

Tagawa, A., Yasuda, M., Kume, S., Yamahara, K., Nakazawa, J., Chin-Kanasaki, M., et al. (2016). Impaired Podocyte Autophagy Exacerbates Proteinuria in Diabetic Nephropathy. *Diabetes* 65, 755–767. doi:10.2337/db15-0473

Tang, H., Lei, C.-T., Ye, C., Gao, P., Wan, C., Chen, S., et al. (2017). MDM2 Is Implicated in High-Glucose-Induced Podocyte Mitotic Catastrophe *via* Notch1 Signalling. *J. Cel. Mol. Med.* 21, 3435–3444. doi:10.1111/jcmm.13253

Tharaux, P.-L., and Huber, T. B. (2012). How many ways can a podocyte die? *Semin. Nephrol.* 32, 394–404. doi:10.1016/j.semnephrol.2012.06.011

Thomasova, D., Bruns, H. A., Kretschmer, V., Ebrahim, M., Romoli, S., Liapis, H., et al. (2015). Murine Double Minute-2 Prevents P53-Overactivation-Related Cell Death (Podoptosis) of Podocytes. *Jasn* 26, 1513–1523. doi:10.1681/ASN.2014040345

Tian, X., Kim, J. J., Monkley, S. M., Gotoh, N., Nandez, R., Soda, K., et al. (2014). Podocyte-associated Talin1 Is Critical for Glomerular Filtration Barrier Maintenance. *J. Clin. Invest.* 124, 1098–1113. doi:10.1172/jci69778

Topham, P. S., Haydar, S. A., Kuphal, R., Lightfoot, J. D., and Salant, D. J. (1999). Complement-mediated Injury Reversibly Disrupts Glomerular Epithelial Cell Actin Microfilaments and Focal Adhesions. *Kidney Int.* 55, 1763–1775. doi:10.1046/j.1523-1755.1999.00407.x

Trimarchi, H. (2017). Podocyturia: Potential Applications and Current Limitations. *Wjn* 6, 221–228. doi:10.5527/wjn.v6.i5.221

Vakifahmetoglu, H., Olsson, M., and Zhivotovsky, B. (2008). Death through a Tragedy: Mitotic Catastrophe. *Cel Death Differ* 15, 1153–1162. doi:10.1038/cdd.2008.47

Vogelmann, S. U., Nelson, W. J., Myers, B. D., and Lemley, K. V. (2003). Urinary Excretion of Viable Podocytes in Health and Renal Disease. *Am. J. Physiology-Renal Physiol.* 285, F40–F48. doi:10.1152/ajprenal.00404.2002

von Moltke, J., Ayres, J. S., Kofoed, E. M., Chavarría-Smith, J., and Vance, R. E. (2013). Recognition of Bacteria by Inflammasomes. *Annu. Rev. Immunol.* 31, 73–106. doi:10.1146/annurev-immunol-032712-095944

Westman, J., Grinstein, S., and Marques, P. E. (2019). Phagocytosis of Necrotic Debris at Sites of Injury and Inflammation. *Front. Immunol.* 10, 3030. doi:10.3389/fimmu.2019.03030

Wharram, B. L., Goyal, M., Wiggins, J. E., Sanden, S. K., Hussain, S., Filipiak, W. E., et al. (2005). Podocyte Depletion Causes Glomerulosclerosis: Diphtheria Toxin-Induced Podocyte Depletion in Rats Expressing Human Diphtheria Toxin Receptor Transgene. *Jasn* 16, 2941–2952. doi:10.1681/asn.2005010055

Wu, L., Feng, Z., Cui, S., Hou, K., Tang, L., Zhou, J., et al. (2013). Rapamycin Upregulates Autophagy by Inhibiting the mTOR-ULK1 Pathway, Resulting in Reduced Podocyte Injury. *PLoS One* 8, e63799. doi:10.1371/journal.pone.0063799

Xia, M., Conley, S. M., Li, G., Li, P.-L., and Boini, K. M. (2014). Inhibition of Hyperhomocysteinemia-Induced Inflammasome Activation and Glomerular Sclerosis by NLRP3 Gene Deletion. *Cell Physiol Biochem* 34, 829–841. doi:10.1159/000363046

Xiong, W., Meng, X.-F., and Zhang, C. (2020). Inflammasome Activation in Podocytes: a New Mechanism of Glomerular Diseases. *Inflamm. Res.* 69, 731–743. doi:10.1007/s00011-020-01354-w

Xu, Y., Gao, H., Hu, Y., Fang, Y., Qi, C., Huang, J., et al. (2019). High Glucose-Induced Apoptosis and Necroptosis in Podocytes Is Regulated by UCHL1 *via* RIPK1/RIPK3 Pathway. *Exp. Cel Res.* 382, 111463. doi:10.1016/j.yexcr.2019.06.008

Yan, G., Elbadawi, M., and Efferth, T. (2020). Multiple Cell Death Modalities and Their Key Features (Review). *World Acad. Sci. J.* 2, 39–48. doi:10.3892/wasj.2020.40

Yasuda-Yamahara, M., Kume, S., Tagawa, A., Maegawa, H., and Uzu, T. (2015). Emerging Role of Podocyte Autophagy in the Progression of Diabetic Nephropathy. *Autophagy* 11, 2385–2386. doi:10.1080/15548627.2015.1115173

Yi, M., Zhang, L., Liu, Y., Livingston, M. J., Chen, J.-K., Nahman, N. S., et al. (2017). Autophagy Is Activated to Protect against Podocyte Injury in Adriamycin-Induced Nephropathy. *Am. J. Physiology-Renal Physiol.* 313, F74–f84. doi:10.1152/ajprenal.00114.2017

Yu, C.-C., Fornoni, A., Weins, A., Hakroush, S., Maiguel, D., Sageshima, J., et al. (2013). Abatacept in B7-1-Positive Proteinuric Kidney Disease. *N. Engl. J. Med.* 369, 2416–2423. doi:10.1056/NEJMoa1304572

Yu, P., Zhang, X., Liu, N., Tang, L., Peng, C., and Chen, X. (2021). Pyroptosis: Mechanisms and Diseases. *Signal. Transduct Target. Ther.* 6, 128. doi:10.1038/s41392-021-00507-5

Zhan, J.-F., Huang, H.-W., Huang, C., Hu, L.-L., and Xu, W.-W. (2020). Long Non-coding RNA NEAT1 Regulates Pyroptosis in Diabetic Nephropathy *via* Mediating the miR-34c/NLRP3 Axis. *Kidney Blood Press. Res.* 45, 589–602. doi:10.1159/000508372

Zhang, C., Boini, K. M., Xia, M., Abais, J. M., Li, X., Liu, Q., et al. (2012). Activation of Nod-like Receptor Protein 3 Inflammasomes Turns on Podocyte Injury and Glomerular Sclerosis in Hyperhomocysteinemia. *Hypertension* 60, 154–162. doi:10.1161/hypertensionaha.111.189688

Zhang, K.-j., Wu, Q., Jiang, S.-m., Ding, L., Liu, C.-x., Xu, M., et al. (2021). Pyroptosis: A New Frontier in Kidney Diseases. *Oxidative Med. Cell Longevity* 2021, 1–12. doi:10.1155/2021/6686617

Conflict of Interest: The authors declare that the research was conducted in the absence of any commercial or financial relationships that could be construed as a potential conflict of interest.

Publisher's Note: All claims expressed in this article are solely those of the authors and do not necessarily represent those of their affiliated organizations, or those of the publisher, the editors and the reviewers. Any product that may be evaluated in this article, or claim that may be made by its manufacturer, is not guaranteed or endorsed by the publisher.

frontiers in Cell and Developmental Biology

REVIEW
published: 21 February 2022
doi: 10.3389/fcell.2022.837828

Using *Drosophila* Nephrocytes to Understand the Formation and Maintenance of the Podocyte Slit Diaphragm

Joyce van de Leemput[1,2†], *Pei Wen*[1,2†] *and Zhe Han*[1,2*†]

[1]*Center for Precision Disease Modeling, Department of Medicine, University of Maryland School of Medicine, Baltimore, MD, United States,* [2]*Division of Endocrinology, Diabetes and Nutrition, Department of Medicine, University of Maryland School of Medicine, Baltimore, MD, United States*

OPEN ACCESS

Edited by:
Mario Ollero, INSERM U955 Institut Mondor de Recherche Biomédicale (IMRB), France

Reviewed by:
Roland Wedlich-Söldner, University of Münster, Germany
José Carlos Pastor-Pareja, Tsinghua University, China

***Correspondence:**
Zhe Han
zhan@som.umaryland.edu

†ORCID ID:
Joyce van de Leemput, orcid.org/0000-0003-1903-7295
Pei Wen, orcid.org/0000-0001-7065-6396
Zhe Han, orcid.org/0000-0002-5177-7798

Specialty section:
This article was submitted to Cell Death and Survival, a section of the journal Frontiers in Cell and Developmental Biology

Received: *17 December 2021*
Accepted: *01 February 2022*
Published: *21 February 2022*

Citation:
van de Leemput J, Wen P and Han Z (2022) Using Drosophila Nephrocytes to Understand the Formation and Maintenance of the Podocyte Slit Diaphragm. Front. Cell Dev. Biol. 10:837828. doi: 10.3389/fcell.2022.837828

The podocyte slit diaphragm (SD) is an essential component of the glomerular filtration barrier and its disruption is a common cause of proteinuria and many types of kidney disease. Therefore, better understanding of the pathways and proteins that play key roles in SD formation and maintenance has been of great interest. Podocyte and SD biology have been mainly studied using mouse and other vertebrate models. However, vertebrates are limited by inherent properties and technically challenging *in vivo* access to the podocytes. *Drosophila* is a relatively new alternative model system but it has already made great strides. Past the initial obvious differences, mammalian podocytes and fly nephrocytes are remarkably similar at the genetic, molecular and functional levels. This review discusses SD formation and maintenance, and their dependence on cell polarity, the cytoskeleton, and endo- and exocytosis, as learned from studies in fly nephrocytes and mammalian podocytes. In addition, it reflects on the remaining gaps in our knowledge, the physiological implications for glomerular diseases and how we can leverage the advantages *Drosophila* has to offer to further our understanding.

Keywords: kidney, mammalian podocytes, Drosophila nephrocytes, slit diaphragm, apical-basal polarity, cytoskeleton, endocytosis and exocytosis, glomerular diseases

INTRODUCTION

Glomerulopathy and chronic kidney disease are marked by injury and loss of podocytes. Podocytes are specialized epithelial cells that wrap around the glomerular capillaries. The podocytes tightly adhere to the outer capillary surface where they form interlaced foot processes, thus making close contacts with neighboring podocytes to form the slit diaphragms (SDs). The SDs, together with the capillary fenestrated endothelial cells and the glomerular basement membrane (GBM), form the glomerular filtration unit (Pollak et al., 2014; Kawasaki et al., 2019) (**Figure 1**). The filtration unit is essential for kidney function to remove toxins and waste from the bloodstream while recycling vital nutrients. These processes to maintain homeostasis of fluids (e.g. blood pressure), salts and hormones are highly conserved from Metazoa to mammals. Under stress or toxic conditions, the podocytes undergo active morphological changes during which the cells smoothen and loose their elaborate branches in a process known as foot process effacement (Garg, 2018). Because podocyte inter-foot connections are crucial to SD structural integrity, effacement inherently leads to disruption of the glomerular filtration structure and ultimately loss of kidney function. Mammalian

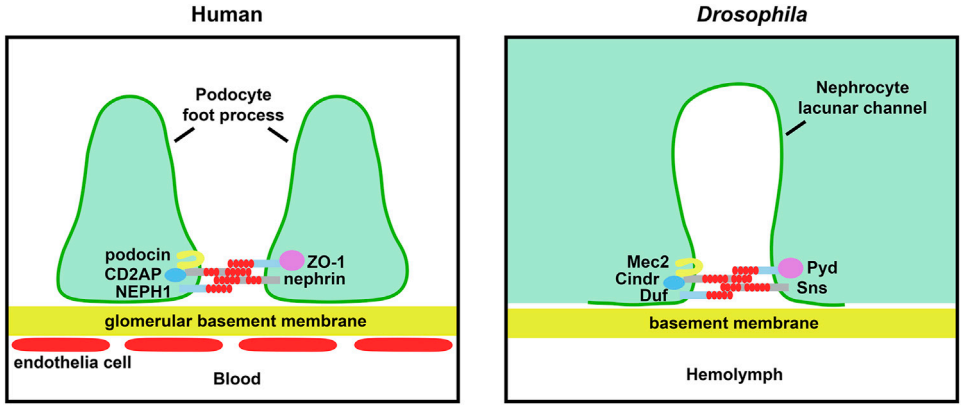

FIGURE 1 | Schematic of renal filtration structure and essential slit diaphragm proteins. The left panel shows the glomerular filtration barrier structure in human. The blood is filtered through fenestrated endothelial cells, glomerular basement membrane and slit diaphragm between the podocyte foot processes. The right panel shows the filtration structure in the *Drosophila* nephrocyte. The hemolymph is filtered through the basement membrane and slit diaphragm located at the opening of the lacunar channels. The core components of the slit diaphragm are highly conserved between fly and human.

model systems for the podocyte slit diaphragm, both *in vitro* and *in vivo*, have greatly increased our understanding. However, each system came with its own strengths and limitations. For example, the *in vitro* system provides ready access to podocytes, but their key characteristics are often rapidly lost under cell culture conditions (Agarwal et al., 2020). On the other hand, while the *in vivo* system studies podocytes in their physiological environment, the cells have been notoriously difficult to access for *in vivo* imaging (Siegerist et al., 2018). The fruit fly (i.e. vinegar flies; *Drosophila melanogaster*) is a relatively new model to the field. Here we describe the similarities and differences between the fly nephrocyte and the mammalian (mouse) podocyte filtration structures, as well as the contributions made by fly studies of SD formation and maintenance. Further, we discuss what these findings mean for human glomerular disease research, and ultimately patients, and speculate on how the unmatched fly toolkit could be employed to answer remaining questions.

MAMMALIAN MODEL SYSTEMS TO STUDY PODOCYTES AND THE SLIT DIAPHRAGM

Mammalian models, like mouse and rat, have taught us a lot about podocytes and kidney function. Yet, intrinsic (long gestation, small litter size, high maintenance costs and limited specialized genetic tools) and experimental (difficult access to the podocytes) limitations have impeded progress. *In vitro* studies of podocytes have met their own technical challenges pertaining to the difficulty to maintain fully differentiated cells. Podocytes in culture tend to lose their most characteristic features within days, including cell polarity, the intricate foot process morphology, and intact functional SD structures. A landmark publication (Mundel et al., 1997) demonstrated that by omitting sub-cultivation of primary rat or human podocytes, columnar cells could differentiate into mature podocytes. Podocytes were designated mature based on the formation of extensive arborized processes and the expression of Synaptopodin [previously Podocyte protein, 44kDa (PP44) (Mundel et al., 1997b) and Desmin; neither protein was detected in cells with columnar morphology. However, podocyte differentiation also induced cell cycle arrest, thus limiting the number of cells available for subsequent assays (Mundel et al., 1997a). This led some researchers to develop immortalized podocyte cell lines, which came with their own set of limitations (Agarwal et al., 2020). The immortalized lines are generated through insertion of an immortalizing gene [*simian virus 40 (SV40) large tumor antigen (Tag)*] that is not naturally present in the podocyte, therefore random insertion of this gene can lead to off-target effects. The uncontrolled proliferation led to altered podocyte physiology, to prevent this conditional immortalized human podocyte cell lines using a temperature sensitive SV40 gene (*SV40-T*) have been generated. The conditional lines express Nephrin and Podocin, and using this approach podocyte lines have been derived from patients with congenital genetic syndrome (Saleem et al., 2002). These conditional lines have to be continuously monitored for spontaneous transformation, especially in podocytes cultures exceeding 30 passages (Saleem et al., 2002; Agarwal et al., 2020). Other *in vitro* disadvantages might be remedied by using more complex culture systems that mimic the circulatory system and other components of the glomerular filtration unit to better resemble physiological conditions as in, for example, the podocyte organoid models currently under development (Nishinakamura, 2019). By culturing under flow conditions, some kidney organoids include glomerular vascular development (Homan et al., 2019), other models are capable of producing functional renin, the first and rate-limiting enzyme of the renin-angiotensin system (RAS) which regulates blood pressure (Shankar et al., 2021). These technical feats require high levels of expertise and are time, cost, and labor intensive, thus limiting their widespread application. The technical difficulties in obtaining *in vivo* access to podocytes in mammalian models, and in maintaining mature podocytes *in vitro*, have spurred the development of alternative models like zebrafish (*Danio rerio*) and fruit flies (*Drosophila*).

CONSERVATION OF THE SLIT DIAPHRAGM BETWEEN *DROSOPHILA* AND MAMMALS

The fly equivalent of podocytes are the nephrocytes. In fact, the fly has two types of nephrocytes, those located around the connection site of the esophagus and proventriculus known as garland cells, and those located near the heart known as pericardial nephrocytes (Denholm and Skaer, 2009). Of note, unlike podocytes, the nephrocytes are not physically connected to the fly excretory and osmoregulatory system known as the Malpighian tubules (mammalian liver and kidneys). This difference means that mammalian podocytes form an *inter*cellular filtration system, between adjacent foot processes. These foot processes cover the glomerular basement membrane, which acts as a negatively charged filter prior to SD access (Haraldsson et al., 2008). At the SD, blood proteins are filtered by size for entry into the urinary space where the proteins get reabsorbed in the renal proximal tubule to retain vital nutrients. Fly nephrocytes, on the other hand, have a cell surface covered by membrane ingressions that form labyrinthine channels with a fingerprint-like pattern. *Auto*cellular filtration barriers span the openings of these labyrinthine, or lacunar, channels where hemolymph proteins get reabsorbed *via* endocytosis (Kawasaki et al., 2019) (**Figure 1**). The nephrocytes are encased in the basement membrane (Kawasaki et al., 2019), where it might perform a similar function to the podocyte glomerular basement membrane. Unfortunately, the nephrocyte basement membrane remains a grossly understudied area. Given the close interaction between the SD and the basement membrane and their size-charge filtration activities, respectively, further study of the basement membrane will undoubtedly benefit our understanding of the SD in development and diseases.

The fly might not have a defined kidney as such, but the pathways governing filtration of its hemolymph (fly equivalent of blood) are remarkably conserved among flies and mammals. Insect nephrocytes have been described as early as the 1800s. Initially they were identified as phagocytic cells able to take up foreign and toxic compounds from the hemolymph (Leydig, 1866; Balbiani, 1886; Hollande, 1921; Crossley, 1972). However, it was not until landmark publications in 2009 (Weavers et al., 2009; Zhuang et al., 2009) that their similarity to mammalian podocytes was fully appreciated and their potential as a model system recognized. These studies showed that both podocytes and nephrocytes have a specialized size-selective filtration barrier, and that the fly nephrocyte has orthologs for the main mammalian proteins composing the SD, including fly Sns (mammalian Nephrin), Duf [Kin of irre (kirre)] (mammalian KIRREL1; NEPH1), Cindr (mammalian CD2AP), Pyd (mammalian ZO-1), and Mec2 (mammalian Podocin). The studies also demonstrated that these proteins form similar multi-protein complexes in both species, that altered expression of these complexes leads to defective filtration and disrupts hemolymph homeostasis, and that Sticks and stones (Sns) and Dumbfounded (Duf), similar to their mammalian Nephrin and Nephrin-like 1 (NEPH1) counterparts, are key to SD formation (Weavers et al., 2009; Zhuang et al., 2009). Together these studie demonstrated the strong similarities between the fly nephrocyte and mammalian podocyte SD structures. Moreover, the width of the SD structure in podocytes and nephrocytes is comparable at just under 40 nm (Kawasaki et al., 2019), and podocytes and pericardial nephrocytes share a ~70 kD size selection filtration cut-off (garland nephrocytes filtrate at a 66–80 kD size limit) (Hermle et al., 2017). The highly conserved genes, pathways, filtration structure and function, combined with the highly accessible nephrocytes (facilitated by the open circulatory system in fly, whereas podocytes are locked away inside glomeruli), have made the fly a powerful model to study podocyte development and disease.

ROLE FOR CORE COMPONENTS OF THE SLIT DIAPHRAGM IN ITS ASSEMBLY

Zonula occludens-1 (ZO-1) and NEPH1 are two core components of the SD main filtration unit (**Figure 1** and **Table 1**). It has been shown these proteins themselves play critical roles in junctional remodeling and formation of the SD (Carrasco-Rando et al., 2019). Nephrocytes deficient for Sns or Duf, fly orthologs of mammalian Nephrin and NEPH1 respectively, show a near complete lack of SD structures at the labyrinthine lacunar channels and display a significantly impaired filtration function (Weavers et al., 2009; Zhuang et al., 2009). In addition, ZO-1 localization to the podocyte membrane is dependent on NEPH1-ZO-1 complex formation (Wagner et al., 2008). Similarly, in fly nephrocytes localization of Duf is dependent on Pyd (mammalian ZO-1) during formation of the lacunar channel filtration unit (Carrasco-Rando et al., 2019). For both mammalian podocytes and fly nephrocytes this transition from junctional complex (Cadherin-based) to SDs is reversible (Carrasco-Rando et al., 2019). In fact, the reversed process underlies foot process effacement which is a common hallmark of glomerular diseases. In podocytes, CD2-associated protein (CD2AP) direct interaction with Nephrin and Podocin was shown to be important for SD structural integrity (Schwarz et al., 2001; Shih et al., 2001). Similarly, a genetic interaction study in nephrocytes, showed that the fly ortholog CIN85 and CD2AP related (Cindr) (mammalian CD2AP) interacts with Mechanosensory protein 2 (Mec2) (mammalian Podocin) Fly nephrocytes deficient for Cindr showed collapsed lacunar channels and effacement of SDs, culminating in severe functional defects, and reduced lifespan (Fu et al., 2017b). Nephrocytes from flies on a chronic high sucrose diet, a model for diabetic nephropathy, showed reduced Sns. Further, the study showed that the transcription factor Knot (Kn) [mammalian Early B cell factor 2 (EBF2)], negatively regulated Sns expression in fly nephrocytes in a high dietary sugar dependent manner. The same negative correlation was found for EBF2 in regulating the level of Nephrin in glomeruli of a patient with diabetic nephropathy (Na et al., 2015). Together these findings indicate an important role for these core filtration proteins in SD formation and possibly maintenance (**Figure 1**).

TABLE 1 | Essential slit diaphragm proteins.

Human protein	Fly ortholog	DIOPT score	Protein function	Function in podocytes/nephrocytes
Nephrin	Sns	14	Cell junction	SD Component
NEPH1	Duf	11	Cell junction	SD Component
ZO-1	Pyd	11	Cell junction	SD Component
CD2AP	Cindr	8	Cell junction	SD Component
Podocin	Mec2	3	Cell junction	SD Component
PRKCI (aPKC)	aPKC	12	Cell polarity	SD Formation
PARD6 (G/B/A)	Par-6	12	Cell polarity	SD Formation
PARD3	Baz	13	Cell polarity	SD Formation
DLG1	Dlg	13	Cell polarity	SD Formation
LLGL1	Lgl	15	Cell polarity	SD Formation
SCRIB	Scrib	7	Cell polarity	SD Formation
MARK1	Par-1	10	Cell polarity	SD Formation
STK11 (LKB1)	Lkb1	12	Cell polarity	SD Formation
CRB1	Crb	9	Cell polarity	SD Formation
PALS1 (MPP5)	Sdt	12	Cell polarity	SD Formation
PATJ	Patj	9	Cell polarity	SD Formation
EZR/RDX/MSN	Moe	13/13/14	Actin regulation	Cytoskeleton
ARHGDIA	RhoGDI	15	Actin regulation	Cytoskeleton
ARHGAP24	RhoGAP92B	1	Actin regulation	Cytoskeleton
KANK1, 2, 4	Kank	10	Actin regulation	Cytoskeleton
MYH9	Zip	11	Actin regulation	Cytoskeleton
ACTN4	Actn	11	Actin regulation	Cytoskeleton
MYO1E	Myo61F	3	Actin regulation	Cytoskeleton
INF2	Form3	7	Actin regulation	Cytoskeleton
CLTA	Chc	13	Endocytosis	SD Maintenance
CLTC	Clc	14	Endocytosis	SD Maintenance
DYNAMIN	Shi	13	Endocytosis	SD Maintenance
AP2B1	AP-1-2β	12	Endocytosis	SD Maintenance
AP2A2	AP-2α	13	Endocytosis	SD Maintenance
AP2M1	AP-2μ	13	Endocytosis	SD Maintenance
AP2S1	AP-2σ	14	Endocytosis	SD Maintenance
AUXILIN	Aux	11	Endocytosis	SD Maintenance
HSPA8	Hsc70-4	12	Endocytosis	SD Maintenance
PICALM (AP180)	Lap	12	Endocytosis	SD Maintenance
RAB5B	Rab5	13	Endocytosis	SD Maintenance
RBSN	Rbsn-5	11	Endocytosis	SD Maintenance
PIK3C3 (VPS34)	Pi3K59F (Vps34)	15	Endocytosis	SD Maintenance
GAPVD1	Gapvd1	14	Endocytosis	SD Maintenance
AMN	dAmn	11	Endocytosis	SD Maintenance
CUBN	Cubn	12	Endocytosis	SD Maintenance
CUBN	Cubn-2	9	Endocytosis	SD Maintenance
RPH3a	Rph	10	Endocytosis	SD Maintenance
RAB3A	Rab3	12	Endocytosis	SD Maintenance
RAB11A	Rab11	13	Recycling	SD Maintenance
EXOC1	Sec3	14	Recycling	SD Maintenance
EXOC2	Sec5	14	Recycling	SD Maintenance
EXOC3	Sec6	14	Recycling	SD Maintenance
EXOC4	Sec8	14	Recycling	SD Maintenance
EXOC5	Sec10	14	Recycling	SD Maintenance
EXOC6	Sec15	13	Recycling	SD Maintenance
EXOC7	Exo70	15	Recycling	SD Maintenance
EXOC8	Exo84	14	Recycling	SD Maintenance
TBC1D8B	Tbc1d8b	13	Recycling	SD Maintenance

DIOPT, Drosophila *RNAi Screening Center (DRSC) integrative ortholog prediction tool (Hu et al., 2011); SD, slit diaphragm.*

THE IMPORTANCE OF APICAL-BASAL POLARITY FOR SLIT DIAPHRAGM FORMATION

Podocytes have an epithelial origin, starting out as cells with columnar morphology that support cell-cell junctions at the apical surface. These epithelial cells completely transform during development, turning into podocytes with bulbous cell bodies and intricate protrusions that form intercellular junctions (i.e. SDs) at their basal foot processes. This transformation requires (re-)localization of many apical junction proteins to the basal side of the podocyte, where they are gradually

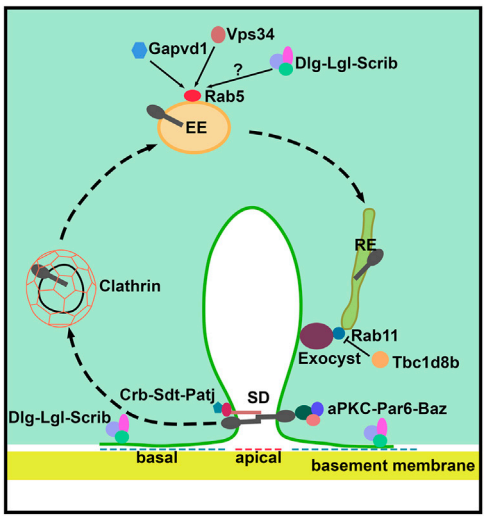

FIGURE 2 | Schematic of slit diaphragm formation and maintenance in *Drosophila* nephrocytes. The apical polarity Crumbs (Crb) and aPKC complexes are localized at the slit diaphragm and define the apical region of the nephrocyte which is important during slit diaphragm formation. The basolateral Scribble (Scrib) complex localizes to the basal region of the nephrocyte between neighboring slit diaphragms. The clathrin-mediated endocytosis, Rab5-dependent early endosomes, Rab11-dependent recycling endosomes and the exocyst complex are critical for slit diaphragm maintenance. Gapvd1, Vps34 (Pi3K59F), and possibly the Scrib basal polarity complex, positively regulate Rab5-dependent early endosome trafficking. Tbc1d8b negatively regulates the function of Rab11 in slit diaphragm recycling. SD, slit diaphragm; EE, early endosome; and, RE, recycling endosome.

replaced by the SD (Ichimura et al., 2017). Even though nephrocytes are not derived from epithelial progenitor cells, they do show the distinct apical-basal polarity (Heiden et al., 2021). The apical and basal plasma membrane domains are defined by the junctional zone and SD/lacunar channel diaphragms in mammalian podocytes and fly nephrocytes, respectively. Moreover, apical-basal polarity in both cell types is governed by the same classical polarity proteins, which have been found to play key roles in SD assembly, maintenance and endocytosis (Michgehl et al., 2017; Heiden et al., 2021) (**Figure 2** and **Table 1**).

The Role of Apical Polarity Proteins

The apical polarity Crumbs (CRB) and Partitioning defective (PAR)-atypical Protein kinase C (aPKC) complexes have been implicated in podocyte health, and SD formation and maintenance. The polarity protein known as Protein crumbs homolog (CRB) is an evolutionary highly conserved protein that is important during epithelial morphogenesis. The genes encoding components of the CRB complex, including fly Crumbs (gene *crb*), Stardust (gene *sdt*) and Bazooka (gene *baz*), were initially discovered in a systematic screen for fly developmental mutants (Wieschaus and Nüsslein-Volhard, 2016). The genes encoding the CRB complex proteins were noted for their disruptive effect on epidermal structure and integrity when mutated. The fly and mammalian CRB complexes share core components, including Sdt [mammalian Protein associated with LIN-7 1 (PALS1)], Serine/threonine-protein kinase Par-6 (Par-6), and Pals1-associated tight junction protein (Patj) (Hochapfel et al., 2017; Michgehl et al., 2017). Fly nephrocytes deficient for *crb* displayed reduced SD structures, disturbed morphology of foot processes and a marked decreased filtration rate (*ex vivo*). This could be attenuated by expressing either human *CRB2* or *CRB3*, which encode the two CRB proteins expressed in podocytes (Hochapfel et al., 2017). Mammalian PALS1 (a.k.a. MPP5) is a core component of the CRB complex in the nephron. Mice with nephron-specific *Pals1* haploinsufficiency suffered from renal cyst formation and severe defects in renal barrier function, indicative of abnormal SDs, resulting in early death (6–8 weeks) (Weide et al., 2017). Similarly, the PALS1 fly homologous protein Sdt was found to be essential in regulating epithelial cell polarity and for SD structural formation in nephrocytes (Bachmann et al., 2001; Hong et al., 2001). Deficiency for *sdt* led to destabilization and endocytosis of Crb in fly epithelial cells (Lin et al., 2015), with mis-localization of Crb (and Patj) to the cytosol and vesicles, and strikingly decreased expression in the nephrocytes, while Sns remained at the cortex (Hochapfel et al., 2017). Moreover, Crb regulates early- and late-endosome formation in nephrocytes, indicating a role in SD maintenance and function (Hochapfel et al., 2017). Regarding the PAR polarity complex, studies in mouse podocytes have shown PAR complex components PAR3, PAR6 and aPKC interact with NEPH1-Nephrin at the SD, and that this interaction is required to establish the structures for the foot processes and SD filtration barriers which facilitate glomerular maturation (Hartleben et al., 2008, 2013). Even though aPKCλ/ι and aPKCζ isoforms are very similar in structure, both are needed to stabilize the NEPH1-Nephrin complex at the SD (Hartleben et al., 2013). Recently, *in vivo* studies have shown similar processes are active in fly nephrocytes. The studies demonstrated that fly Par-6, aPKC and Baz (mammalian PAR-3) are essential for localization of Sns (mammalian Nephrin) at the nephrocyte cortex (Heiden et al., 2021). In addition, the Par-aPKC complex has been shown to be important in endocytosis and SD structural integrity in nephrocytes (Heiden et al., 2021). Together, these studies suggest a role for PAR-aPKC in SD maintenance and function as well as formation.

The Role of Basolateral Polarity Proteins

In addition to the apical polarity regulators, basolateral polarity determinants were found to be essential for slit diaphragm formation. The actions of the apical CRB and PAR-aPKC complexes are balanced by the basolateral Scribble complex. The Scribble complex, comprising Discs large (Dlg), Scribble (Scrib), and Lethal giant larvae (Lgl), was first discovered in *Drosophila* (Hadorn, 1937; Scharrer and Hadorn, 1938; Stewart et al., 1972; Bilder and Perrimon, 2000), with subsequent uncovering of their mammalian orthologs [*see* (Su et al., 2012) for a detailed review]. The balancing actions of the apical and basal complexes was recently demonstrated in fly nephrocytes, which showed that the basolateral polarity proteins Dlg, Scrib, Lgl, and Par1 are required for SD formation (Mysh and Poulton,

2021). Subcellular localization and genetic-interaction data suggested interaction between basolateral and apical protein functions. However, the authors caution that it remains to be determined whether these effects are due to direct interaction of the basolateral and apical protein complexes or if they are mediated through their interaction with the SD (Mysh and Poulton, 2021). Furthermore, the study showed that nephrocytes deficient for the basolateral polarity proteins, particularly Dlg and Par1, displayed mis-localized SD proteins. These nephrocytes showed fewer lacunar channels and SD structures. Instead, the SD components were located in cytoplasmic vesicles adjacent to Rab5-positive vesicles (early endosomes). Based on these findings the authors proposed that the basolateral proteins mediate the organization and function of the endocytic pathway (Mysh and Poulton, 2021). The importance of endocytosis and various Rab family members, including Rab5, in maintaining SD structural integrity—by ensuring localization of key SD proteins—and supporting nephrocyte function has been recently reported in fly (Wen et al., 2020). Furthermore, a separate study in nephrocytes, which used a combination of expansion microscopy and functional assays, showed that the basolateral polarity regulators Dlg, Lgl, Lkb1, and to a greater extent Par-1 and Scrib, are essential for proper Sns distribution (Heiden et al., 2021). Deficiency for any of these polarity proteins led to reduced presence of Sns at the cell surface, with Sns re-localized to intracellular vesicles. Despite the greatly reduced SDs in these nephrocytes—observed as a severely disturbed Sns distribution on the nephrocyte cell surface that typically presents as a fingerprint-like pattern—uptake seemed mostly intact in functional assays of endocytosis (Heiden et al., 2021). Notably, mouse podocytes deficient for *Scrib* (Hartleben et al., 2012) or *Dlg5* (Yu et al., 2016) did not disrupt cell polarity, SD structural integrity or podocyte function (no detectable proteinuria). A plausible explanation [suggested by (Mysh and Poulton, 2021)] for the lacking effect in mice is the genetic redundancy for basolateral polarity components observed in mouse and human, which suggests protein family members might compensate for any deficiency. Indeed, Scrib belongs to the LAP family with four family members [SCRIB, Leucine-rich repeat-containing protein 1 (LRRC1), LRRC7, and Erbb2-interacting protein (Erbin)], and the DLG protein family contains five members (DLG1-5) in mammals. The fly genome, on the other hand, is overall much more compact with little genetic redundancy. It comprises two LAP orthologs (Scrib, and Lap1) and two Dlg protein family members (Dlg1 and Dlg5) (https://flybase.org; http://www.flyrnai.org/diopt). To determine whether these components of basal polarity play similar roles in mammalian podocytes as their roles in fly nephrocytes will require further investigation that combines multiple family members within one model. Interestingly, the apical polarity complexes, CRB and PAR-aPKC, similarly mediate endocytosis (Hochapfel et al., 2017; Heiden et al., 2021), suggesting intersection of the basal (Scrib, Dlg) and apical (Crb, Par-aPKC) polarity pathways. Additional studies are needed to determine how these apical-basal polarity components interact with the SD structural proteins and other podocyte/nephrocyte functional components in the pathomechanisms underlying glomerular diseases.

SLIT DIAPHRAGM DEPENDENCE ON THE CYTOSKELETON FOR FORMATION AND FUNCTION

The role of the cytoskeleton in podocyte development and function cannot be overstated. During development the podocytes undergo huge morphological changes, transforming from simple columnar epithelial cells into the fully differentiated podocytes marked by a bulbous cell body and complex network of protrusions (foot processes). In addition to structure and shape, the podocyte cytoskeleton is also integral to forming the refined polar organization required to obtain the intricate arborization of mature podocytes. Furthermore, the cytoskeleton plays a crucial role in podocyte functioning by ensuring adhesion of the foot processes to the basement membrane, which is essential for the formation of the main filtration structures (slit diaphragms), as well as for adequate signaling responses to external stimuli (Welsh and Saleem, 2011; Endlich et al., 2017; Blaine and Dylewski, 2020). To achieve its complex morphology, each podocyte cellular compartment carries a distinct combination of cytoskeletal components. The major extending, primary processes, that protrude from the bulbous cell body, contain a microtubule and intermediate filament cytoskeleton, while the finer branches, known as secondary foot processes, are mainly structured by Actin filaments (Drenckhahn and Franke, 1988; Schell and Huber, 2017).

The Cytoskeleton and the Slit Diaphragm

Core SD components Duf and Sns are members of the immunoglobulin superfamily that is known to mediate cell adhesion, among others, and to influence cytoskeletal organization through adaptor proteins. In nephrocytes, it has been shown that Pyd-P, a specific isoform of Pyd, might serve as such an intracellular Actin-associated adaptor protein for Duf, this interaction mediates Duf-Sns assembly at the SD. Indeed Pyd is a component of both adherens junctions and the SD filtration barrier, this dual function might facilitate the recruitement and organization of the nephrocyte cytoskeleton (Carrasco-Rando et al., 2019). Similarly, in podocytes disruption of the NEPH1-ZO-1 complex (fly Duf-Pyd) leads to mis-localized NEPH1 and its reduced presence at the SD (Wagner et al., 2008). Moesin is a member of the Ezrin, Radixin, Moesin (ERM) protein family. These proteins interact with transmembrane proteins and membrane associated cytoplasmic proteins on one side, and the filamentous Actin cytoskeleton on the other (Tsukita and Yonemura, 1999). Ezrin is highly expressed in podocytes, where it has been reported to act in several complexes, including with the Na^+/H^+ exchanger regulatory factor (NHEFR2) and Podocalyxin. The function of Ezrin in podocytes might be multi-fold. Interestingly, a study in mice showed *Ezrin* deficiency (knockdown) possibly protects podocytes from morphological defects by inhibiting Rac1 activation (Hatano et al., 2018). The fly homolog for all three ERM family proteins is Moesin (Moe).

Nephrocytes deficient for *Moe* (RNAi) displayed a disrupted Actin cytoskeleton and SD structures (Hochapfel et al., 2017). Furthermore, these nephrocytes showed reduced early (Rab5-positive) and, to lesser extent, late (Rab7-positive) endosomal vesicles. A phenotype reminiscent of nephrocytes deficient for *crb* (RNAi) in the same study. In fact, *Moe*-deficient nephrocytes showed decreased cortical Crb expression, and *vice versa*. Moreover, the phenotype in *crb*-deficient nephrocytes could be attenuated by simultaneous overexpression of *Moe*. These interdependencies were shown to be contingent on the intracellular FERM-binding domain of Crb (Wei et al., 2015; Hochapfel et al., 2017). Fly and mouse studies have demonstrated Crb is competitively regulated by Moesin (Actin cytoskeleton) and aPKC (apical polarity) (Whiteman et al., 2014; Sherrard and Fehon, 2015). Further studies are needed to identify the molecular pathways underlying Crb and Moesin-mediated endocytosis, and their possible ties to mechanisms of cellular polarity. Another example of the involvement of the cytoskeleton at the SD is the functional interactions of Dynamin (a GTPase), Synaptojanin and Endophilin. These proteins are known for their role in synaptic vesicle recycling in neurons, where they are critical for membrane fission during Clathrin-dependent endocytosis and vesicular trafficking. Their function is Actin-dependent, and their regulatory complexes and pathways are highly conserved from yeast to mammals (Kaksonen and Roux, 2018). A study in mice podocytes showed that Dynamin, Synaptojanin and Endophilin, similar to neurons, act at the intersection of endocytosis and the Actin cytoskeleton, and are critical for SD formation. Mice deficient for any of these proteins displayed substantial proteinuria at birth. They further found reduced turnover of Nephrin (fly Sns) on the surface of podocyte foot processes (Soda et al., 2012). Subsequently, Dynamin-1 was shown to regulate the formation and maintenance of the microtubule network in rat glomerular podocytes (La et al., 2020). These Dynamin protein interactions in podocytes are highly conserved. In flies, Dynamin is known as Shibire (Shi), which was similarly shown to be required for SD protein endocytosis in nephrocytes (Wang et al., 2021). Given the high conservation of these endocytosis and vesicular trafficking pathways, the fly nephrocyte could provide a valuable model for further studies.

Systematic Studies Into Podocyte/Nephrocyte Cytoskeletal Proteins

Systematic studies to identify the proteins essential for podocyte structure and function have uncovered multiple Actin cytoskeleton-related proteins. One such study carried out an *in vitro* genetic screen based on podocyte adhesion to various substrates. Among the genes affecting adhesion were several encoding Actin regulatory proteins (Cinà et al., 2019), including: Integrin-linked protein (ILK) which mediates Actin filament rearrangement (Qian et al., 2005); Parvin alpha (PARVA), an Actin-binding protein; and, PDZ and LIM domain 2 (PDLIM2), an adaptor protein of the Actin cytoskeleton that promotes cell attachment. Another study used flies combined with RNAi and conditional CRISPR/Cas9 in nephrocytes to test 29 genes associated with steroid-resistant nephrotic syndrome (SRNS) (Hermle et al., 2017). Of these, 16, when deficient in fly nephrocytes, caused loss-of-function based on a tracer endocytosis assay. These genes encoded fly orthologs of proteins in the SD complex, proteins involved in endocytosis, and proteins that regulate the Actin cytoskeleton, among others, the latter included: orthologs for mammalian α-Actinin-4 (ACTN4), Rho GTPase-activating protein 24 (ARHGAP24), Myosin-9 (MYH9), and Anillin (ANLN). A second study in fly, systematically tested 40 genes previously associated with nephrotic syndrome, including several not studied *in vivo* before (Fu et al., 2017b). Nephrocyte-specific RNAi silencing revealed that 85% of the disease-associated genes were required for nephrocyte uptake function. These included seven that encode proteins known to regulate Actin cytoskeletal dynamics: RhoGDI [mammalian Rho GDP-dissociation inhibitor 1 (ARHGDIA)] and Kank [mammalian KN motif and ankyrin repeat domain-containing proteins 1 (KANK1)] (both previously shown), as well as Zip (mammalian MYH9), Actn (mammalian ACTN4), integrins Mew [mammalian Integrin alpha-3 (ITGA3)] and Mys [mammalian Integrin beta-4 (ITGB4)], homeobox transcription factors CG32105 [mammalian LIM homeobox transcription factor 1-beta (LMX1B); important for maintenance of the Actin cytoskeleton and regulation of the SD]. Nephrocytes deficient for these genes, displayed disrupted SDs and lacunar channel structures as well as functional deficits (Fu et al., 2017b).

These findings likely describe just a fraction of the structural and functional (e.g. protein trafficking) contributions of the cytoskeleton in podocytes/nephrocytes. Much remains to be learned, such as how disruption of the microtubule cytoskeleton affects apical-basal polarity and thus podocyte/nephrocyte maturation and formation of the SD. The nephrocyte cytoskeleton, especially the microtubule network, remains a greatly understudied area. However, the fly shares many of the proteins and interactions that form and regulate the cytoskeleton. The fly could rapidly accommodate extensive initial screens of genetic interactions with components of the cytoskeleton prior to further study in more expensive and time-consuming mammalian model systems.

ENDOCYTOSIS AND EXOCYTOSIS SUSTAIN SLIT DIAPHRAGM DYNAMICS AND MAINTENANCE

The SD is highly dynamic and requires rapid turnover of its core components to ensure responsive uptake of proteins from blood, and to safeguard podocyte homeostasis. Therefore, SD maintenance is heavily dependent upon endocytosis and exocytosis (**Figure 2** and **Table 1**). The class III Phosphoinositide 3-kinase vacuolar proteins sorting 34 (Vps34; a.k.a. fly Pi3K59F; a.k.a. mammalian PIK3C3) has been found to be one such protein indispensable for SD maintenance. A study using both mouse and fly models demonstrated a key role for Vps34 in regulating endocytosis and autophagosome-autolysosome formation in podocytes and

nephrocytes, respectively (Bechtel et al., 2013). In both cells, *Vps34*-deficiency resulted in severe disruption of the early (Rab5-positive) endosomal compartment. The *Vps34*-deficient fly nephrocytes revealed a disruption between Rab5 and Rab7-positive endosomal compartments, these mis-localized proteins are likely indicative of disrupted vesicular transport which ultimately leads to diminished fluid-phase uptake. The mouse podocyte data indicated endosomal deficits, rather than aberrant autophagosome formation and autophagic flux, as the primary cause of the extensive vacuolization and foot process effacement. Mice with podocytes deficient for VPS34 suffered from proteinuria, glomerular scarring, and early lethality (Bechtel et al., 2013). Of note, a class II Phosphoinositide, 3-kinase C2 α (PI3KC2α), was found to be essential for podocyte morphology and function in mice, as deficiency led to chronic renal failure, marked by podocyte loss (atrophy), widespread foot process effacement, and modest proteinuria (Harris et al., 2011). While these findings implicate PI3KC2α in podocyte maintenance, it remains to be seen how the associated morphological disruption might affect SD structural integrity. The endocytosis and exocytosis pathways are highly conserved. Indeed, a systematic study of 27 *Drosophila* Rab GTPases, found nearly half were expressed in, and required for, nephrocyte function (Fu et al., 2017c). The study identified Rabs 1, 5, 7, 11, and 35 as essential. Notably these include Rabs that mediate early and late endosomes and the recycling vesicle trafficking pathways. Furthermore, *Rabphilin 3A* (*RPH3A*) which encodes a Rab small GTPase family effector protein has been implicated in SD functional integrity (Selma-Soriano et al., 2020). RPH3A forms a complex with Rab3A, which is known for its role in vesicle docking/fusion reactions during endocytosis and exocytosis at the neuronal synapse. Expression of the RPH3a-Rab3a complex was shown around vesicles located in the foot processes of mouse, rat, and human podocytes in tissue samples (Rastaldi et al., 2003). However, the effect of a RPH3a-mediated pathomechanism might have on podocytes remained unknown. A recent study in fly showed that Rph (mammalian RPH3A) colocalized with endocytic pathways proteins, Rab3 and Hepatocyte growth factor-regulate tyrosine kinase substrate (Hrs). Hrs plays a role in endocytic sorting of ubiquitinated membrane proteins (Selma-Soriano et al., 2020). Nephrocytes deficient for Rph, displayed a reduced number of endosomes with reduced uptake of toxins, and reduced expression of SD core components like Cubn and Sns. Indeed, lacunar channels and SD structures in these nephrocytes were disrupted, which led to an overall loss of nephrocytes in the flies (Selma-Soriano et al., 2020). Finally, studies have shown the importance of both endocytosis and vesicle recycling to maintain the structural integrity of the SD (Wen et al., 2020; Wang et al., 2021). The exocyst complex is an octameric protein complex important for exocytosis and recycling that tethers the vesicles to the plasma membrane thus mediating fusion. Mice deficient for *Exoc5*, one of the exocyst complex proteins, displayed severe proteinuria and glomerular defects (Nihalani et al., 2019). The components that make up the exocyst complex are highly conserved. In fact, silencing each of the genes encoding the exocyst components in fly nephrocytes demonstrated the importance of the exocyst complex for lacunar channel membrane invagination and SD structural integrity. Flies deficient for exocyst components showed mis-localization of key SD proteins and dysfunctional nephrocytes with significantly reduced protein uptake. The study further showed that SD proteins partially co-localized with exocyst components Sec15, Rab5, and Rab11 (Wen et al., 2020). Together, the data suggest that slit diaphragm proteins are endocytosed through Clathrin-mediated endocytosis, then enter Rab5-labelled early endosomes, and are sorted into Rab11-dependent recycling endosomes. Rab11 then interacts with the Sec15 subunit of the exocyst complex, which tethers the recycling endosome to the cell membrane and promotes the fusion of their respective membranes. This facilitates recycling of the slit diaphragm proteins back to the plasma membrane (Wen et al., 2020). The key proteins of this endocytosis and recycling route are known to regulate cellular trafficking. It remains unclear whether they have any direct interactions with slit diaphragm proteins or carry out podocyte-specific functions.

CHALLENGES IN SLIT DIAPHRAGM RESEARCH AND ADVANTAGES OF USING *DROSOPHILA*

To date few, if any, studies have distinguished between the proteins important for SD assembly versus those in maintenance or function. Most glomerular model studies have focused on foot process effacement, a later stage outcome, rather than SD assembly. The aPKC double mutant (aPKCλ/ι and aPKCζ) study in mice (Hartleben et al., 2013) was able to investigate stages prior to effacement by focusing on the late capillary loop stage, i.e. the stage of immature glomeruli where cell division is arrested and typical podocyte differentiation markers like Nephrin and Podocin are expressed. The study made a strong case for a role for aPKCs and the apicobasal polarity PAR complex in SD formation, however, the study did not investigate whether aPKC proteins play a role in SD maintenance. A separate study found that mouse podocytes deficient for aPKCλ show SD disassembly, disrupted apico-basal cell polarity, and focal segmental glomerulosclerosis (FSGS; scarring, i.e. sclerosis, of the kidney), indicating a role in SD maintenance (Hirose et al., 2009). The study further found evidence for a direct interaction between the aPKC-PAR3 complex and the core SD Nephrin-Podocin complex. Through this interaction, aPKC-PAR3 regulates Nephrin and Podocin distribution and Nephrin accumulation at the plasma membrane (Hirose et al., 2009). These studies highlight the importance of the temporal component. The timecourse of events is especially relevant in differentiating between SD formation and maintenance. The same group studied VPS34 and its role in podocyte homeostasis and related SD maintenance (Bechtel et al., 2013). Their previous work had shown that constitutive knockout of *Vps34* led to embryonic death (day 7.5–8) in mice (Zhou et al., 2010), therefore, this time they used a conditional mouse model with podocyte-specific knockdown of *Vps34*. The conditional model revealed a crucial

role for VPS34-mediated endocytosis in podocyte function and SD structural integrity. This latter study exemplifies the importance of the spatial, i.e. tissue specific, component of studies into podocyte development and SD formation. These temporal and spatial aspects are technically difficult, time-consuming, and costly to study in mammalian models. Fortunately, the fly offers a well-founded alternative.

Drosophila offers a plethora of inducible systems for genetic manipulation, while its fast lifecycle offers the opportunity for detailed timecourse studies with reasonable effort and cost. In fact, the timing of the developmental stages in fly are so well defined that many stage-specific drivers for gene expression are readily available (*Gal4*-UAS system) (Brand and Perrimon, 1993). Alternatively, one could use temperature sensitive RNAi, regulated by simply housing the flies at different temperatures. Moreover, cell subtype-specific genetic manipulation can be achieved by crossing any of the numerous split-Gal4 fly lines in which Gal4 activity is dependent upon two enhancers, instead of one (Luan et al., 2006). These tools enable exploration of all the nuances of the spatial and temporal effects of protein deficiency, and to distinguish the processes of development (assembly/formation) versus those of maturation and maintenance. Their potential was demonstrated in our recent study into the role of exocyst genes in nephrocyte filtration function which used temperature sensitive RNAi (Wen et al., 2020). The flies were crossed and initially kept at 25°C (inactive RNAi), then embryos were collected and maintained at 29°C at which temperature the UAS-RNAi-targeting transgene, with a nephrocyte-specific driver (*Dot*-Gal4), was active for functional assays. This tightly controlled system enabled distinction between SD formation and SD maintenance, and thereby demonstrated the importance of the exocyst complex in maintaining the filtration (SD) and absorption (lacunar channels) functions in fly nephrocytes. In another study, we used temperature sensitive Gal80 combined with the ubiquitous *Tubulin* promoter to initiate knock down of *Clathrin* (*Clc*) after SD assembly, to specifically study the role of Clc in SD maintenance (Wang et al., 2021). Furthermore, by combining the fly *in vivo* platform with biochemistry applications, such as TurboID and APEX, one could identify the components that play key roles during SD assembly. TurboID is an engineered biotin ligase that uses ATP to convert biotin into biotin-AMP, which covalently labels proximal proteins (Uçkun et al., 2021; Zhang et al., 2021), while APEX is an engineered peroxidase that can convert exogenous biotin for unselective covalent labelling of proximal proteins (Lobingier et al., 2017). Either biotinylated complex can then be enriched using Streptavidin beads for subsequent analysis by mass spectrometry to achieve live-cell proteomics. These technologies enable precise spatial (cell type-specific) and temporal (developmental stage-specific) resolution.

A GLOMERULAR DISEASES PERSPECTIVE

A key characteristic shared across glomerular diseases is foot process effacement. It signifies the podocyte response to injury and is marked by loss of the interdigitating pattern of foot processes typically observed between adjacent podocytes. This process disrupts SD structural integrity, which leads to reduced SD presence and thus podocyte functional deficits. The disrupted filtration capacity in return results in proteinuria. If untreated, this process progresses to podocyte detachment and culminates in end-stage renal failure. Given the essential nature of the SD to podocyte function, it is not surprising that many of the genes described above for their roles in SD formation and maintenance have been implicated in glomerular diseases.

Slit Diaphragm Core Components in Disease

Renal disease-associated genetic variants have been found in key components of the SD such as Nephrin (NPHS1) and Podocin (NPHS2), as well as CD2AP. *NPHS1* genetic variants are causative of congenital nephrotic syndrome of the Finnish type (Kestilä et al., 1998), in which podocytes from human embryos carrying an NPHS1 mutation displayed reduced Nephrin expression (20%) and altered (cilia-specific) α-Tubulin distribution, indicative of incomplete podocyte maturation (Vukojevic et al., 2018). *NPHS2* genetic variants have been shown to cause autosomal recessive SRNS, marked by childhood onset of proteinuria with rapid progression (Boute et al., 2000). Mutations in *CD2AP* have been found in patients with SRNS and FSGS (Gigante et al., 2009). Fly nephrocytes with *cindr* (ortholog of *CD2AP*) deficiency showed severely disrupted lacunar channels and loss of SD structural integrity. Notably, these phenotypes could be rescued by expressing human reference *CD2AP*, but not by a patient allele carrying a *CD2AP* mutation (Fu et al., 2017b), thus providing a beautiful example of patient-specific, i.e. precision disease, modeling using fly nephrocytes.

Apical-Basal Polarity Proteins in Disease

Regarding the polarity proteins, variants in both apical and the balancing basolateral components have been implicated in glomerular diseases. On the apical side, variants in *CRB2*, a key Crumbs complex member, have been linked to SRNS (Ebarasi et al., 2015) and congenital nephrosis, Finnish type (Slavotinek et al., 2015). In addition, the Crumbs and PAR apical polarity complexes have been, directly or indirectly, linked to renal cyst disease. For example, *PALS1-interacting proteins Nephrocystin-1 (NPHP1)* and *NPHP4* have been associated with nephronophthisis (NPHP), an autosomal recessive ciliopathic childhood cystic kidney disease (Wolf and Hildebrandt, 2011). On the basolateral side, variants in *DLG5* have been linked to sporadic FSGS (Yu et al., 2016). Initial functional studies using mouse podocytes deficient for *Dlg5* (shRNA) did not show any phenotype (Yu et al., 2016), possibly due to genetic redundancy. However, recent studies in fly, which has a much more compact genome, have revealed nephrocytes deficient for *Dlg* display collapse of SD structural integrity and disrupted endocytosis (Heiden et al., 2021; Mysh and Poulton, 2021).

Cytoskeletal Proteins in Disease

Several podocyte cytoskeletal proteins have been linked to proteinuria and glomerular disease [for a comprehensive review *see* (Blaine and Dylewski, 2020)]. Variants in *anillin* (*ANLN*), a cell cycle protein that binds F-actin, were shown to cause familial FSGS. Functional studies found that the mutated protein has reduced CD2AP binding affinity. CD2AP is the major binding partner of Endophilin and an SD-associated scaffold protein. *Anln* deficiency in mice resulted in disrupted filtration barrier integrity, foot process effacement, and severe edema (Gbadegesin et al., 2014). Mutations in *ACTN4*, which encodes an Actin-filament crosslinking protein, caused idiopathic FSGS with autosomal dominant inheritance in three families suffering from increased urinary protein excretion and decreased kidney function, with ultimate progression to end-stage renal failure (Kaplan et al., 2000). An Actin-regulating protein encoded by *inverted formin 2* (*INF2*) has been associated with FSGS. Linkage analysis and subsequent sequencing identified nine independent missense mutations in highly conserved amino acid residues across multiple unrelated families (Brown et al., 2010). Since then, at least 45 pathogenic mutations in *IFN2* have been identified in isolated FSGS (Labat-de-Hoz and Alonso, 2020). Four patient variants in *INF2* have been studied in *Drosophila* nephrocytes for *in vivo* validation. Nephrocytes expressing these variants showed a disrupted Actin cytoskeleton, in which the level of Actin accumulation in the cytosol correlated with the presumed impact of the mutation on INF2 activation. Furthermore, they showed that these *INF2* mutations were similarly correlated to reduced Sns at the cell surface, indicative of disrupted SD structures (Bayraktar et al., 2020). Further, variants in *MYH9*, which encodes an Actin-binding cytoskeleton regulatory protein, have been associated with FSGS in the African American population. Of interest, the MYH9 risk alleles were found more frequently among African Americans, whereas the protective alleles were more frequent among European Americans (Kopp et al., 2008). Another study associated variants in *MYH9* with Alport-like-syndrome (a.k.a. Fechtner syndrome; FTNS), a rare disorder with a renal component. The genetic variants were not fully penetrant for the renal phenotype, but a subset of the patients carrying *MYH9* variants suffered from nephritis, including display of foot process effacement, loss of SDs, proteinuria, and renal failure (Ghiggeri et al., 2003).

In vitro studies have shown that podocytes are typically in a RhoA-dependent stationary rest state. In response to stress they become migratory and CDC42 and RAC1-dependent (Mundel and Reiser, 2010). This switch might drive foot process effacement. Indeed, several Rho GTPase signaling regulators have been implicated in glomerular diseases. For example, Rho GTPase ARHGAP24 was identified as an Actin regulatory protein in podocytes, and *ARHGAP24* mutations have been found in FSGS patients and associated with reduced RAC1-GAP activity (Akilesh et al., 2011). Another example is ARHGDIA, which forms a complex with Rho GTPase. Mutations in *ARHGDIA* were found in patients with SRNS. The ARHGDIA mutations resulted in impeded interaction with RAC1 and CDC42 and increased migration of human immortalized podocytes (*in vitro*) (Gee et al., 2013). Further study found that cultured mouse immortalized podocytes carrying *Arhgdia* mutations showed RAC1 hyperactivity, as well as impaired Actin polymerization, decreased cell size, increased cellular projections, and reduced motility. This study further showed that ARHGDIA mRNA expression increased as the podocytes matured with RAC1 activity limited to immature podocytes, suggesting ARHGDIA typically suppresses RAC1 activity (Auguste et al., 2016). Note the different effect of mutant *ARHGDIA* on podocyte motility reported in each study. These conflicting results might be due to methodological differences between the two studies. Both studies used immortalized podocytes lines in which human *ARHGDIA* carrying patient mutations was overexpressed. However, they differ in that the mouse podocyte study knocked down endogenous *Arhgdia* expression (shRNA) (Auguste et al., 2016), whereas the human podocyte study did not (Gee et al., 2013). The mouse study reported trending reduced motility for three *ARHGDIA* variants based on a wound healing assay, including the two variants from the human podocyte study. However, they only provided real-time migration data for the third variant. The human podocyte study applied the real-time migration assay to both variants. Whether these methodological differences account for the opposing motility findings, or if an unknown biological process is the cause warrants further investigation. The last example is the *KANK* family genes. Recessive mutations in *KANK1*, *KANK2*, and *KANK4* have been identified in patients with SRNS. Knockdown of *kank2* in zebrafish caused a nephrotic syndrome phenotype, marked by proteinuria and podocyte foot process effacement. *Drosophila* has one homolog (*dKank*), and knockdown of *dKank* (RNAi) in flies resulted in disrupted lacunar channel and SD filtration structures. Additional assays in rat glomeruli and cultured human podocytes showed KANK2 interacts with ARHGDIA, with knockdown of *KANK2* (*in vitro*) leading to increased active (GTP-bound) RhoA and decreased podocyte motility (Gee et al., 2015).

Endocytosis and Exocytosis Pathway Proteins in Disease

A variant in *RPH3A* has been associated with increased risk for microalbuminuria. Both in subjects with a microalbuminuric and in those with a normoalbuminuric metabolomic profile the variant was associated with urinary albumin excretion. Increased levels of albumin in urine have been associated with cardiovascular and renal disease (Marrachelli et al., 2014). Moreover, expression of the RPH3A-RAB3 complex was decreased in podocytes of a mouse model for FSGS (growth-hormone transgenic mice), and RPH3A protein expression was increased in biopsied tissue from patients with glomerular diseases, where the expression inversely correlated to the amount of urinary proteins (Rastaldi et al., 2003). Mutations in genes encoding the RAB5 (early endocytosis)-interacting proteins—GTPase-activating protein and VPS9 domain-containing protein 1 (GAPVD1) and Rabankyrin-5 (ANKFY1)—were found to cause SRNS in patients (Hermle et al., 2018). These variants were shown to reduce protein affinity for active RAB5 and an inability to rescue the migratory defect in podocytes deficient for either *GAPVD1* or *ANKFY1*. Of note, in rat glomeruli, GAPVD1 was shown to directly interact with Nephrin, a core component of the

SD (Hermle et al., 2018). Mutations in the gene encoding TBC1 domain family member 8B (TBC1D8B), a regulator of RAB11 (recycling endosomes), have been identified in multiple families with SNRS (Kampf et al., 2019). Mutant TBC1D8B showed reduced affinity for RAB11 and Nephrin, and *Drosophila* nephrocytes deficient for *Tbc1d8b* showed mis-localized Sns (mammalian Nephrin) and impaired protein uptake function (Kampf et al., 2019). Additional variants in endocytosis proteins important for SD maintenance and function have been associated with nephrotic syndrome in patients, including variants in Myosin-1E (Myo1E; binds Dynamin and Synaptojanin) (Mele et al., 2011; Sanna-Cherchi et al., 2011), and CD2AP (a major binding partner of Endophilin) (Kim et al., 2003). Finally, exome sequencing revealed a mutation in *EXOC8* to segregate with disease in a family with Joubert syndrome (Dixon-Salazar et al., 2012). EXOC8 is a component of the exocyst complex, that mediates vesicle tethering for fusion in endocytosis and recycling.

HOW THE FRUIT FLY CAN CONTRIBUTE TO THE STUDY OF HUMAN GLOMERULAR DISEASES

Identification and Validation of Candidate Genes for Glomerular Diseases Using the Fly System

One of the first studies using flies to model glomerular diseases, applied an unbiased genetic screen of over 1,000 RNAi transgenic lines spanning the fly genome (Zhang et al., 2013). Transgenic flies carried an ANF secretion peptide with RFP reporter driven by the myosin heavy chain enhancer (*MHC-ANF*-RFP), combined with RNAi (UAS-RNAi) driven by the *Hand* pericardial cell marker (*Hand*-GFP, Dot-Gal4). The secreted ANF-RFP accumulates in the nephrocytes and serves as a measure of nephrocyte function. The embryos from these RNAi crosses were rapidly assessed for RFP accumulation in the pericardial nephrocytes, with follow-up RFP up-take measurements in newly hatched adults. The screen identified over 70 genes required for nephrocyte function, all of which have highly conserved human homologs (Zhang et al., 2013). Remarkably, the RNAi lines available from *Drosophila* resource stock centres, like the Vienna Drosophila Resource Center (VDRC; Austria) and the Bloomington Drosophila Stock Center (BDSC; Indiana University, United States), collectively cover over 90% of the fly protein-coding genes. These resources will be invaluable in unbiased approaches to identify the genetic interactors of glomerular disease genes, and to gain insight in the underlying pathological molecular pathways.

The previous examples described studies that have linked genetic variants with various glomerular diseases using patient samples. Several of those studies included subsequent functional validation using *in vitro* (human) cell culture or *in vivo* animal models, such as mouse, rat, zebrafish, and flies. However, many more genes await genetic validation and subsequent mechanistic study. *Drosophila* could provide a fast and cost-effective means to achieve this, due to the highly conserved genes, pathways, and functionality between nephrocytes and podocytes. The fly can be used to rapidly survey large numbers of genes as demonstrated in an *in vivo* genetic screen of 40 genes associated with nephrotic syndrome, which validated the involvement in nephrocyte function for 34 of the genes (85%) (Fu et al., 2017b); and, in an *in vivo* RNAi screen of 29 genes with variants associated with SRNS that validated 16 genes (55%) to exert significant roles in nephrocyte function and SD structural integrity (Hermle et al., 2017). Other studies using flies have uncovered potential therapeutic targets, such as one into recessive mutations in *KANK* family members in patients with nephrotic syndrome (Gee et al., 2015). The variants were found to act through dysregulated Rho GTPase signalling, suggesting (ant)agonists of Rho GTPase activity might provide therapeutic benefit in patients with *KANK* mutations. Of note, KANK2 was shown to interact with ARHGDIA (Gee et al., 2015), a known regulator of Rho GTPases in podocytes that had been previously shown to cause SRNS (Gee et al., 2013). Once candidates have been validated in fly and their initial function has been established, they can be moved forward to the more expensive and time-consuming studies in mammalian model systems. Furthermore, for various existing fly models for glomerular disease the effect of their genetic variants on nephrocyte uptake function and the structural integrity of the SD has not yet been studied. Such as the fly model to study the APOL1 risk alleles associated with glomerular diseases in persons of recent African ancestry. These flies show biphasic age-related changes in nephrocyte uptake function (Fu et al., 2017a). Of note, the effect of APOL1 risk alleles on nephrocyte function has not yet been correlated to structural changes in the SD. These studies could reveal additional mechanism regulating SD assembly and maintenance, and provide insight into the interaction of known pathways.

Fly to Delineate the Genetic Intricacies Underlying Glomerular Diseases

Glomerular diseases caused by defective SDs typically share proteinuria and renal failure in their clinical profile. However, the shared structural cause, a defective SD, is the culmination of varying underlying disease mechanisms. Glomerular disease modelling is further complicated by variants in a single gene leading to different outcomes. For example, variants in *INF2* have been associated with both FSGS and Charcot-Marie-Tooth disease, a neurological disorder with nephrotic pathology (typically FSGS). One study screened over 50 autosomal dominant *INF2* mutants from patients in HeLa *INF2* KO cells, and further assessed a few variants in *Drosophila* nephrocytes and one in patient urine-derived epithelial cells (Bayraktar et al., 2020). The fly data demonstrated intracellular accumulation of Actin in nephrocytes carrying an *INF2* patient variant. Furthermore, the Actin accumulation quantitatively correlated with disrupted localization of Nephrin to the plasma membrane. Together the findings enabled a clear distinction between those variants causing primary FSGS and those that cause FSGS with the neurological disorder, as well as the definition of subsets of

INF2 variants based on their level of activation and intracellular Actin accumulation (Bayraktar et al., 2020). Furthermore, in other cases the genetic cause of glomerular disease lies in multiple genes (polygenic). For example, using comprehensive modelling in flies, variants in *Adducin-γ* [*ADD3*; *hu li tai shao* (*hts*) in fly] and *Lysine Acetyltransferase 2B* (*KAT2B*; *Gcn5* in fly) were shown to act synergistically in kidney and heart dysfunction comorbid with *ADD3*-associated phenotypes (Gonçalves et al., 2018). Or in the case of *MYH9* where the same genetic variant resulted in diverse phenotypic outcomes (all carriers displayed platelet and leukocyte abnormalities, but only a subset suffered from proteinuria and renal failure among other symptoms), suggesting that additional genetic and/or environmental factors contribute to disease outcomes (Ghiggeri et al., 2003). Technical limitations and time constrictions make modeling in mice unfeasible for these applications. The fly on the other hand allows for fast screening of multiple variants for various phenotypic outcomes, and new lines can be rapidly generated to carry patient (-specific) variants in multiple genes.

Drosophila Enables Rapid, Scale-Able, *in vivo* Drug Screens

Several studies have used *Drosophila* nephrocytes to complement a mammalian model system. One such study used a combination of *in vitro* podocyte and *ex vivo* nephrocyte models to investigate the phosphorylation of SD proteins Nephrin and NEPH1 in maintenance of the Actin cytoskeleton (Solanki et al., 2021). Fly nephrocytes were treated with hepatocyte growth factor (HGF) following chemically induced injury with protamine sulfate, which resulted in severe Actin cytoskeletal disorganization. They demonstrated HGF-induced phosphorylation of Sns (mammalian Nephrin) and Duf (mammalian NEPH1) mediated nephrocyte recovery. The same response was observed when treating immortalized human podocytes *in vitro*, thus exemplifying the molecular conservation between nephrocytes and podocytes and the potential to use nephrocytes in drug screens. Another study identified variants in *aarF domain containing kinase 4* (*ADCK4*) in multiple patients with familial SRNS (Ashraf et al., 2013). They used flies and zebrafish for functional validation and demonstrated phenotypic attenuation by dietary supplementation with CoQ10. *ADCK4* encodes a kinase that acts in the biosynthesis of coenzyme Q (ubiquinone); while not a direct SD component, a later study in *Drosophila* showed CoQ10 pathway gene deficiency leads to abnormal localization of SDs, collapse of lacunar channels, and dysmorphic mitochondria, as well as increased autophagy and mitophagy, ROS, and sensitivity to oxidative stress (Zhu et al., 2017c). Similarly, these effects in fly nephrocytes could be attenuated by dietary supplementation with CoQ10. Moreover, the latter study showed that expressing the human *COQ2* reference gene was able to attenuate the protein uptake defect in *Coq2*-deficient nephrocytes, whereas expressing a patient allele carrying a *COQ2* variant could not (Zhu et al., 2017c). This study is notable for demonstrating the possibility of using *Drosophila* to generate precision disease models, designed to study patient-specific mutations and underlying mechanisms, and to identify therapeutic targets and screen compounds for their effectivity in reversing the phenotypes. These genetic and pharmacological *in vivo* screens in *Drosophila* can be readily scaled up to comprise well over 100 genes as we have shown in studies into candidate genes for congenital heart disease (CHD) to demonstrate their importance in nephrocyte function (Zhu et al., 2017b; 2017a). This study also provided functional validation for the CHD patient-derived $WDR5^{K7Q}$ allele. Replacing endogenous *wds* expression with the patient allele could not restore the cardiac phenotype induced by *wds* deficiency, whereas the human reference allele could (Zhu et al., 2017a). In a recent a study, we used transgenic flies carrying the human $KRAS^{G12V}$ leukemia-variant in both genetic and chemical inhibitor screens, which independently revealed the importance of hypoxia signalling in mediating RAS-induced cancer phenotypes (Zhu et al., 2022). Together these studies show how fly can help in studying human glomerular diseases, for both functional validation and precision disease modelling, as well as for therapeutic drug screens.

CONCLUDING REMARKS

The genetic, molecular, structural, as well as the genetic deficiency-induced phenotypic similarities, make the *Drosophila* nephrocyte a well-suited model to study the SD in development and disease. Especially the many genetic tools that enable defined temporal and spatial control put the fly in a strong position to study the intricacies of SD formation vs. maintenance. Moreover, the fly system is ideally equipped for rapid, extensive genetic and pharmacological *in vivo* screens, and can be used to study the interplay of multiple components at the SD. Finally, the fly provides a powerful system to take glomerular disease studies into the future of precision disease modeling to identify and tailor therapeutics to the individual patient.

AUTHOR CONTRIBUTIONS

JvdL, PW, and ZH drafted and revised this manuscript. All authors read and approved the final version for publication.

FUNDING

This work was supported by National Institutes of Health grants R01 DK098410 (ZH) and R01 DK120908 (ZH).

ACKNOWLEDGMENTS

The authors would like to acknowledge the invaluable contributions of the FlyBase (Larkin et al., 2021) and UniProt Knowledgebase (uniProtKB) (UniProt Consortium, 2021) resources to their ongoing research and this manuscript.

REFERENCES

Agarwal, S., Sudhini, Y. R., Reiser, J., and Altintas, M. M. (2020). From Infancy to Fancy-A Glimpse into the Evolutionary Journey of Podocytes in Culture. *Kidney 360* 2, 385–397. doi:10.34067/kid.0006492020

Akilesh, S., Suleiman, H., Yu, H., Stander, M. C., Lavin, P., Gbadegesin, R., et al. (2011). Arhgap24 Inactivates Rac1 in Mouse Podocytes, and a Mutant Form Is Associated with Familial Focal Segmental Glomerulosclerosis. *J. Clin. Invest.* 121, 4127–4137. doi:10.1172/jci46458

Ashraf, S., Gee, H. Y., Woerner, S., Xie, L. X., Vega-Warner, V., Lovric, S., et al. (2013). ADCK4 Mutations Promote Steroid-Resistant Nephrotic Syndrome through CoQ10 Biosynthesis Disruption. *J. Clin. Invest.* 123, 5179–5189. doi:10.1172/jci69000

Auguste, D., Maier, M., Baldwin, C., Aoudjit, L., Robins, R., Gupta, I. R., et al. (2016). Disease-causing Mutations of RhoGDIα Induce Rac1 Hyperactivation in Podocytes. *Small GTPases* 7, 107–121. doi:10.1080/21541248.2015.1113353

Bachmann, A., Schneider, M., Theilenberg, E., Grawe, F., and Knust, E. (2001). Drosophila Stardust Is a Partner of Crumbs in the Control of Epithelial Cell Polarity. *Nature* 414, 638–643. doi:10.1038/414638a

Balbiani, C. R. (1886). Études bactériologiques sur les arthropodes. *Comptes rendus hebdomadaires des séances de l'Académie des Sci.* 103, 952–954.

Bayraktar, S., Nehrig, J., Menis, E., Karli, K., Janning, A., Struk, T., et al. (2020). A Deregulated Stress Response Underlies Distinct INF2-Associated Disease Profiles. *Jasn* 31, 1296–1313. doi:10.1681/asn.2019111174

Bechtel, W., Helmstädter, M., Balica, J., Hartleben, B., Kiefer, B., Hrnjic, F., et al. (2013). Vps34 Deficiency Reveals the Importance of Endocytosis for Podocyte Homeostasis. *Jasn* 24, 727–743. doi:10.1681/asn.2012070700

Bilder, D., and Perrimon, N. (2000). Localization of Apical Epithelial Determinants by the Basolateral PDZ Protein Scribble. *Nature* 403, 676–680. doi:10.1038/35001108

Blaine, J., and Dylewski, J. (2020). Regulation of the Actin Cytoskeleton in Podocytes. *Cells* 9, 1700. doi:10.3390/cells9071700

Boute, N., Gribouval, O., Roselli, S., Benessy, F., Lee, H., Fuchshuber, A., et al. (2000). NPHS2, Encoding the Glomerular Protein Podocin, Is Mutated in Autosomal Recessive Steroid-Resistant Nephrotic Syndrome. *Nat. Genet.* 24, 349–354. doi:10.1038/74166

Brand, A. H., and Perrimon, N. (1993). Targeted Gene Expression as a Means of Altering Cell Fates and Generating Dominant Phenotypes. *Development* 118, 401–415. doi:10.1242/dev.118.2.401

Brown, E. J., Schlöndorff, J. S., Becker, D. J., Tsukaguchi, H., Tonna, S. J., Uscinski, A. L., et al. (2010). Mutations in the Formin Gene INF2 Cause Focal Segmental Glomerulosclerosis. *Nat. Genet.* 42, 72–76. doi:10.1038/ng.505

Carrasco-Rando, M., Prieto-Sánchez, S., Culi, J., Tutor, A. S., and Ruiz-Gómez, M. (2019). A Specific Isoform of Pyd/ZO-1 Mediates Junctional Remodeling and Formation of Slit Diaphragms. *J. Cel Biol.* 218, 2294–2308. doi:10.1083/jcb.201810171

Cinà, D. P., Ketela, T., Brown, K. R., Chandrashekhar, M., Mero, P., Li, C., et al. (2019). Forward Genetic Screen in Human Podocytes Identifies Diphthamide Biosynthesis Genes as Regulators of Adhesion. *Am. J. Physiol. Ren. Physiol.* 317, F1593–F1604. doi:10.1152/ajprenal.00195.2019

Consortium, Uni. Prot. (2021). UniProt: the Universal Protein Knowledgebase in 2021. *Nucleic Acids Res.* 49, D480–D489. doi:10.1093/nar/gkaa1100

Crossley, A. C. (1972). The Ultrastructure and Function of Pericardial Cells and Other Nephrocytes in an Insect: *Calliphora erythrocephala*. *Tissue and Cell* 4, 529–560. doi:10.1016/s0040-8166(72)80029-6

Denholm, B., and Skaer, H. (2009). Bringing Together Components of the Fly Renal System. *Curr. Opin. Genet. Develop.* 19, 526–532. doi:10.1016/j.gde.2009.08.006

Dixon-Salazar, T. J., Silhavy, J. L., Udpa, N., Schroth, J., Bielas, S., Schaffer, A. E., et al. (2012). Exome Sequencing Can Improve Diagnosis and Alter Patient Management. *Sci. Transl. Med.* 4, 138ra78. doi:10.1126/scitranslmed.3003544

Drenckhahn, D., and Franke, R. P. (1988). Ultrastructural Organization of Contractile and Cytoskeletal Proteins in Glomerular Podocytes of Chicken, Rat, and Man. *Lab. Invest.* 59, 673–682.

Ebarasi, L., Ashraf, S., Bierzynska, A., Gee, H. Y., McCarthy, H. J., Lovric, S., et al. (2015). Defects of CRB2 Cause Steroid-Resistant Nephrotic Syndrome. *Am. J. Hum. Genet.* 96, 153–161. doi:10.1016/j.ajhg.2014.11.014

Endlich, K., Kliewe, F., and Endlich, N. (2017). Stressed Podocytes-Mechanical Forces, Sensors, Signaling and Response. *Pflugers Arch. - Eur. J. Physiol.* 469, 937–949. doi:10.1007/s00424-017-2025-8

Fu, Y., Zhu, J.-Y., Richman, A., Zhang, Y., Xie, X., Das, J. R., et al. (2017a). APOL1-G1 in Nephrocytes Induces Hypertrophy and Accelerates Cell Death. *Jasn* 28, 1106–1116. doi:10.1681/asn.2016050550

Fu, Y., Zhu, J.-Y., Richman, A., Zhao, Z., Zhang, F., Ray, P. E., et al. (2017b). A Drosophila Model System to Assess the Function of Human Monogenic Podocyte Mutations that Cause Nephrotic Syndrome. *Hum. Mol. Genet.* 26, 768–780. doi:10.1093/hmg/ddw428

Fu, Y., Zhu, J.-Y., Zhang, F., Richman, A., Zhao, Z., and Han, Z. (2017c). Comprehensive Functional Analysis of Rab GTPases in Drosophila Nephrocytes. *Cell Tissue Res* 368, 615–627. doi:10.1007/s00441-017-2575-2

Garg, P. (2018). A Review of Podocyte Biology. *Am. J. Nephrol.* 47 (Suppl. 1), 3–13. doi:10.1159/000481633

Gbadegesin, R. A., Hall, G., Adeyemo, A., Hanke, N., Tossidou, I., Burchette, J., et al. (2014). Mutations in the Gene that Encodes the F-Actin Binding Protein Anillin Cause FSGS. *Jasn* 25, 1991–2002. doi:10.1681/asn.2013090976

Gee, H. Y., Saisawat, P., Ashraf, S., Hurd, T. W., Vega-Warner, V., Fang, H., et al. (2013). ARHGDIA Mutations Cause Nephrotic Syndrome via Defective RHO GTPase Signaling. *J. Clin. Invest.* 123, 3243–3253. doi:10.1172/jci69134

Gee, H. Y., Zhang, F., Ashraf, S., Kohl, S., Sadowski, C. E., Vega-Warner, V., et al. (2015). KANK Deficiency Leads to Podocyte Dysfunction and Nephrotic Syndrome. *J. Clin. Invest.* 125, 2375–2384. doi:10.1172/jci79504

Ghiggeri, G. M., Caridi, G., Magrini, U., Sessa, A., Savoia, A., Seri, M., et al. (2003). Genetics, Clinical and Pathological Features of Glomerulonephrites Associated with Mutations of Nonmuscle Myosin IIA (Fechtner Syndrome). *Am. J. Kidney Dis.* 41, 95–104. doi:10.1053/ajkd.2003.50028

Gigante, M., Pontrelli, P., Montemurno, E., Roca, L., Aucella, F., Penza, R., et al. (2009). CD2AP Mutations Are Associated with Sporadic Nephrotic Syndrome and Focal Segmental Glomerulosclerosis (FSGS). *Nephrol. Dial. Transplant.* 24, 1858–1864. doi:10.1093/ndt/gfn712

Gonçalves, S., Patat, J., Guida, M. C., Lachaussée, N., Arrondel, C., Helmstädter, M., et al. (2018). A Homozygous KAT2B Variant Modulates the Clinical Phenotype of ADD3 Deficiency in Humans and Flies. *Plos Genet.* 14, e1007386.

Hadorn, E. (1937). An Accelerating Effect of Normal "Ring-Glands" on Puparium-Formation in Lethal Larvae of Drosophila Melanogaster. *Proc. Natl. Acad. Sci.* 23, 478–484. doi:10.1073/pnas.23.9.478

Haraldsson, B., Nyström, J., and Deen, W. M. (2008). Properties of the Glomerular Barrier and Mechanisms of Proteinuria. *Physiol. Rev.* 88, 451–487. doi:10.1152/physrev.00055.2006

Harris, D. P., Vogel, P., Wims, M., Moberg, K., Humphries, J., Jhaver, K. G., et al. (2011). Requirement for Class II Phosphoinositide 3-Kinase C2α in Maintenance of Glomerular Structure and Function. *Mol. Cel. Biol.* 31, 63–80. doi:10.1128/mcb.00468-10

Hartleben, B., Schweizer, H., Lübben, P., Bartram, M. P., Möller, C. C., Herr, R., et al. (2008). Neph-Nephrin Proteins Bind the Par3-Par6-Atypical Protein Kinase C (aPKC) Complex to Regulate Podocyte Cell Polarity. *J. Biol. Chem.* 283, 23033–23038. doi:10.1074/jbc.m803143200

Hartleben, B., Widmeier, E., Suhm, M., Worthmann, K., Schell, C., Helmstädter, M., et al. (2013). aPKCλ/ι and aPKCζ Contribute to Podocyte Differentiation and Glomerular Maturation. *Jasn* 24, 253–267. doi:10.1681/asn.2012060582

Hartleben, B., Widmeier, E., Wanner, N., Schmidts, M., Kim, S. T., Schneider, L., et al. (2012). Role of the Polarity Protein Scribble for Podocyte Differentiation and Maintenance. *PLoS One* 7, e36705. doi:10.1371/journal.pone.0036705

Hatano, R., Takeda, A., Abe, Y., Kawaguchi, K., Kazama, I., Matsubara, M., et al. (2018). Loss of Ezrin Expression Reduced the Susceptibility to the Glomerular Injury in Mice. *Sci. Rep.* 8, 4512. doi:10.1038/s41598-018-22846-0

Heiden, S., Siwek, R., Lotz, M.-L., Borkowsky, S., Schröter, R., Nedvetsky, P., et al. (2021). Apical-basal Polarity Regulators Are Essential for Slit Diaphragm Assembly and Endocytosis in Drosophila Nephrocytes. *Cell. Mol. Life Sci.* 78, 3657–3672. doi:10.1007/s00018-021-03769-y

Hermle, T., Braun, D. A., Helmstädter, M., Huber, T. B., and Hildebrandt, F. (2017). Modeling Monogenic Human Nephrotic Syndrome in the Drosophila Garland Cell Nephrocyte. *Jasn* 28, 1521–1533. doi:10.1681/asn.2016050517

Hermle, T., Schneider, R., Schapiro, D., Braun, D. A., van der Ven, A. T., Warejko, J. K., et al. (2018). GAPVD1 and ANKFY1 Mutations Implicate RAB5

Regulation in Nephrotic Syndrome. *Jasn* 29, 2123–2138. doi:10.1681/asn.2017121312

Hirose, T., Satoh, D., Kurihara, H., Kusaka, C., Hirose, H., Akimoto, K., et al. (2009). An Essential Role of the Universal Polarity Protein, aPKCλ, on the Maintenance of Podocyte Slit Diaphragms. *PLoS One* 4, e4194. doi:10.1371/journal.pone.0004194

Hochapfel, F., Denk, L., Mendl, G., Schulze, U., Maaßen, C., Zaytseva, Y., et al. (2017). Distinct Functions of Crumbs Regulating Slit Diaphragms and Endocytosis in Drosophila Nephrocytes. *Cel. Mol. Life Sci.* 74, 4573–4586. doi:10.1007/s00018-017-2593-y

Hollande, C. (1921). Arch d'Anat Micr, Paris. *Arch. D'anat Micr, Paris* 18, 85.

Homan, K. A., Gupta, N., Kroll, K. T., Kolesky, D. B., Skylar-Scott, M., Miyoshi, T., et al. (2019). Flow-enhanced Vascularization and Maturation of Kidney Organoids In Vitro. *Nat. Methods* 16, 255–262. doi:10.1038/s41592-019-0325-y

Hong, Y., Stronach, B., Perrimon, N., Jan, L. Y., and Jan, Y. N. (2001). Drosophila Stardust Interacts with Crumbs to Control Polarity of Epithelia but Not Neuroblasts. *Nature* 414, 634–638. doi:10.1038/414634a

Hu, Y., Flockhart, I., Vinayagam, A., Bergwitz, C., Berger, B., Perrimon, N., et al. (2011). An Integrative Approach to Ortholog Prediction for Disease-Focused and Other Functional Studies. *BMC Bioinformatics* 12, 357. doi:10.1186/1471-2105-12-357

Ichimura, K., Kakuta, S., Kawasaki, Y., Miyaki, T., Nonami, T., Miyazaki, N., et al. (2017). Morphological Process of Podocyte Development Revealed by Block-Face Scanning Electron Microscopy. *J. Cel Sci.* 130, 132–142. doi:10.1242/jcs.187815

Kaksonen, M., and Roux, A. (2018). Mechanisms of Clathrin-Mediated Endocytosis. *Nat. Rev. Mol. Cel Biol.* 19, 313–326. doi:10.1038/nrm.2017.132

Kampf, L. L., Schneider, R., Gerstner, L., Thünauer, R., Chen, M., Helmstädter, M., et al. (2019). TBC1D8B Mutations Implicate RAB11-dependent Vesicular Trafficking in the Pathogenesis of Nephrotic Syndrome. *Jasn* 30, 2338–2353. doi:10.1681/asn.2019040414

Kaplan, J. M., H Kim, S., North, K. N., Rennke, H., A Correia, L., Tong, H.-Q., et al. (2000). Mutations in ACTN4, Encoding α-actinin-4, Cause Familial Focal Segmental Glomerulosclerosis. *Nat. Genet.* 24, 251–256. doi:10.1038/73456

Kawasaki, Y., Matsumoto, A., Miyaki, T., Kinoshita, M., Kakuta, S., Sakai, T., et al. (2019). Three-dimensional Architecture of Pericardial Nephrocytes in *Drosophila melanogaster* Revealed by FIB/SEM Tomography. *Cel Tissue Res* 378, 289–300. doi:10.1007/s00441-019-03037-3

Kestilä, M., Lenkkeri, U., Männikkö, M., Lamerdin, J., McCready, P., Putaala, H., et al. (1998). Positionally Cloned Gene for a Novel Glomerular Protein--nephrin--is mutated in congenital nephrotic syndrome. *Mol. Cel* 1, 575–582.

Kim, J. M., Wu, H., Green, G., Winkler, C. A., Kopp, J. B., Miner, J. H., et al. (2003). CD2-associated protein haploinsufficiency is linked to glomerular disease susceptibility. *Science* 300, 1298–1300. doi:10.1126/science.1081068

Kopp, J. B., Smith, M. W., Nelson, G. W., Johnson, R. C., Freedman, B. I., Bowden, D. W., et al. (2008). MYH9 is a major-effect risk gene for focal segmental glomerulosclerosis. *Nat. Genet.* 40, 1175–1184. doi:10.1038/ng.226

La, T. M., Tachibana, H., Li, S. A., Abe, T., Seiriki, S., Nagaoka, H., et al. (2020). Dynamin 1 is important for microtubule organization and stabilization in glomerular podocytes. *FASEB j.* 34, 16449–16463. doi:10.1096/fj.202001240rr

Labat-de-Hoz, L., and Alonso, M. A. (2020). The formin INF2 in disease: progress from 10 years of research. *Cel. Mol. Life Sci.* 77, 4581–4600. doi:10.1007/s00018-020-03550-7

Larkin, A., Marygold, S. J., Antonazzo, G., Attrill, H., dos Santos, G., Garapati, P. V., et al. (2021). FlyBase: updates to the *Drosophila melanogaster* knowledge base. *Nucleic Acids Res.* 49, D899–D907. doi:10.1093/nar/gkaa1026

Leydig, F. (1866). "Traité D'histologie de L'homme et des Animaux," in *Traité D'histologie*. Paris: Bailliére.

Lin, Y. H., Currinn, H., Pocha, S. M., Rothnie, A., Wassmer, T., and Knust, E. (2015). AP-2-complex-mediated endocytosis of Drosophila Crumbs regulates polarity by antagonizing Stardust. *J. Cel Sci.* 128, 4538–4549. doi:10.1242/jcs.174573

Lobingier, B. T., Hüttenhain, R., Eichel, K., Miller, K. B., Ting, A. Y., von Zastrow, M., et al. (2017). An approach to spatiotemporally resolve protein interaction networks in living cells. *Cell* 169, 350–360. doi:10.1016/j.cell.2017.03.022

Luan, H., Peabody, N. C., Vinson, C. R., and White, B. H. (2006). Refined spatial manipulation of neuronal function by combinatorial restriction of transgene expression. *Neuron* 52, 425–436. doi:10.1016/j.neuron.2006.08.028

Marrachelli, V. G., Monleon, D., Rentero, P., Mansego, M. L., Morales, J. M., Galan, I., et al. (2014). Genomic and metabolomic profile associated to microalbuminuria. *PLoS One* 9, e98227. doi:10.1371/journal.pone.0098227

Mele, C., Iatropoulos, P., Donadelli, R., Calabria, A., Maranta, R., Cassis, P., et al. (2011). MYO1EMutations and Childhood Familial Focal Segmental Glomerulosclerosis. *N. Engl. J. Med.* 365, 295–306. doi:10.1056/nejmoa1101273

Michgehl, U., Pavenstädt, H., and Vollenbröker, B. (2017). Cross talk between the Crumbs complex and Hippo signaling in renal epithelial cells. *Pflugers Arch. - Eur. J. Physiol.* 469, 917–926. doi:10.1007/s00424-017-2004-0

Mundel, P., Reiser, J., and Kriz, W. (1997a). Induction of differentiation in cultured rat and human podocytes. *Jasn* 8, 697–705. doi:10.1681/asn.v85697

Mundel, P., Heid, H. W., Mundel, T. M., Kruger, M., Reiser, J., and Kriz, W. (1997b). Synaptopodin: An Actin-Associated Protein in Telencephalic Dendrites and Renal Podocytes. *J. Cell Biol.* 139 (1), 193–204. doi:10.1083/jcb.139.1.193

Mundel, P., and Reiser, J. (2010). Proteinuria: an enzymatic disease of the podocyte. *Kidney Int.* 77, 571–580. doi:10.1038/ki.2009.424

Mysh, M., and Poulton, J. S. (2021). The Basolateral Polarity Module Promotes Slit Diaphragm Formation in Drosophila Nephrocytes, a Model of Vertebrate Podocytes. *Jasn* 32, 1409–1424. doi:10.1681/asn.2020071050

Na, J., Sweetwyne, M. T., Park, A. S. D., Susztak, K., and Cagan, R. L. (2015). Diet-Induced Podocyte Dysfunction in Drosophila and Mammals. *Cel Rep.* 12, 636–647. doi:10.1016/j.celrep.2015.06.056

Nihalani, D., Solanki, A. K., Arif, E., Srivastava, P., Rahman, B., Zuo, X., et al. (2019). Disruption of the exocyst induces podocyte loss and dysfunction. *J. Biol. Chem.* 294, 10104–10119. doi:10.1074/jbc.ra119.008362

Nishinakamura, R. (2019). Human kidney organoids: progress and remaining challenges. *Nat. Rev. Nephrol.* 15, 613–624. doi:10.1038/s41581-019-0176-x

Pollak, M. R., Quaggin, S. E., Hoenig, M. P., and Dworkin, L. D. (2014). The glomerulus: the sphere of influence. *Cjasn* 9, 1461–1469. doi:10.2215/cjn.09400913

Qian, Y., Zhong, X., Flynn, D. C., Zheng, J. Z., Qiao, M., Wu, C., et al. (2005). ILK mediates actin filament rearrangements and cell migration and invasion through PI3K/Akt/Rac1 signaling. *Oncogene* 24, 3154–3165. doi:10.1038/sj.onc.1208525

Rastaldi, M. P., Armelloni, S., Berra, S., Li, M., Pesaresi, M., Poczewski, H., et al. (2003). Glomerular podocytes possess the synaptic vesicle molecule Rab3A and its specific effector rabphilin-3a. *Am. J. Pathol.* 163, 889–899. doi:10.1016/s0002-9440(10)63449-9

Saleem, M. A., O'Hare, M. J., Reiser, J., Coward, R. J., Inward, C. D., Farren, T., et al. (2002). A conditionally immortalized human podocyte cell line demonstrating nephrin and podocin expression. *Jasn* 13, 630–638. doi:10.1681/asn.v133630

Sanna-Cherchi, S., Burgess, K. E., Nees, S. N., Caridi, G., Weng, P. L., Dagnino, M., et al. (2011). Exome sequencing identified MYO1E and NEIL1 as candidate genes for human autosomal recessive steroid-resistant nephrotic syndrome. *Kidney Int.* 80, 389–396. doi:10.1038/ki.2011.148

Scharrer, B., and Hadorn, E. (1938). The structure of the ring-gland (corpus allatum) in normal and lethal larvae of *Drosophila melanogaster*. *Proc. Natl. Acad. Sci.* 24, 236–242. doi:10.1073/pnas.24.6.236

Schell, C., and Huber, T. B. (2017). The Evolving Complexity of the Podocyte Cytoskeleton. *Jasn* 28, 3166–3174. doi:10.1681/asn.2017020143

Schwarz, K., Simons, M., Reiser, J., Saleem, M. A., Faul, C., Kriz, W., et al. (2001). Podocin, a raft-associated component of the glomerular slit diaphragm, interacts with CD2AP and nephrin. *J. Clin. Invest.* 108, 1621–1629. doi:10.1172/jci200112849

Selma-Soriano, E., Llamusi, B., Fernández-Costa, J. M., Ozimski, L. L., Artero, R., and Redón, J. (2020). Rabphilin involvement in filtration and molecular uptake in Drosophila nephrocytes suggests a similar role in human podocytes. *Dis. Model. Mech.* 13, 41509. doi:10.1242/dmm.041509

Shankar, A. S., Du, Z., Mora, H. T., van den Bosch, T. P. P., Korevaar, S. S., Van den Berg-Garrelds, I. M., et al. (2021). Human kidney organoids produce functional renin. *Kidney Int.* 99, 134–147. doi:10.1016/j.kint.2020.08.008

Sherrard, K. M., and Fehon, R. G. (2015). The transmembrane protein Crumbs displays complex dynamics during follicular morphogenesis and is regulated competitively by Moesin and aPKC. *Development* 142, 1869–1878. doi:10.1242/dev.115329

Shih, N.-Y., Li, J., Cotran, R., Mundel, P., Miner, J. H., and Shaw, A. S. (2001). CD2AP localizes to the slit diaphragm and binds to nephrin via a novel

C-terminal domain. *Am. J. Pathol.* 159, 2303–2308. doi:10.1016/s0002-9440(10)63080-5

Siegerist, F., Endlich, K., and Endlich, N. (2018). Novel Microscopic Techniques for Podocyte Research. *Front. Endocrinol.* 9, 379. doi:10.3389/fendo.2018.00379

Slavotinek, A., Kaylor, J., Pierce, H., Cahr, M., DeWard, S. J., Schneidman-Duhovny, D., et al. (2015). CRB2 mutations produce a phenotype resembling congenital nephrosis, Finnish type, with cerebral ventriculomegaly and raised alpha-fetoprotein. *Am. J. Hum. Genet.* 96, 162–169. doi:10.1016/j.ajhg.2014.11.013

Soda, K., Balkin, D. M., Ferguson, S. M., Paradise, S., Milosevic, I., Giovedi, S., et al. (2012). Role of dynamin, synaptojanin, and endophilin in podocyte foot processes. *J. Clin. Invest.* 122, 4401–4411. doi:10.1172/jci65289

Solanki, A. K., Arif, E., Srivastava, P., Furcht, C. M., Rahman, B., Wen, P., et al. (2021). Phosphorylation of slit diaphragm proteins NEPHRIN and NEPH1 upon binding of HGF promotes podocyte repair. *J. Biol. Chem.* 297, 101079. doi:10.1016/j.jbc.2021.101079

Stewart, M., Murphy, C., and Fristrom, J. W. (1972). The recovery and preliminary characterization of X chromosome mutants affecting imaginal discs ofDrosophila melanogaster. *Develop. Biol.* 27, 71–83. doi:10.1016/0012-1606(72)90113-3

Su, W. H., Mruk, D. D., Wong, E. W., Lui, W. Y., and Cheng, C. Y. (2012). Polarity protein complex Scribble/Lgl/Dlg and epithelial cell barriers. *Adv. Exp. Med. Biol.* 763, 149–170. doi:10.1007/978-1-4614-4711-5_7

Tsukita, S., and Yonemura, S. (1999). Cortical actin organization: lessons from ERM (ezrin/radixin/moesin) proteins. *J. Biol. Chem.* 274, 34507–34510. doi:10.1074/jbc.274.49.34507

Uçkun, E., Wolfstetter, G., Anthonydhason, V., Sukumar, S. K., Umapathy, G., Molander, L., et al. (2021). In Vivo profiling of the Alk proximitome in the developing Drosophila brain. *J. Mol. Biol.* 433, 167282. doi:10.1016/j.jmb.2021.167282

Vukojevic, K., Raguz, F., Saraga, M., Filipovic, N., Bocina, I., Kero, D., et al. (2018). Glomeruli from patients with nephrin mutations show increased number of ciliated and poorly differentiated podocytes. *Acta Histochem.* 120, 748–756. doi:10.1016/j.acthis.2018.08.015

Wagner, M. C., Rhodes, G., Wang, E., Pruthi, V., Arif, E., Saleem, M. A., et al. (2008). Ischemic injury to kidney induces glomerular podocyte effacement and dissociation of slit diaphragm proteins Neph1 and ZO-1. *J. Biol. Chem.* 283, 35579–35589. doi:10.1074/jbc.m805507200

Wang, L., Wen, P., van de Leemput, J., Zhao, Z., and Han, Z. (2021). Slit diaphragm maintenance requires dynamic clathrin-mediated endocytosis facilitated by AP-2, Lap, Aux and Hsc70-4 in nephrocytes. *Cell Biosci* 11, 83. doi:10.1186/s13578-021-00595-4

Weavers, H., Prieto-Sánchez, S., Grawe, F., Garcia-López, A., Artero, R., Wilsch-Bräuninger, M., et al. (2009). The insect nephrocyte is a podocyte-like cell with a filtration slit diaphragm. *Nature* 457, 322–326. doi:10.1038/nature07526

Wei, Z., Li, Y., Ye, F., and Zhang, M. (2015). Structural basis for the phosphorylation-regulated interaction between the cytoplasmic tail of cell polarity protein crumbs and the actin-binding protein moesin. *J. Biol. Chem.* 290, 11384–11392. doi:10.1074/jbc.m115.643791

Weide, T., Vollenbröker, B., Schulze, U., Djuric, I., Edeling, M., Bonse, J., et al. (2017). Pals1 Haploinsufficiency Results in Proteinuria and Cyst Formation. *Jasn* 28, 2093–2107. doi:10.1681/asn.2016040474

Welsh, G. I., and Saleem, M. A. (2011). The podocyte cytoskeleton-key to a functioning glomerulus in health and disease. *Nat. Rev. Nephrol.* 8, 14–21. doi:10.1038/nrneph.2011.151

Wen, P., Zhang, F., Fu, Y., Zhu, J.-Y., and Han, Z. (2020). Exocyst Genes Are Essential for Recycling Membrane Proteins and Maintaining Slit Diaphragm in Drosophila Nephrocytes. *Jasn* 31, 1024–1034. doi:10.1681/asn.2019060591

Whiteman, E. L., Fan, S., Harder, J. L., Walton, K. D., Liu, C.-J., Soofi, A., et al. (2014). Crumbs3 is essential for proper epithelial development and viability. *Mol. Cel. Biol.* 34, 43–56. doi:10.1128/mcb.00999-13

Wieschaus, E., and Nüsslein-Volhard, C. (2016). The Heidelberg Screen for Pattern Mutants of Drosophila: A Personal Account. *Annu. Rev. Cel Dev. Biol.* 32, 1–46. doi:10.1146/annurev-cellbio-113015-023138

Wolf, M. T. F., and Hildebrandt, F. (2011). Nephronophthisis. *Pediatr. Nephrol.* 26, 181–194. doi:10.1007/s00467-010-1585-z

Yu, H., Artomov, M., Brähler, S., Stander, M. C., Shamsan, G., Sampson, M. G., et al. (2016). A role for genetic susceptibility in sporadic focal segmental glomerulosclerosis. *J. Clin. Invest.* 126, 1067–1078. doi:10.1172/jci82592

Zhang, B., Zhang, Y., and Liu, J.-L. (2021). Highly effective proximate labeling in Drosophila. *G3 Genes|Genomes|Genetics* 11, jkab077. doi:10.1093/g3journal/jkab077

Zhang, F., Zhao, Y., and Han, Z. (2013). An In Vivo Functional Analysis System for Renal Gene Discovery in Drosophila Pericardial Nephrocytes. *Jasn* 24, 191–197. doi:10.1681/asn.2012080769

Zhou, X., Wang, L., Hasegawa, H., Amin, P., Han, B.-X., Kaneko, S., et al. (2010). Deletion of PIK3C3/Vps34 in sensory neurons causes rapid neurodegeneration by disrupting the endosomal but Not the autophagic pathway. *Proc. Natl. Acad. Sci.* 107, 9424–9429. doi:10.1073/pnas.0914725107

Zhu, J.-Y., Fu, Y., Nettleton, M., Richman, A., and Han, Z. (2017a). High Throughput In Vivo Functional Validation of Candidate Congenital Heart Disease Genes in Drosophila. *Elife* 6, 22617. doi:10.7554/eLife.22617

Zhu, J.-Y., Fu, Y., Richman, A., and Han, Z. (2017b). Validating Candidate Congenital Heart Disease Genes in Drosophila. *Bio-protocol* 7, 2350. doi:10.21769/BioProtoc.2350

Zhu, J.-Y., Fu, Y., Richman, A., Zhao, Z., Ray, P. E., and Han, Z. (2017c). A Personalized Model of COQ2 Nephropathy Rescued by the Wild-Type COQ2 Allele or Dietary Coenzyme Q10 Supplementation. *Jasn* 28, 2607–2617. doi:10.1681/asn.2016060626

Zhu, J.-Y., Huang, X., Fu, Y., Wang, Y., Zheng, P., Liu, Y., et al. (2022). Pharmacological or genetic inhibition of hypoxia signaling attenuates oncogenic RAS-induced cancer phenotypes. *Dis. Model. Mech.* 15, 48953. doi:10.1242/dmm.048953

Zhuang, S., Shao, H., Guo, F., Trimble, R., Pearce, E., and Abmayr, S. M. (2009). Sns and Kirre, theDrosophilaorthologs of Nephrin and Neph1,direct adhesion, fusion and formation of a slit diaphragm-like structure in insect nephrocytes. *Development* 136, 2335–2344. doi:10.1242/dev.031609

Conflict of Interest: The authors declare that the research was conducted in the absence of any commercial or financial relationships that could be construed as a potential conflict of interest.

Publisher's Note: All claims expressed in this article are solely those of the authors and do not necessarily represent those of their affiliated organizations, or those of the publisher, the editors and the reviewers. Any product that may be evaluated in this article, or claim that may be made by its manufacturer, is not guaranteed or endorsed by the publisher.

frontiers in Cell and Developmental Biology

REVIEW
published: 24 February 2022
doi: 10.3389/fcell.2022.838272

The Pathology Lesion Patterns of Podocytopathies: How and why?

Fiammetta Ravaglia[1], Maria Elena Melica[2], Maria Lucia Angelotti[2], Letizia De Chiara[2], Paola Romagnani[2,3] and Laura Lasagni[2]**

[1]Nephrology and Dialysis Unit, Santo Stefano Hospital, Prato, Italy, [2]Department of Experimental and Clinical Biomedical Sciences "Mario Serio", University of Florence, Florence, Italy, [3]Nephrology Unit, Meyer Children's Hospital, Florence, Italy

Podocytopathies are a group of proteinuric glomerular disorders driven by primary podocyte injury that are associated with a set of lesion patterns observed on kidney biopsy, i.e., minimal changes, focal segmental glomerulosclerosis, diffuse mesangial sclerosis and collapsing glomerulopathy. These unspecific lesion patterns have long been considered as independent disease entities. By contrast, recent evidence from genetics and experimental studies demonstrated that they represent signs of repeated injury and repair attempts. These ongoing processes depend on the type, length, and severity of podocyte injury, as well as on the ability of parietal epithelial cells to drive repair. In this review, we discuss the main pathology patterns of podocytopathies with a focus on the cellular and molecular response of podocytes and parietal epithelial cells.

Keywords: podocytopathies, minimal change disease, focal segmental glomerulosclerosis, diffuse mesangial sclerosis, collapsing glomerulopathy, minimal change, parietal epithelial cells, renal progenitor

OPEN ACCESS

Edited by:
Mario Ollero, INSERM U955 Institut Mondor de Recherche Biomédicale (IMRB), France

Reviewed by:
Aihua Zhang, Nanjing Children's Hospital, China
Miriam Zacchia, University of Campania Luigi Vanvitelli, Italy
Sandeep Mallipattu, Stony Brook University, United States

****Correspondence:***
Fiammetta Ravaglia
ravaglia.fiammetta@gmail.com
Laura Lasagni
laura.lasagni@unifi.it

Specialty section:
This article was submitted to Cell Death and Survival, a section of the journal Frontiers in Cell and Developmental Biology

Received: *17 December 2021*
Accepted: *07 February 2022*
Published: *24 February 2022*

Citation:
Ravaglia F, Melica ME, Angelotti ML, De Chiara L, Romagnani P and Lasagni L (2022) The Pathology Lesion Patterns of Podocytopathies: How and why? Front. Cell Dev. Biol. 10:838272. doi: 10.3389/fcell.2022.838272

INTRODUCTION

Podocytes are differentiated epithelial cells whose number is determined shortly before birth as nephrogenesis ceases (Bertram et al., 2011). Podocytes have a limited capacity to complete successful cytokinesis as cell division requires a rearrangement of the podocyte actin cytoskeleton, disrupting the podocyte foot processes (Lasagni et al., 2013). Consequently, direct or indirect podocyte injury, which causes cytoskeleton rearrangement, poses a serious threat to kidney barrier function maintenance, which is reflected in glomerular proteinuria levels.

Podocyte injury can be caused by immunologic, infectious or toxic agents, as well as patient specific characteristics such as obesity or haemodynamic modifications (Kopp et al., 2020). In addition, genetic analysis techniques have broadened the known causes of podocytopathies adding genetic variants to the list. Currently, more than fifty podocyte-expressed genes have been identified as directly linked to podocytopathies as well as syndromal non-podocyte-specific genes, phenocopies with other underlying genetic abnormalities and susceptibility genes (i.e., apolipoprotein L1 (APOL1) variants) leading to a complete revision of carrier risk stratification (Freedman et al., 2014; Warejko et al., 2018; Landini et al., 2020). Podocyte injury can be observed in the setting of all forms of immune complex glomerulonephritis (i.e., lupus nephritis, membranous nephropathy) and in metabolic disorders (diabetes, amyloidosis) and is a key event in chronic kidney disease progression (Kopp et al., 2020). The latter will not be the topic of this review. We will rather focus on disorders that have podocyte as a primary target of injury and that are associated with a variety of lesion patterns that renal pathology struggles to classify (Ahn and Bomback, 2020). These histopathological lesion patterns range from 1) minimal changes (MC), traditionally referred to as "minimal change disease" (MCD) and defined as minimal alterations visible only by ultrastructural analysis; 2) focal segmental glomerulosclerosis (FSGS) where sclerotic lesions are restricted to a

subset of the glomeruli; 3) diffuse mesangial sclerosis (DMS) characterized by mesangial matrix increase and podocyte hypertrophy; and lastly 4) collapsing glomerulopathy (CG) which presents as collapse of the glomerular capillaries and hyperplasia of parietal epithelial cells (PECs) migrating to the tuft forming "pseudocrescents" (Barisoni et al., 2007). These glomerular histopathological lesion patterns can be collectively viewed as podocytopathies and their progression to chronic kidney disease is related to the amount of podocyte loss (Kopp et al., 2020). In addition to podocytes and PECs, glomerular endothelial cells and mesangial cells likely contribute to the progression of podocytopathies (Chung et al., 2020). However, as a comprehensive analysis of all the cell types involved in the disease progression is beyond the scope of this review, we will focus our discussion on the PEC-podocyte axis.

Several lines of evidence support the podocyte depletion hypothesis (Kim et al., 2001; Wharram et al., 2005; Fukuda et al., 2012a). In particular, the Wiggins group (Wharram et al., 2005) elegantly showed the consequences of podocyte loss: less than 20% of podocyte loss is associated with a normal glomerulus at light microscopy or with mesangial expansion, whereas loss of more than 20% of podocytes leads to segmental denudation of glomerular basement membrane with consequent adhesions between the Bowman capsule and the glomerular capillary loop. Once the process is initiated sclerosis follows. Segmental sclerosis occurs if podocyte loss is less than 40%, while global sclerosis occurs if podocyte loss exceeds 60% (Wharram et al., 2005).

A subpopulation of PECs endowed with progenitor characteristics can replace, at least to some extent, lost podocytes (Peired et al., 2013; Zhang et al., 2013; Eng et al., 2015; Lasagni et al., 2015; Romoli et al., 2018; Kaverina et al., 2019). However, PECs may also have a detrimental role, as proliferation of activated PECs can also be a crucial determinant of glomerulosclerosis (Lasagni et al., 2015; Eymael et al., 2018).

Collectively, the aim of this review is to: 1) discuss the current concept of histopathological pattern recognition; 2) introduce the importance of PECs in the formation and identification of these peculiar lesions; 3) consider the relationship between PECs and podocytes as an important determinant of disease progression.

MINIMAL CHANGES

How—Pathology

By definition, glomerular appearance observed by light microscopy in minimal changes is normal, while tubular compartment showed vacuolar, lipoid changes in the proximal tubules defined as lipoid nephrosis (Munk, 1918).

Ultrastructural examination is required to identify the only consistent glomerular pathologic feature of minimal changes, which is simplification of podocyte shape at ultrastructural level without glomerular abnormalities at light microscopy. By electron microscopy, this feature is visualized as effacement of the discrete foot processes and it may be associated to coarsening, i.e., retraction, shortening and widening of foot processes (De Vriese et al., 2018). Foot process simplification and effacement are the earliest morphological patterns of podocyte injury and are clinically associated with highly selective nephrotic-range proteinuria (Vivarelli et al., 2017). Extension of foot process effacement and coarsening is an issue. It has been hypothesized that the surface area extension of capillary loops involved in this process could differentiate the MC lesion pattern from FSGS (De Vriese et al., 2018). Specifically, MC lesion would show widespread foot process effacement and coarsening, involving at least more than half of the capillary loop surface area, while FSGS would show more segmental alterations (Deegens et al., 2008; da Silva et al., 2020) as in maladaptive FSGS increased fluid shear stress is typically a segmental phenomenon (Kriz and Lemley, 2017a). Nevertheless, such an assessment is prone to inaccuracy considering that the ultrastructural analysis is bidimensional and it is limited in the number of glomeruli analyzed (i.e., no more than one or two glomeruli). In addition, no correlation between foot process effacement measured by electron microscopy and proteinuria severity exists, suggesting that this evaluation alone is not sufficient to allow clinical-pathological correlations (Royal et al., 2020).

Foot process effacement is also associated with microfilament aggregation at the base of epithelial cells and filtration slit distortion, resulting in a reduction in the number of slit diaphragms (Patrakka et al., 2002). This, in turn, causes a displacement of the diaphragms in a ladder-like formation toward the pore apex (Patrakka et al., 2002). In addition, podocytes may show other non-specific structural alterations including hypertrophy, microvillous transformation, formation of vacuoles and the presence of resorption droplets (Royal et al., 2020). However, these alterations do not prevent podocytes from fully covering the glomerular basement membrane. Accordingly, in MC lesions, areas of glomerular basement membrane denudation (Lahdenkari et al., 2004) due to reduction in podocyte density or to net podocyte loss compared to healthy controls do not occur (Szeto et al., 2015) (**Figure 1**).

Finally, immunofluorescence for immunoglobulins and complement fractions on kidney biopsy is generally negative (Vivarelli et al., 2017). However, recent findings of nephrin autoantibodies in a subset of patients with MC lesions at light microscopy and podocyte-associated punctate IgG at immunofluorescence provide support for an autoimmune etiology (Watts et al., 2021). Collectively, the lack of pathological features detectable by light microscopy and immunohistochemistry in biopsies of patients with MC lesions complicates the diagnostic process. Ongoing studies are attempting to identify new biomarkers to predict outcomes or individualize treatments. Nevertheless, podocyte injury at kidney biopsy may be difficult to identify and characterize, mostly due to the focal nature of the damage, inadequate sampling and specific shortcomings linked to traditional techniques, as previously mentioned. Recently, the combination of optical clearing techniques with state-of-the-art microscopy permitted morphometric analysis in thick tissues with a resolution up to nanoscale levels (Angelotti et al., 2021). This technique permits

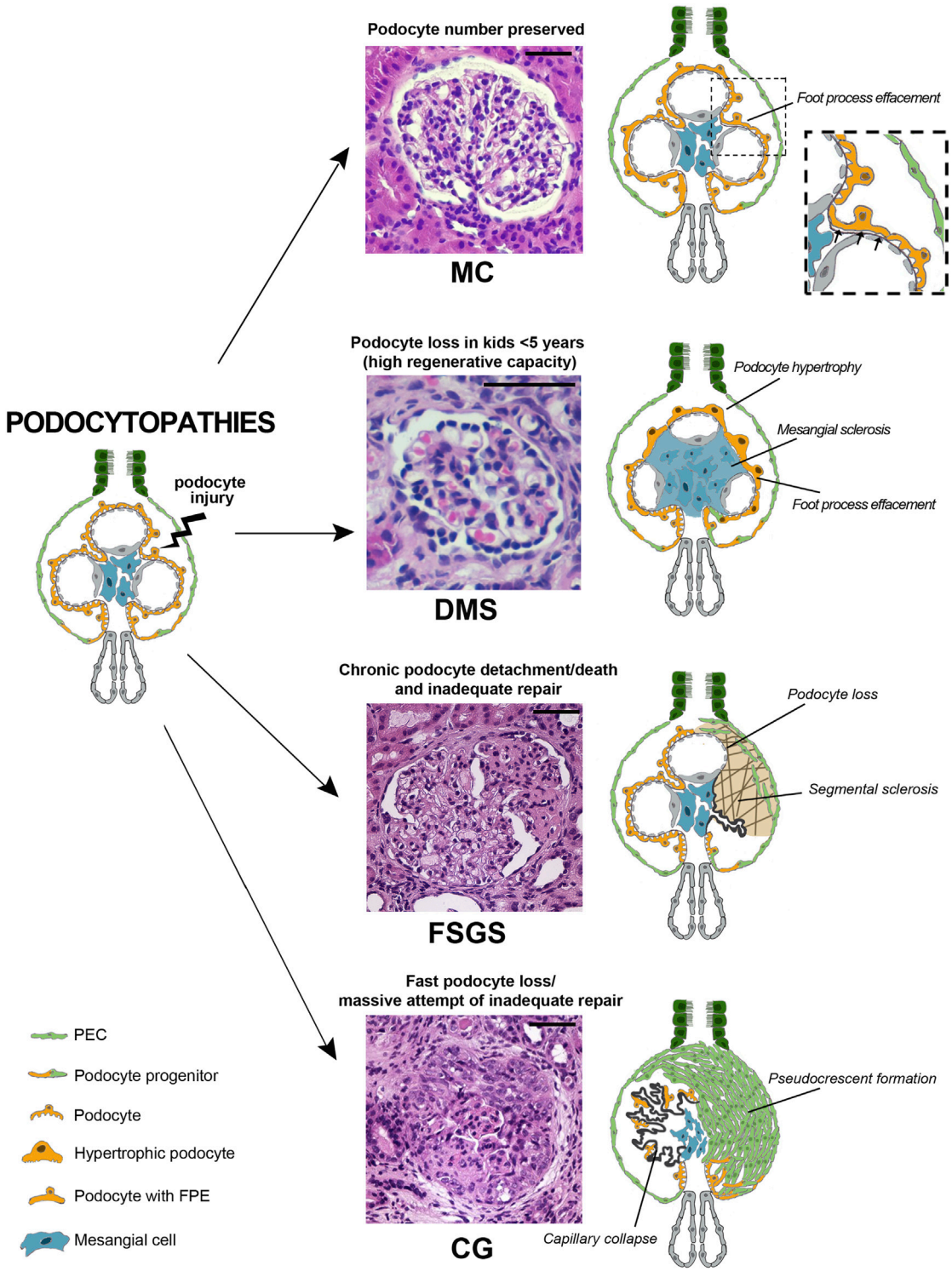

FIGURE 1 | Podocytopathies result from the equilibrium between the nature of injury and the glomerular capacity of repair. When podocyte injury does not determine net cell loss, no changes are present on light microscopy and only foot process effacement is detectable, as in minimal changes (MC). In a setting of fast podocyte loss in kids younger than 5 years old, massive attempt of repair takes place. Immature podocytes are generated and are visible as a halo of hypertrophic podocytes overlying capillary loops as in diffuse mesangial sclerosis (DMS). When severity or chronicity of podocyte injury overcomes the capacity of PECs to replace detached or loss podocytes, glomerular basement membrane denudation triggers an injury cascade. This results in the segmental solidification of the tuft with accumulation of extracellular matrix characteristic of focal segmental glomerulosclerosis (FSGS). Finally, if fast podocyte loss occurs in individuals where the regenerative capacity is inadequate, generation of new podocytes is hampered and proliferating progenitors accumulate in Bowman space in the form of pseudocrescents resulting in collapsing glomerulopathy (CG) (Hematoxylin and eosin stains, magnifications 40x. Bars= 50 μm). (Abbreviations: MC= minimal changes, DMS= diffuse mesangial sclerosis, FSGS= focal segmental glomerulosclerosis, CG= collapsing glomerulopathy, PEC= parietal epithelial cell, FPE= foot process effacement).

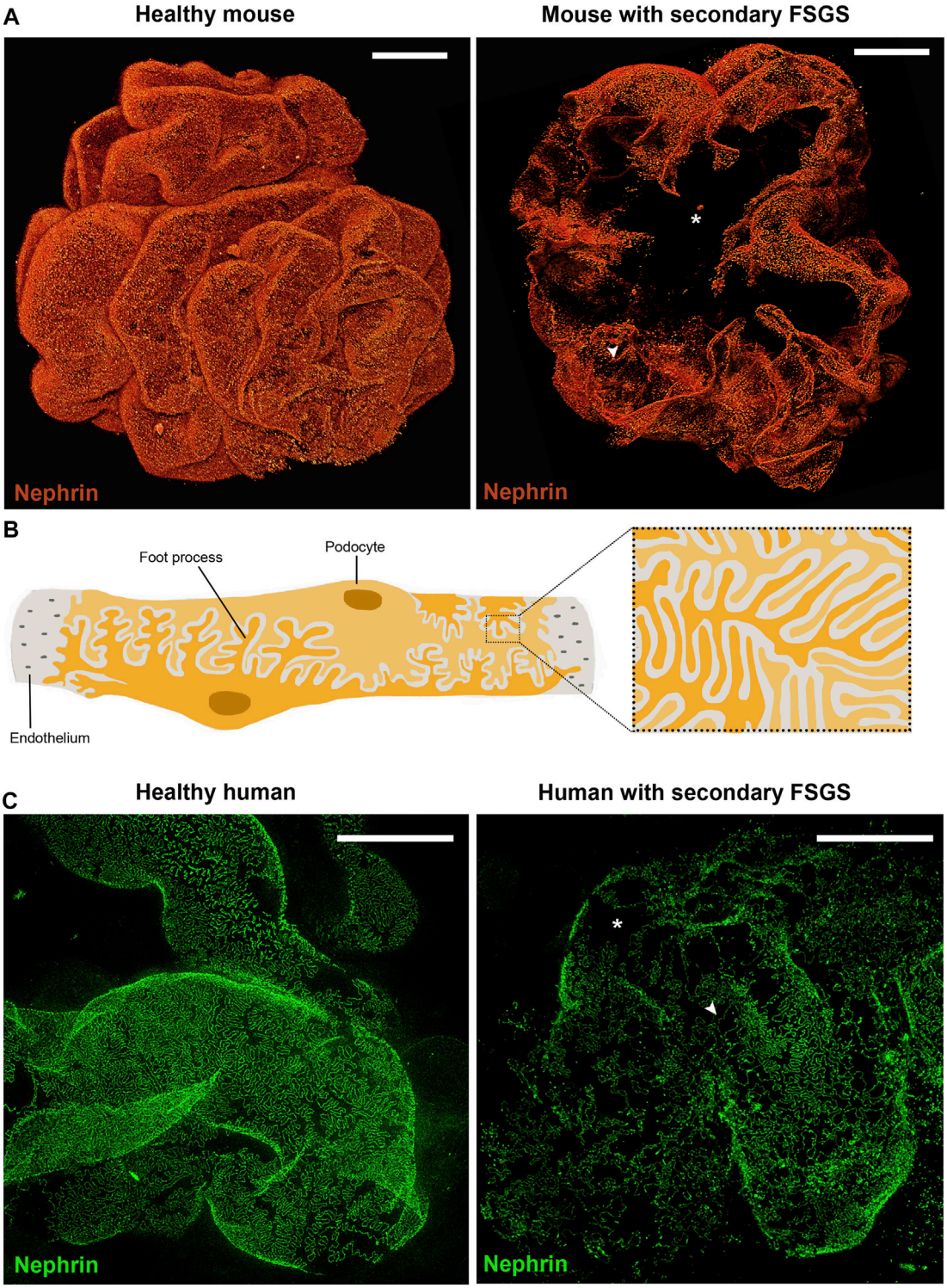

FIGURE 2 | Podocytes are crucial for integrity of the filtration barrier. **(A)** Three-dimensional reconstruction of whole mouse glomeruli stained for nephrin upon optical tissue clearing by using confocal microscopy. The signal represents nephrin protein within the slit diaphragm. Z-series stacks were obtained from 80-μm kidney slices with images collected at 1 μ m intervals. On the left a representative glomerulus from a healthy mouse shows an intact filtration barrier. On the right a representative glomerulus from a mouse with secondary FSGS (obesity- related diabetic mouse, db/db mouse) shows large denudated areas with podocyte loss (asterisk) and foot process effacement (arrowhead). **(B)** Schematic drawing of representative podocytes, with their interdigitating foot processes, wrapped around a glomerular capillary loop. **(C)** Representative images of human podocyte foot processes by using STED-super resolution microscopy upon tissue clearing. Z-series stacks were obtained from 5-μm kidney slices. The green signal represents nephrin protein. On the left a representative image of a normal human kidney obtained from a patient who underwent nephrectomy for localized renal tumor. On the right a representative image of a kidney biopsy obtained from a patient with secondary FSGS, showing denudated areas with podocyte loss (asterisk) and foot process effacement (arrowhead) (Bars= 20 μm).

imaging of large tissue areas and to resolve fine structural details at once. Therefore, we can visualize the slit diaphragm 3D, giving direct evidence of structural changes or podocyte loss (**Figure 2**) (Artelt et al., 2018; Tesch et al., 2021).

Why—Experimental Evidence

Podocyte foot process effacement is the ultrastructural hallmark of MC lesion, however, the process leading to podocyte effacement is not clear (Purohit et al., 2021). Immunologic dysregulations and modifications of the podocyte are thought to synergize in altering the integrity of the glomerular barrier and therefore determining proteinuria (Purohit et al., 2021). Animal models could potentially provide valuable insights into physiopathology of the MC lesion, but we lack an animal model fitting the specific MC characteristics, i.e., abrupt onset selective nephrotic-range proteinuria, diffuse foot process effacement but no podocytopenia, low rates of disease progression, and steroid sensitivity (Chugh et al., 2012). In fact, all mouse models of chronic and heavy proteinuria eventually develop FSGS following an initial phase with only diffuse podocyte foot process effacement, offering the opportunity to elucidate mechanisms of progression rather than that of acute renal damage. The models most broadly employed by researchers are the Puromycin Aminonucleoside (PAN) model, in which single low-dose injection of toxic agent directed against podocyte molecules induces transient proteinuria and foot process effacement, without inducing podocyte loss (Kim et al., 2001; Pippin et al., 2009) and the diphtheria toxin (DT) model, in which DT injection into rats expressing human diphtheria toxin receptor transgene results in dose-dependent podocyte depletion (Wharram et al., 2005). In particular, in the DT model, less than 20% of podocyte depletion results in mesangial expansion, transient proteinuria, and normal kidney function. The continuum between the MC lesion and FSGS in these models supports the hypothesis that in some patients these two lesion patterns represent different pathology manifestations of the same injury (Maas et al., 2016).

Long before animal models, the possible link between MC and FSGS lesions had already been suggested in the first clinical report of nephrotic syndrome in the 1970s (Habib and Kleinknecht, 1971). Afterwards, identification of FSGS in patients that previously exhibited MC biopsy pattern was reported in children who underwent repeated kidney biopsies during the course of steroid sensitive nephrotic syndrome (Tejani, 1985) and in serial post-transplantation biopsies of patients with FSGS recurrence (Charnaya and Moudgil, 2017), supporting evidence of an evolving process (Maas et al., 2016). During the progression from MC to FSGS lesion, the glomeruli significantly increase their volumes and podocyte hypertrophy appears as a distinguishing feature of FSGS *vs.* MC (Fogo et al., 1990). This would suggest that interventions aimed at regulating glomerular volume and podocyte hypertrophy could represent an effective strategy to sustain podocyte survival and to prevent podocytopenia (Puelles et al., 2019; Banu et al., 2021). However, this adaptive response of podocytes is only sustainable until a threshold is reached, after which the podocyte detaches and progression to FSGS occurs. Podocyte detachment is thought to occur through a substantial increase in the mechanical forces of fluid filtration (Saga et al., 2021). Evaluation of mechanical properties of podocytes and of their response to external mechanical stimuli has shown how circumferential wall tension as well as fluid shear stress play an important role in podocytopathies and progression from MC to FSGS lesion (Kriz and Lemley, 2017b; Embry et al., 2018; Calizo et al., 2019). It is also possible that in MC podocyte loss occurs but it is not detectable either because it does not differ from normal physiological turnover of healthy glomeruli or because the progenitors succeed in replacing lost podocytes. Indeed, many studies reported the PEC capacity to differentiate into mature podocytes after glomerular injury, replacing at least in part the lost podocytes (Peired et al., 2013; Zhang et al., 2013; Eng et al., 2015; Lasagni et al., 2015; Romoli et al., 2018; Kaverina et al., 2019).

If the cause of podocyte injury is reversible, we observe a return to normal of foot processes together with a complete proteinuria remission and a favorable prognosis. In case of irreversible podocyte injury, podocyte loss can still be partially compensated by progenitor replacement (Nagata, 2016; Kopp et al., 2020). When podocyte loss reaches its tipping point (more than 20% of podocytes are lost), PECs are unable to fully compensate for podocyte loss. In such cases, the MC lesion represents the first stage of a condition that will progress towards more severe patterns of injury characterized by more prominent podocyte loss (i.e., FSGS) (**Figure 1** and **Table 1**).

DIFFUSE MESANGIAL SCLEROSIS

How—Pathology

DMS is found in children younger than 5 years old with nephrotic syndrome progressing to end stage kidney disease during childhood (Wiggins, 2007). DMS is defined by the presence of diffuse mesangial sclerosis in kidney biopsy, with the deeper glomeruli being the least affected. The term DMS relies on the late appearance of the lesion, but does not give any clue on its pathogenesis (Barisoni et al., 2007).

Glomeruli in DMS appear as a halo-shaped distribution of podocytes surrounding a matrix-containing glomerular center (**Figure 1**). Initially, the matrix has a fibrillary appearance, but at later stages, the mesangial extracellular matrix accumulation becomes more prominent as capillary lumens obliterate with progressive tuft contraction. In parallel, podocytes show absence of foot processes and glomerular capillary loops tend to collapse with progressive podocyte hypertrophy and mild hyperplasia, remaining visible even in advanced disease stages (Barisoni et al., 2007). The tubules are dilated and atrophic, sometimes containing hyaline casts (Charles Jennette et al., 2015). Non-diagnostic deposits of IgM and C3 are seen in the mesangium of the less affected glomeruli and in the periphery of the sclerotic glomeruli (Charles Jennette et al., 2015). Electron microscopy shows mesangial collagen fibrils. The glomerular basement membrane is split and wavy because of zones of subepithelial lucent widening and segmental denudation due to foot process detachment (Charles Jennette et al., 2015).

TABLE 1 | Animal models and clinical evidence supporting the proposed pathomechanisms for development of pathology lesion patterns associated with podocytopathies.

Minimal changes (foot process effacement and podocyte loss lower than 20%)			
		Evidence	**Study limitations**
Minimal changes develops in absence of podocyte loss or for loss lower than 20%	Animal models	Development of FPE and proteinuria following low dose injection of toxic agents and dose dependent podocyte depletion shows normal glomeruli when podocyte loss is absent or limited Kim et al. (2001); Wharram et al. (2005); Pippin et al. (2009); Banu et al. (2021)	After an initial phase with only FPE, FSGS develops in this model
	Clinical evidence	Normal glomeruli on light microscopy in biopsies of patients	Alteration missing owing to sampling error
		Absence of podocyte excretion or low levels of podocyte mRNAs in urine of patients with minimal changes Szeto et al. (2015)	Podocytes die but do not detach from GBM
Minimal changes progress toward focal segmental sclerosis	Animal models	FSGS develops after an initial phase with only FPE in all the animal models with persistent proteinuria Kim et al. (2001); Wharram et al. (2005); Pippin et al. (2009)	NA
		Podocyte depletion and FSGS development are dose-dependent Kim et al. (2001); Wharram et al. (2005)	NA
	Clinical evidence	Appearance of FSGS in second biopsies in patients previously diagnosed with MC Tejani, (1985) and in post-transplant biopsies of patients with FSGS recurrence after diagnosis of MC Maas et al. (2016); Charnaya and Moudgil, (2017)	FSGS is missed owing to sampling error
Diffuse Mesangial Sclerosis (podocytes loss in the setting of high podocyte replacement-early childhood)			
		Evidence	**Study limitations**
Diffuse mesangial sclerosis develops following podocyte loss	Animal models	Mesangial expansion is the first evidence of podocyte loss by 20% or less Wharram et al. (2005)	Podocyte loss induced in adult rats do not reproduce human DMS
	Clinical evidence	Podocyte excretion in urine of patients with DMS Ikezumi et al. (2014)	NA
High capacity to generate new podocyte by PECs during childhood	Animal models	Generation of podocytes from PECs during kidney development before birth Wanner et al. (2014) and during postnatal glomerular growth Appel et al. (2009)	Lineage tracing of PECs started before birth Wanner et al. (2014)
		Generation of 10% of podocytes from genetically tagged PECs during postnatal glomerular growth Lasagni et al. (2015)	NA
	Clinical evidence	Less-differentiated podocyte phenotype and increased expression of the PEC progenitor marker Pax2 in glomeruli of patients with DMS Yang et al. (1999)	NA
		Proliferating cells positive for claudin-1 in glomeruli of children with DMS Ikezumi et al. (2014)	NA
FSGS (chronic severe podocyte loss and PEC activation with inadequate podocyte replacement)			
		Evidence	**Study limitations**
FSGS lesions develop following chronic severe podocyte loss and PECs activation but inefficient differentiation with inadequate podocyte replacement	Animal models	FSGS develops for podocyte depletion between 21 and 40% Wharram et al. (2005) or for chronic proteinuria Kim et al. (2001); Pippin et al. (2009), and results in PEC activation and glomerulosclerosis Puelles et al. (2019)	NA
		Podocyte depletion and FSGS development are dose-dependent Kim et al. (2001); Wharram et al. (2005); Pippin et al. (2009); Fukuda et al. (2012b)	NA
		CD44 and CD9 expression in PECs during FSGS Okamoto et al. (2013); Lazareth et al. (2019)	NA
		Lesions in FSGS are generated by genetically tagged PECs Lasagni et al. (2015); Romoli et al. (2018)	NA
		Generation of podocytes from PECs in FSGS Eng et al. (2015); Kaverina et al. (2019) and during aging Kaverina et al. (2020)	NA
		Pharmacological treatment induces remission of proteinuria and increase in podocyte number enhancing generation of	NA

(Continued on following page)

TABLE 1 | (*Continued*) Animal models and clinical evidence supporting the proposed pathomechanisms for development of pathology lesion patterns associated with podocytopathies.

		podocytes by genetically labelled PECs Lasagni et al. (2015); Romoli et al. (2018)	
		Increased podocyte density and/or in number of PEC progenitors in response to pharmacological treatment Peired et al. (2013); Zhang et al. (2013); Zhang et al. (2012); Hudkins et al. (2020); Zhang et al. (2015); Motrapu et al. (2020)	No lineage tracing to determine the origin of new podocytes
	Clinical evidence	Reduced number of podocytes in biopsies Motrapu et al. (2020)	Semi-quantitative podocyte counting
		Presence of podocytes and podocyte mRNA in urine of patients affected by FSGS Szeto et al. (2015)	NA
		CD44 and CD9 expression in glomeruli of FSGS patients Lazareth et al. (2019); Fatima et al. (2012)	NA
		Markers of PEC progenitor in FSGS lesions from biopsies of patients Smeets et al. (2014); Dijkman et al. (2005); Smeets et al. (2009)	NA
		Increase in podocyte number, remission and regression of functional parameters of CKD in patients with diabetic and nondiabetic nephropathies Fioretto et al. (1998); Remuzzi et al. (2006); Takahashi et al. (2007); Cortinovis et al. (2016); Boffa et al. (2003); Ma et al. (2005); Fogo, (2001); Yang and Fogo, (2014)	NA
Collapsing glomerulopathy (severe podocyte loss and dysregulated PEC/RPC activation)			
		Evidence	**Study limitations**
Collapsing glomerulopathy develops following severe podocyte loss and pseudocrescents originate from the proliferation of PECs progenitors	Animal models	Global glomerulosclerosis for podocyte depletion >40% Wharram et al. (2005)	NA
		Extensive podocyte loss and simultaneous PEC hyperplasia in collapsing FSGS Suzuki et al. (2009)	NA
		Podocyte loss triggers the activation of a distinct PEC subpopulation Pace et al. (2021)	NA
		PEC to podocyte differentiation in HIV nephropathy Dai et al. (2017)	No lineage tracing to determine the origin of new podocytes
		Presence of cells expressing PEC and podocyte markers in glomeruli of HIV transgenic mice expressing APOL1 Kumar et al. (2018)	
	Clinical evidence	Expression of PEC progenitor markers in proliferating cells of pseudocrescent Lazareth et al. (2019); Dijkman et al. (2006); Smeets et al. (2009); Smeets et al. (2004)	NA
		Presence of PEC expressing PEC and podocyte markers in glomeruli of patients with HIVAN Kumar et al. (2018)	NA

(Abbreviations: FPE= foot process effacement, FSGS= focal segmental glomerulosclerosis, GBM= glomerular basement membrane, MC= minimal changes, DMS= diffuse mesangial sclerosis, PEC= parietal epithelial cell, CKD= chronic kidney disease, APOL1= apolipoprotein L1, HIVAN= HIV associated nephropathy).

Why—Experimental Evidence

Genetic mutations causing DMS have given an insight in podocyte biology. For instance, truncating mutations in phospholipase C epsilon (PLCε1) expressed by podocytes in the developing glomerulus; mutations in WT1, a major podocyte transcription factor present early in podocyte development, or mutations in b2laminin (LAMB2) gene involved in glomerular basement membrane expansion and assembly, are associated with the DMS pattern of injury in humans (Boyer et al., 2010; Lehnhardt et al., 2015; Matejas et al., 2010) and in mouse models (Atchison et al., 2020; Ratelade et al., 2010; Lin et al., 2018). These mutations result in arrested development of glomeruli (Hinkes et al., 2006; Yang et al., 1999) that are not able to prevent protein leakage while filtering, causing massive proteinuria responsible for fast podocyte loss and rapid progression to end stage kidney disease. In particular, glomeruli in kidneys of patients with DMS linked to WT1 mutations show a relatively less-differentiated podocyte phenotype and immunostaining reveals increased expression of the PEC progenitor marker Pax2 (Yang et al., 1999), suggesting migration and attempt of PECs to differentiate into podocytes. Interestingly, gene expression analysis of isolated glomeruli of DMS mouse model obtained introducing a heterozygous WT1 mutation, identified increased expression of Cyp26a1 in podocytes of mutated mice (Ratelade et al., 2010). This resulted in a decrease of the concentration of *all-trans*-retinoic acid—an inducer of PEC progenitor differentiation into podocytes (Peired et al., 2013; Zhang et al., 2012; Dai et al.,

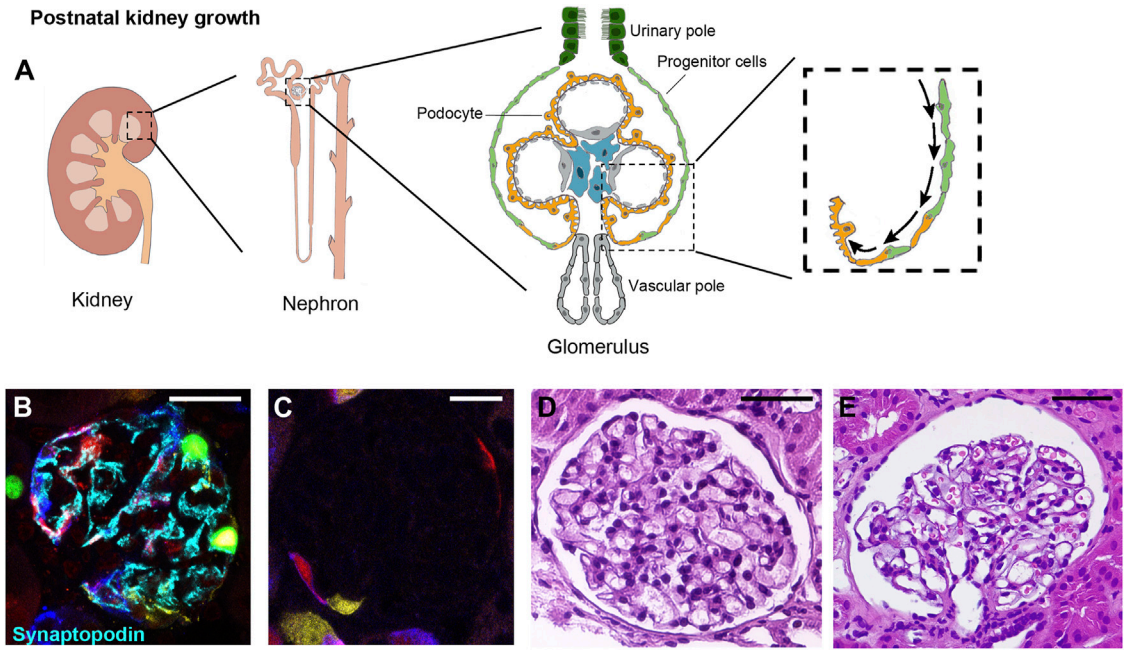

FIGURE 3 | Progenitor cells generate novel podocytes during postnatal kidney growth. **(A)** The kidney is composed of functional units, nephrons, each of which is made of a glomerulus and a tubule. The glomerulus is composed of a tuft of capillaries covered by visceral epithelial cells, the podocytes, and surrounded by the Bowman capsule lined on the inner surface by flat epithelial cells, parietal epithelial cells (PEC). A subpopulation of PEC localized at the urinary pole is endowed with progenitor characteristics and progressively differentiate into podocytes toward the vascular pole of the glomerulus. This occurs as the kidney grows, during childhood and adolescence in mouse models and in humans. In **(B,C)** representative glomeruli from transgenic *Pax2.rtTA;TetO.Cre;R26.Confetti* mice, an established mouse model of renal progenitor cell lineage tracing. In this model, green, yellow, cyan or red fluorescent protein is randomly expressed by Pax2- expressing cells. Pax2 is expressed by PEC progenitor cells during kidney development but is lost upon their differentiation into mature podocytes in the post-natal kidney (*magnification 63x*). In **(B)** a representative glomerulus of *Pax2.rtTA;TetO.Cre;R26.Confetti* mouse, induced at postnatal day P5 (when the generation of new glomeruli from the metanephric mesenchyme has already ended) for 10 days and tracked until 5 weeks of age. Fluorescent Pax2+ cells are present in the parietal epithelium of the Bowman capsule as well as inside the glomerulus. These intraglomerular Pax2-derived cells expressed synaptopodin (cyan), demonstrating their podocyte nature. In (C) a representative glomerulus of a *Pax2.rtTA;TetO.Cre;R26.Confetti* adult mouse induced at 5 weeks of age for 10 days, showing Pax2+ cells only in Bowman capsule. Podocytes are not labeled. **(D,E)** In humans, the observation that the number of podocytes increases during glomerular growth and maturation in the early years after birth, suggest the involvement of a podocyte progenitor pool during postnatal kidney growth. In D a glomerulus of a 4 years old normal human kidney and in E a glomerulus of a 25 years old normal human kidney from two patients who underwent nephrectomy for localized renal tumor (Hematoxylin and eosin stain, magnification 40 x. Bars= 20 μm in B and C, bars= 50 μm in D and E).

2017)—in the glomerular milieu, supporting the hypothesis that a hampered differentiation of PEC progenitors into podocytes could be involved in the development of DMS. In adult animals, mesangial expansion is the first indirect evidence of podocyte loss up to 20% of the podocyte compartment (Wharram et al., 2005). Indeed, in the attempt to maintain the capillary loop open despite the podocyte loss, the mesangium assumes a more prominent fibrillary appearance and expands (Wharram et al., 2005). Reduced number of podocytes, associated with excretion of urinary podocytes, was observed also in glomeruli with severe sclerosis in children with DMS (Ikezumi et al., 2014). Interestingly, some glomeruli showed hypercellular lesions with proliferating cells that stained positive for the PEC marker claudin-1 (Ikezumi et al., 2014), suggesting that podocyte loss and the consequent proliferation of PECs are common processes in the pathogenesis of DMS. Several studies have shown that around 10% of podocytes are formed after birth from PEC progenitors localized at the urinary pole of the Bowman capsule, that progressively differentiate into podocytes, migrating from the urinary pole towards the vascular pole of the glomerulus (Lasagni et al., 2015; Appel et al., 2009; Wanner et al., 2014) (**Figure 3**). PEC differentiation into podocytes happens substantially to support the increase of kidney dimension as the kidney grows, during childhood and adolescence in mouse models (Lasagni et al., 2015; Appel et al., 2009; Wanner et al., 2014) (**Figure 3**). Similarly in humans, the finding that podocytes increase in numbers during the first years after birth (Puelles et al., 2015), suggests the involvement of a podocyte progenitor subpopulation driving postnatal glomerular growth (**Figure 3**). These observations suggest that kidneys from children <5 years are endowed with a higher capacity to generate new podocytes from PECs deriving from the ongoing growth process. This explains why even severe podocyte loss driven by major genetic alterations of the podocyte in young children is associated with a pattern of injury characterized by mesangial expansion and the signs of a massive podocyte turnover. Indeed, in the context of repair attempt by PECs, the initial mesangial adaptive response paralleled by massive introduction of new podocytes along the glomerular basement membrane is enough to prevent scarring

and maintain kidney function despite heavy proteinuria in young children (**Figure 1** and **Table 1**). Unfortunately, due to the frequent underlying genetic cause connected to DMS, new podocytes originated by PECs carry the same functional problem of the lost ones, damping the regenerative potential of these patients and progressively leading first to FSGS and then to end stage kidney disease.

FOCAL SEGMENTAL GLOMERULOSCLEROSIS

How—Pathology

The pathognomonic characteristic of FSGS is segmental solidification of the glomerular capillary tuft with hyalinosis and intracapillary foam cells, podocyte hypertrophy and extracellular matrix accumulation in the mesangium, often presented with an adhesion between the capillary tuft and the Bowman capsule (Rosenberg and Kopp, 2017) (**Figure 1**). Tubulointerstitial scarring is usually associated with glomerular disease and its presence in kidney biopsies with MC lesion suggests FSGS presence on unsampled glomeruli (Rosenberg and Kopp, 2017). Indeed, sampling constitutes an issue in FSGS, as distribution of segmental sclerosis starts in the juxtamedullary glomeruli and progresses towards the outer cortex at later disease stages (Rosenberg and Kopp, 2017). In addition, focality of sclerotic lesions is greater in children than in adults (Fogo, 2015).

Positive staining for IgM and C3 may be revealed by immunofluorescence, and it is believed to represent macromolecular trapping rather than specific deposition (De Vriese et al., 2021). On ultrastructural analysis, electron-dense material may be found in the mesangium and in the subendothelial compartment, consistent with hyalinosis (Barisoni et al., 2007).

FSGS is a pattern of injury shared by different diseases with variable clinical courses. To address this heterogeneity, the first attempt to classify FSGS relied on pathologic presentation describing five variants (D'Agati et al., 2004): the perihilar variant, with FSGS lesion located at the vascular pole; the tip lesion variant, with lesion located at the urinary pole; the cellular variant, characterized by endocapillary hypercellularity; the collapsing variant, characterized by collapse of the capillary tuft with epithelial cell hypertrophy and hyperplasia; and lastly FSGS not otherwise specified if lesions do not fit in the other variants mentioned (D'Agati et al., 2004). Unfortunately, with the exception of the tip lesion variant, which is usually associated with response to steroid treatment, the other variants have not provided sufficient help in patient stratification, mostly because the not otherwise specified variant represents by far the most frequent one. However, the common feature of FSGS is absolute or relative podocyte depletion as also demonstrated by the presence of podocyturia in FSGS patients (Szeto et al., 2015).

Why—Experimental Evidence

Podocyte injury is a major trigger of glomerulosclerosis but alone may not be sufficient to cause sclerosis as observed in the MC lesion. Additional cellular processes, including podocyte detachment are necessary to reach a critical threshold of podocyte depletion (Wharram et al., 2005), after which glomerulosclerosis occurs. The FSGS lesion is not due to a specific glomerular disease. Indeed, several conditions are well-described causative insults that lead to podocyte depletion such as hyperglycemia and insulin signaling, mechanical stress, angiotensin II, calcium signaling, viral infection, toxins, oxidants, and immunological injury (Zhong et al., 2019). Thus, a wide range of disease states can lead to the development of the FSGS injury pattern, the common denominator being that the initiating events take place in podocytes. FSGS animal models provided the proof-of-concept that podocyte depletion is a major factor mediating proteinuria and glomerulosclerosis. In particular, in the DT model, 21–40% podocyte depletion showed mesangial expansion, capsular adhesions, focal segmental glomerulosclerosis, mild persistent proteinuria and normal renal function, while more than 40% podocyte depletion showed segmental to global glomerulosclerosis with sustained high-grade proteinuria and reduced renal function (Wharram et al., 2005). Nevertheless, following podocyte loss, subsequent local responses are also critical for segmental sclerosis to occur. Indeed, following loss of podocyte coverage due to death or detachment, the uncovered glomerular basement membrane loses structural support by overlying podocytes at these sites (Jefferson and Shankland, 2014). Consequently, the capillary loop may bulge toward the Bowman capsule and an early connection, tuft adhesion, forms between PECs and the uncovered glomerular basement membrane or between podocytes and PECs (Löwen et al., 2021). As a response, PECs become focally activated, *de novo* express the specific markers CD9 and CD44 (Okamoto et al., 2013; Lazareth et al., 2019; Ito et al., 2020), migrate to a visceral location and deposit matrix. Interestingly, the CD44 marker is scarcely expressed by PECs in human MC lesion and may represent a useful marker to distinguish the MC and FSGS lesions in human biopsies (Smeets et al., 2014; Kuppe et al., 2015).

Several studies suggested that the presence of PECs on the glomerular tuft represents an attempt to replenish the podocyte pool (Romoli et al., 2018; Lasagni et al., 2015; Peired et al., 2013; Kaverina et al., 2019; Eng et al., 2015; Zhang et al., 2013; Kaverina et al., 2020). The capacity of a PEC subset to differentiate into podocytes and restore the podocyte number is the likely explanation for the clinical observations of remission and regression of functional parameters of chronic kidney disease in patients with diabetic and nondiabetic nephropathies (Cortinovis et al., 2016; Fioretto et al., 1998; Remuzzi et al., 2006; Takahashi et al., 2007), as well as for podocyte number restoration observed in response to pharmacological treatment in experimental models of diabetic and non-diabetic kidney disease (Zhang et al., 2012; Hudkins et al., 2020; Zhang et al., 2015). Recent results elucidated the podocyte-progenitor cross-talk revealing mediators of progenitor quiescence during homeostasis and mechanisms by which podocyte loss triggers the activation of the progenitor population in the setting of podocyte injury (Peired et al., 2021). In addition, they also provide possible explanation of why in certain conditions podocyte replacement by PECs may not be successful and lead

to development of the FSGS lesion (Peired et al., 2021). In healthy conditions, the constitutive production of CXCL12 by podocytes maintains local podocyte progenitors in a quiescent state (Romoli et al., 2018), while the reduced expression of CXCL12 consequent to podocyte loss, promotes activation, migration and differentiation of PECs into podocytes (Romoli et al., 2018). Podocyte loss also permits the passage through the damaged glomerular filtration barrier of circulating retinol that is subsequently transformed into the Bowman space in retinoic acid that acts as an inducer of progenitor differentiation into podocytes (Peired et al., 2013; Zhang et al., 2012; Dai et al., 2017). The availability of retinoic acid for PECs is strongly reduced in the presence of a high-grade proteinuria, due to the retinoic acid sequestration operated by albumin in the Bowman space (Peired et al., 2013), with a consequent inefficient progenitor-to-podocyte differentiation. This observation likely explains the well-known clinical observation that high proteinuria associates with FSGS progression, while reduction of proteinuria by renin-angiotensin system blockers retards progression and restores podocyte number (Fogo, 2015; Boffa et al., 2003; Ma et al., 2005). Interestingly, increasing progenitor responsiveness to retinoic acid signaling through pharmacological approaches, such as administration of 6-bromo-indirubin-3′-oxime, mitigates glomerulosclerosis progression in non-diabetic (Lasagni et al., 2015) and diabetic mouse models (Motrapu et al., 2020), demonstrating that the progenitor-to-podocyte axis is a potential therapeutic target. PEC differentiation into podocytes appears strongly dependent on mechanical conditions present inside the glomerulus, such as its stiffness (Melica et al., 2019), that changes during the course of several diseases (Embry et al., 2018; Wyss et al., 2011) and precedes the appearance of glomerular sclerosis, as observed in the early phase of a HIV-associated nephropathy model (Embry et al., 2018). In conclusion, the FSGS pattern represents the pathology expression of a scar generated by a chronic podocyte loss (Motrapu et al., 2020) that exceeds the capacity for podocyte replacement provided by PECs, either because the podocyte loss is severe or because the capacity of PECs to differentiate into podocytes is hampered by an excessive proteinuria or an altered glomerular basement membrane stiffness (**Table 1**). Interestingly, juxtamedullary nephrons that show low numbers of PECs with progenitor capacity are particularly sensitive to development of sclerosis (Romoli et al., 2018) while superficial and mid-cortical nephrons harbor a higher number of podocyte progenitors, explaining the reported increased regenerative capacity of these glomeruli, and their resistance to development of FSGS lesions (Romoli et al., 2018). However, when podocyte loss overcomes PEC capacity of regeneration, glomerular basement membrane denudation occurs followed by synechia formation and ultimately sclerosis resulting in FSGS pattern (**Figure 1**).

COLLAPSING GLOMERULOPATHY

How—Pathology

CG is a pathology pattern characterized by the presence of segmental capillary tuft collapse (wrinkling and folding) in at least one glomerulus, in association with podocyte hypertrophy and/or hyperplasia (D'Agati et al., 2004). The Columbia classification had the merit to recognize the collapsing pattern as part of the same family of FSGS (D'Agati et al., 2004). Afterwards, terminology has evolved in collapsing glomerulopathy to underline the rapid and catastrophic collapsing nature of the pathological process. CG is histologically defined by the formation of a pseudocrescent, i.e., a massive proliferation of cuboidal undifferentiated epithelial cell in the Bowman space, leading to a collapse of the capillary loops, regardless of the extracellular matrix accumulation eventually leading to focal and global glomerulosclerosis (Muehlig et al., 2021) (**Figure 1**). This pattern of injury represents a common endpoint from multiple etiologies (APOL1 risk variants, infections, drugs, ischemia, hematologic neoplasia and autoimmune disease), suggesting a common pathological mechanism rather than a specific cause (Nicholas Cossey et al., 2017).

Why—Experimental Evidence

Immunohistochemistry and ultrastructural studies suggested that a primary damage to podocytes alone is sufficient to initiate the events underlying the formation of pseudocrescents (Henderson et al., 2008). Although the swollen and proliferating abnormal cells within the Bowman space involved in pseudocrescent formation lacked the expression of podocyte markers, they were previously regarded as "dysregulated or dedifferentiated" podocytes that had re-entered the cell cycle to proliferate (Barisoni et al., 1999). This assumption was mostly based on their occasional positivity for the cell cycle marker Ki67. However, positivity for Ki67 indicates cell cycle entry and not necessarily mitosis (Lazzeri et al., 2019). Indeed, after injury, podocytes can re-enter the S phase of the cell cycle (Frank et al., 2022) to undergo hypertrophy, and stain for Ki67 (Marshall and Shankland, 2006). However, if they are forced to bypass the G2/M cell cycle checkpoint, podocytes undergo aberrant mitosis and consequent detachment or death for mitotic catastrophe (Barisoni et al., 2000; Suzuki et al., 2009; Lasagni et al., 2013; Liapis et al., 2013; Al Hussain et al., 2017). Thus, consistent with their status of highly differentiated post-mitotic cells, staining for cell cycle markers in podocytes should not be interpreted as a sign of mitosis. On the contrary, it may be suggestive of an endoreplication process as shown in multiple organs (Lazzeri et al., 2019; Bischof et al., 2021).

A typical clinical condition associated with collapsing pattern of injury at kidney biopsy is viral-mediated nephropathy, such as that observed with HIV, Parvovirus and SARS-CoV-2 infection (Muehlig et al., 2021). Pseudocrescents, collapse of the capillary loops and podocyte multinucleation are predominant features of HIV-associated nephropathy (Barisoni et al., 2000; Suzuki et al., 2009; Lasagni et al., 2013; Liapis et al., 2013; Al Hussain et al., 2017). Indeed, virus-induced podocyte mitosis is catastrophic and induces podocyte death. In addition, immunohistochemical studies in idiopathic, HIV-associated, and pamidronate-associated CG have shown that cells comprising the pseudocrescents in human biopsies express proteins characteristic of PECs, such as cytokeratin, Pax2, CD24, and

specific glycosylated isoform of CD133 (glycCD133), suggesting that cells within the pseudocrescents have a parietal epithelial rather than podocyte origin (Dijkman et al., 2005; Dijkman et al., 2006; Smeets et al., 2009). Lineage tracing by genetic tagging employing both podocyte and PEC-specific reporter mice in a model mimicking CG finally proved that hyperplastic cells were not podocyte-derived, but of PEC origin (Suzuki et al., 2009). Moreover, a recent multiomics study reported that podocyte-specific knockdown of Krüppel-like factor 4 contributes to podocyte loss triggering the activation of a distinct PEC subpopulation, suggesting that in this disorder PEC proliferation and pseudocrescent formation represent a response to podocyte injury and loss (Pace et al., 2021).

Experimental evidence demonstrated that, collapsing nephropathy and pseudocrescents originate from the proliferation of a specific PEC subpopulation expressing CD133 and Pax2 markers and representing renal progenitor cells that abnormally shift their reactions from reparative to detrimental (Yang et al., 2002; Smeets et al., 2004). It is unclear which factors are responsible for tilting the balance. It was proposed that pseudocrescents originate from PEC progenitors as a dysregulated response to the massive and fast podocyte detachment occurring in conditions of direct podocyte injury caused by drugs exposure, immune-mediated disorders or viral infections that cause a fast, massive podocyte loss leading to capillary collapse (Al Hussain et al., 2017; Kopp et al., 2020). In viral glomerulopathies, type I interferons (IFNs) are important mediators of viral infection (Anders et al., 2010). Indeed, in the biopsy of a patient with monogenic type I interferonopathy, MxA, a protein involved in antiviral immunity and induced by type I IFNs, was selectively expressed in CD133 positive PECs but not in podocytes (Fenaroli et al., 2021). *In vivo*, in a model of Adriamycin nephropathy, the injection of either IFN-α and IFN-β aggravated proteinuria and glomerulosclerosis and correlated not only with the triggering of local inflammation inside the glomerulus but also with a direct effect on podocytes and PECs (Migliorini et al., 2013). IFN- β specifically promoted podocyte loss by inducing mitotic catastrophe in podocytes (Migliorini et al., 2013). IFN- α affected PEC proliferation and migration (Migliorini et al., 2013). Both IFNs also impaired the differentiation of renal progenitors into mature podocytes, a mechanism that favors focal scarring over glomerular repair (Migliorini et al., 2013). Collapsing glomerulopathy has also been described in patients receiving exogenous IFN therapy administered for various medical conditions (Markowitz et al., 2010), further confirming that IFNs are critical mediators of the collapsing pattern of injury. Moreover, a growing body of evidence supports the role of IFNs as inducers of CG in individuals with the APOL1 high-risk genotype (Abid et al., 2020). APOL1 risk variants G1 and G2 are known to result in risk for kidney disease in patients of African ancestry and associate with a heterogeneous pattern of injury. Collapsing glomerulopathy is the most fulminant pattern of injury associated with APOL1-nephropathy (Abid et al., 2020). This form of glomerulopathy is observed mostly in diseases that have increased IFN levels, such as HIV infection and systemic lupus erythematosus (Larsen et al., 2013; Abid et al., 2020; Goyal and Singhal, 2021). APOL1 regulates PEC molecular phenotype through modulation of miR-193a expression through reciprocal feedback (Kumar et al., 2018). Indeed, PEC differentiation into podocytes is accompanied by a decrease in miR-193a expression (Kietzmann et al., 2015). Similarly, the suppression of miR-193a enhances APOL1 expression (Jessee and Kopp, 2018). Taken altogether, these observations suggest that the expression of APOL1 in PECs contributes to their differentiation into podocytes and the absence of APOL1 promotes PEC phenotype maintenance (Kumar et al., 2018). These data support the hypothesis that in the presence of massive and fast podocyte detachment observed in the collapsing pattern of injury, APOL1 risk variants aggravate the clinical outcome by hampering *de novo* formation of podocytes. Rapid and massive podocyte loss does not allow a mesangial adaptive response and abruptly stimulates the podocyte-progenitor feedback (Kietzmann et al., 2015; Jessee and Kopp, 2018; Kumar et al., 2018; Goyal and Singhal, 2021). The PEC compartment responds promptly with proliferation but it fails to complete the differentiation process towards mature podocytes. This results in obliteration of Bowman capsule with immature elements further compressing the glomerular tuft that lacks support from external and internal sides (**Figure 1** and **Table 1**).

CONCLUSIONS

Altogether, these observations suggest that podocytopathies represent a complex group of disorders of the glomerular epithelial compartment, where the equilibrium between the nature, the length and the severity of podocyte injury as well as the efficiency of the repair response provided by PECs ultimately determines the pattern of injury observed at the biopsy as well as renal prognosis. A variety of genetic variants contributes to both podocyte injury and PEC repair response affecting kidney disease progression. Standard pathology techniques are not able to identify the ongoing evolution of these alterations but merely show the histological appearance that results from the process. In MC lesion only the slit diaphragm is damaged, and the structural alterations are reversible, either because the podocyte is not lost, or because PECs succeed in differentiating into new podocytes and maintaining full coverage of the filtration barrier. In FSGS, the balance between podocyte injury and replacement is lost, triggering a vicious circle where proteinuria prevents PEC progenitor cells from appropriately facing podocyte loss. In contrast, if PECs succeed in generating new podocytes, scar formation can be contained and limited to a certain extent. However, this high

regenerative potential is restricted to a specific and relatively short age span, explaining why DMS is observed only in children. Finally, a fast and massive podocyte loss determining the collapse of the glomerular capillary loops is the key mechanism of CG. The ability of PECs to proliferate is retained, but the capacity to differentiate into mature podocytes is prevented, causing massive PEC activation, ultimately resulting in pseudocrescents that are typical of CG. Understanding the molecular and cellular alterations that lead to the generation of these patterns of injury can help the clinicians to convey the right diagnosis and the researchers to identify novel potential therapeutic targets for podocytopathies.

AUTHOR CONTRIBUTIONS

All authors listed have made a substantial, direct, and intellectual contribution to the work and approved it for publication.

FUNDING

This study was supported by the European Research Council (ERC) under the European Union's Horizon 2020 research and innovation programme (grant agreement N° 101019891, SIMPOSION). M.E.M. was supported by a FIRC-AIRC fellowship for Italy.

REFERENCES

Abid, Q., Best Rocha, A., Larsen, C. P., Schulert, G., Marsh, R., Yasin, S., et al. (2020). APOL1-Associated Collapsing Focal Segmental Glomerulosclerosis in a Patient with Stimulator of Interferon Genes (STING)-Associated Vasculopathy with Onset in Infancy (SAVI). *Am. J. Kidney Dis.* 75, 287–290. doi:10.1053/j.ajkd.2019.07.010

Ahn, W., and Bomback, A. S. (2020). Approach to Diagnosis and Management of Primary Glomerular Diseases Due to Podocytopathies in Adults: Core Curriculum 2020. *Am. J. Kidney Dis.* 75, 955–964. doi:10.1053/j.ajkd.2019.12.019

Al Hussain, T., Al Mana, H., Hussein, M. H., and Akhtar, M. (2017). Podocyte and Parietal Epithelial Cell Interactions in Health and Disease. *Adv. Anat. Pathol.* 24, 24–34. doi:10.1097/pap.0000000000000125

Anders, H.-J., Lichtnekert, J., and Allam, R. (2010). Interferon-α and -β in Kidney Inflammation. *Kidney Int.* 77, 848–854. doi:10.1038/ki.2010.71

Angelotti, M. L., Antonelli, G., Conte, C., and Romagnani, P. (2021). Imaging the Kidney: from Light to Super-resolution Microscopy. *Nephrol. Dial. Transpl.* 36, 19–28. doi:10.1093/ndt/gfz136

Appel, D., Kershaw, D. B., Smeets, B., Yuan, G., Fuss, A., Frye, B., et al. (2009). Recruitment of Podocytes from Glomerular Parietal Epithelial Cells. *J. Am. Soc. Nephrol.* 20, 333–343. doi:10.1681/asn.2008070795

Artelt, N., Siegerist, F., Ritter, A. M., Grisk, O., Schlüter, R., Endlich, K., et al. (2018). Comparative Analysis of Podocyte Foot Process Morphology in Three Species by 3D Super-resolution Microscopy. *Front. Med.* 5, 292. doi:10.3389/fmed.2018.00292

Atchison, D. K., O'Connor, C. L., Menon, R., Otto, E. A., Ganesh, S. K., Wiggins, R. C., et al. (2020). Hypertension Induces Glomerulosclerosis in Phospholipase C-E1 Deficiency. *Am. J. Physiology-Renal Physiol.* 318, F1177–F1187. doi:10.1152/ajprenal.00541.2019

Banu, K., Lin, Q., Basgen, J. M., Planoutene, M., Wei, C., Reghuvaran, A. C., et al. (2021). AMPK Mediates Regulation of Glomerular Volume and Podocyte Survival. *JCI Insight* 6, e150004. doi:10.1172/jci.insight.150004

Barisoni, L., Kriz, W., Mundel, P., and D'Agati, V. (1999). The Dysregulated Podocyte Phenotype. *J. Am. Soc. Nephrol.* 10, 51–61. doi:10.1681/asn.v10151

Barisoni, L., Mokrzycki, M., Sablay, L., Nagata, M., Yamase, H., and Mundel, P. (2000). Podocyte Cell Cycle Regulation and Proliferation in Collapsing Glomerulopathies. *Kidney Int.* 58, 137–143. doi:10.1046/j.1523-1755.2000.00149.x

Barisoni, L., Schnaper, H. W., and Kopp, J. B. (2007). A Proposed Taxonomy for the Podocytopathies: a Reassessment of the Primary Nephrotic Diseases. *Clin. J. Am. Soc. Nephrol.* 2, 529–542. doi:10.2215/cjn.04121206

Bertram, J. F., Douglas-Denton, R. N., Diouf, B., Hughson, M. D., and Hoy, W. E. (2011). Human Nephron Number: Implications for Health and Disease. *Pediatr. Nephrol.* 26, 1529–1533. doi:10.1007/s00467-011-1843-8

Bischof, C., Mirtschink, P., Yuan, T., Wu, M., Zhu, C., Kaur, J., et al. (2021). Mitochondrial-cell Cycle Cross-Talk Drives Endoreplication in Heart Disease. *Sci. Transl Med.* 13, eabi7964. doi:10.1126/scitranslmed.abi7964

Boffa, J.-J., Lu, Y., Placier, S., Stefanski, A., Dussaule, J.-C., and Chatziantoniou, C. (2003). Regression of Renal Vascular and Glomerular Fibrosis: Role of Angiotensin II Receptor Antagonism and Matrix Metalloproteinases. *J. Am. Soc. Nephrol.* 14, 1132–1144. doi:10.1097/01.asn.0000060574.38107.3b

Boyer, O., Benoit, G., Gribouval, O., Nevo, F., Pawtowski, A., Bilge, I., et al. (2010). Mutational Analysis of the PLCE1 Gene in Steroid Resistant Nephrotic Syndrome. *J. Med. Genet.* 47, 445–452. doi:10.1136/jmg.2009.076166

Calizo, R. C., Bhattacharya, S., van Hasselt, J. G. C., Wei, C., Wong, J. S., Wiener, R. J., et al. (2019). Disruption of Podocyte Cytoskeletal Biomechanics by Dasatinib Leads to Nephrotoxicity. *Nat. Commun.* 10, 2061. doi:10.1038/s41467-019-09936-x

Charnaya, O., and Moudgil, A. (2017). Hypertension in the Pediatric Kidney Transplant Recipient. *Front. Pediatr.* 5, 86. doi:10.3389/fped.2017.00086

Chugh, S. S., Clement, L. C., and Macé, C. (2012). New Insights into Human Minimal Change Disease: Lessons from Animal Models. *Am. J. Kidney Dis.* 59, 284–292. doi:10.1053/j.ajkd.2011.07.024

Chung, J.-J., Goldstein, L., Chen, Y.-J. J., Lee, J., Webster, J. D., Roose-Girma, M., et al. (2020). Single-Cell Transcriptome Profiling of the Kidney Glomerulus Identifies Key Cell Types and Reactions to Injury. *J. Am. Soc. Nephrol.* 31, 2341–2354. doi:10.1681/asn.2020020220

Cortinovis, M., Ruggenenti, P., and Remuzzi, G. (2016). Progression, Remission and Regression of Chronic Renal Diseases. *Nephron* 134, 20–24. doi:10.1159/000445844

D'Agati, V. D., Fogo, A. B., Bruijn, J. A., and Jennette, J. C. (2004). Pathologic Classification of Focal Segmental Glomerulosclerosis: a Working Proposal. *Am. J. Kidney Dis.* 43, 368–382. doi:10.1053/j.ajkd.2003.10.024

da Silva, C. A., Monteiro, M. L. G. d. R., Araújo, L. S., Urzedo, M. G., Rocha, L. B., Dos Reis, M. A., et al. (2020). *In Situ* evaluation of Podocytes in Patients with Focal Segmental Glomerulosclerosis and Minimal Change Disease. *PLoS One* 15, e0241745. doi:10.1371/journal.pone.0241745

Dai, Y., Chen, A., Liu, R., Gu, L., Sharma, S., Cai, W., et al. (2017). Retinoic Acid Improves Nephrotoxic Serum-Induced Glomerulonephritis through Activation of Podocyte Retinoic Acid Receptor α. *Kidney Int.* 92, 1444–1457. doi:10.1016/j.kint.2017.04.026

De Vriese, A. S., Sethi, S., Nath, K. A., Glassock, R. J., and Fervenza, F. C. (2018). Differentiating Primary, Genetic, and Secondary FSGS in Adults: A Clinicopathologic Approach. *J. Am. Soc. Nephrol.* 29, 759–774. doi:10.1681/asn.2017090958

De Vriese, A. S., Wetzels, J. F., Glassock, R. J., Sethi, S., and Fervenza, F. C. (2021). Therapeutic Trials in Adult FSGS: Lessons Learned and the Road Forward. *Nat. Rev. Nephrol.* 17, 619–630. doi:10.1038/s41581-021-00427-1

Deegens, J. K. J., Dijkman, H. B. P. M., Borm, G. F., Steenbergen, E. J., van den Berg, J. G., Weening, J. J., et al. (2008). Podocyte Foot Process Effacement as a Diagnostic Tool in Focal Segmental Glomerulosclerosis. *Kidney Int.* 74, 1568–1576. doi:10.1038/ki.2008.413

Dijkman, H. B. P. M., Weening, J. J., Smeets, B., Verrijp, K. C. N., van Kuppevelt, T. H., Assmann, K. K. J. M., et al. (2006). Proliferating Cells in HIV and Pamidronate-Associated Collapsing Focal Segmental Glomerulosclerosis Are Parietal Epithelial Cells. *Kidney Int.* 70, 338–344. doi:10.1038/sj.ki.5001574

Dijkman, H., Smeets, B., van der Laak, J., Steenbergen, E., and Wetzels, J. (2005). The Parietal Epithelial Cell Is Crucially Involved in Human Idiopathic Focal Segmental glomerulosclerosis11See Editorial by Schwartz, P. 1894. *Kidney Int.* 68, 1562–1572. doi:10.1111/j.1523-1755.2005.00568.x

Embry, A. E., Liu, Z., Henderson, J. M., Byfield, F. J., Liu, L., Yoon, J., et al. (2018). Similar Biophysical Abnormalities in Glomeruli and Podocytes from Two Distinct Models. *J. Am. Soc. Nephrol.* 29, 1501–1512. doi:10.1681/asn.2017050475

Eng, D. G., Sunseri, M. W., Kaverina, N. V., Roeder, S. S., Pippin, J. W., and Shankland, S. J. (2015). Glomerular Parietal Epithelial Cells Contribute to Adult Podocyte Regeneration in Experimental Focal Segmental Glomerulosclerosis. *Kidney Int.* 88, 999–1012. doi:10.1038/ki.2015.152

Eymael, J., Sharma, S., Loeven, M. A., Wetzels, J. F., Mooren, F., Florquin, S., et al. (2018). CD44 Is Required for the Pathogenesis of Experimental Crescentic Glomerulonephritis and Collapsing Focal Segmental Glomerulosclerosis. *Kidney Int.* 93, 626–642. doi:10.1016/j.kint.2017.09.020

Fatima, H., Moeller, M. J., Smeets, B., Yang, H.-C., D'Agati, V. D., Alpers, C. E., et al. (2012). Parietal Epithelial Cell Activation Marker in Early Recurrence of FSGS in the Transplant. *Clin. J. Am. Soc. Nephrol.* 7, 1852–1858. doi:10.2215/cjn.10571011

Fenaroli, P., Rossi, G. M., Angelotti, M. L., Antonelli, G., Volpi, S., Grossi, A., et al. (2021). Collapsing Glomerulopathy as a Complication of Type I Interferon-Mediated Glomerulopathy in a Patient with RNASEH2B-Related Aicardi-Goutières Syndrome. *Am. J. Kidney Dis.* 78, 750–754. doi:10.1053/j.ajkd.2021.02.330

Fioretto, P., Steffes, M. W., Sutherland, D. E. R., Goetz, F. C., and Mauer, M. (1998). Reversal of Lesions of Diabetic Nephropathy after Pancreas Transplantation. *N. Engl. J. Med.* 339, 69–75. doi:10.1056/nejm199807093390202

Fogo, A. B. (2015). Causes and Pathogenesis of Focal Segmental Glomerulosclerosis. *Nat. Rev. Nephrol.* 11, 76–87. doi:10.1038/nrneph.2014.216

Fogo, A. B. (2001). Progression and Potential Regression of Glomerulosclerosis. *Kidney Int.* 59, 804–819. doi:10.1046/j.1523-1755.2001.059002804.x

Fogo, A., Hawkins, E. P., Berry, P. L., Glick, A. D., Chiang, M. L., MacDonell, R. C., Jr., et al. (1990). Glomerular Hypertrophy in Minimal Change Disease Predicts Subsequent Progression to Focal Glomerular Sclerosis. *Kidney Int.* 38, 115–123. doi:10.1038/ki.1990.175

Frank, C. N., Hou, X., Petrosyan, A., Villani, V., Zhao, R., Hansen, J. R., et al. (2022). Effect of Disease Progression on the Podocyte Cell Cycle in Alport Syndrome. *Kidney Int.* 101, 106–118. doi:10.1016/j.kint.2021.08.026

Freedman, B. I., Langefeld, C. D., Andringa, K. K., Croker, J. A., Williams, A. H., Garner, N. E., et al. (2014). End-Stage Renal Disease in African Americans with Lupus Nephritis Is Associated WithAPOL1. *Arthritis Rheumatol.* 66, 390–396. doi:10.1002/art.38220

Fukuda, A., Chowdhury, M. A., Venkatareddy, M. P., Wang, S. Q., Nishizono, R., Suzuki, T., et al. (2012b). Growth-dependent Podocyte Failure Causes Glomerulosclerosis. *J. Am. Soc. Nephrol.* 23, 1351–1363. doi:10.1681/asn.2012030271

Fukuda, A., Wickman, L. T., Venkatareddy, M. P., Sato, Y., Chowdhury, M. A., Wang, S. Q., et al. (2012a). Angiotensin II-dependent Persistent Podocyte Loss from Destabilized Glomeruli Causes Progression of End Stage Kidney Disease. *Kidney Int.* 81, 40–55. doi:10.1038/ki.2011.306

Goyal, R., and Singhal, P. C. (2021). APOL1 Risk Variants and the Development of HIV-associated Nephropathy. *FEBS J.* 288, 5586–5597. doi:10.1111/febs.15677

Habib, R., and Kleinknecht, C. (1971). The Primary Nephrotic Syndrome of Childhood. Classification and Clinicopathologic Study of 406 Cases. *Pathol. Annu.* 6, 417–474.

Henderson, J. M., Al-Waheeb, S., Weins, A., Dandapani, S. V., and Pollak, M. R. (2008). Mice with Altered α-actinin-4 Expression Have Distinct Morphologic Patterns of Glomerular Disease. *Kidney Int.* 73, 741–750. doi:10.1038/sj.ki.5002751

Hinkes, B., Wiggins, R. C., Gbadegesin, R., Vlangos, C. N., Seelow, D., Nürnberg, G., et al. (2006). Positional Cloning Uncovers Mutations in PLCE1 Responsible for a Nephrotic Syndrome Variant that May Be Reversible. *Nat. Genet.* 38, 1397–1405. doi:10.1038/ng1918

Hudkins, K. L., Wietecha, T. A., Steegh, F., and Alpers, C. E. (2020). Beneficial Effect on Podocyte Number in Experimental Diabetic Nephropathy Resulting from Combined Atrasentan and RAAS Inhibition Therapy. *Am. J. Physiology-Renal Physiol.* 318, F1295–F1305. doi:10.1152/ajprenal.00498.2019

Ikezumi, Y., Suzuki, T., Karasawa, T., Kaneko, U., Yamada, T., Hasegawa, H., et al. (2014). Glomerular Epithelial Cell Phenotype in Diffuse Mesangial Sclerosis: a Report of 2 Cases with Markedly Increased Urinary Podocyte Excretion. *Hum. Pathol.* 45, 1778–1783. doi:10.1016/j.humpath.2014.03.017

Ito, N., Sakamoto, K., Hikichi, C., Matsusaka, T., and Nagata, M. (2020). Biphasic MIF and SDF1 Expression during Podocyte Injury Promote CD44-Mediated Glomerular Parietal Cell Migration in Focal Segmental Glomerulosclerosis. *Am. J. Physiology-Renal Physiol.* 318, F741–F753. doi:10.1152/ajprenal.00414.2019

Jefferson, J. A., and Shankland, S. J. (2014). The Pathogenesis of Focal Segmental Glomerulosclerosis. *Adv. Chronic Kidney Dis.* 21, 408–416. doi:10.1053/j.ackd.2014.05.009

Jessee, J., and Kopp, J. B. (2018). APOL1-miR-193 Axis as a Bifunctional Regulator of the Glomerular Parietal Epithelium. *Am. J. Pathol.* 188, 2461–2463. doi:10.1016/j.ajpath.2018.08.002

Kaverina, N. V., Eng, D. G., Freedman, B. S., Kutz, J. N., Chozinski, T. J., Vaughan, J. C., et al. (2019). Dual Lineage Tracing Shows that Glomerular Parietal Epithelial Cells Can Transdifferentiate toward the Adult Podocyte Fate. *Kidney Int.* 96, 597–611. doi:10.1016/j.kint.2019.03.014

Kaverina, N. V., Eng, D. G., Miner, J. H., Pippin, J. W., and Shankland, S. J. (2020). Parietal Epithelial Cell Differentiation to a Podocyte Fate in the Aged Mouse Kidney. *Aging* 12, 17601–17624. doi:10.18632/aging.103788

Kietzmann, L., Guhr, S. S. O., Meyer, T. N., Ni, L., Sachs, M., Panzer, U., et al. (2015). MicroRNA-193a Regulates the Transdifferentiation of Human Parietal Epithelial Cells toward a Podocyte Phenotype. *J. Am. Soc. Nephrol.* 26, 1389–1401. doi:10.1681/asn.2014020190

Kim, Y. H., Goyal, M., Kurnit, D., Wharram, B., Wiggins, J., Holzman, L., et al. (2001). Podocyte Depletion and Glomerulosclerosis Have a Direct Relationship in the PAN-Treated Rat. *Kidney Int.* 60, 957–968. doi:10.1046/j.1523-1755.2001.060003957.x

Kopp, J. B., Anders, H.-J., Susztak, K., Podestà, M. A., Remuzzi, G., Hildebrandt, F., et al. (2020). Podocytopathies. *Nat. Rev. Dis. Primers* 6, 68. doi:10.1038/s41572-020-0196-7

Kriz, W., and Lemley, K. V. (2017b). Mechanical Challenges to the Glomerular Filtration Barrier: Adaptations and Pathway to Sclerosis. *Pediatr. Nephrol.* 32, 405–417. doi:10.1007/s00467-016-3358-9

Kriz, W., and Lemley, K. V. (2017a). Potential Relevance of Shear Stress for Slit Diaphragm and Podocyte Function. *Kidney Int.* 91, 1283–1286. doi:10.1016/j.kint.2017.02.032

Kumar, V., Vashistha, H., Lan, X., Chandel, N., Ayasolla, K., Shoshtari, S. S. M., et al. (2018). Role of Apolipoprotein L1 in Human Parietal Epithelial Cell Transition. *Am. J. Pathol.* 188, 2508–2528. doi:10.1016/j.ajpath.2018.07.025

Kuppe, C., Gröne, H.-J., Ostendorf, T., van Kuppevelt, T. H., Boor, P., Floege, J., et al. (2015). Common Histological Patterns in Glomerular Epithelial Cells in Secondary Focal Segmental Glomerulosclerosis. *Kidney Int.* 88, 990–998. doi:10.1038/ki.2015.116

Lahdenkari, A.-T., Lounatmaa, K., Patrakka, J., Holmberg, C., Wartiovaara, J., Kestila, M., et al. (2004). Podocytes Are Firmly Attached to Glomerular Basement Membrane in Kidneys with Heavy Proteinuria. *J. Am. Soc. Nephrol.* 15, 2611–2618. doi:10.1097/01.asn.0000139478.03463.d9

Landini, S., Mazzinghi, B., Becherucci, F., Allinovi, M., Provenzano, A., Palazzo, V., et al. (2020). Reverse Phenotyping after Whole-Exome Sequencing in Steroid-Resistant Nephrotic Syndrome. *Clin. J. Am. Soc. Nephrol.* 15, 89–100. doi:10.2215/cjn.06060519

Larsen, C. P., Beggs, M. L., Saeed, M., and Walker, P. D. (2013). Apolipoprotein L1 Risk Variants Associate with Systemic Lupus Erythematosus-Associated Collapsing Glomerulopathy. *J. Am. Soc. Nephrol.* 24, 722–725. doi:10.1681/asn.2012121180

Lasagni, L., Angelotti, M. L., Ronconi, E., Lombardi, D., Nardi, S., Peired, A., et al. (2015). Podocyte Regeneration Driven by Renal Progenitors Determines Glomerular Disease Remission and Can Be Pharmacologically Enhanced. *Stem Cel Rep.* 5, 248–263. doi:10.1016/j.stemcr.2015.07.003

Lasagni, L., Lazzeri, E., J. Shankland, S., Anders, H.-J., and Romagnani, P. (2013). Podocyte Mitosis - a Catastrophe. *Curr. Mol. Med.* 13, 13–23. doi:10.2174/156652413804486250

Lazareth, H., Henique, C., Lenoir, O., Puelles, V. G., Flamant, M., Bollée, G., et al. (2019). The Tetraspanin CD9 Controls Migration and Proliferation of Parietal Epithelial Cells and Glomerular Disease Progression. *Nat. Commun.* 10, 3303. doi:10.1038/s41467-019-11013-2

Lazzeri, E., Angelotti, M. L., Conte, C., Anders, H.-J., and Romagnani, P. (2019). Surviving Acute Organ Failure: Cell Polyploidization and Progenitor Proliferation. *Trends Mol. Med.* 25, 366–381. doi:10.1016/j.molmed.2019.02.006

Lehnhardt, A., Karnatz, C., Ahlenstiel-Grunow, T., Benz, K., Benz, M. R., Budde, K., et al. (2015). Clinical and Molecular Characterization of Patients with Heterozygous Mutations in Wilms Tumor Suppressor Gene 1. *Clin. J. Am. Soc. Nephrol.* 10, 825–831. doi:10.2215/cjn.10141014

Liapis, H., Romagnani, P., and Anders, H.-J. (2013). New Insights into the Pathology of Podocyte Loss. *Am. J. Pathol.* 183, 1364–1374. doi:10.1016/j.ajpath.2013.06.033

Lin, M.-H., Miller, J. B., Kikkawa, Y., Suleiman, H. Y., Tryggvason, K., Hodges, B. L., et al. (2018). Laminin-521 Protein Therapy for Glomerular Basement Membrane and Podocyte Abnormalities in a Model of Pierson Syndrome. *J. Am. Soc. Nephrol.* 29, 1426–1436. doi:10.1681/asn.2017060690

Löwen, J., Gröne, E. F., Gross-Weissmann, M.-L., Bestvater, F., Gröne, H.-J., and Kriz, W. (2021). Pathomorphological Sequence of Nephron Loss in Diabetic Nephropathy. *Am. J. Physiology-Renal Physiol.* 321, F600–F616. doi:10.1152/ajprenal.00669.2020

Ma, L.-J., Nakamura, S., Aldigier, J. C., Rossini, M., Yang, H., Liang, X., et al. (2005). Regression of Glomerulosclerosis with High-Dose Angiotensin Inhibition Is Linked to Decreased Plasminogen Activator Inhibitor-1. *J. Am. Soc. Nephrol.* 16, 966–976. doi:10.1681/asn.2004060492

Maas, R. J., Deegens, J. K., Smeets, B., Moeller, M. J., and Wetzels, J. F. (2016). Minimal Change Disease and Idiopathic FSGS: Manifestations of the Same Disease. *Nat. Rev. Nephrol.* 12, 768–776. doi:10.1038/nrneph.2016.147

Markowitz, G. S., Nasr, S. H., Stokes, M. B., and D'Agati, V. D. (2010). Treatment with IFN-α, -β, or -γ Is Associated with Collapsing Focal Segmental Glomerulosclerosis. *Clin. J. Am. Soc. Nephrol.* 5, 607–615. doi:10.2215/cjn.07311009

Marshall, C. B., and Shankland, S. J. (2006). Cell Cycle and Glomerular Disease: a Minireview. *Nephron Exp. Nephrol.* 102, e39–e48. doi:10.1159/000088400

Matejas, V., Hinkes, B., Alkandari, F., Al-Gazali, L., Annexstad, E., Aytac, M. B., et al. (2010). Mutations in the Human Laminin β2 (LAMB2) Gene and the Associated Phenotypic Spectruma. *Hum. Mutat.* 31, 992–1002. doi:10.1002/humu.21304

Melica, M. E., La Regina, G., Parri, M., Peired, A. J., Romagnani, P., and Lasagni, L. (2019). Substrate Stiffness Modulates Renal Progenitor Cell Properties via a ROCK-Mediated Mechanotransduction Mechanism. *Cells* 8, 1561. doi:10.3390/cells8121561

Migliorini, A., Angelotti, M. L., Mulay, S. R., Kulkarni, O. O., Demleitner, J., Dietrich, A., et al. (2013). The Antiviral Cytokines IFN-α and IFN-β Modulate Parietal Epithelial Cells and Promote Podocyte Loss. *Am. J. Pathol.* 183, 431–440. doi:10.1016/j.ajpath.2013.04.017

Motrapu, M., Świderska, M. K., Mesas, I., Marschner, J. A., Lei, Y., Martinez Valenzuela, L., et al. (2020). Drug Testing for Residual Progression of Diabetic Kidney Disease in Mice beyond Therapy with Metformin, Ramipril, and Empagliflozin. *J. Am. Soc. Nephrol.* 31, 1729–1745. doi:10.1681/asn.2019070703

Muehlig, A. K., Gies, S., Huber, T. B., and Braun, F. (2021). Collapsing Focal Segmental Glomerulosclerosis in Viral Infections. *Front. Immunol.* 12, 800074. doi:10.3389/fimmu.2021.800074

Munk, F. (1918). *Pathologie und klinik der Nephrosen, Nephritiden und Schrumpfnieren*. Berlin, Wien: Urban & Schwarzenberg.

Nagata, M. (2016). Podocyte Injury and its Consequences. *Kidney Int.* 89, 1221–1230. doi:10.1016/j.kint.2016.01.012

Nicholas Cossey, L., Larsen, C. P., and Liapis, H. (2017). Collapsing Glomerulopathy: a 30-year Perspective and Single, Large center Experience. *Clin. Kidney J.* 10, 443–449. doi:10.1093/ckj/sfx029

Okamoto, T., Sasaki, S., Yamazaki, T., Sato, Y., Ito, H., and Ariga, T. (2013). Prevalence of CD44-Positive Glomerular Parietal Epithelial Cells Reflects Podocyte Injury in Adriamycin Nephropathy. *Nephron Exp. Nephrol.* 124, 11–18. doi:10.1159/000357356

Pace, J. A., Bronstein, R., Guo, Y., Yang, Y., Estrada, C. C., Gujarati, N., et al. (2021). Podocyte-specific KLF4 Is Required to Maintain Parietal Epithelial Cell Quiescence in the Kidney. *Sci. Adv.* 7, eabg6600. doi:10.1126/sciadv.abg6600

Patrakka, J., Lahdenkari, A.-T., Koskimies, O., Holmberg, C., Wartiovaara, J., and Jalanko, H. (2002). The Number of Podocyte Slit Diaphragms Is Decreased in Minimal Change Nephrotic Syndrome. *Pediatr. Res.* 52, 349–355. doi:10.1203/00006450-200209000-00007

Peired, A., Angelotti, M. L., Ronconi, E., la Marca, G., Mazzinghi, B., Sisti, A., et al. (2013). Proteinuria Impairs Podocyte Regeneration by Sequestering Retinoic Acid. *J. Am. Soc. Nephrol.* 24, 1756–1768. doi:10.1681/asn.2012090950

Peired, A. J., Melica, M. E., Molli, A., Nardi, C., Romagnani, P., and Lasagni, L. (2021). Molecular Mechanisms of Renal Progenitor Regulation: How Many Pieces in the Puzzle. *Cells* 10, 59. doi:10.3390/cells10010059

Pippin, J. W., Brinkkoetter, P. T., Cormack-Aboud, F. C., Durvasula, R. V., Hauser, P. V., Kowalewska, J., et al. (2009). Inducible Rodent Models of Acquired Podocyte Diseases. *Am. J. Physiology-Renal Physiol.* 296, F213–F229. doi:10.1152/ajprenal.90421.2008

Puelles, V. G., van der Wolde, J. W., Wanner, N., Scheppach, M. W., Cullen-McEwen, L. A., Bork, T., et al. (2019). mTOR-mediated Podocyte Hypertrophy Regulates Glomerular Integrity in Mice and Humans. *JCI Insight* 4, e99271. doi:10.1172/jci.insight.99271

Puelles, V. G., Douglas-Denton, R. N., Cullen-McEwen, L. A., Li, J., Hughson, M. D., Hoy, W. E., et al. (2015). Podocyte Number in Children and Adults: Associations with Glomerular Size and Numbers of Other Glomerular Resident Cells. *J. Am. Soc. Nephrol.* 26, 2277–2288. doi:10.1681/asn.2014070641

Purohit, S., Piani, F., Ordoñez, F. A., de Lucas-Collantes, C., Bauer, C., and Cara-Fuentes, G. (2021). Molecular Mechanisms of Proteinuria in Minimal Change Disease. *Front. Med.* 8, 761600. doi:10.3389/fmed.2021.761600

Ratelade, J., Arrondel, C., Hamard, G., Garbay, S., Harvey, S., Biebuyck, N., et al. (2010). A Murine Model of Denys-Drash Syndrome Reveals Novel Transcriptional Targets of WT1 in Podocytes. *Hum. Mol. Genet.* 19, 1–15. doi:10.1093/hmg/ddp462

Remuzzi, G., Benigni, A., and Remuzzi, A. (2006). Mechanisms of Progression and Regression of Renal Lesions of Chronic Nephropathies and Diabetes. *J. Clin. Invest.* 116, 288–296. doi:10.1172/jci27699

Charles Jennette, J., Olson, J. L., Silva, F. G., and D'Agati, V. D. (2014). eds. 7th edition. 2014. Lippincott Williams8Wilki.

Romoli, S., Angelotti, M. L., Antonelli, G., Kumar Vr, S., Mulay, S. R., Desai, J., et al. (2018). CXCL12 Blockade Preferentially Regenerates Lost Podocytes in Cortical Nephrons by Targeting an Intrinsic Podocyte-Progenitor Feedback Mechanism. *Kidney Int.* 94, 1111–1126. doi:10.1016/j.kint.2018.08.013

Rosenberg, A. Z., and Kopp, J. B. (2017). Focal Segmental Glomerulosclerosis. *Clin. J. Am. Soc. Nephrol.* 12, 502–517. doi:10.2215/cjn.05960616

Royal, V., Zee, J., Liu, Q., Avila-Casado, C., Smith, A. R., Liu, G., et al. (2020). Ultrastructural Characterization of Proteinuric Patients Predicts Clinical Outcomes. *J. Am. Soc. Nephrol.* 31, 841–854. doi:10.1681/asn.2019080825

Saga, N., Sakamoto, K., Matsusaka, T., and Nagata, M. (2021). Glomerular Filtrate Affects the Dynamics of Podocyte Detachment in a Model of Diffuse Toxic Podocytopathy. *Kidney Int.* 99, 1149–1161. doi:10.1016/j.kint.2020.12.034

Smeets, B., Angelotti, M. L., Rizzo, P., Dijkman, H., Lazzeri, E., Mooren, F., et al. (2009). Renal Progenitor Cells Contribute to Hyperplastic Lesions of Podocytopathies and Crescentic Glomerulonephritis. *J. Am. Soc. Nephrol.* 20, 2593–2603. doi:10.1681/asn.2009020132

Smeets, B., Stucker, F., Wetzels, J., Brocheriou, I., Ronco, P., Gröne, H.-J., et al. (2014). Detection of Activated Parietal Epithelial Cells on the Glomerular Tuft Distinguishes Early Focal Segmental Glomerulosclerosis from Minimal Change Disease. *Am. J. Pathol.* 184, 3239–3248. doi:10.1016/j.ajpath.2014.08.007

Smeets, B., Te Loeke, N. A., Dijkman, H. B., Steenbergen, M. L., Lensen, J. F., Begieneman, M. P., et al. (2004). The Parietal Epithelial Cell: a Key Player in the Pathogenesis of Focal Segmental Glomerulosclerosis in Thy-1.1 Transgenic Mice. *J. Am. Soc. Nephrol.* 15, 928–939. doi:10.1097/01.asn.0000120559.09189.82

Suzuki, T., Matsusaka, T., Nakayama, M., Asano, T., Watanabe, T., Ichikawa, I., et al. (2009). Genetic Podocyte Lineage Reveals Progressive Podocytopenia with Parietal Cell Hyperplasia in a Murine Model of Cellular/collapsing Focal Segmental Glomerulosclerosis. *Am. J. Pathol.* 174, 1675–1682. doi:10.2353/ajpath.2009.080789

Szeto, C.-C., Wang, G., Chow, K.-M., Lai, F. M.-M., Ma, T. K.-W., Kwan, B. C.-H., et al. (2015). Podocyte mRNA in the Urinary Sediment of Minimal Change Nephropathy and Focal Segmental Glomerulosclerosis. *Clin. Nephrol.* 84, 198–205. doi:10.5414/cn108607

Takahashi, H., Ichihara, A., Kaneshiro, Y., Inomata, K., Sakoda, M., Takemitsu, T., et al. (2007). Regression of Nephropathy Developed in Diabetes by (Pro)renin Receptor Blockade. *J. Am. Soc. Nephrol.* 18, 2054–2061. doi:10.1681/asn.2006080820

Tejani, A. (1985). Morphological Transition in Minimal Change Nephrotic Syndrome. *Nephron* 39, 157–159. doi:10.1159/000183363

Tesch, F., Siegerist, F., Hay, E., Artelt, N., Daniel, C., Amann, K., et al. (2021). Super-resolved Local Recruitment of CLDN5 to Filtration Slits Implicates a Direct Relationship with Podocyte Foot Process Effacement. *J. Cel Mol Med* 25, 7631–7641. doi:10.1111/jcmm.16519

Vivarelli, M., Massella, L., Ruggiero, B., and Emma, F. (2017). Minimal Change Disease. *Clin. J. Am. Soc. Nephrol.* 12, 332–345. doi:10.2215/cjn.05000516

Wanner, N., Hartleben, B., Herbach, N., Goedel, M., Stickel, N., Zeiser, R., et al. (2014). Unraveling the Role of Podocyte Turnover in Glomerular Aging and Injury. *J. Am. Soc. Nephrol.* 25, 707–716. doi:10.1681/asn.2013050452

Warejko, J. K., Tan, W., Daga, A., Schapiro, D., Lawson, J. A., Shril, S., et al. (2018). Whole Exome Sequencing of Patients with Steroid-Resistant Nephrotic Syndrome. *Clin. J. Am. Soc. Nephrol.* 13, 53–62. doi:10.2215/cjn.04120417

Watts, A., Keller, K., Lerner, G., Rosales, I., Collins, A., Sekulic, M., et al. (2021). Discovery of Autoantibodies Targeting Nephrin in Minimal Change Disease Supports a Novel Autoimmune Etiology. *J. Am. Soc. Nephrol.* 33, 238–252. doi:10.1681/asn.2021060794

Wharram, B. L., Goyal, M., Wiggins, J. E., Sanden, S. K., Hussain, S., Filipiak, W. E., et al. (2005). Podocyte Depletion Causes Glomerulosclerosis: Diphtheria Toxin-Induced Podocyte Depletion in Rats Expressing Human Diphtheria Toxin Receptor Transgene. *J. Am. Soc. Nephrol.* 16, 2941–2952. doi:10.1681/asn.2005010055

Wiggins, R.-C. (2007). The Spectrum of Podocytopathies: a Unifying View of Glomerular Diseases. *Kidney Int.* 71, 1205–1214. doi:10.1038/sj.ki.5002222

Wyss, H. M., Henderson, J. M., Byfield, F. J., Bruggeman, L. A., Ding, Y., Huang, C., et al. (2011). Biophysical Properties of normal and Diseased Renal Glomeruli. *Am. J. Physiology-Cell Physiol.* 300, C397–C405. doi:10.1152/ajpcell.00438.2010

Yang, H.-C., and Fogo, A. B. (2014). Mechanisms of Disease Reversal in Focal and Segmental Glomerulosclerosis. *Adv. Chronic Kidney Dis.* 21, 442–447. doi:10.1053/j.ackd.2014.04.001

Yang, Y., Gubler, M.-C., and Beaufils, H. (2002). Dysregulation of Podocyte Phenotype in Idiopathic Collapsing Glomerulopathy and HIV-Associated Nephropathy. *Nephron* 91, 416–423. doi:10.1159/000064281

Yang, Y., Jeanpierre, C., Dressler, G. R., Lacoste, M., Niaudet, P., and Gubler, M.-C. (1999). WT1 and PAX-2 Podocyte Expression in Denys-Drash Syndrome and Isolated Diffuse Mesangial Sclerosis. *Am. J. Pathol.* 154, 181–192. doi:10.1016/s0002-9440(10)65264-9

Zhang, J., Pippin, J. W., Krofft, R. D., Naito, S., Liu, Z.-H., and Shankland, S. J. (2013). Podocyte Repopulation by Renal Progenitor Cells Following Glucocorticoids Treatment in Experimental FSGS. *Am. J. Physiology-Renal Physiol.* 304, F1375–F1389. doi:10.1152/ajprenal.00020.2013

Zhang, J., Pippin, J. W., Vaughan, M. R., Krofft, R. D., Taniguchi, Y., Romagnani, P., et al. (2012). Retinoids Augment the Expression of Podocyte Proteins by Glomerular Parietal Epithelial Cells in Experimental Glomerular Disease. *Nephron Exp. Nephrol.* 121, e23–e37. doi:10.1159/000342808

Zhang, J., Yanez, D., Floege, A., Lichtnekert, J., Krofft, R. D., Liu, Z.-H., et al. (2015). ACE-inhibition Increases Podocyte Number in Experimental Glomerular Disease Independent of Proliferation. *J. Renin Angiotensin Aldosterone Syst.* 16, 234–248. doi:10.1177/1470320314543910

Zhong, J., Whitman, J. B., Yang, H.-C., and Fogo, A. B. (2019). Mechanisms of Scarring in Focal Segmental Glomerulosclerosis. *J. Histochem. Cytochem.* 67, 623–632. doi:10.1369/0022155419850170

Conflict of Interest: The authors declare that the research was conducted in the absence of any commercial or financial relationships that could be construed as a potential conflict of interest.

Publisher's Note: All claims expressed in this article are solely those of the authors and do not necessarily represent those of their affiliated organizations, or those of the publisher, the editors and the reviewers. Any product that may be evaluated in this article, or claim that may be made by its manufacturer, is not guaranteed or endorsed by the publisher.

frontiers in Cell and Developmental Biology

PERSPECTIVE
published: 03 March 2022
doi: 10.3389/fcell.2022.854998

Cell Hypertrophy: A "Biophysical Roadblock" to Reversing Kidney Injury

Angelo Michele Lavecchia[1], *Kostas Pelekanos*[2], *Fabio Mavelli*[3] *and Christodoulos Xinaris*[1]*

[1]Laboratory of Organ Regeneration, Department of Molecular Medicine, Istituto di Ricerche Farmacologiche Mario Negri IRCCS, Centro Anna Maria Astori, Bergamo, Italy, [2]Independent scholar, Nicosia, Cyprus, [3]Department of Chemistry, University of Bari Aldo Moro, Bari, Italy

In anamniotes cell loss can typically be compensated for through proliferation, but in amniotes, this capacity has been significantly diminished to accommodate tissue complexity. In order to cope with the increased workload that results from cell death, instead of proliferation highly specialised post-mitotic cells undergo polyploidisation and hypertrophy. Although compensatory hypertrophy is the main strategy of repair/regeneration in various parenchymal tissues, the long-term benefits and its capacity to sustain complete recovery of the kidney has not been addressed sufficiently. In this perspective article we integrate basic principles from biophysics and biology to examine whether renal cell hypertrophy is a sustainable adaptation that can efficiently regenerate tissue mass and restore organ function, or a maladaptive detrimental response.

Keywords: hypertrophy, regeneration, metabolism, podocytes, proximal tubular epithelial cells, kidney injury

OPEN ACCESS

Edited by:
Hans Kristian Lorenzo, Université Paris-Saclay, France

Reviewed by:
Elena Lazzeri, University of Florence, Italy

***Correspondence:**
Christodoulos Xinaris
christodoulos.xinaris@marionegri.it

Specialty section:
This article was submitted to Cell Death and Survival, a section of the journal Frontiers in Cell and Developmental Biology

Received: *14 January 2022*
Accepted: *10 February 2022*
Published: *03 March 2022*

Citation:
Lavecchia AM, Pelekanos K, Mavelli F and Xinaris C (2022) Cell Hypertrophy: A "Biophysical Roadblock" to Reversing Kidney Injury. Front. Cell Dev. Biol. 10:854998. doi: 10.3389/fcell.2022.854998

INTRODUCTION

In response to injury, anamniotes–i.e., fish and amphibians–compensate for cell loss through proliferation and differentiation, which allows them to partially or completely regenerate tissues and organs (Brockes and Kumar, 2008; Gemberling et al., 2013). Adult mammals, on the other hand, have lost this capacity, partially due to endothermy (Hirose et al., 2019; Nguyen et al., 2021), and because of the cumulative structural and functional complexity of organs (Jaźwińska and Sallin, 2016). In response to injuries, the highly specialised and terminally differentiated cells of mammalian organs, in order to cope with the increased workload, typically undergo hypertrophy and/or polyploidisation. This allows complex organs, such as the mammalian kidney, to deal with the increased workload without significantly compromising structure and function, which makes this trait vital for tissues where the architecture is implicitly and linearly correlated with function.

In response to injury, podocytes undergo polyploidy by DNA synthesis and G2/M arrest, and grow in size until they eventually coat the areas that were depleted (Najafian et al., 2011; Lasagni et al., 2013; Benedetti et al., 2019). Interestingly, recent studies have proposed that detached podocytes can be replaced by neighbouring podocyte progenitors. Two podocyte progenitor pools have been proposed: parietal epithelial cells (PECs) (Sagrinati et al., 2006; Appel et al., 2009) and cells of renin lineage (CoRL) (Pippin et al., 2015; Eng et al., 2018). Although the common developmental programme of PECs and podocytes (Grouls et al., 2012; Meyer-Schwesinger, 2016) can partially justify the ability of PEC progenitors to transdifferentiate into podocytes, their substantial involvement in glomerulus repopulation has been inconsistent (Berger et al., 2014; Wanner et al., 2014). Furthermore, a number of studies have suggested not only that PECs are not involved in podocyte regeneration, but that they contribute to the development of crescent, glomerulosclerosis and extracapillary proliferation (Smeets et al., 2004; Smeets et al., 2011; Gaut et al., 2014; Sakamoto et al., 2014). Studies in CoRL have also

provided conflicting results and, most importantly, have not shown through which developmental programme CoRL can transdifferentiate into podocytes (Meyer-Schwesinger, 2016). Finally, very recent studies–which support earlier evidence that renin cells are pericytes (Brunskill et al., 2011; Stefanska et al., 2016)—have shown that CoRL transdifferentiated exclusively to mesangial cells (Steglich et al., 2020). We could consider several variables in any attempt to explain these inconsistencies, such as intrinsic methodological differences in species and models, the timing of analysis, and the severity of injury/disease–but so far, the main recovery mechanism of injured glomeruli seems to be podocyte hypertrophy.

Hypertrophy has also been associated with tubular injury–the most common cause of acute kidney injury (AKI). AKI is typically reversible because the mammalian renal tubule has conserved an extraordinary capacity for regeneration. The dominant dogma is that tubular regeneration after AKI can be achieved thanks to the surviving epithelial cells, which dedifferentiate, proliferate, migrate, and re-differentiate into newly generated tubular cells (Vogetseder et al., 2008; Chang-Panesso et al., 2019). However, recent studies have proposed that renal functional recovery after AKI occurs mainly through tubular cell hypertrophy, and with a minimal contribution from resident progenitor cells (Lazzeri et al., 2018). While the conundrum of tubular repair/regeneration is still being investigated vigorously, the presence of hypertrophy in proximal tubules has long been demonstrated in several models (Wolf et al., 1993; Kobayashi et al., 1995), indicating that under certain conditions (in terms of the type, severity and duration of the stress) proximal tubular epithelial cells (PTECs) undergo hypertrophy to replenish the lost tissue mass. Either if we accept that dedifferentiated proximal tubule epithelial or intratubular progenitor cells are responsible for cell replacement, hypertrophy may depend on stimulus intensity: mild stimuli may cause reversible damage that is completely repaired through proliferation, while stronger stimuli that cause extensive cell depletion may induce hypertrophy of surviving cells to grow and restore critical tissue mass.

The above findings suggest that podocytes and proximal tubular cells share some common mechanisms of response to injury, including hypertrophy and possibly a limited contribution by progenitor cells. One crucial question that has not been investigated sufficiently is whether renal cell hypertrophy is a long-standing repair/regeneration adaptation. If so, tissue mass replacement and organ recovery could indeed be mediated by hypertrophy, which would otherwise be a maladaptation and incompatible with reversibility after injury and complete recovery. Here we will try to address this question by examining podocyte and PTEC hypertrophy from the biophysic and energetic perspectives.

WHY DOES THE SIZE OF CELLS MATTER?

A cell can be considered an open chemical reactor that uses the energy input from the environment in the form of light radiation, nutrients, osmotic gradient and electrostatic potential to sustain an internal metabolic network that transforms nutrients into all the cell constituents, and at the same time produces heat, osmotic work and by-products. These are in turn exchanged with the environment in order to maintain homeostasis and keep a tissue/organ at a constant temperature.

Now we will examine whether hypertrophy of surviving cells can lead the organ to a better or poorer homeostatic condition compared to the original condition.

For the sake of simplicity, we will consider a section of an organ with a volume V as an assembly of cells in a spherical shape (**Figure 1A**) with an average radius r_0. Therefore, if the cells are identical, the number of cells that form the organ section can be estimated using the relationship:

$$V = n\left(\frac{4}{3}\pi r_0^3\right) \tag{1}$$

while the total surface area of the cell membrane will be:

$$A_0 = n\left(4\pi r_0^2\right) \tag{2}$$

If we assume that a number k of cells is now lost, to maintain the volume of the organ section constant the neighbouring cells must grow and occupy the empty volume. Therefore, now each cell will exhibit a larger radius r so the volume of this section is:

$$V = (n-k)\frac{4}{3}\pi r^3 \tag{3}$$

From relations **Eqs 1**, **3** we deduce:

$$r = \left(\frac{n}{n-k}\right)^{\frac{1}{3}} r_0 \tag{4}$$

So now the total area A of the cell membrane will be:

$$A = (n-k)4\pi r^2 \tag{5}$$

Dividing A_0/A we get:

$$\frac{A_0}{A} = \left(\frac{n}{n-k}\right)^{\frac{1}{3}} \tag{6}$$

Since $(\frac{n}{n-k}) > 1$ we deduce that $A < A_0$, that is, while the total volume of the organ section V remains constant, which corresponds to the overall volume of the cells, the total membrane surface of the cell assembly is reduced.

It is important to highlight that both the substrate transport and the heat transfer in a cell occur through its membrane towards and from the environment, and the rate of these processes is therefore proportional to the cell surface area. Hence, a section of an organ which consists of a high number of small cells is more efficient in conserving a homeostatic condition than the same section with a lower number of larger cells (**Figure 1A**).

Scaling down to the level of a single cell, it is important to underline that cells need catalysts (enzymes), which enable chemical reactions to take place in a reasonable timeframe, to maintain the organ's function and structure in a condition of homeostatis (Himeoka and Kaneko, 2014). From this point of

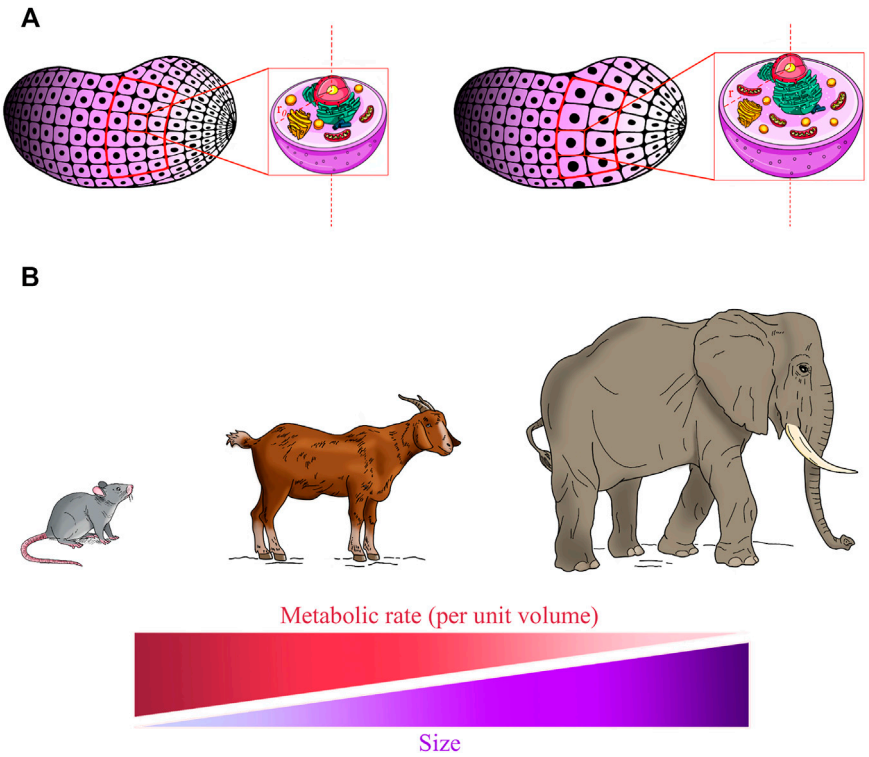

FIGURE 1 | Living system's size affects homeostatic balance and metabolic rate. **(A)** An ideal condition in which an organ section consists of "*n*" identical spherical cells with an average radius "r_O" (left panel, red frame). In response to injury, the surviving cells grow to radius "*r*" (right panel, red frame) to compensate for tissue loss. As the cell grows bigger, the volume increases more rapidly (r^3) than does the surface area (r^2), and so the relative amount of surface area available to pass materials to a unit volume of the cell decreases. As the tissue section remains constant, the total membrane surface of the cells is reduced and this results in the decreased efficiency of the tissue in preserving homeostasis. Moreover, intracellular transport distances and diffusion times of oxygen and nutrients are increased and the metabolic rate decreased, negatively affecting overall cell efficiency in conserving cellular homeostatic conditions. **(B)** Allometric laws are among the most fundamental features of life and it is believed that they can be applied to all size scales. Allometric scaling of the metabolism predicts that the metabolic rate per mass unit declines with the increase in size in living systems.

view there are two key factors that enable cells to achieve a stationary condition within a reasonable timeframe: (i) nutrient flow through the membrane, in order to have enough energy input and (ii) maintenance of catalyst abundance.

Assuming that when the cell grows in volume it maintains a constant density of enzymes–that is, the number of enzymes scales with the volume–this means the enzymatic rate per unit volume remains the same. Thus, if a cell increases its volume by a factor of $\lambda_v \equiv (\frac{v}{v_0}) = (\frac{r}{r_0})^3$, v_o being the initial volume and r_0 being the initial radius, then the nutrient flow f through the membrane should grow by at least the same factor:

$$f \sim \lambda v f_0 \tag{7}$$

to sustain the internal metabolism at the same homeostatic condition. On the other hand, if cells keep the spherical shape, the area of the membrane grows only by a factor of $\lambda_A \equiv (\frac{a}{a_0}) = (\frac{r}{r_0})^2$ with a_0 being the initial surface area of the single cell.

$$\frac{\lambda_v}{\lambda_A} = \frac{r}{r_0} > 1 \tag{8}$$

Since the flow through a surface is proportional to the surface area, we can claim that as a cell grows in volume, it is harder to satisfy relation **Eq. 7** because of relation **Eq. 8** and thus the cell cannot remain as metabolically efficient, under conditions of homeostasis, as the original smaller cells.

Each internal region of the cell must be served (in terms of nutrients and oxygen) by a part of the cell surface. As the cell grows bigger, its internal volume enlarges and the cell membrane expands; however, the volume increases more rapidly (r^3) than does the surface area (r^2), and so the relative amount of surface area available to pass materials to a unit volume (surface-to-volume ratio) of the cell steadily decreases. Thus, less and less material will be able to cross the membrane quickly enough to accommodate the increased cellular volume.

To better illustrate this effect, a simple metabolic pathway involving three enzymes and supported by the flow of nutrient N from the outside is presented in **Figure 2A**. N diffuses across the cell membrane at rate b_N and is then converted to the intermediate M by the first enzyme with rate v_1. In turn M can be converted into metabolites P or Q by the second and the

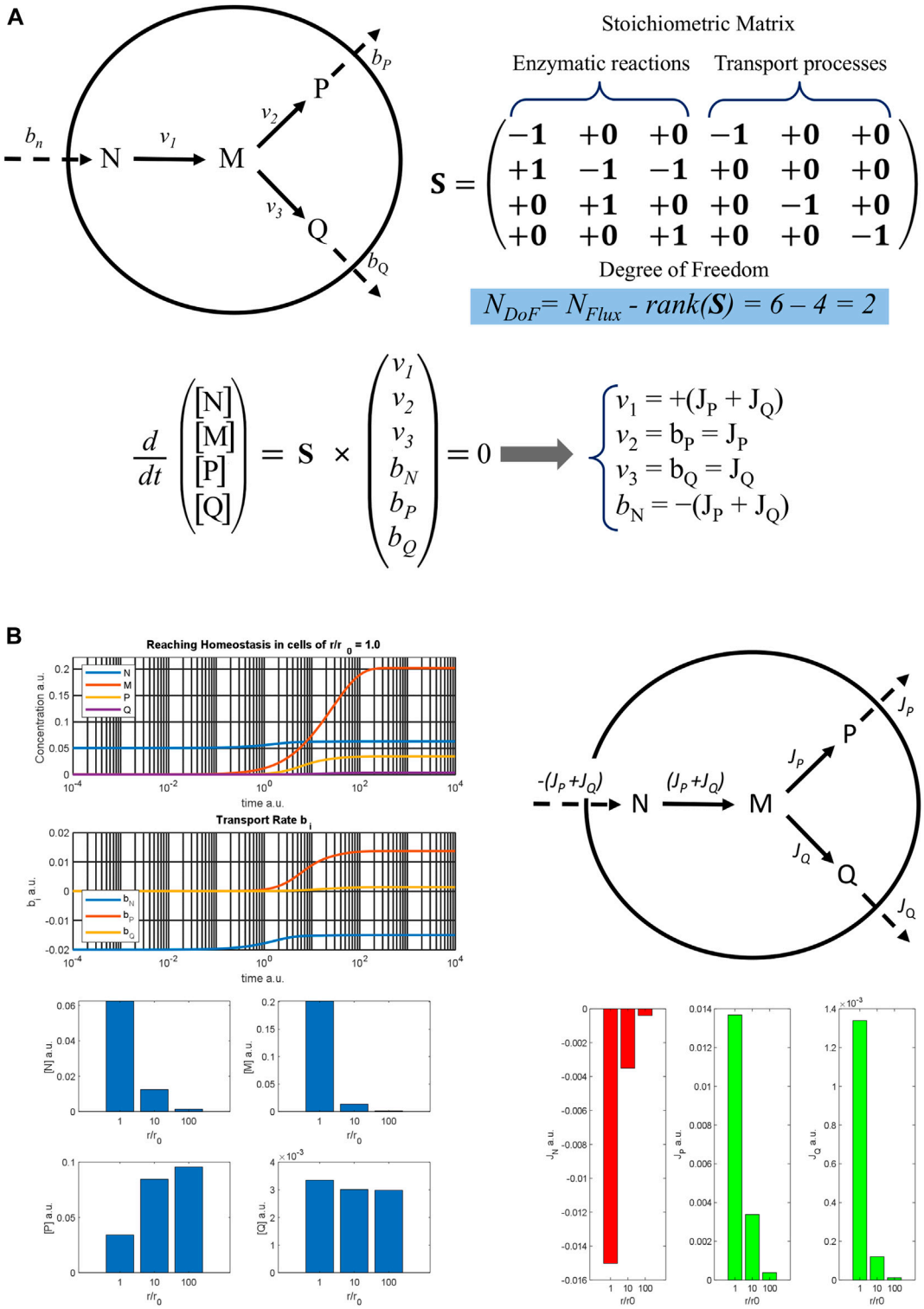

FIGURE 2 | Metabolic model of a three-enzyme pathway **(A)** A three-enzyme metabolic pathway model is reported with the result of the flux balance analysis. The rank of the stoichiometric matrix **S** is 4, so that the degree of freedom of the algebraic system obtained by applying the stationary condition for homeostasis is 2. Therefore, only two fluxes, J_P and J_Q must be determined to know the stationary rates of all the processes at homeostasis. **(B)** On the top left, the time courses of the metabolite concentrations and of the rates of the transport processes are reported against time, showing a cell with a normal radius r_0 as it reaches homeostasis; on the top right, a metabolic map with the flux distribution at homeostasis is sketched; on the bottom left, stationary concentrations of different metabolites are shown, and on the bottom right the values of the fluxes are reported as diverse histograms for cells with an increasing ratio of r/r_0.

third enzymes, with rates v_2 and v_3, respectively, according to the metabolic map. It is assumed that P and Q diffuse through the cell surface with b_P and b_Q transport rates, while the cell membrane is impermeable to the intermediate M. Analysing the stoichiometric matrix, the degree of freedom of this metabolic pathway is 2, which means that only two fluxes (i.e., process rates in stationary conditions) must be determined to define all the process velocities at homeostasis. The distribution of the fluxes on the metabolic map is reported at the top right of **Figure 2B**, showing the input flux of the nutrient N, negative value, and the two outflows of the metabolites P and Q, positive values.

Based on this metabolic map, a dynamic model was implemented assuming a reversible Michaelis-Menten kinetic mechanism for each enzyme and using some hypothetical parameters. The time trend of metabolite concentrations and transport rates is reported at the top left of **Figure 2B**. The graph shows that the system reaches a stable stationary condition, which is cellular homeostasis. Assuming a spherical shape and increasing the cellular radius r, the dynamic simulation was repeated for r/r_0 ratios equal to 10 and 100 and the homeostatic values obtained are reported in the bar graphs below. As can be seen, the outflows flux J_P and J_Q decrease markedly when the r/r_0 ratio increases, as does the absolute value of the input flux $|JN| = (J_P + J_Q)$. This determines the reduction of the steady concentration both of N and M. On the other hand, the stationary concentration values of P and Q change quite little being the reduction of the enzymatic rate, due to the decrease in [M], balanced by the reduction of the outcoming fluxes. Therefore, both the efficiency and the composition of the cell in homeostasis are perturbed by the hypertrophic growth of the cell. Moreover, the J_P/J_Q ratio also changes, going from 10.2, when $r/r_0 = 1$, to 32.0 when $r/r_0 = 100$, also exhibiting a different flux distribution at homeostasis.

It is worth mentioning that in this simple model we have not taken into account molecular diffusion in the cellular milieu by assuming these very fast processes. Indeed, the intracellular transport distances and diffusion times of oxygen and nutrients increase too, and the transport of metabolites and oxygen becomes limiting. As such, the large cells have a decreased size-normalised metabolic rate, as measured by oxygen consumption (Rubner, 1883; Kleiber, 1932). This phenomenon, known as allometric scaling of metabolism, is one of the most fundamental features of life, and is believed to apply to all size scales of biological systems (West et al., 2002; West and Brown, 2005) (**Figures 1A,B**). The size-dependent limitations in nutrient and oxygen transport impose a limit on the metabolism and thus on cell size, and as such the optimal cell size must be at a point where the metabolic (i.e., mitochondrial functionality) and cellular fitness (i.e., viability) are maximised (Miettinen and Björklund, 2016; Miettinen and Björklund, 2017). This size must perfectly reflect the optimal size for its functions (Ginzberg et al., 2015). Hence, the third claim is that the hypertrophied version of our hypothetical cell type–if it grows isometrically (in terms of cellular and organelle content; **Figure 1A**)—would in principle perform with a suboptimal metabolism, function and viability.

Based on the above claims, we can support the net thesis that for a given function or functions, a cell type has a biophysically optimal size where metabolic efficiency and cell-size-dependent homeostatic conditions are maximised. Any deviation from this size would theoretically reflect substantial alterations to cellular and organismal homeostasis.

IS HYPERTROPHY BIOPHYSICALLY AND METABOLICALLY EFFICIENT FOR PODOCYTES AND PTECS?

For podocytes and PTECs–the functions of which entail adequately covering a given area (basement membranes)—functionality is linearly correlated with their size and must be maximised at a biophysically optimal cell size. Therefore, hypertrophied podocytes and PTECs operate under kinetically unfavourable conditions and at a suboptimal metabolic rate, which makes hypertrophy incompatible with complete organ repair/regeneration and reversible injuries. As such, hypertrophy cannot be used to explain conditions where kidney function is largely restored, like typical AKI.

One could argue against these claims by maintaining that profound cellular remodelling (in terms of shape and organelles) takes place during hypertrophy, as happens during cell proliferation, to allow hypertrophic cells to perform optimally without having irreversible effects on homeostasis. It is believed that proliferating cells overcome this metabolic barrier by undergoing allometric mitochondrial remodelling (Miettinen and Björklund, 2016; Miettinen and Björklund, 2017). Although cellular protein and organelle content increases isometrically (linearly; as in the **Figure 1A**) across a wide range of cell types (Savage et al., 2007), increased mitochondrial connectivity can alleviate energy transport limitations, enabling a higher metabolic rate and larger cell size, and thus allowing cells to grow and divide. In essence, this is a transient condition that allows proliferating cells to give rise to 2 daughter cells that will inherit their mother's low metabolic rate and, as they grow, to reset their mitochondrial activity to match their size (Miettinen and Björklund, 2016; Miettinen and Björklund, 2017). Likewise, mitochondrial dynamics can explain the transient growth of skeletal muscle in response to exercise, regeneration and the growth of amphibian limbs and other cases of physiological growth (Drake et al., 2016; Qin et al., 2021). However, unlike these cell types, hypertrophied podocytes and PTECs maintain a biophysically suboptimal metabolism and size, and a permanently inefficient homeostatic status. In addition, podocytes have relatively low density of mitochondria compared to PTECs (Na et al., 2021) and their metabolism seems to be mainly based on glycolysis (Brinkkoetter et al., 2019). Although it remains intensely debated what the actual source of ATP in podocytes is (Ozawa et al., 2015; Gujarati et al., 2020; Audzeyenka et al., 2021; Na et al., 2021), based on the above premises we could safely deduce that presumptive increased mitochondrial connectivity could not have a substantial impact on metabolic functionality and cellular fitness (even if such mitochondrial remodelling existed in podocytes). On the other hand, PTECs have a high number of mitochondria and their metabolism relies mostly on beta-oxidation of fatty acids under physiological conditions (Faivre et al., 2021). During AKI PTECs undergo rapid fragmentation of mitochondria (Brooks et al., 2009; Xiao et al., 2014; Clark and Parikh, 2020) and a metabolic shift toward glycolysis (Lan et al., 2016; Faivre

et al., 2021)—which again undermines the hypothesis of mitochondria remodelling. Most importantly, the transient metabolic switch seems to be indispensable during the early phases after injury and is reversed in normally recovering tubules but, if persistent, could lead to mitochondrial dysfunction and failure in tubular repair (Lan et al., 2016). Hence, from a biophysical and energetic perspective, although renal cell hypertrophy enables tissue mass replacement, it is a roadblock to complete repair and recovery.

It has been suggested that hypertrophy is an adaptive evolutionary response that allows for tissue growth, repair and regeneration in various species and taxa. For example, mammary epithelial cells through polyploidization and hypertrophy can increase DNA and transcriptional/translational capacity to rapidly increase secretion of their products (Rios et al., 2016), while liver co-ordinately combines proliferation, stem/progenitor cell differentiation and polyploidization-mediated hypertrophy to completely restore tissue mass and function. The short lifespan and the ability of liver cells to undergo reductive mitoses and proliferate, as well as the nature of their functionality, make liver hypertrophy an excellent adaptive strategy for coping rapidly with increased workload demands or injuries (Donne et al., 2020; Matsumoto et al., 2020). On the other hand, in organs with very limited regenerative potential and strong interdependence between architecture and function, as the heart, although cell hypertrophy can temporally normalize wall tension and function, when is persistent and especially when accompanied by adoption of a low energy profile, becomes maladaptive and often leads to failure and death (Frey and Olson, 2003; Pantos et al., 2008).

Is hypertrophy an adaptation or maladaptation in the mammalian kidney? Unlike amphibians and fish, which can regenerate whole organs, terrestrial animals cannot regenerate whole nephrons *de novo* without influencing homeostasis, because of the complexity and interdependence of architecture and function. Therefore, natural selection would have favoured genes that block mitosis and orchestrate a metabolic and structural profile that would allow for growth without cytokinesis (Mourouzis et al., 2020; Mantzouratou et al., 2022). This adaptation in turn improved the reproductive value of individual organisms that were capable of renal cell hypertrophy at least until the end of their reproductive lives. After this period, the detrimental consequences of hypertrophy (e.g., fibrosis and apoptosis) are indifferent to the pressures of natural selection–as happens with many other maladaptive traits found in ageing and cancer–and for these reasons hypertrophy is a common trait in most mammalian species, despite this trade-off.

DISCUSSION

The main conclusions/deductions of our analysis are as follows: (i) podocyte hypertrophy is not a biophysically or metabolically efficient condition, but a slowly debilitating process. Moreover, as podocyte progenitors do not substantially and substantively contribute to renal repair/regeneration, we maintain that the main evolutionary adaptation for injured glomeruli is hypertrophy, which straightforwardly antagonises functionality and fitness; (ii) tubular cell hypertrophy is not a permanent solution for AKI either; the lack of evidence supporting a supposition that these cells undergo mitochondrial remodelling, which would enable them to optimally perform at a larger size, further weakens the hypothesis that hypertrophy can mediate tissue replacement in reversible tubular injuries. This, in combination with the minor contribution of progenitor cells to tubular recovery (Lazzeri et al., 2018), suggests that the main mechanisms of complete tubular recovery are not related to hypertrophy, but probably dedifferentiation/proliferation and re-differentiation instead. Tubular hypertrophy does indeed exist, but presumably it occurs as a consequence of severe injuries, resulting in a sub-critical number of surviving cells that are not able to regenerate tissue mass through proliferation.

One criticism of our analysis could be the simplicity of the model; cells are conceived of as ideal spheres and we do not take into consideration other parameters, like changes in cell shape and morphology. Nevertheless, the overarching objective was to put the general sense of hypertrophy into a kinetic/energetic perspective for our readers, in a simplified, but conceptually sturdy manner. Other biological elements (like growth factors, receptors, cytokines) are purposely not considered either, as they do not autonomously define the optimal size (Ginzberg et al., 2015). Although further mathematical and biological analyses are needed to definitely explain the role of hypertrophy in glomerular and tubular injuries and repair/regeneration, this new perspective provides a solid theoretical and conceptual platform for explaining the physiological role and evolutionary significance of hypertrophy in kidney injuries.

DATA AVAILABILITY STATEMENT

The original contributions presented in the study are included in the article/supplementary material, further inquiries can be directed to the corresponding author.

AUTHOR CONTRIBUTIONS

AL, KP, FM, CX contributed to design and writing of the study. AL contributed to the development of the biological aspect of the study and to writing the manuscript. KP and FM developed the biophysical aspect and contributed to writing the manuscript. CX conceived the central idea and wrote the manuscript. All authors contributed to manuscript revision and read and approved the submitted version.

FUNDING

AL is the recipient of a fellowship from Fondazione Aiuti per la Ricerca sulle Malattie Rare, Bergamo, Italy. AL and CX's research is funded by Euronanomed (an ERA-NET grant, EURONANOMED 2019-049/REASON), Associazione per la Ricerca sul Diabete Italia (ARDI), Fondazione Terzi-Albini.

ACKNOWLEDGMENTS

The authors wish to thank Kerstin Mierke for the excellent editing work on the manuscript and Elena Bisato for the fundamental contribution to the figure preparation.

REFERENCES

Appel, D., Kershaw, D. B., Smeets, B., Yuan, G., Fuss, A., Frye, B., et al. (2009). Recruitment of Podocytes from Glomerular Parietal Epithelial Cells. *J. Am. Soc. Nephrol.* 20, 333–343. doi:10.1681/ASN.2008070795

Audzeyenka, I., Rachubik, P., Typiak, M., Kulesza, T., Topolewska, A., Rogacka, D., et al. (2021). Hyperglycemia Alters Mitochondrial Respiration Efficiency and Mitophagy in Human Podocytes. *Exp. Cel Res.* 407, 112758. doi:10.1016/j.yexcr.2021.112758

Benedetti, V., Lavecchia, A. M., Locatelli, M., Brizi, V., Corna, D., Todeschini, M., et al. (2019). Alteration of Thyroid Hormone Signaling Triggers the Diabetes-Induced Pathological Growth, Remodeling, and Dedifferentiation of Podocytes. *JCI Insight* 4, 130249. doi:10.1172/jci.insight.130249

Berger, K., Schulte, K., Boor, P., Kuppe, C., van Kuppevelt, T. H., Floege, J., et al. (2014). The Regenerative Potential of Parietal Epithelial Cells in Adult Mice. *J. Am. Soc. Nephrol.* 25, 693–705. doi:10.1681/ASN.2013050481

Brinkkoetter, P. T., Bork, T., Salou, S., Liang, W., Mizi, A., Özel, C., et al. (2019). Anaerobic Glycolysis Maintains the Glomerular Filtration Barrier Independent of Mitochondrial Metabolism and Dynamics. *Cel Rep.* 27, 1551–1566. e5. doi:10.1016/j.celrep.2019.04.012

Brockes, J. P., and Kumar, A. (2008). Comparative Aspects of Animal Regeneration. *Annu. Rev. Cel Dev. Biol.* 24, 525–549. doi:10.1146/annurev.cellbio.24.110707.175336

Brooks, C., Wei, Q., Cho, S.-G., and Dong, Z. (2009). Regulation of Mitochondrial Dynamics in Acute Kidney Injury in Cell Culture and Rodent Models. *J. Clin. Invest.* 119, 1275–1285. doi:10.1172/JCI37829

Brunskill, E. W., Sequeira-Lopez, M. L. S., Pentz, E. S., Lin, E., Yu, J., Aronow, B. J., et al. (2011). Genes that Confer the Identity of the Renin Cell. *J. Am. Soc. Nephrol.* 22, 2213–2225. doi:10.1681/ASN.2011040401

Chang-Panesso, M., Kadyrov, F. F., Lalli, M., Wu, H., Ikeda, S., Kefaloyianni, E., et al. (2019). FOXM1 Drives Proximal Tubule Proliferation during Repair from Acute Ischemic Kidney Injury. *J. Clin. Invest.* 129, 5501–5517. doi:10.1172/JCI125519

Clark, A. J., and Parikh, S. M. (2020). Mitochondrial Metabolism in Acute Kidney Injury. *Semin. Nephrol.* 40, 101–113. doi:10.1016/j.semnephrol.2020.01.002

Donne, R., Saroul-Aïnama, M., Cordier, P., Celton-Morizur, S., and Desdouets, C. (2020). Polyploidy in Liver Development, Homeostasis and Disease. *Nat. Rev. Gastroenterol. Hepatol.* 17, 391–405. doi:10.1038/s41575-020-0284-x

Drake, J. C., Wilson, R. J., and Yan, Z. (2016). Molecular Mechanisms for Mitochondrial Adaptation to Exercise Training in Skeletal Muscle. *FASEB j.* 30, 13–22. doi:10.1096/fj.15-276337

Eng, D. G., Kaverina, N. V., Schneider, R. R. S., Freedman, B. S., Gross, K. W., Miner, J. H., et al. (2018). Detection of Renin Lineage Cell Transdifferentiation to Podocytes in the Kidney Glomerulus with Dual Lineage Tracing. *Kidney Int.* 93, 1240–1246. doi:10.1016/j.kint.2018.01.014

Faivre, A., Verissimo, T., Auwerx, H., Legouis, D., and de Seigneux, S. (2021). Tubular Cell Glucose Metabolism Shift during Acute and Chronic Injuries. *Front. Med.* 8, 742072. doi:10.3389/fmed.2021.742072

Frey, N., and Olson, E. N. (2003). Cardiac Hypertrophy: the Good, the Bad, and the Ugly. *Annu. Rev. Physiol.* 65, 45–79. doi:10.1146/annurev.physiol.65.092101.142243

Gaut, J. P., Hoshi, M., Jain, S., and Liapis, H. (2014). Claudin 1 and Nephrin Label Cellular Crescents in Diabetic Glomerulosclerosis. *Hum. Pathol.* 45, 628–635. doi:10.1016/j.humpath.2013.10.030

Gemberling, M., Bailey, T. J., Hyde, D. R., and Poss, K. D. (2013). The Zebrafish as a Model for Complex Tissue Regeneration. *Trends Genet.* 29, 611–620. doi:10.1016/j.tig.2013.07.003

Ginzberg, M. B., Kafri, R., and Kirschner, M. (2015). On Being the Right (Cell) Size. *Science* 348, 1245075. doi:10.1126/science.1245075

Grouls, S., Iglesias, D. M., Wentzensen, N., Moeller, M. J., Bouchard, M., Kemler, R., et al. (2012). Lineage Specification of Parietal Epithelial Cells Requiresβ-Catenin/Wnt Signaling. *J. Am. Soc. Nephrol.* 23, 63–72. doi:10.1681/ASN.2010121257

Gujarati, N. A., Vasquez, J. M., Bogenhagen, D. F., and Mallipattu, S. K. (2020). The Complicated Role of Mitochondria in the Podocyte. *Am. J. Physiology-Renal Physiol.* 319, F955–F965. doi:10.1152/ajprenal.00393.2020

Himeoka, Y., and Kaneko, K. (2014). Entropy Production of a Steady-Growth Cell with Catalytic Reactions. *Phys. Rev. E* 90, 042714. doi:10.1103/PhysRevE.90.042714

Hirose, K., Payumo, A. Y., Cutie, S., Hoang, A., Zhang, H., Guyot, R., et al. (2019). Evidence for Hormonal Control of Heart Regenerative Capacity during Endothermy Acquisition. *Science* 364, 184–188. doi:10.1126/science.aar2038

Jaźwińska, A., and Sallin, P. (2016). Regeneration versus Scarring in Vertebrate Appendages and Heart. *J. Pathol.* 238, 233–246. doi:10.1002/path.4644

Kleiber, M. (1932). Body Size and Metabolism. *Hilgardia* 6, 315–353. doi:10.3733/hilg.v06n11p315

Kobayashi, S., Clemmons, D. R., Nogami, H., Roy, A. K., and Venkatachalam, M. A. (1995). Tubular Hypertrophy Due to Work Load Induced by Furosemide Is Associated with Increases of IGF-1 and IGFBP-1. *Kidney Int.* 47, 818–828. doi:10.1038/ki.1995.124

Lan, R., Geng, H., Singha, P. K., Saikumar, P., Bottinger, E. P., Weinberg, J. M., et al. (2016). Mitochondrial Pathology and Glycolytic Shift during Proximal Tubule Atrophy after Ischemic AKI. *J. Am. Soc. Nephrol.* 27, 3356–3367. doi:10.1681/ASN.2015020177

Lasagni, L., Lazzeri, E., J. Shankland, S., Anders, H.-J., and Romagnani, P. (2013). Podocyte Mitosis - a Catastrophe. *Curr. Mol. Med.* 13, 13–23. doi:10.2174/156652413804486250

Lazzeri, E., Angelotti, M. L., Peired, A., Conte, C., Marschner, J. A., Maggi, L., et al. (2018). Endocycle-related Tubular Cell Hypertrophy and Progenitor Proliferation Recover Renal Function after Acute Kidney Injury. *Nat. Commun.* 9, 1344. doi:10.1038/s41467-018-03753-4

Mantzouratou, P., Lavecchia, A. M., and Xinaris, C. (2022). Thyroid Hormone Signalling in Human Evolution and Disease: A Novel Hypothesis. *J. Clin. Med.* 11, 43. doi:10.3390/jcm11010043

Matsumoto, T., Wakefield, L., Tarlow, B. D., and Grompe, M. (2020). *In Vivo* Lineage Tracing of Polyploid Hepatocytes Reveals Extensive Proliferation during Liver Regeneration. *Cell Stem Cell* 26, 34–47. e3. doi:10.1016/j.stem.2019.11.014

Meyer-Schwesinger, C. (2016). The Role of Renal Progenitors in Renal Regeneration. *Nephron* 132, 101–109. doi:10.1159/000442180

Miettinen, T. P., and Björklund, M. (2016). Cellular Allometry of Mitochondrial Functionality Establishes the Optimal Cell Size. *Develop. Cel* 39, 370–382. doi:10.1016/j.devcel.2016.09.004

Miettinen, T. P., and Björklund, M. (2017). Mitochondrial Function and Cell Size: An Allometric Relationship. *Trends Cel Biol.* 27, 393–402. doi:10.1016/j.tcb.2017.02.006

Mourouzis, I., Lavecchia, A. M., and Xinaris, C. (2020). Thyroid Hormone Signalling: From the Dawn of Life to the Bedside. *J. Mol. Evol.* 88, 88–103. doi:10.1007/s00239-019-09908-1

Na, K. R., Jeong, J. Y., Shin, J. A., Chang, Y.-K., Suh, K.-S., Lee, K. W., et al. (2021). Mitochondrial Dysfunction in Podocytes Caused by CRIF1 Deficiency Leads to Progressive Albuminuria and Glomerular Sclerosis in Mice. *Int. J. Mol. Sci.* 22, 4827. doi:10.3390/ijms22094827

Najafian, B., Alpers, C. E., and Fogo, A. B. (2011). Pathology of Human Diabetic Nephropathy. *Contrib. Nephrol.* 170, 36–47. doi:10.1159/000324942

Nguyen, P. D., de Bakker, D. E. M., and Bakkers, J. (2021). Cardiac Regenerative Capacity: an Evolutionary Afterthought? *Cell. Mol. Life Sci.* 78, 5107–5122. doi:10.1007/s00018-021-03831-9

Ozawa, S., Ueda, S., Imamura, H., Mori, K., Asanuma, K., Yanagita, M., et al. (2015). Glycolysis, but Not Mitochondria, Responsible for Intracellular ATP Distribution in Cortical Area of Podocytes. *Sci. Rep.* 5, 18575. doi:10.1038/srep18575

Pantos, C., Mourouzis, I., Xinaris, C., Papadopoulou-Daifoti, Z., and Cokkinos, D. (2008). Thyroid Hormone and "Cardiac Metamorphosis": Potential Therapeutic Implications. *Pharmacol. Ther.* 118, 277–294. doi:10.1016/j.pharmthera.2008.02.011

Pippin, J. W., Kaverina, N. V., Eng, D. G., Krofft, R. D., Glenn, S. T., Duffield, J. S., et al. (2015). Cells of Renin Lineage Are Adult Pluripotent Progenitors in Experimental Glomerular Disease. *Am. J. Physiology-Renal Physiol.* 309, F341–F358. doi:10.1152/ajprenal.00438.2014

Qin, T., Fan, C.-M., Wang, T.-Z., Sun, H., Zhao, Y.-Y., Yan, R.-J., et al. (2021). Single-cell RNA-Seq Reveals Novel Mitochondria-Related Musculoskeletal Cell Populations during Adult Axolotl Limb Regeneration Process. *Cell Death Differ* 28, 1110–1125. doi:10.1038/s41418-020-00640-8

Rios, A. C., Fu, N. Y., Jamieson, P. R., Pal, B., Whitehead, L., Nicholas, K. R., et al. (2016). Essential Role for a Novel Population of Binucleated Mammary Epithelial Cells in Lactation. *Nat. Commun.* 7, 11400. doi:10.1038/ncomms11400

Rubner, M. (1883). Ueber den Einfluss der Körpergrösse auf Stoff- und Kraftwechsel. *Z. für Biologie* 19, 535–562.

Sagrinati, C., Netti, G. S., Mazzinghi, B., Lazzeri, E., Liotta, F., Frosali, F., et al. (2006). Isolation and Characterization of Multipotent Progenitor Cells from the Bowman's Capsule of Adult Human Kidneys. *J. Am. Soc. Nephrol.* 17, 2443–2456. doi:10.1681/ASN.2006010089

Sakamoto, K., Ueno, T., Kobayashi, N., Hara, S., Takashima, Y., Pastan, I., et al. (2014). The Direction and Role of Phenotypic Transition between Podocytes and Parietal Epithelial Cells in Focal Segmental Glomerulosclerosis. *Am. J. Physiology-Renal Physiol.* 306, F98–F104. doi:10.1152/ajprenal.00228.2013

Savage, V. M., Allen, A. P., Brown, J. H., Gillooly, J. F., Herman, A. B., Woodruff, W. H., et al. (2007). Scaling of Number, Size, and Metabolic Rate of Cells with Body Size in Mammals. *Proc. Natl. Acad. Sci.* 104, 4718–4723. doi:10.1073/pnas.0611235104

Smeets, B., Kuppe, C., Sicking, E.-M., Fuss, A., Jirak, P., van Kuppevelt, T. H., et al. (2011). Parietal Epithelial Cells Participate in the Formation of Sclerotic Lesions in Focal Segmental Glomerulosclerosis. *J. Am. Soc. Nephrol.* 22, 1262–1274. doi:10.1681/ASN.2010090970

Smeets, B., Te Loeke, N. A. J. M., Dijkman, H. B. P. M., Steenbergen, M. L. M., Lensen, J. F. M., Begieneman, M. P. V., et al. (2004). The Parietal Epithelial Cell: a Key Player in the Pathogenesis of Focal Segmental Glomerulosclerosis in Thy-1.1 Transgenic Mice. *J. Am. Soc. Nephrol.* 15, 928–939. doi:10.1097/01.asn.0000120559.09189.82

Stefanska, A., Kenyon, C., Christian, H. C., Buckley, C., Shaw, I., Mullins, J. J., et al. (2016). Human Kidney Pericytes Produce Renin. *Kidney Int.* 90, 1251–1261. doi:10.1016/j.kint.2016.07.035

Steglich, A., Hickmann, L., Linkermann, A., Bornstein, S., Hugo, C., and Todorov, V. T. (2020). "Beyond the Paradigm: Novel Functions of Renin-Producing Cells," in *Reviews of Physiology, Biochemistry and Pharmacology*. Editor S. H. F. Pedersen (Cham: Springer International Publishing), 53–81. doi:10.1007/112_2020_27

Vogetseder, A., Picard, N., Gaspert, A., Walch, M., Kaissling, B., and Le Hir, M. (2008). Proliferation Capacity of the Renal Proximal Tubule Involves the Bulk of Differentiated Epithelial Cells. *Am. J. Physiology-Cell Physiol.* 294, C22–C28. doi:10.1152/ajpcell.00227.2007

Wanner, N., Hartleben, B., Herbach, N., Goedel, M., Stickel, N., Zeiser, R., et al. (2014). Unraveling the Role of Podocyte Turnover in Glomerular Aging and Injury. *J. Am. Soc. Nephrol.* 25, 707–716. doi:10.1681/ASN.2013050452

West, G. B., and Brown, J. H. (2005). The Origin of Allometric Scaling Laws in Biology from Genomes to Ecosystems: towards a Quantitative Unifying Theory of Biological Structure and Organization. *J. Exp. Biol.* 208, 1575–1592. doi:10.1242/jeb.01589

West, G. B., Woodruff, W. H., and Brown, J. H. (2002). Allometric Scaling of Metabolic Rate from Molecules and Mitochondria to Cells and Mammals. *Proc. Natl. Acad. Sci.* 99 (Suppl. 1), 2473–2478. doi:10.1073/pnas.012579799

Wolf, G., Mueller, E., Stahl, R. A., and Ziyadeh, F. N. (1993). Angiotensin II-Induced Hypertrophy of Cultured Murine Proximal Tubular Cells Is Mediated by Endogenous Transforming Growth Factor-Beta. *J. Clin. Invest.* 92, 1366–1372. doi:10.1172/JCI116710

Xiao, X., Hu, Y., Quirós, P. M., Wei, Q., López-Otín, C., and Dong, Z. (2014). OMA1 Mediates OPA1 Proteolysis and Mitochondrial Fragmentation in Experimental Models of Ischemic Kidney Injury. *Am. J. Physiology-Renal Physiol.* 306, F1318–F1326. doi:10.1152/ajprenal.00036.2014

Conflict of Interest: The authors declare that the research was conducted in the absence of any commercial or financial relationships that could be construed as a potential conflict of interest.

Publisher's Note: All claims expressed in this article are solely those of the authors and do not necessarily represent those of their affiliated organizations, or those of the publisher, the editors and the reviewers. Any product that may be evaluated in this article, or claim that may be made by its manufacturer, is not guaranteed or endorsed by the publisher.

frontiers in Cell and Developmental Biology

REVIEW
published: 07 March 2022
doi: 10.3389/fcell.2022.832887

Podocyte Injury in Diabetic Kidney Disease: A Focus on Mitochondrial Dysfunction

Simeng Liu[1], *Yanggang Yuan*[1], *Yi Xue*[2], *Changying Xing*[1]* *and Bo Zhang*[1,3]*

[1]Department of Nephrology, The First Affiliated Hospital of Nanjing Medical University, Nanjing Medical University, Nanjing, China, [2]Suzhou Hospital of Integrated Traditional Chinese and Western Medicine, Suzhou, China, [3]Department of Nephrology, Pukou Branch of JiangSu Province Hospital (Nanjing Pukou Central Hospital), Nanjing, China

Podocytes are a crucial cellular component in maintaining the glomerular filtration barrier, and their injury is the major determinant in the development of albuminuria and diabetic kidney disease (DKD). Podocytes are rich in mitochondria and heavily dependent on them for energy to maintain normal functions. Emerging evidence suggests that mitochondrial dysfunction is a key driver in the pathogenesis of podocyte injury in DKD. Impairment of mitochondrial function results in an energy crisis, oxidative stress, inflammation, and cell death. In this review, we summarize the recent advances in the molecular mechanisms that cause mitochondrial damage and illustrate the impact of mitochondrial injury on podocytes. The related mitochondrial pathways involved in podocyte injury in DKD include mitochondrial dynamics and mitophagy, mitochondrial biogenesis, mitochondrial oxidative phosphorylation and oxidative stress, and mitochondrial protein quality control. Furthermore, we discuss the role of mitochondria-associated membranes (MAMs) formation, which is intimately linked with mitochondrial function in podocytes. Finally, we examine the experimental evidence exploring the targeting of podocyte mitochondrial function for treating DKD and conclude with a discussion of potential directions for future research in the field of mitochondrial dysfunction in podocytes in DKD.

Keywords: podocytes, diabetic kidney disease, mitochondrial dysfunction, therapeutic strategies, injury

OPEN ACCESS

Edited by:
Mario Ollero,
INSERM U955 Institut Mondor de Recherche Biomédicale (IMRB), France

Reviewed by:
Hua Su,
Huazhong University of Science and Technology, China
Carole Henique,
INSERM U955 Institut Mondor de Recherche Biomédicale (IMRB), France

***Correspondence:**
Changying Xing
cyxing62@126.com
Bo Zhang
zhangbo@jsph.org.cn

Specialty section:
This article was submitted to Cell Death and Survival, a section of the journal Frontiers in Cell and Developmental Biology

Received: *10 December 2021*
Accepted: *07 February 2022*
Published: *07 March 2022*

Citation:
Liu S, Yuan Y, Xue Y, Xing C and Zhang B (2022) Podocyte Injury in Diabetic Kidney Disease: A Focus on Mitochondrial Dysfunction. Front. Cell Dev. Biol. 10:832887. doi: 10.3389/fcell.2022.832887

INTRODUCTION

Diabetic kidney disease (DKD) is the leading cause of end-stage renal disease (ESRD), and it affects nearly 30–40% of patients with diabetes (Alicic et al., 2017). Although remarkable progress in drug therapy has reduced the rate of diabetes-related cardiovascular complications, the incidence of DKD and renal failure has continued to rise (Gregg et al., 2014). The principal feature of DKD is an abnormality of the glomerular filtration barrier (GFB), leading to the leakage of protein (proteinuria), metabolites and ions into the urine. Proteinuria simultaneously acts as a major, independent risk factor for the progression of DKD to ESRD. Podocytes form the outer part and ensure the mechanical stability of the GFB, therefore preventing protein loss into the urine. Podocyte dysfunction is one of the earliest glomerular morphologic changes and it plays a key role in DKD progression (Wang et al., 2012; Reidy et al., 2014; Qi et al., 2017).

Mitochondria, the main energy-producing organelles, play a central role in cell survival and death signalling. Mitochondria respond to pathophysiologic cues by altering their content, fusion, fission, mitophagy, and the unfolded protein response (UPR). Hyperglycemia is the most predominant clinical abnormality in diabetes, and it has been viewed as one of the leading risk

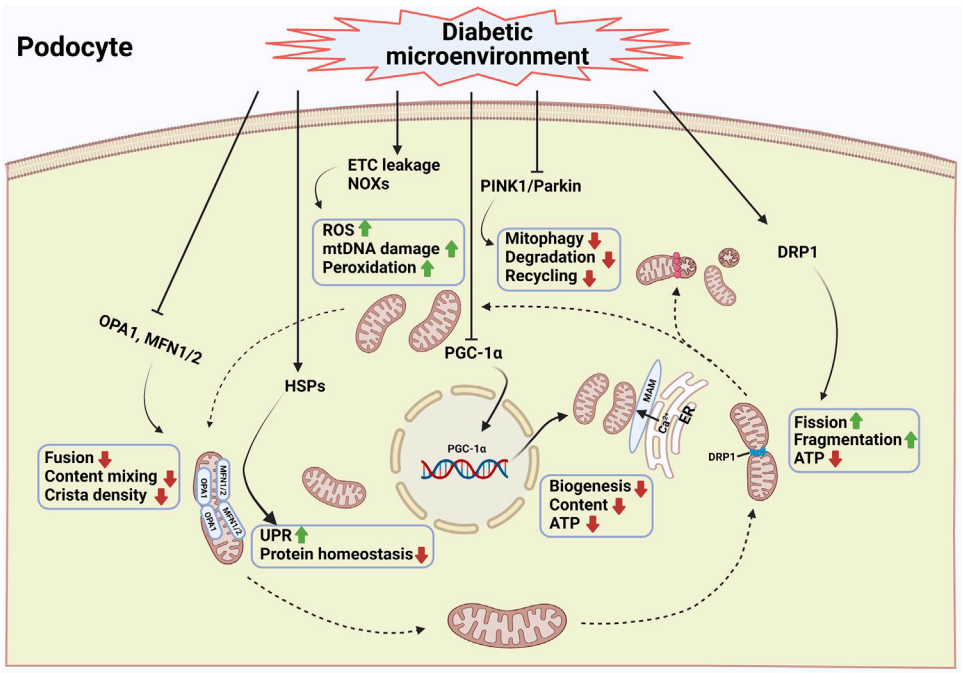

FIGURE 1 | Mitochondrial damage of podocytes during diabetic kidney disease. Mitochondria are highly dynamic organelles that respond to pathophysiologic cues by altering mitochondrial content, fusion, fission, mitophagy, and the unfolded protein response. Fission and fusion complement each other to maintain mitochondrial morphology, whereas mitophagy selectively clears damaged mitochondria from the network (Nisoli et al., 2004). Excessive mitochondrial fission combined with decreased mitochondrial fusion is a prototypical feature of podocytes in diabetic kidney disease (Wang et al., 2012; Ayanga et al., 2016; Qin et al., 2019; Audzeyenka et al., 2021). In addition, the inhibition of mitophagy leads to the lack of a proper mitochondrial turnover in the diabetic kidney (Li et al., 2016; Li W. et al., 2017). Another key feature of mitochondrial dysfunction of podocytes in diabetic kidney disease is the reduced efficiency of mitochondrial biogenesis (Sun et al., 2014; Li S.-Y. et al., 2017; Zhang et al., 2018). Under high glucose condition, intracellular ROS production, mitochondrial DNA damage and protein and lipid peroxidation were enhanced (Tan et al., 2010; Dugan et al., 2013; Coughlan et al., 2016). In addition, mitochondrial protein homeostasis is challenging because of the continuous exposure of mitochondrial proteins to mitochondrial ROS. Mitochondria within a cell cannot exist in isolation. They interact with endoplasmic reticulum via the formation of mitochondrial-associated membranes (MAMs). The disturbance of MAMs leads to abnormal intracellular Ca^{2+} influx, mitochondrial damage, and apoptosis (Inoue et al., 2019). A combination of the above factors resulted in podocyte injury and the progression of diabetic kidney disease. The podocyte mitochondria in diabetic condition is illustrated schematically with blue frame and text. DRP1, dynamin-1-like protein; MFNs, mitofusin proteins 1 and 2; ETC, electron transport chain; HSPs, heat shock proteins; MAM, mitochondria associated ER membrane; NOXs, NADPH oxidases; OPA1, optic atrophy protein 1; PGC-1α, peroxisome proliferator activated receptor γ coactivator-1α; PINK1, PTEN-induced putative kinase protein 1; ROS, reactive oxygen species; UPR, unfolded protein response (Created with BioRender.com).

factors for the pathogenesis of DKD. High glucose (HG) toxicity is mediated by many abnormal glucose metabolic pathways or signalling pathways that can induce reactive oxygen species (ROS) overproduction and mitochondrial damage (Qi et al., 2017). These factors may in turn cause oxidative stress, inflammation, and cell apoptosis. Indirect evidence for mitochondrial dysfunction of podocytes involved in DKD from diabetic models has been accumulating (Susztak et al., 2006; Wang et al., 2012; Ayanga et al., 2016; Qin et al., 2020; Wei et al., 2020), and studies have directly observed mitochondrial dysfunction in clinical samples from patients with DKD (Sharma et al., 2013; Czajka et al., 2015). A variety of mitochondrial dysfunction pathways have been identified as the main molecular causes of podocyte injury, such as elevated mitochondrial ROS production (Jha et al., 2016), imbalanced mitochondrial dynamics (Ayanga et al., 2016) and decreased mitochondrial biogenesis (Bhargava and Schnellmann 2017; Qin et al., 2020). Notably, mitochondrial dysfunction induced by glucose toxicity is usually considered to be an irreversible process owing to the persistence of epigenetic reprogramming (Reidy et al., 2014). For example, Chen *et al.* found persistent differential methylation at several loci over more than 16–17 years in a same cohort (Chen et al., 2016).

Podocytes are terminally differentiated with poor capacity to re-enter the cell cycle and proliferate. Mitochondrial dysfunction is the major contributor to podocyte injury and death, where an abnormal energy supply may lead to irreversible cellular injury (Carney 2015; Arif et al., 2019). Podocytes require a substantial amount of energy to maintain the complex cellular morphology of tertiary foot processes. Mitochondrial DNA mutations could cause podocyte dysfunction and breakdown of the GFB (Heeringa et al., 2011), and data from animal models support this hypothesis (Baek et al., 2018; Widmeier et al., 2020). The above findings support mitochondria involvement in the pathogenesis of podocyte injury, and regulating podocyte energy metabolism by targeting mitochondria may promote podocyte recovery from injury.

The regulation of podocyte mitochondrial dysfunction in patients with DKD has been extensively studied in the past few years, but few reviews have thoroughly summarized the progress in this area. In this review, we summarize the latest research progress on the causes of acquired mitochondrial dysfunction in podocytes in DKD (**Figure 1**). A comprehensive investigation of mitochondrial damage and its potential regulatory mechanisms could provide a deeper understanding of podocyte injury and possible therapeutic options that could have a positive impact on the treatment of DKD.

MITOCHONDRIAL QUALITY CONTROL AND PODOCYTES INJURY IN DKD

Mitochondrial Dynamics and Mitophagy

Mitochondria are dynamic organelles that frequently change their content and distribution within the cell. Dynamic remodelling of mitochondrial networks by fission, fusion and mitophagy promotes the maintenance of cellular function and survival under different physiological conditions. Mitochondrial fission and fusion processes appear to be accompanied by mitophagy. Fission and fusion complement each other to maintain mitochondrial morphology, whereas mitophagy selectively clears damaged mitochondria from the network (Nisoli et al., 2004). Of note, mitochondrial fission is thought to be a central process required for mitochondrial autophagy whereas mitochondrial elongation through fusion inhibits mitophagy. Accordingly, mutations in genes encoding fission and fusion proteins are associated with genetic diseases, highlighting the importance of sustaining mitochondrial dynamics (Sheffer et al., 2016; Gerber et al., 2017).

Fission and Fusion

Fission is the division of mitochondria in two by cleavage of the inner mitochondrial membrane (IMM) and outer mitochondrial membrane (OMM) and fusion is the combination of two mitochondria into one by the joining of the OMM and IMM. Fission is necessary to facilitate the autophagic removal of damaged mitochondria. Fission and fusion are complementary processes. Rather than being phenomenological, mitochondrial dynamics also influence mitochondrial functions and energy metabolism in many ways.

Mitochondrial fusion is regulated by several proteins, including mitofusin1 (MFN1) and mitofusin2 (MFN2) located in the OMM and optic atrophy protein 1 (OPA1) located in the IMM (Song et al., 2015). MFN1 is necessary for OMM fusion, whereas OPA1 is important for IMM fusion. Mice deficient in either MFN1 or MFN2 die in utero in midgestation (Chen et al., 2003). The precise role of MFN2 in fusion is not yet clear and it may be involved in the interaction between mitochondria and other organelles [in particular with the endoplasmic reticulum (ER)] (de Brito and Scorrano 2008). Fusion allows for content mixing, thus buffering the effect of damaged mitochondrial DNA, proteins, lipids and metabolites and maintaining normal mitochondrial activity (Youle and van der Bliek 2012; Pickles et al., 2018). MFN1 and MFN2 initiate the fusion process by tethering OMMs of adjacent mitochondria, and external stimuli, such as oxidative stress, can enhance OMM fusion (Shutt et al., 2012). Then, OPA1 completes the fusion process at IMMs. IMM fusion is more complicated than OMM fusion maintaining crista structures of the IMM. Deletion of OPA1 induces mitochondrial fragmentation and also results in decreased cristae density, in which the IMM becomes vesicular (Meeusen et al., 2006).

Mitochondrial fission is primarily driven by dynamin-related protein 1 (Drp1), a gtpase that dynamically associates with the ER and mitochondria (Ji et al., 2017). Drp1 translocates from the cytosol to the surface of the OMM, binding to its receptors in the OMM, including mitochondrial fission factor (MFF) (Otera et al., 2010; Sheng et al., 2019), mitochondrial dynamics proteins 49 and 51 (MID49/51) (Palmer et al., 2013) and mitochondrial fission 1 protein (Fis1) (James et al., 2003). Following this binding, Drp1 oligomerizes to form a constrictive ring around the mitochondrion to physically constrict and sever the mitochondrion (Kalia et al., 2018; Adachi et al., 2020). Drp1 is essential for embryonic development, and genetic knockout of Drp1 in mice is embryonically lethal at approximately embryonic Days 11.5–12 (Wakabayashi et al., 2009). However, cultured mammalian cells can survive without Drp1 and undergo mitochondrial fission *in vitro* (Kraus et al., 2021). Therefore, the functional role of mitochondrial fission is easier to detect *in vivo* studies in which damaged mitochondrial networks impair a variety of cellular biological activities, such as autophagy and apoptosis. Mitochondrial fission is necessary to surveil and isolate damaged mitochondria, which plays a key role in the quality control of the mitochondrial network (Bhargava and Schnellmann 2017). These daughter mitochondria with high membrane potential may recover by fusion (Abrisch et al., 2020) while unbalanced and depolarized daughter mitochondria are degraded through mitophagy to sustain a population of healthy mitochondria (Dikic and Elazar 2018; Kraus et al., 2021).

Defective mitochondrial dynamics have harmful effects on mitochondrial homeostasis and have been closely linked to the pathogenesis of numerous diseases, including cancer, cardiovascular diseases, and CKD (Galloway et al., 2012). Recently, several studies have proposed that excessive mitochondrial fission and enhanced fragmented mitochondria in podocytes are characteristic features of kidney injury before the obvious clinical manifestations of DKD (Wang et al., 2012; Ayanga et al., 2016; Qin et al., 2019). Drp1-specific knockdown in podocytes or pharmacologic inhibition of Drp1 by mitochondrial division inhibitor 1 (Mdivi-1) in diabetic mice confers protection against DKD with decreased albuminuria and improved morphology compared to diabetic control mice (Ayanga et al., 2016). Accordingly, podocytes isolated from Drp1 knockout mice demonstrated more elongated mitochondria and ATP production was restored, unlike in podocytes isolated from wild-type mice. Furthermore, the herbal alkaloid berberine could significantly protect podocytes via inhibiting Drp1-mediated mitochondrial fission and cell apoptosis, suggesting its use as a new therapeutic drug to treat DKD (Qin et al., 2019). Collectively, the data available indicate

that mitochondrial fragmentation contributes critically to podocyte injury in DKD. Research is, however, still in an early stage.

Mediators that increase the expression of Drp1 or promote Drp1 translocation to the OMM both contribute to mitochondrial fission (Ayanga et al., 2016; Deng et al., 2020). Drp1 activity and translocation can be affected by posttranslational modifications, such as phosphorylation (Wang et al., 2012; Sabouny and Shutt 2020), *O*-GlcNAcylation (Gawlowski et al., 2012), and sumoylation (Zunino et al., 2007; Braschi et al., 2009). Among these post-translational modifications, Drp1 phosphorylation seems to play a central regulatory role, which can exert either activating or inhibitory effect depending on the specific site modified. Several phosphorylation sites have been identified in Drp1, including Ser-579, Ser-40, Ser-585, Ser-44, Ser-592, Ser-656, Ser-616, Ser-637, and Ser-693 (Qi et al., 2019). Among these sites, both Ser-616 and Ser-637 have been extensively reported in various diseases, while only Ser-637 was deeply examined in podocytes. Drp1 is a cytosolic protein, and phosphorylation at Ser637 of Drp1 promotes Drp1 translocation to mitochondrion to induce fission in response to HG conditions in podocytes (Ayanga et al., 2016). Similarly, activated A-kinase anchoring protein 1 (AKAP1) promotes the phosphorylation of Drp1 at Ser637, which promotes the transposition of Drp1 to the OMM and results in mitochondrial dysfunction events in HG-induced podocyte injury (Chen et al., 2020). However, another study, inconsistent with these findings, found that Drp1 phosphorylation at Ser637 by phosphoprotein kinase A (PKA) inhibits its gtpase activity and inhibits fission (Cribbs and Strack 2007). In contrast, Drp1 dephosphorylation at the same site by the Ca^{2+}-dependent phosphatase calcineurin activates Drp1 and promotes fission (Cereghetti et al., 2008). A possible explanation for these conflicting results could be that the effects of Drp1 phosphorylation at this residue are likely cellular context- and external stimulus-dependent (Galvan et al., 2017). Because of the complexity of the posttranslational modification, the external stimuli that trigger this pathway remains largely unknown and needs investigation.

Mitophagy

Mitophagy is the best-described form of selective autophagy. It specifically degrades long-lived or damaged mitochondria via the formation of intracellular organelles-mitophagosomes. Mitophagosomes ultimately fuse with lysosomes, finally resulting in content degradation. The half-life of mitochondria is 10–25 days in the human body, and mitophagy serves as a master regulator in the maintenance of the quality of the mitochondrial pool in response to metabolic demand. If mitochondria are damaged beyond repair, mitochondria are eliminated through mitophagy to prevent ROS production, provide raw materials for metabolic needs and contribute to mitochondrial biogenesis. Abnormal or excessive mitophagy has been implicated in numerous human disorders (Palikaras et al., 2018).

Generally, mitophagy is divided into PTEN-induced putative kinase protein 1 (PINK1)/Parkin-dependent or PINK1/Parkin-independent (receptor-mediated) pathways. PINK1/Parkin-dependent mitophagy can be initiated by a loss of mitochondrial membrane potential (MMP), while the activation of the PINK1/Parkin-independent pathway is regulated through receptors that are anchored on the cytosolic surface of the OMM such as BNIP3L, BCL2-L13, and FUNDC1 (Ng et al., 2021). Mitophagy in most cell types is induced by the PINK1/Parkin-mediated pathway. Under physiological conditions, the mitophagy signal protein PINK1 is translocated from the cytosol to the IMM and then degraded by mitochondrial proteasomes (Greene et al., 2012). As PINK1 import is dependent on an intact MMP, mitochondrial damage or depolarization hampers its translocation and results in its accumulation on the OMM (Choi 2020). Then PINK1 recruits the E3 ubiquitin ligase Parkin to the mitochondria and prompts its phosphorylation/activation, which ubiquitinates lysine residues in the N-termini of OMM proteins, thereby targeting the mitochondria for degradation by autophagosomes (Randow and Youle 2014; Choi 2020). Meanwhile, simultaneous phosphorylation of ubiquitin chains by PINK1 might further facilitate Parkin activation and recruitment (Lazarou et al., 2015).

Autophagy is well known to be exacerbated in podocytes in DKD (Liu et al., 2019), and relatively few studies have explored the effect of mitophagy on podocytes in DKD. Mitophagy is considered as a defense mechanism under pathological conditions. Thus, we can infer that mitophagy is induced to ensure mitochondrial quality control by clearing damaged mitochondria during the initial stage of DKD. However, as the disease progresses, the increased number of damaged mitochondria might exceed the eliminated capacity of mitophagy, or mitophagy might also become impaired, then the apoptotic pathway is activated to minimize tissue damage. It has been demonstrated that HG accelerates mitochondrial dysfunction and podocyte apoptosis by inhibiting mitophagy activity (Li et al., 2016; Li W. et al., 2017). Overexpression of forkhead-box class O1 (FOXO1) in podocytes activates PINK1/parkin-dependent mitophagy, which degrades dysfunctional mitochondria and alleviates podocyte injury in diabetic mice and cultured podocytes, supporting the hypothesis of an important role of FOXO1 in the regulation of mitophagy in podocytes (Li W. et al., 2017). Progranulin (PGRN), an autocrine growth factor, has been known to be involved in the development and/or progression of various inflammatory diseases including renal ischemia/reperfusion injury and diabetic complications (Xu et al., 2015; Zhou et al., 2015; Choi et al., 2020). In diabetic mice, knockout of PGRN, which is significantly reduced in DKD, aggravated mitochondrial dysfunction in podocytes (Zhou et al., 2019). Treatment with recombinant human PGRN promoted mitophagy and mitochondrial biogenesis, thereby alleviating mitochondrial dysfunction and podocyte injury. A potential mechanism by which PGRN protects mitochondria is mediated via PGRN–SIRT1–PGC1α regulation of FOXO1 (Zhou et al., 2019).

Mitochondrial Biogenesis

Mitochondrial biogenesis replicates mtDNA, generates new and functional mitochondria, and increases ATP production by the

proliferation of pre-existing organelles (Jiang et al., 2020). Mitochondrial biogenesis and its concomitant cellular processes enhance metabolic pathways and antioxidant defense mechanisms that mitigate injury from tissue hypoxia, excess production of ROS, and glucose or fatty acid overload, all of which contribute to the pathogenesis of kidney disease, including DKD. The process of mitochondrial biogenesis is largely regulated by networks of transcription factors that link external cues to cell energy demand and adaptive responses (Galvan et al., 2017).

Peroxisome proliferator-activated receptor γ coactivator-1α (PGC-1α) is a prominent transcriptional coactivator that interacts with other transcription factors to regulate mitochondrial biogenesis in a variety of cells including podocytes (Svensson et al., 2016; Li S.-Y. et al., 2017). PGC-1α acts as the "master regulator" in stimulating the expression of mitochondrial genes as well as nuclear genes in response to extracellular signals, energetic demand, or mitochondrial dysfunction. Several experimental models of DKD exhibit reduced efficiency of mitochondrial biogenesis, decreased PGC-1α levels, and defective mitochondrial function (Sun et al., 2014; Li S.-Y. et al., 2017; Zhang et al., 2018). The downregulation of PGC-1α and its downstream signalling cascades has been proposed to be the key contributor to renal lipid overload, mitochondrial loss and dysfunction, eventually leading to podocyte injury and destruction of the GFB (Long et al., 2016; Li S.-Y. et al., 2017; Li and Susztak 2018). Endogenous expression of PGC-1α in podocytes exhibited protective effects against kidney fibrosis in mice with DKD (Zhang et al., 2018). Furthermore, PGC-1α is negatively regulated by upstream open reading frames (uORFs) (Dumesic et al., 2019), Smad3, and NF-κB (Dai et al., 2021). PGC-1α expression is positively regulated by AMPK (Dugan et al., 2013), sirtuins (Yacoub et al., 2014), Ewing sarcoma breakpoint region 1 (EWSR1) (Park et al., 2015), PGRN (Zhou et al., 2019), G protein-coupled bile acid receptor TGR5 (Wang et al., 2016), and induced-by-high-glucose 1 (IHG-1) (Hickey et al., 2011), which subsequently activates nuclear respiratory factors (NRFs), improving mitochondrial DNA expression and protein translation and thus promoting mitochondrial biogenesis. For example, it has been demonstrated the activation of TGR5 with its agonist INT-777 can induce mitochondrial biogenesis and attenuate renal oxidative stress in db/db mice and human podocyte cell line (Wang et al., 2016).

The activation of peroxisome proliferator-activated receptors (PPARs) and oestrogen-related receptors (ERRs) is also involved in the regulation of mitochondrial biogenesis, sometimes by these receptors co-operating with PGC-1α (Fan and Evans 2015). ERRs upregulate the entire gene network necessary for biogenesis, but in contrast to ERRs, PPARs are not sufficient by themselves to fully induce biogenesis (Weinberg 2011). Numerous studies have demonstrated that the activity of PPARγ, the third member of the PPARs (PPARα, PPARβ/δ and PPARγ), is pivotal in protecting podocytes (Agrawal et al., 2021). PPARγ attenuates the renal effects of aging and generally promotes mitochondrial biogenesis by inducing PGC-1α (Hondares et al., 2006; Weinberg 2011). PGC-1α can directly bind to nuclear receptors PPARs and ERRs and coactivate the transcription of genes. PPARγ agonists (such as thiazolidinediones) have been shown to delay DKD progression in patients with type 2 diabetes mellitus and in various animal models of diabetes (Yang et al., 2012).

Furthermore, multiple other factors act directly or indirectly to regulate mitochondrial biogenesis in podocytes. Mitochondrial glycerol 3-phosphate dehydrogenase (mGPDH) is defined as a component in the respiratory chain, which guarantees the appropriate production of energy in a cell. Recently, Qu *et al.* verified that podocyte-dominated expression of mGPDH was downregulated in DKD, and activation of mGPDH induced mitochondrial biogenesis and reinforced mitochondrial function (Qu et al., 2021). The role of transcription factor EB (TFEB) as a key regulator of the autophagy-lysosome pathway has been widely investigated (Sardiello et al., 2009; Settembre et al., 2011). TFEB can regulate mitochondrial biogenesis in PGC-1α-dependent or PGC-1α-independent pathways (Kang et al., 2019; Wang S. et al., 2020). Adenosine is significantly increased in response to various cellular damages. Treatment of db/db mice with the adenosine receptor A_3AR antagonist LJ-2698 has a renoprotective effect by modulating PGC-1α (Dorotea et al., 2018).

PGC-1α interacts with many transcription factors and is implicated in complex biological functions. Currently, there are no drugs that specifically target PGC-1α in clinical trials. It is reasonable to assume that a strategy targeting upstream or downstream molecules of PGC-1α pathway is possible. It should be noted, however, that podocytes may have a narrow PGC-1α tolerance and that excessive PGC-1α may alter mitochondrial properties. It has been proven that transgenic overexpression of PGC-1α in podocytes causes uncontrolled mitochondrial proliferation and glomerulopathy in mice (Li S.-Y. et al., 2017).

Oxidative Phosphorylation and ROS Production

The term ROS encompasses a wide range of highly reactive, oxygen-containing molecules, including free radical species, such as hydroxyl radicals and superoxide radicals, and non-radical species, such as hydrogen peroxide. ROS are well known for their role in mitochondrial dysfunction and the development of diabetic microvascular complications, including DKD. ROS are historically considered toxic by-products of pathological cellular metabolism, but the current consensus is that ROS have physiological functions at low levels and take part in promoting the proliferation and survival of cells in response to stress. However, if ROS generation is not balanced through appropriate regulation of synthesis and degradation, oxidative stress may occur. ROS levels that exceed the antioxidant capacity are a sign of mitochondrial dysfunction and a risk factor for DKD (Dugan et al., 2013; Coughlan et al., 2016).

There are several sources of ROS in human cells, but the main endogenous ROS are generated from mitochondria via the respiratory chain (Scialo et al., 2016). Hyperglycemia is a representative hallmark of diabetes and is closely linked to

excessive ROS, which is an important pathway contributing to the pathogenesis of diabetes associated complications. Under diabetic conditions, excessive glucose enters into the tricarboxylic acid cycle (TAC), which results in more NADH or $FADH_2$ entering the mitochondrial electron transport chain. Under this condition, electron transfer is obstructed, and some of them escape to generate superoxide in both the intermembrane space and matrix, which results in excessive production of ROS (Brownlee 2005). It has been firmly established that HG exposure of glomerular podocytes results in an increased ROS level. Overproduction of ROS in the presence of HG induces mtDNA damage and protein and lipid peroxidation, subsequently resulting in mitochondrial dysfunction and podocyte injury. Notably, glucose-induced excessive ROS production plays a central role in initiating podocyte apoptosis and podocyte depletion followed by progression to renal damage (Susztak et al., 2006; Fakhruddin et al., 2017). Pyruvate kinase isoform M2 (PKM2) is a rate-limiting glycolytic enzyme. Qi *et al.* shows that podocyte-specific *Pkm2*-knockout in mice aggravates albuminuria and pathological severity of DKD (Qi et al., 2017). PKM2 activator (TEPP-46) can significantly ameliorate mitochondrial dysfunction by increasing glucose metabolic flux, preventing the elevation of ROS production, inducing mitochondrial biogenesis (Qi et al., 2017). In addition, treatment with antioxidants, such as Grape seed proanthocyanidin extracts (Bao et al., 2014), INO-1001 or PJ-34 (Szabo et al., 2006), has been shown to restore mitochondrial dysfunction and attenuate kidney injury in animal models of DKD.

The NADPH oxidase (Nox) family is another important endogenous source of ROS production. The mammalian Nox has seven isoforms: Nox1 to Nox5, Duox1, and Duox2. Nox4 is the predominant form within the kidney, whereas Nox1, Nox2 and Nox5 are also expressed in the kidney (Holterman et al., 2015). NOXs, particularly NOX4, have been reported to be pathologically relevant sources of ROS in HG-induced podocytes leading to mitochondrial damage and podocyte apoptosis. Furthermore, *in vivo* studies, genetic deletion of NOX4 in podocytes or treatment with a novel NOX1/4 inhibitor (GKT137831) reduced oxidative stress, podocyte injury and the development of DKD (Jha et al., 2014; Jha et al., 2016; Gray et al., 2017). Similar results were obtained using salvianolate, a prescribed Chinese medicine derived from Danshen, through regulation of NOX4 activity in db/db mice (Liang et al., 2021).

As described above, PGC-1α is considered to be a master, upstream transcriptional regulator of oxidative phosphorylation and mitochondrial biogenesis (Galvan et al., 2017) and PGC-1α levels were reduced in DKD (Sun et al., 2014; Zhang et al., 2018). Endogenous PGC-1α also exhibited protective effects against renal fibrosis in diabetic mice through an anti-oxidative mechanism (Zhang et al., 2018). Recently, a study highlighted that PGC-1α-mediated mitochondrial bioenergetics could play a pivotal role in lipid disorder-induced podocyte injury and the development of DKD, whereas restoring PGC-1α activity and a balanced energy supply via berberine may be a novel therapeutic strategy for the treatment of DKD (Qin et al., 2020).

The family of NAD^+-dependent deacetylases known as sirtuins (SIRT1-7) has an essential role in the regulation of mitochondrial function of podocytes in DKD (Hershberger et al., 2017; Fan et al., 2019; Zhang et al., 2019). It has been reported that Sirt6 alleviates HG-induced mitochondrial damage and oxidative stress in podocytes through AMPK activation (Fan et al., 2019). Importantly, SIRT1-mediated deacetylation of PGC-1α could ameliorate HG-induced podocyte damage (Cai et al., 2016; Zhang et al., 2019) and resveratrol, an activator of SIRT1, demonstrated significant protection of mitochondrial function in diabetic mice with DKD through SIRT1/PGC-1α-regulated attenuation of mitochondrial oxidative stress (Zhang et al., 2019; Wang F. et al., 2020). Furthermore, one other group found that salidroside, an active component from Rhodiola rosea L., ameliorates diabetic nephropathy by stimulating the Sirt1/PGC-1α axis in diabetic mice (Liang et al., 2021). The above results revealed the protective role of PGC-1α in regulating mitochondrial homeostasis in podocytes and identified potential targets for the treatment of DKD.

ROS act as a master switch for activating inflammatory responses by activating multiple downstream pathways, including nucleotide leukin-rich polypeptide 3 (NLRP3), NF-κB, and Toll-like receptor (TLR). Upon stimulation, NLRP3 can form a NLRP3 inflammasome to act as a cytosolic multiprotein caspase-activating complex platform and subsequently lead to the activation of Caspase-1. Activation of Caspase-1 can lead to the maturation and release of interleukin (IL)-1β and IL-18 (Davis et al., 2011). In a type 2 diabetic model, excessive activation of NLRP3 was associated with chronic inflammation, cell death, and fibrosis. Accumulating data suggest that mitochondrial ROS could activate the NLRP3 inflammasome in glucose or advanced glycation end product stressed podocytes (Shahzad et al., 2015; Yu et al., 2019; Wu et al., 2021). Treatment of db/db mice with the NLRP3 inflammasome inhibitor (MCC950) could attenuate podocyte damage and improve kidney function by inhibiting lipid accumulation in DKD (Wu et al., 2021). Another study reported that luteolin, a natural flavonoid found in various fruits and vegetables, attenuated HG-induced podocyte damage by suppressing the NLRP3 inflammasome pathway (Yu et al., 2019).

Mitochondrial Protein Quality Control

The mitochondrial proteome comprises approximately 1,200 proteins in humans (Rath et al., 2021). Mitochondrial function strongly relies on protein homeostasis within organelles. Mitochondria are comprised of proteins encoded by two genomes, mitochondrial and nuclear, but approximately 99% of mitochondrial proteins are encoded by the nuclear genome, and they are synthesized in the cytosol (Song et al., 2021). Hence, the synchronization of gene expression between the nucleus and mitochondria and efficient import of the encoded mitochondrial proteins into the specific locations in the mitochondria from the cytosol are essential for mitochondrial protein homeostasis. To repair or degrade misfolded and damaged proteins, mitochondria rely on several quality control pathways, including mitochondrial molecular chaperones promoting folding of misfolded proteins and ATP-dependent proteases degrading misfolded or damaged

TABLE 1 | Potential approaches to target podocyte mitochondrial dysfunction in clinical studies.

Agent	Mechanism of action	*In vivo* and clinical studies	References
Coenzyme Q10	Antioxidant	1) Decreases albuminuria and prevents detrimental changes in mitochondrial function rodent models with DKD 2) Reduces albuminuria in paediatric patients with COQ6 glomerulopathy or ADCK4 mutation	Sourris et al. (2012), Stanczyk et al. (2018), Feng et al. (2017)
Lademirsen	Inhibits microRNA-21	1) Down-regulation of miR-21 inhibits the progression of DKD in streptozotocin- induced diabetic nephropathy rats 2) Phase II study (NCT02855268) in patients with Alport syndrome	Gomez et al. (2015); Chen et al. 2018)
Bardoxolone methyl	Activates of Nrf2 and inhibits the expression of Drp1 and mitochondrial fission	1) Decreased albuminuria and has a renoprotective role for podocytes and diabetic glomerulopathy in diabetic nephropathy mice 2) Phase III study (NCT03550443) in patients with diabetic kidney disease	Fang et al. (2021), Zhou et al. (2020)

mitochondrial proteins (Vazquez-Calvo et al., 2020). Disturbances in mitochondrial protein homeostasis lead to proteotoxic insults and cell injury (Cybulsky 2017). Notably, mitochondrial protein homeostasis is challenging under HG conditions. As described above, HG exposure of podocytes leads to elevated ROS, whereas continuous intracellular ROS elevation can impair protein function and induce inflammatory responses, leading to cellular death.

Most mitochondrial proteins are synthesized in the cytosol, and then precursor proteins are bound to molecular chaperones and imported into mitochondria. Molecular chaperones are enzymes whose functions are responsible for stabilizing, folding, and unfolding precursor proteins. Heat shock proteins (HSPs) are highly conserved proteins that act as molecular chaperones and play a vital role in protein homeostasis (Young et al., 2003; Song et al., 2021). Increased levels of HSP25, HSP60, and HSP70 are observed in the diabetic outer medulla, but no differences were detected in the glomeruli in response to diabetes (Barutta et al., 2008). Only the phosphorylated form of HSP27 is increased in the podocytes of diabetic animals (Barutta et al., 2008).

The major response to excessive amounts of unfolded or misfolded proteins is activation of UPR pathway. There are two distinct UPRs—the endoplasmic reticulum unfolded protein response (UPRER) and the mitochondrial unfolded protein response (UPRmt)—that stabilize, renature, and degrade unfolded proteins in the mitochondria and the ER, respectively. However, prolonged and severe UPR can lead to an excessive ER stress and result in pro-apoptotic cell death. Although the UPRER and UPRmt involve chaperones and proteases specific to each organelle, both pathways interact and influence each other upon activation in response to extrinsic stimuli (Senft and Ronai 2015; Tang et al., 2021). Notably, the sustained UPRER pathway has been implicated in the pathogenesis of podocyte injury and DKD (Cybulsky 2017; Kang et al., 2017; Wang et al., 2021). Therefore, activation of the UPRmt might have also occurred in DKD. One study in a rat model of streptozotocin-induced diabetes showed that exposure to HG activated the UPRER pathway in renal podocytes, whereas treatment with an endogenous peptide (intermedin), which has anti-inflammatory and antioxidant properties, blocked such ER stress responses and alleviated podocyte apoptosis (Wang et al., 2021). The regulation of mitochondrial protein quality control in polypeptide sorting, folding, transportation and subsequent assembly into multiprotein complexes during mitochondrial biogenesis is essential for mitochondrial function and cellular survival. However, the functional association between the mitochondrial protein quality control system, podocyte injury and DKD remains poorly understood.

MITOCHONDRIA-ASSOCIATED ENDOPLASMIC RETICULUM MEMBRANES

To maintain homeostasis, organelles work cooperatively (Inoue et al., 2019). Certainly, mitochondria within a cell cannot exist in isolation. They interact with other subcellular organelles, particularly with the ERs. Recently, an emerging concept is that the ER and mitochondria are organized as a complex network through direct interactions at membrane contact sites called MAMs (mitochondria associated ER membranes) (Kornmann et al., 2009). At the MAMs, the membrane of the juxtaposed ER and mitochondria are separated by only 10–25 nm. This proximity not only allows direct contact of proteins and lipids but also exchanges of Ca^{2+} in the ER with those in the OMM (Csordas et al., 2006). Perturbations in MAMs and increased ER-mitochondria contacts have been reported in various neurodegenerative disorders (Parakh and Atkin 2021) and metabolic disorders (Yang et al., 2020), as well as DKD (Yang et al., 2021). The disturbance of MAMs leads to abnormal intracellular Ca^{2+} levels, mitochondrial damage, ER stress, autophagy, and apoptosis (Inoue et al., 2019).

Calcium signalling plays a vital role in many cellular physiological pathways. In pathological states, calcium signals can precipitate mitochondrial damage and trigger cell death, particularly when accompanied by energetic deprivation and oxidative stress (Bhosale et al., 2015). Therefore, the role of mitochondria as sensors and modulators of calcium signalling is extremely important. An increase in the inflow of Ca^{2+} into mitochondria from the juxtaposed ER takes place through this specialized proximity during various common stresses. An appropriate elevation in Ca^{2+} concentration activates TAC

TABLE 2 | Potential approaches to target podocyte mitochondrial dysfunction in preclinical developments.

Agent	Classification	Mechanism of action	DKD model	References
Mitochondria-targeted antioxidant	Salvianolate	Modulates NOX4 activity and ameliorates oxidative injury	Db/db mice and human podocyte cell line	Liang et al. (2021)
	MCC950	Inhibits NLRP3 inflammasome and suppresses lipid accumulation, ROS generation and NF-κB p65 activation	Db/db mice and mouse podocyte cell line	Wu et al. (2021)
	Berberine	Activates the PGC-1α signalling pathway and promotes mitochondrial fatty acid oxidation	Db/db mice and mouse podocyte cell line	Qin et al. (2020)
	Resveratrol	Activates SIRT1 and suppresses oxidative stress	Db/db mice and human podocyte cell line	Wang et al. (2020a), Zhang et al. (2019)
	GKT137831	Inhibits Nox1/4 activity and suppresses ROS generation	Streptozotocin-induced diabetic mice and human podocyte cell line	Jha et al. (2014)
	INO-1001 and PJ-34	Inhibits poly (ADP-ribose) polymerase activity and blocks the ROS generation	Db/db mice and mouse podocyte cell line	Szabo et al. (2006)
	Grape seed proanthocyanidin extracts	Activates the AMPK-SIRT1-PGC-1a signaling pathway and inhibits oxidative stress	Streptozotocin-induced diabetic mice	Bao et al. (2014)
Inhibits mitochondrial fission	Mdivi-1	Inhibits DRP1 activity and suppresses mitochondrial fission	Db/db mice and primary mouse podocyte	Ayanga et al. (2016)
	Berberine	Inhibits palmitic acid-induced activation of DRP1 activity and suppresses mitochondrial fission	Db/db mice and mouse podocyte cell line	Qin et al. (2019)
Promotes mitochondrial biogenesis	LJ-2698	Inhibits adenosine receptor activity and promotes mitochondrial biogenesis	Db/db mice	Dorotea et al. (2018)
	Salidroside	Stimulates the Sirt1/PGC-1 axis and promotes mitochondrial biogenesis	Streptozotocin-induced diabetic mice	Xue et al. (2019)
	TEPP-46	Activates pyruvate kinase M2 and induces mitochondrial biogenesis	Streptozotocin-induced diabetic mice, mouse and human podocyte cell lines	Qi et al. (2017)
	INT-777	Activates G protein-coupled receptor TGR5 and induces mitochondrial biogenesis	Db/db mice and human podocyte cell line	Wang et al. (2016)

dehydrogenase to promote ATP production. However, an excessive elevation in Ca^{2+} concentration opens the mitochondrial permeability transition pore and releases cytochrome c simultaneously, leading to cellular apoptosis (Inoue et al., 2019). In the unilateral ureteral obstruction model, mitochondria and the ER form a pathological feedback loop by Ca^{2+} dysregulation and ER stress pathways, resulting in the impairment of both organelles (Martinez-Klimova et al., 2020). Ca^{2+} channel transient receptor potential cation channel subfamily V member 1 (TRPV1), a channel modulating the intracellular Ca^{2+} concentration, can be activated by multiple endogenous stimuli, including pressure, force, and exogenous stimuli, such as capsaicin (Nieto-Posadas et al., 2011). Activation of the TRPV1 channel by capsaicin can play a robust therapeutic role in HG-induced mitochondrial damage in podocytes, accompanied by decreased MAM formation and reduced Ca^{2+} transport from the ER to mitochondria (Wei et al., 2020).

As described above, mitophagy refers to a protective effect in response to diverse stimuli, including hypoxia, ROS, and energy stresses (Tang et al., 2020). ER-mitochondria contact sites are essential for organelle quality control by involving in mitophagy (Hamasaki et al., 2013). Researchers have demonstrated that many proteins involved in mitophagy are recruited to MAMs following mitophagic stimuli, in turn, recruited autophagy-associated proteins promote the formation of MAMs and autophagosomes (Yao et al., 2021). Currently, the FUNDC1-mediated pathway is one of the well-studied pathways of the PINK1/Parkin-independent mitophagy as described above. FUNDC1 has been proven to accumulate at MAMs, which can initiate mitochondrial division prior to mitophagy (Wu et al., 2016). FUNDC1-dependent mitophagy plays a protective role in acute reperfusion injury and chronic metabolic syndrome via its sustaining mitochondrial homeostasis activity. As shown in proximal tubule-specific Fundc1 knockout mice, ischemic preconditioning activates FUNDC1-dependent mitophagy, and FUNDC1 deficiency abolishes the benefits of ischemic preconditioning against renal ischemia reperfusion injury. Mechanistically, FUNDC1 deficiency provoked compromised mitochondrial quality control, manifested by abnormal mitochondrial quality and excessive Drp1-dependent mitochondrial fission (Wang J. et al., 2020). Although more studies on the role of MAMs in mitophagy in DKD are needed, the available evidence suggests that MAMs provide a platform for autophagy-associated proteins to perform their biological functions.

Mitochondria are highly plastic organelles that undergo fission and fusion to optimize their function (Youle and van der Bliek 2012). Disturbances of mitochondrial dynamics, featuring excessive mitochondrial fission, are noted in glomerular podocytes in diabetic nephropathy (Ni et al., 2017; Ma et al., 2019; Qin et al., 2019). As described previously, mitofusin 2 (Mfn2) is enriched at the ER-mitochondria interface and plays a key role in the maintenance of mitochondrial fusion and fission

(de Brito and Scorrano 2008). MAMs are involved in the early steps of mitochondrial fission by marking the division sites (Csordas et al., 1999). Despite these interesting findings, the precise role and regulation of MAMs in the development and progression of DKD await further investigation.

TARGETING MITOCHONDRIAL DYSFUNCTION

Although the precise roles of mitochondrial function in podocyte health and disease are not completely understood, targeting mitochondria could be a very promising strategy to treat podocyte dysfunction. Various therapeutic strategies that target mitochondria are under investigation for the treatment of podocyte dysfunction and/or DKD. Emerging data from preclinical and preliminary clinical data suggest that targeting mitochondrial dysfunction is a sound rationale. Several investigational drugs are in different stages of clinical evaluation. Although some of these drugs are currently used in clinical trials for the treatment of other CKDs, preclinical data suggest that these therapies are also promising agents for the treatment of DKD by targeting the mitochondrial function of podocytes.

Antioxidants are the oldest class of drugs used to counteract ROS generation and treat mitochondrial dysfunction. Currently, the majority of ongoing clinical trials for the treatment of mitochondrial diseases are still based on the use of antioxidants (Forbes and Thorburn 2018). In mitochondria, Coenzyme Q10 (CoQ10; ubiquinone) is a pivotal component of the mitochondrial respiratory chain with powerful antioxidant capacity, as it shuttles electrons from both complexes I and II to complex III of the electron transport chain. Knockout of genes involved in coding the CoQ10 biosynthesis pathway enzymes in glomerular podocytes is sufficient to induce the typical phenotypes of nephrotic syndrome and focal segmental glomerular sclerosis (Widmeier et al., 2019; Widmeier et al., 2020). CoQ10 therapy of rodent models with DKD could significantly decrease albuminuria and prevent detrimental changes in mitochondrial function, indicating its potent protective effect on the GFB and podocytes (Sourris et al., 2012). Case reports and case series have reported the treatment with CoQ10 or its synthetic analogue idebenone significantly reduced albuminuria in paediatric patients with COQ6 glomerulopathy or ADCK4 mutation (Feng et al., 2017; Stanczyk et al., 2018). CoQ10 is not water soluble, which limits its transport to the IMM. More recently, more soluble and hydrophilic 2,4-dihydroxybenzoic acid (2,4-diHB) has been shown to have a strong effect in rescuing podocyte function and preventing renal disease caused by primary dysfunction in the CoQ10 biosynthesis pathway (Widmeier et al., 2019; Widmeier et al., 2020). These findings warrant further evaluation in prospective human studies in the near future. MicroRNA-21 (miR-21) has been widely studied in kidney disease because of its important antiapoptotic effects (Chen et al., 2018; Wang et al., 2019). MiR-21 expression is upregulated in kidney tissues of DKD patients and HG-treated podocytes, and the down-regulation of miR-21 inhibited the progression of DKD (Chen et al., 2018). Furthermore, miR-21 is involved in the regulation of mitochondrial dysfunction by disrupting ROS homeostasis (La Sala et al., 2018). Lademirsen is an antisense oligonucleotide that inhibits miR-21, and there is some evidence that it can enhance mitochondrial function in podocytes; it is currently under clinical evaluation in Alport syndrome patients (NCT02855268) (Gomez et al., 2015). Nuclear respiratory factor 2 (Nrf2), a master regulator of the stress response, is relatively inactive under non-stressed conditions. Activation of Nrf2 inhibits the expression of Drp1 and mitochondrial fission, leading to enhanced mitochondrial fusion and survival (Zhu et al., 2019). Drp1 hyperactivation and excessive/pathological mitochondrial fission occur in various DKD models, and selective activation of Nrf2 is sufficient for its anti-senescent and podocyte protective effects (Fang et al., 2021). Due to this, its potential as a therapeutic target in DKD has been increasingly discussed. Bardoxolone methyl is a novel, small-molecule inhibitor of Nrf2 that improves kidney function in several glomerular diseases and is under clinical evaluation in patients with chronic kidney disease (NCT03749447) or DKD (NCT03550443) (Zhou et al., 2020; Daehn and Duffield 2021) (**Table 1**).

In addition, although several previous and current drugs to treat DKD do not directly target mitochondrial function, they play a protective role under conditions that affect mitochondria. For example, the Study of Diabetic Nephropathy with Antrasentan (SONAR) trial found that the endothelin A receptor (EAR) antagonist atrasentan reduced the risk of renal events by 35% in patients with DKD (Heerspink et al., 2019). Analysis of urinary metabolites from DKD patients treated with atrasentan revealed that it might prevent the progression of mitochondrial dysfunction (Pena et al., 2017). Similar results were obtained in DKD patients treated with sodium glucose cotransporter 2 (SGLT2) inhibitors, such as dapagliflozin, canagliflozin, and empagliflozin (Liu et al., 2020; Liu et al., 2021). Currently, there are no studies investigating the effect of EAR antagonists or SGLT2 inhibitors on the mitochondrial function of podocytes. This may be worthy of further study.

Despite the fact that direct targeting of mitochondrial function as a therapeutic approach is not satisfactory, the development of specific molecules targeting mitochondria and mitochondria-associated signalling pathways for therapeutic gain is a rapidly evolving field. In recent years, numerous specific molecules and treatment strategies targeting various aspects of mitochondrial dysfunction have been reported. The targets involve many genes controlling mitochondrial biogenesis and energy homeostasis, including PGC-1α, Drp1 and ROS. The molecular targets, mechanisms of action and therapeutic effects of these preclinical drugs are summarized in **Table 2**.

None of the existing drugs could be specifically targeted to mitochondrial health of podocytes. Nevertheless, a success in one of these ongoing clinical trials will provide important new insights into the development of innovative regimens for podocyte dysfunction. Therefore, there is a continuing need to identify novel and more specific targets to target

mitochondria to widen the scope of current treatments for DKD. In addition to identifying effective therapeutic agents, considering the optimal timing for these interventions is also needed. Predictive biomarkers that can help guide decision-making to target mitochondrial dysfunction to prevent DKD are likewise lacking.

FUTURE DIRECTIONS

Although increasing amounts of evidence has demonstrated that mitochondrial dysfunction of podocytes is involved in the development and progression of DKD, our understanding of the role of mitochondrial damage in DKD remains limited. There are several unanswered questions in this area. First, it is clear that mitochondrial dysfunction is a common pathological hallmark and occurs early in DKD. Although much is known about mitochondrial dynamics, mitophagy, ROS production and biogenesis, the exact role and interaction of each process in DKD remains unclear. Second, despite evidence that MAMs play an important role during the development and progression of DKD, their precise role remains largely unclear. The relationship between the MAMs and mitochondrial dysfunction has attracted increasing attention. A further understanding of the role of the MAMs in mediating mitochondrial dysfunction under hyperglycemic condition might lead to new therapeutic options for DKD. Third, there are currently no mitochondria-targeting therapeutic agents approved for DKD. Modern small-molecule drug design, advances in nucleic acid-based therapeutics, and novel nano-drug delivery systems have greatly assisted in enhancing bioavailablity and mitochondrial targeting during the development of more effective therapeutic agents. We can therefore expect many more innovations to occur in the near future.

AUTHOR CONTRIBUTIONS

BZ, CX, and YY conceived the study. SL wrote and revised the manuscript. BZ and YX revised the manuscript. All the authors contributed to the article and approved the submitted version.

FUNDING

This study was supported by grants from the "PRO•Run" Fund of the Nephrology Group of CEBM (KYS 2021-03-02-14), and the National Natural Science Foundation of China (Nos. 81670628, 81870469).

REFERENCES

Abrisch, R. G., Gumbin, S. C., Wisniewski, B. T., Lackner, L. L., and Voeltz, G. K. (2020). Fission and Fusion Machineries Converge at ER Contact Sites to Regulate Mitochondrial Morphology. *J. Cell Biol* 219, e201911122. doi:10.1083/jcb.201911122

Adachi, Y., Kato, T., Yamada, T., Murata, D., Arai, K., Stahelin, R. V., et al. (2020). Drp1 Tubulates the ER in a GTPase-independent Manner. *Mol. Cell* 80, 621–632. doi:10.1016/j.molcel.2020.10.013

Agrawal, S., He, J. C., and Tharaux, P.-L. (2021). Nuclear Receptors in Podocyte Biology and Glomerular Disease. *Nat. Rev. Nephrol.* 17, 185–204. doi:10.1038/s41581-020-00339-6

Alicic, R. Z., Rooney, M. T., and Tuttle, K. R. (2017). Diabetic Kidney Disease: Challenges, Progress, and Possibilities. *Cjasn* 12, 2032–2045. doi:10.2215/CJN.11491116

Arif, E., Solanki, A. K., Srivastava, P., Rahman, B., Fitzgibbon, W. R., Deng, P., et al. (2019). Mitochondrial Biogenesis Induced by the β2-adrenergic Receptor Agonist Formoterol Accelerates Podocyte Recovery from Glomerular Injury. *Kidney Int.* 96, 656–673. doi:10.1016/j.kint.2019.03.023

Audzeyenka, I., Rachubik, P., Typiak, M., Kulesza, T., Topolewska, A., Rogacka, D., et al. (2021). Hyperglycemia Alters Mitochondrial Respiration Efficiency and Mitophagy in Human Podocytes. *Exp. Cell Res.* 407, 112758. doi:10.1016/j.yexcr.2021.112758

Ayanga, B. A., Badal, S. S., Wang, Y., Galvan, D. L., Chang, B. H., Schumacker, P. T., et al. (2016). Dynamin-Related Protein 1 Deficiency Improves Mitochondrial Fitness and Protects against Progression of Diabetic Nephropathy. *Jasn* 27, 2733–2747. doi:10.1681/ASN.2015101096

Baek, J.-H., Gomez, I. G., Wada, Y., Roach, A., Mahad, D., and Duffield, J. S. (2018). Deletion of the Mitochondrial Complex-IV Cofactor Heme A:Farnesyltransferase Causes Focal Segmental Glomerulosclerosis and Interferon Response. *Am. J. Pathol.* 188, 2745–2762. doi:10.1016/j.ajpath.2018.08.018

Bao, L., Cai, X., Dai, X., Ding, Y., Jiang, Y., Li, Y., et al. (2014). Grape Seed Proanthocyanidin Extracts Ameliorate Podocyte Injury by Activating Peroxisome Proliferator-Activated Receptor-γ Coactivator 1α in Low-Dose Streptozotocin-And High-Carbohydrate/high-Fat Diet-Induced Diabetic Rats. *Food Funct.* 5, 1872–1880. doi:10.1039/c4fo00340c

Barutta, F., Pinach, S., Giunti, S., Vittone, F., Forbes, J. M., Chiarle, R., et al. (2008). Heat Shock Protein Expression in Diabetic Nephropathy. *Am. J. Physiology-Renal Physiol.* 295, F1817–F1824. doi:10.1152/ajprenal.90234.2008

Bhargava, P., and Schnellmann, R. G. (2017). Mitochondrial Energetics in the Kidney. *Nat. Rev. Nephrol.* 13, 629–646. doi:10.1038/nrneph.2017.107

Bhosale, G., Sharpe, J. A., Sundier, S. Y., and Duchen, M. R. (2015). Calcium Signaling as a Mediator of Cell Energy Demand and a Trigger to Cell Death. *Ann. N.Y. Acad. Sci.* 1350, 107–116. doi:10.1111/nyas.12885

Braschi, E., Zunino, R., and McBride, H. M. (2009). MAPL Is a New Mitochondrial SUMO E3 Ligase that Regulates Mitochondrial Fission. *EMBO Rep.* 10, 748–754. doi:10.1038/embor.2009.86

Brownlee, M. (2005). The Pathobiology of Diabetic Complications: a Unifying Mechanism. *Diabetes* 54, 1615–1625. doi:10.2337/diabetes.54.6.1615

Cai, X., Bao, L., Ren, J., Li, Y., and Zhang, Z. (2016). Grape Seed Procyanidin B2 Protects Podocytes from High Glucose-Induced Mitochondrial Dysfunction and Apoptosis via the AMPK-SIRT1-PGC-1α axis *In Vitro*. *Food Funct.* 7, 805–815. doi:10.1039/c5fo01062d

Carney, E. F. (2015). Glomerular Disease: Autophagy Failure and Mitochondrial Dysfunction in FSGS. *Nat. Rev. Nephrol.* 11, 66. doi:10.1038/nrneph.2014.233

Cereghetti, G. M., Stangherlin, A., de Brito, O. M., Chang, C. R., Blackstone, C., Bernardi, P., et al. (2008). Dephosphorylation by Calcineurin Regulates Translocation of Drp1 to Mitochondria. *Proc. Natl. Acad. Sci.* 105, 15803–15808. doi:10.1073/pnas.0808249105

Chen, H., Detmer, S. A., Ewald, A. J., Griffin, E. E., Fraser, S. E., and Chan, D. C. (2003). Mitofusins Mfn1 and Mfn2 Coordinately Regulate Mitochondrial Fusion and Are Essential for Embryonic Development. *J. Cell Biol* 160, 189–200. doi:10.1083/jcb.200211046

Chen, X., Zhao, L., Xing, Y., and Lin, B. (2018). Down-regulation of microRNA-21 Reduces Inflammation and Podocyte Apoptosis in Diabetic Nephropathy by Relieving the Repression of TIMP3 Expression. *Biomed. Pharmacother.* 108, 7–14. doi:10.1016/j.biopha.2018.09.007

Chen, Z., Ma, Y., Yang, Q., Hu, J., Feng, J., Liang, W., et al. (2020). AKAP1 Mediates High Glucose-induced Mitochondrial Fission through the Phosphorylation of Drp1 in Podocytes. *J. Cell Physiol* 235, 7433–7448. doi:10.1002/jcp.29646

Chen, Z., Miao, F., Paterson, A. D., Lachin, J. M., Zhang, L., Schones, D. E., et al. (2016). Epigenomic Profiling Reveals an Association between Persistence of DNA Methylation and Metabolic Memory in the DCCT/EDIC Type 1 Diabetes Cohort. *Proc. Natl. Acad. Sci. USA* 113, E3002–E3011. doi:10.1073/pnas.1603712113

Choi, J. P., Park, S. Y., Moon, K. A., Ha, E. H., Woo, Y. D., Chung, D. H., et al. (2020). Macrophage-derived Progranulin Promotes Allergen-induced Airway Inflammation. *Allergy* 75, 1133–1145. doi:10.1111/all.14129

Choi, M. E. (2020). Autophagy in Kidney Disease. *Annu. Rev. Physiol.* 82, 297–322. doi:10.1146/annurev-physiol-021119-034658

Coughlan, M. T., Higgins, G. C., Nguyen, T.-V., Penfold, S. A., Thallas-Bonke, V., Tan, S. M., et al. (2016). Deficiency in Apoptosis-Inducing Factor Recapitulates Chronic Kidney Disease via Aberrant Mitochondrial Homeostasis. *Diabetes* 65, 1085–1098. doi:10.2337/db15-0864

Cribbs, J. T., and Strack, S. (2007). Reversible Phosphorylation of Drp1 by Cyclic AMP-dependent Protein Kinase and Calcineurin Regulates Mitochondrial Fission and Cell Death. *EMBO Rep.* 8, 939–944. doi:10.1038/sj.embor.7401062

Csordas, G., Thomas, A. P., and Hajnoczky, G. (1999). Quasi-synaptic Calcium Signal Transmission between Endoplasmic Reticulum and Mitochondria. *EMBO J.* 18, 96–108. doi:10.1093/emboj/18.1.96

Csorda´s, G., Renken, C., Va´rnai, P., Walter, L., Weaver, D., Buttle, K. F., et al. (2006). Structural and Functional Features and Significance of the Physical Linkage between ER and Mitochondria. *J. Cell Biol* 174, 915–921. doi:10.1083/jcb.200604016

Cybulsky, A. V. (2017). Endoplasmic Reticulum Stress, the Unfolded Protein Response and Autophagy in Kidney Diseases. *Nat. Rev. Nephrol.* 13, 681–696. doi:10.1038/nrneph.2017.129

Czajka, A., Ajaz, S., Gnudi, L., Parsade, C. K., Jones, P., Reid, F., et al. (2015). Altered Mitochondrial Function, Mitochondrial DNA and Reduced Metabolic Flexibility in Patients with Diabetic Nephropathy. *EBioMedicine* 2, 499–512. doi:10.1016/j.ebiom.2015.04.002

Daehn, I. S., and Duffield, J. S. (2021). The Glomerular Filtration Barrier: a Structural Target for Novel Kidney Therapies. *Nat. Rev. Drug Discov.* 20, 770–788. doi:10.1038/s41573-021-00242-0

Dai, W., Lu, H., Chen, Y., Yang, D., Sun, L., and He, L. (2021). The Loss of Mitochondrial Quality Control in Diabetic Kidney Disease. *Front. Cell Dev. Biol.* 9, 706832. doi:10.3389/fcell.2021.706832

Davis, B. K., Wen, H., and Ting, J. P.-Y. (2011). The Inflammasome NLRs in Immunity, Inflammation, and Associated Diseases. *Annu. Rev. Immunol.* 29, 707–735. doi:10.1146/annurev-immunol-031210-101405

de Brito, O. M., and Scorrano, L. (2008). Mitofusin 2 Tethers Endoplasmic Reticulum to Mitochondria. *Nature* 456, 605–610. doi:10.1038/nature07534

Deng, Q., Wen, R., Liu, S., Chen, X., Song, S., Li, X., et al. (2020). Increased Long Noncoding RNA Maternally Expressed Gene 3 Contributes to Podocyte Injury Induced by High Glucose through Regulation of Mitochondrial Fission. *Cell Death Dis* 11, 814. doi:10.1038/s41419-020-03022-7

Dikic, I., and Elazar, Z. (2018). Mechanism and Medical Implications of Mammalian Autophagy. *Nat. Rev. Mol. Cell Biol* 19, 349–364. doi:10.1038/s41580-018-0003-4

Dorotea, D., Cho, A., Lee, G., Kwon, G., Lee, J., Sahu, P. K., et al. (2018). Orally Active, Species-independent Novel A3 Adenosine Receptor Antagonist Protects against Kidney Injury in Db/db Mice. *Exp. Mol. Med.* 50, 1–14. doi:10.1038/s12276-018-0053-x

Dugan, L. L., You, Y.-H., Ali, S. S., Diamond-Stanic, M., Miyamoto, S., DeCleves, A.-E., et al. (2013). AMPK Dysregulation Promotes Diabetes-Related Reduction of Superoxide and Mitochondrial Function. *J. Clin. Invest.* 123, 4888–4899. doi:10.1172/JCI66218

Dumesic, P. A., Egan, D. F., Gut, P., Tran, M. T., Parisi, A., Chatterjee, N., et al. (2019). An Evolutionarily Conserved uORF Regulates PGC1α and Oxidative Metabolism in Mice, Flies, and Bluefin Tuna. *Cell Metab.* 30, 190–200. doi:10.1016/j.cmet.2019.04.013

Fakhruddin, S., Alanazi, W., and Jackson, K. E. (2017). Diabetes-Induced Reactive Oxygen Species: Mechanism of Their Generation and Role in Renal Injury. *J. Diabetes Res.* 2017, 1–30. doi:10.1155/2017/8379327

Fan, W., and Evans, R. (2015). PPARs and ERRs: Molecular Mediators of Mitochondrial Metabolism. *Curr. Opin. Cell Biol.* 33, 49–54. doi:10.1016/j.ceb.2014.11.002

Fan, Y., Yang, Q., Yang, Y., Gao, Z., Ma, Y., Zhang, L., et al. (2019). Sirt6 Suppresses High Glucose-Induced Mitochondrial Dysfunction and Apoptosis in Podocytes through AMPK Activation. *Int. J. Biol. Sci.* 15, 701–713. doi:10.7150/ijbs.29323

Fang, Y., Chen, B., Gong, A. Y., Malhotra, D. K., Gupta, R., Dworkin, L. D., et al. (2021). The Ketone Body β-hydroxybutyrate Mitigates the Senescence Response of Glomerular Podocytes to Diabetic Insults. *Kidney Int.* 100, 1037–1053. doi:10.1016/j.kint.2021.06.031

Feng, C., Wang, Q., Wang, J., Liu, F., Shen, H., Fu, H., et al. (2017). Coenzyme Q10 Supplementation Therapy for 2 Children with Proteinuria Renal Disease and ADCK4 Mutation: Case Reports and Literature Review. *Medicine (Baltimore)* 96, e8880. doi:10.1097/MD.0000000000008880

Forbes, J. M., and Thorburn, D. R. (2018). Mitochondrial Dysfunction in Diabetic Kidney Disease. *Nat. Rev. Nephrol.* 14, 291–312. doi:10.1038/nrneph.2018.9

Galloway, C. A., Lee, H., Nejjar, S., Jhun, B. S., Yu, T., Hsu, W., et al. (2012). Transgenic Control of Mitochondrial Fission Induces Mitochondrial Uncoupling and Relieves Diabetic Oxidative Stress. *Diabetes* 61, 2093–2104. doi:10.2337/db11-1640

Galvan, D. L., Green, N. H., and Danesh, F. R. (2017). The Hallmarks of Mitochondrial Dysfunction in Chronic Kidney Disease. *Kidney Int.* 92, 1051–1057. doi:10.1016/j.kint.2017.05.034

Gawlowski, T., Suarez, J., Scott, B., Torres-Gonzalez, M., Wang, H., Schwappacher, R., et al. (2012). Modulation of Dynamin-Related Protein 1 (DRP1) Function by Increased O-Linked-β-N-Acetylglucosamine Modification (O-GlcNAc) in Cardiac Myocytes. *J. Biol. Chem.* 287, 30024–30034. doi:10.1074/jbc.M112.390682

Gerber, S., Charif, M., Chevrollier, A., Chaumette, T., Angebault, C., Kane, M. S., et al. (2017). Mutations in DNM1L, as in OPA1, Result in Dominant Optic Atrophy Despite Opposite Effects on Mitochondrial Fusion and Fission. *Brain* 140, 2586–2596. doi:10.1093/brain/awx219

Gomez, I. G., MacKenna, D. A., Johnson, B. G., Kaimal, V., Roach, A. M., Ren, S., et al. (2015). Anti-microRNA-21 Oligonucleotides Prevent Alport Nephropathy Progression by Stimulating Metabolic Pathways. *J. Clin. Invest.* 125, 141–156. doi:10.1172/JCI75852

Gray, S. P., Jha, J. C., Kennedy, K., van Bommel, E., Chew, P., Szyndralewiez, C., et al. (2017). Combined NOX1/4 Inhibition with GKT137831 in Mice Provides Dose-dependent reno- and Atheroprotection Even in Established Micro- and Macrovascular Disease. *Diabetologia* 60, 927–937. doi:10.1007/s00125-017-4215-5

Greene, A. W., Grenier, K., Aguileta, M. A., Muise, S., Farazifard, R., Haque, M. E., et al. (2012). Mitochondrial Processing Peptidase Regulates PINK1 Processing, Import and Parkin Recruitment. *EMBO Rep.* 13, 378–385. doi:10.1038/embor.2012.14

Gregg, E. W., Li, Y., Wang, J., Rios Burrows, N., Ali, M. K., Rolka, D., et al. (2014). Changes in Diabetes-Related Complications in the United States, 1990-2010. *N. Engl. J. Med.* 370, 1514–1523. doi:10.1056/NEJMoa1310799

Hamasaki, M., Furuta, N., Matsuda, A., Nezu, A., Yamamoto, A., Fujita, N., et al. (2013). Autophagosomes Form at ER-Mitochondria Contact Sites. *Nature* 495, 389–393. doi:10.1038/nature11910

Heeringa, S. F., Chernin, G., Chaki, M., Zhou, W., Sloan, A. J., Ji, Z., et al. (2011). COQ6 Mutations in Human Patients Produce Nephrotic Syndrome with Sensorineural Deafness. *J. Clin. Invest.* 121, 2013–2024. doi:10.1172/JCI45693

Heerspink, H. J. L., Parving, H. H., Andress, D. L., Bakris, G., Correa-Rotter, R., Hou, F. F., et al. (2019). Atrasentan and Renal Events in Patients with Type 2 Diabetes and Chronic Kidney Disease (SONAR): a Double-Blind, Randomised, Placebo-Controlled Trial. *Lancet* 393, 1937–1947. doi:10.1016/S0140-6736(19)30772-X

Hershberger, K. A., Martin, A. S., and Hirschey, M. D. (2017). Role of NAD+ and Mitochondrial Sirtuins in Cardiac and Renal Diseases. *Nat. Rev. Nephrol.* 13, 213–225. doi:10.1038/nrneph.2017.5

Hickey, F. B., Corcoran, J. B., Docherty, N. G., Griffin, B., Bhreathnach, U., Furlong, F., et al. (2011). IHG-1 Promotes Mitochondrial Biogenesis by Stabilizing PGC-1α. *Jasn* 22, 1475–1485. doi:10.1681/ASN.2010111154

Holterman, C. E., Read, N. C., and Kennedy, C. R. J. (2015). Nox and Renal Disease. *Clin. Sci. (Lond).* 128, 465–481. doi:10.1042/CS20140361

Hondares, E., Mora, O., Yubero, P., de la Concepcio´n, M. R., Iglesias, R., Giralt, M., et al. (2006). Thiazolidinediones and Rexinoids Induce Peroxisome

Proliferator-Activated Receptor-Coactivator (PGC)-1α Gene Transcription: An Autoregulatory Loop Controls PGC-1α Expression in Adipocytes via Peroxisome Proliferator-Activated Receptor-γ Coactivation. *Endocrinology* 147, 2829–2838. doi:10.1210/en.2006-0070

Inoue, T., Maekawa, H., and Inagi, R. (2019). Organelle Crosstalk in the Kidney. *Kidney Int.* 95, 1318–1325. doi:10.1016/j.kint.2018.11.035

James, D. I., Parone, P. A., Mattenberger, Y., and Martinou, J.-C. (2003). hFis1, a Novel Component of the Mammalian Mitochondrial Fission Machinery. *J. Biol. Chem.* 278, 36373–36379. doi:10.1074/jbc.M303758200

Jha, J. C., Gray, S. P., Barit, D., Okabe, J., El-Osta, A., Namikoshi, T., et al. (2014). Genetic Targeting or Pharmacologic Inhibition of NADPH Oxidase Nox4 Provides Renoprotection in Long-Term Diabetic Nephropathy. *Jasn* 25, 1237–1254. doi:10.1681/ASN.2013070810

Jha, J. C., Thallas-Bonke, V., Banal, C., Gray, S. P., Chow, B. S. M., Ramm, G., et al. (2016). Podocyte-specific Nox4 Deletion Affords Renoprotection in a Mouse Model of Diabetic Nephropathy. *Diabetologia* 59, 379–389. doi:10.1007/s00125-015-3796-0

Ji, W.-K., Chakrabarti, R., Fan, X., Schoenfeld, L., Strack, S., and Higgs, H. N. (2017). Receptor-mediated Drp1 Oligomerization on Endoplasmic Reticulum. *J. Cell Biol* 216, 4123–4139. doi:10.1083/jcb.201610057

Jiang, M., Bai, M., Lei, J., Xie, Y., Xu, S., Jia, Z., et al. (2020). Mitochondrial Dysfunction and the AKI-To-CKD Transition. *Am. J. Physiology-Renal Physiol.* 319, F1105–F1116. doi:10.1152/ajprenal.00285.2020

Kalia, R., Wang, R. Y.-R., Yusuf, A., Thomas, P. V., Agard, D. A., Shaw, J. M., et al. (2018). Structural Basis of Mitochondrial Receptor Binding and Constriction by DRP1. *Nature* 558, 401–405. doi:10.1038/s41586-018-0211-2

Kang, M.-K., Park, S.-H., Kim, Y.-H., Lee, E.-J., Antika, L. D., Kim, D. Y., et al. (2017). Chrysin Ameliorates Podocyte Injury and Slit Diaphragm Protein Loss via Inhibition of the PERK-eIF2α-ATF-CHOP Pathway in Diabetic Mice. *Acta Pharmacol. Sin* 38, 1129–1140. doi:10.1038/aps.2017.30

Kang, Y., Li, Y., Zhang, T., Chi, Y., and Liu, M. (2019). Effects of Transcription Factor EB on Oxidative Stress and Apoptosis Induced by High Glucose in Podocytes. *Int. J. Mol. Med.* 44, 447–456. doi:10.3892/ijmm.2019.4209

Kornmann, B., Currie, E., Collins, S. R., Schuldiner, M., Nunnari, J., Weissman, J. S., et al. (2009). An ER-Mitochondria Tethering Complex Revealed by a Synthetic Biology Screen. *Science* 325, 477–481. doi:10.1126/science.1175088

Kraus, F., Roy, K., Pucadyil, T. J., and Ryan, M. T. (2021). Function and Regulation of the Divisome for Mitochondrial Fission. *Nature* 590, 57–66. doi:10.1038/s41586-021-03214-x

La Sala, L., Mrakic-Sposta, S., Micheloni, S., Prattichizzo, F., and Ceriello, A. (2018). Glucose-sensing microRNA-21 Disrupts ROS Homeostasis and Impairs Antioxidant Responses in Cellular Glucose Variability. *Cardiovasc. Diabetol.* 17, 105. doi:10.1186/s12933-018-0748-2

Lazarou, M., Sliter, D. A., Kane, L. A., Sarraf, S. A., Wang, C., Burman, J. L., et al. (2015). The Ubiquitin Kinase PINK1 Recruits Autophagy Receptors to Induce Mitophagy. *Nature* 524, 309–314. doi:10.1038/nature14893

Li, S.-Y., Park, J., Qiu, C., Han, S. H., Palmer, M. B., Arany, Z., et al. (2017a). Increasing the Level of Peroxisome Proliferator-Activated Receptor γ Coactivator-1α in Podocytes Results in Collapsing Glomerulopathy. *JCI Insight* 2, e92930. doi:10.1172/jci.insight.92930

Li, S.-Y., and Susztak, K. (2018). The Role of Peroxisome Proliferator-Activated Receptor γ Coactivator 1α (PGC-1α) in Kidney Disease. *Semin. Nephrol.* 38, 121–126. doi:10.1016/j.semnephrol.2018.01.003

Li, W., Du, M., Wang, Q., Ma, X., Wu, L., Guo, F., et al. (2017b). FoxO1 Promotes Mitophagy in the Podocytes of Diabetic Male Mice via the PINK1/Parkin Pathway. *Endocrinology* 158, 2155–2167. doi:10.1210/en.2016-1970

Li, W., Wang, Q., Du, M., Ma, X., Wu, L., Guo, F., et al. (2016). Effects of Overexpressing FoxO1 on Apoptosis in Glomeruli of Diabetic Mice and in Podocytes Cultured in High Glucose Medium. *Biochem. Biophysical Res. Commun.* 478, 612–617. doi:10.1016/j.bbrc.2016.07.115

Liang, Y., Liu, H., Fang, Y., Lin, P., Lu, Z., Zhang, P., et al. (2021). Salvianolate Ameliorates Oxidative Stress and Podocyte Injury through Modulation of NOX4 Activity in Db/db Mice. *J. Cell Mol Med* 25, 1012–1023. doi:10.1111/jcmm.16165

Liu, H., Sridhar, V. S., Montemayor, D., Lovblom, L. E., Lytvyn, Y., Ye, H., et al. (2021). Changes in Plasma and Urine Metabolites Associated with Empagliflozin in Patients with Type 1 Diabetes. *Diabetes Obes. Metab.* 23, 2466–2475. doi:10.1111/dom.14489

Liu, W. J., Gan, Y., Huang, W. F., Wu, H.-l., Zhang, X.-q., Zheng, H. J., et al. (2019). Lysosome Restoration to Activate Podocyte Autophagy: a New Therapeutic Strategy for Diabetic Kidney Disease. *Cell Death Dis* 10, 806. doi:10.1038/s41419-019-2002-6

Liu, X., Xu, C., Xu, L., Li, X., Sun, H., Xue, M., et al. (2020). Empagliflozin Improves Diabetic Renal Tubular Injury by Alleviating Mitochondrial Fission via AMPK/SP1/PGAM5 Pathway. *Metabolism* 111, 154334. doi:10.1016/j.metabol.2020.154334

Long, J., Badal, S. S., Ye, Z., Wang, Y., Ayanga, B. A., Galvan, D. L., et al. (2016). Long Noncoding RNA Tug1 Regulates Mitochondrial Bioenergetics in Diabetic Nephropathy. *J. Clin. Invest.* 126, 4205–4218. doi:10.1172/JCI87927

Ma, Y., Chen, Z., Tao, Y., Zhu, J., Yang, H., Liang, W., et al. (2019). Increased Mitochondrial Fission of Glomerular Podocytes in Diabetic Nephropathy. *Endocr. Connect.* 8, 1206–1212. doi:10.1530/EC-19-0234

Martínez-Klimova, E., Aparicio-Trejo, O. E., Gómez-Sierra, T., Jiménez-Uribe, A. P., Bellido, B., and Pedraza-Chaverri, J. (2020). Mitochondrial Dysfunction and Endoplasmic Reticulum Stress in the Promotion of Fibrosis in Obstructive Nephropathy Induced by Unilateral Ureteral Obstruction. *Biofactors* 46, 716–733. doi:10.1002/biof.1673

Meeusen, S., DeVay, R., Block, J., Cassidy-Stone, A., Wayson, S., McCaffery, J. M., et al. (2006). Mitochondrial Inner-Membrane Fusion and Crista Maintenance Requires the Dynamin-Related GTPase Mgm1. *Cell* 127, 383–395. doi:10.1016/j.cell.2006.09.021

Ng, M. Y. W., Wai, T., and Simonsen, A. (2021). Quality Control of the Mitochondrion. *Dev. Cell* 56, 881–905. doi:10.1016/j.devcel.2021.02.009

Ni, Z., Tao, L., Xiaohui, X., Zelin, Z., Jiangang, L., Zhao, S., et al. (2017). Polydatin Impairs Mitochondria Fitness and Ameliorates Podocyte Injury by Suppressing Drp1 Expression. *J. Cell. Physiol.* 232, 2776–2787. doi:10.1002/jcp.25943

Nieto-Posadas, A., Jara-Oseguera, A., and Rosenbaum, T. (2011). TRP Channel Gating Physiology. *Ctmc* 11, 2131–2150. doi:10.2174/156802611796904870

Nisoli, E., Falcone, S., Tonello, C., Cozzi, V., Palomba, L., Fiorani, M., et al. (2004). Mitochondrial Biogenesis by NO Yields Functionally Active Mitochondria in Mammals. *Proc. Natl. Acad. Sci.* 101, 16507–16512. doi:10.1073/pnas.0405432101

Otera, H., Wang, C., Cleland, M. M., Setoguchi, K., Yokota, S., Youle, R. J., et al. (2010). Mff Is an Essential Factor for Mitochondrial Recruitment of Drp1 during Mitochondrial Fission in Mammalian Cells. *J. Cell Biol* 191, 1141–1158. doi:10.1083/jcb.201007152

Palikaras, K., Lionaki, E., and Tavernarakis, N. (2018). Mechanisms of Mitophagy in Cellular Homeostasis, Physiology and Pathology. *Nat. Cell Biol* 20, 1013–1022. doi:10.1038/s41556-018-0176-2

Palmer, C. S., Elgass, K. D., Parton, R. G., Osellame, L. D., Stojanovski, D., and Ryan, M. T. (2013). Adaptor Proteins MiD49 and MiD51 Can Act Independently of Mff and Fis1 in Drp1 Recruitment and Are Specific for Mitochondrial Fission. *J. Biol. Chem.* 288, 27584–27593. doi:10.1074/jbc.M113.479873

Parakh, S., and Atkin, J. D. (2021). The Mitochondrial-Associated ER Membrane (MAM) Compartment and its Dysregulation in Amyotrophic Lateral Sclerosis (ALS). *Semin. Cell Dev. Biol.* 112, 105–113. doi:10.1016/j.semcdb.2021.02.002

Park, J. H., Kang, H.-J., Lee, Y. K., Kang, H., Kim, J., Chung, J. H., et al. (2015). Inactivation of EWS Reduces PGC-1α Protein Stability and Mitochondrial Homeostasis. *Proc. Natl. Acad. Sci. USA* 112, 6074–6079. doi:10.1073/pnas.1504391112

Pena, M. J., de Zeeuw, D., Andress, D., Brennan, J. J., Correa-Rotter, R., Coll, B., et al. (2017). The Effects of Atrasentan on Urinary Metabolites in Patients with Type 2 Diabetes and Nephropathy. *Diabetes Obes. Metab.* 19, 749–753. doi:10.1111/dom.12864

Pickles, S., Vigié, P., and Youle, R. J. (2018). Mitophagy and Quality Control Mechanisms in Mitochondrial Maintenance. *Curr. Biol.* 28, R170–R185. doi:10.1016/j.cub.2018.01.004

Qi, W., Keenan, H. A., Li, Q., Ishikado, A., Kannt, A., Sadowski, T., et al. (2017). Pyruvate Kinase M2 Activation May Protect against the Progression of Diabetic Glomerular Pathology and Mitochondrial Dysfunction. *Nat. Med.* 23, 753–762. doi:10.1038/nm.4328

Qi, Z., Huang, Z., Xie, F., and Chen, L. (2019). Dynamin-related Protein 1: A Critical Protein in the Pathogenesis of Neural System Dysfunctions and Neurodegenerative Diseases. *J. Cell Physiol* 234, 10032–10046. doi:10.1002/jcp.27866

Qin, X., Jiang, M., Zhao, Y., Gong, J., Su, H., Yuan, F., et al. (2020). Berberine Protects against Diabetic Kidney Disease via Promoting PGC-1α-regulated Mitochondrial Energy Homeostasis. *Br. J. Pharmacol.* 177, 3646–3661. doi:10.1111/bph.14935

Qin, X., Zhao, Y., Gong, J., Huang, W., Su, H., Yuan, F., et al. (2019). Berberine Protects Glomerular Podocytes via Inhibiting Drp1-Mediated Mitochondrial Fission and Dysfunction. *Theranostics* 9, 1698–1713. doi:10.7150/thno.30640

Qu, H., Gong, X., Liu, X., Zhang, R., Wang, Y., Huang, B., et al. (2021). Deficiency of Mitochondrial Glycerol 3-Phosphate Dehydrogenase Exacerbates Podocyte Injury and the Progression of Diabetic Kidney Disease. *Diabetes* 70, 1372–1387. doi:10.2337/db20-1157

Randow, F., and Youle, R. J. (2014). Self and Nonself: How Autophagy Targets Mitochondria and Bacteria. *Cell Host & Microbe* 15, 403–411. doi:10.1016/j.chom.2014.03.012

Rath, S., Sharma, R., Gupta, R., Ast, T., Chan, C., Durham, T. J., et al. (2021). MitoCarta3.0: an Updated Mitochondrial Proteome Now with Sub-organelle Localization and Pathway Annotations. *Nucleic Acids Res.* 49, D1541–D1547. doi:10.1093/nar/gkaa1011

Reidy, K., Kang, H. M., Hostetter, T., and Susztak, K. (2014). Molecular Mechanisms of Diabetic Kidney Disease. *J. Clin. Invest.* 124, 2333–2340. doi:10.1172/JCI72271

Sabouny, R., and Shutt, T. E. (2020). Reciprocal Regulation of Mitochondrial Fission and Fusion. *Trends Biochem. Sci.* 45, 564–577. doi:10.1016/j.tibs.2020.03.009

Sardiello, M., Palmieri, M., di Ronza, A., Medina, D. L., Valenza, M., Gennarino, V. A., et al. (2009). A Gene Network Regulating Lysosomal Biogenesis and Function. *Science* 325, 473–477. doi:10.1126/science.1174447

Scialo, F., Sriram, A., Fernández-Ayala, D., Gubina, N., Lõhmus, M., Nelson, G., et al. (2016). Mitochondrial ROS Produced via Reverse Electron Transport Extend Animal Lifespan. *Cell Metab.* 23, 725–734. doi:10.1016/j.cmet.2016.03.009

Senft, D., and Ronai, Z. e. A. (2015). UPR, Autophagy, and Mitochondria Crosstalk Underlies the ER Stress Response. *Trends Biochem. Sci.* 40, 141–148. doi:10.1016/j.tibs.2015.01.002

Settembre, C., Di Malta, C., Polito, V. A., Arencibia, M. G., Vetrini, F., Erdin, S., et al. (2011). TFEB Links Autophagy to Lysosomal Biogenesis. *Science* 332, 1429–1433. doi:10.1126/science.1204592

Shahzad, K., Bock, F., Dong, W., Wang, H., Kopf, S., Kohli, S., et al. (2015). Nlrp3-inflammasome Activation in Non-myeloid-derived Cells Aggravates Diabetic Nephropathy. *Kidney Int.* 87, 74–84. doi:10.1038/ki.2014.271

Sharma, K., Karl, B., Mathew, A. V., Gangoiti, J. A., Wassel, C. L., Saito, R., et al. (2013). Metabolomics Reveals Signature of Mitochondrial Dysfunction in Diabetic Kidney Disease. *Jasn* 24, 1901–1912. doi:10.1681/ASN.2013020126

Sheffer, R., Douiev, L., Edvardson, S., Shaag, A., Tamimi, K., Soiferman, D., et al. (2016). Postnatal Microcephaly and Pain Insensitivity Due to a De Novo heterozygousDNM1Lmutation Causing Impaired Mitochondrial Fission and Function. *Am. J. Med. Genet.* 170, 1603–1607. doi:10.1002/ajmg.a.37624

Sheng, J., Li, H., Dai, Q., Lu, C., Xu, M., Zhang, J., et al. (2019). DUSP1 Recuses Diabetic Nephropathy via Repressing JNK-Mff-mitochondrial Fission Pathways. *J. Cell Physiol* 234, 3043–3057. doi:10.1002/jcp.27124

Shutt, T., Geoffrion, M., Milne, R., and McBride, H. M. (2012). The Intracellular Redox State Is a Core Determinant of Mitochondrial Fusion. *EMBO Rep.* 13, 909–915. doi:10.1038/embor.2012.128

Song, J., Herrmann, J. M., and Becker, T. (2021). Quality Control of the Mitochondrial Proteome. *Nat. Rev. Mol. Cell Biol* 22, 54–70. doi:10.1038/s41580-020-00300-2

Song, M., Dorn, G. W., and 2nd (2015). Mitoconfusion: Noncanonical Functioning of Dynamism Factors in Static Mitochondria of the Heart. *Cell Metab.* 21, 195–205. doi:10.1016/j.cmet.2014.12.019

Sourris, K. C., Harcourt, B. E., Tang, P. H., Morley, A. L., Huynh, K., Penfold, S. A., et al. (2012). Ubiquinone (Coenzyme Q10) Prevents Renal Mitochondrial Dysfunction in an Experimental Model of Type 2 Diabetes. *Free Radic. Biol. Med.* 52, 716–723. doi:10.1016/j.freeradbiomed.2011.11.017

Stańczyk, M., Bałasz-Chmielewska, I., Lipska-Ziętkiewicz, B., and Tkaczyk, M. (2018). CoQ10-related Sustained Remission of Proteinuria in a Child with COQ6 Glomerulopathy-A Case Report. *Pediatr. Nephrol.* 33, 2383–2387. doi:10.1007/s00467-018-4083-3

Sun, W., Wang, Y., Miao, X., Wang, Y., Zhang, L., Xin, Y., et al. (2014). Renal Improvement by Zinc in Diabetic Mice Is Associated with Glucose Metabolism Signaling Mediated by Metallothionein and Akt, but Not Akt2. *Free Radic. Biol. Med.* 68, 22–34. doi:10.1016/j.freeradbiomed.2013.11.015

Susztak, K., Raff, A. C., Schiffer, M., and Böttinger, E. P. (2006). Glucose-induced Reactive Oxygen Species Cause Apoptosis of Podocytes and Podocyte Depletion at the Onset of Diabetic Nephropathy. *Diabetes* 55, 225–233. doi:10.2337/diabetes.55.01.06.db05-0894

Svensson, K., Schnyder, S., Cardel, B., and Handschin, C. (2016). Loss of Renal Tubular PGC-1α Exacerbates Diet-Induced Renal Steatosis and Age-Related Urinary Sodium Excretion in Mice. *PLoS One* 11, e0158716. doi:10.1371/journal.pone.0158716

Szabo´, C., Biser, A., Benkő, R., Böttinger, E., and Suszta´k, K. (2006). Poly(ADP-ribose) Polymerase Inhibitors Ameliorate Nephropathy of Type 2 Diabetic Leprdb/db Mice. *Diabetes* 55, 3004–3012. doi:10.2337/db06-0147

Tan, A. L. Y., Sourris, K. C., Harcourt, B. E., Thallas-Bonke, V., Penfold, S., Andrikopoulos, S., et al. (2010). Disparate Effects on Renal and Oxidative Parameters Following RAGE Deletion, AGE Accumulation Inhibition, or Dietary AGE Control in Experimental Diabetic Nephropathy. *Am. J. Physiology-Renal Physiol.* 298, F763–F770. doi:10.1152/ajprenal.00591.2009

Tang, C., Cai, J., Yin, X.-M., Weinberg, J. M., Venkatachalam, M. A., and Dong, Z. (2021). Mitochondrial Quality Control in Kidney Injury and Repair. *Nat. Rev. Nephrol.* 17, 299–318. doi:10.1038/s41581-020-00369-0

Tang, C., Livingston, M. J., Liu, Z., and Dong, Z. (2020). Autophagy in Kidney Homeostasis and Disease. *Nat. Rev. Nephrol.* 16, 489–508. doi:10.1038/s41581-020-0309-2

Vazquez-Calvo, C., Suhm, T., Büttner, S., and Ott, M. (2020). The Basic Machineries for Mitochondrial Protein Quality Control. *Mitochondrion* 50, 121–131. doi:10.1016/j.mito.2019.10.003

Wakabayashi, J., Zhang, Z., Wakabayashi, N., Tamura, Y., Fukaya, M., Kensler, T. W., et al. (2009). The Dynamin-Related GTPase Drp1 Is Required for Embryonic and Brain Development in Mice. *J. Cell Biol* 186, 805–816. doi:10.1083/jcb.200903065

Wang, F., Li, R., Zhao, L., Ma, S., and Qin, G. (2020a). Resveratrol Ameliorates Renal Damage by Inhibiting Oxidative Stress-Mediated Apoptosis of Podocytes in Diabetic Nephropathy. *Eur. J. Pharmacol.* 885, 173387. doi:10.1016/j.ejphar.2020.173387

Wang, J., Shen, L., Hong, H., Li, J., Wang, H., and Li, X. (2019). Atrasentan Alleviates High Glucose-Induced Podocyte Injury by the microRNA-21/forkhead Box O1 axis. *Eur. J. Pharmacol.* 852, 142–150. doi:10.1016/j.ejphar.2019.03.013

Wang, J., Zhu, P., Li, R., Ren, J., and Zhou, H. (2020b). Fundc1-dependent Mitophagy Is Obligatory to Ischemic Preconditioning-Conferred Renoprotection in Ischemic AKI via Suppression of Drp1-Mediated Mitochondrial Fission. *Redox Biol.* 30, 101415. doi:10.1016/j.redox.2019.101415

Wang, S., Chen, Y., Li, X., Zhang, W., Liu, Z., Wu, M., et al. (2020c). Emerging Role of Transcription Factor EB in Mitochondrial Quality Control. *Biomed. Pharmacother.* 128, 110272. doi:10.1016/j.biopha.2020.110272

Wang, W., Wang, Y., Long, J., Wang, J., Haudek, S. B., Overbeek, P., et al. (2012). Mitochondrial Fission Triggered by Hyperglycemia Is Mediated by ROCK1 Activation in Podocytes and Endothelial Cells. *Cell Metab.* 15, 186–200. doi:10.1016/j.cmet.2012.01.009

Wang, X. X., Edelstein, M. H., Gafter, U., Qiu, L., Luo, Y., Dobrinskikh, E., et al. (2016). G Protein-Coupled Bile Acid Receptor TGR5 Activation Inhibits Kidney Disease in Obesity and Diabetes. *Jasn* 27, 1362–1378. doi:10.1681/ASN.2014121271

Wang, Y., Tian, J., Mi, Y., Ren, X., Lian, S., Kang, J., et al. (2021). Experimental Study on Renoprotective Effect of Intermedin on Diabetic Nephropathy. *Mol. Cell Endocrinol.* 528, 111224. doi:10.1016/j.mce.2021.111224

Wei, X., Wei, X., Lu, Z., Li, L., Hu, Y., Sun, F., et al. (2020). Activation of TRPV1 Channel Antagonizes Diabetic Nephropathy through Inhibiting Endoplasmic Reticulum-Mitochondria Contact in Podocytes. *Metabolism* 105, 154182. doi:10.1016/j.metabol.2020.154182

Weinberg, J. M. (2011). Mitochondrial Biogenesis in Kidney Disease: Figure 1. *Jasn* 22, 431–436. doi:10.1681/ASN.2010060643

Widmeier, E., Airik, M., Hugo, H., Schapiro, D., Wedel, J., Ghosh, C. C., et al. (2019). Treatment with 2,4-Dihydroxybenzoic Acid Prevents FSGS Progression

and Renal Fibrosis in Podocyte-specific Coq6 Knockout Mice. *Jasn* 30, 393–405. doi:10.1681/ASN.2018060625

Widmeier, E., Yu, S., Nag, A., Chung, Y. W., Nakayama, M., Fernández-del-Río, L., et al. (2020). ADCK4 Deficiency Destabilizes the Coenzyme Q Complex, Which Is Rescued by 2,4-Dihydroxybenzoic Acid Treatment. *Jasn* 31, 1191–1211. doi:10.1681/ASN.2019070756

Wu, M., Yang, Z., Zhang, C., Shi, Y., Han, W., Song, S., et al. (2021). Inhibition of NLRP3 Inflammasome Ameliorates Podocyte Damage by Suppressing Lipid Accumulation in Diabetic Nephropathy. *Metabolism* 118, 154748. doi:10.1016/j.metabol.2021.154748

Wu, W., Li, W., Chen, H., Jiang, L., Zhu, R., and Feng, D. (2016). FUNDC1 Is a Novel Mitochondrial-Associated-Membrane (MAM) Protein Required for Hypoxia-Induced Mitochondrial Fission and Mitophagy. *Autophagy* 12, 1675–1676. doi:10.1080/15548627.2016.1193656

Xu, L., Zhou, B., Li, H., Liu, J., Du, J., Zang, W., et al. (2015). Serum Levels of Progranulin Are Closely Associated with Microvascular Complication in Type 2 Diabetes. *Dis. Markers* 2015, 1–9. doi:10.1155/2015/357279

Xue, H., Li, P., Luo, Y., Wu, C., Liu, Y., Qin, X., et al. (2019). Salidroside Stimulates the Sirt1/PGC-1α axis and Ameliorates Diabetic Nephropathy in Mice. *Phytomedicine* 54, 240–247. doi:10.1016/j.phymed.2018.10.031

Yacoub, R., Lee, K., and He, J. C. (2014). The Role of SIRT1 in Diabetic Kidney Disease. *Front. Endocrinol.* 5, 166. doi:10.3389/fendo.2014.00166

Yang, J., Zhou, Y., and Guan, Y. (2012). PPARγ as a Therapeutic Target in Diabetic Nephropathy and Other Renal Diseases. *Curr. Opin. Nephrol. Hypertens.* 21, 97–105. doi:10.1097/MNH.0b013e32834de526

Yang, M., Han, Y., Luo, S., Xiong, X., Zhu, X., Zhao, H., et al. (2021). MAMs Protect against Ectopic Fat Deposition and Lipid-Related Kidney Damage in DN Patients. *Front. Endocrinol.* 12, 609580. doi:10.3389/fendo.2021.609580

Yang, S., Zhou, R., Zhang, C., He, S., and Su, Z. (2020). Mitochondria-Associated Endoplasmic Reticulum Membranes in the Pathogenesis of Type 2 Diabetes Mellitus. *Front. Cell Dev. Biol.* 8, 571554. doi:10.3389/fcell.2020.571554

Yao, R.-Q., Ren, C., Xia, Z.-F., and Yao, Y.-M. (2021). Organelle-specific Autophagy in Inflammatory Diseases: a Potential Therapeutic Target Underlying the Quality Control of Multiple Organelles. *Autophagy* 17, 385–401. doi:10.1080/15548627.2020.1725377

Youle, R. J., and van der Bliek, A. M. (2012). Mitochondrial Fission, Fusion, and Stress. *Science* 337, 1062–1065. doi:10.1126/science.1219855

Young, J. C., Hoogenraad, N. J., and Hartl, F. U. (2003). Molecular Chaperones Hsp90 and Hsp70 Deliver Preproteins to the Mitochondrial Import Receptor Tom70. *Cell* 112, 41–50. doi:10.1016/s0092-8674(02)01250-3

Yu, Q., Zhang, M., Qian, L., Wen, D., and Wu, G. (2019). Luteolin Attenuates High Glucose-Induced Podocyte Injury via Suppressing NLRP3 Inflammasome Pathway. *Life Sci.* 225, 1–7. doi:10.1016/j.lfs.2019.03.073

Zhang, L., Liu, J., Zhou, F., Wang, W., and Chen, N. (2018). PGC-1α Ameliorates Kidney Fibrosis in Mice with Diabetic Kidney Disease through an Antioxidative Mechanism. *Mol. Med. Rep.* 17, 4490–4498. doi:10.3892/mmr.2018.8433

Zhang, T., Chi, Y., Kang, Y., Lu, H., Niu, H., Liu, W., et al. (2019). Resveratrol Ameliorates Podocyte Damage in Diabetic Mice via SIRT1/PGC-1α Mediated Attenuation of Mitochondrial Oxidative Stress. *J. Cell Physiol* 234, 5033–5043. doi:10.1002/jcp.27306

Zhou, D., Zhou, M., Wang, Z., Fu, Y., Jia, M., Wang, X., et al. (2019). PGRN Acts as a Novel Regulator of Mitochondrial Homeostasis by Facilitating Mitophagy and Mitochondrial Biogenesis to Prevent Podocyte Injury in Diabetic Nephropathy. *Cell Death Dis* 10, 524. doi:10.1038/s41419-019-1754-3

Zhou, H., Wang, Y., You, Q., and Jiang, Z. (2020). Recent Progress in the Development of Small Molecule Nrf2 Activators: a Patent Review (2017-present). *Expert Opin. Ther. Patents* 30, 209–225. doi:10.1080/13543776.2020.1715365

Zhou, M., Tang, W., Fu, Y., Xu, X., Wang, Z., Lu, Y., et al. (2015). Progranulin Protects against Renal Ischemia/reperfusion Injury in Mice. *Kidney Int.* 87, 918–929. doi:10.1038/ki.2014.403

Zhu, Y., Li, M., Lu, Y., Li, J., Ke, Y., and Yang, J. (2019). Ilexgenin A Inhibits Mitochondrial Fission and Promote Drp1 Degradation by Nrf2-induced PSMB5 in Endothelial Cells. *Drug Dev. Res.* 80, 481–489. doi:10.1002/ddr.21521

Zunino, R., Schauss, A., Rippstein, P., Andrade-Navarro, M., and McBride, H. M. (2007). The SUMO Protease SENP5 Is Required to Maintain Mitochondrial Morphology and Function. *J. Cell Sci* 120, 1178–1188. doi:10.1242/jcs.03418

Conflict of Interest: The authors declare that the research was conducted in the absence of any commercial or financial relationships that could be construed as a potential conflict of interest.

Publisher's Note: All claims expressed in this article are solely those of the authors and do not necessarily represent those of their affiliated organizations, or those of the publisher, the editors and the reviewers. Any product that may be evaluated in this article, or claim that may be made by its manufacturer, is not guaranteed or endorsed by the publisher.

frontiers in Cell and Developmental Biology

ORIGINAL RESEARCH
published: 18 March 2022
doi: 10.3389/fcell.2022.790365

Rap1 Activity Is Essential for Focal Adhesion and Slit Diaphragm Integrity

*Mee-Ling Maywald[1], Cara Picciotto[1], Carolin Lepa[1], Luisa Bertgen[1], Farwah Sanam Yousaf[1], Andrea Ricker[2], Jürgen Klingauf[2], Michael P. Krahn[3], Hermann Pavenstädt[1] and Britta George[1]**

[1]Medizinische Klinik D, University Hospital Münster, Münster, Germany, [2]Institute of Medical Physics and Biophysics, Westfälische Wilhelms-University Münster, Münster, Germany, [3]Medizinische Klinik D, Medical Cell Biology, University Hospital Münster, Münster, Germany

Glomerular podocytes build, with their intercellular junctions, part of the kidney filter. The podocyte cell adhesion protein, nephrin, is essential for developing and maintaining slit diaphragms as functional loss in humans results in heavy proteinuria. Nephrin expression and function are also altered in many adult-onset glomerulopathies. Nephrin signals from the slit diaphragm to the actin cytoskeleton and integrin β1 at focal adhesions by recruiting Crk family proteins, which can interact with the Rap guanine nucleotide exchange factor 1 C3G. As Rap1 activity affects focal adhesion formation, we hypothesize that nephrin signals *via* Rap1 to integrin β. To address this issue, we combined *Drosophila in vivo* and mammalian cell culture experiments. We find that Rap1 is necessary for correct targeting of integrin β to focal adhesions in *Drosophila* nephrocytes, which also form slit diaphragm-like structures. In the fly, the Rap1 activity is important for signaling of the nephrin ortholog to integrin β, as well as for nephrin-dependent slit diaphragm integrity. We show by genetic interaction experiments that Rap1 functions downstream of nephrin signaling to integrin β and downstream of nephrin signaling necessary for slit diaphragm integrity. Similarly, in human podocyte culture, nephrin activation results in increased activation of Rap1. Thus, Rap1 is necessary for downstream signal transduction of nephrin to integrin β.

Keywords: nephrin, podocyte, nephrocyte, Rap1, integrin β

OPEN ACCESS

Edited by:
Hans Kristian Lorenzo, Université Paris-Saclay, France

Reviewed by:
Lewis Kaufman, Icahn School of Medicine at Mount Sinai, United States
René-Marc Mège, Centre National de la Recherche Scientifique (CNRS), France

****Correspondence:***
Britta George
Britta.George@ukmuenster.de

Specialty section:
This article was submitted to Cell Death and Survival, a section of the journal Frontiers in Cell and Developmental Biology

Received: *06 October 2021*
Accepted: *24 February 2022*
Published: *18 March 2022*

Citation:
Maywald M-L, Picciotto C, Lepa C, Bertgen L, Yousaf FS, Ricker A, Klingauf J, Krahn MP, Pavenstädt H and George B (2022) Rap1 Activity Is Essential for Focal Adhesion and Slit Diaphragm Integrity. Front. Cell Dev. Biol. 10:790365. doi: 10.3389/fcell.2022.790365

INTRODUCTION

Diseases of the renal glomerulus often result in end-stage renal disease (Wiggins, 2007). In many diseases of the glomerulus, a specialized glomerular epithelial cell called podocyte plays a central role (Pavenstädt et al., 2003; Wiggins, 2007). The loss of podocytes into the urine is a pathophysiological component and a progressive factor for many glomerular pathologies (Pavenstädt et al., 2003). Podocytes are cells with a complex morphology with cellular processes that branch into foot processes (Pavenstädt et al., 2003). With their foot processes, podocytes wrap the glomerular capillaries where blood is filtered, and primary urine is generated (Scott and Quaggin, 2015). Neighboring podocyte foot processes are connected by the slit diaphragm, a specialized intercellular junction. The slit diaphragm is built by cell adhesion molecules such as nephrin and Neph1, as well as other proteins (Pavenstädt et al., 2003). Nephrin is essential for the kidney filter as mutations result in nephrotic syndrome in early childhood, which is recapitulated in nephrin knockout mice (Kestilä et al., 1998; Hamano et al., 2002). Furthermore, nephrin expression is altered in many adult-onset glomerular diseases (George and Holzman, 2012).

Nephrin is an Ig-domain family protein that functions as a transmembrane receptor in complex with Neph1 and the stomatin-family protein podocin, which anchors nephrin and Neph1 in the lipid raft membranes at the slit diaphragm (Barletta et al., 2003; Garg et al., 2007a). Among other post-translational modifications, nephrin can be phosphorylated by the tyrosine kinase Fyn, which then results in the recruitment of several signaling proteins, including the guanine nucleotide exchange factor for the small GTPase Rap1 called Rapgef1 (thereafter called C3G) (Huber et al., 2003; Verma et al., 2003; Jones et al., 2006; Verma et al., 2006; Garg et al., 2007b; Zhu et al., 2008; Jones et al., 2009; Garg et al., 2010; Zhu et al., 2010; Venkatareddy et al., 2011; George et al., 2012; George et al., 2014; Ni et al., 2016; Martin et al., 2018; Dlugos et al., 2019; Zhu et al., 2019). This initiates distinct downstream signaling events, which regulate actin cytoskeletal organization, cell survival, nephrin trafficking, slit diaphragm integrity, and integrin β1 targeting (Huber et al., 2003; Verma et al., 2003; Jones et al., 2006; Verma et al., 2006; Garg et al., 2007b; Zhu et al., 2008; Jones et al., 2009; Garg et al., 2010; Zhu et al., 2010; Venkatareddy et al., 2011; George et al., 2012; George et al., 2014; Ni et al., 2016; Martin et al., 2018; Dlugos et al., 2019; Zhu et al., 2019).

Small GTPases are versatile regulators of many cellular processes. Their action can be fine-tuned by guanine nucleotide exchange factors (GEFs) and GTPase activating proteins (GAPs). Exchange factors activate small GTPases by catalyzing the exchange of GDP by GTP while GAPs inactivate their specific GTPase by catalyzing the hydrolyzation of GTP to GDP and phosphate. The small GTPase Rap1 is ubiquitously expressed and plays important roles in controlling metabolic processes, cytoskeletal rearrangements, cell division, substratum adhesion, intercellular junction regulation, and cell motility (Lagarrigue et al., 2016; Jaskiewicz et al., 2018). In podocytes, Rap1 interacts with nephrin via the adapter protein MAGI-1, thereby regulating slit diaphragm integrity (Ni et al., 2016). Another MAGI family protein, MAGI-2, forms a complex with the Rap1 activating protein Rapgef2 to regulate Rap1 activity (Zhu et al., 2019). In mice, knockout of Rap1A and Rap1B results in disruption of slit diaphragm integrity and development of focal segmental glomerulosclerosis (FSGS)—a chronic glomerular disease with scarring, sclerotic lesions (Potla et al., 2014).

Focal adhesions are contacts between cells and the extracellular matrix (Ginsberg, 2014). Integrins are transmembrane proteins that establish these contacts (Ginsberg, 2014). α- and β-integrins heterodimerize, thereby recruiting adapter proteins, which transmit signals to the actin cytoskeleton and intercellular junctions of the cells, among others (Ginsberg, 2014). In podocytes, integrin β1 is one of the major β-integrins (Sachs and Sonnenberg, 2013). Integrin function is essential to podocytes as knockout of integrin β1 in mice results in early proteinuria as a sign of defective slit diaphragm development (Pozzi et al., 2009). These mice show a progressive podocyte loss presumably due to adhesion defects (Pozzi et al., 2009). Nephrin transduces signals to integrin β1 at focal adhesions by recruiting the Rap1 activating GEF C3G, which results in activation and correct targeting of integrin β1 (Dlugos et al., 2019).

While Rap1 plays a role in nephrin signaling that mediates slit diaphragm integrity (Ni et al., 2016), the role of Rap1 for nephrin signal transduction to integrin β at focal adhesions is not defined yet. Employing the *Drosophila* nephrocyte model, we show that Rap1 is necessary for mediating signals that correctly target integrin β to focal adhesions. Furthermore, Rap1 activity is relevant for nephrin signaling to regulate slit diaphragm integrity. By genetic interaction experiments, we show that Rap1 functions downstream of nephrin to regulate integrin β function at focal adhesions in nephrocytes. Likewise, we show that nephrin activation in podocyte culture results in increased activation of Rap1.

METHODS

Fly Husbandry and Genetics

For the transgenic RNAi and overexpression studies, the *UAS-Gal4* system was employed. Flies were kept at 25°C or 29°C on standard food. RNAi stocks were obtained from the Vienna Drosophila Resource Center (Vienna, Austria): control RNAi targeting *orco* (100825), *rap1* RNAi (20761), *rap1* RNAi (110757) and *magi* RNAi (41735). UAS-Rap1^{V12} (constitutively active), UAS-Rap1^{N17} (dominant-negative), and UAS-Rap1 (wild-type) were a gift from Ulrike Gaul (LMU, Munich, Germany). The overexpression control UAS RFP (30556) was obtained from the Bloomington Stock Center (Bloomington, United States). UAS Sns and Sns-Gal4 driver lines were provided from Tobias Huber (UKE, Hamburg, Germany). For the rescue experiments, driver lines were recombined with the specific RNAi fly lines.

Generation of Transgenic Flies

The pENTR™/DTOPO® Kit (ThermoFisher) was used for cloning of h-Rap1B V12, h-Rap1B N17, and h-Rap1B WT into pENTR (human Rap1B DNA was provided from Andreas Püschel, WestfälischeWilhelms-Universität Münster, Germany). Cloning into the destination vector was performed using the Gateway technology (Invitrogen). UAS-h-Rap1B^{V12}, UAS-h-Rap1B^{N17}, and UAS-h-Rap1B (wild-type) transgenic fly lines were generated using *ΦC31*-mediated germline transformation using landing sites *attP40* and *attP2*.

Immunofluorescence Analysis

Wandering third instar larvae were dissected and the garland cell nephrocytes fixed in 4% paraformaldehyde (PFA) for 15 min. After washing in PBS-T (PBS + 0.1% Triton), nephrocytes were incubated in the primary antibody at 4° overnight, followed by washes in PBS-T. The secondary antibody incubation lasted for 2.5 h at room temperature. After washes with PBS-T, they were mounted in Mowiol. Anti-Sns [custom generated (Dlugos et al., 2019)], anti-Pyd (PYD2) and anti-integrin β (CF.6G11) (all from Developmental Studies Hybridoma Bank, United States) were used as primary antibodies. Anti-Sns antibodies were diluted 1:100, anti-Pyd antibodies 1:20, anti-integrin β antibodies 1:100 in PBS-T. Goat-anti-mouse Alexa^{488}, goat-anti-rabbit Alexa^{594}, and DAPI (all from Invitrogen) were used as secondary antibodies and diluted 1:1000 in 10% goat serum in PBS-T.

Confocal Microscopy

Tangential und surface section images of the nephrocytes were obtained using a confocal microscope (Leica SP8). 1.5× zoom was set for the tangential section and 4× zoom for the surface section. For imaging, the integrated module LIGHTNING was applied. Image processing was done by LasX and ImageJ Software.

Transmission Electron Microscopy

Wandering third instar larvae were dissected, and garland cell nephrocytes were fixed in 2% glutaraldehyde in Sørensen buffer overnight. Next, nephrocytes were washed with Sørensen buffer, osmium tetroxide 1% in Sørensen buffer was applied for 1 h, and samples were again washed with Sørensen buffer. Samples were then dehydrated in an ascending alcohol series and infiltrated with epon using a series of mixtures of epon and the intermedium propylene oxide and pure epon. After embedding in epon and polymerization at 60°C for 36 h, samples were cut in ultra-thin slices of 60 nm and contrasted with uranyl acetate for 20 min and lead citrate for 90 s. Images were taken with a transmission electron microscope (Phillips CM10 equipped with TVIPS CAM F416).

Statistical Analysis

Quantification of slit diaphragms visualized across 1 µm was performed manually (LasX Software, EM measure). The Mann–Whitney *U* test was used to determine the statistical significance between two interventions. Slit diaphragms were quantified in 14 nephrocytes from 20 different animals for each of three independent crosses per genotype. Slit diaphragms were counted perpendicularly across 5 µm cell membrane in five different areas of each cell. To detect integrin β localization upon downregulation of rap1, ROIs were selected at the cell cortex and the cytosol close to the nucleus. The integrin reorganization was then calculated as previously described (Bayraktar et al., 2020): ROI at cell cortex + background area/ROI at cytosol + background area. Slit diaphragms were counted per µm basement membrane for 10 nephrocytes, each of 20–30 animals employing transmission electron microscopy images. Basement membrane length was quantified using ImageJ.

Cell Culture

Human immortalized podocytes were cultured as previously described (Dlugos et al., 2019). Stable podocyte cell lines allowing doxycycline-dependent expression of CD16-CD7-Nephrin Cytoplasmic Domain (NCD) or CD16-CD7-HA (pInducer-21-puro-CD16-CD7-NCD or pInducer-21-puro-CD16-CD7-HA) were generated by lentiviral gene transfer as previously described (Dlugos et al., 2019).

Nephrin Activation Assay

Activation of nephrin was performed as previously described (Dlugos et al., 2019). In short, either CD16-CD7-NCD or CD16-CD7-HA (as control) stable cell lines cultured on 10 cm dishes were cooled down to 4°C for 5 min, incubated with an anti-CD16 antibody (#555404, BD Pharming, 4 µl per ml medium) on ice for 30 min, and then further incubated with an anti-IgG antibody (#ab6708, Abcam, 3 µl per ml medium) for another 5 min at 37°C. The first incubation step allows the anti-CD16 antibody to bind to the CD16 domain of the chimeric proteins and leads to a first clustering of the proteins. The second incubation step allows the binding of the anti-IgG antibody to the bound anti-CD16 antibodies for an enhancement of clusters, which initiates recruitment of Src kinases and consecutive phosphorylation of the intracellular nephrin domain (Verma et al., 2003; Jones et al., 2006; Verma et al., 2006).

Active Rap1 Detection

After nephrin activation by clustering, cells were directly cooled down on ice, media was removed, and cells were washed with ice-cold PBS. Cells were then lysed in 500 µl ice-cold IP buffer (20 mM Tris-HCl, pH 7.4; 20 mM NaCl; 1 mM EDTA; 50 mM NaF; 15 mM $Na_4P_2O_7$; 1% (v/v) Triton X-100) containing protease inhibitor (cOmplete™ protease inhibitor cocktail, Roche Diagnostics) and phosphatase inhibitors (phosphatase inhibitor cocktail 2 and phosphatase inhibitor cocktail 3, Sigma Aldrich) and manually scratched from the plates. Further mechanical lysis was achieved by dragging the lysates through a 26, G needle. Lysates were kept on ice for 30 min, whereby they were vortexed every 3 to 5 min and were then centrifuged for 15 min at 14.000 × g and 4°C. The supernatant was transferred into a new reaction tube containing Sepharose G beads (GE Healthcare), which were washed three times for 5 min rotating in 1 ml IP buffer. 5% of the lysate was kept aside as input. 1 µl of active Rap1-GTP antibody (#26912, NewEast Biosciences) was added to 30 µl of beads slurry and lysate. Immunoprecipitation was performed rotating at 4°C for 1 h. Afterward, beads were washed three times at 4°C, rotating with 1 ml IP buffer each time, containing protease and phosphatase inhibitors. Following the washing steps 2× Laemmli was added to the beads, and the samples were boiled at 95°C for 5 min. Immunoblotting was performed as previously described (Dlugos et al., 2019). Primary antibodies were diluted 1:1000 in 5% bovine serum albumin in TBST. The following antibodies were used: Rap1A/B (#2399S, Cell Signaling Technologies), nephrin (#BP5030, OriGene), p-nephrin (#ab80298, Abcam), HA (#11867423001, Roche), β-tubulin (#T8328, Sigma Aldrich).

RESULTS

Rap1 Is Essential for Correct Targeting of Integrin β in Nephrocytes

We recently showed that nephrin activation results in the activation of integrin β1 in podocytes (Dlugos et al., 2019). C3G appears to play a role in this pathway (Dlugos et al., 2019). C3G is an activator of the small GTPase Rap1 (Radha et al., 2011). However, the role of Rap1 in nephrin signaling to focal adhesions in podocytes is unclear. To analyze the function of Rap1 in nephrin signaling to integrin β, we combined the use of

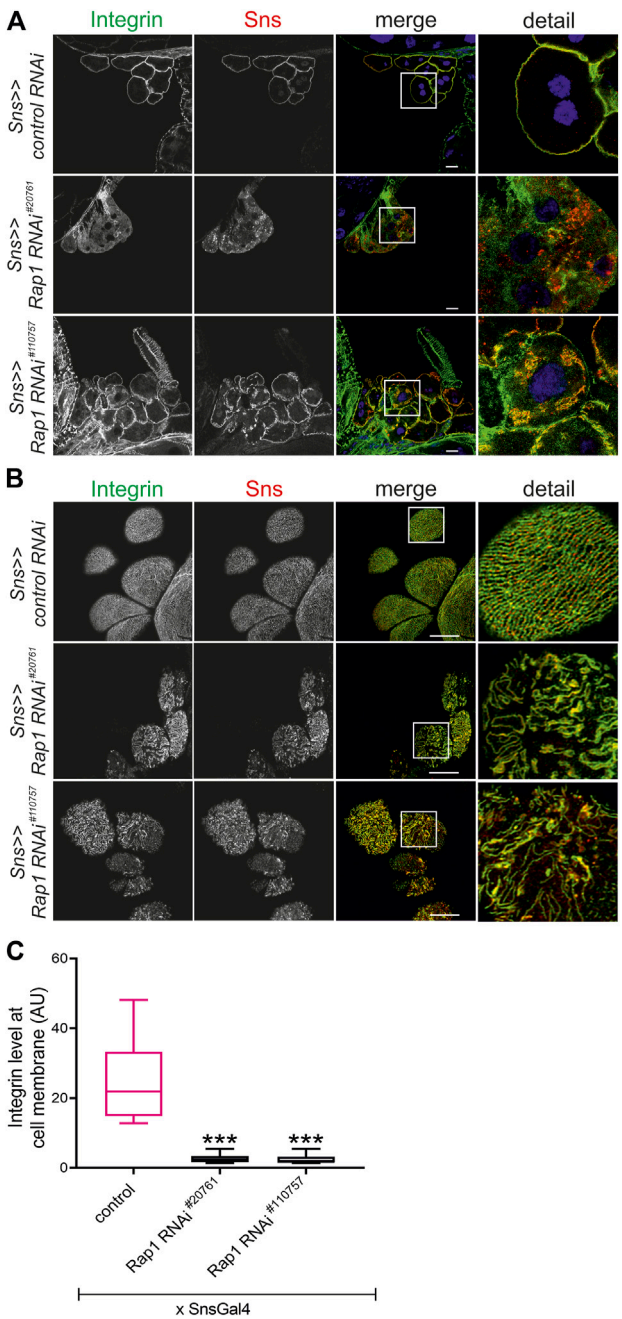

FIGURE 1 | Knockdown of *rap1* results in altered targeting of integrin β. **(A)** Immunofluorescence analysis of tangential sections **(A)** or surface sections **(B)** of *control* (*sns >> control RNAi*) or *rap1* knockdown nephrocytes (*sns>>rap1 RNAi*) is shown. Knockdown in nephrocytes was accomplished by employing *sns-GAL4* and two different RNAi hairpins (#20761 and #110757). Nephrocytes of wandering third instar larvae were dissected, and immunofluorescence analysis was performed with antibodies specific for integrin β (green) and Sns (red). Merged images and higher magnifications of the marked area (detail) are shown. Scale bars in **(A,B)**: 10 µm, $n = 3$. **(C)** The intensity of integrin fluorescence at the cell membrane compared to the cytosol was evaluated for all genotypes shown in **(A)** and presented as a box plot with minimum and maximum in arbitrary units (AU). The control is marked in pink. *** indicates a p-value < 0.001.

two model systems: podocyte culture and the *in vivo Drosophila* nephrocyte model. The nephrocyte expresses a slit diaphragm-like structure based on sticks and stones (Sns, ortholog of nephrin) and Kin-of-irre (Kirre, ortholog of Neph1) (Weavers et al., 2009; Zhuang et al., 2009). Like in podocytes, the nephrocyte slit diaphragm functions as a size and charge-selective barrier (Zhang et al., 2013a). In analogy to podocytes, nephrocytes express the cytoskeletal adapters Cindr (ortholog of CD2AP), Myoblast city (Mbc), Nck ortholog), and Mec-2 (ortholog of podocin) (Weavers et al., 2009; Zhuang et al., 2009). Thus, this model is currently often employed as an *in vivo* model for analyzing the slit diaphragm in a genetically tractable system (Zhang et al., 2013a; Zhang et al., 2013b; Fu et al., 2017; Hermle et al., 2017; Hochapfel et al., 2017).

To test whether Rap1 is essential for targeting of integrin β, we downregulated endogenous *rap1* exclusively in nephrocytes employing the *UAS-Gal4* system with a nephrocyte-specific driver (*sns-Gal4*) and two independent dsRNA lines targeting *rap1*. The localization of myospheroid, the *Drosophila* ortholog of integrin β, was determined in nephrocytes of third instar larvae using confocal microscopy. In tangential sections, integrin β exclusively accumulated at the cell cortex in control nephrocytes while nephrocytes with knockdown of *rap1* showed diffuse cytoplasmic staining of integrin β with some aggregates (**Figure 1A**). When imaging the surface of nephrocytes, integrin β presented in a typical fingerprint-like pattern in control nephrocytes (**Figure 1B**), whereas its localization was severely altered with diffuse targeting of integrin β in *rap1* knockdown nephrocytes (**Figure 1B**). Integrin accumulation at the plasma membrane was quantified in tangential sections (**Figure 1C**) (Bayraktar et al., 2020). To confirm that integrin β mistargeting is a specific effect of *rap1* downregulation, we performed rescue experiments of the *rap1* knockdown by expressing human Rap1B, which is not targeted by the dsRNA specific to the *Drosophila rap1* gene. Nephrocytes expressing a control element [*UAS-RFP*, called *control OE* (overexpression)] instead of human Rap1B on *rap1* knockdown background were prepared, and immunofluorescence analysis was performed with antibodies specific for integrin β (genotype: *sns-Gal4, UAS rap1RNAi^{20761}/UAS RFP* or *sns-Gal4, UAS rap1RNAi^{110757}/UAS RFP*). Analysis of tangential (**Figure 2A**, **Supplementary Figure S1A**) and surface sections (**Figure 2B**, **Supplementary Figure S1B**) of nephrocytes confirmed that downregulation of *rap1* resulted in diffuse targeting of integrin β. Upon knockdown of *rap1* and concomitant expression of *UAS-h-Rap1B*, the phenotype induced by silencing of *rap1* was partly rescued. In these animals, integrin β was localized correctly at the plasma membrane (**Figure 2A**, **Supplementary Figure S1A**) and was found in the fingerprint-like pattern in surface sections (**Figure 2B**, **Supplementary Figure S1B**) (genotypes: *sns-Gal4, rap1RNAi^{20761}/UAS h-Rap1B; UAS h-Rap1B/Tm6b* or *sns-Gal4, rap1RNAi^{110757}/UAS h-Rap1B; UAS h-Rap1B/Tm6b).* We quantified the number of foot processes per 1 µm of the basement membrane, which confirmed the qualitative results (**Figure 2C**, **Supplementary Figure S1C**).

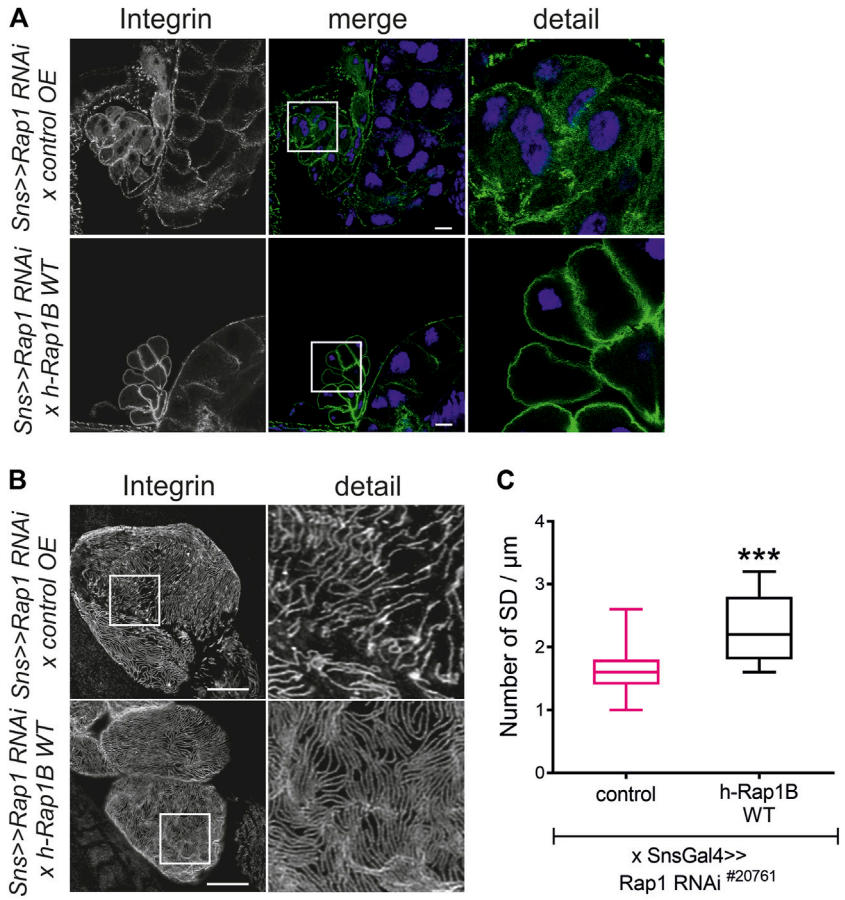

FIGURE 2 | Human Rap1B can rescue *rap1* loss of function-induced mislocalization of integrin β. Immunofluorescence analysis of tangential **(A)** or surface sections **(B)** of *rap1* knockdown nephrocytes (*sns>>rap1 RNAi*) with a genetic element for overexpression of human Rap1B (*UAS h-Rap1B WT*) or a control transgene (*control OE*) is shown. Knockdown of *rap1* (#20761) in nephrocytes was accomplished by employing *sns-GAL4*. Wandering third instar larvae were dissected, and immunofluorescence analysis was performed with antibodies specific for integrin β. Merged images and higher magnifications of the marked area (detail) are shown. Scale bars in **(A,B)**: 10 µm, $n = 3$. **(C)** Statistical evaluation of the number of slit diaphragms (SD) per µm nephrocyte surface area of the genotypes shown in **(A,B)** depicted as a box plot with minimum and maximum. The control is marked in pink. $^{***}p < 0.001$.

Rap1 Activity Is Necessary for Targeting of Integrin β

The activation state of small GTPases is tightly regulated by activating and inactivating factors (Lagarrigue et al., 2016; Jaskiewicz et al., 2018). To deduce whether the activity state of Rap1 is important for correct targeting of integrin β, we expressed wild-type *Drosophila* Rap1, dominant-negative Rap1^{N17} with amino acid substitution of serine to asparagine at position 17, constitutively active Rap1^{V12} with amino acid substitution of glycine to valine at position 12 or RFP as a control in wild-type nephrocytes. Compared to the control (genotype: *sns-Gal4/UAS RFP*), overexpression of *rap1* resulted in moderate mistargeting of integrin β, which was more severe when overexpressing either constitutively active or dominant-negative Rap1 (genotypes: *sns-Gal4/UAS d-rap1* or *sns-Gal4/UAS d-rap1N17* or *sns-Gal4; d-rap1V12*) (**Figures 3A–C**). To test whether ectopic expression of human Rap1B variants exerts a similar phenotype to their *Drosophila* orthologs, we expressed human h-Rap1B, h-Rap1B^{V12}, h-Rap1B^{N17}, or RFP as a control on the wild-typic background (genotypes: *sns-Gal4/UAS RFP* or *sns-Gal4/UAS h-Rap1B; UAS h-Rap1B* or *sns-Gal4/UAS h-Rap1B^{N17}; UAS h-Rap1B^{N17} or sns-Gal4/UAS h-Rap1B^{V12}; UAS h-Rap1B^{V12}*). Tangential sections (**Figure 4A**) or surface sections (**Figures 4B,C**) showed that misexpression of all three h-Rap1B variants resulted in mistargeting of integrin β, demonstrating that the function of *rap1* in focal adhesion integrity appears to be conserved.

Rap1 Activity Is Essential for Nephrocyte Slit Diaphragm Integrity

In mice, Rap1 is essential for slit diaphragm integrity (Potla et al., 2014). In the *Drosophila* nephrocyte model, the role of Rap1 in slit diaphragm integrity has not yet been characterized. Knockdown of *rap1* by two different *dsRNA* in nephrocytes *in vivo* employing *sns-Gal4* resulted in incorrect targeting of the slit diaphragm proteins Sns and Pyd (the fly ortholog of Zonula occludens (ZO-1) in tangential and surface sections

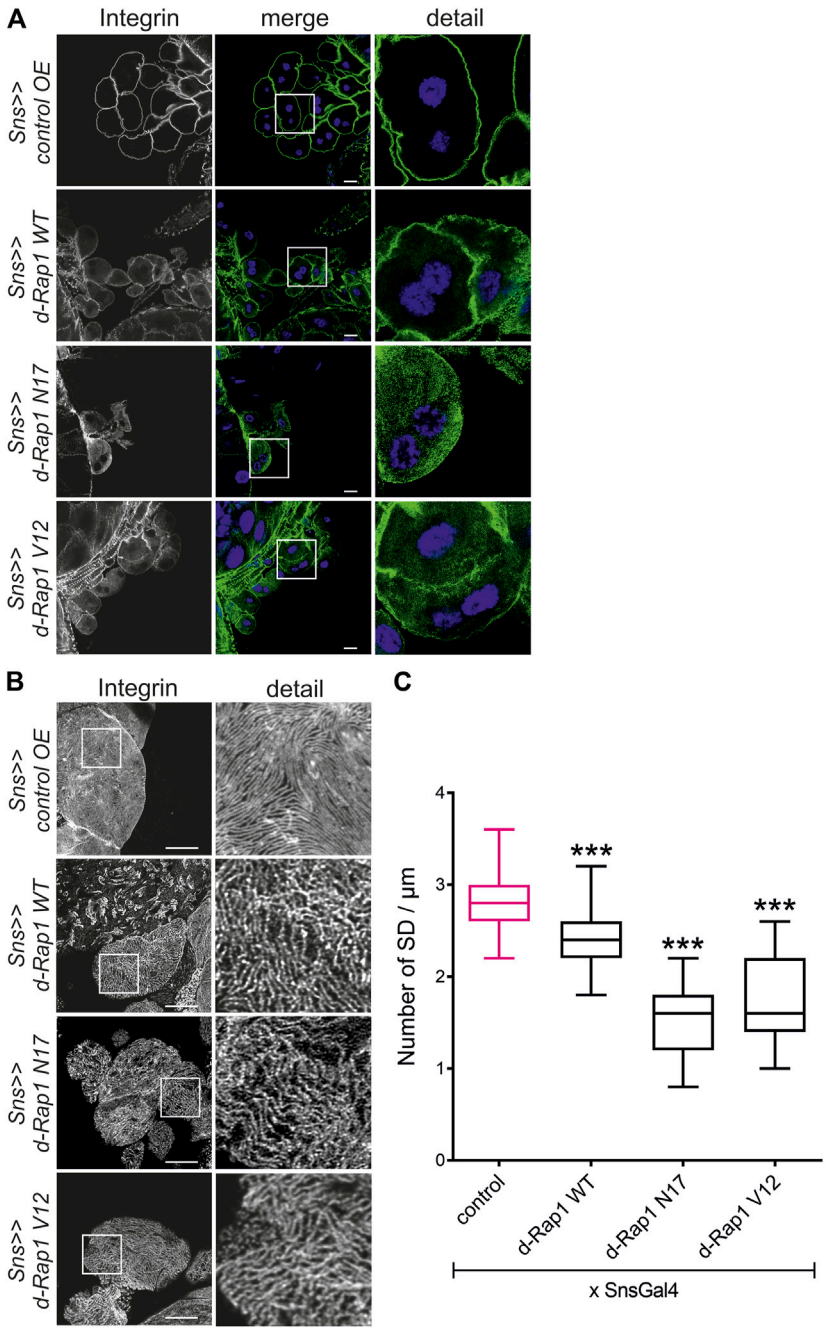

FIGURE 3 | Imbalance in *rap1* activity results in altered targeting of integrin β. Immunofluorescence analysis of tangential **(A)** or surface sections **(B)** of control nephrocytes (*sns>>control OE*), nephrocytes with overexpression of *Drosophila rap1* (*sns>>d-rap1 WT*), of *Drosophila* dominant-negative *rap1* (*sns>>d-rap1 N17*), or of *Drosophila* constitutively active *rap1* (*sns>>d-rap1 V12*). Knockdown in nephrocytes was accomplished by employing *sns-GAL4*. Wandering third instar larvae were dissected, and immunofluorescence analysis was performed with antibodies specific for integrin β. Merged images and higher magnifications of the marked area (detail) are shown. Scale bars in **(A,B)**: 10 µm, $n = 3$. **(C)** Statistical evaluation of the number of slit diaphragms (SD) per µm nephrocyte surface area of the genotypes shown in **(A,B)** depicted as a box plot with minimum and maximum. The control is marked in pink. ***$p < 0.001$.

(**Supplementary Figures S2A,B**). Next, we analyzed whether the expression of h-Rap1B can rescue the *rap1* knockdown phenotype of slit diaphragm protein mistargeting. This showed that expression of h-Rap1B could rescue the *rap1* knockdown-related phenotype of Sns and Pyd mistargeting induced by two independent *dsRNA* (**Supplementary Figures S3A,B, S4A,B**). Thus, the *Drosophila* nephrocyte model recapitulates the phenotypes induced by Rap1 loss of function in mice. We then utilized the nephrocyte model to characterize the role of Rap1 for slit diaphragm integrity further. It is presently not

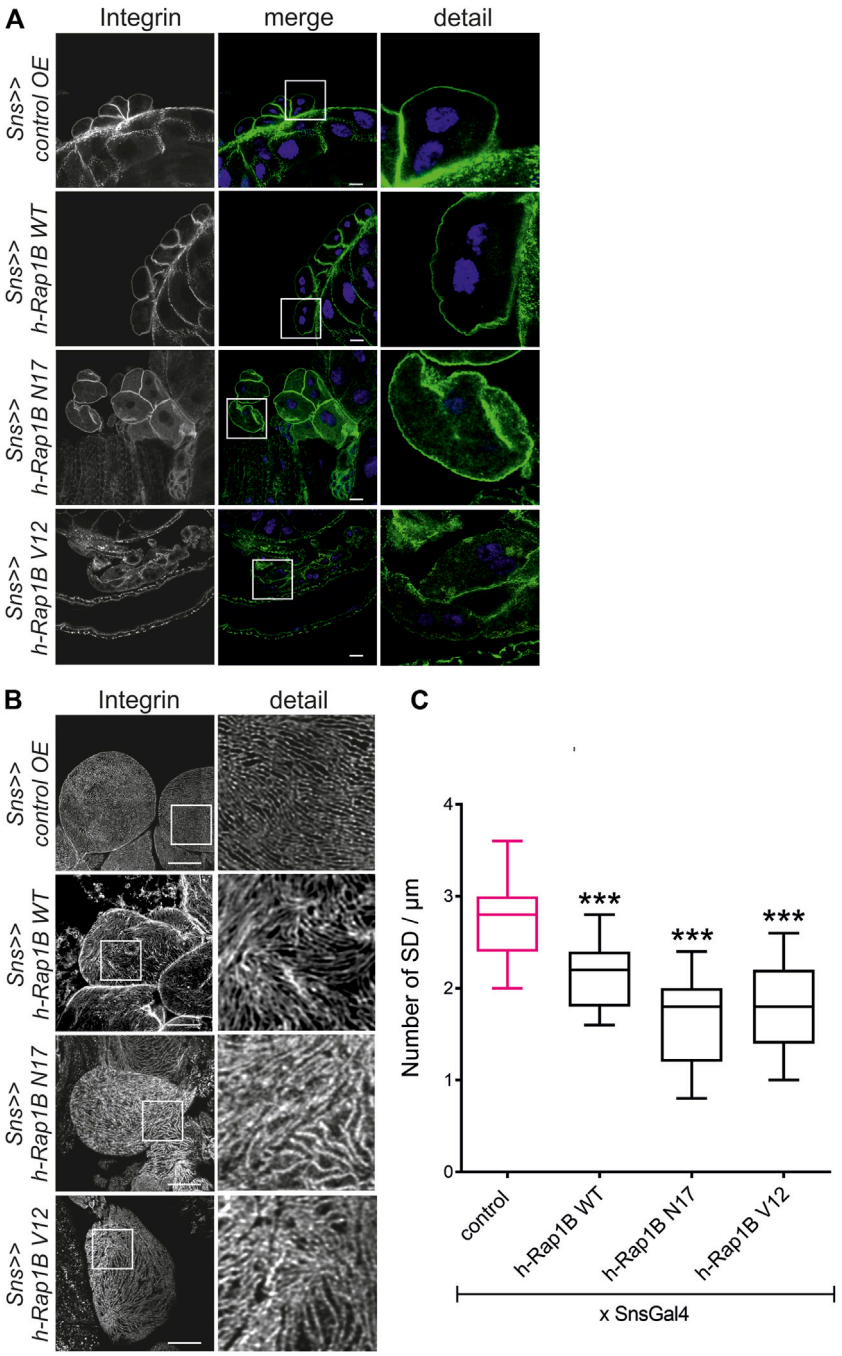

FIGURE 4 | Misexpression of human Rap1B results in altered targeting of integrin β. Immunofluorescence analysis of tangential **(A)** or surface sections **(B)** of control nephrocytes (*sns>>control OE*), nephrocytes with overexpression of wild-type human Rap1B (*sns>>h-Rap1B WT*), of human dominant-negative Rap1B (*sns>>h-Rap1B N17*), or of human constitutively active Rap1B (*sns>>h-Rap1B V12*). Knockdown in nephrocytes was accomplished by employing *sns-GAL4*. Wandering third instar larvae were dissected, and immunofluorescence analysis was performed with antibodies specific for integrin β. Merged images and higher magnifications of the marked area (detail) are shown. Scale bars in **(A,B)**: 10 µm, $n = 3$. **(C)** Statistical evaluation of the number of slit diaphragms (SD) per µm nephrocyte surface area of the genotypes shown in **(A,B)** depicted as a box plot with minimum and maximum. The control is marked in pink. ***$p < 0.001$.

clear whether a balanced Rap1 activity is crucial for slit diaphragm integrity in mammalian podocytes *in vivo* or *Drosophila* nephrocytes. In contrast to the overexpression control (RFP), nephrocyte-specific overexpression of *rap1*, $rap1^{V12}$, and $rap1^{N17}$ on the wild-typic background resulted in mistargeting of slit diaphragm proteins, Sns and Pyd. Similar to targeting of integrin β to focal adhesions, targeting of Sns and Pyd to the slit diaphragm was

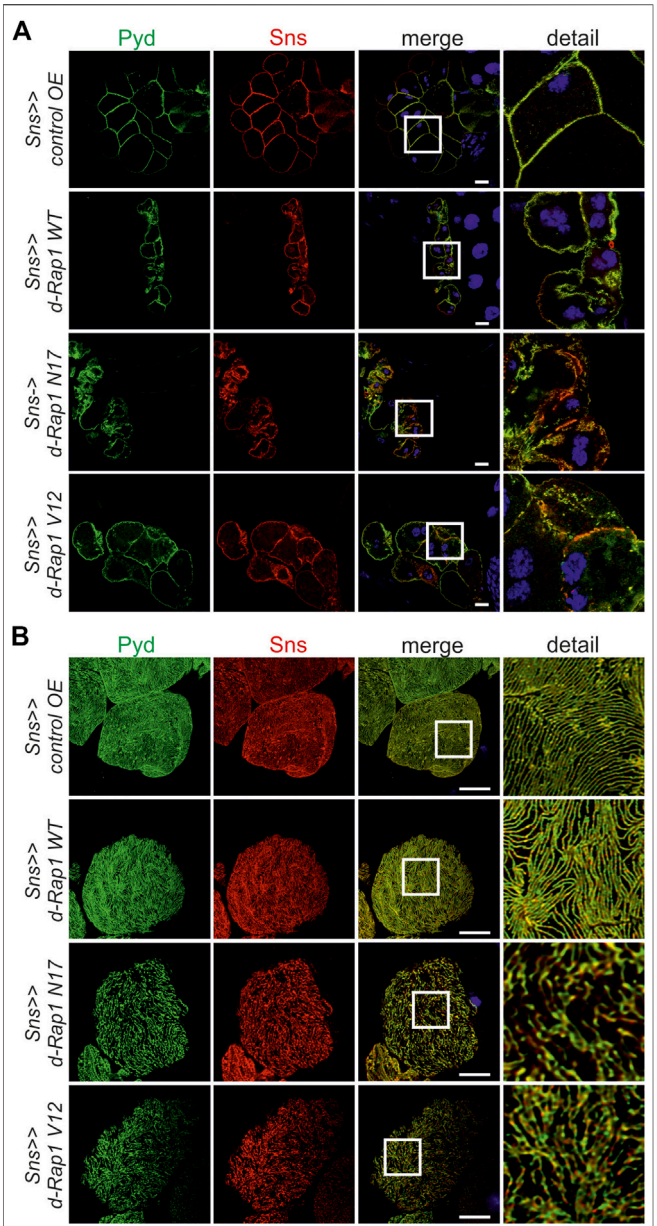

FIGURE 5 | Imbalance of *rap1* activity leads to mistargeting of slit diaphragm proteins Pyd and Sns. Immunofluorescence analysis of tangential **(A)** or surface sections **(B)** of control nephrocytes (*sns>>control OE*), nephrocytes with overexpression of *Drosophila* wild-type *rap1* (*sns>>d-rap1 WT*), of *Drosophila* dominant-negative *rap1* (*sns>>d-rap1 N17*), or of *Drosophila* constitutively active *rap1* (*sns>>d-rap1 V12*). Knockdown in nephrocytes was accomplished by employing *sns-GAL4*. Wandering third instar larvae were dissected, and immunofluorescence analysis was performed with antibodies specific for Pyd (zonula occludens-1 (ZO-1) ortholog) and Sns (nephrin ortholog) as slit diaphragm markers. Merged images and higher magnifications of the marked area are shown in the right columns. Scale bars in **(A,B)**: 10 µm, $n = 3$.

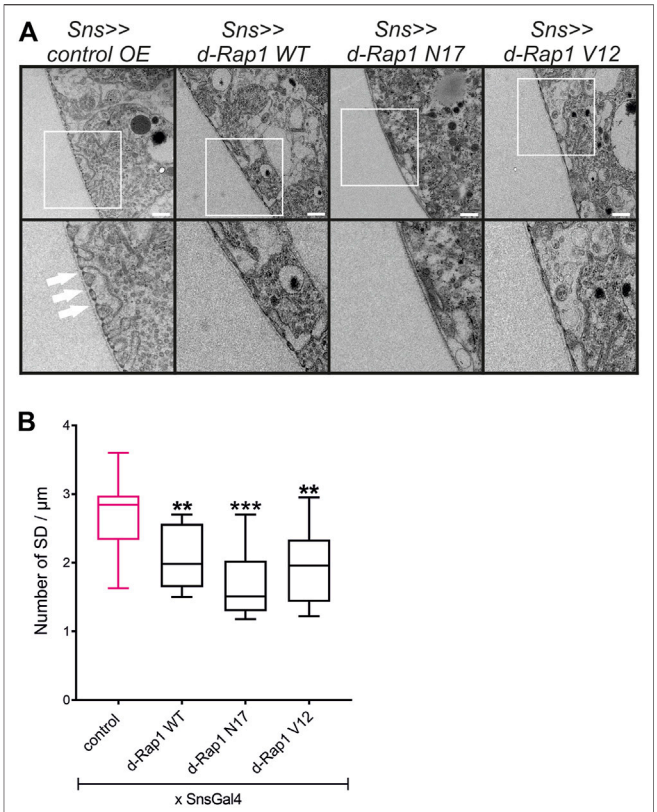

FIGURE 6 | Imbalance of *d-rap1* activity leads to loss of slit diaphragms and lacunae. **(A)** TEM analysis of dissected control nephrocytes (*sns>>control OE*), nephrocytes with overexpression of *Drosophila* wild-type *rap1* (*sns>>d-rap1 WT*), of *Drosophila* dominant-negative *rap1* (*sns>>d-rap1 N17*), or of *Drosophila* constitutively active *rap1* (*sns>>d-rap1 V12*). Knockdown in nephrocytes was accomplished by employing *sns-GAL4*. White arrows exemplarily indicate slit diaphragms. Scale bars: upper panel 500 nm, lower panel zoom compared to the upper panel 2×. $n = 3$. **(B)** Statistical evaluation of the number of slit diaphragms (SD) per µm basement membrane of the genotypes shown in **(A)** depicted as a box plot with minimum and maximum. The control is marked in pink. $^{**}p < 0.01$, $^{***}p < 0.001$.

disturbed by expressing wild-type *rap1* or the constitutively active or dominant-negative forms of *rap1* (**Figures 5A,B**). To analyze whether this correlates with the breakdown of slit diaphragms, we performed transmission electron microscopy (TEM) analysis. Nephrocyte-specific overexpression of either wild-type, dominant-negative or constitutively active *rap1* led to a reduction of slit diaphragms per µm basement membrane (**Figures 6A,B**). In analogy, misexpression of wild-type human Rap1B, constitutively active h-Rap1B^{V12} or dominant-negative h-Rap1B^{N17} on wild-typic background resulted in misexpression of Sns and Pyd and breakdown of slit diaphragms (**Supplementary Figures S5A,B, S6**). Thus, slit diaphragm integrity appears to be regulated by Rap1 activity.

Rap1 Functions Downstream of Nephrin During Signaling to Integrin β and Is Essential for Nephrin-Mediated Slit Diaphragm Integrity

It is well known that *Drosophila* is excellently suited to genetically dissect complex signaling cascades (Simon et al., 1991; Fortini et al., 1992; Brunner et al., 1994). The ability to suppress a

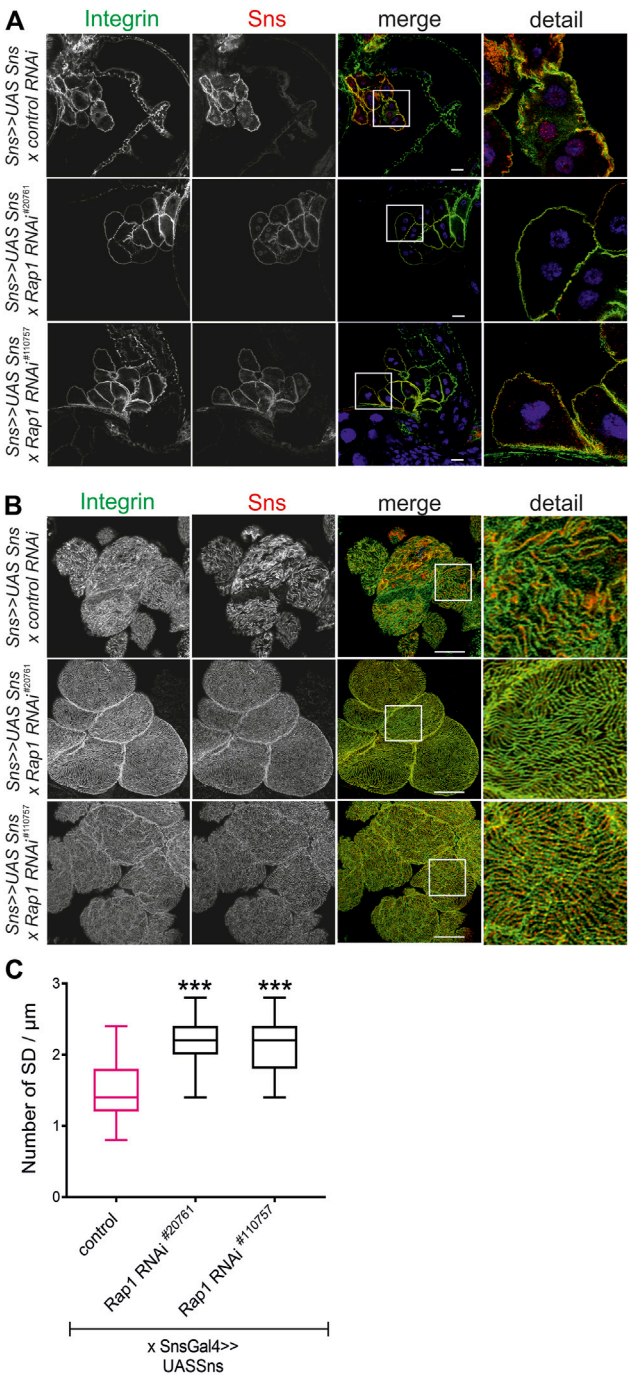

FIGURE 7 | Rap1 functions downstream of nephrin in signaling to integrin β. Immunofluorescence analysis of tangential **(A)** or surface sections **(B)** of nephrocytes overexpressing *sns* (*sns>>UAS Sns x control RNAi*) or nephrocytes with overexpression of sns and knockdown of *rap1* (*sns>>UAS Sns x Rap1 RNAi*^{20761} or *sns>>UAS Sns x Rap1 RNAi*^{110757}). Knockdown in nephrocytes was accomplished by employing *sns-GAL4*. Wandering third instar larvae were dissected, and immunofluorescence analysis was performed with antibodies specific for integrin β (green) and Sns (red). Merged images and higher magnifications of the marked area are shown. Scale bars **(A,B)**: 10 µm, $n = 3$. **(C)** Statistical evaluation of the number of slit diaphragms (SD) per µm nephrocyte surface area of the genotypes shown in **(A,B)** depicted as a box plot with minimum and maximum. The control is marked in pink. ***$p < 0.001$.

phenotype caused by overexpression of a given gene (gain-of-function phenotype) by suppressing another gene is evidence that the two genes interact (Simon et al., 1991; Fortini et al., 1992; Brunner et al., 1994). We employed this technique to test whether the nephrin ortholog *sns* genetically interacts with *rap1*. Flies overexpressing *sns* in nephrocytes were crossed with flies with nephrocyte-specific knockdown of *rap1* (*sns-Gal4*, *UAS-sns*; *UAS-d-rap1RNAi*^{110757} or *sns-Gal4*, *UAS-sns*; *UAS-d-rap1 RNAi*^{20761}) and compared to flies with overexpression of *sns* and a control *UAS-dsRNA* element (*sns-Gal4*, *UAS-sns*; *UAS-control RNAi*). While flies overexpressing *sns* in a background of a control *UAS-dsRNA* element showed mistargeting of integrin β in nephrocytes, flies that overexpress *sns* in the background of *rap1* suppression showed a normal integrin β localization in nephrocytes (**Figures 7A–C**). Importantly, two independent UAS-dsRNA elements tested could rescue integrin β targeting, implying that Rap1 functions downstream of Sns in signaling to integrin β at focal adhesions. Downregulation of *rap1* was also able to partly rescue Sns and Pyd targeting on an *sns* gain-of-function genetic background (**Supplementary Figures S7A,B**). Thus, Rap1 also functions downstream of Sns during signaling that regulates slit diaphragm morphology.

Slit diaphragm integrity and integrin targeting were also rescued when overexpressing *d-rap1* on the *sns* knockdown background (*sns-Gal4>>sns RNAi x UAS-d-rap1*, control: *sns-Gal4>>sns RNAi x UAS-control*) (**Figures 8A–C**). This confirms that Rap1 fulfills functions downstream of Sns.

In mammalian podocytes, Rap1 activity is also regulated via the scaffold proteins, MAGI-1 and MAGI-2. *Drosophila* has only one MAGI ortholog. To test whether dMAGI is essential for slit diaphragm integrity in nephrocytes, we performed a knockdown of the MAGI ortholog by RNAi in nephrocytes (*sns-Gal4*). Immunofluorescence analysis of *magi* knockdown nephrocytes showed a slightly reduced number of slit diaphragms when stained for Sns and Pyd to visualize slit diaphragms (**Supplementary Figure S8**). Thus, MAGI is also necessary for an intact slit diaphragm in nephrocytes.

Nephrin Activation Results in Increased Active Rap1 in Podocytes

To confirm that nephrin activation results in signaling that leads to activation of Rap1 in mammalian podocytes, we employed a podocyte culture system where nephrin signal transduction can be activated (**Figure 9A**) (Jones et al., 2006; Verma et al., 2006; George et al., 2012; George et al., 2014). Cultured human podocytes that inducibly express a chimeric nephrin protein by doxycycline (dox) treatment consisting of a CD16 extracellular domain, a CD7 transmembrane domain, and the cytoplasmic domain of nephrin (CD16-CD7-NCD). Incubation with anti-CD16 antibody induces clustering of chimeric nephrin, initiating recruitment of Src kinases to the nephrin intracellular domain and consecutive phosphorylation on activating tyrosine residues known to bind to cytoskeletal adapter proteins such as Nck, Crk1/2, CrkL, phospho-inositol-3-kinase (pi3k), and other signaling intermediaries (Jones et al., 2006; Verma et al., 2006; George et al., 2012;

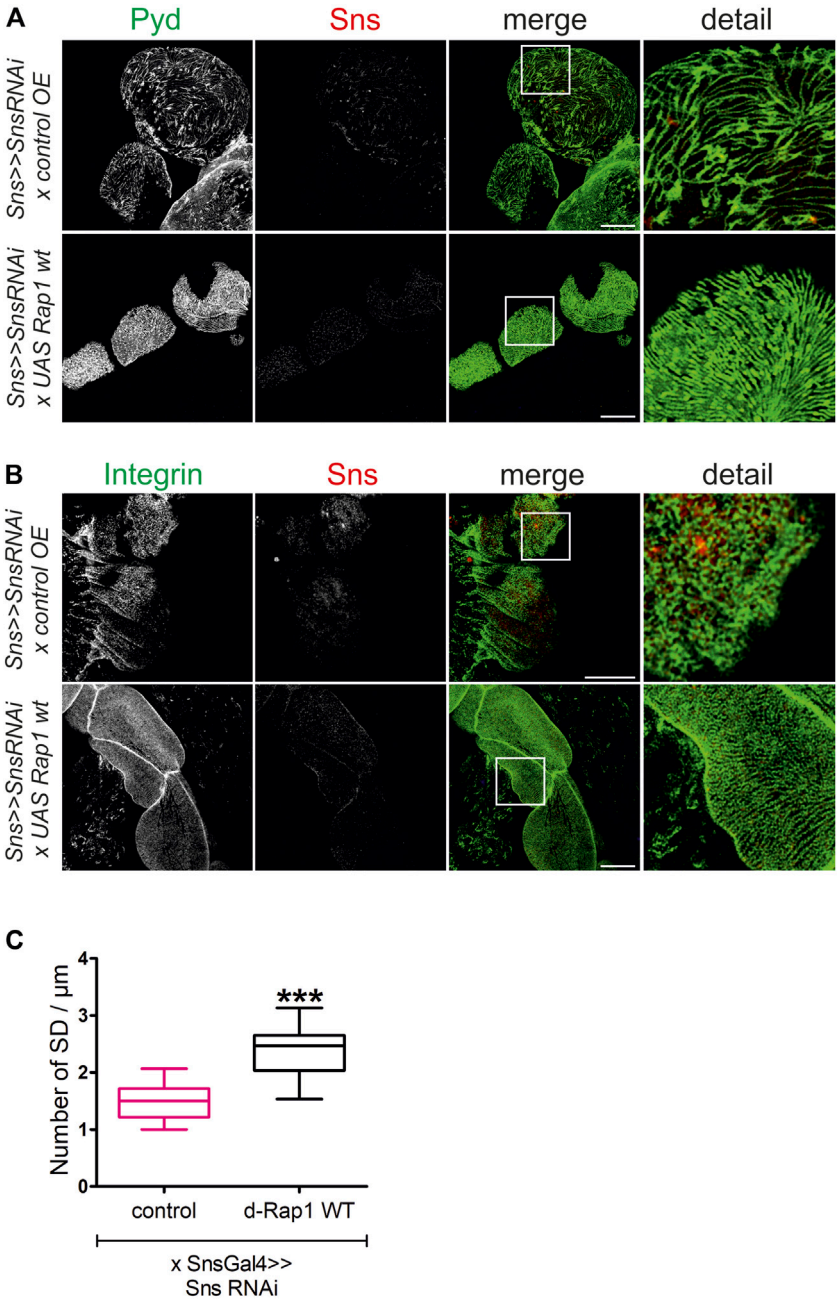

FIGURE 8 | *Rap1* overexpression can rescue the loss of slit diaphragms and integrin targeting induced by *sns* downregulation. Immunofluorescence analysis of surface sections of nephrocytes with knockdown of *sns* and overexpression of a control element or overexpression of *Drosophila rap1* (*sns>>UAS snsRNAi x UAS RFP* or *sns>>UAS snsRNAi x UASdRap1*). Knockdown in nephrocytes was accomplished by employing *sns-GAL4*. Wandering third instar larvae were dissected, and immunofluorescence analysis was performed with antibodies specific for Pyd (green) and Sns (red) **(A)** or integrin β (green) and Sns (red) **(B)**. Merged images and higher magnifications of the marked area are shown. Scale bars **(A,B)**: 10 µm, $n = 3$. **(C)** Statistical evaluation of the number of slit diaphragms (SD) per µm nephrocyte surface area of the genotypes shown in **(A)** depicted as a box plot with minimum and maximum. The control is marked in pink. $^{***}p < 0.001$.

George et al., 2014). As controls, podocytes inducibly expressing CD16-CD7-HA, where the cytoplasmic domain of nephrin is replaced by HA-tag, were used. Podocyte lines were treated with dox to induce the expression of either CD16-CD7-NCD or CD16-CD7-HA followed by incubation with antibodies specific for CD16 and secondary IgG to trigger clustering. Podocyte lysates were then subjected to immunoprecipitation employing an antibody specific for GTP-bound, active Rap1A/B followed by immunoblotting with an antibody recognizing total Rap1A/B. Furthermore, immunoblots were performed with antibodies specific for nephrin, phospho-nephrin (pNephrin), HA, total Rap1A/B, and β-tubulin to control loading. This

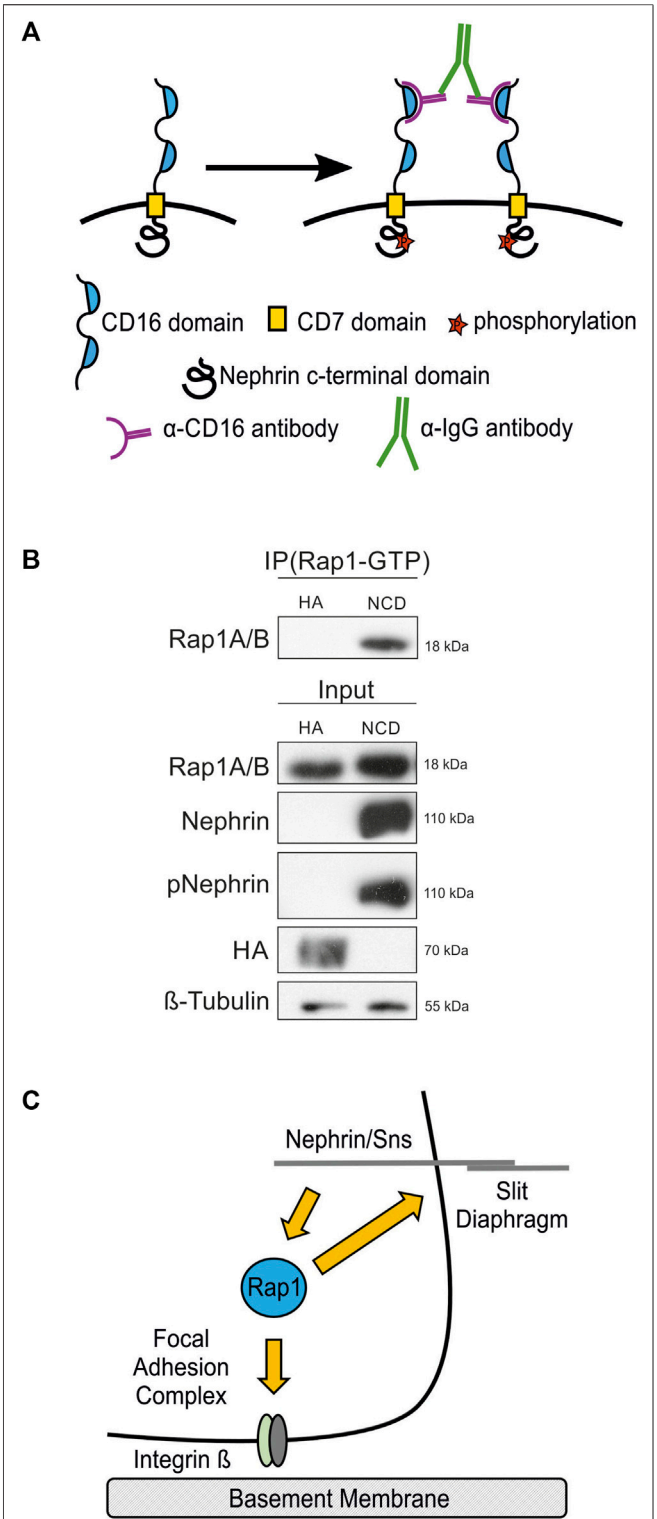

FIGURE 9 | Nephrin activation results in increased active Rap1 in human podocytes. **(A)** A nephrin clustering assay was performed by adding anti-CD16 antibody and secondary anti-IgG antibody to the media of cultured podocytes, which induces clustering of nephrin proteins followed by recruitment of Src kinases and consecutive phosphorylation of nephrin on tyrosine residues. **(B)** Immunoblot with antibodies specific for Rap1A/B

(*Continued*)

FIGURE 9 | following immunoprecipitation (IP Rap1-GTP) with an antibody specific for active Rap1A/B of podocyte lysates. Employed were human podocyte lines that inducibly express either chimeric CD16-CD7-nephrin cytoplasmic domain (NCD) or CD16-CD7-HA (HA) as a control following doxycycline treatment followed by clustering of nephrin. Immunoblots of these lysates were also performed with antibodies specific for Rap1A/B, nephrin, phospho-nephrin (pNephrin), HA, and β-tubulin (Input), $n = 3$. **(C)** Schematic of the hypothesis that the small GTPase Rap1 functions downstream of nephrin in signaling to integrin β at focal adhesions and in signaling at the slit diaphragm.

showed that the amount of the active form of Rap1-GTP was increased following activation of nephrin (**Figure 9B**).

DISCUSSION

By employing the *Drosophila* nephrocyte model, we showed that Rap1 is necessary for typical integrin localization in nephrocytes. Rap1 activity is essential for nephrin signaling to integrin β and nephrin signaling to regulate slit diaphragm integrity. We show by genetic interaction experiments that Rap1 functions downstream in nephrin signaling to integrin β at focal adhesions. In podocyte culture, nephrin activation results in increased activation of Rap1. Thus, the GTPase Rap1 is a novel intermediary in the signaling pathway from nephrin at the slit diaphragm to integrin β at focal adhesions (**Figure 9C**).

Drosophila nephrocytes emerged as a genetically tractable model to dissect slit diaphragm biology and nephrin signal transduction as nephrocytes exhibit slit diaphragms where, similar to mammals, the principal junction proteins and their cytoskeletal adaptors are present (Weavers et al., 2009; Zhuang et al., 2009; Dlugos et al., 2019). The short generation time of *Drosophila* makes it feasible to identify novel mediators in signaling pathways. In a previous study, we identified the small GTPase Rap1 to be necessary for slit diaphragm function and protein uptake in nephrocytes (Dlugos et al., 2019). *Drosophila* genetics make it possible to dissect whether genes act in the same pathway by genetic interaction experiments (Simon et al., 1991; Fortini et al., 1992; Brunner et al., 1994). By increasing nephrin expression and simultaneous downregulation of the *rap1* expression level, we showed that Rap1 acts downstream of nephrin signal transduction to integrin β and in nephrin signaling necessary for slit diaphragm integrity. Dismantling signaling cascades diminutively is essential to discover potential novel drug targets for glomerular disease therapy.

In other cell models, the role of Rap1 in governing the inside-out activation of integrin dimers that consist of a β1, β2, or β3 subunit is well-established (Bos et al., 2003; Caron, 2003; Dustin et al., 2004; Bos, 2005). In blood cells, Rap1 regulates integrin activation *via* the Rap1-GTP-interacting adapter molecule (RIAM) and consecutive activation of integrin by talin (Lagarrigue et al., 2016). Conversely, Rap1 does not appear to play a role in signaling from integrin to adhesion proteins at intercellular junctions (Balzac et al., 2005). Thus, the role of Rap1 in integrin regulation and function is currently judged to be unidirectional (Balzac et al., 2005). This is

interesting, as integrin ligation indeed transduces signals that result in nephrin phosphorylation at the slit diaphragm (Verma et al., 2016), but mediators of this are not yet identified. Previously, we showed that the Rap1 activator C3G acts downstream of nephrin in the signaling pathway to integrin β (Dlugos et al., 2019). Now, we find that Rap1 regulates signaling of nephrin at the intercellular junction in nephrocytes that modulates the targeting of integrin β at focal adhesions clarifying inside-out signal transduction of integrin β in nephrocytes and podocytes.

Rap1 also plays an important role in regulating intercellular junctions (Retta et al., 2006). In endothelial cells, Rap1 activity controls endothelial barrier function by tightening VE-cadherin-based cell–cell adhesion (Cullere et al., 2005; Fukuhara et al., 2005). In contrast to the unilateral function of Rap1 in integrin activation regulation, its role at intercellular junctions appears to be bidirectional. Rap1 is also a target of E-cadherin in outside-in signaling following junction disassembly and E-cadherin endocytosis in endothelial cells (Balzac et al., 2005). In podocytes, nephrin interacts with the adapter protein MAGI-1, thereby recruiting Rap1 (Ni et al., 2016). Rap1 activity is modulated by the Rap1 activating factor Rapgef2 (Zhu et al., 2019). In mice, knockout of Rap1A and Rap1B results in disruption of slit diaphragm integrity and development of focal segmental glomerulosclerosis (FSGS) (Potla et al., 2014). Mutations in the gene encoding MAGI-2 in humans result in nephrotic syndrome, a glomerular pathology where the breakdown of the podocyte intercellular junction and consecutive filtration barrier dysfunction result in loss of protein into the urine (Ashraf et al., 2018). The chronic nephrotic syndrome often leads to chronic glomerular disease. We now show that the Rap1 activity balance is central for an intact slit diaphragm. Both increased and decreased Rap1 activities result in a phenotype of an effaced slit diaphragm. This implies that Rap1 activity is tightly regulated in the nephrin signaling pathway that regulates intercellular junction integrity and the pathway from nephrin to integrin β that governs focal adhesion composition.

We observe a similar phenotype of Sns or Rap1 gain and loss of function. This may indicate that Sns and Rap1 functions are tightly regulated by the cell, and physiological protein levels and activity are necessary for nephrocytes or podocytes. It is not uncommon that signaling cascades are dysregulated by either excess or lack of a signaling component (Reichardt et al., 2000; Feng, 2012; Toker and Chin, 2014; Wang et al., 2014). Many proteins function in multi-protein complexes. Stoichiometric changes in protein complex composition may result in dysfunction of the respective protein complex independent of the cause being excess or lack of one protein component. This could also be the case for Sns and Rap1. In contrast, we cannot rule out that overexpression of either Sns or Rap1 may cause a dominant-negative effect and thus exhibit similar phenotypes as the respective knockdowns. Furthermore, it needs to be noted that, by employing a dominant-negative or constitutively active form of Rap1, we analyzed the impact of very high or low levels of Rap1 activity on focal adhesion and slit diaphragm integrity. To conclude that Rap1 activity has to be tightly balanced in podocytes and nephrocytes to mediate focal adhesion and slit diaphragm integrity, more modest changes in Rap1 activity need to be assayed.

As MAGI is involved in nephrin-dependent Rap1 regulation and slit diaphragm integrity in mammalian podocytes, it is not surprising that dMAGI is also necessary for intact slit diaphragms in nephrocytes. The nephrocyte model can thus be employed to further characterize the role of MAGI in nephrin signaling in future studies. It will be very interesting to distinguish whether MAGI and C3G act in the same pathway down-stream of Sns or whether MAGI and C3G fulfil functions in separate pathways.

Podocyte loss is a central progression factor of chronic glomerular disease (Wiggins, 2007). Mechanisms that regulate podocyte detachment are not well understood. We now dissect a pathway from nephrin *via* Rap1 that regulates integrin β targeting and potentially podocyte adhesion. It will be interesting to further characterize this signaling pathway and its role in different glomerular diseases as this may uncover interesting targets to modify podocyte loss in glomerular disease.

DATA AVAILABILITY STATEMENT

The original contributions presented in the study are included in the **Supplementary Material,** further inquiries can be directed to the corresponding author.

AUTHOR CONTRIBUTIONS

M-LM, CP, CL, and BG designed the experiments. M-LM, CP, CL, FSY, LB, and AR performed the research. JK and MPK helped with analytical tools or new reagents. M-LM, CP, CL, LB, FSY, JK, HP, MPK, and BG analyzed the data. M-LM, CL, and BG wrote the manuscript.

FUNDING

This work was supported by grants to BG from the German Research Foundation (GE 2158/3-1; GE 2158/3-3) and the funds of Innovative Medical Research of the University of Münster Medical School to BG (GE 112002 and GE 111303) and M-LM (ED 521801).

ACKNOWLEDGMENTS

This work contains parts of the PhD thesis of CP and the MD thesis of FSY. We thank Christian Klämbt and Thomas Weide for critically reading the manuscript.

SUPPLEMENTARY MATERIAL

The Supplementary Material for this article can be found online at: https://www.frontiersin.org/articles/10.3389/fcell.2022.790365/full#supplementary-material

REFERENCES

Ashraf, S., Kudo, H., Rao, J., Kikuchi, A., Widmeier, E., Lawson, J. A., et al. (2018). Mutations in Six Nephrosis Genes Delineate a Pathogenic Pathway Amenable to Treatment. *Nat. Commun.* 9 (1), 1960. doi:10.1038/s41467-018-04193-w

Balzac, F., Avolio, M., Degani, S., Kaverina, I., Torti, M., Silengo, L., et al. (2005). E-cadherin Endocytosis Regulates the Activity of Rap1: a Traffic Light GTPase at the Crossroads between Cadherin and Integrin Function. *J. Cel Sci* 118 (20), 4765–4783. doi:10.1242/jcs.02584

Barletta, G.-M., Kovari, I. A., Verma, R. K., Kerjaschki, D., and Holzman, L. B. (2003). Nephrin and Neph1 Co-localize at the Podocyte Foot Process Intercellular Junction and Form Cis Hetero-Oligomers. *J. Biol. Chem.* 278 (21), 19266–19271. doi:10.1074/jbc.m301279200

Bayraktar, S., Nehrig, J., Menis, E., Karli, K., Janning, A., Struk, T., et al. (2020). A Deregulated Stress Response Underlies Distinct INF2-Associated Disease Profiles. *J. Am. Soc. Nephrol.* 31 (6), 1296–1313. doi:10.1681/asn.2019111174

Bos, J. L., de Bruyn, K., Enserink, J., Kuiperij, B., Rangarajan, S., Rehmann, H., et al. (2003). The Role of Rap1 in Integrin-Mediated Cell Adhesion. *Biochem. Soc. Trans.* 31, 83–86. doi:10.1042/bst0310083

Bos, J. L. (2005). Linking Rap to Cell Adhesion. *Curr. Opin. Cel Biol.* 17, 123–128. doi:10.1016/j.ceb.2005.02.009

Brunner, D., Oellers, N., Szabad, J., Biggs, W. H., Zipursky, S. L., and Hafen, E. (1994). A Gain-Of-Function Mutation in Drosophila MAP Kinase Activates Multiple Receptor Tyrosine Kinase Signaling Pathways. *Cell* 76 (5), 875–888. doi:10.1016/0092-8674(94)90362-x

Caron, E. (2003). Cellular Functions of the Rap1 GTP-Binding Protein: a Pattern Emerges. *J. Cel Sci* 116, 435–440. doi:10.1242/jcs.00238

Cullere, X., Shaw, S. K., Andersson, L., Hirahashi, J., Luscinskas, F. W., and Mayadas, T. N. (2005). Regulation of Vascular Endothelial Barrier Function by Epac, a cAMP-Activated Exchange Factor for Rap GTPase. *Blood* 105, 1950–1955. doi:10.1182/blood-2004-05-1987

Dlugos, C. P., Picciotto, C., Lepa, C., Krakow, M., Stöber, A., Eddy, M.-L., et al. (2019). Nephrin Signaling Results in Integrin β1 Activation. *J. Am. Soc. Nephrol.* 30 (6), 1006–1019. doi:10.1681/asn.2018040362

Dustin, M. L., Bivona, T. G., and Philips, M. R. (2004). Membranes as Messengers in T Cell Adhesion Signaling. *Nat. Immunol.* 5, 363–372. doi:10.1038/ni1057

Feng, G.-S. (2012). Conflicting Roles of Molecules in Hepatocarcinogenesis: Paradigm or Paradox. *Cancer Cell* 21 (2), 150–154. doi:10.1016/j.ccr.2012.01.001

Fortini, M. E., Simon, M. A., and Rubin, G. M. (1992). Signalling by the Sevenless Protein Tyrosine Kinase Is Mimicked by Rasl Activation. *Nature* 355, 559–561. doi:10.1038/355559a0

Fu, Y., Zhu, J.-y., Zhang, F., Richman, A., Zhao, Z., and Han, Z. (2017). Comprehensive Functional Analysis of Rab GTPases in Drosophila Nephrocytes. *Cell Tissue Res* 368 (3), 615–627. doi:10.1007/s00441-017-2575-2

Fukuhara, S., Sakurai, A., Sano, H., Yamagishi, A., Somekawa, S., Takakura, N., et al. (2005). Cyclic AMP Potentiates Vascular Endothelial Cadherin-Mediated Cell-Cell Contact to Enhance Endothelial Barrier Function through an Epac-Rap1 Signaling Pathway. *Mol. Cel Biol* 25, 136–146. doi:10.1128/mcb.25.1.136-146.2005

Garg, P., Verma, R., Cook, L., Soofi, A., Venkatareddy, M., George, B., et al. (2010). Actin-depolymerizing Factor Cofilin-1 Is Necessary in Maintaining Mature Podocyte Architecture. *J. Biol. Chem.* 285 (29), 22676–22688. doi:10.1074/jbc.m110.122929

Garg, P., Verma, R., and Holzman, L. B. (2007). Slit Diaphragm Junctional Complex and Regulation of the Cytoskeleton. *Nephron Exp. Nephrol.* 106 (2), e67–72. doi:10.1159/000101795

Garg, P., Verma, R., Nihalani, D., Johnstone, D. B., and Holzman, L. B. (2007). Neph1 Cooperates with Nephrin to Transduce a Signal that Induces Actin Polymerization. *Mol. Cel Biol* 27 (24), 8698–8712. doi:10.1128/mcb.00948-07

George, B., Fan, Q., Dlugos, C. P., Soofi, A. A., Zhang, J., Verma, R., et al. (2014). Crk1/2 and CrkL Form a Hetero-Oligomer and Functionally Complement Each Other during Podocyte Morphogenesis. *Kidney Int.* 85 (6), 1382–1394. doi:10.1038/ki.2013.556

George, B., and Holzman, L. B. (2012). Signaling from the Podocyte Intercellular Junction to the Actin Cytoskeleton. *Semin. Nephrol.* 32 (4), 307–318. doi:10.1016/j.semnephrol.2012.06.002

George, B., Verma, R., Soofi, A. A., Garg, P., Zhang, J., Park, T.-J., et al. (2012). Crk1/2-dependent Signaling Is Necessary for Podocyte Foot Process Spreading in Mouse Models of Glomerular Disease. *J. Clin. Invest.* 122 (2), 674–692. doi:10.1172/jci60070

Ginsberg, M. H. (2014). Integrin Activation. *BMB Rep.* 47 (12), 655–659. doi:10.5483/bmbrep.2014.47.12.241

Hamano, Y., Grunkemeyer, J. A., Sudhakar, A., Zeisberg, M., Cosgrove, D., Morello, R., et al. (2002). Determinants of Vascular Permeability in the Kidney Glomerulus. *J. Biol. Chem.* 277 (34), 31154–31162. doi:10.1074/jbc.m204806200

Hermle, T., Braun, D. A., Helmstädter, M., Huber, T. B., and Hildebrandt, F. (2017). Modeling Monogenic Human Nephrotic Syndrome in the Drosophila Garland Cell Nephrocyte. *J. Am. Soc. Nephrol.* 28 (5), 1521–1533. doi:10.1681/asn.2016050517

Hochapfel, F., Denk, L., Mendl, G., Schulze, U., Maaßen, C., Zaytseva, Y., et al. (2017). Distinct Functions of Crumbs Regulating Slit Diaphragms and Endocytosis in Drosophila Nephrocytes. *Cell. Mol. Life Sci.* 74 (24), 4573–4586. doi:10.1007/s00018-017-2593-y

Huber, T. B., Hartleben, B., Kim, J., Schmidts, M., Schermer, B., Keil, A., et al. (2003). Nephrin and CD2AP Associate with Phosphoinositide 3-OH Kinase and Stimulate AKT-dependent Signaling. *Mol. Cel Biol* 23 (14), 4917–4928. doi:10.1128/mcb.23.14.4917-4928.2003

Jaskiewicz, A., Pajak, B., and Orzechowski, A. (2018). The Many Faces of Rap1 GTPase. *Int. J. Mol. Sci.* 19, 1–20. doi:10.3390/ijms19102848

Jones, N., Blasutig, I. M., Eremina, V., Ruston, J. M., Bladt, F., Li, H., et al. (2006). Nck Adaptor Proteins Link Nephrin to the Actin Cytoskeleton of Kidney Podocytes. *Nature* 440 (7085), 818–823. doi:10.1038/nature04662

Jones, N., New, L. A., Fortino, M. A., Eremina, V., Ruston, J., Blasutig, I. M., et al. (2009). Nck Proteins Maintain the Adult Glomerular Filtration Barrier. *J. Am. Soc. Nephrol.* 20 (7), 1533–1543. doi:10.1681/asn.2009010056

Kestilä, M., Lenkkeri, U., Männikkö, M., Lamerdin, J., McCready, P., Putaala, H., et al. (1998). Positionally Cloned Gene for a Novel Glomerular Protein-Nephrin-Is Mutated in Congenital Nephrotic Syndrome. *Mol. Cel* 1 (4), 575–582. doi:10.1016/s1097-2765(00)80057-x

Lagarrigue, F., Kim, C., and Ginsberg, M. H. (2016). The Rap1-RIAM-Talin axis of Integrin Activation and Blood Cell Function. *Blood* 128 (4), 479–487. doi:10.1182/blood-2015-12-638700

Martin, C. E., Petersen, K. A., Aoudjit, L., Tilak, M., Eremina, V., Hardy, W. R., et al. (2018). ShcA Adaptor Protein Promotes Nephrin Endocytosis and Is Upregulated in Proteinuric Nephropathies. *J. Am. Soc. Nephrol.* 29 (1), 92–103. doi:10.1681/asn.2017030285

Ni, J., Bao, S., Johnson, R. I., Zhu, B., Li, J., Vadaparampil, J., et al. (2016). MAGI-1 Interacts with Nephrin to Maintain Slit Diaphragm Structure through Enhanced Rap1 Activation in Podocytes. *J. Biol. Chem.* 291 (47), 24406–24417. doi:10.1074/jbc.m116.745026

Pavenstädt, H., Kriz, W., and Kretzler, M. (2003). Cell Biology of the Glomerular Podocyte. *Physiol. Rev.* 83 (1), 253–307. doi:10.1152/physrev.00020.2002

Potla, U., Ni, J., Vadaparampil, J., Yang, G., Leventhal, J. S., Campbell, K. N., et al. (2014). Podocyte-specific RAP1GAP Expression Contributes to Focal Segmental Glomerulosclerosis-Associated Glomerular Injury. *J. Clin. Invest.* 124 (4), 1757–1769. doi:10.1172/jci67846

Pozzi, A., Jarad, G., Moeckel, G. W., Coffa, S., Zhang, X., Gewin, L., et al. (2009). Beta1 Integrin Expression by Podocytes Is Required to Maintain Glomerular Structural Integrity. *Dev. Biol.* 316 (2), 288–301. doi:10.1016/j.ydbio.2008.01.022

Radha, V., Mitra, A., Dayma, K., and Sasikumar, K. (2011). Signalling to Actin: Role of C3G, a Multitasking Guanine-Nucleotide-Exchange Factor. *Biosci. Rep.* 31 (4), 231–244. doi:10.1042/bsr20100094

Reichardt, H. M., Umland, T., Bauer, A., Kretz, O., and Schütz, G. (2000). Mice with an Increased Glucocorticoid Receptor Gene Dosage Show Enhanced Resistance to Stress and Endotoxic Shock. *Mol. Cel Biol* 20 (23), 9009–9017. doi:10.1128/mcb.20.23.9009-9017.2000

Retta, S. F., Balzac, F., and Avolio, M. (2006). Rap1: a Turnabout for the Crosstalk between Cadherins and Integrins. *Eur. J. Cel Biol* 85 (3–4), 283–293. doi:10.1016/j.ejcb.2005.09.007

Sachs, N., and Sonnenberg, A. (2013). Cell-matrix Adhesion of Podocytes in Physiology and Disease. *Nat. Rev. Nephrol.* 9 (4), 200–210. doi:10.1038/nrneph.2012.291

Scott, R. P., and Quaggin, S. E. (2015). The Cell Biology of Renal Filtration. *J. Cel Biol* 209 (2), 199–210. doi:10.1083/jcb.201410017

Simon, M. A., Bowtell, D. D. L., Dodson, G. S., Laverty, T. R., and Rubin, G. M. (1991). Ras1 and a Putative Guanine Nucleotide Exchange Factor Perform Crucial Steps in Signaling by the Sevenless Protein Tyrosine Kinase. *Cell* 67, 701–716. doi:10.1016/0092-8674(91)90065-7

Toker, A., and Chin, Y. R. (2014). Akt-ing up on SRPK1: Oncogene or Tumor Suppressor? *Mol. Cel* 54 (3), 329–330. doi:10.1016/j.molcel.2014.04.020

Venkatareddy, M., Cook, L., Abuarquob, K., Verma, R., and Garg, P. (2011). Nephrin Regulates Lamellipodia Formation by Assembling a Protein Complex that Includes Ship2, Filamin and Lamellipodin. *PLoS One* 6 (12), e28710. doi:10.1371/journal.pone.0028710

Verma, R., Wharram, B., Kovari, I., Kunkel, R., Nihalani, D., Wary, K. K., et al. (2003). Fyn Binds to and Phosphorylates the Kidney Slit Diaphragm Component Nephrin. *J. Biol. Chem.* 278 (23), 20716–20723. doi:10.1074/jbc.m301689200

Verma, R., Kovari, I., Soofi, A., Nihalani, D., Patrie, K., and Holzman, L. B. (2006). Nephrin Ectodomain Engagement Results in Src Kinase Activation, Nephrin Phosphorylation, Nck Recruitment, and Actin Polymerization. *J. Clin. Invest.* 116 (5), 1346–1359. doi:10.1172/jci27414

Verma, R., Venkatareddy, M., Kalinowski, A., Patel, S. R., and Garg, P. (2016). Integrin Ligation Results in Nephrin Tyrosine Phosphorylation *In Vitro*. *PLoS One* 11 (2), e0148906–19. doi:10.1371/journal.pone.0148906

Wang, P., Zhou, Z., Hu, A., Ponte de Albuquerque, C., Zhou, Y., Hong, L., et al. (2014). Both Decreased and Increased SRPK1 Levels Promote Cancer by Interfering with PHLPP-Mediated Dephosphorylation of Akt. *Mol. Cel* 54 (3), 378–391. doi:10.1016/j.molcel.2014.03.007

Weavers, H., Prieto-Sánchez, S., Grawe, F., Garcia-López, A., Artero, R., Wilsch-Bräuninger, M., et al. (2009). The Insect Nephrocyte Is a Podocyte-like Cell with a Filtration Slit Diaphragm. *Nature* 457 (7227), 322–326. doi:10.1038/nature07526

Wiggins, R.-C. (2007). The Spectrum of Podocytopathies: A Unifying View of Glomerular Diseases. *Kidney Int.* 71 (12), 1205–1214. doi:10.1038/sj.ki.5002222

Zhang, F., Zhao, Y., and Han, Z. (2013). An *In Vivo* Functional Analysis System for Renal Gene Discovery in Drosophila Pericardial Nephrocytes. *J. Am. Soc. Nephrol.* 24 (2), 1–7. doi:10.1681/asn.2012080769

Zhang, F., Zhao, Y., Chao, Y., Muir, K., and Han, Z. (2013). Cubilin and Amnionless Mediate Protein Reabsorption inDrosophilaNephrocytes. *J. Am. Soc. Nephrol.* 24 (2), 209–216. doi:10.1681/asn.2012080795

Zhu, J., Sun, N., Aoudjit, L., Li, H., Kawachi, H., Lemay, S., et al. (2008). Nephrin Mediates Actin Reorganization via Phosphoinositide 3-kinase in Podocytes. *Kidney Int.* 73 (5), 556–566. doi:10.1038/sj.ki.5002691

Zhu, J., Attias, O., Aoudjit, L., Jiang, R., Kawachi, H., and Takano, T. (2010). p21-Activated Kinases Regulate Actin Remodeling in Glomerular Podocytes. *Am. J. Physiology-Renal Physiol.* 298 (4), F951–F961. doi:10.1152/ajprenal.00536.2009

Zhu, B., Cao, A., Li, J., Young, J., Wong, J., Ashraf, S., et al. (2019). Disruption of MAGI2-RapGEF2-Rap1 Signaling Contributes to Podocyte Dysfunction in Congenital Nephrotic Syndrome Caused by Mutations in MAGI2. *Kidney Int.* 96, 642–655. doi:10.1016/j.kint.2019.03.016

Zhuang, S., Shao, H., Guo, F., Trimble, R., Pearce, E., and Abmayr, S. M. (2009). Sns and Kirre, theDrosophilaorthologs of Nephrin and Neph1,direct Adhesion, Fusion and Formation of a Slit Diaphragm-like Structure in Insect Nephrocytes. *Development* 136 (14), 2335–2344. doi:10.1242/dev.031609

Conflict of Interest: The authors declare that the research was conducted in the absence of any commercial or financial relationships that could be construed as a potential conflict of interest.

Publisher's Note: All claims expressed in this article are solely those of the authors and do not necessarily represent those of their affiliated organizations or those of the publisher, the editors, and the reviewers. Any product that may be evaluated in this article, or claim that may be made by its manufacturer, is not guaranteed or endorsed by the publisher.

frontiers | Frontiers in Cell and Developmental Biology

ORIGINAL RESEARCH
published: 20 April 2022
doi: 10.3389/fcell.2022.855340

SARS-CoV-2 Employ BSG/CD147 and ACE2 Receptors to Directly Infect Human Induced Pluripotent Stem Cell-Derived Kidney Podocytes

Titilola D. Kalejaiye[1], *Rohan Bhattacharya*[1,2], *Morgan A. Burt*[1], *Tatianna Travieso*[3,4], *Arinze E. Okafor*[1], *Xingrui Mou*[1], *Maria Blasi*[3,4] *and Samira Musah*[1,2,5,6,7]*

[1]Department of Biomedical Engineering, Pratt School of Engineering, Duke University, Durham, NC, United States, [2]Center for Biomolecular and Tissue Engineering, Duke University, Durham, NC, United States, [3]Division of Infectious Diseases, Department of Medicine, Duke University School of Medicine, Durham, NC, United States, [4]Duke Human Vaccine Institute, Duke University Medical Center, Durham, NC, United States, [5]Division of Nephrology, Department of Medicine, Duke University School of Medicine, Durham, NC, United States, [6]Developmental and Stem Cell Biology Program, Duke University, Durham, NC, United States, [7]Department of Cell Biology, Duke University, Durham, NC, United States

OPEN ACCESS

Edited by:
Hans Kristian Lorenzo, Université Paris-Saclay, France

Reviewed by:
Rajkumar S. Kalra, Okinawa Institute of Science and Technology Graduate University, Japan
José M. Reyes-Ruiz, Instituto Mexicano del Seguro Social (IMSS), Mexico

***Correspondence:**
Samira Musah
samira.musah@duke.edu

Specialty section:
This article was submitted to Cell Death and Survival, a section of the journal Frontiers in Cell and Developmental Biology

Received: 15 January 2022
Accepted: 18 March 2022
Published: 20 April 2022

Citation:
Kalejaiye TD, Bhattacharya R, Burt MA, Travieso T, Okafor AE, Mou X, Blasi M and Musah S (2022) SARS-CoV-2 Employ BSG/CD147 and ACE2 Receptors to Directly Infect Human Induced Pluripotent Stem Cell-Derived Kidney Podocytes. Front. Cell Dev. Biol. 10:855340. doi: 10.3389/fcell.2022.855340

Severe acute respiratory syndrome coronavirus 2 (SARS-CoV-2) causes the Coronavirus disease 2019 (COVID-19), which has resulted in over 5.9 million deaths worldwide. While cells in the respiratory system are the initial target of SARS-CoV-2, there is mounting evidence that COVID-19 is a multi-organ disease. Still, the direct affinity of SARS-CoV-2 for cells in other organs such as the kidneys, which are often targeted in severe COVID-19, remains poorly understood. We employed a human induced pluripotent stem (iPS) cell-derived model to investigate the affinity of SARS-CoV-2 for kidney glomerular podocytes, and examined the expression of host factors for binding and processing of the virus. We studied cellular uptake of the live SARS-CoV-2 virus as well as a pseudotyped virus. Infection of podocytes with live SARS-CoV-2 or spike-pseudotyped lentiviral particles revealed cellular uptake even at low multiplicity of infection (MOI) of 0.01. We found that direct infection of human iPS cell-derived podocytes by SARS-CoV-2 virus can cause cell death and podocyte foot process retraction, a hallmark of podocytopathies and progressive glomerular diseases including collapsing glomerulopathy observed in patients with severe COVID-19 disease. We identified BSG/CD147 and ACE2 receptors as key mediators of spike binding activity in human iPS cell-derived podocytes. These results show that SARS-CoV-2 can infect kidney glomerular podocytes *in vitro* via multiple binding interactions and partners, which may underlie the high affinity of SARS-CoV-2 for kidney tissues. This stem cell-derived model is potentially useful for kidney-specific antiviral drug screening and mechanistic studies of COVID-19 organotropism.

Keywords: SARS-CoV-2, podocytes, S-pseudotyped virus, ACE2, BSG/CD147, organotropism, kidney disease, *in vitro* disease model

INTRODUCTION

The Coronavirus disease 2019 (COVID-19)—caused by the severe acute respiratory syndrome coronavirus 2 (SARS-CoV-2)—has affected more than 441 million people and caused over 5.9 million deaths worldwide (Johns Hopkins University and Medicine, 2021) (retrieved 3 March 2022). Although SARS-CoV-2 primarily infects cells in the respiratory tract, other tissues and organs have also been shown to be highly vulnerable to the virus resulting in a broad array of complications in the renal, cardiovascular, gastrointestinal and nervous systems (Gupta et al., 2020; Naicker et al., 2020; Zhang et al., 2020) particularly in elderly cases and in those with comorbidities (Deshmukh et al., 2021). Several *in vitro* studies have examined the impact of SARS-CoV-2 infection in lung and cardiac cells (Sharma et al., 2020; Sungnak et al., 2020; Yang et al., 2020; Marchiano et al., 2021). SARS-CoV-2 viral RNA from tissues of living and dead patients of COVID-19 has been detected in multiple organs including the kidneys (Puelles et al., 2020; Musah, 2021; Peiris et al., 2021). Intriguingly, acute kidney injury (Akilesh et al., 2021) and cardiac injury are common in COVID-19 patients (Cheng et al., 2020; Singh et al., 2020; Diao et al., 2021; Sharma et al., 2021) and have been associated with increased morbidity and mortality (Braun et al., 2020; Shi et al., 2020; Peiris et al., 2021). Additionally, collapsing glomerulopathy or COVID-19-associated nephropathy (COVAN) has been reported in COVID-19 patients (Velez et al., 2020; Sharma et al., 2021). COVAN resembles human immunodeficiency virus (HIV) -associated nephropathy (HIVAN), a kidney disease caused by HIV infection (Wyatt et al., 2008) resulting in CKD and kidney failure (Genovese et al., 2010). Notably, collapsing glomerulopathy constitutes a new renal manifestation of COVID-19 (Akilesh et al., 2021) that may also arise from genetic predisposition (Wu et al., 2020; Sharma et al., 2021).

Within the kidney, podocytes and proximal tubules play important roles in renal filtration, reabsorption and excretion (Pan et al., 2020). The glomerulus, a network of capillaries, is the primary site for blood filtration. The glomerular filtration barrier consists of interdigitated podocytes separated from fenestrated glomerular endothelial cells by the glomerular basement membrane (GBM), all of which function together to facilitate the selective filtration of toxins and waste from the blood (Lennon et al., 2014; Musah et al., 2017; Petrosyan et al., 2019). The kidney's glomerular podocytes are particularly vulnerable to bacterial and viral attacks and injury which can result in retraction of podocyte foot processes and effacement, causing abnormal leakage of proteins into the urine (proteinuria) (Jefferson et al., 2011). Given that SARS-CoV-2 has been found in nephrin-positive cells of the kidneys of COVID-19 patients (Puelles et al., 2020), we hypothesized that podocytes could be direct targets for SARS-CoV-2 infection.

SARS-CoV-2 organotropism (cell types or tissues permissive to viral infection) is influenced by the expression of suitable receptors on the cell surface and the presence of a host-encoded protease proximally positioned to the site of receptor binding to enable cleavage of the Spike (S) protein for viral processing (Singh et al., 2020; Tang et al., 2020). Angiotensin-Converting Enzyme 2 (ACE2) is widely recognized as a key receptor for SARS-CoV-2 binding to cells and tissues (Fehr and Perlman, 2015; Hoffmann et al., 2020; Lan et al., 2020; Moore and June, 2020; Walls et al., 2020). Basigin (BSG, also known as CD147 or EMMPRIN), a transmembrane glycoprotein has also been shown to be an alternate route for SARS-CoV and SARS-CoV-2 invasion of host cells (Chen et al., 2005; Wang et al., 2020). For instance, BSG/CD147 is shown to interact with S protein *in vitro* and facilitate entry of SARS-CoV and SARS-CoV-2 in Vero and HEK 293T cell (Vankadari and Wilce, 2020; Wang et al., 2020). Other receptors such as Neuropilin 1, a pleiotropic transmembrane peptide growth factor in fibroblasts, endothelial cells, and hepatocytes (Glinka et al., 2010) has been shown to enhance SARS-CoV-2 entry and infectivity when co-expressed with ACE2 and TMPRSS2 (Cantuti-Castelvetri et al., 2020). Additionally, CD209/DC-SIGN interacts with spike receptor binding domain (S-RBD) and can mediate SARS-CoV-2 entry into human cells (Amraei et al., 2021). Once the viral spike protein binds to the host receptor (Wrapp et al., 2020), the activity of proteases such as Transmembrane Serine Protease 2 (TMPRSS2) or Cathepsin L (CTSL) promote fusion and internalization of the receptor-viral spike complex (Wysocki et al., 2021).

Understanding the susceptibility of organ-specific cell types to SARS-CoV-2 infection and COVID-19 disease mechanisms rely on the availability of robust experimental models that can closely mimic the functional phenotype and developmental status of human cells and tissues. However, functional *in vitro* models are lacking for many tissues. For instance, the lack of appropriate *in vitro* models contributes to the poor understanding of how SARS-CoV-2 invades the human kidney tissues including the specialized group of visceral epithelial cells called podocytes. Podocytes encase the glomerular capillaries and play a vital role in regulating the removal of toxins and waste products from blood. These cells, are also susceptible to disease including those arising from drug toxicities and viral infections. As a result, there is a dire need to study SARS-CoV-2 infection in human kidney podocytes. Because stem cells can self-renew indefinitely and differentiate into almost any cell type when provided appropriate signals, they serve as virtually unlimited supply of organ-specific cells including podocytes (Musah et al., 2017). Derivatives of human pluripotent stem cells have also been used for disease modelling and drug discovery assays (Ilic and Ogilvie, 2017; Bhattacharya et al., 2021; Okafor et al., 2021; Kalejaiye et al., 2022). We previously developed a method to directly differentiate human iPS cells into cells that exhibit morphological, molecular, and functional characteristics of the mature human kidney glomerular podocytes (Musah et al., 2017; Musah et al., 2018; Burt et al., 2020). Herein, we employed this model to study the susceptibility of human kidney podocytes to SARS-CoV-2 infection. We also investigated the expression and involvement of host receptors and processing enzymes in SARS-CoV-2 binding to human kidney podocytes.

MATERIALS AND METHODS

Cell Culture

All cell lines used for this study were obtained under appropriate material transfer agreements and approved by all involved

institutional review boards. All cells were tested for and shown to be devoid of *mycoplasma* contamination (*Mycoplasma* PCR Detection Kit from abm, G238). Human colon epithelial (Caco-2) (ATCC, HTB-37) and human embryonic kidney (HEK 293T) (ATCC, CRL-3216) cell lines were cultured in high-glucose Dulbecco's Modified Eagle Medium (DMEM; Gibco, 12634010) media supplemented with 10% fetal bovine serum (FBS; Gibco; 10082147) with L-Glutamine (Gibco; 25030081) and 1X Penicillin/Streptomycin (Gibco; 15140122). HEK 293T cells were split (1:10) while Caco-2 cells were split (1: 5) every 3 days. Human lung (Calu-3) (ATCC, HTB-55) cells were cultured in Minimum Essential Media (MEM) (Gibco; 11095080) supplemented with 10% FBS with 1 mM sodium pyruvate (Gibco; 11360070), MEM non-essential amino acids (NEAA) (Gibco; 11140050) with 1X Penicillin/Streptomycin. Human induced pluripotent stem (Human iPS) cell line used for this study (PGP1—the Personal Genome Project (Ball et al., 2012)) were tested and shown to be free of *mycoplasma* contamination. The cell line had normal karyotype. Human iPS cells were cultured in mTeSR1 (StemCell Technologies; 85870) medium without antibiotics and split (1:6) every 4–5 days. All cells were incubated in a 37°C incubator with 5% CO_2.

Differentiation of Human iPS Cells Into Podocytes

Mature human glomerular podocytes were generated using previously published protocol (Musah et al., 2017; Musah et al., 2018; Burt et al., 2020). Briefly, human induced pluripotent stem (iPS) cells cultured on Matrigel-coated plates were dissociated with warm enzyme-free dissociation buffer (Gibco; 13150-016) and centrifuged twice at 200x*g* for 5 min each in advanced DMEM/F12 (Gibco; 12634010). The DMEM/F12 was aspirated off and the cells were resuspended in mesoderm induction media (consisting of DMEM/F12 with GlutaMax (Gibco; 10565042) supplemented with 100 ng/ml activin A (Invitrogen; PHC9564), 3 μM CHIR99021 (Stemgent; 04-0004), 10 μM Y27632 (TOCRIS; 1254) and 1X B27 serum-free supplement (Gibco; 17504044) and plated at a seeding density of 100,000 cells per well of a 12-well plate. The cells were cultured in the mesoderm induction medium for 2 days with daily medium change and after 2 days, intermediate mesoderm differentiation was initiated by feeding the cells with intermediate mesoderm induction medium (containing DMEM/F12 with GlutaMax supplemented with 100 ng/ml BMP7 (Invitrogen; Phc9543), 3 μM CHIR99021 and 1X B27 serum-free supplement) for a minimum of 14 days. Podocyte induction was initiated by dissociating the intermediate mesoderm cells with 0.05% trysin-EDTA (Gibco; 25300-054) for 5 min with subsequent quenching of the enzyme with 10% FBS in DMEM/F12 (trypsin neutralizing solution). Adhered cells were gently scraped using a cell lifter and the cell suspension was pipetted up and down using a P1000 barrier tip to dislodge cells and obtain individualized cells. The cell suspension was transferred into a 50 ml falcon tube containing 30 ml DMEM/F12 and centrifuged twice at 200x*g* for 5 min each. The cell pellet was resuspended in podocyte induction mediaand plated on a freshly prepared laminin-511-E8-coated plates at a seeding density of 100,000 cells per well of a 12 well plate. The cells were fed podocyte induction media containing advanced DMEM/F12 with GlutaMax supplemented with 100 ng/ml BMP7, 100 ng/ml activin A, 50 ng/ml VEGF (Gibco; PHC9394), 3 μM CHIR99021, 1X B27 serum-free supplement, and 0.1 μM all-trans retinoic acid (Stem Cell Technologies; 72262) for 5 days. Mature podocytes were maintained in CultureBoost-R (Cell Systems; 4Z0-500).

Production of SARS-CoV-2 S-Pseudotyped Lentiviral Particles

The SARS-CoV-2 S-pseudotyped lentiviral particles were generated by transfecting HEK 293T cells. Briefly, HEK 293T cells were seeded in DMEM-10 growth media in 75 cm^3 flask and propagated to about 65%–75% confluent. The cells were then transfected with the plasmids required for the lentiviral production using Lipofectamine 3000 reagent (Invitrogen; L3000015) in Opti-MEM (Gibco; 31985070) following manufacturer's instructions. Briefly, 20 μg of plasmid DNA (total plasmid mix) per flask was mixed in Opti-MEM and P3000 reagent and incubated at room temperature for 5 min. Plasmids mix for each transfection consisted of psPax2 (packaging; Addgene plasmid # 12260), pCMV-SCoV-2S (Spike envelope plasmid; Sinobiologicals—# VG40589-UT) and pLJM1-EGFP (reporter; Addgene plasmid #19319) in a ratio of 1:1:2, respectively. After 5 min incubation, the plasmid DNA mix in Opti-MEM- P3000 media was then mixed with the transfection reagent (Opti-MEM and Lipofectamine 3000 reagent) and incubated at room temperature for 10-15 min. Appropriate volumes of transfection mixture was used to transfect HEK 293Tcells in each flask and incubated in a 37°C incubator with 5% CO_2 for 6 h. Lentivirus pseudotyped with the vesicular stomatitis virus spike G (pCMV-VSV-G; Addgene plasmid # 8454) was used as positive control and a "bald" lentivirus lacking the envelope was used as a negative control.

At 6 h post-transfection, the culture medium was replaced with fresh pre-warmed DMEM-10. After an additional 24 h (30 h post-transfection) and 48 h (54 h post-transfection), the lentiviral particles were harvested by collecting the supernatant from each flask, centrifuged at 1000x*g* for 5 min and filtered through a 0.45 μm SFCA low protein-binding filter. Samples were then subjected to ultracentrifugation over a 28% sucrose cushion (Sucrose/PBS; Sigma S7903-1KG) at 100,000x*g* for 3 h at 4°C. The pellet was resuspended in 1X Tris buffered saline (TBS, Bio-Rad; 1706345), and then aliquoted and stored at −80°C to avoid repeated freeze-thaw cycles.

Infection of Cells With S-Pseudotyped Virus

Cells were cultured in the appropriate culture media and infected with S-pseudotyped, positive control or bald virus in the presence of polybrene (Sigma; TR-1003) to a final concentration of 5 μg/ml.

SARS-CoV-2 Expansion in Vero E6 Cells and Titration

All experiments with the live virus were performed under Biosafety Level 3 (BSL-3) in the Duke Regional Biocontainment Laboratory at the Duke Human Vaccine

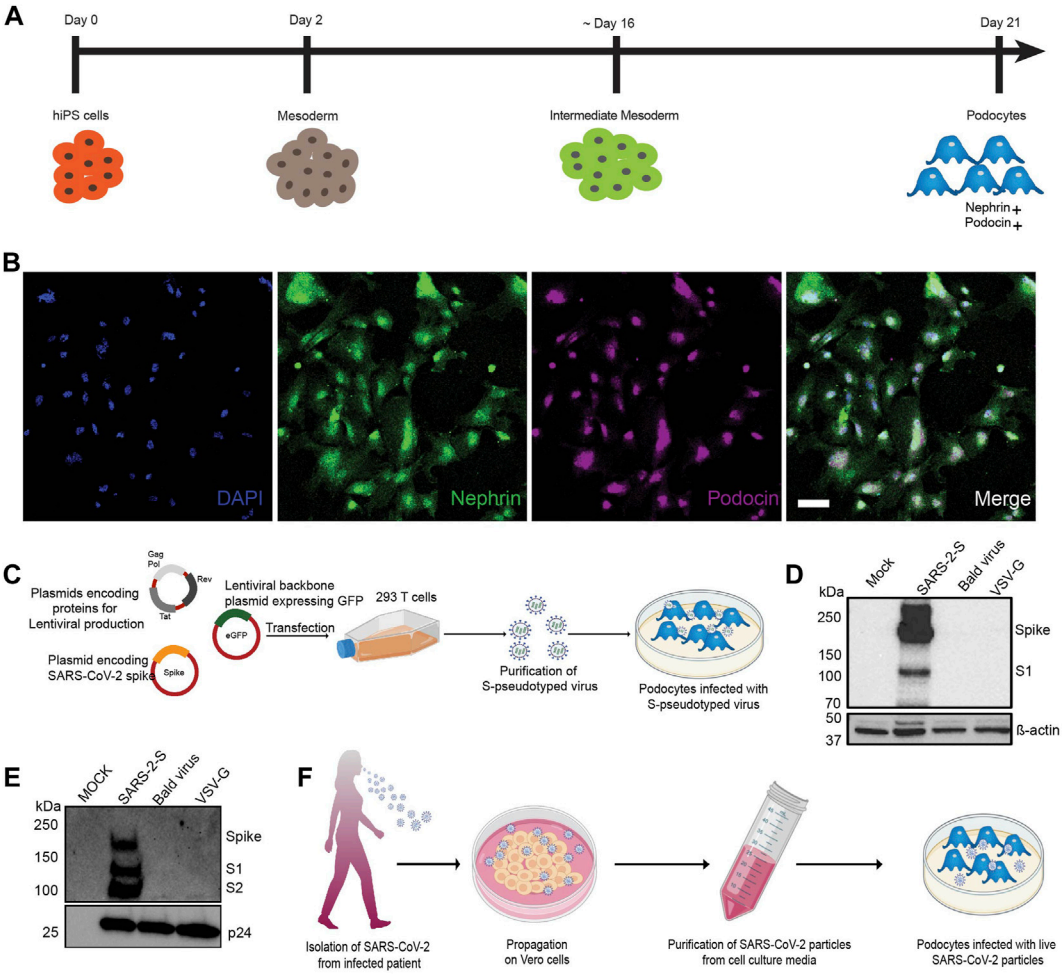

FIGURE 1 | Establishment of a method to examine susceptibility of human iPS cell-derived podocytes to SARS-CoV-2 infection. **(A)** Schematic overview of the protocol for the differentiation of mature podocytes from human iPS cells; adapted from (Musah et al., 2017). **(B)** Human iPS cell-derived podocytes express the lineage specific markers nephrin (green) and podocin (magenta). Cells were counterstained with DAPI (blue) nuclear marker. Scale bar, 100 µm. **(C)** Schematic depicting the lentiviral vectors used to produce S-pseudotyped virus from 293T cells and infection of human iPS cell-derived podocytes *in vitro*. **(D,E)** Western blot confirming the successful transfection of 293T cells and production of S-pseudotyped virus indicated by the presence of Spike protein (190kDa) and its cleavage products S1 (~110 kDa) in both **(D)** the cell lysates (β-actin used as loading control) and **(E)** purified viral particle (normalized to HIV viral protein p24) with extra band for S2 (~100 kDa). Mock for figure D represents lysate from untransfected cells while in E, mock represents pseudoviral particle dissolving media (TBS); SARS-2-S represent lysate from cells transfected with spike expressing plasmid or S-pseudotyped particle; Bald virus represent lysate from cells transfected with no envelope plasmid or the resulting pseudovirus particle without viral envelope protein; VSV-G represent lysate from cells transfected with plasmid expressing VSV-G or pseudotyped particle with VSV-G envelope **(F)** Schematic showing propagation of patient-derived SARS-CoV-2 virus in Vero E6 cells followed by purification and infection of human iPS cell-derived podocytes *in vitro*.

Institute (DHVI) in compliance with the BSL-3 laboratory safety protocols and guidelines from the CDC for handling SARS-CoV-2.

SARS-CoV-2 USA-WA1/2020 (BEI Resources; NR-52281) was propagated in Vero E6 cells at a MOI of 0.001 in DMEM supplemented with 2% FBS, 1X Penicillin/Streptomycin, 1 mM Sodium pyruvate and 1X Non-Essential Amino Acid (NEAA) at 37°C in 5% CO_2. Four days post infection (pi), supernatant containing the released virus were harvested, centrifuged at 1,500 rpm for 5 min and filtered through a 0.22 µM filter. Samples were aliquoted and stored at −80°C until further use.

Plaque assay was done to determine the titer of the viral stock. Briefly, 0.72×10^6 Vero E6 cells were seeded in 24 well plates. The virus stock was diluted serially (10-fold), and the dilutions were used to infect monolayer of Vero E6 cells at 37°C in 5% CO_2. After an hour of incubation, cells were overlayed with media containing carboxy-methyl cellulose (CMC) (0.6% CMC), MEM supplemented with 2% fetal bovine serum (FBS), 1 mM sodium pyruvate (Gibco), 1X NEAA (Gibco), 0.3% sodium bicarbonate (Gibco) and 1X GlutaMAX (Gibco) with 1X Penicillin/Streptomycin. After 4 days of incubation at 37°C in 5% CO_2, cells were stained with 1% crystal violet in 10% neutral

buffered formalin (NBF) and the number of plaque forming units per ml (pfu/ml) was determined.

Infection of Human iPS Cell-Derived Podocytes With Live Virus

1×10^5 intermediate mesoderm cells were differentiated to podocytes (per well of a 12 well plate). After 5 days of induction, podocytes were incubated with the SARS-CoV-2 virus at an MOI 0.01, 0.1 or 1.0 at 37°C and 5% CO_2 with intermittent plate rocking. To obtain the desired MOI, SARS-CoV-2 was diluted in CultureBoost-R and incubated with the podocytes for 1 h at 37°C. After 1 h of incubation, the virus-containing supernatant was aspirated, and cells were washed twice with 1X PBS. Fresh maintenance medium was then added, and cells incubated for either 24, 48 or 72 h at 37°C and 5% CO_2. Uninfected controls were incubated with CultureBoost-R only.

Infectious Viral Titer of Supernatant

Cellular supernatant was collected from podocytes infected with SARS-CoV-2 virus at MOI of 0.01, 0.1 and 1.0, at 24 hrs, 48 and 72 hrs post infection. The supernatant was clarified by centrifugation at 1,500 rpm for 5 min and the infectious viral titer was measured by plaque assay as described above.

qRT-PCR for Detection of Intracellular and Cell-free Viral RNA

SARS-CoV-2 RNA was extracted from the supernatant or cell pellet of infected podocytes using the QIAamp viral RNA mini kit (Qiagen; 52904). qRT-PCR was performed with primers specific for target genes (see **Supplementary Table S1** for the list of primers) using the Luna universal One-Step RT-qPCR kit (NEB; E3005). Experiment was performed using the QuantStudio3 (Applied Biosystems) with the following thermal cycling steps; 55°C for 10 min, 95°C for 1 min and 40 cycles of 95°C for 10 s and 60°C for 1 min according to manufacturer's protocol.

qRT-PCR and qPCR Analysis of Infected Cells

Cell pellets were washed and lysed using RA1 RNA extraction buffer and purified using the NucleoSpin RNA kit (MAcherey-Nagel; 740955.250) following the manufacturer's instructions. RNA from infected and control podocytes were harvested using NucleoSpin RNA kit. The RNA was quantified by nanodrop (Thermo Fisher). 0.5–1 μg of RNA was converted to cDNA for qPCR. cDNA synthesis was done using SuperScript III Reverse Transcriptase (Invitrogen; 18080-085) and qPCR was performed using qPCR SYBR Master Mix (Promega; A6001). Quantitative PCR was performed with QuantStudio3 (Applied Biosystems) using the thermal cycling steps; 50°C for 2 min, 95°C for 10 min and 40 cycles of 95°C for 15 s and 60°C for 1 min. Delta cycle threshold (ΔCt) was determined relative to GAPDH. Viral RNA from pseudovirus infected cells was also quantified by qRT-PCR using the Lenti-X qRT-PCR titration kit (Clontech; 631235) following manufacturer's instruction. Primer sequences are provided in the **Supplementary Table S1**.

Western Blot Analyses

For Western blotting, cells were first lysed using RIPA buffer (Sigma; R0278-500ML) supplemented with protease inhibitor cocktail (Roche) at 4°C with shaking for 30 min for protein extraction. Pierce BCA protein assay Kit (Thermo Fisher; 23227) was used for protein quantification. 15 μg of the extracted protein samples were boiled for 5 min at 95°C in 1X Laemlli buffer (BioRad; 1610747), run on mini-PROTEAN TGX precast gels (Bio-Rad; 4568083) and then transferred to PVDF membrane blot (Bio-Rad; 1620175). The blots were blocked in 5% non-fat milk made in TBS-T (50 mM Tris-HCl, 150 mM NaCl, 0.1% Tween-20) for 1 h and incubated with the primary antibodies in blocking buffer overnight at 4°C (see **Supplementary Table S2** for the antibody dilutions). The next day, horseradish-peroxidase-conjugated rabbit anti-goat (R&D Systems; HAF017), goat anti-rabbit (CST; 7074) or goat anti-mouse (CST; 7076) antibody was added, and the blot was incubated for 1 h at room temperature. The membranes were developed with the SuperSignal West Femto substrate (Thermo Fisher; 34095) by following manufacturer's protocol. The chemi-luminiscent signals were acquired using a GelDoc Imager (Bio-Rad).

Identification of Spike Associated Host Factors Expressed by Podocyte

To identify podocyte host factors that could facilitate viral entry and replication, we integrated the BioGRID interaction database with transcriptomic data previously generated in our lab. BioGRID is an expansive database of experimentally verified protein-protein and genetic interactions as assembled and curated from tens of thousands of studies (Oughtred et al., 2019). Firstly the latest release of the BioGRID interaction database (as at when this study was carried out) for coronaviruses was downloaded from the archive at https://downloads.thebiogrid.org/Download/BioGRID/Release-Archive/BIOGRID-3.5.188/BIOGRID-CORONAVIRUS-3.5.188.tab3.zip. The interaction network file was then opened using Cytoscape (v3.8.0) and filtered to obtain only edges linking human proteins to the SARS-CoV2 spike protein.

We extracted podocyte gene expression data for spike-binding proteins and integrated it with the network table obtained from BioGRID. The microarray transcriptomic data for human iPS cell-derived podocytes used in this study had been generated in a previous study (Musah et al., 2018). The podocyte microarray gene expression data were analyzed using standard pipeline. Briefly, the raw expression data were normalized by robust multiarray averaging (Irizarry et al., 2003) and the Human Gene 2.0 ST Affymetrix array mapping obtained from the ENSEMBL mart database was used to map probe IDs to gene IDs. The podocyte transcriptomic data was analyzed using the Bioconductor packages, oligo (v3.11), biomaRt, and pd.hugene.2.0.st (Carvalho and Irizarry, 2010). The expression data for

these proteins were then used to annotate a network visualization of these interactions on Cytoscape.

Immunofluorescence Imaging

For immunofluorescent imaging, human iPS cell-derived podocytes (infected and control) were fixed with 4% paraformaldehyde (PFA) in PBS for 20–30 min at room temperature and permeabilized using 0.125% Triton X-100 (Sigma-Aldrich) in PBS for 5 min. Cells were blocked with 1% BSA/PBS-T for 30 min at room temperature and then incubated with primary antibody diluted in the blocking buffer overnight at 4°C. After overnight incubation, cells were incubated with Alexa Fluor-488 or Alexa Fluor-594 donkey (Invitrogen, 1:1000) secondary antibodies diluted in blocking buffer for 1 h at room temperature. Cells were afterwards counterstained with 4′,6-diamidino-2-phenylindole (DAPI, Invitrogen, D1306). The primary antibodies used were anti-Nephrin (Progen, GP-N2); anti-Podocin (Abcam, ab50339); anti-SARS-CoV2 spike (ProSci, 3525); anti-SARS-CoV-2 N protein (Sinobiological, 40143-R019); anti-GFP (Millipore, SAB4301138); Human/Mouse/Rat/Hamster ACE-2 (R&D systems, AF933), Human TRA-1-85/CD147 (R&D systems, MAB3195), Cathepsin L (Santa Cruz Biotechnology, sc-32320), TMPRSS2 (Santa Cruz Biotechnology, sc-515727) and DC-SIGN/CD209 (Santa Cruz Biotechnology, sc-65740). Images were acquired using an M7000 epifluorescence microscope (Invitrogen, AMF7000) equipped with 10×/0.30 LWDPH with 7.13 mm WD and 20×/0.45 LWDPH with 6.12 mm WD objectives. Confocal images were captured using a Zeiss 880 inverted confocal Airyscan with a 10×/0.30 EC Plan-Neofluar air lens with 5.2 mm objective at the Duke Light Microscopy Core Facility.

Blocking of ACE2 and BSG/CD147 Protein With Antibodies

For the blocking of ACE2 and/or BSG/CD147 epitope, we infected podocytes with the S-pseudotyped lentivirus. Approximately 1.5 h prior to infecting cells, antibody dilutions were prepared in the CultureBoost-R. We performed the blocking experiment using an ACE2 polyclonal goat antibody (R&D systems; AF933) and CD147 (BSG) mouse monoclonal antibody (Human TRA-1-85/CD147 MAb (Clone TRA-1-85)-R&D systems; MAB3159). The human iPS cell-induced podocytes were pre-treated with serial dilutions of ACE2 antibody, BSG/CD147 antibody or both for 1 h. Unblocked cells and uninfected (mock) cells were used as control. After 1 h of incubation, the pseudoviral particles (MOI- 0.02) were added to each well and incubated for 48–60 h. After 60 h, cells were washed and lysed in RNA extraction buffer. RNA was purified using the Macherey Nagel RNA extraction kit following manufacturer's instruction and viral RNA uptake was quantified using the Luna universal One-Step RT-qPCR kit (NEB; E3005).

Quantification and Statistical Analysis

All experiments were done in 3 independent biological replicates unless otherwise indicated. N = 3. One-way analysis of variance (ANOVA) with Šidák's posttest or multiple *t*-test was used to test for statistical significance. Only p values of 0.05 or lower were considered statistically significant ($p > 0.05$ [ns, not significant], $p < 0.05$ [*], $p < 0.01$ [**], $p < 0.001$ [***], $p < 0.0001$ [****]). For all statistical analyses, the GraphPad Prism 9 software package was used.

RESULTS

Human iPS Cell-Derived Podocytes Are Permissive to S-Pseudotyped Viral Infection

Using our previously described protocol, (Musah et al., 2017; Musah et al., 2018; Burt et al., 2020). we differentiated human iPS cells into mature glomerular podocytes (**Figure 1A**) that exhibited highly specialized morphological features and expressed podocyte-specific markers including nephrin and podocin (**Figure 1B**).

The spike surface envelope glycoprotein (S) facilitates binding and entry of coronavirus including SARS-CoV and SARS-CoV-2 into cells (Wrapp et al., 2020) and it exhibits capabilities for receptor binding and membrane fusion (Masters and Perlman, 2013; Millet and Whittaker, 2015). We initially employed S-pseudotyped virus to study viral entry and uptake into podocytes. To generate the S-pseudotyped virus, we used an HIV-1-based S-pseudotyped lentiviral vector as illustrated in **Figure 1C**. Control pseudotyped viruses were generated using the vesicular stomatitis virus glycoprotein (VSV-G; control envelope) plasmid and a "bald" virus lacking an envelope protein. Western blot analysis of 293T cell lysates confirmed the presence of spike protein in only the cells that were transfected with the spike plasmid and not in the cell lysates obtained from VSV-G or bald virus transfection (**Figure 1D**). Western blot analysis of the 293T cell supernatant from S-pseudotyped particle produced three major bands at 190, 110, and 100 kDa representing the full-length and cleaved S proteins (S1 and S2, respectively) as well as the HIV gag protein (p24). These results confirmed the incorporation of the S protein in the pseudoviral particles and the successful generation of S-pseudotyped virus with the SARS-CoV-2 spike protein (SARS-2-S) (**Figure 1E**). As expected, the VSV-G and bald pseudoviruses produced only a band for HIV p24 and no band was detected in the mock (medium control) (**Figure 1E**). Live virus infection of human iPS cell-derived podocytes was performed using SARS-CoV-2 strain USA-WA1/2020 grown on Vero E6 cells as illustrated in **Figure 1F**.

We initially inoculated human iPS cell-derived podocytes with the S-pseudotyped virus to examine their permissiveness to the virus. The total viral RNA copies in transduced cells were quantified by qRT-PCR using the Lenti-X qRT-PCR titration kit every 24 h post infection (h.p.i) for up to 72 h.p.i. Interestingly, we observed an exponential increase in the number of intracellular RNA copies with each additional day of exposure (**Figure 2A**), confirming an increase in viral uptake with incubation time. Consistent with these results, Western blot quantification of the relative amount of Gag-p24 taken up by the podocytes each day post-infection (**Figure 2B**) corroborated

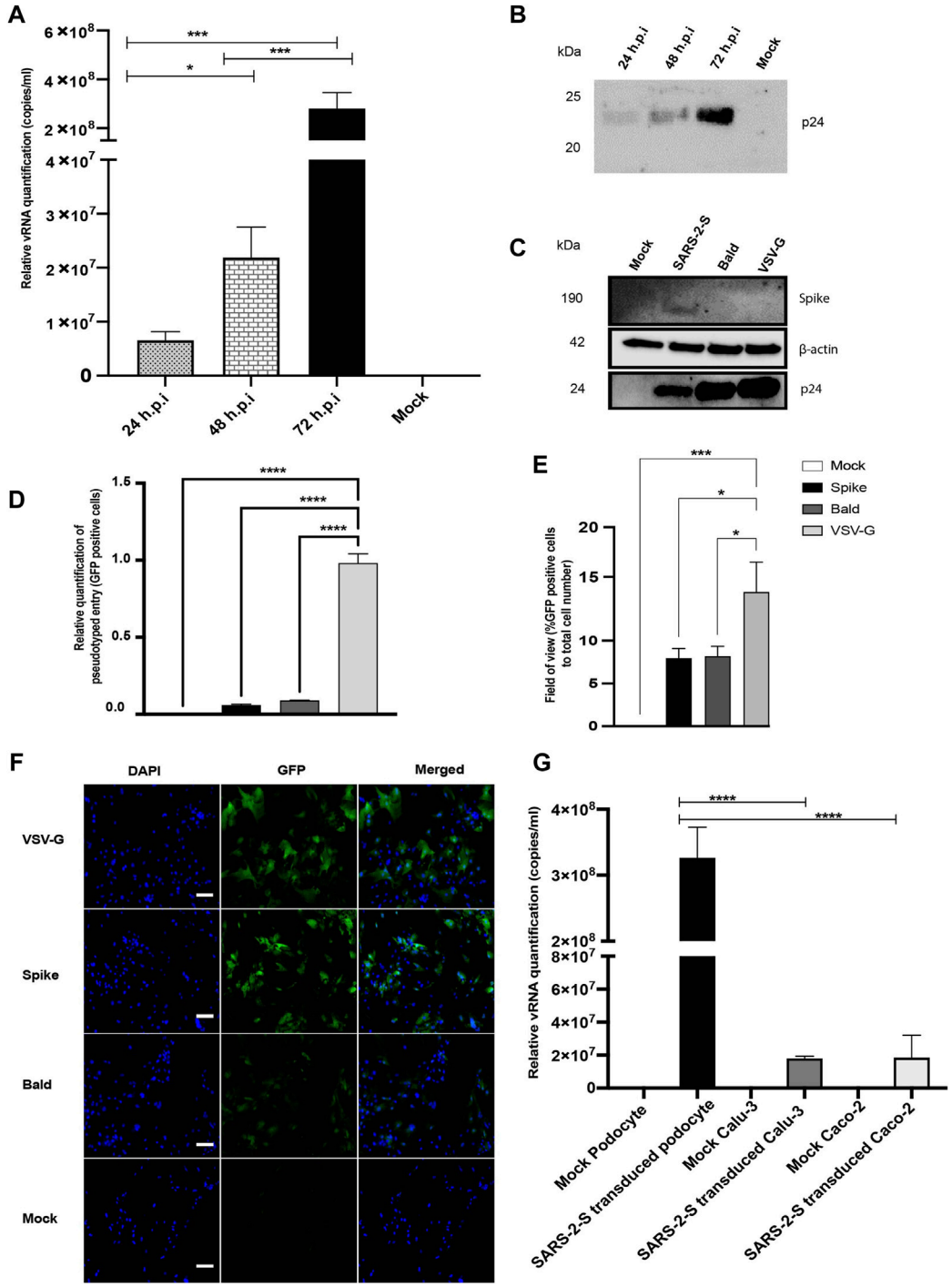

FIGURE 2 | SARS-CoV-2 S-pseudovirus infection of human iPS cell-derived podocytes**. (A)** qRT-PCR analysis using Lenti-X titration kit revealed time-dependent increase in the copies of viral RNA in human iPS cell-derived podocytes infected with the S-pseudovirus. **(B)** Western blot confirmed time-dependent increase of S-pseudovirus particles in human iPS cell-derived podocytes, where p24 (GAG) is a marker for the pseudoviral capsid protein. **(C)** Western blot from cell lysates of mock and infected (S-, Bald and VSV-G pseudotyped) podocytes confirming the presence of SARS-CoV-2 spike proteins in S-pseudotyped infected podocytes, HIV viral protein p24 visible in all pseudotyped infected cells but not in mock and β-actin used as loading control present in all cell lysates **(D)** qRT-PCR data measuring the levels of EGFP using GFP specific primers **(E)** Percentage of EGFP positive cells compared to total cell number **(F)** Immunofluorescent staining showing DAPI, EGFP and merged in pseudotyped infected cells and mock. Scale bar: 100 μm. **(G)** qRT-PCR results showing significantly higher number of S-pseudotyped copies in human iPS cell-derived podocytes compared to Calu-3 and Caco-2 cell lines, 72 h post infection (h.p.i.). The statistical test was done by One-way ANOVA with Sidak's multiple comparison test. Error bars indicate standard deviation of the mean. Only p values of 0.05 or lower were considered statistically significant ($p > 0.05$ [ns, not significant], $p < 0.05$ [*], $p < 0.01$ [**], $p < 0.001$ [***], $p < 0.0001$ [****]).

the results of relative viral RNA quantification shown in **Figure 2A**. Furthermore, Western blot analysis of protein lysates generated from uninfected (mock) podocytes, or podocytes infected with S-pseudotyped, bald pseudotyped and VSV-G pseudotyped virus for 72 h revealed bands that correspond to the spike protein only in the lysate from podocytes infected with the S-pseudotyped virus. β-actin (used as loading control) was present in all cell lysates while the band for p24 was observed only in the lysates from the pseudotyped virus infected cells (**Figure 2C**).

We quantified GFP transcript levels from pseudovirus infected and uninfected cells using qRT-PCR (**Figure 2D**). When compared to levels of viral uptake (corresponding to the GFP mRNA levels) in VSV-G pseudotyped infected cells, there was a significantly lower uptake in cells infected with S-pseudotyped virus, which is expected since entry of VSV-G typed virus does not require specialized receptors as S-pseudotyped viruses do. GFP-positive cells were imaged by fluorescence microscopy and quantified relative to the total cell counts (**Figures 2E,F**).

To examine how the levels of viral uptake in the podocytes compare to other organ-specific cell types, we examined pseudoviral uptake in Calu-3 and Caco-2 cells. Intriguingly, there was significantly more viral uptake in the podocytes than Calu-3 and Caco-2 cells (p-value < 0.0001 for both) (**Figure 2G**).

Live SARS-CoV-2 Virus Infects and Replicates in Human iPS Cell-Derived Podocytes

To explore the susceptibility of human iPS cell-derived podocytes to live SARS-CoV-2, podocytes were incubated with SARS-CoV-2 strain USA-WA1/2020 at MOI of 0.01, 0.1 or 1.0 for 1 h. All steps with live virus were strictly performed in Duke's BSL3 facility following the guidelines provided by Duke University's Biosafety committee and the CDC. The range of MOIs chosen was based on previously established models of infection kinetics (Goswami et al., 2021). After 1 h incubation, cells were washed with PBS and then incubated with fresh culture medium for 24, 48 and 72 h (**Supplementary Figure S1A**). At 24-, 48- and 72-h post-infection, total RNA was extracted from both the cell pellets and the supernatant to evaluate both intracellular and extracellular viral RNA (vRNA) levels.

We quantified the intracellular and extracellular vRNA copies at 24, 48 and 72 h.p.i. by qRT-PCR using primers specific for SARS-CoV-2 spike and nucleocapsid genes. Analysis of cell pellets collected at 24 and 48 h.p.i demonstrated high levels of viral RNA transcripts in cells infected with MOI of 1.0 (**Figures 3A,B**). At 72 h.p.i., higher levels of viral RNA transcripts were detected in the cells infected with MOI of 0.01 (**Figure 3C**). At 72 h.p.i, lower levels of viral RNA were detected in the intracellular fractions from the higher MOI of 0.1 and 1.0 conditions likey due to increased cellular toxicity, leading to a decrease in the number of healthy cells available for additional rounds of viral propagation. These results indicate increased susceptibility of podocytes to primary infection with SARS-CoV-2 even at MOI as low as 0.01. Quantification of the levels of spike and nucleocapsid in cell supernatants revealed an inverse trend (for 72 h.p.i) whereby significantly higher amounts of vRNA was detected in supernatants from cells infected with a MOI of 1.0 than in the cells infected with a MOI of 0.1 or 0.01 at 24, 48 and 72 h.p.i. (**Supplementary Figures S1B–D**).

We next performed plaque assays to measure the amount of infectious SARS-CoV-2 particles released from infected podocytes (**Supplementary Figures S1E–G**, respectively). Ten-fold dilutions of each cell supernatant were assessed in duplicates as previously described (Goswami et al., 2021). The number of plaque forming units (PFU) was significantly higher in the cells infected with MOI of 0.1 at 72 h.p.i compared to 24 and 48 h.p.i. (**Figure 3D**). However, a lower number of PFU was observed in cells infected with MOI of 1.0 compared to cells infected with MOI of 0.1 at 72h.p.i. (**Supplementary Figure S1G**). These data suggest that the higher vRNA levels observed in **Supplementary Figures S1B–D** accounts for vRNA released from dying cells that is not incorporated in new infectious particles. Taken together, these results confirm that podocytes are highly permissible host to SARS-CoV-2 infection and replication.

In probing cell viability after SARS-CoV-2 infection, we observed significantly (p-value < 0.0001) more cell death in the infected wells compared to controls (**Supplementary Figure S2A**). We then quantified the mRNA levels of apoptotic genes as well as necroptotic genes to examine whether SARS-CoV-2 can trigger both apoptosis and necroptosis (a form of cell death mediating secretion of inflammatory cytokines) (Pasparakis and Vandenabeele, 2015) in the infected podocytes. It was previously shown that SARS-CoV-2 can trigger apoptosis in Calu-3 cells through caspase-8 activation and that the process was dependent on viral replication (Shufen Li et al., 2020). We observed a significant increase in Caspase 8 mRNA (p-value < 0.005) at MOI of 0.01, but not caspase 7, suggesting that the activation of cellular apoptosis is dependent on viral replication (**Supplementary Figure S2B**). To determine whether SARS-CoV-2 infected podocytes undergo necroptosis, we assessed mRNA expression of the mixed lineage kinase domain-like (MLKL) and the receptor-interacting protein kinase-3 (RIPK3), two effectors of necroptosis. There was a significant upregulation of MLKL (p-value < 0.0001) and RIPK3 (p-value < 0.0014) in the MOI of 0.01 infected cells (**Supplementary Figure S2B**), where higher levels of intracellular vRNA were detected (**Figure 3C**). These results are consistent with a prior report using Calu-3 cells, where activation of necroptosis pathway was shown to be dependent on viral replication (Shufen Li et al., 2020). Conversely, no upregulation of MLKL or RIPK3 mRNA was observed in podocytes infected with either 0.1 or 1.0 MOI of SARS-CoV-2, (**Supplementary Figure S2B**), presumably due to the lower levels of viral replication in those conditions (**Figure 3C**). These data suggest that SARS-CoV-2 infection activates necroptosis and apoptosis pathways in podocytes.

SARS-CoV-2 Infection Alters Podocyte-Specific Gene Expression

Changes in the expression levels of podocyte-specific genes and proteins often correlate with the onset and progression of podocytopathies (Langham et al., 2002; Sung et al., 2006b; Niranjan et al., 2008). Additionally, defects in podocyte

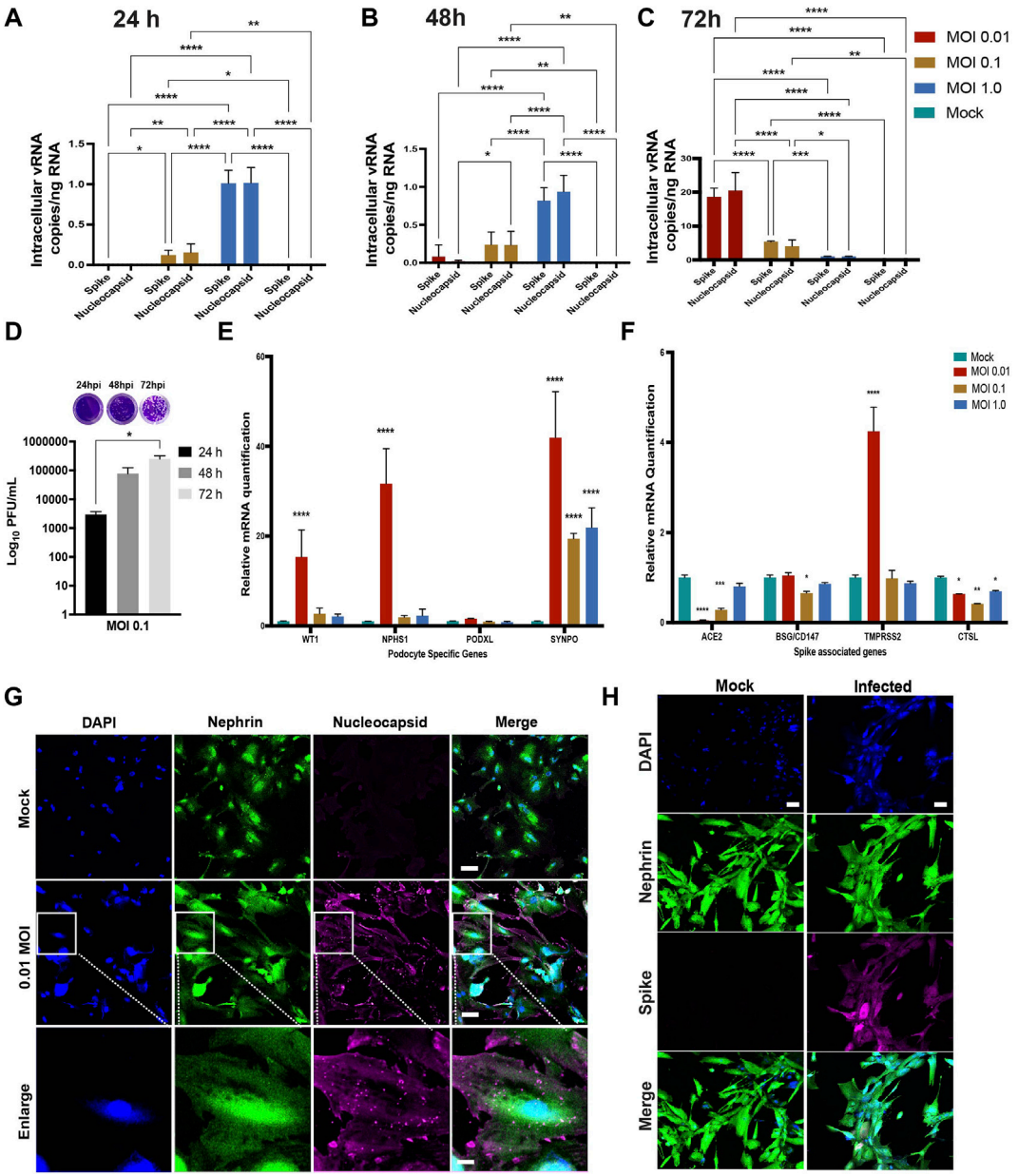

FIGURE 3 | Susceptibility of human iPS cell-derived podocytes to infection by live SARS-CoV-2. qPCR analysis of human iPS cell-derived podocytes infected with SARS-CoV-2 revealed intracellular uptake of the virus for 24 h.p.i **(A)**, 48 h.p.i **(B)** and 72 h.p.i **(C)**. **(D)** plaque assay quantification from supernatant obtained from infected podocytes at 24, 48 and 72 h.p.i. **(E)** qPCR analysis of podocyte-specific genes revealed that both synaptopodin (SYNPO) and podocalyxin (PODXL) are significantly upregulated after infection with SARS-CoV-2 at MOI of 0.01, whereas SYNPO is significantly upregulated at multiple MOIs, and PODXL shows no significant changes with viral infection. **(F)** The expression of spike-associated genes (ACE2, BSG/CD147) and spike processing genes (TMPRSS2, CTSL) are significantly impacted by infection at MOIs of 0.01 and 0.1, respectively. **(G)** Human iPS cell-derived podocytes treated with SARS-CoV-2 (at MOI of 0.01) immunostain positive for Nucleocapsid protein (magenta), indicating successful infection with the virus. The cells were immunostained also for the podocyte marker Nephrin (green) and counterstained with DAPI (blue). Scale bar: 100 μm **(H)** Spike positive cells Nephrin and DAPI as nuclear counterstain in the infected podocytes. Scale bar: 100 μm. One-way analysis of variance (ANOVA) with Sidak's multiple comparison test was used to determine statistical significance. Only p values of 0.05 or lower were considered statistically significant ($p > 0.05$ [ns, not significant], $p < 0.05$ [*], $p < 0.01$ [**], $p < 0.001$ [***], $p < 0.0001$ [****]). Error bars indicate standard deviation of the mean.

structure and function leads to their detachment from the glomerular basement membrane and subsequent loss of the cells into urine, and the onset of glomerulopathies (Kim et al., 2001; Wharram et al., 2005; Matovinović, 2009).

Quantification of podocyte lineage identification genes (WT1, NPHS1, PODXL and SYNPO) after SARS-CoV-2 viral infection at MOI of 0.01 revealed significant increase in WT1, NPHS1 and SYNPO and a moderate increase in PODXL expression levels

(**Figure 3E**). The increased expression of NPHS1 may result from compensatory mechanism to help maintain podocyte physiology post-infection and minimize destabilization of their cellular phenotype as previously reported in a diabetic model of podocyte injury (Sung et al., 2006a). The increase in nephrin gene expression also correlates to the presence of more foot-like processes in the podocytes infected with SARS-CoV-2 at an MOI of 0.01 (**Supplementary Figure S2C**). However, at MOI of 1.0, we observed changes reminiscent of foot process retraction with a concomitant reduction in nephrin mRNA expression (**Figure 3E**; **Supplementary Figure S2C**) indicating a possible maladaptive response with increased viral infection burden. These results indicate that SARS-CoV-2 infection of human iPS cell-derived podocytes leads to dynamic changes in the expression of podocyte-specific genes. Together, our results suggest that infection of podocytes by SARS-CoV-2 results in disrupted molecular profile as well as structural changes which can lead to cell detachment and death (**Supplementary Figure S2A**).

We also quantified the relative expression of BSG/CD147, ACE2 (given its involvement in SARS-CoV-2 binding and infection of many cell types) (Hoffmann et al., 2020; Shang et al., 2020a; Yanwei Li et al., 2020; Shang et al., 2020b), as well as cell surface protease TMPRSS2 (Wysocki et al., 2021) and endosomal Cathepsin L (CTSL) in podocytes infected with SARS-CoV-2 for 72 h using different MOIs (**Figure 3F**). We observed that infection at MOI of 0.01 and 0.1 lead to significant reduction in ACE2 expression when compared to uninfected podocytes. Compared to the mock condition, the expression levels of BSG/CD147 remained unchanged for MOI of 0.01 and 1.0, but decreased significantly when the podocytes were infected at an MOI of 0.1. Additionally, TMPRSS2 expression was significantly increased with SARS-CoV-2 infection at MOI of 0.01 but remained relatively similar to the mock condition when the cells were infected at MOI of 0.1 and 1.0. CTSL expression was significantly reduced in all three MOIs. It has been previously shown that COVID-19 infection associates with decreased ACE2 expression due to the internalization of the virus-receptor complex (Gheblawi et al., 2020). Our results show that at MOI of 0.01, expression of ACE2 decreases but that of TMPRSS2 increases, suggesting enhanced enzymatic activity necessary to cleave Spike for processing. These results also show that the low MOI of 0.01 is sufficient for the infection of human iPS cell-derived podocytes with SARS-CoV-2 and indicate that SARS-CoV-2 infection of the podocytes leads to dynamic changes in the expression of spike-binding factors (**Figure 3F**) as well as podocyte-specific genes (**Figure 3E**).

Immunofluorescence analysis of the SARS-CoV-2 infected human iPS cell-derived podocytes showed positive immunostaining of the nucleocapsid and spike proteins, suggesting the presence of viral proteins within the cytoplasm even at low MOI of 0.01 (**Figures 3G,H**). This result further confirmed our observation that SARS-CoV-2 can establish active infection in human iPS cell-derived podocytes. The infected podocytes also exhibited plaque-like regions (**Supplementary Figure S2D**) and pronounced DAPI staining and spreading indicating more nuclear content in SARS-CoV-2 infected podocytes compared to the mock samples (**Figures 3G,H**; **Supplementary Figure S2E**). Changes in nuclear content of the podocytes correlates with enhanced viral replication (De Wilde et al., 2017), that could have led to the genotypic changes in these cells. We used the JACoP plug-in for ImageJ to set thresholds for colocalization analysis and to derive the Pearson's correlation coefficient (Bolte and Cordelières, 2006). We calculated the Pearson's coefficient between ACE2 and BSG/CD147 in the control podocyte and obtained a value of 0.81. This confirms a strong positive correlation between ACE2 and BSG/CD147. We then checked for the coefficient between SARS-CoV-2 protein Nucleocapsid and BSG/CD147 in the infected sample and obtained a value of 0.698 which indicates a positive relationship between the molecular components. The coefficient for SARS-CoV-2 protein Nucleocapsid and ACE2 in the infected sample was found to be 0.581, indicating a less positive correlation, which could be due to the reduced expression of ACE2 in infected samples as previously reported in an independent study showing that ACE2 expression is altered in disease conditions or during viral infections (Kuba et al., 2005; Glowacka et al., 2010; Gheblawi et al., 2020). Representative images from our calculations of the Pearson's correlation coefficient are shown in **Supplementary Figure S3A** for ACE2 and BSG/CD147, **Supplementary Figure S3B** for Nucleocapsid and BSG/CD147 and **Supplementary Figure S3C** for Nucleocapsid and ACE2.

Human iPS Cell-Derived Podocytes Express Several Spike-Interacting Factors

Previous studies have identified specific host factors that can facilitate entry of SARS-CoV-2 virus into various tissues and cell types (Cantuti-Castelvetri et al., 2020; Vankadari and Wilce, 2020; Wang et al., 2020; Amraei et al., 2021). To examine whether iPS cell-derived podocytes express host factors that can facilitate entry of SARS-CoV-2 virus, we first explored BioGRID (a database of molecular interactions) and identified twenty-four spike-interacting factors involved in SARS-CoV-2 binding and processing (**Supplementary Figure S4A**; **Supplementary Table S3**). We then examined the gene expression levels of the twenty-four spike-interacting factors in human iPS cell-derived podocytes using our previously generated microarray data (**Figure 4A**) (Musah et al., 2018). Intriguingly, the podocytes expressed twenty (out of twenty-four) spike-interacting factors (**Figure 4A**; **Supplementary Table S3**). These results indicate that human iPS cells possess many of the factors involved in SARS-CoV-2 binding and processing, which further supports our data from above showing high SARS-CoV-2 infectivity in the podocytes.

Comparative Analysis of Spike Interacting Factors in Podocytes and Other Cell Lines

ACE2 is expressed in a variety of human tissues and has been shown to function by counter-balancing the renin-angiotensin-aldosterone system (Hikmet et al., 2020; Yanwei Li et al., 2020). We quantified the basal mRNA expression levels of ACE2, BSG/CD147 and other spike-associated genes in different human cell

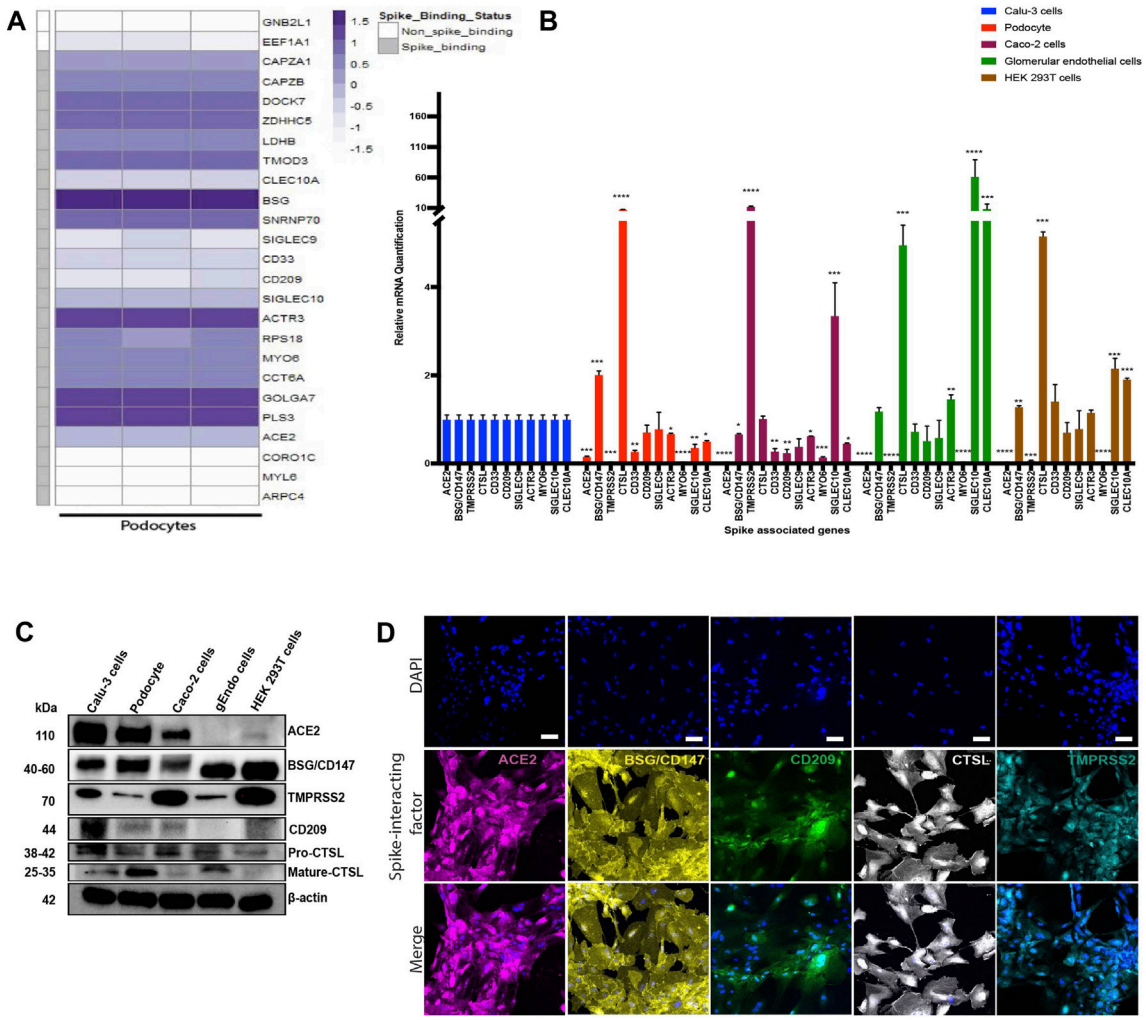

FIGURE 4 | Transcriptomic and protein level analyses of spike-interacting factors in mature podocytes differentiated from human iPS cells. **(A)** Heatmap showing expression levels of spike associated genes from three biological human iPS cell-derived podocyte samples. SIGLEC9, Sialic acid-binding Ig-like lectin 9; CAPZA1, F-actin-capping protein subunit alpha-1; CLEC10A, C-type lectin domain family 10 member A; CD33, Myeloid cell surface antigen CD33; TMOD3, Tropomodulin-3; ACE2, Angiotensin Converting Enzyme 2; BSG/CD147, Basigin/CD147 molecule; CD209, CD209 Antigen; MYO6, Unconventional myosin-VI; PLS3, Plastin-3; LDHB, L-lactate dehydrogenase B chain; GNB2L1/RACK, Receptor of activated protein C kinase 1; SNRNP70, U1 small nuclear ribonucleoprotein 70 kDa; DOCK7, Dedicator of cytokinesis protein 7; RPS18, 40S ribosomal protein S18; CAPZB, F-actin-capping protein subunit beta; GOLGA7, Golgin subfamily A member 7; ZDHHC5, Palmitoyltransferase ZDHHC5; SIGLEC10, Sialic acid-binding Ig-like lectin 10; ACTR3, Actin-related protein 3; MYL6, Myosin light polypeptide 6; CORO1C, Coronin-1C; ARPC4, Actin-related protein 2/3 complex subunit 4; CCT6A, T-complex protein 1 subunit zeta; **(B)** qPCR quantification of nine of the human spike-associated gene from **(A)** including Transmembrane Serine Protease 2 (TMPRSS2) or cathepsin L (CTSL) in human iPS cell-derived podocytes, Calu-3, Caco-2, glomerular endothelial cells, and HEK 293T cells (normalized to Calu-3 groups). **(C)** Western blot analysis to evaluate protein expression of ACE2, BSG/CD147, CD209, TMPRSS2 and CTSL in the different cell type used; Calu-3, human iPS cell-derived podocytes, Caco-2, glomerular endothelial (gEndos) cells, and HEK 293T cells. **(D)** Immunocytochemistry analysis of ACE2, BSG/CD147, CD209, TMPRSS2 and CTSL expression in iPS cell-derived podocytes. Scale bar: 100 μm. One-way analysis of variance (ANOVA) with Sidak's multiple comparison test was used to determine statistical significance. Only p values of 0.05 or lower were considered statistically significant ($p > 0.05$ [ns, not significant], $p < 0.05$ [*], $p < 0.01$ [**], $p < 0.001$ [***], $p < 0.0001$ [****]). Error bars indicate standard deviation of the mean.

types (**Figure 4B**). The expression of these genes is important for the uptake and cleavage of the spike glycoprotein, fusion of SARS-CoV-2 and cell membranes, and subsequent release of viral genome into the cytoplasm of an infected cell (Millet and Whittaker, 2015).

Studies have shown that some cells with little to no ACE2 expression can still be infected with SARS-CoV-2 (Hikmet et al., 2020; Singh et al., 2020), suggesting that other class of receptors might facilitate viral infection in ACE2-deficient cell types. Additionally, it has been shown that the expression levels of viral uptake receptors can vary significantly between different cell types (Cantuti-Castelvetri et al., 2020; Wang et al., 2020). These findings suggest that ACE2 may not be the only receptor for SARS-CoV-2 in some cells, and that there could be multiple mechanisms for viral infection and processing. We examined expression levels of several of the factors in multiple cell types

(podocytes, Calu-3, Caco-2, glomerular endothelium, and HEK 293T) to help understand the levels of tissue or cell-type specificity (**Figure 4B**). We found that there was no ACE2 expression in HEK 293T cells and glomerular endothelial cells and only little expression in Caco-2 cells compared to Calu-3. Intriguingly, ACE2 expression in human iPS cell-derived podocytes is approximately 10 times lower than the expression level in Calu-3 cells and slightly higher than the expression level in Caco-2 cells.

We observed a significantly low expression level of TMPRRS2 in the podocytes compared to Calu-3 cells (**Figure 4B**). A lower level expression of TMPRRS2 was also previously reported for cardiomyocytes derived from human embryonic stem cell (hESC-CMs) and a different endosomal viral processing protease was shown to be much more highly expressed (Marchiano et al., 2021). Our qPCR results showed a significantly higher expression of CTSL in podocytes when compared to Calu-3 cells (**Figure 4B**), suggesting that the mechanism of SARS-CoV-2 entry in podocytes might be different from the TMPRRS2-dependent mechanisms observed in lung epithelial cells (Hoffmann et al., 2020; Shang et al., 2020a).

It is likely that SARS-CoV-2 infection of podocytes relies on ACE2, BSG/CD147 and other genes that might direct membrane fusion and/or entry through the endo-lysosomal pathway. Together, these results show that human iPS cell-derived podocytes express proteins that make them susceptible to SARS-CoV-2 infection, like human iPS cell derived cardiomyocytes (Sharma et al., 2020; Marchiano et al., 2021). The expression of CD209, which is recognized as an alternative receptor for lung and kidney epithelial and endothelial cells (Amraei et al., 2021), was comparable between Calu-3 cells, human iPS cell-derived podocytes, glomerular endothelial cells and HEK 293T cells but significantly lower in Caco-2 cells (**Figure 4B**). The mRNA expression of the other genes, SIGLEC9, ACTR3, MYO6, SIGLEC10 and CLEC10A, varied between the different cell types (**Figure 4B**). We then validated the relative protein level expression of three uptake (ACE2, BSG/CD147, CD209) and two processing (TMPRSS2, and CTSL) factors in podocytes and other cell types (Calu-3, Caco-2, glomerular endothelia and 293T cells). Western blot analysis confirmed higher expression of ACE2 protein in Calu-3 and then podocytes, and little to no expression in glomerular endothelial cells (gEndos) (**Figure 4C**). This result also demonstrated that podocytes express more ACE2 than Caco-2 cells, consistent with the gene expression data in **Figure 4B**. Additionally, the Western blot data for BSG/CD147 corroborated the mRNA data showing higher expression in podocytes than Calu-3 and Caco-2. **Figure 4C** also shows the expression of CD209 in podocytes and the other cell types. We observed relatively low gene and protein level expression of TMPRSS2 in podocytes when compared to the other cell types. Although mature CTSL protein is present in podocytes, Calu-3 and glomerular endothelia cells, pro-CTSL is present in all the cell types which may explain the presence of the CTSL mRNA in all the cell types even when they do not express mature CTSL protein. It has been suggested that SARS-CoV-2 entry into host cells depends on the presence of cholesterol-rich lipid rafts, which facilitates membrane fusion through proteases such as TMPRSS2 or endosomal pathway using Cathepsin B&L (Palacios-Rápalo et al., 2021). Our results suggests low levels of TMPRSS2 expression in podocyte, and we speculate that the use of BSG/CD147 as a receptor and CTSL as a processing enzyme for viral entry mediated by S protein might be a preferred mechanism for the podocytes. Finally, expression of all these proteins was also validated using immunocytochemistry in podocytes (**Figure 4D**), Calu-3 (**Supplementary Figure S4B**), Caco-2 (**Supplementary Figure S4C**), glomerular endothelial (S**upplementary Figure S4D**) and 293T (**Supplementary Figure S4E**) cells. These findings strongly indicate that human kidney podocytes employ multiple spike-binding receptors (in addition to ACE2) for SARS-CoV-2 viral uptake.

Receptor Antibodies can Reduce SARS-CoV-2 Pseudovirus Entry Into Human iPS Cell-Derived Podocytes

Based on the hypothesis that SARS-CoV-2 could exploit both ACE2 and BSG/CD147 receptors for viral uptake in human iPS cell-derived podocytes, we investigated whether antibodies against these two spike receptors can block the entry of S-pseudotyped virus in the cells. We used anti-hACE2 and anti-CD147 (anti-BSG) antibodies at varying concentrations to block ACE2 and BSG/CD147 receptors from interacting with pseudoviral particles.

When the podocytes were blocked with ACE2 or BSG/CD147 antibody at varying concentrations (from 0.1 to 5 μg/ml), we observed a concentration-dependent and statistically significant decrease in viral uptake (**Figure 5A**). The highest concentration of the antibody (5 μg/ml) was most effective for blocking the receptors while significantly (p-value < 0.0001) reducing cellular uptake of the virus (**Figure 5A**). These results confirm that ACE2 and BSG/CD147 facilitate S-pseudotyped viral update in podocytes. The observed high expression of BSG/CD147 receptor in podocytes revealed by microarray (**Figure 4A**), qPCR data (**Figure 4B**), Western blotting (**Figure 4C**) and immunocytochemistry (**Figure 4D**) further suggest that these receptors interact with the spike protein of SARS-CoV-2 and facilitate its uptake and entry into the cells. As a result, blocking with anti-BSG/CD147 significantly decreased viral uptake similar to that observed with ACE2 blocking.

To examine if blocking with both anti-ACE2 and anti-BSG had a synergistic effect, the podocytes were simultaneously pretreated with both the antibodies and then infected with the virus. We observed similar trend where the lowest viral uptake was at 5 μg/ml (**Figure 5A**). This result suggests that both ACE2 and BSG/CD147 are involved in SARS-CoV-2 internalization in human iPS cell-derived podocytes.

Next, we examined whether the expression of the key viral entry genes, ACE2, BSG/CD147, TMPRSS2 and CTSL are altered during antibody blocking. Exposure of podocytes to the pseudoviral particles after blocking with 5 μg/ml anti-ACE2 antibodies showed significant downregulation of BSG/CD147 and TMPRSS2 transcripts, but upregulation of CTSL

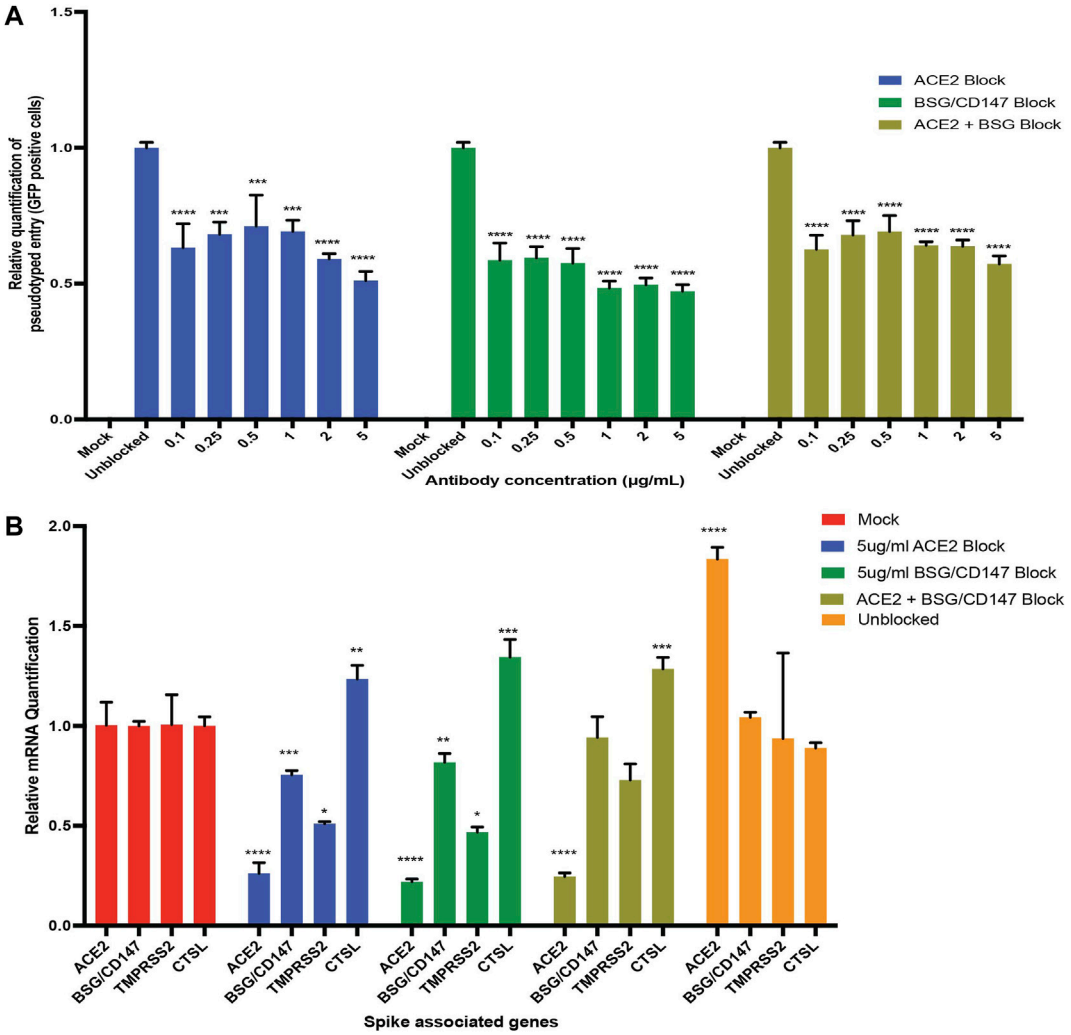

FIGURE 5 | Antibody blocking reveal roles of ACE2 and BSG/CD147 receptors in viral uptake. **(A)** qPCR quantification of S-pseudotyped entry relative to antibody concentration (normalized to unblocked samples). Human iPS cell-derived podocytes were incubated with different dilutions of anti-ACE2, anti-BSG or both for an hour followed by infection with S-pseudotyped virus at MOI 0.02 for 60 h **(B)** qPCR quantification of Spike binding receptor genes (ACE2, BSG/CD147) and Spike processing factor genes (TMPRSS2, CTSL) at 5 µg/ml for both anti-ACE2 antibody blockage and anti-BSG antibody blockage showing significant changes in gene expression with optimal receptor blockage when compared to unblocked samples (normalized to mock groups). One-way analysis of variance (ANOVA) with Sidak's multiple comparison test was used to determine statistical significance. Only p values of 0.05 or lower were considered statistically significant ($p > 0.05$ [ns, not significant], $p < 0.05$ [*], $p < 0.01$ [**], $p < 0.001$ [***], $p < 0.0001$ [****]). Error bars indicate standard deviation of the mean.

compared to unblocked cells (**Figure 5B**). Similarly, exposure of podocytes to the pseudoviral particles after blocking with 5 µg/ml anti-CD147 antibodies showed significant downregulation of ACE2 and TMPRSS2 transcripts, but upregulation of CTSL compared to the unblocked cells. The successful blocking of ACE2 or CD147 anti-ACE2 or anti-CD147 (anti-BSG) antibodies respectively was as expected and is also shown in **Figure 5B**. However, when podocytes were exposed to 5 µg/ml of both anti-ACE2 and anti-CD147 (anti-BSG) antibodies, the level of ACE2 decreased as expected, but the level of BSG/CD147 unexpectedly remained high and was comparable to the unblocked cells (**Figure 5B**). The level of CTSL was higher than the unblocked cells when they were simultaneousy exposed to both antibodies.

These findings supports recent report that abundance of ACE2 correlates with with the levels of BSG/CD147 and that the two receptors are being co-regulated (Fenizia et al., 2021). Since viral entry was not fully inhibited when both receptors were blocked, it is possible that other types of receptors facilitate SARS-COV-2 viral entry in podocytes when ACE2 and BSG/CD147 are blocked.

DISCUSSION

The global pandemic caused by SARS-CoV-2 has resulted in the loss of millions of lives and caused devastating social and economic burdens. The disease mostly presents as a

respiratory illness, similar to viral pneumonia, and in more severe cases as acute respiratory distress syndrome (ARDS) (De Wilde et al., 2017; Gupta et al., 2020; Simoneau and Ott, 2020). In addition, several COVID-19 patients simultaneously experience renal, cardiac, neurological, digestive, and/or pancreatic complications (Gupta et al., 2020; Singh et al., 2020). Although the onset of acute kidney injury and collapsing glomerulopathy (Velez et al., 2020) have been clinically associated with the severe form of COVID-19 (Braun et al., 2020), it remains unknown how the kidneys are specifically targeted by the virus, and whether podocytes—the specialized epithelial cells that help form the blood filtration barrier in the kidneys—can be directly infected by the virus.

To address some of these important questions, we have shown in this paper that human iPS cell-derived podocytes are highly susceptible to SARS-CoV-2 infection. Initial viral infection of cells at low MOIs (<1.0) allows additional rounds of virus replication in in a 2D culture, as the replicating virus can enter adjacent cells that were not infected during primary infection. Indeed, we observed higher levels of intracellular vRNA and higher number of PFU at 72 h.p.i. in cells infected with MOI of 0.01 of SARS-CoV-2 compared to MOI of 1.0. These results are relevant and consistent with a recent report showing that SARS-CoV-2 isolated from COVID-19 autopsied kidney could extensively infect kidney tubular cells *in vitro* and lead to extensive viral replication that produced 1000-fold increase in the amount of viral RNA, confirming the presence of infectious virus in the kidneys (Braun et al., 2020).

Due to the lower ACE2 mRNA expression in podocytes when compared to Calu-3, we evaluated the extent of viral infections using various MOIs from 0.01 to 1.0, as it was initially unknown if human iPS cell-derived podocytes would be permissive to direct infection with SARS-CoV-2. Typically, high MOIs (e.g., 1.0 or more) are required if the cell type is minimally permissive to viral infection (Simoneau and Ott, 2020) as observed for some organoid models (Huang et al., 2020; Monteil et al., 2020) within which cell-type-specific responses could not be fully evaluated due to high levels of heterogeneity (Bar-Ephraim et al., 2020). We show, however, that specialized podocytes derived from human iPS cells can be directly infected with SARS-CoV-2 at low MOIs of 0.01–1.0 (**Figures 3A–C**). The level of the cellular uptake of viral particles can be quantified using multiple assays including immunofluorescence microscopy (for the structural protein N or S, or against dsRNA intermediate), by quantitative RT-PCR of vRNA and plaque assay to quantify infection in the supernatant (Simoneau and Ott, 2020). Indeed, we confirmed viral uptake by the human iPS cell-derived podocytes using qRT-PCR at 24, 48 and 72 h.p.i. (**Figures 3A–C**), plaque assay (**Figure 3D**) and immunofluorescence microscopy analysis with both anti-N and -S antibodies (**Figures 3F,G**). In addition, our investigation of how infection alters the expression of the spike-associated genes revealed a significant reduction in ACE2 expression when compared to uninfected samples (**Figure 4B**). This is in line with down regulation of ACE2 expression upon SARS-CoV spike protein binding which promotes lung injury (Glowacka et al., 2010) as well as reduction in ACE2 expression due to SARS-CoV replication in Vero cells (Kuba et al., 2005).

Our results also revealed that human iPS cell-derived podocytes express lower levels of ACE2 (Mizuiri and Ohashi, 2015) and TMPRSS2 when compared to Calu-3 (**Figures 4B,C**). Since SARS-CoV-2 -host interaction is vital for viral pathogenesis, ultimately determining the outcome of infection (De Wilde et al., 2017), and the functional activity of the virus depends on the proteolytic processing during cell entry (Simmons et al., 2005; Kang et al., 2020), we next sought to identify other factors that could mediate viral entry in iPS cell-derived podocytes. We utilized BioGRID analysis to gain insight into SARS-CoV-2—host interactions by mapping out spike-binding proteins expressed in podocytes. Viral processing factors have been shown to be co-expressed with the type of spike binding receptor used by a given cell (Muus et al., 2020; Marchiano et al., 2021; Wysocki et al., 2021). In this study, we identified BSG/CD147 as a mediator of SARS-CoV-2 entry into podocytes along with ACE2 (**Figure 5A**). Our results add to the repertoire of cells that employ BSG/CD147 as a receptor for viral entry as recently reported for Calu-3 cells (Fenizia et al., 2021). Thus, our results indicate that SARS-CoV-2 employs multiple receptors and viral processing mechanisms to directly infect human iPS cell-derived podocytes.

The importance of employing cell models with mature phenotypes, which has historically been difficult for organoids and other iPS derived cell models, cannot be over-emphasized. For example iPS cell-derived renal organoids generate glomeruli with transcriptomic signatures similar to fetal stages (Homan et al., 2019) which poses a question as to whether human iPS cell-derived cells can recapitulate the biology of SARS-CoV-2 infection in adults since vertical infection of the fetus is still unclear (Lamouroux et al., 2020) but remains a possibility (Chen et al., 2020; Muus et al., 2020). Furthermore, this points to the tissue-specific viral tropisms that may determine whether a productive infection is established in any given tissue. Therefore, it is important to understand these non-canonical SARS-CoV-2 entry-mediating proteins (i.e., other than ACE2 and TMPRSS2) so that we can establish effective methods to block viral replication in those tissues in which ACE2/TMPRSS are poorly expressed or not employed for viral infection.

Aside from being a receptor for SARS-CoV-2, ACE2 plays important role in different tissues in controlling blood pressure (Wysocki et al., 2010; Wang et al., 2020; Wysocki et al., 2021) or preventing heart failure and kidney injury (Wong et al., 2007; Batlle et al., 2012; Mizuiri and Ohashi, 2015). As such, development of drugs to block ACE2 might have a negative effect on its other protective functions. BSG/CD147 has been implicated in tumor metastasis, inflammation and viral infection (Pushkarsky et al., 2001; Chen et al., 2005; Douglas et al., 2014; Zhang et al., 2018) and also previously shown to facilitate SARS-CoV invasion in host cells (Chen et al., 2005; Wang et al., 2020). Our results shows that antibody blocking of BSG/CD147 receptors significantly reduces SARS-CoV-2 viral uptake in human iPS cell-derived podocytes. Thus, BSG/CD147 could potentially be a useful target for antiviral therapeutics including those aimed to address SARS-CoV-2 infections and

COVID-19 disease. On the other hand, BSG/CD147, which belongs to the Ig superfamily is expressed in several tissues like the brain, heart, liver, kidney etc and might play a complex role in COVID-19 and possibly contribute to the worse prognosis of patients with other co-morbidities (Radzikowska et al., 2020; Fenizia et al., 2021). Given the high coregulation between ACE2 and BSG/CD147, it might be beneficial to explore additional cell-entry mechanisms to inform future therapeutic strategies for the prevention and treatment of SARS-CoV-2 infection in human tissues and organs.

DATA AVAILABILITY STATEMENT

The original contributions presented in the study are included in the article/**Supplementary Material**, further inquiries can be directed to the corresponding author.

AUTHOR CONTRIBUTIONS

TK and SM conceived the strategy for this study, designed the experiments, interpreted the results, and wrote the manuscript. TK performed the experiments with assistance from co-authors. TK and RB differentiated podocytes from human iPS cells; TK and MB designed BSL3-level experiments for SARS-CoV-2 viral infection of cells, MB performed the infection experiments, and TK and MB analyzed the data; TT performed viral RNA isolation from podocytes infected with live virus; RB created the schematic illustrations. XM, helped with confocal microscopy; MAB. and TK analysed microscopy data. AO performed the BioGRID analysis and generated heatmaps from microarray data previously generated by SM; All authors contributed to data analyses, figure preparations, discussion of results and the writing and editing of the manuscript.

FUNDING

SM is a recipient of the Whitehead Scholarship in Biomedical Research, a Chair's Research Award from the Department of Medicine at Duke University, a MEDx Pilot Grant on Biomechanics in Injury or injury repair, a Burroughs Wellcome Fund PDEP Career Transition Ad Hoc Award, a Duke Incubation Fund from the Duke Innovation & Entrepreneurship Initiative, a Genentech Research Award, and a George M. O'Brien Kidney Center Pilot Grant (P30 DK081943). RB is a recipient of the Lew's Predoctoral Fellowship in the Center for Biomolecular and Tissue Engineering (CBTE) at Duke University (T32 Support NIH Grant T32GM800555); MAB is a recipient of an NSF graduate research fellowship; and XM is a recipient of the graduate research fellowship from the International Foundation for Ethical Research, Inc. MB is supported by National Institute of Diabetes and Digestive and Kidney Diseases grant number R01DK130381. This study received funding from the International Foundation for Ethical Research, Inc. The funder was not involved in the study design, collection, analysis, interpretation of data, the writing of this article or the decision to submit it for publication.

ACKNOWLEDGMENTS

The authors thank all the members of Musah Lab at Duke University for comments on the manuscript, and Dr. X. Campilongo for helpful comments on the manuscript. Confocal microscopy was performed at the Duke Light Microscopy Core facility (Durham, NC). The following reagent was deposited by the Centers for Disease Control and Prevention and obtained through BEI Resources, NIAID, NIH: SARS-Related Coronavirus 2, Isolate USA-WA1/2020, NR-52281, and was provided by MB. Work with live SARS-CoV-2 isolate (USA-WA1/2020; BEI Resources NR-52281) was performed under Biosafety Level-3 (BSL3) in the Duke Regional Biocontainment Laboratory (RBL), which received partial support for construction from the National Institutes of Health, National Institute of Allergy and Infectious Diseases (UC6-AI058607, G20-AI167200).

SUPPLEMENTARY MATERIAL

The Supplementary Material for this article can be found online at: https://www.frontiersin.org/articles/10.3389/fcell.2022.855340/full#supplementary-material

REFERENCES

Akilesh, S., Nast, C. C., Yamashita, M., Henriksen, K., Charu, V., Troxell, M. L., et al. (2021). Multicenter Clinicopathologic Correlation of Kidney Biopsies Performed in COVID-19 Patients Presenting with Acute Kidney Injury or Proteinuria. *Am. J. Kidney Dis.* 77 (1), 82–93.e1. doi:10.1053/j.ajkd.2020.10.001

Amraei, R., Yin, W., Napoleon, M. A., Suder, E. L., Berrigan, J., Zhao, Q., et al. (2021). CD209L/L-SIGN and CD209/DC-SIGN Act as Receptors for SARS-CoV-2. *ACS Cent. Sci.* 7 (7), 1156–1165. doi:10.1021/acscentsci.0c01537

Ball, M. P., Thakuria, J. V., Zaranek, A. W., Clegg, T., Rosenbaum, A. M., Wu, X., et al. (2012). A Public Resource Facilitating Clinical Use of Genomes. *Proc. Natl. Acad. Sci. U.S.A.* 109 (30), 11920–11927. doi:10.1073/pnas.1201904109

Bar-Ephraim, Y. E., Kretzschmar, K., and Clevers, H. (2020). Organoids in Immunological Research. *Nat. Rev. Immunol.* 20 (5), 279–293. doi:10.1038/s41577-019-0248-y

Batlle, D., Wysocki, J., Soler, M. J., and Ranganath, K. (2012). Angiotensin-converting Enzyme 2: Enhancing the Degradation of Angiotensin II as a Potential Therapy for Diabetic Nephropathy. *Kidney Int.* 81 (6), 520–528. doi:10.1038/ki.2011.381

Bhattacharya, R., Bonner, M. G., and Musah, S. (2021). Harnessing Developmental Plasticity to Pattern Kidney Organoids. *Cell stem cell* 28 (4), 587–589. doi:10.1016/j.stem.2021.03.009

Bolte, S., and Cordelières, F. P. (2006). A Guided Tour into Subcellular Colocalization Analysis in Light Microscopy. *J. Microsc.* 224 (3), 213–232. doi:10.1111/j.1365-2818.2006.01706.x

Braun, F., Lütgehetmann, M., Pfefferle, S., Wong, M. N., Carsten, A., Lindenmeyer, M. T., et al. (2020). SARS-CoV-2 Renal Tropism Associates with Acute Kidney Injury. *Lancet* 396 (10251), 597–598. doi:10.1016/S0140-6736(20)31759-1

Burt, M., Bhattachaya, R., Okafor, A. E., and Musah, S. (2020). Guided Differentiation of Mature Kidney Podocytes from Human Induced Pluripotent Stem Cells under Chemically Defined Conditions. *J. Vis. Exp.* (161), e61299. doi:10.3791/61299

Cantuti-Castelvetri, L., Ojha, R., Pedro, L. D., Djannatian, M., Franz, J., Kuivanen, S., et al. (2020). Neuropilin-1 Facilitates SARS-CoV-2 Cell Entry and Infectivity. *Science* 370(6518), 856–860. doi:10.1126/science.abd2985

Carvalho, B. S., and Irizarry, R. A. (2010). A Framework for Oligonucleotide Microarray Preprocessing. *Bioinformatics* 26 (19), 2363–2367. doi:10.1093/bioinformatics/btq431

Chen, Z., Mi, L., Xu, J., Yu, J., Wang, X., Jiang, J., et al. (2005). Function of HAb18G/CD147 in Invasion of Host Cells by Severe Acute Respiratory Syndrome Coronavirus. *J. Infect. Dis.* 191 (5), 755–760. doi:10.1086/427811

Chen, H., Guo, J., Wang, C., Luo, F., Yu, X., Zhang, W., et al. (2020). Clinical Characteristics and Intrauterine Vertical Transmission Potential of COVID-19 Infection in Nine Pregnant Women: a Retrospective Review of Medical Records. *Lancet* 395 (10226), 809–815. doi:10.1016/s0140-6736(20)30360-3

Cheng, Y., Luo, R., Wang, K., Zhang, M., Wang, Z., Dong, L., et al. (2020). Kidney Disease Is Associated with In-Hospital Death of Patients with COVID-19. *Kidney Int.* 97 (5), 829–838. doi:10.1016/j.kint.2020.03.005

De Wilde, A. H., Snijder, E. J., Kikkert, M., and van Hemert, M. J. (2017). Host Factors in Coronavirus Replication. *Curr. Top. Microbiol. Immunol.* 419, 1–42. doi:10.1007/82_2017_25

Deshmukh, V., Motwani, R., Kumar, A., Kumari, C., and Raza, K. (2021). Histopathological Observations in COVID-19: A Systematic Review. *J. Clin. Pathol.* 74 (2), 76–83. doi:10.1136/jclinpath-2020-206995

Diao, B., Wang, C., Wang, R., Feng, Z., Zhang, J., Yang, H., et al. (2021). Human Kidney Is a Target for Novel Severe Acute Respiratory Syndrome Coronavirus 2 Infection. *Nat. Commun.* 12 (1), 2506. doi:10.1038/s41467-021-22781-1

Douglas, A. D., Williams, A. R., Knuepfer, E., Illingworth, J. J., Furze, J. M., Crosnier, C., et al. (2014). Neutralization of Plasmodium Falciparum Merozoites by Antibodies against PfRH5. *J. Immunol.* 192 (1), 245–258. doi:10.4049/jimmunol.1302045

Fehr, A. R., and Perlman, S. (2015). Coronaviruses: an Overview of Their Replication and Pathogenesis. *Methods Mol. Biol.* 1282, 1–23. doi:10.1007/978-1-4939-2438-7_1

Fenizia, C., Galbiati, S., Vanetti, C., Vago, R., Clerici, M., Tacchetti, C., et al. (2021). SARS-CoV-2 Entry: At the Crossroads of CD147 and ACE2. *Cells* 10 (6), 1434. doi:10.3390/cells10061434

Genovese, G., Friedman, D. J., Ross, M. D., Lecordier, L., Uzureau, P., Freedman, B. I., et al. (2010). Association of Trypanolytic ApoL1 Variants with Kidney Disease in African Americans. *Science* 329 (5993), 841–845. doi:10.1126/science.1193032

Gheblawi, M., Wang, K., Viveiros, A., Nguyen, Q., Zhong, J.-C., Turner, A. J., et al. (2020). Angiotensin-Converting Enzyme 2: SARS-CoV-2 Receptor and Regulator of the Renin-Angiotensin System. *Circ. Res.* 126 (10), 1456–1474. doi:10.1161/circresaha.120.317015

Glinka, Y., Stoilova, S., Mohammed, N., and Prud'homme, G. J. (2010). Neuropilin-1 Exerts Co-receptor Function for TGF-Beta-1 on the Membrane of Cancer Cells and Enhances Responses to Both Latent and Active TGF-Beta. *Carcinogenesis* 32 (4), 613–621. doi:10.1093/carcin/bgq281

Glowacka, I., Bertram, S., Herzog, P., Pfefferle, S., Steffen, I., Muench, M. O., et al. (2010). Differential Downregulation of ACE2 by the Spike Proteins of Severe Acute Respiratory Syndrome Coronavirus and Human Coronavirus NL63. *J. Virol.* 84 (2), 1198–1205. doi:10.1128/jvi.01248-09

Goswami, R., Russell, V. S., Tu, J. J., Thomas, C., Hughes, P., Kelly, F., et al. (2021). Oral Hsp90 Inhibitor SNX-5422 Attenuates SARS-CoV-2 Replication and Dampens Inflammation in Airway Cells. *iScience* 24 (12), 103412. doi:10.1016/j.isci.2021.103412

Gupta, A., Madhavan, M. V., Sehgal, K., Nair, N., Mahajan, S., Sehrawat, T. S., et al. (2020). Extrapulmonary Manifestations of COVID-19. *Nat. Med.* 26 (7), 1017–1032. doi:10.1038/s41591-020-0968-3

Hikmet, F., Méar, L., Edvinsson, Å., Micke, P., Uhlén, M., and Lindskog, C. (2020). The Protein Expression Profile of ACE2 in Human Tissues. *Mol. Syst. Biol.* 16 (7), e9610. doi:10.15252/msb.20209610

Hoffmann, M., Kleine-Weber, H., Schroeder, S., Krüger, N., Herrler, T., Erichsen, S., et al. (2020). SARS-CoV-2 Cell Entry Depends on ACE2 and TMPRSS2 and Is Blocked by a Clinically Proven Protease Inhibitor. *cell* 181 (2), 271–280.e8. doi:10.1016/j.cell.2020.02.052

Homan, K. A., Gupta, N., Kroll, K. T., Kolesky, D. B., Skylar-Scott, M., Miyoshi, T., et al. (2019). Flow-enhanced Vascularization and Maturation of Kidney Organoids *In Vitro*. *Nat. Methods* 16 (3), 255–262. doi:10.1038/s41592-019-0325-y

Huang, J., Hume, A. J., Abo, K. M., Werder, R. B., Villacorta-Martin, C., Alysandratos, K.-D., et al. (2020). SARS-CoV-2 Infection of Pluripotent Stem Cell-Derived Human Lung Alveolar Type 2 Cells Elicits a Rapid Epithelial-Intrinsic Inflammatory Response. *Cell Stem Cell* 27 (6), 962–973.e7. doi:10.1016/j.stem.2020.09.013

Ilic, D., and Ogilvie, C. (2017). Concise Review: Human Embryonic Stem Cells-What Have We Done? what Are We Doing? where Are We Going? *Stem cells* 35 (1), 17–25. doi:10.1002/stem.2450

Irizarry, R. A., Hobbs, B., Collin, F., Beazer-Barclay, Y. D., Antonellis, K. J., Scherf, U., et al. (2003). Exploration, Normalization, and Summaries of High Density Oligonucleotide Array Probe Level Data. *Biostatistics* 4 (2), 249–264. doi:10.1093/biostatistics/4.2.249

Jefferson, J. A., Nelson, P. J., Najafian, B., and Shankland, S. J. (2011). Podocyte Disorders: Core Curriculum 2011. *Am. J. Kidney Dis.* 58 (4), 666–677. doi:10.1053/j.ajkd.2011.05.032

Johns Hopkins University and Medicine (2021). *COVID-19 Dashboard by the Center for Systems Science and Engineering*. Baltimore, MD: CSSE at Johns Hopkins University JHU. Available at: https://coronavirus.jhu.edu/map.html.

Kalejaiye, T. D., Holmes, J. A., Bhattacharya, R., and Musah, S. (2022). "Reconstitution of the Kidney Glomerular Capillary wall," in *Regenerative Nephrology* (Elsevier), 331–351. doi:10.1016/b978-0-12-823318-4.00007-x

Kang, Y.-L., Chou, Y.-y., Rothlauf, P. W., Liu, Z., Soh, T. K., Cureton, D., et al. (2020). Inhibition of PIKfyve Kinase Prevents Infection by Zaire Ebolavirus and SARS-CoV-2. *Proc. Natl. Acad. Sci. U.S.A.* 117 (34), 20803–20813. doi:10.1073/pnas.2007837117

Kim, Y. H., Goyal, M., Kurnit, D., Wharram, B., Wiggins, J., Holzman, L., et al. (2001). Podocyte Depletion and Glomerulosclerosis Have a Direct Relationship in the PAN-Treated Rat. *Kidney Int.* 60 (3), 957–968. doi:10.1046/j.1523-1755.2001.060003957.x

Kuba, K., Imai, Y., Rao, S., Gao, H., Guo, F., Guan, B., et al. (2005). A Crucial Role of Angiotensin Converting Enzyme 2 (ACE2) in SARS Coronavirus-Induced Lung Injury. *Nat. Med.* 11 (8), 875–879. doi:10.1038/nm1267

Lamouroux, A., Attie-Bitach, T., Martinovic, J., Leruez-Ville, M., and Ville, Y. (2020). Evidence for and against Vertical Transmission for Severe Acute Respiratory Syndrome Coronavirus 2. *Am. J. Obstet. Gynecol.* 223 (1), 91.e1–91.e4. doi:10.1016/j.ajog.2020.04.039

Lan, J., Ge, J., Yu, J., Shan, S., Zhou, H., Fan, S., et al. (2020). Structure of the SARS-CoV-2 Spike Receptor-Binding Domain Bound to the ACE2 Receptor. *Nature* 581 (7807), 215–220. doi:10.1038/s41586-020-2180-5

Langham, R. G., Kelly, D. J., Cox, A. J., Thomson, N. M., Holthöfer, H., Zaoui, P., et al. (2002). Proteinuria and the Expression of the Podocyte Slit Diaphragm Protein, Nephrin, in Diabetic Nephropathy: Effects of Angiotensin Converting Enzyme Inhibition. *Diabetologia* 45 (11), 1572–1576. doi:10.1007/s00125-002-0946-y

Lennon, R., Randles, M. J., and Humphries, M. J. (2014). The Importance of Podocyte Adhesion for a Healthy Glomerulus. *Front. Endocrinol.* 5, 160. doi:10.3389/fendo.2014.00160

Marchiano, S., Hsiang, T.-Y., Khanna, A., Higashi, T., Whitmore, L. S., Bargehr, J., et al. (2021). SARS-CoV-2 Infects Human Pluripotent Stem Cell-Derived Cardiomyocytes, Impairing Electrical and Mechanical Function. *Stem Cel Rep.* 16, 478–492. doi:10.1016/j.stemcr.2021.02.008

Masters, P. S., and Perlman, S. (2013). "Coronaviridae," in *Fields Virology* 6th ed. Ediotors Knipe, D. M, and Howley, P. M. (Lippincott Williams & Wilkins) 1, 825–858.

Matovinović, M. S. (2009). 1. Pathophysiology and Classification of Kidney Diseases. *Ejifcc* 20 (1), 2–11.

Millet, J. K., and Whittaker, G. R. (2015). Host Cell Proteases: Critical Determinants of Coronavirus Tropism and Pathogenesis. *Virus. Res.* 202, 120–134. doi:10.1016/j.virusres.2014.11.021

Mizuiri, S., and Ohashi, Y. (2015). ACE and ACE2 in Kidney Disease. *Wjn* 4 (1), 74. doi:10.5527/wjn.v4.i1.74

Monteil, V., Kwon, H., Prado, P., Hagelkrüys, A., Wimmer, R. A., Stahl, M., et al. (2020). Inhibition of SARS-CoV-2 Infections in Engineered Human Tissues Using Clinical-Grade Soluble Human ACE2. *Cell* 181 (4), 905–913.e7. doi:10.1016/j.cell.2020.04.004

Moore, J. B., and June, C. H. (2020). Cytokine Release Syndrome in Severe COVID-19. *Science* 368 (6490), 473–474. doi:10.1126/science.abb8925

Musah, S., Mammoto, A., Ferrante, T. C., Jeanty, S. S. F., Hirano-Kobayashi, M., Mammoto, T., et al. (2017). Mature Induced-Pluripotent-Stem-Cell-Derived Human Podocytes Reconstitute Kidney Glomerular-Capillary-wall Function on a Chip. *Nat. Biomed. Eng.* 1 (5), 1–12. doi:10.1038/s41551-017-0069

Musah, S., Dimitrakakis, N., Camacho, D. M., Church, G. M., and Ingber, D. E. (2018). Directed Differentiation of Human Induced Pluripotent Stem Cells into Mature Kidney Podocytes and Establishment of a Glomerulus Chip. *Nat. Protoc.* 13 (7), 1662–1685. doi:10.1038/s41596-018-0007-8

Musah, S. (2021). Uncovering SARS-CoV-2 Kidney Tropism. *Nat. Rev. Mol. Cel Biol.* 22, 509. doi:10.1038/s41580-021-00370-w

Muus, C., Luecken, M. D., Eraslan, G., Waghray, A., Heimberg, G., Sikkema, L., et al. (2020). Integrated Analyses of Single-Cell Atlases Reveal Age, Gender, and Smoking Status Associations with Cell Type-specific Expression of Mediators of SARS-CoV-2 Viral Entry and Highlights Inflammatory Programs in Putative Target Cells. *bioRxiv* 1–65. doi:10.1101/2020.04.19.049254

Naicker, S., Yang, C.-W., Hwang, S.-J., Liu, B.-C., Chen, J.-H., and Jha, V. (2020). The Novel Coronavirus 2019 Epidemic and Kidneys. *Kidney Int.* 97 (5), 824–828. doi:10.1016/j.kint.2020.03.001

Niranjan, T., Bielesz, B., Gruenwald, A., Ponda, M. P., Kopp, J. B., Thomas, D. B., et al. (2008). The Notch Pathway in Podocytes Plays a Role in the Development of Glomerular Disease. *Nat. Med.* 14 (3), 290–298. doi:10.1038/nm1731

Okafor, A. E., Bhattacharya, R., and Musah, S. (2021). "Models of Kidney Glomerulus Derived from Human-Induced Pluripotent Stem Cells," in *iPSCs in Tissue Engineering*. Editor A. Birbrair (Academic Press), 329–370. doi:10.1016/b978-0-12-823809-7.00013-x

Oughtred, R., Stark, C., Breitkreutz, B.-J., Rust, J., Boucher, L., Chang, C., et al. (2019). The BioGRID Interaction Database: 2019 Update. *Nucleic Acids Res.* 47 (D1), D529–D541. doi:10.1093/nar/gky1079

Palacios-Rápalo, S. N., Jesús-González, D., Adrián, L., Cordero-Rivera, C. D., Farfan-Morales, C. N., Osuna-Ramos, J. F., et al. (2021). Cholesterol-Rich Lipid Rafts as Platforms for SARS-CoV-2 Entry. *Front. Immunol.* 12, 796855. doi:10.3389/fimmu.2021.796855

Pan, X.-w., Xu, D., Zhang, H., Zhou, W., Wang, L.-h., and Cui, X.-g. (2020). Identification of a Potential Mechanism of Acute Kidney Injury during the COVID-19 Outbreak: a Study Based on Single-Cell Transcriptome Analysis. *Intensive Care Med.* 46 (6), 1114–1116. doi:10.1007/s00134-020-06026-1

Pasparakis, M., and Vandenabeele, P. (2015). Necroptosis and its Role in Inflammation. *Nature* 517 (7534), 311–320. doi:10.1038/nature14191

Peiris, S., Mesa, H., Aysola, A., Manivel, J., Toledo, J., Borges-Sa, M., et al. (2021). Pathological Findings in Organs and Tissues of Patients with COVID-19: A Systematic Review. *PLoS One* 16 (4), e0250708. doi:10.1371/journal.pone.0250708

Petrosyan, A., Cravedi, P., Villani, V., Angeletti, A., Manrique, J., Renieri, A., et al. (2019). A Glomerulus-On-A-Chip to Recapitulate the Human Glomerular Filtration Barrier. *Nat. Commun.* 10 (1), 3656–3673. doi:10.1038/s41467-019-11577-z

Puelles, V. G., Lütgehetmann, M., Lindenmeyer, M. T., Sperhake, J. P., Wong, M. N., Allweiss, L., et al. (2020). Multiorgan and Renal Tropism of SARS-CoV-2. *N. Engl. J. Med.* 383 (6), 590–592. doi:10.1056/NEJMc2011400

Pushkarsky, T., Zybarth, G., Dubrovsky, L., Yurchenko, V., Tang, H., Guo, H., et al. (2001). CD147 Facilitates HIV-1 Infection by Interacting with Virus-Associated Cyclophilin A. *Proc. Natl. Acad. Sci. U.S.A.* 98 (11), 6360–6365. doi:10.1073/pnas.111583198

Radzikowska, U., Ding, M., Tan, G., Zhakparov, D., Peng, Y., Wawrzyniak, P., et al. (2020). Distribution of ACE2, CD147, CD26, and Other SARS-CoV-2 Associated Molecules in Tissues and Immune Cells in Health and in Asthma, COPD, Obesity, Hypertension, and COVID-19 Risk Factors. *Allergy* 75 (11), 2829–2845. doi:10.1111/all.14429

Shang, J., Wan, Y., Luo, C., Ye, G., Geng, Q., Auerbach, A., et al. (2020a). Cell Entry Mechanisms of SARS-CoV-2. *Proc. Natl. Acad. Sci. U.S.A.* 117 (21), 11727–11734. doi:10.1073/pnas.2003138117

Shang, J., Ye, G., Shi, K., Wan, Y., Luo, C., Aihara, H., et al. (2020b). Structural Basis of Receptor Recognition by SARS-CoV-2. *Nature* 581 (7807), 221–224. doi:10.1038/s41586-020-2179-y

Sharma, A., Garcia, G., Wang, Y., Plummer, J. T., Morizono, K., Arumugaswami, V., et al. (2020). Human iPSC-Derived Cardiomyocytes Are Susceptible to SARS-CoV-2 Infection. *Cel Rep. Med.* 1 (4), 100052. doi:10.1016/j.xcrm.2020.100052

Sharma, P., Ng, J. H., Bijol, V., Jhaveri, K. D., and Wanchoo, R. (2021). Pathology of COVID-19-Associated Acute Kidney Injury. *Clin. kidney J.* 14 (Suppl 1), i30–i39. doi:10.1093/ckj/sfab003

Shi, S., Qin, M., Shen, B., Cai, Y., Liu, T., Yang, F., et al. (2020). Association of Cardiac Injury with Mortality in Hospitalized Patients with COVID-19 in Wuhan, China. *JAMA Cardiol.* 5 (7), 802–810. doi:10.1001/jamacardio.2020.0950

Li, S., Zhang, Y., Guan, Z., Li, H., Ye, M., Chen, X., et al. (2020). SARS-CoV-2 Triggers Inflammatory Responses and Cell Death through Caspase-8 Activation. *Sig Transduct Target. Ther.* 5 (1), 235. doi:10.1038/s41392-020-00334-0

Simmons, G., Gosalia, D. N., Rennekamp, A. J., Reeves, J. D., Diamond, S. L., and Bates, P. (2005). Inhibitors of Cathepsin L Prevent Severe Acute Respiratory Syndrome Coronavirus Entry. *Proc. Natl. Acad. Sci. U.S.A.* 102 (33), 11876–11881. doi:10.1073/pnas.0505577102

Simoneau, C. R., and Ott, M. (2020). Modeling Multi-Organ Infection by SARS-CoV-2 Using Stem Cell Technology. *Cell stem cell* 27 (6), 859–868. doi:10.1016/j.stem.2020.11.012

Singh, M., Bansal, V., and Feschotte, C. (2020). A Single-Cell RNA Expression Map of Human Coronavirus Entry Factors. *Cel Rep.* 32 (12), 108175. doi:10.1016/j.celrep.2020.108175

Sung, S. H., Ziyadeh, F. N., Wang, A., Pyagay, P. E., Kanwar, Y. S., and Chen, S. (2006a). Blockade of Vascular Endothelial Growth Factor Signaling Ameliorates Diabetic Albuminuria in Mice. *Jasn* 17 (11), 3093–3104. doi:10.1681/ASN.2006010064

Sung, S. H., Ziyadeh, F. N., Wang, A., Pyagay, P. E., Kanwar, Y. S., and Chen, S. (2006b). Blockade of Vascular Endothelial Growth Factor Signaling Ameliorates Diabetic Albuminuria in Mice. *Jasn* 17 (11), 3093–3104. doi:10.1681/asn.2006010064

Sungnak, W., Huang, N., Bécavin, C., Berg, M., Queen, R., Litvinukova, M., et al. (2020). SARS-CoV-2 Entry Factors Are Highly Expressed in Nasal Epithelial Cells Together with Innate Immune Genes. *Nat. Med.* 26, 681–687. doi:10.1038/s41591-020-0868-6

Tang, T., Bidon, M., Jaimes, J. A., Whittaker, G. R., and Daniel, S. (2020). Coronavirus Membrane Fusion Mechanism Offers a Potential Target for Antiviral Development. *Antiviral Res.* 178, 104792. doi:10.1016/j.antiviral.2020.104792

Vankadari, N., and Wilce, J. A. (2020). Emerging COVID-19 Coronavirus: Glycan Shield and Structure Prediction of Spike Glycoprotein and its Interaction with Human CD26. *Emerging Microbes Infections* 9 (1), 601–604. doi:10.1080/22221751.2020.1739565

Velez, J. C. Q., Caza, T., and Larsen, C. P. (2020). COVAN Is the New HIVAN: the Re-emergence of Collapsing Glomerulopathy with COVID-19. *Nat. Rev. Nephrol.* 16 (10), 565–567. doi:10.1038/s41581-020-0332-3

Walls, A. C., Park, Y.-J., Tortorici, M. A., Wall, A., McGuire, A. T., and Veesler, D. (2020). Structure, Function, and Antigenicity of the SARS-CoV-2 Spike Glycoprotein. *Cell* 181 (2), 281–292.e6. doi:10.1016/j.cell.2020.02.058

Wang, K., Chen, W., Zhang, Z., Deng, Y., Lian, J.-Q., Du, P., et al. (2020). CD147-spike Protein Is a Novel Route for SARS-CoV-2 Infection to Host Cells. *Sig Transduct Target. Ther.* 5 (1), 283. doi:10.1038/s41392-020-00426-x

Wharram, B. L., Goyal, M., Wiggins, J. E., Sanden, S. K., Hussain, S., Filipiak, W. E., et al. (2005). Podocyte Depletion Causes Glomerulosclerosis: Diphtheria Toxin-Induced Podocyte Depletion in Rats Expressing Human Diphtheria Toxin Receptor Transgene. *Jasn* 16 (10), 2941–2952. doi:10.1681/asn.2005010055

Wong, D. W., Oudit, G. Y., Reich, H., Kassiri, Z., Zhou, J., Liu, Q. C., et al. (2007). Loss of Angiotensin-Converting Enzyme-2 (Ace2) Accelerates Diabetic Kidney Injury. *Am. J. Pathol.* 171 (2), 438–451. doi:10.2353/ajpath.2007.060977

Wrapp, D., Wang, N., Corbett, K. S., Goldsmith, J. A., Hsieh, C.-L., Abiona, O., et al. (2020). Cryo-EM Structure of the 2019-nCoV Spike in the Prefusion Conformation. *Science* 367 (6483), 1260–1263. doi:10.1126/science.abb2507

Wu, H., Larsen, C. P., Hernandez-Arroyo, C. F., Mohamed, M. M. B., Caza, T., Sharshir, M. d., et al. (2020). AKI and Collapsing Glomerulopathy Associated with COVID-19 and APOL1 High-Risk Genotype. *Jasn* 31 (8), 1688–1695. doi:10.1681/asn.2020050558

Wyatt, C. M., Klotman, P. E., and D'Agati, V. D. (2008). HIV-associated Nephropathy: Clinical Presentation, Pathology, and Epidemiology in the Era of Antiretroviral Therapy. *Semin. Nephrol.* 28 (6), 513–522. doi:10.1016/j.semnephrol.2008.08.005

Wysocki, J., Ye, M., Rodriguez, E., González-Pacheco, F. R., Barrios, C., Evora, K., et al. (2010). Targeting the Degradation of Angiotensin II with Recombinant Angiotensin-Converting Enzyme 2: Prevention of Angiotensin II–dependent Hypertension. *Hypertension* 55 (1), 90–98. doi:10.1161/hypertensionaha.109.138420

Wysocki, J., Ye, M., Hassler, L., Gupta, A. K., Wang, Y., Nicoleascu, V., et al. (2021). A Novel Soluble ACE2 Variant with Prolonged Duration of Action Neutralizes SARS-CoV-2 Infection in Human Kidney Organoids. *Jasn* 32, 795–803. ASN.2020101537. doi:10.1681/ASN.2020101537

Yang, L., Han, Y., Nilsson-Payant, B. E., Gupta, V., Wang, P., Duan, X., et al. (2020). A Human Pluripotent Stem Cell-Based Platform to Study SARS-CoV-2 Tropism and Model Virus Infection in Human Cells and Organoids. *Cell stem cell* 27 (1), 125–136. e127. doi:10.1016/j.stem.2020.06.015

Li, Y., Zhou, W., Yang, L., and You, R. (2020). Physiological and Pathological Regulation of ACE2, the SARS-CoV-2 Receptor. *Pharmacol. Res.* 157, 104833. doi:10.1016/j.phrs.2020.104833

Zhang, M.-Y., Zhang, Y., Wu, X.-D., Zhang, K., Lin, P., Bian, H.-J., et al. (2018). Disrupting CD147-RAP2 Interaction Abrogates Erythrocyte Invasion by Plasmodium Falciparum. *blood* 131 (10), 1111–1121. doi:10.1182/blood-2017-08-802918

Zhang, C., Shi, L., and Wang, F.-S. (2020). Liver Injury in COVID-19: Management and Challenges. *Lancet Gastroenterol. Hepatol.* 5 (5), 428–430. doi:10.1016/S2468-1253(20)30057-1

Conflict of Interest: SM is an inventor on a patent regarding podocyte differentiation.

The remaining authors declare that the research was conducted in the absence of any commercial or financial relationships that could be construed as a potential conflict of interest.

Publisher's Note: All claims expressed in this article are solely those of the authors and do not necessarily represent those of their affiliated organizations, or those of the publisher, the editors and the reviewers. Any product that may be evaluated in this article, or claim that may be made by its manufacturer, is not guaranteed or endorsed by the publisher.

frontiers | Frontiers in Cell and Developmental Biology

ORIGINAL RESEARCH
published: 10 May 2022
doi: 10.3389/fcell.2022.884509

The Lipid-Binding Defective Dynamin 2 Mutant in Charcot-Marie-Tooth Disease Impairs Proper Actin Bundling and Actin Organization in Glomerular Podocytes

Eriko Hamasaki[1†], Natsuki Wakita[1†], Hiroki Yasuoka[1], Hikaru Nagaoka[2], Masayuki Morita[2], Eizo Takashima[2], Takayuki Uchihashi[3], Tetsuya Takeda[1], Tadashi Abe[1], Ji-Won Lee[4], Tadahiro Iimura[4], Moin A Saleem[5], Naohisa Ogo[6], Akira Asai[6], Akihiro Narita[7], Kohji Takei[1] and Hiroshi Yamada[1]**

[1]Department of Neuroscience, Graduate School of Medicine, Dentistry and Pharmaceutical Sciences, Okayama University, Okayama, Japan, [2]Division of Malaria Research, Proteo-Science Center, Ehime University, Matsuyama, Japan, [3]Department of Physics, Nagoya University, Nagoya, Japan, [4]Department of Pharmacology, Faculty and Graduate School of Dental Medicine, Hokkaido University, Sapporo, Japan, [5]Bristol Renal, Translational Health Sciences, Bristol Medical School, University of Bristol, Bristol, United Kingdom, [6]Center for Drug Discovery, Graduate School of Pharmaceutical Sciences, University of Shizuoka, Shizuoka, Japan, [7]Graduate School of Science, Nagoya University, Nagoya, Japan

OPEN ACCESS

Edited by:
Hans Kristian Lorenzo,
Université Paris-Saclay, France

Reviewed by:
Oliver Daumke,
Max Delbrueck Center for Molecular Medicine, Germany
Ana María Cárdenas,
Universidad de Valparaiso, Chile

***Correspondence:**
Kohji Takei
kohji@md.okayama-u.ac.jp
Hiroshi Yamada
hiroyama@md.okayama-u.ac.jp

†These authors have contributed equally to this work

Specialty section:
This article was submitted to Cell Death and Survival, a section of the journal Frontiers in Cell and Developmental Biology

Received: 26 February 2022
Accepted: 06 April 2022
Published: 10 May 2022

Citation:
Hamasaki E, Wakita N, Yasuoka H, Nagaoka H, Morita M, Takashima E, Uchihashi T, Takeda T, Abe T, Lee J-W, Iimura T, Saleem MA, Ogo N, Asai A, Narita A, Takei K and Yamada H (2022) The Lipid-Binding Defective Dynamin 2 Mutant in Charcot-Marie-Tooth Disease Impairs Proper Actin Bundling and Actin Organization in Glomerular Podocytes. Front. Cell Dev. Biol. 10:884509. doi: 10.3389/fcell.2022.884509

Dynamin is an endocytic protein that functions in vesicle formation by scission of invaginated membranes. Dynamin maintains the structure of foot processes in glomerular podocytes by directly and indirectly interacting with actin filaments. However, molecular mechanisms underlying dynamin-mediated actin regulation are largely unknown. Here, biochemical and cell biological experiments were conducted to uncover how dynamin modulates interactions between membranes and actin in human podocytes. Actin-bundling, membrane tubulating, and GTPase activities of dynamin were examined *in vitro* using recombinant dynamin 2-wild-type (WT) or dynamin 2-K562E, which is a mutant found in Charcot-Marie-Tooth patients. Dynamin 2-WT and dynamin 2-K562E led to the formation of prominent actin bundles with constant diameters. Whereas liposomes incubated with dynamin 2-WT resulted in tubule formation, dynamin 2-K562E reduced tubulation. Actin filaments and liposomes stimulated dynamin 2-WT GTPase activity by 6- and 20-fold, respectively. Actin-filaments, but not liposomes, stimulated dynamin 2-K562E GTPase activity by 4-fold. Self-assembly-dependent GTPase activity of dynamin 2-K562E was reduced to one-third compared to that of dynamin 2-WT. Incubation of liposomes and actin with dynamin 2-WT led to the formation of thick actin bundles, which often bound to liposomes. The interaction between lipid membranes and actin bundles by dynamin 2-K562E was lower than that by dynamin 2-WT. Dynamin 2-WT partially colocalized with stress fibers and actin bundles based on double immunofluorescence of human podocytes. Dynamin 2-K562E expression resulted in decreased stress fiber density and the formation of aberrant actin clusters. Dynamin 2-K562E colocalized with α-actinin-4 in aberrant actin clusters. Reformation of stress fibers after cytochalasin D-induced actin depolymerization and washout was less effective in

dynamin 2-K562E-expressing cells than that in dynamin 2-WT. Bis-T-23, a dynamin self-assembly enhancer, was unable to rescue the decreased focal adhesion numbers and reduced stress fiber density induced by dynamin 2-K562E expression. These results suggest that the low affinity of the K562E mutant for lipid membranes, and atypical self-assembling properties, lead to actin disorganization in HPCs. Moreover, lipid-binding and self-assembly of dynamin 2 along actin filaments are required for podocyte morphology and functions. Finally, dynamin 2-mediated interactions between actin and membranes are critical for actin bundle formation in HPCs.

Keywords: dynamin, podocyte, actin, bundle, GTPase, CMT

INTRODUCTION

Glomerular podocytes are highly differentiated epithelial cells that line the urinary side of the glomerular basement membrane. They participate in filtration of blood plasma to form primary urine. Podocytes have a complex architecture. They consist of major primary processes that branch to form secondary and tertiary foot processes. These secondary and tertiary branches interdigitate with those of neighboring podocytes to form and maintain the glomerular slit diaphragms (Pavenstädt et al., 2003). Foot processes of podocytes are mainly supported by the actin cytoskeleton, including actin bundles and cortical actin mesh structures (Sever and Schiffer, 2018). Proper regulation of the actin cytoskeleton is crucial for maintaining the unique morphology and the filtering function of podocytes.

Dynamins are endocytic proteins that form vesicles by fission of invaginated plasma membranes (Antonny et al., 2016). Dynamins are divided into three isoforms in mammals (Ferguson and De Camilli, 2012). Dynamin 1 is enriched in the brain, dynamin 2 is expressed in all cells, and dynamin 3 localizes to the brain, lung, and testis (Nakata et al., 1993). All dynamin isoforms contain an N-terminal GTPase domain, a middle domain (MD), phosphoinositide-binding pleckstrin homology (PH) domain, GTPase effector domain (GED), and C-terminal proline and arginine-rich domain (PRD) which interacts with variety of proteins containing the Src-homology-3 domain (**Figure 1A**; Ferguson and De Camilli, 2012). Crystallographically, the three α-helix of MD and the single α-helix in GED form four-helix bundle structure termed the "stalk", which provides interface required for dimerization and self-assembly (Faelber et al., 2011; Ford et al., 2011). In unassembled dynamin, PH domain is at "closed" position, at which it is folded back onto the stalk preventing oligomerization of dynamin. Upon binding of dynamin to phosphatidylinositol (4,5) bisphosphate (PIP_2) -containing membrane, the PH domain is displaced to "open" dynamin conformation capable of self-assembly (Srinivasan et al., 2016; Kong et al., 2018). Mutations in dynamin 2 gene cause autosomal dominantly inherited diseases, Charcot-Marie-Tooth disease (CMT) (Züchner et al., 2005), and centronuclear myopathy (CNM) (Bitoun et al., 2005), which are characterized by degenerative changes of peripheral nerves and muscles respectively. Although both CMT mutations and CNM mutations are mostly found in the PH domain, the two group of mutations are differentially located. While CNM mutations are present in PH domain-stalk interface, CMT mutations, including K562E used in this study, are located at the opposite side of PH domain implicated in membrane binding (Faelber et al., 2011; Tassin et al., 2021).

All dynamins function in endocytosis by participating in membrane fission (Antonny et al., 2016), and recognition of phosphoinositides by dynamin's PH domain, especially, electrically polarised seven-stranded β-sandwich, is crucial for this function (Vallis et al., 1999). Dynamins are also involved in the regulation of the cytoskeleton. Dynamin directly or indirectly interacts with actin (Sever et al., 2013), and thus regulates actin dynamics in lamellipodia and dorsal membrane ruffles (Cao et al., 1998; McNiven et al., 2000), invadopodia (Baldassarre et al., 2003), podosomes (Ochoa et al., 2000), growth cones (Torre et al., 1994; Kurklinsky et al., 2011; Yamada et al., 2013), phagocytic cups (Gold et al., 1999; Otsuka et al., 2009), and filopodia of cancer cells (Yamada et al., 2016a). It is recently shown that dynamin helix bundles 12-16 actin filaments, and the dynamin-enriched actin bundle was present at the fusogenic synapse (Zhang et al., 2020).

Dynamin maintains the integrity and structure of the glomerular filtration barrier by regulating actin and microtubule cytoskeleton in addition to endocytosis. Podocyte-specific double knockouts of dynamin 1 and dynamin 2 in mice result in severe proteinuria and renal failure, which are caused by the disruption of glomerular slit diaphragms (Soda et al., 2012). In addition, a reduction in cellular dynamin levels by cathepsin L expression causes proteinuria in mice (Sever et al., 2007). Dynamin has been implicated in the turnover of nephrin on the surface of podocyte foot processes via endocytosis (Soda et al., 2012). Dynamin 1 in podocyte is involved in cellular protrusion formation by regulating microtubule organization and stabilization (La et al., 2020). Furthermore, dynamin participates in the maintenance of the structure of foot processes through direct and indirect interactions with actin filaments (Gu et al., 2010). Bis-T-23 was originally reported as a potent dynamin inhibitor of lipid-stimulated GTPase activity (Hill et al., 2005). Subsequently, Gu et al. found that Bis-T-23 promotes dynamin's oligomerization *in vitro* (Gu et al., 2017), and increases the formation of stress fibers and focal adhesions in mouse podocyte cells (Gu et al., 2014). Because of these effects of Bis-T-23 on dynamin and dynamin-regulated actin-rich structures, Bis-T-23 is shown to improve proteinuria in several animal models (Schiffer et al., 2015). However, a mode of action for actin regulation by dynamin 2 remains to be elucidated.

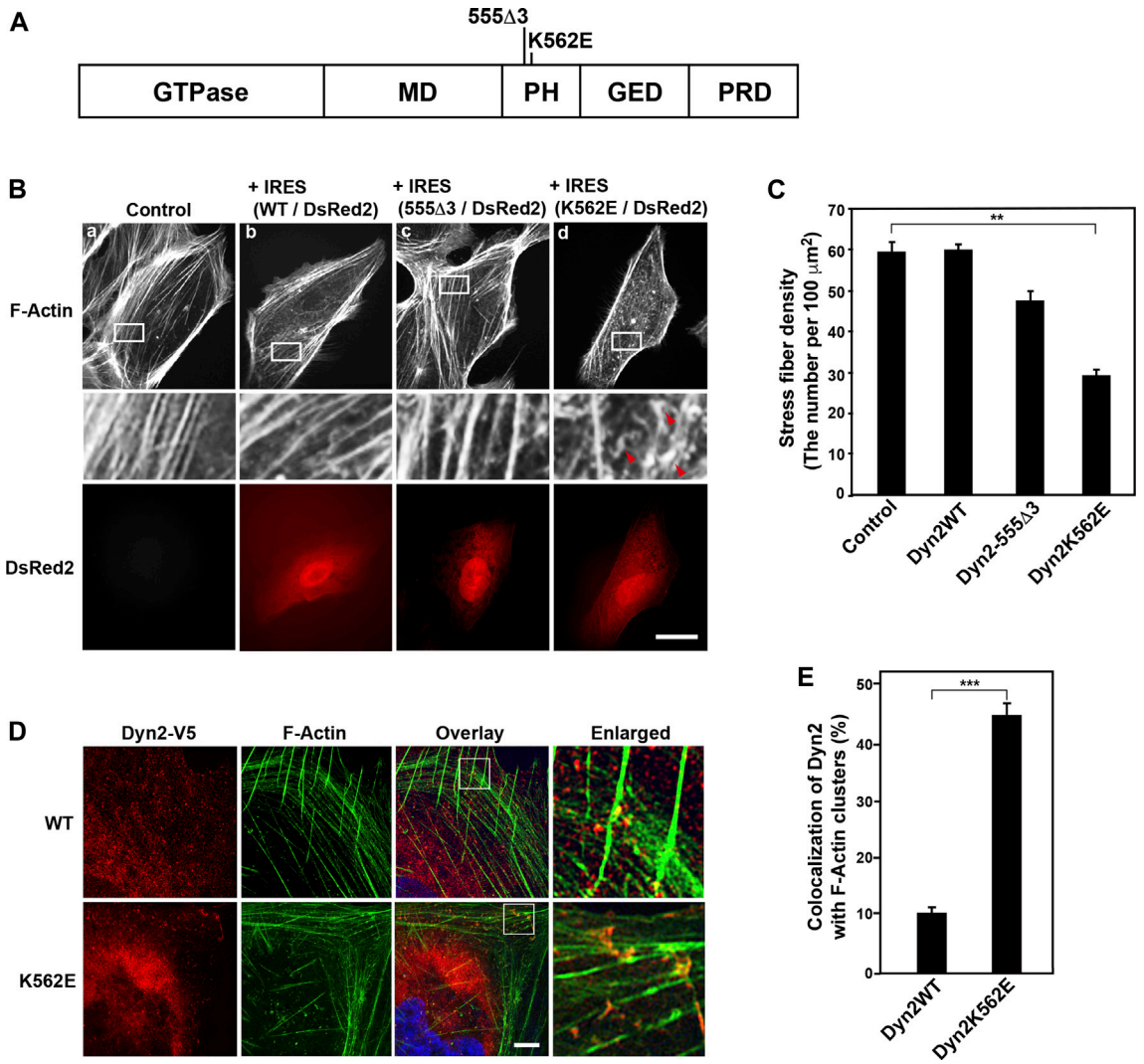

FIGURE 1 | Expression of the dynamin 2 (Dyn2)-K562E mutant leads to the formation of aberrant actin bundles and a decrease in stress fiber density in human podocyte cells. **(A)** Domain structure of dynamin 2 and the location of the 555Δ3 and K562E mutations in rat dynamin 2. GTPase domain, MD = Middle Domain; PH = Pleckstrin Homology domain; GED = GTPase Effector Domain; PRD = Proline arginin-Rich Domain. **(B)** Alexa Fluor 488-phalloidin-labeled actin filaments in HPCs. HPCs were transfected with dynamin 2-WT (WT) **(b)**, 555Δ3 **(c)**, or K562E **(d)** expression constructs cloned into the pIRES-DsRed2 vector. Non-transfected cells (Controls) are shown in **(a)**. White rectangular areas in the top panels correspond to enlarged images in the middle panels. Stress fibers are clearly observed in control and dynamin 2-WT-expressing cells. Note the reduction in actin bundles and stress fibers, and the presence of F-Actin clusters (red arrowheads) in K562E mutant-expressing cells **(d)**. Dynamin-transfected cells were identified by DsRed2 expression (bottom panels). Actin clusters were shown by arrowheads. Scale bars: 20 μm in top and bottom panels and 3.6 μm in middle panels. **(C)** Stress fiber density in control HPCs and those expressing the various dynamin 2 constructs. Data are means ± S.E.M. of 33 cells (control), 101 cells (dynamin 2-WT), 39 cells (dynamin 2-555Δ3) or 105 cells (dynamin 2-K562E) from three independent experiments. (**$p < 0.01$). **(D)** Super-resolution microscopy images of V5-tagged dynamin 2-WT or K562E, and actin filaments (F-Actin) in HPCs processed by double-immunofluorescence. White squares in the overlay images correspond to the enlarged images on the right. Scale bars: 5 μm, 1 μm in enlarged panels. **(E)** Quantification of the colocalization of dynamin 2-WT or K562E, and actin filaments in HPCs. Data are mean ± S.E.M. of 51 cells in dynamin 2-WT and 50 cells in K562E from three independent experiments. For each sample, colocalization was determined in three randomly selected areas per cell (21 μm^2). (***$p < 0.001$).

Our previous studies show that the dynamin 2 CMT mutant K562E decreases the formation of stress fibers and triggers the assembly of aberrant actin clusters in U2OS cells (Yamada et al., 2016b). In the present study, biochemical and cell biological experiments were used to uncover the mode of action for actin regulation by dynamin 2 by comparing the effects of dynamin 2-WT on actin filaments to those of K562E in conditionally immortalized human podocytes (HPCs). Expression of dynamin 2-K562E resulted in decreased formation of stress fibers and the appearance of aberrant actin clusters. Bis-T-23 was less effective on the self-assembly of dynamin 2-K562E *in vitro*, it was unable to reverse the aberrant actin structures in dynamin 2-K562E expressing cells. Furthermore, *in vitro* experiments revealed defects in the interaction of actin bundles formed by dynamin 2-K562E to lipid membranes. These results suggest that the self-assembly and membrane interaction properties of dynamin 2 are

crucial for actin regulation, which is a prerequisite for maintaining the unique morphology and filtering function of podocytes.

EXPERIMENTAL METHODS

Antibodies and Reagents

Rabbit polyclonal anti-V5 antibody (AB3792), rabbit polyclonal anti-α-actinin-4 antibody (0042-05), and mouse monoclonal antibody against paxillin (AHO0492) were purchased from Sigma-Aldrich, immunoGlobe, and Thermo Fisher Scientific, respectively. Alexa Fluor 488-conjugated goat anti-mouse IgG (A11001), Rhodamine Red X-conjugated goat anti-rabbit IgG (R6394), and Alexa Fluor 488-phalloidin (A12379) were purchased from Life Technologies. The rabbit polyclonal antibodies against mouse IgG (31450) and goat IgG (31402), and goat polyclonal antibody against rabbit IgG (31460) were purchased from Thermo Fisher Scientific. The mouse monoclonal antibodies against beta-actin (A5441) and cytochalasin D (C8273) were purchased from Sigma-Aldrich. Bis-T-23 (2-cyano-N-{3-[2-cyano-3-(3,4,5-trihydroxyphenyl) acryloylamino] propyl}-3-(3,4,5 trihydroxyphenyl) acrylamide) (ab146050) was purchased from Abcam, and stored frozen as a 50 mM stock solution in dimethyl sulfoxide (DMSO).

Cell Culture

The conditionally immortalized HPC line was cultured as described previously (Saleem et al., 2002). Briefly, the cells were cultured on type I collagen-coated plastic dishes (356450, Corning Inc.) in Roswell Park Memorial Institute (RPMI) 1640 medium (189-02025, Fujifilm Wako Pure Chemicals Co. Ltd.) containing 10% fetal bovine serum (26140079, Thermo Fisher Scientific), 100 U/ml penicillin, 100 μg/ml streptomycin (15140122, Thermo Fisher Scientific), and ITS-G (Insulin-Transferrin-Selenium mixture) (100×, 41400045, Thermo Fisher Scientific), and maintained at 33°C and 5% CO_2. To induce differentiation, podocytes were cultured at 37°C in medium lacking ITS-G for 7–14 days. Under these conditions, the cells stopped proliferating and were positive for synaptopodin.

Purification of Recombinant Proteins

His-tagged dynamin 2b was expressed using the Bac-to-Bac baculovirus expression system (Thermo Fisher Scientific) and purified as described previously (Yamada et al., 2016a). The purified dynamin proteins were concentrated using Centriplus YM50 (4310, Merck-Millipore). His-tagged rat dynamin 2-WT or dynamin 2-K562E was expressed using a wheat germ cell-free expression system (CellFree Sciences). Dynamin 2-WT or dynamin 2-K562E was resolved in 100 mM NaCl, 50 mM Tris, 500 mM imidazole, pH8.0, and stored at 4°C until use. We used dynamin 2-WT and K562E produced by a wheat germ cell free expression system except **Supplementary Figures S2E, F**, and baculovirus protein expression system was used for **Supplementary Figures S2E, F**.

Liposome Preparation

Liposomes were prepared as previously described (Takeda et al., 2018). 10% (mol/mol) PIP_2 (Cat. No 524644, Calbiochem), 80% phosphatidylethanolamine (PE; 840022C, Avanti Polar Lipids), 10% cholesterol (700000, Avanti Polar Lipids) were mixed in chloroform. Then chloroform was evaporated using slow-flow nitrogen gas to produce lipid film on the glass and then completely dried under vacuum for at least 1 day. The dried lipid was rehydrated by water-saturated nitrogen gas followed by addition of 500 μl of filtered 100 mM KCl, 10 mM Tris-HCl, pH 7.5 for 2 h at 37°C. The resultant membrane vesicles were passed through 0.4 μm- or 1 μm-polycarbonate filters respectively 11 times using Avanti Mini extruder. To visualize liposomes under fluorescent microscope, 1% Rhodamine-labeled PE was added to liposomes.

Complementary DNA Constructs and Transfection

Rat dynamin 2-WT, 555Δ3, and K562E cloned into pcDNA4 V5/His are described in Yamada et al. (2016b). Rat dynamin 2-WT was subcloned into pIRES2-DsRed2 as an EcoRI-SmaI fragment (Clontech Laboratories). Mutations were introduced with QuikChange II XL (Agilent Technologies, Santa Clara, CA) following the manufacturer's instructions, and mutation accuracy was verified by DNA sequencing. Vectors containing dynamin 2-WT and the site-directed mutants were transfected into cells using Lipofectamine LTX reagent (Thermo Fisher Scientific) according to the manufacturer's protocol. After transfection for 2 days, the cells were processed by double immunofluorescence.

Fluorescence Microscopy

HPCs were fixed in 4% paraformaldehyde and processed for immunofluorescence as described previously (Yamada et al., 2016a). For cytochalasin D washout experiments, HPCs were incubated in 5 μM cytochalasin D at 37°C for 30 min. Cytochalasin D-containing medium was then replaced with fresh cytochalasin D-free medium. Cells were further incubated for 60 min after cytochalasin D washout, and then fixed with 4% paraformaldehyde in phosphate buffered saline (PBS; 145 mM NaCl, 10 mM phosphate buffer, pH7.4).

For Bis-T-23 treatment, HPCs were incubated in 50 μM Bis-T-23 at 37°C for 30 min, and then fixed with 4% paraformaldehyde in PBS. After fixation, cells were subjected to double-immunofluorescence. Samples were examined with a spinning-disc confocal microscope system (X-Light Confocal Imager; CREST OPTICS S.P.A., Rome, Italy), which consisted of an inverted microscope (IX-71; Olympus Optical Co., Ltd., Tokyo, Japan) and an iXon + camera (Oxford Instruments, Oxfordshire, United Kingdom). The confocal system was controlled by the MetaMorph software (Molecular Devices, Sunnyvale, CA, United States). When necessary, images were processed with Adobe Photoshop CS3 or Illustrator CS3 software. The N-SIM system (NIKON Corp., Tokyo, Japan) was used for super-resolution microscopy.

Determination of Phosphate Concentration

Dynamin 2-WT or K562E (1.5 μM) was incubated with actin filaments (1 μM) in buffer (100 mM KCl, 2 mM $MgCl_2$, 0.2 mM $CaCl_2$, 10 mM Tris-HCl, pH 7.5, 0.62 mM ATP, 0.5 mM DTT) at 4°C for 16 h. The dynamin 2-actin filament mixture (160 μl) was then incubated in the presence of 1 mM GTP at 37°C for 15 min. GTP hydrolysis was measured using a colorimetric assay to detect inorganic phosphate (Pi) release as previously described (Leonard et al., 2005).

Quantification of Actin Bundles by a Low-Speed Sedimentation Assay

Non-muscle actin (APHL99, Cytoskeleton Inc.) was polymerized in F-buffer (50 mM KCl, 2 mM $MgCl_2$, 0.2 mM $CaCl_2$, 10 mM Tris-HCl, pH7.5, 0.5 mM DTT, 1 mM ATP) for 1 h. Dynamin 2-WT or K562E (1 μM) was then incubated with actin filaments (3 μM) in F-buffer for 1 h. Actin bundles were sedimented by low-speed centrifugation at 14,000 × g for 1 h. The pellet and supernatant were separated by SDS-PAGE, stained with SYPRO Orange (S6650, Thermo Fisher Scientific), and quantified by densitometry using Image J. All steps were carried out at room temperature.

Transmission Electron Microscopy

Negative staining was performed according to Yamada et al. (Yamada et al., 2013). The dynamin 2-WT- or K562E-induced actin-bundling assays were conducted by incubating 1.5 μM of the dynamins with 1 μM actin filaments in F-buffer containing 50 mM or 100 mM KCl at 4°C for 16 h. The samples were absorbed onto a Formvar- and carbon-coated copper grid. To observe the effect of GTP hydrolysis on actin bundle morphology, GTP or GMP-PNP at the indicated concentrations were added onto the grid and incubated for 1 min or 5 min, respectively. The grids were then stained with 3% uranyl acetate in double deionized H_2O for 2 min. Grids were imaged with a transmission electron microscope (TEM) (H-7650, Hitachi High-Tech Corp., Tokyo, Japan) at a voltage of 120 kV.

Atomic Force Microscopy (AFM)

The laboratory-built AFM observation was performed as follows (Takeda et al., 2018). First, after incubation with a mixture of dynamin 2-WT/K562E and actin filament in F-buffer containing 50 mM KCl, a glass stage with a diameter of 2 mm was immersed in the solution, and the complex is fixed to the glass substrate by centrifugation (6,000 × g for 20 min). After that, the samples were washed by the F-buffer and fixed with the F-buffer with 0.01% glutaraldehyde solution. Then AFM images were obtained in the F-buffer at room temperature.

Morphometry

Cells were stained with Alexa Fluor 488-phalloidin, and analyzed by fluorescent confocal microscopy to determine stress fiber density. The number of stress fibers in three randomly selected areas (10 μm × 10 μm) per cell was counted. Data were analyzed from three independent experiments. The extent of colocalization of dynamin 2-WT or K562E with F-actin or α-actinin-4 was assessed by imaging immunostained cells, and measuring the immunoreactivities in three randomly selected areas (5 × 5 μm) per cell. To quantify focal adhesions, cells immunostained with dynamin 2-WT or K562E, and paxillin, were imaged. The number of clear dots per cell was counted. we performed morphological analysis again. For quantification of liposomes bound to actin filaments, images of the mixture, including dynamin 2-WT or K562E, and F-actin with rhodamine-labelled liposomes, were taken with a confocal microscope at a 1000× magnification. The corresponding pixels to liposomes colocalizing at F-actin were extracted using Metamorph software from double-fluorescent overlay image (1024 × 1024 pixel) of liposome (red) and actin filament (green) and then calculated the total amount of colocalizing liposomes with F-actin. We normalized the total amount of colocalizing liposomes with F-actin by the same amount of F-actin in each condition. We quantified the pitch in dynamin-induced actin bundles by visually scanning negatively-stained samples at the electron microscope according to Takei et al. (Takei et al., 1999).

Statistical Analysis

Data were analyzed for statistical significance using KaleidaGraph software for Macintosh, version 4.1 (Synergy Software Inc., Essex Junction, VT, United States). Student's t-tests were used to analyze statistical significance between two groups. An analysis of variance and Tukey's honest significant difference post-hoc test were used to compare several groups. All data are displayed as means ± standard error of the means (S.E.M.) with $p < 0.05$ considered statistically significant.

RESULTS

Expression of Dynamin 2-K562E Results in Aberrant Actin Stress Fibers and Actin Clusters in Human Podocyte Cells

Our previous studies show that dynamin 2-K562E, a point mutation in dynamin 2 PH domain, induces aberrant actin filament structures in U2OS cells (Yamada et al., 2016b). To investigate the mode of action for dynamin 2 mutation-triggered changes in actin morphology in HPCs, we first examined actin filament distribution in dynamin 2-WT- or K562E-expressing cells by double-immunofluorescence microscopy. Dynamin 2-WT and K562E were compared to dynamin 2-555Δ3, which is a deletion mutant that affects microtubule organization (**Figures 1A, Bc**; Tanabe and Takei 2009). DsRed2 was co-expressed with the dynamin 2-WT and mutant constructs to identify cells expressing the exogenous proteins. Control HPCs, untransfected, formed the typical parallel arrangement of stress fibers and actin bundles (**Figure 1Ba**). The organization of the actin cytoskeleton in cells expressing dynamin 2-WT was similar to that of control cells (**Figure 1Bb**). Furthermore, actin filament distribution in 555Δ3-expressing cells was similar to that of control or dynamin 2-WT-expressing cells (**Figures 1Bc, C**). By contrast, stress fiber density was approximately 50% lower in K562E-expressing cells than that of control or dynamin 2-WT-expressing cells (**Figures 1Bd, C**). Dynamin 2-WT was observed as fine dots distributed throughout the cell when imaged by super-resolution microscopy. The dot-like dynamin 2-WT structures partially colocalized with stress fibers and actin bundles (**Figures 1D** upper panels, **E**). By contrast, K562E-expressing cells showed numerous actin filament clusters, and aberrant stress fibers accumulating with K562E-dynamin 2 (**Figures 1D** bottom panels, **E**). The results indicate that K562E-dynamin 2 causes distinct effects on the organization of the actin cytoskeleton in HPCs.

Dynamin 2 is Involved in Stress Fiber Formation in Human Podocytes

Given the appearance of aberrant stress fibers and actin clusters in dynamin 2-K562E-expressing HPCs, we next asked whether the dynamin mutant affects stress fiber formation. Actin filaments,

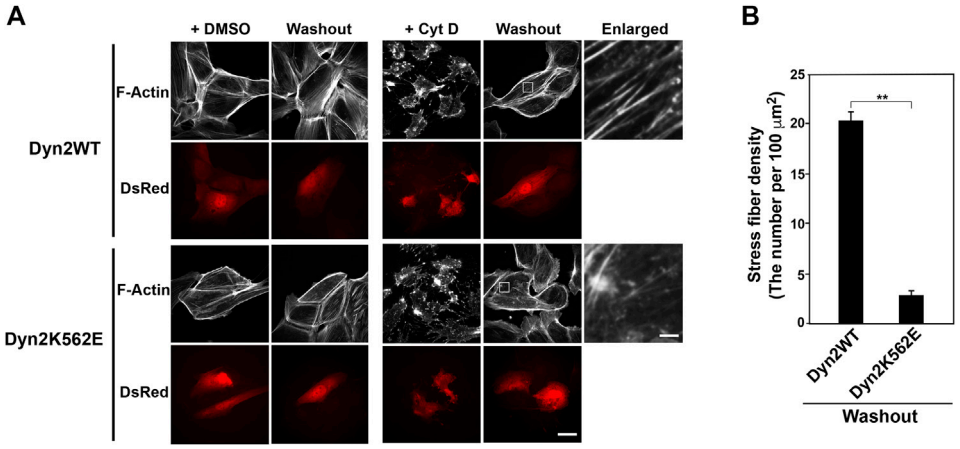

FIGURE 2 | Stress fiber formation decreases in dynamin 2 (Dyn2)-K562E-expressing HPCs. **(A)** Double-immunofluorescence images of HPCs transfected with dynamin 2-WT or K562E cloned into the pIRES-DsRed2 vector as in **Figure 1B**. HPCs were treated with or without 5 μM cytochalasin D (Cyt D) for 30 min. Washout experiments involved changing the Cyt D-containing medium with Cyt D-free medium. After 60 min, actin filaments were stained with Alexa Fluor 488-phalloidin (Washout). Cells were treated with the solvent control (DMSO) solution represent the negative controls. Scale bars: 20 and 1.8 μm in enlarged panels. **(B)** Stress fiber density in dynamin 2-WT- or K562E-expressing HPCs after washing out of Cyt D. Data are means ± S.E.M. of 24 cells (dynamin 2-WT) or 27 cells (dynamin 2-K562E) from three independent experiments. (**$p < 0.01$).

including stress fibers, are disrupted by the actin polymerization inhibitor cytochalasin D (Brenner and Korn, 1979). Reformation of stress fibers after removing cytochalasin D from the medium was examined. As shown in **Figure 2A**, cytochalasin D treatment for 30 min resulted in the disruption of stress fibers and actin bundles in dynamin 2-WT- and dynamin 2-K562E-expressing HPCs. Dynamin 2-WT-expressing cells reformed clear stress fibers 1 hour after removal of cytochalasin D. On the other hand, stress fiber reformation was lower in dynamin 2-K562E-expressing cells than that in dynamin 2-WT-expressing cells (**Figure 2B**). Thus, dynamin 2 is required in the early stages of stress fiber reformation.

The dynamin polymerization enhancer, Bis-T-23, promotes the formation of stress fibers and focal adhesions in mouse podocyte cells (Schiffer et al., 2015; Gu et al., 2017). Here, Bis-T-23 enhanced stress fiber formation in dynamin 2-K562E-expressing and dynamin 2-WT-expressing HPCs (**Figures 3A,B**). However, Bis-T-23-induced stress fiber formation in dynamin 2-K562E-expressing HPCs was lower than that in dynamin 2-WT-expressing HPCs. Bis-T-23 had the same effect on focal adhesion formation in dynamin 2-K562E-expressing and dynamin 2-WT-expressing HPCs (**Figures 3C,D**).

The Dynamin 2 Ring-Like Structure Directly Bundles Actin Filaments

To determine if dynamin 2 directly affects actin filaments, we examined *in vitro* the GTPase activities and membrane deformation activities of recombinant dynamin 2-WT and dynamin 2-K562E. Purified dynamin 2-WT showed high GTPase activity under low ionic strength buffer (**Supplementary Figure S2A**) or in the presence of lipid membranes (**Supplementary Figure S2B**). These findings were consistent with previous reports (Warnock et al., 1997; Leonard et al., 2005). By contrast, GTPase activity of dynamin 2-K562E was approximately one-third that of dynamin 2-WT under low ionic strength buffer (**Supplementary Figure S2A**). Furthermore, liposome-stimulated increase of GTPase activity was not observed in dynamin 2-K562E (**Supplementary Figure S2B**).

For membrane deformation activity assays, liposomes containing PIP_2 were incubated with dynamin 2-WT or dynamin 2-K562E, and examined by TEM. Dynamin 2-WT formed typical membrane tubules decorated with dynamin spiral polymers as reported previously (Chin et al., 2015; **Supplementary Figure S2C**). On the other hand, dynamin 2-K562E hardly tubulated the liposomes, although it slightly deformed spherical liposomes (**Supplementary Figure S2C**). In absence of liposomes, both dynamin 2-WT, dynamin 2-K562E formed ring-shaped polymers under GDP-Pi conditions (**Supplementary Figure S2D**; Carr and Hinshaw, 1997), which suggested that the ability of dynamin 2 to self-assemble into rings is retained in dynamin 2-K562E. We next examined the direct effects of Bis-T-23 on dynamin polymerization. In the presence of Bis-T-23, polymerization of recombinant dynamin 2-WT increased by thirty times in comparison to that without Bis-T-23. On the other hand, polymerization of dynamin 2-K562E slightly increased by three and half times (**Supplementary Figures S2E, F**). These results suggested that self-assembly and membrane tubulating activity of dynamin 2-K562E was defective, and the differential effects of Bis-T-23 *in cellulo* on dynamin 2-WT and dynamin 2-K562E (**Figure 3**) could be attributed to changes in the molecular characteristics of dynamin 2-K562E.

Given that dynamin directly bundles actin filaments (Zhang et al., 2020), we assessed whether dynamin 2-WT or K562E bundles actin

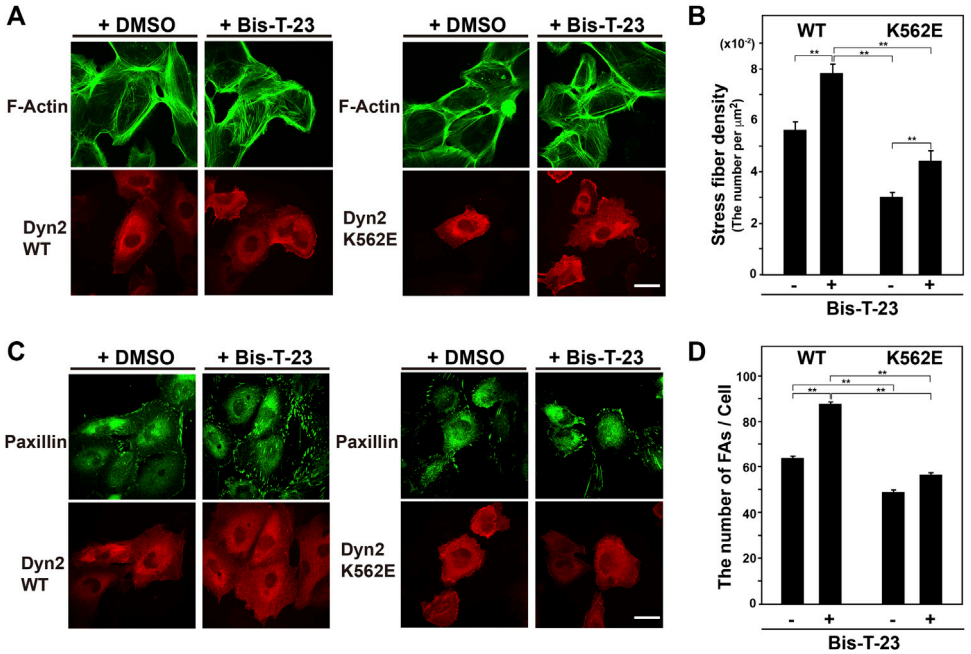

FIGURE 3 | Stress fibers and focal adhesions increase in Bis-T-23-treated HPCs. **(A)** Double-immunofluorescence of V5-tagged dynamin 2 (Dyn2)-WT or K562E (bottom panels) and actin filaments (top panels) in Bis-T-23-treated (50 μM) HPCs and corresponding solvent controls (DMSO). Scale bar: 20 μm. **(B)** Stress fiber density in Bis-T-23-treated dynamin 2-WT- or K562E-expressing HPCs. Data are means ± S.E.M. of 35 cells (dynamin 2-WT/DMSO), 33 cells (dynamin 2-WT/Bis-T-23), 38 cells (dynamin 2-K562E/DMSO) or 35 cells (dynamin 2-K562E/Bis-T-23) from three independent experiments. (**$p < 0.01$). **(C)** Double-immunofluorescence of V5-tagged dynamin 2-WT or K562E (bottom panels) and paxillin (top panels) in Bis-T-23-treated (50 μM) HPCs and corresponding solvent controls (DMSO). Scale bar; 20 μm. **(D)** Number of focal adhesions in Bis-T-23-treated dynamin 2-WT- or K562E-expressing HPCs. Data are means ± S.E.M. of 35 cells (dynamin 2-WT/DMSO), 32 cells (dynamin 2-WT/Bis-T-23), 35 cells (dynamin 2-K562E/DMSO) or 34 cells (dynamin 2-K562E/Bis-T-23) from three independent experiments. (**$p < 0.01$). more than 32 cells from three independent experiments. (**$p < 0.01$).

filaments. Preformed actin filaments were incubated *in vitro* with or without recombinant dynamin 2-WT or K562E, and actin bundle formation was examined by low-speed sedimentation assays. In the absence of dynamin 2 proteins, actin in the pellet after centrifugation at 14,000 x g was around 20% of total actin (**Figure 4A**). In the presence of dynamin 2-WT or dynamin 2-K562E, actin in the pellets increased by 30–40% (**Figure 4A**). These results suggested that dynamin 2-WT and K562E bundle actin filaments to similar extents.

TEM revealed that actin filaments were often tightly bundled by dynamin 2-WT or K562E (**Figure 4B**). The diameter of actin filament bundles in the presence of dynamin 2-WT and dynamin 2-K562E was 41.0 ± 0.6 nm (n = 24) and 41.4 ± 0.5 nm (n = 21), respectively. Periodically arranged dynamins were often observed both in dynamin 2-WT- and dynamin 2-K562E-induced actin bundles (**Figure 4B** inset). Atomic force microscopy (AFM) was used to investigate dynamin and actin filament configurations. AFM revealed that dynamin 2-WT ring-like structures formed spirals, and actin filaments directly bound to the outer rim of the dynamin spirals (**Supplementary Figure S3**). Dynamin 2-K562E bundled actin filaments in the same manner as that of dynamin 2-WT (**Supplementary Figure S3**).

Next, the effect of actin bundles on dynamin GTPase activity was determined. High ion strength buffer conditions containing 100 mM KCl were used to detect actin bundling-dependent GTPase activity because low ionic strength buffer containing 50 mM KCl causes a dynamin 2 self-assembly-dependent increase in GTPase activity (Warnock et al., 1997). Low magnification TEM images showed that dynamin 2-WT bundled actin filaments in the high ion strength buffer. By contrast, actin bundle formation by dynamin 2-K562E was lower than that of dynamin 2-WT (**Figure 4C**). Under the same conditions, concentration of released free phosphate by dynamin 2-WT or dynamin 2-K562E increased 6-fold or 4-fold, respectively, relative to that without actin proteins (**Figure 4D**).

We next examined morphological changes of actin bundles upon GTP hydrolysis of dynamins. The addition of GTP caused the rapid depolymerization of dynamin spiral polymers, and the resulting dispersion of actin bundles (**Figure 4E** middle panels) consistent with recent report (Zhang et al., 2020). This morphological change is likely to be largely dependent on GTP hydrolysis, although the reaction mixture also contains ATP for the purpose of stabilizing actin filaments. It is known that dynamin has much higher affinity to GTP compared to that to ATP (Maeda et al., 1992). Consistently, in the presence of nonhydrolyzable GTP analogue, GMP-PNP, did not result in disassembly of dynamin spiral polymers on the actin bundles (**Figure 4E** bottom panels). The clearance among adjacent dynamin 2-WT polymers in the actin bundles changed from 14.2 ± 0.2 nm (-GTP, n = 24) to 12.9 ± 0.3 nm (+GMP-PNP, n = 27). On the other hand, clearance among adjacent dynamin 2-K562E polymer in the actin bundles changed from 13.9 ± 0.3 nm

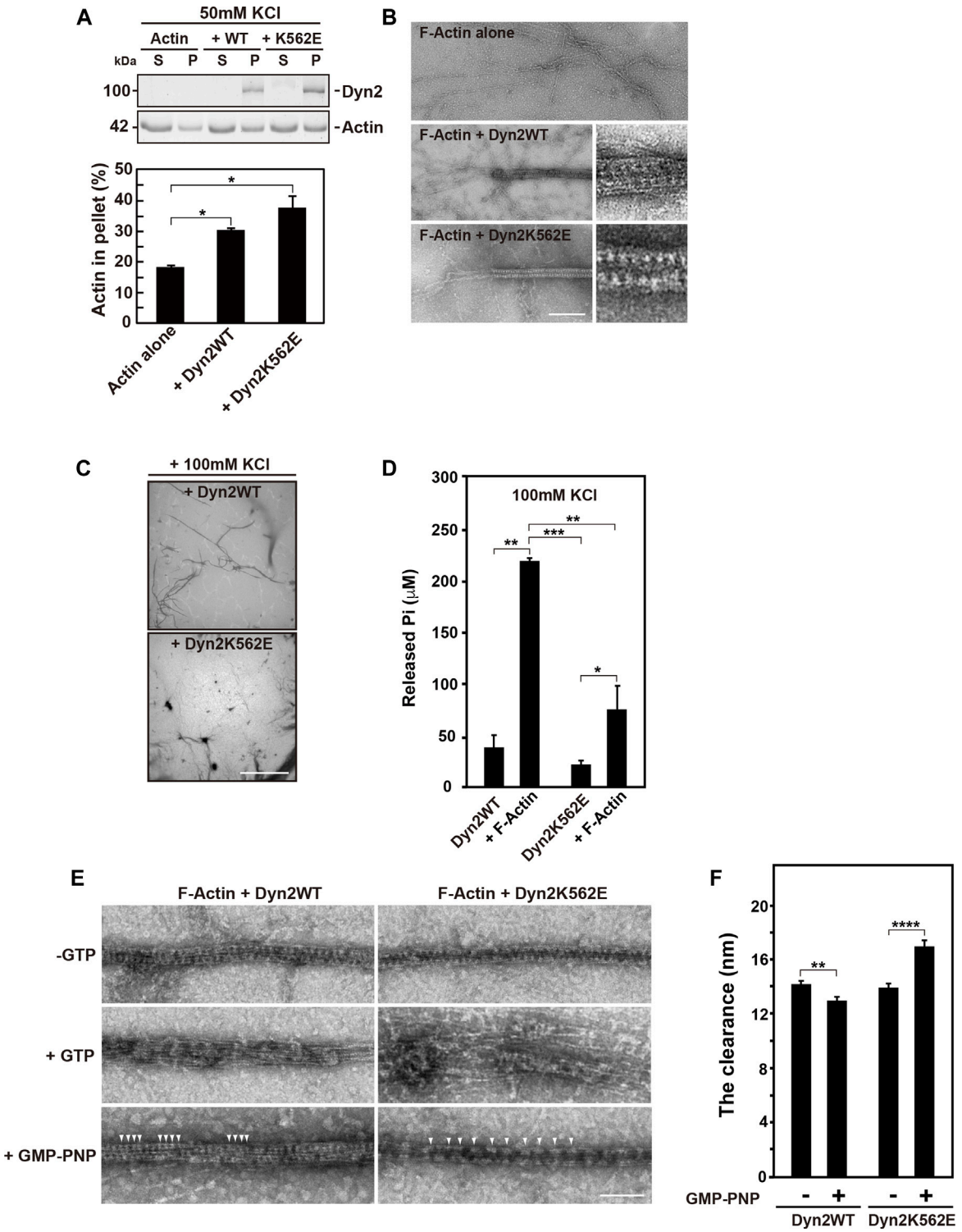

FIGURE 4 | *In vitro* actin bundle formation by dynamin 2 (Dyn2)-WT or K562E. **(A)** Low-speed sedimentation assay for dynamin 2-WT- or K562E-induced actin bundle formation in low ionic strength buffer. The top panel shows actin in the pellet (P) or supernatant (S) fraction in the presence or absence of dynamin. Quantification of actin in the low-speed pellet in actin only, dynamin 2-WT, and K562E samples by densitometry (bottom panel). Data are means ± S.E.M. of three independent experiments. (*; $p < 0.05$). **(B)** Transmission electron micrographs of negatively-stained actin bundles formed by dynamin 2-WT (middle) or K562E (bottom). Scale bar: 200 nm, 50 nm in enlarged images. **(C)** Low magnification electron micrographs of negatively-stained actin bundles show a decrease in actin bundle formation by dynamin 2-K562E in the high ionic strength buffer. Scale bar: 8.5 μm. **(D)** Actin filaments (F-Actin) increases Pi release by dynamin 2-WT or K562E. Data are means ± (*Continued*)

FIGURE 4 | S.E.M. of three independent experiments. (***; $p < 0.001$: **; $p < 0.01$: *; $p < 0.05$). **(E)** Electron micrographs showing morphological changes of dynamin 2-WT- or K562E-induced actin bundles in high ionic strength buffer. A reaction consisting of recombinant dynamin (1.5 μM) and F-Actin (1 μM) was initiated as in D, and the resulting actin bundles were treated with buffer alone, 0.1 mM GTP, or 0.5 mM GMP-PNP at room temperature for 5 min. Dynamin polymers were shown by arrowheads. Scale bar: 100 nm. **(F)** The clearance among adjacent dynamin 2-WT spiral polymer in the actin bundles. Twenty four (dynamin 2-WT/-GTP) or 27 (dynamin 2-WT/GMP-PNP), 21 (dynamin 2-K562E/-GTP) or 35 (dynamin 2-K562E/GMP-PNP) negatively-stained TEM images taken at ×30000 magnification from three independent experiments were used for the quantification. Data are means ± S.E.M. of three independent experiments. (****; $p < 0.0001$: **; $p < 0.01$).

(-GTP, $n = 21$) to 16.9 ± 0.5 nm (+GMP-PNP, $n = 35$) (**Figures 4E** bottom panels, **F**).

Dynamin 2 Crosslinks Actin Bundles and Membranes, and Dynamin 2-K562E Reduces the Association Between Membranes and Actin Bundles

Dynamin binds to membrane phospho-lipids, such as PIP_2 via its PH domain, and this association is essential for membrane deformation (Antonny et al., 2016). We therefore asked whether dynamin 2-induced actin bundles could bind to lipid membranes. Actin filaments did not form bundles or associate with lipid vesicles in the absence of dynamins (**Figure 5A**). In the presence of dynamin 2-WT, almost all actin filaments incorporated into thick actin bundles that colocalized with liposomes (**Figure 5A**). On the other hand, fewer actin bundles formed in the presence of dynamin 2-K562E than that in dynamin 2-WT (**Figure 5A**). Liposomes colocalizing with actin filaments or bundles in the presence of dynamin 2-K562E was approximately 30% of that in the presence of dynamin 2-WT (**Figure 5B**). These results indicate that dynamin 2 has actin-bundling and lipid-binding properties, and that dynamin 2-K562E has lower lipid-binding activity during actin bundling than that of dynamin 2-WT.

DISCUSSION

Two dynamin isoforms, dynamin 1 and dynamin 2, are expressed in podocytes (Soda et al., 2012). Dynamin 2 in podocytes play a role in maintaining the glomerular slit diaphragms by directly regulating actin (Gu et al., 2010; Schiffer et al., 2015) or by modulating endocytosis (Soda et al., 2012). However, the mode of action of actin regulation by dynamin 2 in podocytes remains unsolved. We have investigated the actin regulation by using variety of dynamin 2 CMT mutants to clarify CMT pathogenesis. Among the mutants, we found that expression of K562E, a member of CMT mutant in dynamin 2, resulted in the decrease of stress fibers and formation of actin clusters (Yamada et al., 2016b). We also examined two kinds of CMT mutants, G358R and 555Δ3. These CMT mutations did not affect the actin cytoskeleton (Yamada et al., 2016b). In the present study, we used the K562E mutants to clarify the function of dynamin 2 on actin cytoskeleton by the comparison of dynamin 2-WT and K562E in conditionally immortalized HPCs. Because the CMT mutations in dynamin 2 cause autosomal dominantly inherited

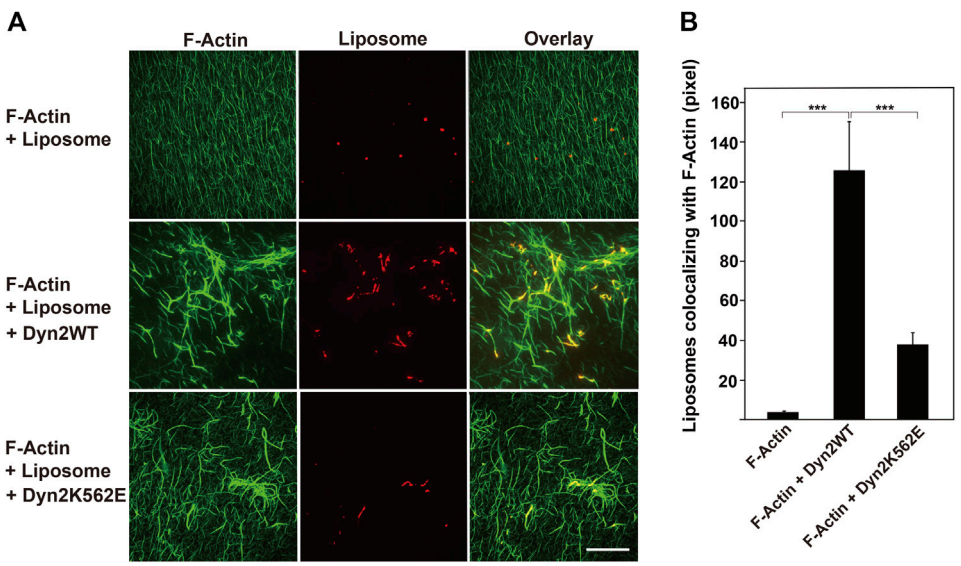

FIGURE 5 | Decreased interaction of actin bundles formed by dynamin 2-K562E with PIP_2-containing lipid vesicles. **(A)** Actin filaments (F-Actin) and lipid vesicles were visualized with Alexa Fluor 488-phalloidin (green) and Rhodamine-phosphatidylethanolamine (PE) (red), respectively. Preformed actin bundles by dynamin 2-WT (middle panels) or dynamin 2-K562E (bottom panels) were mixed with rhodamine-labeled lipid vesicles. Note that thick actin bundles formed by dynamin 2-WT associated with several lipid membranes. In the presence of dynamin 2-K562E, actin bundles were thinner and bound to few lipid vesicles. Scale bar: 20 μm. **(B)** Quantification of liposomes colocalizing with actin filaments. Data are means ± S.E.M. of 10 images (F-Actin), 25 images (F-Actin + Dyn2 WT) or 25 images (F-Actin + Dyn2 K562E) from three independent experiments. (***$p < 0.001$).

diseases (Züchner et al., 2005), the expression of exogenous CMT mutant in cells would represent the pathological phenotype even though the presence of endogenous WT dynamin. In the study, we exogenously expressed dynamin CMT mutant in the presence of endogenous dynamin 2 to access the effect of actin filaments. Dynamin 2-K562E-expressing HPCs had lower stress fibers and actin filaments than those of dynamin 2-WT-expressing HPCs (**Figures 1**, **2**). In addition, dynamin 2-K562E colocalized with aberrant actin clusters and bundles in areas, in which α-actinin-4 was located (**Figure 1** and **Supplementary Figure S1**). Stress fiber reformation was lower in dynamin 2-K562E-expressing HPCs than that in dynamin 2-WT-expressing cells (**Figure 2**). These results suggest that dynamin 2 is involved in stress fiber formation in HPCs.

Bis-T-23, a dynamin polymerization enhancer (Schiffer et al., 2015), stimulated the formation of stress fibers and focal adhesions in dynamin 2-WT-expressing cells (**Figure 3**). On the other hand, Bis-T-23 had less effects on stress fiber formation and focal adhesion in dynamin 2-K562E-expressing cells than that in dynamin 2-WT-expressing cells (**Figure 3**). Moreover, Bis-T-23 was unable to stimulate dynamin 2-K562E polymerization *in vitro* (**Supplementary Figure S2E**). *In vitro* studies revealed lower dynamin 2-K562E self-assembly and membrane tubulation with decreased GTPase activity than that in dynamin 2-WT (**Supplementary Figure S2**). WT and mutant dynamins formed ring-like structures and/or spirals in the presence of actin filaments (**Figure 4**), and bound to actin filaments outside of the dynamin rings (**Figure 4** and **Supplementary Figure S3**). Crosslinking between membranes and actin bundles triggered by dynamin 2-K562E were lower than those of dynamin 2-WT (**Figure 5**). These results indicate that proper self-assembly and association of dynamin 2 to membranes are crucial for actin regulation in HPCs.

Dynamin K562E has its mutation site in the PH domain at the interface of polymerized dynamin and membranes, and the mutant is defective in lipid-binding (Kenniston and Lemmon, 2010). In this study, dynamin 2-K562E hardly generated membrane tubules from liposomes, and therefore the mutant rarely polymerized into regularly arranged spirals on lipid membrane (**Supplementary Figure S2C**). The dynamin 2-K562E mutation in PH domain largely reduced membrane-binding ability, but not affected its actin binding capability (**Figure 4A**). Thus, the defective lipid-induced oligomerization of dynamin 2-K562E mutant might impact the proper formation of actin stress fibers in HPCs. Dynamin might have several putative actin binding sites. Gu and others determined several crucial amino acid residues for actin binding in the dynamin middle domain and upstream of the PH domain (Gu et al., 2010). Furthermore, the proline-rich domain is essential for actin bundling (Zhang et al., 2020). From the study, the K562E mutation seems to rarely affect its actin binding and bundling ability.

AFM revealed that several actin filaments bound to the outer rim of dynamin rings or spirals. Furthermore, actin filaments were not observed inside the dynamin spirals (**Supplementary Figure S3**). There are reports that the dynamin ring bundles actin filaments indirectly and directly (Yamada et al., 2013; Zhang et al., 2020). Dynamin 1 binds to cortactin, which is an actin filament binding protein (Wu and Parsons 1993), and forms a ring-shaped or spiral complex (Yamada et al., 2013). The dynamin-cortactin ring bundles actin filaments inside of the ring. The three-dimensional structure of the dynamin-actin filament complex needs to be determined at higher resolution such as by cryo-electron tomography reconstruction to better understand the nature of actin binding to dynamin.

Differentiated podocytes have a complex architecture with a multitude of foot processes that interdigitate with those of neighbouring podocytes to form and maintain the glomerular slit diaphragms (Pavenstädt et al., 2003). Actin serves as the main cytoskeletal structure in foot processes (Perico et al., 2016). Podocyte-specific conditional double knockouts of dynamins 1 and 2 in mice result in severe proteinuria and renal failure because of disruptions to the glomerular slit diaphragms (Soda et al., 2012). Dynamin 2 is thought to not only strengthen the actin cytoskeleton through its actin-bundling ability, but also promotes the formation of stress fibers and focal adhesions to maintain podocyte morphology and filtration functions. The present study shows that the self-assembly, and the membrane binding are essential characteristics of dynamin for the formation of stress fibers and actin bundles in HPCs.

Dynamin 2 binds to several actin-related proteins, and indirectly or directly regulates actin. Our previous studies report that another dynamin isoform, dynamin 1, is crucial for proper distribution and stability of microtubules in podocytes (La et al., 2020). Dynamin 2-dependent regulatory functions of stress fibers and focal adhesions in coordination with dynamin 1-dependent distribution and stabilization of microtubules, could be essential for normal podocyte function.

DATA AVAILABILITY STATEMENT

The raw data supporting the conclusions of this article will be made available by the authors, without undue reservation.

AUTHOR CONTRIBUTIONS

Yamada H, KT, and EH designed the research and wrote the paper. Yamada H, EH, NW, Yasuoka H, HN, MM, ET, TU, TA, TT, NO, AA, J-WL, TI and AN performed the experiments. NO, AA, and MS contributed new reagents or analytic tools. All authors read and approved the final manuscript.

FUNDING

This work was supported, in part, by grants from the Ministry of Education, Science, Sports, and Culture of Japan (grant numbers 19H03225, 21K19484 to Takei K, 20K08591 to Yamada H and 19K07084 to Abe T), the Okayama University Central Research Laboratory, Ehime University Proteo-Science Center (PROS), and by Joint Research by Exploratory Research Center on Life and Living Systems (ExCELLS) program No 18-305 to Yamada H).

ACKNOWLEDGMENTS

The authors thank Kento Sumida, Sayaka Seiriki, and The Mon La (Okayama University, Okayama, Japan) for technical assistance. The work was supported by Okayama University Central Research Laboratory.

SUPPLEMENTARY MATERIAL

The Supplementary Material for this article can be found online at: https://www.frontiersin.org/articles/10.3389/fcell.2022.884509/full#supplementary-material

REFERENCES

Antonny, B., Burd, C., De Camilli, P., Chen, E., Daumke, O., Faelber, K., et al. (2016). Membrane Fission by Dynamin: What We Know and what We Need to Know. *EMBO J.* 35, 2270–2284. doi:10.15252/embj.201694613

Baldassarre, M., Pompeo, A., Beznoussenko, G., Castaldi, C., Cortellino, S., McNiven, M. A., et al. (2003). Dynamin Participates in Focal Extracellular Matrix Degradation by Invasive Cells. *Mol. Biol. Cel.* 14, 1074–1084. doi:10.1091/mbc.e02-05-0308

Bitoun, M., Maugenre, S., Jeannet, P. Y., Lacène, E., Ferrer, X., Laforêt, P., et al. (2005). Mutations in Dynamin 2 Cause Dominant Centronuclear Myopathy. *Nat. Genet.* 37, 1207–1209. doi:10.1038/ng1657

Brenner, S. L., and Korn, E. D. (1979). Substoichiometric Concentrations of Cytochalasin D Inhibit Actin Polymerization. Additional Evidence for an F-Actin Treadmill. *J. Biol. Chem.* 254, 9982–9985. doi:10.1016/S0021-9258(19)86660-7

Cao, H., Garcia, F., and McNiven, M. A. (1998). Differential Distribution of Dynamin Isoforms in Mammalian Cells. *Mol. Biol. Cel.* 9, 2595–2609. doi:10.1091/mbc.9.9.2595

Carr, J. F., and Hinshaw, J. E. (1997). Dynamin Assembles into Spirals under Physiological Salt Conditions upon the Addition of GDP and γ-Phosphate Analogues. *J. Biol. Chem.* 272, 28030–28035. doi:10.1074/jbc.272.44.28030

Chin, Y. H., Lee, A., Kan, H. W., Laiman, J., Chuang, M. C., Hsieh, S. de T., et al. (2015). Dynamin-2 Mutations Associated with Centronuclear Myopathy Are Hypermorphic and lead to T-Tubule Fragmentation. *Hum. Mol. Genet.* 24, 5542–5554. doi:10.1093/hmg/ddv285

Faelber, K., Posor, Y., Gao, S., Held, M., Roske, Y., Schulze, D., et al. (2011). Crystal Structure of Nucleotide-Free Dynamin. *Nature* 477, 556–560. doi:10.1038/nature10369

Ferguson, S. M., and De Camilli, P. (2012). Dynamin, a Membrane-Remodelling GTPase. *Nat. Rev. Mol. Cel Biol.* 13, 75–88. doi:10.1038/nrm3266

Ford, M. G. J., Jenni, S., and Nunnari, J. (2011). The crystal Structure of Dynamin. *Nature* 477, 561–566. doi:10.1038/nature10441

Gold, E. S., Underhill, D. M., Morrissette, N. S., Guo, J., McNiven, M. A., and Aderem, A. (1999). Dynamin 2 Is Required for Phagocytosis in Macrophages. *J. Exp. Med.* 190, 1849–1856. doi:10.1084/jem.190.12.1849

Gu, C., Chang, J., Shchedrina, V. A., Pham, V. A., Hartwig, J. H., Suphamungmee, W., et al. (2014). Regulation of Dynamin Oligomerization in Cells: The Role of Dynamin-Actin Interactions and its GTPase Activity. *Traffic* 15, 819–838. doi:10.1111/tra.12178

Gu, C., Lee, H. W., Garborcauskas, G., Reiser, J., Gupta, V., and Sever, S. (2017). Dynamin Autonomously Regulates Podocyte Focal Adhesion Maturation. *J. Am. Soc. Nephrol.* 28, 446–451. doi:10.1681/ASN.2016010008

Gu, C., Yaddanapudi, S., Weins, A., Osborn, T., Reiser, J., Pollak, M., et al. (2010). Direct Dynamin-Actin Interactions Regulate the Actin Cytoskeleton. *EMBO J.* 29, 3593–3606. doi:10.1038/emboj.2010.249

Hill, T., Odell, L. R., Edwards, J. K., Graham, M. E., McGeachie, A. B., Rusak, J., et al. (2005). Small Molecule Inhibitors of Dynamin I GTPase Activity: Development of Dimeric Tyrphostins. *J. Med. Chem.* 48, 7781–7788. doi:10.1021/jm040208l

Kenniston, J. A., and Lemmon, M. A. (2010). Dynamin GTPase Regulation Is Altered by PH Domain Mutations Found in Centronuclear Myopathy Patients. *EMBO J.* 29, 3054–3067. doi:10.1038/emboj.2010.187

Kong, L., Sochacki, K. A., Wang, H., Fang, S., Canagarajah, B., Kehr, A. D., et al. (2018). Cryo-EM of the Dynamin Polymer Assembled on Lipid Membrane. *Nature* 560, 258–262. doi:10.1038/s41586-018-0378-6

Kurklinsky, S., Chen, J., and McNiven, M. A. (2011). Growth Cone Morphology and Spreading Are Regulated by a Dynamin-Cortactin Complex at point Contacts in Hippocampal Neurons. *J. Neurochem.* 117, 48–60. doi:10.1111/j.1471-4159.2011.07169.x

La, T. M., Tachibana, H., Li, S. A., Abe, T., Seiriki, S., Nagaoka, H., et al. (2020). Dynamin 1 Is Important for Microtubule Organization and Stabilization in Glomerular Podocytes. *FASEB J.* 34, 16449–16463. doi:10.1096/fj.202001240RR

Leonard, M., Doo Song, B., Ramachandran, R., and Schmid, S. L. (2005). Robust Colorimetric Assays for Dynamin's Basal and Stimulated GTPase Activities. *Methods Enzymol.* 404, 490–503. doi:10.1016/S0076-6879(05)04043-7

Maeda, K., Nakata, T., Noda, Y., Sato-Yoshitake, R., and Hirokawa, N. (1992). Interaction of Dynamin with Microtubules: Its Structure and GTPase Activity Investigated by Using Highly Purified Dynamin. *Mol. Biol. Cel.* 3, 1181–1194. doi:10.1091/mbc.3.10.1181

McNiven, M. A., Kim, L., Krueger, E. W., Orth, J. D., Cao, H., and Wong, T. W. (2000). Regulated Interactions between Dynamin and the Actin-Binding Protein Cortactin Modulate Cell Shape. *J. Cel Biol.* 151, 187–198. doi:10.1083/jcb.151.1.187

Nakata, T., Takemura, R., and Hirokawa, N. (1993). A Novel Member of the Dynamin Family of GTP-Binding Proteins Is Expressed Specifically in the Testis. *J. Cel Sci.* 105, 1–5. doi:10.1242/jcs.105.1.1

Ochoa, G. C., Slepnev, V. I., Neff, L., Ringstad, N., Takei, K., Daniell, L., et al. (2000). A Functional Link between Dynamin and the Actin Cytoskeleton at Podosomes. *J. Cel Biol.* 150, 377–390. doi:10.1083/jcb.150.2.377

Otsuka, A., Abe, T., Watanabe, M., Yagisawa, H., Takei, K., and Yamada, H. (2009). Dynamin 2 Is Required for Actin Assembly in Phagocytosis in Sertoli Cells. *Biochem. Biophys. Res. Commun.* 378, 478–482. doi:10.1016/j.bbrc.2008.11.066

Pavenstädt, H., Kriz, W., and Kretzler, M. (2003). Cell Biology of the Glomerular Podocyte. *Physiol. Rev.* 83, 253–307. doi:10.1152/physrev.00020.2002

Perico, L., Conti, S., Benigni, A., and Remuzzi, G. (2016). Podocyte-Actin Dynamics in Health and Disease. *Nat. Rev. Nephrol.* 12, 692–710. doi:10.1038/nrneph.2016.127

Saleem, M. A., O'Hare, M. J., Reiser, J., Coward, R. J., Inward, C. D., Farren, T., et al. (2002). A Conditionally Immortalized Human Podocyte Cell Line Demonstrating Nephrin and Podocin Expression. *J. Am. Soc. Nephrol.* 13, 630–638. doi:10.1681/ASN.V133630

Schiffer, M., Teng, B., Gu, C., Shchedrina, V. A., Kasaikina, M., Pham, V. A., et al. (2015). Pharmacological Targeting of Actin-Dependent Dynamin Oligomerization Ameliorates Chronic Kidney Disease in Diverse Animal Models. *Nat. Med.* 21, 601–609. doi:10.1038/nm.3843

Sever, S., Altintas, M. M., Nankoe, S. R., Möller, C. C., Ko, D., Wei, C., et al. (2007). Proteolytic Processing of Dynamin by Cytoplasmic Cathepsin L Is a Mechanism for Proteinuric Kidney Disease. *J. Clin. Invest.* 117, 2095–2104. doi:10.1172/JCI32022

Sever, S., Chang, J., and Gu, C. (2013). Dynamin Rings: Not Just for Fission. *Traffic* 14, 1194–1199. doi:10.1111/tra.12116

Sever, S., and Schiffer, M. (2018). Actin Dynamics at Focal Adhesions: A Common Endpoint and Putative Therapeutic Target for Proteinuric Kidney Diseases. *Kidney Int.* 93, 1298–1307. doi:10.1016/j.kint.2017.12.028

Soda, K., Balkin, D. M., Ferguson, S. M., Paradise, S., Milosevic, I., Giovedi, S., et al. (2012). Role of Dynamin, Synaptojanin, and Endophilin in Podocyte Foot Processes. *J. Clin. Invest.* 122, 4401–4411. doi:10.1172/JCI65289

Srinivasan, S., Dharmarajan, V., Reed, D. K., Griffin, P. R., and Schmid, S. L. (2016). Identification and Function of Conformational Dynamics in the Multidomain GTP Ase Dynamin. *EMBO J.* 35, 443–457. doi:10.15252/embj.201593477

Takeda, T., Kozai, T., Yang, H., Ishikuro, D., Seyama, K., Kumagai, Y., et al. (2018). Dynamic Clustering of Dynamin-Amphiphysin Helices Regulates Membrane Constriction and Fission Coupled with GTP Hydrolysis. *Elife* 7, e30246. doi:10.7554/eLife.30246

Takei, K., Slepnev, V. I., Haucke, V., and De Camilli, P. (1999). Functional Partnership between Amphiphysin and Dynamin in Clathrin-Mediated Endocytosis. *Nat. Cel Biol.* 1, 33–39. doi:10.1038/9004

Tanabe, K., and Takei, K. (2009). Dynamic Instability of Microtubules Requires Dynamin 2 and Is Impaired in a Charcot-Marie-Tooth Mutant. *J. Cel Biol.* 185, 939–948. doi:10.1083/jcb.200803153

Tassin, T. C., Barylko, B., Hedde, P. N., Chen, Y., Binns, D. D., James, N. G., et al. (2021). Gain-of-Function Properties of a Dynamin 2 Mutant Implicated in Charcot-Marie-Tooth Disease. *Front. Cel. Neurosci.* 15, 745940. doi:10.3389/fncel.2021.745940

Torre, E., McNiven, M. A., and Urrutia, R. (1994). Dynamin 1 Antisense Oligonucleotide Treatment Prevents Neurite Formation in Cultured Hippocampal Neurons. *J. Biol. Chem.* 269, 32411–32417. doi:10.1016/S0021-9258(18)31650-8

Vallis, Y., Wigge, P., Marks, B., Evans, P. R., and McMahon, H. T. (1999). Importance of the Pleckstrin Homology Domain of Dynamin in Clathrin-Mediated Endocytosis. *Curr. Biol.* 9, 257–263. doi:10.1016/s0960-9822(99)80114-6

Warnock, D. E., Baba, T., and Schmid, S. L. (1997). Ubiquitously Expressed Dynamin-II Has a Higher Intrinsic GTPase Activity and a Greater Propensity for Self-Assembly Than Neuronal Dynamin-I. *Mol. Biol. Cel.* 8, 2553–2562. doi:10.1091/mbc.8.12.2553

Wu, H., and Parsons, J. T. (1993). Cortactin, an 80/85-kilodalton Pp60src Substrate, Is a Filamentous Actin-Binding Protein Enriched in the Cell Cortex. *J. Cel Biol.* 120, 1417–1426. doi:10.1083/jcb.120.6.1417

Yamada, H., Abe, T., Satoh, A., Okazaki, N., Tago, S., Kobayashi, K., et al. (2013). Stabilization of Actin Bundles by a Dynamin 1/Cortactin Ring Complex Is Necessary for Growth Cone Filopodia. *J. Neurosci.* 33, 4514–4526. doi:10.1523/JNEUROSCI.2762-12.2013

Yamada, H., Kobayashi, K., Zhang, Y., Takeda, T., and Takei, K. (2016b). Expression of a Dynamin 2 Mutant Associated with Charcot-Marie-Tooth Disease Leads to Aberrant Actin Dynamics and Lamellipodia Formation. *Neurosci. Lett.* 628, 179–185. doi:10.1016/j.neulet.2016.06.030

Yamada, H., Takeda, T., Michiue, H., Abe, T., and Takei, K. (2016a). Actin Bundling by Dynamin 2 and Cortactin Is Implicated in Cell Migration by Stabilizing Filopodia in Human Non-Small Cell Lung Carcinoma Cells. *Int. J. Oncol.* 49, 877–886. doi:10.3892/ijo.2016.3592

Zhang, R., Lee, D. M., Jimah, J. R., Gerassimov, N., Yang, C., Kim, S., et al. (2020). Dynamin Regulates the Dynamics and Mechanical Strength of the Actin Cytoskeleton as a Multifilament Actin-Bundling Protein. *Nat. Cel Biol.* 22, 674–688. doi:10.1038/s41556-020-0519-7

Züchner, S., Noureddine, M., Kennerson, M., Verhoeven, K., Claeys, K., Jonghe, P. D., et al. (2005). Mutations in the Pleckstrin Homology Domain of Dynamin 2 Cause Dominant Intermediate Charcot-Marie-Tooth Disease. *Nat. Genet.* 37, 289–294. doi:10.1038/ng1514

Conflict of Interest: The authors declare that the research was conducted in the absence of any commercial or financial relationships that could be construed as a potential conflict of interest.

Publisher's Note: All claims expressed in this article are solely those of the authors and do not necessarily represent those of their affiliated organizations, or those of the publisher, the editors and the reviewers. Any product that may be evaluated in this article, or claim that may be made by its manufacturer, is not guaranteed or endorsed by the publisher.

frontiers | Frontiers in Cell and Developmental Biology

ORIGINAL RESEARCH
published: 16 May 2022
doi: 10.3389/fcell.2022.838086

The ShGlom*Assay* Combines High-Throughput Drug Screening With Downstream Analyses and Reveals the Protective Role of Vitamin D3 and Calcipotriol on Podocytes

*Marie-Christin Ristov[1], Tim Lange[1], Nadine Artelt[1], Neetika Nath[2], Andreas W. Kuss[3], Jochen Gehrig[4,5], Maja Lindenmeyer[6], Clemens D. Cohen[7], Sheraz Gul[8], Karlhans Endlich[1], Uwe Völker[3] and Nicole Endlich[1]**

[1]Institute of Anatomy and Cell Biology, University Medicine Greifswald, Greifswald, Germany, [2]Institute of Bioinformatics, University Medicine Greifswald, Greifswald, Germany, [3]Department of Functional Genomics, Interfaculty Institute for Genetics and Functional Genomics, University of Greifswald, Greifswald, Germany, [4]Acquifer Imaging GmbH, Heidelberg, Germany, [5]DITABIS, Digital Biomedical Imaging Systems AG, Pforzheim, Germany, [6]III Department of Medicine, University Medical Center Hamburg-Eppendorf, Hamburg, Germany, [7]Nephrological Center, Medical Clinic and Policlinic IV, University of Munich, Munich, Germany, [8]Fraunhofer Institute for Translational Medicine and Pharmacology, Fraunhofer Cluster of Excellence Immune-Mediated Diseases CIMD, Hamburg, Germany*

OPEN ACCESS

Edited by:
Mario Ollero, INSERM U955 Institut Mondor de Recherche Biomédicale (IMRB), France

Reviewed by:
Isha Sharma, Northwestern University Feinberg School of Medicine, United States
Jeffrey Kopp, National Institute of Diabetes and Digestive and Kidney Diseases (NIH), United States

***Correspondence:**
Nicole Endlich
nicole.endlich@uni-greifswald.de

Specialty section:
This article was submitted to Cell Death and Survival, a section of the journal Frontiers in Cell and Developmental Biology

Received: *17 December 2021*
Accepted: *13 April 2022*
Published: *16 May 2022*

Citation:
Ristov M-C, Lange T, Artelt N, Nath N, Kuss AW, Gehrig J, Lindenmeyer M, Cohen CD, Gul S, Endlich K, Völker U and Endlich N (2022) The ShGlomAssay Combines High-Throughput Drug Screening With Downstream Analyses and Reveals the Protective Role of Vitamin D3 and Calcipotriol on Podocytes. Front. Cell Dev. Biol. 10:838086. doi: 10.3389/fcell.2022.838086

Chronic kidney disease (CKD) is a major public health burden affecting more than 500 million people worldwide. Podocytopathies are the main cause for the majority of CKD cases due to pathogenic morphological as well as molecular biological alterations of postmitotic podocytes. Podocyte de-differentiation is associated with foot process effacement subsequently leading to proteinuria. Since currently no curative drugs are available, high throughput screening methods using a small number of animals are a promising and essential tool to identify potential drugs against CKD in the near future. Our study presents the implementation of the already established mouse Glom*Assay* as a semi-automated high-throughput screening method—shGlom*Assay*—allowing the analysis of several hundreds of FDA-verified compounds in combination with downstream pathway analysis like transcriptomic and proteomic analyses from the same samples, using a small number of animals. In an initial prescreening we have identified vitamin D3 and its analog calcipotriol to be protective on podocytes. Furthermore, by using RT-qPCR, Western blot, and RNA sequencing, we found that mRNA and protein expression of nephrin, the vitamin D receptor and specific podocyte markers were significantly up-regulated due to vitamin D3- and calcipotriol-treatment. In contrast, kidney injury markers were significantly down-regulated. Additionally, we found that vitamin D3 and calcipotriol have had neither influence on the expression of the miR-21 and miR-30a nor on miR-125a/b, a miRNA described to regulate the vitamin D receptor. In summary, we advanced the established mouse Glom*Assay* to a semi-automated high-throughput assay and combined it with downstream analysis techniques by using only a minimum number of animals. Hereby, we identified the vitamin D signaling pathway as podocyte protective and to be counteracting their de-differentiation.

Keywords: podocyte, CKD—chronic kidney disease, differentiation, glomerulus, screening, compound, vitamin D3

INTRODUCTION

With a prevalence of 10% in the Western world, chronic kidney disease (CKD) is a global public health burden (Bikbov et al., 2020). Diabetes mellitus and arterial hypertension constitute to the main risks for the development of CKD. In case of disease progression or when treated inadequately, it increases the risk for cardiovascular diseases and subsequently leads to the total loss of renal function and end-stage kidney disease (ESKD) (Levey et al., 2007; Collister et al., 2016). In 70% of all CKD cases podocytopathies and the associated impairment of the glomerular filtration barrier (GFB) are causal (Wiggins, 2007). The GFB consists of the fenestrated capillary endothelium, the glomerular basement membrane and the highly differentiated, postmitotic podocytes with their interdigitating foot processes. Adjacent foot processes form cell-cell contacts consisting of specific proteins, including nephrin (NPHS1), forming a size-selective slit diaphragm. Structural changes such as effacement of podocyte foot processes or alterations of slit diaphragm proteins like NPHS1 lead to the loss of the interdigitating pattern between the adjacent podocytes, resulting in proteinuria as an indicator of CKD progression (Bose et al., 2017). In most of these cases, podocyte de-differentiation is the major causal event (May et al., 2014).

Insufficient therapeutic approaches in the treatment of CKD and the underlying podocyte lesions, make dialysis and kidney transplantation inevitable for ESKD patients. This highlights the need for drugs, to expand the current treatment options for CKD patients, which in turn requires appropriate high-throughput screening methods (Feder et al., 2016; Bryer and Susztak, 2018).

Current strategies mostly rely on cell line based- or *in vivo* approaches. Most cell lines represent insufficient podocyte characteristics leading to results hardly translatable to clinical entities. Animal trials negotiate this but require large animal quantities making high-throughput approaches close to impossible (Lee et al., 2015; Bryer and Susztak, 2018).

To address this issue, we recently developed an *in situ* screening model using a transgenic mouse strain that expresses the cyan fluorescent protein (CFP) under the control of a *Nphs1* promoter fragment resulting in cyan fluorescent podocytes when *Nphs1* is expressed. *Nphs1* expression is known to be directly related to podocyte differentiation *in vivo* and spontaneously decreases over time in cultured podocytes (Schiwek et al., 2004; Agarwal et al., 2021). So the Glom*Assay* is using the fluorescence intensity of the isolated glomeruli as a read out for podocyte de-/differentiation over time and in the presence of specific compounds (Kindt et al., 2017). Since novel semi-automated imaging approaches and the related data processing progressed quickly over the last years, imaging based high-throughput screening procedures became more practicable.

In the past, studies have investigated vitamin D3 (vit D) and its complex spectrum of action on various organs, finding potential protective properties of this compound on kidney tissue. Besides its classical working modes as a regulator of calcium and phosphate metabolism, alternative biological signaling pathways of this metabolite have been investigated (Lehmann and Meurer, 2010). Recently, some tissue-protective mechanisms of vit D have been discovered. Even though Wang *et al.* provided experimental data showing that vit D in podocytes contributes to the protection of the kidney against diabetic injuries (Wang et al., 2012), it remains a subject of controversy and therefore further studies are necessary to reveal the role of vit D because it might be an option to treat specific kidney diseases.

Taken togehter, this study shows the application of the Glom*Assay* to a semi-automated high-throughput procedure in combination with downstream analysis techniques. This allows the screening of hundreds of potential drugs and the identification of specific pathways, like the vit D and calcipotriol pathway by using a minimum number of animals.

METHODS

Transgenic Mice

Transgenic *Nphs1*:CFP-mice (Wong et al., 2000; Cui et al., 2005) were used in the present study. The housing conditions of mice have been described previously (Kindt et al., 2017). Mice at the age of 6 months were used for experiments. All laboratory animal studies have been approved by local authorities (#A3936/3/1) and adhere to the National Institute of Health's guidelines for the care and use of laboratory animals. All experiments have been carried out in accordance with national animal welfare guidelines (Kilkenny et al., 2010; McGrath and Lilley, 2015).

Glomeruli Isolation and Culture

Glomeruli were isolated as previously described (Kindt et al., 2017). 96-well plates (Greiner Bio-One GmbH, Frickenhausen, Germany) were coated with collagen IV (Corning, New York, United States) and glomeruli were grown with phenol red-free RPMI-1640 medium supplemented with 10% FBS (both Thermo Fisher Scientific, Waltham, MA, United States) at 37°C and 5% CO^2. To prevent glomeruli from drying but still ensure gas exchange, we used adhesive Seals (4titude Ltd., Berlin, Germany). Glomerular viability was verified by propidium iodide (Merck KGaA, Darmstadt, Germany) staining performed after manufacturer's instructions.

Pharmacological Treatment

The isolated glomeruli were treated with the following substances and final concentrations in the corresponding well throughout all experiments. DMSO (Merck KGaA, 0.1%, dissolved in phenol red-free RPMI-1640 medium with 10% FBS) was used as control-treatment, vit D (100 nM, Santa Cruz Biotechnology, Heidelberg, Germany, dissolved in 0.1% DMSO) and calcipotriol (1 µM MedChemExpress, Monmouth Junction, NJ 08852, United States, dissolved in 0.1% DMSO). All treatments were performed on glomeruli of the same mouse. The vit D concentrations are orientated on the Institute of Medicine (IOM) (Ross et al., 2011).

Imaging and Fluorescence Quantification

The Acquifer Imaging Machine (IM, DITABIS, Pforzheim, Germany) was used to measure the fluorescence intensity of glomeruli in 96-well plates. In order to estimate the filling density of glomeruli, overview images were taken with a 2x objective

without autofocus. Subsequently, four sub-positions per well were determined avoiding overlapping to exclude double-measurements. Sub-positioning is illustrated in **Supplementary Figure S1**. Afterwards, 16z-slices with a height of 10 µm per sub-position per well were applied. To quantify fluorescence reporter activity within glomeruli, acquired z-stacks were batch maximum projected using a custom written Perl script in combination with Fiji open-source software (available upon request, DITABIS). Maximum projections of one experimental folder were loaded into a z-stack in Fiji. Each z-slice was duplicated and thresholded using the Triangle method. The area, mean intensity, minimum intensity and the integrated intensity were then measured within the masked region of the original image (**Supplementary Figure S1**). Imaging was performed after 3-, 6- and 9 days past isolation and treatment. These time points have previously been shown to resemble a mild, moderate and strong phenotype, respectively (Kindt et al., 2017).

RT-PCR

For RNA isolation the glomeruli were cultured for 9 days in 6 well plates (SARSTEDT AG & Co. KG, Nümbrecht, Germany) and treated with DMSO 0.1%, vit D 100 nM and calcipotriol 1 µM. Glomeruli were washed twice with PBS prior to RNA isolation. The RNA isolation was performed with TRI-reagent (Merck KGaA) according to manufacturer's protocol. The isolated RNA was measured using a photometer (Eppendorf AG, Hamburg, Germany). The Reverse Transcription Kit (Qiagen, Hilden, Germany) was used to synthesize cDNA from equal amounts of denaturated RNA and ranged from 700 ng to 1 µg. Negative controls included no-template and no-reverse-transcriptase controls. RT-PCR was performed on the Mastercycler gradient (Eppendorf AG) by using 10x DreamTaq Green Buffer and DreamTaq DNA Polymerase (both Thermo Fisher Scientific). For RT-qPCR we used iTaq Universal SYBR Green Supermix and Thermal Cycler iQ5 Multicolor Real-Time PCR Detection System (both Bio-Rad Laboratories GmbH, München, Germany). The following primers were used: mouse *Nphs1*, CFP, and Actb as previously described (Kindt et al., 2017); mouse *Vdr*, forward 5′-TCC GGA GAC TCC TCC TCA AA-3′, reverse 5′-AAA AGA CTG GTT GGA GCG CA-3′, 300 bp product size and mouse *Rxra*, forward 5′- CTC AAT GGC GTC CTC AAG GT-3, reverse 5′-AGG CAG TCC TTG TTG TCT CG-3′, 197 bp product size (both Thermo Fisher Scientific). Ct-values were calculated by the Thermal Cycler iQ5 Multicolor Real-Time PCR Detection System with automatically set thresholds and baselines. Raw Ct-values were normalized against ß-actin as endogenous reference gene and the day 0 control by the ΔΔCt-method. Samples with raw Ct-values ≥38 were excluded from the analysis.

Taqman RT-qPCR

cDNA was synthesized from 10 ng total RNA using Taqman miRNA Assays and the Taqman miRNA Reverse Transcription Kit (Thermo Fisher Scientific). The following Taqman miRNA Assays were used: Hsa-miR-30a-5p: ID #000417; Hsa-miR-21-5p: ID #000397; Hsa-miR-125a-5p: ID #002198; Hsa-miR-125b-5p: ID #000449. RT-reactions were performed after manufacturer's instructions. Negative controls included no template and no reverse transcriptase controls. The qPCR was performed with the Taqman miRNA Assays described above and the Taqman Universal Master Mix II, no UNG (Thermo Fisher Scientific) following the manufacturer's instructions. The reaction volumes contained 1.33 µL undiluted cDNA solution and 18.67 µL Master Mix. The qPCR was performed on the Thermal Cycler iQ5 Multicolor Real-Time PCR Detection System with the following cycler scheme: 10 min at 95°C followed by 45 cycles of 15 s at 95°C and 60 s at 60°C. All samples were run in triplicate. Negative controls included the ones from cDNA synthesis and an extra no template control for the qPCR reaction. Standard curves with standard cDNA samples were used for efficiency determination of every single Taqman miRNA Assay. Ct-values were calculated by the Thermal Cycler iQ5 Multicolor Real-Time PCR Detection System with automatically set thresholds and baselines. Raw Ct-values ≥38 were excluded from analysis. All Ct-values were normalized against day 0 controls and against U6 snRNA as endogenous reference gene by the ΔΔCt-method.

Preparation of Protein Samples

Proteins were isolated from the same samples as the RNA. DNA and protein precipitation were performed using TRI-Reagent (Merck KGaA) according to the manufacturer's protocol with minor changes: the protein pellet was air-dried and dissolved in 8 M thiourea/2 M urea (Merck KGaA) on a shaker (Eppendorf AG, Hamburg, Germany). Afterwards the dissolved pellet was centrifuged at 10,000 × g for 10 min at 4°C to remove insoluble material. The amount of protein was determined using the Bradford Assay (SERVA Electrophoresis GmbH, Heidelberg, Germany).

Western Blots

The Western blots with the corresponding antibodies were performed as described before with some changes: TBST (0.1%) and Clarity Western ECL substrates (Bio-Rad Laboratories GmbH) were used. Blots were stripped for usage of alternative antibodies on the same blot (10). The following antibodies were used as previously described (10): guinea pig anti-NPHS1; mouse anti-CFP; rabbit anti-GAPDH; goat anti-guinea pig; goat anti-mouse; goat anti-rabbit; rabbit anti-VDR (1: 1000, Cell Signaling Technology, Frankfurt am Main, Germany #12550) and rabbit anti-RXRa (1:500, Cell Signaling Technology #3085). Samples were run in Stain-free TGX gels and quantified with Criterion Stain Free Imager (SFI, Bio-Rad Laboratories GmbH). Whole lane intensities were quantified using Fiji. Specific band intensities were quantified using Fiji and target bands were normalized against GAPDH and whole lane intensities. Ratios of vit D-/calcipotriol-treated, normalized intensities against control-treated, normalized intensities were calculated.

RNA Sequencing

RNA sequencing (RNA_Seq) was performed with glomeruli cultured in 6-well plates for 6 days after treatment with vit D 100 nM and DMSO 0.1%. The RNA isolation was performed as

previously described (Kindt et al., 2017). RNA integrity was visualized using an Agilent Bioanalyzer 2100. Before library preparation, 1 μg total RNA was spiked with ERCC (Thermo Fisher Scientific). Subsequently the ribosomal RNA was digested and removed, using a RiboMinus kit (Thermo Fisher Scientific) according to the instructions of the manufacturer. The RNA was then fragmented, barcoded and prepared for sequencing following the TruSeq Stranded Total RNA protocol (Illumina, San Diego, CA, United States). Thus, obtained sequencing libraries were analysed on an Illumina NextSeq machine, using the NextSeq 500/550 High Output Kit v2 (150 cycles, paired end) chemistry (Illumina). For bioinformatic data analysis we performed quality assessments using FASTQC format. This was followed by application of the Trimmomatic package (read trimming tool; (Bolger et al., 2014). With the latter, the following steps were performed: Remove leading low quality or N bases below quality 3 (LEADING:3)—Remove trailing low quality below quality 3 (TRAILING:3)—Scan the read with a 4-base wide sliding window, cutting when the average quality per base drops below 15 (SLIDINGWINDOW:4:15). TopHat (Kim et al., 2013) was used for alignment against the mouse reference genome (mm10). Read counts were determined using R (R Core Team, 2018) DESeq2 (Love et al., 2014) and the transcripts were annotated using AnnotationDbi Bioconductor packages. We thus obtained between 149 × 106 and 168 × 106 reads per sample and the percentage of mapped reads ranged between 94.4 and 95.6 per cent. Gene ontology classification was performed with Panther 16.0 (Mi et al., 2021).

Microarrays on Human Kidney Biopsies

Biopsies were obtained from patients after informed consent and with approval of the local ethics committees and Affymetrix expression microarrays were performed within the scope of the European Renal cDNA Bank—Kröner-Fresenius Biopsy Bank (Cohen et al., 2002; Martini et al., 2014). Following renal biopsy, the tissue was transferred to RNase inhibitor and micro-dissected into glomeruli and tubulointerstitium. As previously reported (Cohen et al., 2006), total RNA was extracted from micro-dissected glomeruli, followed by reverse transcription and linear amplification. In the present study we used published glomerular expression data of patients with from focal segmental glomerulosclerosis (FSGS, n = 23), diabetic nephropathy (DN, n = 14) and minimal change disease (MCD, n = 14). Kidney biopsies from living donors prior to transplantation (LD, n = 42) were used as control (GSE99340, GSE37463, GSE47185, GSE32591). CEL file normalization was performed with the Robust Multichip Average method using RMAExpress (Version 1.0.5) and the human Entrez-Gene custom CDF annotation from Brain Array version 18. The log-transformed dataset was corrected for batch effect using ComBat from the GenePattern pipeline (http://www.broadinstitute.org/cancer/software/genepattern/). To identify differentially expressed genes the SAM (Significance Analysis of Microarrays) method was applied using TiGR (MeV, Version 4.8.1) (Tusher et al., 2001). A q value below 0.05 was considered to be statistically significant.

Statistics

Statistical analyses were performed by using IBM SPSS Statistics 22.0 (SSPS Inc., Chicago, IL, United States). All data are presented by mean ± SD and statistical significance was determined by one-way ANOVA and *post-hoc* Bonferroni. p-values <0.05 were considered as statistically significant.

RESULTS

Application of the Glom*Assay* to a Semi-Automated and High-Throughput Assay

To increase the number of compounds to be screened simultaneously, we adapted the Glom*Assay* (Kindt et al., 2017) from a 15-well to a 96-well plate format. This was achieved by the optimization of image acquisition which was converted from manual confocal microscopy to a semi-automated approach using the Imaging Machine (IM) from Acquifer. Here manual z-stack acquisition is replaced by automated, script-based autofocusing followed by 16-slice z-stack acquisition. Furthermore, we also adapted the manual imaging data analysis and evaluation to a semi-automated Fiji-based approach. By using this assay, we could increase the sample and compound number, lower the number of animals needed to 2–3 mice per plate as well as the manual workload and working time to decrease experimental bias.

Identification of Vit D and Calcipotriol as a Potential Protective Drugs

By using the workflow described before, we measured an increase of the CFP fluorescence after vit D and calcipotriol in an incubation time dependent way. Starting on day 3, the difference in fluorescence intensity between vit D- and DMSO-treated podocytes was 30% (p = 0.008). On day 6, this difference increased to 42% (p <0.000) and on day 9, CFP fluorescence was 38% more intense for vit D-treated glomeruli compared to DMSO-treatment (p <0.001; **Figures 1**,**2**). The difference in fluorescence intensity between calcipotriol-treated glomeruli and DMSO was significant and amounts to 29% on day 3 (p = 0.015) and 44% on day 6 (p <0.001; **Figures 1**,**2**). On day 9, CFP fluorescence was 40% more intense after calcipotriol-treatment compared to DMSO-treated samples (p <0.000; **Figures 1**,**2**).

Vit D- and Calcipotriol-Treatment Increase the mRNA Expression of *Nphs1* and CFP

To verify the effect of vit D and calcipotriol obtained by IM, we determined the mRNA levels by RT-qPCR (**Figures 3B,C,E,G**) and by RT-PCR (**Figures 3A,D,F**).

By treating the podocytes with vit D, the mRNA levels of *Nphs1* were significantly increased compared to the DMSO control (p = 0.039). The treatment with calcipotriol also showed increased expression levels, but these were not in the significant range (p = 0.575; **Figures 3A,B**).

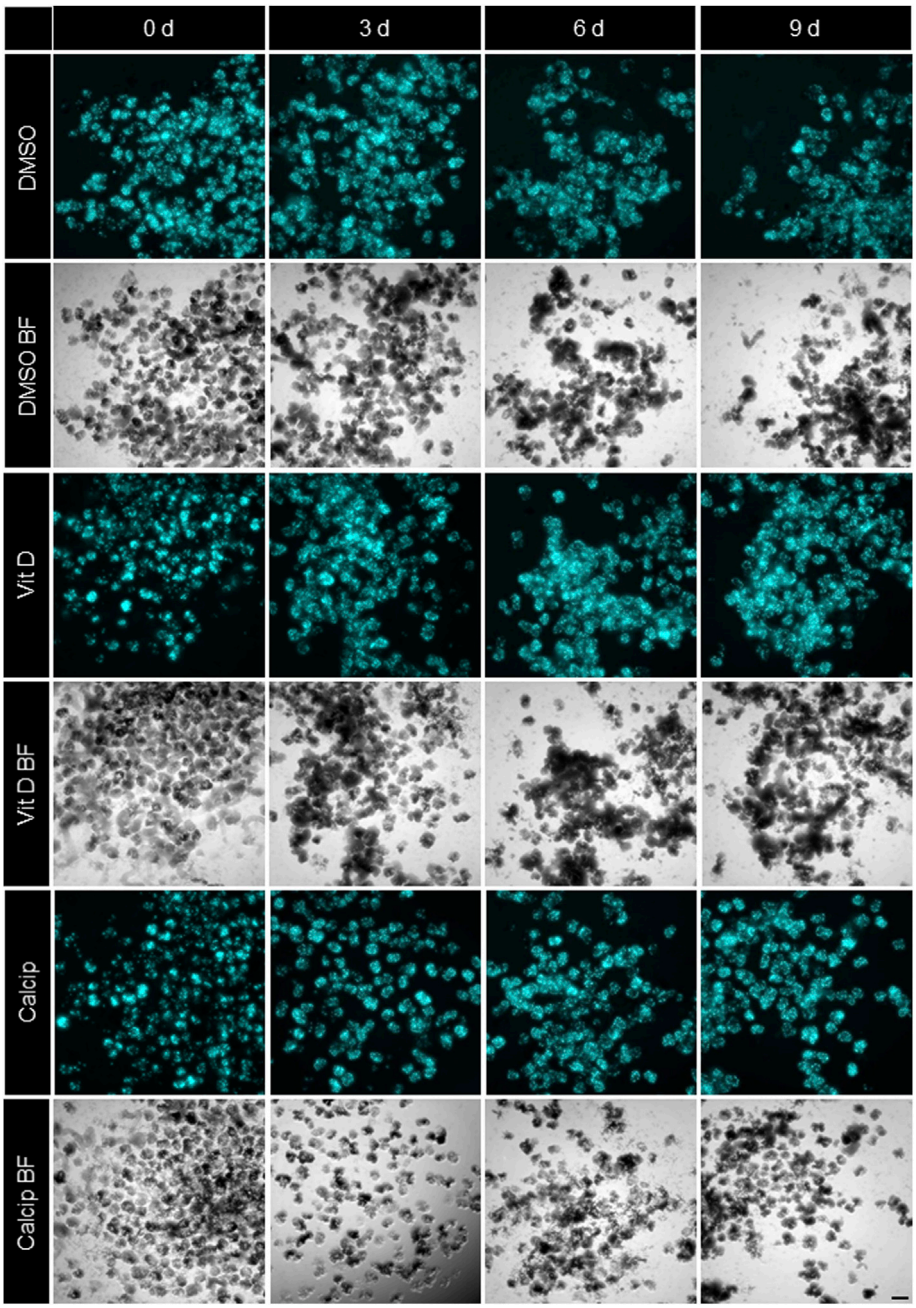

FIGURE 1 | Treatment of isolated glomeruli with vit D and calcipotriol leads to increased CFP fluorescence intensity. Representative Imaging Machine images of cultured glomeruli show different CFP (cyan) fluorescence intensities depending on the treatment. Treatment with vit D 100 nM, 1 μM calcipotriol and 0.1% DMSO. Vit D = vitamin D, calcip = calcipotriol, BF = Brightfield, d = days. Scale bar represents 100 μm. (n = 3)

The mRNA levels of CFP were significantly increased compared to DMSO in both vit D- (p = 0.001) and calcipotriol-treatment (p = 0.012; **Figures 3A,C**).

In order to obtain further information on the underlying signaling pathway, we also determined the mRNA levels of *Vdr* and its nuclear interaction partner *Rxra* by RT-qPCR (**Figures 3D–G**). Both receptors showed no significant differences on the mRNA level between vit D-, calcipotriol- and DMSO-treated glomeruli (**Figures 3E,G**).

Increased Expression Levels of VDR After Treatment of Glomeruli With Vit D or Calcipotriol

To verify the effect of vit D and calcipotriol on the protein level, we also applied Western blot analysis. Data were normalized against GAPDH and against the total protein load. Both normalization methods are shown in **Figures 4A–H**.

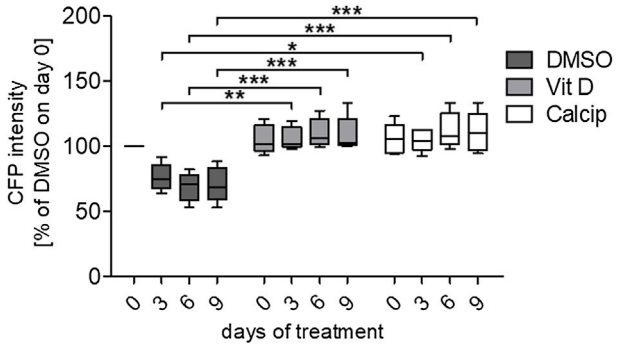

FIGURE 2 | Quantification of the relative CFP intensity after vit D- and calcipotriol-treatment. Vit D- and calcipotriol-treated glomeruli exhibit an enhanced relative CFP intensity compared to DMSO controls. Treatment with vit D 100 nM, 1 μM calcipotriol and 0.1% DMSO. Values presented are medians + Min/Max. *p <0.05; **p <0.01; ***p <0.001. Vit D = vitamin D, calcip = calcipotriol. (n = 5)

The protein expression of CFP was significantly increased after the treatment with vit D compared to DMSO (GAPDH p = 0.007; SFI p = 0.043), regardless of the normalization method (**Figures 4C,D**).

A similar effect was observed for NPHS1 (GAPDH p <0.001; SFI p = 0.002; **Figures 4A,B**) by the treatment of glomeruli with vit D. A treatment of glomeruli with calcipotriol resulted in an increase of CFP expression compared to DMSO, although this effect was only significant when normalized with SFI (p = 0.004; **Figure 4D**). NPHS1 showed a significant increase in protein expression by calcipotriol compared to DMSO, regardless of the normalization method (GAPDH p = 0.002; SFI p = 0.013; **Figure 4B**).

Protein expression levels of RXRa were similar to the mRNA levels. There were no significant differences in the protein levels between vit D and DMSO and between calcipotriol and DMSO independent of the normalization method (**Figures 4E,F**).

On the other hand, protein levels and mRNA levels differed strongly regarding *Vdr*. The protein expression of VDR was significantly increased after the treatment with vit D (GAPDH p <0.001; SFI p <0.001) and calcipotriol (GAPDH p = 0.006; SFI p <0.001) compared to DMSO, regardless of normalization (**Figures 4G,H**). Furthermore, VDR was the only of the 4 tested targets where the protein expression was significantly increased after 9 days of treatment with vit D and calcipotriol compared to day 0 (**Figure 4H**). The significance of this effect was independent of the chosen normalization method for vit D-treatment (GAPDH p = 0.009; SFI p = 0.007) and depended on the chosen normalization method for the treatment with calcipotriol (GAPDH p = 0.573; SFI p <0.001; **Figure 4H**).

Regulated Expression Levels of miRNA-30a, -21, -125a, -125b

To analyze the expression of miR-30a, -21, -125a, -125b in podocyte de-differentiation and to observe the effect of vit D on the expression of these miRs, we measured their expression levels in freshly isolated

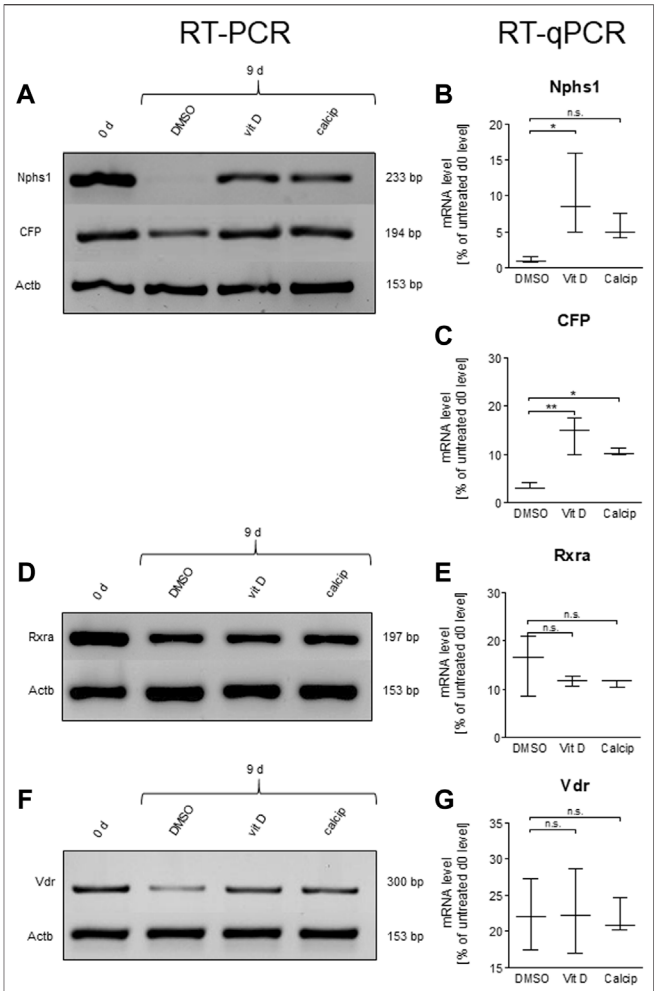

FIGURE 3 | Vit D and calcipotriol increase *Nphs1* and CFP mRNA levels. **(A,D,F)** Representative RT-PCR for *Nphs1*, CFP, *Rxra* and *Vdr* in vit D- and calcipotriol-treated mouse glomeruli after 9 days and untreated glomeruli on day 0. **(B,C,E,G)** Quantification of mRNA levels by RT-qPCR. The mRNA levels of *Nphs1* and CFP are significantly increased by the treatment with vit D (100 nM) and calcipotriol (1 μM) compared to DMSO (0.1%). Values are presented as medians + Min/Max. *p <0.05; **p <0.01; ***p <0.001. Vit D = vitamin D, calcip = calcipotriol. (n = 3).

(day 0) and 9 days cultured glomeruli that were treated with vit D, calcipotriol as well as DMSO (control) by RT-qPCR. MiR-21 was up-regulated after 9 days cultivation under control (13.9-fold, p = 0.006), vit D- (14.9-fold, p = 0.024) and calcipotriol-treatment (19.2-fold, p = 0.011). MiR-30a was down-regulated after 9 days cultivation under control conditions (0.1-fold, p <0.001), vit D (0.2-fold, p <0.001) and calcipotriol (0.2-fold, p <0.001). In contrast, miR-125a was up-regulated after the treatment with DMSO (1.6-fold, p = 0.025), vit D (1.2-fold, p = 0.257) and calcipotriol (1.3-fold, p = 0.244) for 9 days. MiR-125b was also up-regulated after a treatment with DMSO (6.8-fold, p <0.000), vit D and calcipotriol (5.6-fold, p = 0.018; 6.4-fold, p = 0.010, respectively) for 9 days. We could not detect any significant differences between the treatment groups at 9 days (**Figure 5**).

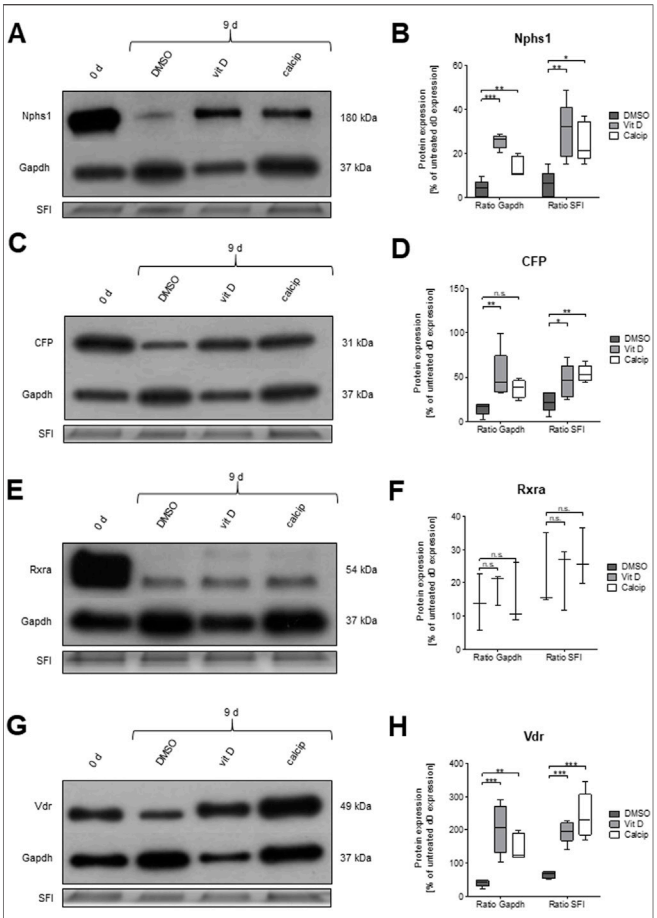

FIGURE 4 | Treatment of glomeruli with vit D and calcipotriol leads to increased protein levels of NPHS1, CFP and VDR after 9 days. **(A,C,E,G)** Representative Western blots for NPHS1, CFP, RXRa, and VDR in vit D- and calcipotriol-treated mouse glomeruli after 9 days and untreated glomeruli on day 0. **(B,D,F,H)** Quantification of Western blot lanes. The protein expression of NPHS1, CFP, and VDR is significantly increased after treatment with vit D and calcipotriol compared to DMSO. Treatment was done with 100 nM vit D, 1 μM calcipotriol, and 0.1% DMSO. Values are presented as medians + Min/Max. *p <0.05; **p <0.01; ***p <0.001. Vit D = vitamin D, calcip = calcipotriol, SFI = Stain Free Imager. (n = 5, 5, 3, 5).

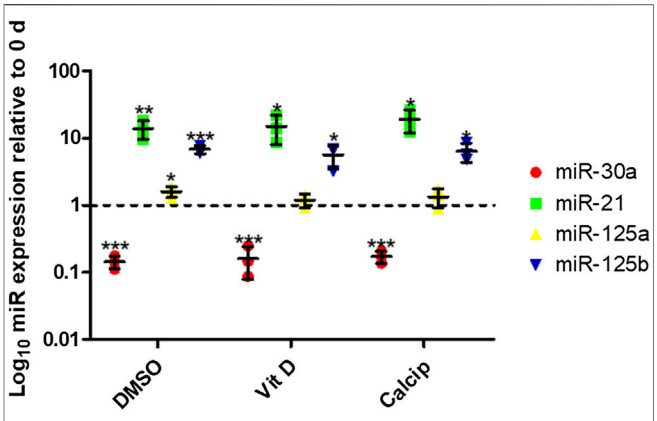

FIGURE 5 | Treatment with vit D and calcipotriol has no effect on specific miR-expression after de-differentiation. After 9 days de-differentiation, miR-30a is down-regulated, while miR-21, miR-125a, and miR-125b are up-regulated. Vit D and calcipotriol showed no significant effect. Treatment with 100 nM vit D, 1 μM calcipotriol, and 0.1% DMSO. Values are presented as $\log_{10}$ mean expression (±SD) of each miRNA relative to day 0-controls. *p <0.05; **p <0.01; ***p <0.001. Vit D = vitamin D, calcip = calcipotriol, 0 days = day 0. (n = 3)

RNA_Seq Reveals an Up-Regulation of Podocyte-Specific Genes

As no differences between vit D- and calcipotriol-treated glomeruli could be detected, we performed RNA_Seq only with vit D-treated glomeruli after 6 days in culture. The raw reads were normalized against the geometric mean and normalized against DMSO-treatment at 6 days. After Benjamini–Hochberg correction, we obtained 113 significantly differentially expressed genes. Data distribution is displayed as Volcano plot and MA plot (**Supplementary Figure S2**). We identified 45 significantly up-regulated and 68 significantly down-regulated genes. Amongst the most up-regulated genes, podocyte-specific markers like *Nphs1*, *Kirrel2* and *Tcf21* were found. We could also find genes involved in epithelial cell differentiation, actin cytoskeleton and extracellular matrix organization (**Figure 6**). Furthermore, we identified disease markers such as *CD163* and *Mmp9* as well as inflammatory and immune cell markers such as *Gatm*, *Clec10a*, *Stab1,* and *Fcna* as the most down-regulated genes. All significantly regulated genes are shown in **Supplementary Table S1**.

Microarrays on Human Kidney Biopsies

Next, we tested for gene expression alteration in glomerular disease for genes found to be regulated by treatment with vit D and calcipotriol. Microarray data of micro-dissected glomeruli of biopsies of patients with FSGS, DN, and MCD were analyzed. Genes known to be up-regulated by the treatment with vit D and calcipotriol in the shGlom*Assay* were found to be down-regulated in disease. For example, the slit diaphragm protein *Nphs1* and the cycline-dependent kinase inhibitor *Cdkn1c* are down-regulated in DN patients in contrast to the vit D-treated glomeruli. On the other hand, *Clec10a*, *Il21r*, *Cenpe*, *Cd163*, *Stab1,* and *Ccl8* which became down-regulated by vit D and calcipotriol, were up-regulated in FSGS and DN patients. Furthermore, the same regulation was found for the cytokine *Ccl8* (in MCD), *Siglec1* (in DN), *Cd38* (in DN-, MCD and FSGS) and *Pf4* (in FSGS) all of which were up-regulated in contrast to the vit D- and calcipotriol-treated glomeruli. We also identified genes that showed the same regulation direction compared to vit D-treated glomeruli like *Ifitm6*, *Kcnk3,* and *Hsd17b11* that were up-regulated in patients with DN and FSGS. *Plcb2* is up-regulated in DN patients only, whereas *Col3a* is up-regulated in all investigated glomerulopathies. *Nfatc2ip* and *Hdac1* are only up-regulated in FSGS patients. In contrast to this, there are only *Gatm* and *Igf1* that showed the same regulation as the vit D-treated glomeruli in patients with from FSGS, MCD, and DN and in FSGS and DN patients, respectively (**Figure 7**, **Supplementary Table S1**).

	Gene name	Fold change
Pro differentiation	Ccl8	0.40
	Igf1	0.62
	Ccr5	0.64
	Trf	0.65
	Aspm	0.67
	Col1a1	0.68
	Gas6	0.69
	Aurka	0.70
	Itgam	0.71
	Fam210b	0.71
	Runx1	0.75
	Zfp703	0.75
	Tnfrsf1b	0.76
	Por	0.79
	Nedd9	1.28
	Cebpd	1.35
	Dcn	1.36
	Net1	1.46
	Ifitm1	1.47
	Hdac1	1.52
	Gdpd5	1.64
Actin cytoskeleton	Arhgap25	0.66
	Diap3	0.69
	Cobl	0.70
	Zyx	0.73
	Plek	0.73
	Gas2l3	0.76
	Nedd9	1.28
	Pdlim2	1.40
Extracellular matrix organization	Mmp9	0.57
	Col1a1	0.68
	Aplp1	1.35
	Fbln2	1.51
	Col3a1	1.53
	Mmp8	2.48
Podocyte	Tcf21	1.40
	Kirrel2	1.67
	Nphs1	2.07
Epithelial cell differentiation	Igf1	0.62
	Hpse	0.69
	Sipa1l3	0.72
	Zfp703	0.75
	Tcf21	1.40
	Hdac1	1.52

FIGURE 6 | Gene clustering of the most regulated genes after RNA_Seq of vit D-treated glomeruli. Gene names and fold change of significantly regulated genes are shown. Gene clustering was performed using Panther 16.0. Treatment with vit D 100 nM and 0.1% DMSO, respectively. Red = significantly up-regulated genes, blue = significantly down-regulated genes.

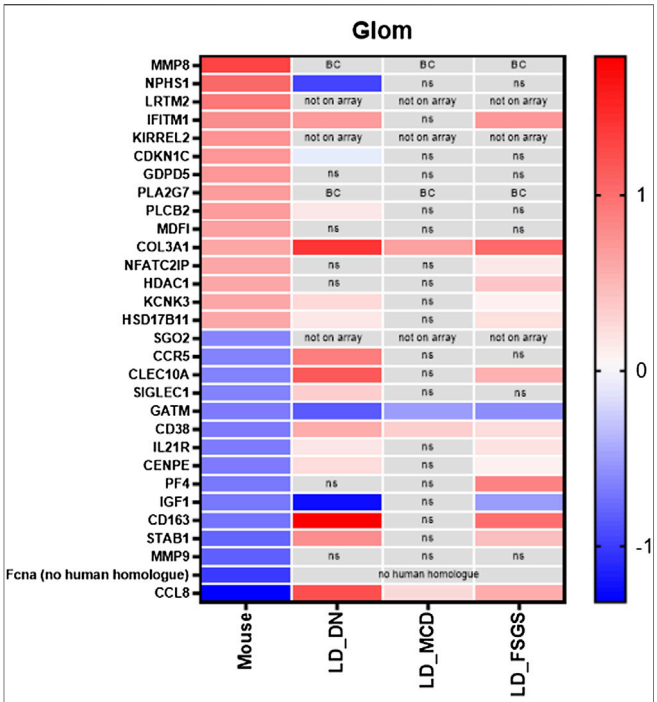

FIGURE 7 | Compilation of the 15 most up-regulated and down-regulated genes and their expression in patients with FSGS, DN and MCD compared to living donors. Data are represented as log fold change, a q-value <5% was considered as significant. Red: up-regulated compared to controls; blue: down-regulated compared to controls. ns: not significant; BC: below cutoff, LD = living donors.

DISCUSSION

Glomerulopathies are the main cause for the development of CKD. De-differentiation of podocytes is the leading mechanism and plays a key role in the development of various renal diseases such as diabetic glomerulopathy. Until today, there are no healing or protective drugs available. Therefore, great efforts must be made to identify chemical compounds and their signaling pathways that can stop and reverse this de-differentiation process, making screening models indispensable.

Our group has developed a screening model, the Glom*Assay*, using isolated glomeruli from transgenic *Nphs1*:CFP-mice to study the effect of pharmaceutical substances on podocyte differentiation *in situ*. This assay can be used to evaluate the effect of compounds on the interaction between podocytes, endothelial cells, and mesangial cells, resembling the *in vivo* situation better than permanent podocyte cell lines (Kindt et al., 2017).

Since we wanted to increase the number of drugs that could be screened simultaneously, we further developed the Glom*Assay* by the use of a semi-automated imaging machine. To address this, we have established a semi-quantitative and high-throughput screening platform (shGlom*Assay*). The shGlom*Assay* screening platform bridges the gap between the use of immortalized podocyte cell lines (Yamauchi et al., 2006) and whole animal experiments. This is a major step forward because, on the one

hand, currently available podocyte cell lines are hardly comparable with podocytes *in vivo* and *in situ*. The expression of podocyte-specific proteins like TCF21 and NPHS1 is either completely lost or severely reduced in theses cell lines, the morphology of these podocytes is completely different to *in vivo* podocytes and the matrix composition, which has an important influence on podocyte differentiation, is not comparable (Agarwal et al., 2021). On the other hand, especially rodent models require a high number of animals, aggravating applicability due to the high time requirements, animal right restrictions, ethical issues and readout systems.

In contrast to this, the shGlom*Assay* allows the analysis of a huge variety of different compounds on podocyte differentiation by combining the advantages of *in vitro* and *in vivo* models (Kindt et al., 2017).

Our screening by the shGlom*Assay* identified a podocyte protective effect of vit D, a compound whose effect on podocytes has been controversially discussed in the past. Besides its role in calcium and phosphate metabolism, renoprotective properties of vit D have been found in previous work (Wang et al., 2012). However, high vit D levels are also thought to be associated with severe kidney damage and even kidney failure, which is often related to genetic polymorphisms (Tripathi et al., 2010; Kramer, 2015; Wani et al., 2016).

By using the *s*hGlom*Assay*, we observed that the podocyte-specific CFP fluorescence, driven by the *Nphs1* promoter, is significantly increased after treatment with vit D as well as its analogue calcipotriol compared to controls. This indicates that vit D as well as calcipotriol strongly up-regulate the *Nphs1* expression of *in situ* podocytes. This is in agreement with the observation of Shi et al. showing that the treatment of spontaneously hypertensive rats with vit D resulted in a decrease of proteinuria, increase of serum albumin, as well as a reduction of podocyte injury compared to untreated rats (Shi et al., 2018). Here in our shGlom*Assay*, we could show that the mRNA and protein levels of CFP and *Nphs1* increased simultaneously by the treatment with vit D and calcipotriol. Although *Nphs1* mRNA levels were not significantly increased after calcipotriol-treatment, they showed a clear trend towards up-regulation. This was also confirmed by the significantly increased protein levels in Western blot analysis. In a diabetic rat model, it was demonstrated that the glucose-mediated down-regulation of *Nphs1* could be ameliorated by treatment with a vit D analogue (Trohatou et al., 2017). We could show that the difference in CFP expression reflects NPHS1 expression making the shGlom*Assay* an ideal model for drug screening. It was further shown in animal models as well as in patients that NPHS1 is an essential slit diaphragm protein which is compromised during de-differentiation. A sufficient expression of this specific protein is necessary to maintain the complex podocyte morphology and function of the GFB (Patrakka and Tryggvason, 2007). Putaala and coworkers generated *Nphs1*-deficient mice which died within 24 h after birth and they showed electron microscopically effaced podocytes (Putaala et al., 2001). Gene mutations of *Nphs1* are also associated with missing slit diaphragms and proteinuria (Patrakka et al., 2000). Since impaired *Nphs1* expression is closely related to the development of CKD, it was important to further investigate the regulatory mechanisms of this protein. Deb and coworkers have already demonstrated that vit D influences *Nphs1* expression by acting on a vit D response element in the proximal *Nphs1* promoter (Deb et al., 2011). This effect may indicate that the de-differentiation of vit D- and calcipotriol-treated podocytes progresses more slowly as compared to controls. This is important and supported by the RNA_Seq data of the glomeruli in the shGlom*Assay* showing an up-regulation of podocyte genes like *Nphs1*, *Kirrel2*, *Tcf21,* and *Mmp8* and a down-regulation of genes that are involved in inflammation and fibrosis after vit D-treatment (**Supplementary Table S1**). Additionally, we found that vit D-treated glomeruli showed adverse regulation of genes that are involved in kidney diseases which was revealed by microarrays of FSGS, DN, and MCD patients (**Supplementary Table S1**).

Since it is published that vit D binds to the *Vdr* and the *Vdr*/*Rxra* heterodimer, we studied the expression of these receptors under our shGlom*Assay* conditions (Christakos et al., 2016). We observed a significant increase of *Vdr* due to the treatment of vit D as well as calcipotriol, which is in agreement with the results received from spontaneously hypertensive rats (Shi et al., 2018).

While *Vdr* is regulated by the treatment with vit D and calcipotriol, surprisingly, no changes in the *Rxra* expression was observed. This suggested an involvement of another unknown protein in the vit D signaling pathway. Since Okamura and colleagues have shown that vit D-induced *Nphs1* expression can be the result of the interaction of the retinoic acid receptor (*Rara*) and *Vdr* in a *Rxra*-independent way (Okamura et al., 2009), we explored this in our study. However, RNA_Seq data have shown that there is no significant regulation for both receptors.

Recently, miRNAs have been shown to play a pivotal role in podocyte homeostasis and in vit D signaling which underlies a complex regulatory network. In the present study, we selected two miRNAs known as typical kidney injury biomarkers. First of all, miR-30a is known to be down-regulated in de-differentiated podocytes and in kidney diseases (Wu et al., 2014). Here in our shGlom*Assay*, we also found a significant down-regulation of miR-30a after 9 days. In contrast, miR-21, described to be a kidney injury marker (Peters et al., 2020) and up-regulated in urinary exosomes of kidney patients (Lange et al., 2019), was also significantly up-regulation in the shGlom*Assay*.

Other miRs, like miR-125a and miR-125b which are known to target *Vdr* (Zenata and Vrzal, 2017), were found to be regulated in our model. Our experiments show that miR-125b, which seems to have a higher impact on *Vdr* translation than miR-125a (Zenata and Vrzal, 2017), was up-regulated in our shGlom*Assay* already under control conditions. However, vit D-treatment had no effect on the expression of miR-30a, miR-21, miR-125a and miR-125b which was surprising because miR-125b has previously been described to regulate the *Vdr* as well as Cyp24a1, a vit D inactivator (40) and is itself regulated by vit D (Giangreco et al., 2013).

In summary, we have shown that our previously described Glom*Assay* can be adapted to a high throughput compound screening model identifying compounds that are important for

podocyte differentiation. We also confirmed the protective effect of vit D and calcipotriol in our model and identified new target genes involved in this signaling pathway.

DATA AVAILABILITY STATEMENT

The datasets presented in this study can be found in online repositories. The names of the repository/repositories and accession number(s) can be found below: Zenodo; doi: 10.5281/zenodo.6358568.

ETHICS STATEMENT

The animal study was reviewed and approved by the National Institute of Health's guidelines for the care and use of laboratory animals.

AUTHOR CONTRIBUTIONS

Project planning was conducted by NE, TL, and M-CR. The manuscript was written by M-CR, TL, and NE. The Figures were designed by M-CR, TL, and ML. M-CR performed mouse glomeruli isolations. M-CR performed Acquifer imaging machine experiments and data analysis. The Fiji analysis script was designed by JG, M-CR, and TL performed RT-(q)PCR and Western blot experiments. TL performed miRNA experiments and statistical analysis. Glomeruli isolations for RNA_Seq were performed by NA. RNA_Seq and corresponding data analysis was performed by NN and AK. Library planning and composition was done by SG, ML, and CC handled and analyzed human biopsies and corresponding data. NE, KE, and UV supervised the project and have proofread the manuscript. The manuscript is approved by all authors.

FUNDING

This work was supported by a grant of the Federal Ministry of Education and Research (BMBF grant 01GM1518B TP2, STOP-FSGS) and EFR GHS-200-032 to NE, CC, and ML are supported by the Else Kröner-Fresenius Foundation. The present study was also supported by the Dr. Büchtemann Stiftung and the Südmeyer Stiftung.

ACKNOWLEDGMENTS

The authors thank Claudia Weber, Mandy Weise and Oliver Zabel for technical assistance. We thank all participating centers of the European Renal cDNA Bank–Kröner-Fresenius Biopsy Bank (ERCB-KFB) and their patients for their cooperation. Active members at the time of the study are listed in ref. (Martini et al. JASN 2014; Vol 25, No 11, 2559–2572).

SUPPLEMENTARY MATERIAL

The Supplementary Material for this article can be found online at: https://www.frontiersin.org/articles/10.3389/fcell.2022.838086/full#supplementary-material

REFERENCES

Agarwal, S., Sudhini, Y. R., Reiser, J., and Altintas, M. M. (2021). From Infancy to Fancy: A Glimpse into the Evolutionary Journey of Podocytes in Culture. *Kidney360* 2, 385–397. doi:10.34067/KID.0006492020

Bikbov, B., Purcell, C. A., Levey, A. S., Smith, M., Abdoli, A., Abebe, M., et al. (2020). Global, Regional, and National burden of Chronic Kidney Disease, 1990-2017: a Systematic Analysis for the Global Burden of Disease Study 2017. *Lancet* 395, 709–733. doi:10.1016/S0140-6736(20)30045-3

Bolger, A. M., Lohse, M., and Usadel, B. (2014). Trimmomatic: a Flexible Trimmer for Illumina Sequence Data. *Bioinformatics* 30, 2114–2120. doi:10.1093/bioinformatics/btu170

Bose, M., Almas, S., and Prabhakar, S. (2017). Wnt Signaling and Podocyte Dysfunction in Diabetic Nephropathy. *J. Investig. Med.* 65, 1093–1101. doi:10.1136/jim-2017-000456

Bryer, J. S., and Susztak, K. (2018). Screening Drugs for Kidney Disease: Targeting the Podocyte. *Cell Chem. Biol.* 25, 126–127. doi:10.1016/j.chembiol.2018.01.018

Christakos, S., Dhawan, P., Verstuyf, A., Verlinden, L., and Carmeliet, G. (2016). Vitamin D: Metabolism, Molecular Mechanism of Action, and Pleiotropic Effects. *Physiol. Rev.* 96, 365–408. doi:10.1152/physrev.00014.2015

Cohen, C. D., Frach, K., Schlöndorff, D., and Kretzler, M. (2002). Quantitative Gene Expression Analysis in Renal Biopsies: a Novel Protocol for a High-Throughput Multicenter Application. *Kidney Int.* 61, 133–140. doi:10.1046/j.1523-1755.2002.00113.x

Cohen, C. D., Klingenhoff, A., Boucherot, A., Nitsche, A., Henger, A., Brunner, B., et al. (2006). Comparative Promoter Analysis Allows De Novo Identification of Specialized Cell junction-associated Proteins. *Proc. Natl. Acad. Sci. U.S.A.* 103, 5682–5687. doi:10.1073/pnas.0511257103

Collister, D., Ferguson, T., Komenda, P., and Tangri, N. (2016). The Patterns, Risk Factors, and Prediction of Progression in Chronic Kidney Disease: A Narrative Review. *Semin. Nephrol.* 36, 273–282. doi:10.1016/j.semnephrol.2016.05.004

Cui, S., Li, C., Ema, M., Weinstein, J., and Quaggin, S. E. (2005). Rapid Isolation of Glomeruli Coupled with Gene Expression Profiling Identifies Downstream Targets in Pod1 Knockout Mice. *Jasn* 16, 3247–3255. doi:10.1681/ASN.2005030278

Deb, D. K., Wang, Y., Zhang, Z., Nie, H., Huang, X., Yuan, Z., et al. (2011). Molecular Mechanism Underlying 1,25-dihydroxyvitamin D Regulation of Nephrin Gene Expression. *J. Biol. Chem.* 286, 32011–32017. doi:10.1074/jbc.M111.269118

Feder, J., Nadel, M. V., and Krishnan, M. (2016). A Matter of Choice: Opportunities and Obstacles Facing People with ESRD. *Cjasn* 11, 536–538. doi:10.2215/CJN.04470415

Giangreco, A. A., Vaishnav, A., Wagner, D., Finelli, A., Fleshner, N., van der Kwast, T., et al. (2013). Tumor Suppressor microRNAs, miR-100 and -125b, Are Regulated by 1,25-dihydroxyvitamin D in Primary Prostate Cells and in Patient Tissue. *Cancer Prev. Res.* 6, 483–494. doi:10.1158/1940-6207.CAPR-12-0253

Kilkenny, C., Browne, W., Cuthill, I. C., Emerson, M., and Altman, D. G. (2010). Animal Research: Reporting *In Vivo* Experiments: the ARRIVE Guidelines. *Br. J Pharmacol.* 160, 1577–1579. doi:10.1111/j.1476-5381.2010.00872.x

Kim, D., Pertea, G., Trapnell, C., Pimentel, H., Kelley, R., and Salzberg, S. L. (2013). TopHat2: Accurate Alignment of Transcriptomes in the Presence of Insertions, Deletions and Gene Fusions. *Genome Biol.* 14, R36. doi:10.1186/gb-2013-14-4-r36

Kindt, F., Hammer, E., Kemnitz, S., Blumenthal, A., Klemm, P., Schlüter, R., et al. (2017). A Novel Assay to Assess the Effect of Pharmaceutical Compounds on the Differentiation of Podocytes. *Br. J. Pharmacol.* 174, 163–176. doi:10.1111/bph.13667

Kramer, J. (2015). Vitamin-D-Substitution: Immer Notwendig? *Dtsch Med. Wochenschr* 140, 1661–1666. doi:10.1055/s-0041-103272

Lange, T., Artelt, N., Kindt, F., Stracke, S., Rettig, R., Lendeckel, U., et al. (2019). MiR-21 Is Up-regulated in Urinary Exosomes of Chronic Kidney Disease Patients and after Glomerular Injury. *J. Cell Mol Med* 23, 4839–4843. doi:10.1111/jcmm.14317

Lee, H. W., Khan, S. Q., Faridi, M. H., Wei, C., Tardi, N. J., Altintas, M. M., et al. (2015). A Podocyte-Based Automated Screening Assay Identifies Protective Small Molecules. *Jasn* 26, 2741–2752. doi:10.1681/ASN.2014090859

Lehmann, B., and Meurer, M. (2010). Vitamin D Metabolism. *Dermatol. Ther.* 23, 2–12. doi:10.1111/j.1529-8019.2009.01286.x

Levey, A. S., Atkins, R., Coresh, J., Cohen, E. P., Collins, A. J., Eckardt, K.-U., et al. (2007). Chronic Kidney Disease as a Global Public Health Problem: Approaches and Initiatives - a Position Statement from Kidney Disease Improving Global Outcomes. *Kidney Int.* 72, 247–259. doi:10.1038/sj.ki.5002343

Love, M. I., Huber, W., and Anders, S. (2014). Moderated Estimation of Fold Change and Dispersion for RNA-Seq Data with DESeq2. *Genome Biol.* 15 (12), 550. doi:10.1186/s13059-014-0550-8

Martini, S., Nair, V., Keller, B. J., Eichinger, F., Hawkins, J. J., Randolph, A., et al. (2014). Integrative Biology Identifies Shared Transcriptional Networks in CKD. *Jasn* 25, 2559–2572. doi:10.1681/ASN.2013080906

May, C. J., Saleem, M., and Welsh, G. I. (2014). Podocyte Dedifferentiation: a Specialized Process for a Specialized Cell. *Front. Endocrinol.* 5, 148. doi:10.3389/fendo.2014.00148

McGrath, J. C., and Lilley, E. (2015). Implementing Guidelines on Reporting Research Using Animals (ARRIVE etc.): New Requirements for Publication in BJP. *Br. J. Pharmacol.* 172, 3189–3193. doi:10.1111/bph.12955

Mi, H., Ebert, D., Muruganujan, A., Mills, C., Albou, L.-P., Mushayamaha, T., et al. (2021). PANTHER Version 16: a Revised Family Classification, Tree-Based Classification Tool, Enhancer Regions and Extensive API. *Nucleic Acids Res.* 49, D394–D403. doi:10.1093/nar/gkaa1106

Okamura, M., Takano, Y., Saito, Y., Yao, J., and Kitamura, M. (2009). Induction of Nephrin Gene Expression by Selective Cooperation of the Retinoic Acid Receptor and the Vitamin D Receptor. *Nephrol. Dial. Transpl.* 24, 3006–3012. doi:10.1093/ndt/gfp243

Patrakka, J., Kestilä, M., Wartiovaara, J., Ruotsalainen, V., Tissari, P., Lenkkeri, U., et al. (2000). Congenital Nephrotic Syndrome (NPHS1): Features Resulting from Different Mutations in Finnish Patients. *Kidney Int.* 58, 972–980. doi:10.1046/j.1523-1755.2000.00254.x

Patrakka, J., and Tryggvason, K. (2007). Nephrin - a Unique Structural and Signaling Protein of the Kidney Filter. *Trends Mol. Med.* 13, 396–403. doi:10.1016/j.molmed.2007.06.006

Peters, L. J. F., Floege, J., Biessen, E. A. L., Jankowski, J., and van der Vorst, E. P. C. (2020). MicroRNAs in Chronic Kidney Disease: Four Candidates for Clinical Application. *Ijms* 21, 6547. doi:10.3390/ijms21186547

Putaala, H., Soininen, R., Kilpeläinen, P., Wartiovaara, J., and Tryggvason, K. (2001). The Murine Nephrin Gene Is Specifically Expressed in Kidney, Brain and Pancreas: Inactivation of the Gene Leads to Massive Proteinuria and Neonatal Death. *Hum. Mol. Genet.* 10, 1–8. doi:10.1093/hmg/10.1.1

R Core Team (2018). *R: A Language and Environment for Statistical Computing*. Vienna, Austria. Online verfügbar unter https://www.R-project.org.

Ross, A. C., Manson, J. E., Abrams, S. A., Aloia, J. F., Brannon, P. M., Clinton, S. K., et al. (2011). The 2011 Report on Dietary Reference Intakes for Calcium and Vitamin D from the Institute of Medicine: what Clinicians Need to Know. *J. Clin. Endocrinol. Metab.* 96, 53–58. doi:10.1210/jc.2010-2704

Schiwek, D., Endlich, N., Holzman, L., Holthöfer, H., Kriz, W., and Endlich, K. (2004). Stable Expression of Nephrin and Localization to Cell-Cell Contacts in Novel Murine Podocyte Cell Lines. *Kidney Int.* 66, 91–101. doi:10.1111/j.1523-1755.2004.00711.x

Shi, W., Guo, L., Liu, G., Peng, T., Li, H., Xie, T., et al. (2018). Protective Effect of Calcitriol on Podocytes in Spontaneously Hypertensive Rat. *J. Chin. Med. Assoc.* 81, 691–698. doi:10.1016/j.jcma.2018.01.010

Tripathi, G., Sharma, R., Sharma, R. K., Gupta, S. K., Sankhwar, S. N., and Agrawal, S. (2010). Vitamin D Receptor Genetic Variants Among Patients with End-Stage Renal Disease. *Ren. Fail.* 32, 969–977. doi:10.3109/0886022X.2010.501934

Trohatou, O., Tsilibary, E.-F., Charonis, A., Iatrou, C., and Drossopoulou, G. (2017). Vitamin D3 Ameliorates Podocyte Injury through the Nephrin Signalling Pathway. *J. Cel. Mol. Med.* 21, 2599–2609. doi:10.1111/jcmm.13180

Tusher, V. G., Tibshirani, R., and Chu, G. (2001). Significance Analysis of Microarrays Applied to the Ionizing Radiation Response. *Proc. Natl. Acad. Sci. U.S.A.* 98, 5116–5121. doi:10.1073/pnas.091062498

Wang, Y., Deb, D. K., Zhang, Z., Sun, T., Liu, W., Yoon, D., et al. (2012). Vitamin D Receptor Signaling in Podocytes Protects against Diabetic Nephropathy. *Jasn* 23, 1977–1986. doi:10.1681/ASN.2012040383

Wani, M., Wani, I., Banday, K., and Ashraf, M. (2016). The Other Side of Vitamin D Therapy: a Case Series of Acute Kidney Injury Due to Malpractice-Related Vitamin D Intoxication. *Clin Nephrol.* 86 (2016), 236–241. doi:10.5414/CN108904

Wiggins, R.-C. (2007). The Spectrum of Podocytopathies: a Unifying View of Glomerular Diseases. *Kidney Int.* 71, 1205–1214. doi:10.1038/sj.ki.5002222

Wong, M. A., Cui, S., and Quaggin, S. E. (2000). Identification and Characterization of a Glomerular-specific Promoter from the Human Nephrin Gene. *Am. J. Physiology-Renal Physiol.* 279, F1027–F1032. doi:10.1152/ajprenal.2000.279.6.F1027

Wu, J., Zheng, C., Fan, Y., Zeng, C., Chen, Z., Qin, W., et al. (2014). Downregulation of microRNA-30 Facilitates Podocyte Injury and Is Prevented by Glucocorticoids. *Jasn* 25, 92–104. doi:10.1681/ASN.2012111101

Yamauchi, K., Takano, Y., Kasai, A., Hayakawa, K., Hiramatsu, N., Enomoto, N., et al. (2006). Screening and Identification of Substances that Regulate Nephrin Gene Expression Using Engineered Reporter Podocytes. *Kidney Int.* 70, 892–900. doi:10.1038/sj.ki.5001625

Zenata, O., and Vrzal, R. (2017). Fine Tuning of Vitamin D Receptor (VDR) Activity by post-transcriptional and post-translational Modifications. *Oncotarget* 8, 35390–35402. doi:10.18632/oncotarget.15697

Conflict of Interest: JG is an employee of the DITABIS AG, Pforzheim, Germany and the ACQUIFER Imaging GmbH, Heidelberg, Germany.

The remaining authors declare that the research was conducted in the absence of any commercial or financial relationships that could be construed as a potential conflict of interest.

Publisher's Note: All claims expressed in this article are solely those of the authors and do not necessarily represent those of their affiliated organizations, or those of the publisher, the editors and the reviewers. Any product that may be evaluated in this article, or claim that may be made by its manufacturer, is not guaranteed or endorsed by the publisher.

frontiers | Frontiers in Cell and Developmental Biology

ORIGINAL RESEARCH
published: 30 May 2022
doi: 10.3389/fcell.2022.800574

Curcumin Blocks High Glucose-Induced Podocyte Injury via RIPK3-Dependent Pathway

*Hyunsoo Chung[1†], Seong-Woo Lee[2,3†], Miri Hyun[2†], So Young Kim[2], Hyeon Gyu Cho[1], Eun Soo Lee[4,5], Jeong Suk Kang[2,6], Choon Hee Chung[4,5] and Eun Young Lee[1,2,3,6]**

[1]College of Medicine, Soonchunhyang University, Cheonan, South Korea, [2]Department of Internal Medicine, Soonchunhyang University Cheonan Hospital, Cheonan, South Korea, [3]BK21 Four Project, College of Medicine, Soonchunhyang University, Cheonan, South Korea, [4]Department of Internal Medicine, Yonsei University Wonju College of Medicine, Wonju, South Korea, [5]Institution of Genetic Cohort, Yonsei University Wonju College of Medicine, Wonju, South Korea, [6]Institute of Tissue Regeneration, College of Medicine, Soonchunhyang University, Cheonan, South Korea

OPEN ACCESS

Edited by:
Mario Ollero,
INSERM U955 Institut Mondor de Recherche Biomédicale (IMRB), France

Reviewed by:
Xue-Kai Wang,
Chinese Academy of Medical Sciences and Peking Union Medical College, China
Yuan Li,
Nanjing Medical University, China
Vivek Soni,
Guru Ghasidas Vishwavidyalaya, India

***Correspondence:**
Eun Young Lee
eylee@sch.ac.kr

†These authors have contributed equally to this work and share first authorship

Specialty section:
This article was submitted to Cell Death and Survival, a section of the journal Frontiers in Cell and Developmental Biology

Received: 23 October 2021
Accepted: 08 March 2022
Published: 30 May 2022

Citation:
Chung H, Lee S-W, Hyun M, Kim SY, Cho HG, Lee ES, Kang JS, Chung CH and Lee EY (2022) Curcumin Blocks High Glucose-Induced Podocyte Injury via RIPK3-Dependent Pathway. Front. Cell Dev. Biol. 10:800574. doi: 10.3389/fcell.2022.800574

Podocyte loss is well known to play a critical role in the early progression of diabetic nephropathy. A growing number of studies are paying attention to necroptosis, a programmed form of cell necrosis as a mechanism of podocyte loss. Although necroptosis is a recently established concept, the significance of receptor interacting serine/threonine kinase 3 (*RIPK3*), a gene that encodes for the homonymous enzyme RIPK3 responsible for the progression of necroptosis, is well studied. Curcumin, a natural hydrophobic polyphenol compound responsible for the yellow color of *Curcuma longa,* has drawn attention due to its antioxidant and anti-inflammatory effects on cells prone to necroptosis. Nonetheless, effects of curcumin on high glucose-induced podocyte necroptosis have not been reported yet. Therefore, this study investigated RIPK3 expression in high glucose-treated podocytes to identify the involvement of necroptosis *via* the RIPK3 pathway and the effects of curcumin treatment on RIPK3-dependent podocytopathy in a hyperglycemic environment. The study discovered that increased reactive oxygen species (ROS) in renal podocytes induced by high glucose was improved after curcumin treatment. Curcumin treatment also significantly restored the upregulated levels of VEGF, TGF-β, and CCL2 mRNAs and the downregulated level of nephrin mRNA in cultured podocytes exposed to a high glucose environment. High glucose-induced changes in protein expression of TGF-β, nephrin, and CCL2 were considerably reverted to their original levels after curcumin treatment. Increased expression of RIPK3 in high glucose-stimulated podocytes was alleviated by curcumin treatment as well as N-acetyl cysteine (NAC, an antioxidant) or GSK′872 (a RIPK3 inhibitor). Consistent with this, the increased necroptosis-associated molecules, such as RIPK3, pRIPK3, and pMLKL, were also restored by curcumin in high glucose-treated mesangial cells. DCF-DA assay confirmed that such a result was attributed to the reduction of RIPK3 through the antioxidant effect of curcumin. Further observations of DCF-DA-sensitive intracellular ROS in NAC-treated and GSK′872-treated podocyte groups showed a reciprocal regulatory relationship between ROS and RIPK3. The treatment of curcumin and GSK′872 in podocytes incubated with high glucose protected from excessive intracellular superoxide anion production. Taken together, these results indicate that

curcumin treatment can protect against high glucose-induced podocyte injuries by suppressing the abnormal expression of ROS and RIPK3. Thus, curcumin might be a potential therapeutic agent for diabetic nephropathy as an inhibitor of RIPK3.

Keywords: diabetic nephropathy, curcumin, necroptosis, RIPK3, antioxidant

INTRODUCTION

Diabetic nephropathy (DN) is the major cause of mortality in patients with diabetes (Dabla, 2010). Diabetes-induced chronic hyperglycemia can cause metabolic and hemodynamic abnormalities with an increase in reactive oxygen species (ROS), leading to abnormal changes in renal podocytes and DN, whose main symptoms are increased renal albuminuria and declining renal function (Dabla, 2010; Cao and Cooper, 2011).

Podocytes play multiple roles in maintaining kidney functions (Anil Kumar et al., 2014). They also play a vital role in the pathogenesis of DN. Podocytes can maintain the size of a protein and the charge of the glomerular filtration barrier, which forms a filtration unit of the kidney (Anil Kumar et al., 2014). In addition, podocytes are involved in the maintenance of capillary loop shape, the maintenance and synthesis of the GBM (glomerular basement membrane), and the production of VEGF (vascular endothelial growth factor) (Wolf et al., 2005; Jefferson et al., 2011). A decrease in the number of glomerular podocytes is positively related to the emergence of DN in diabetic patients. It is also known to play a significant role in the progression of DN (Susztak et al., 2006).

Necroptosis is a nonapoptotic form of programmed cell death with necrotic morphology. It has been demonstrated that necroptosis plays a significant role in various pathological processes, including acute renal injury (Xu et al., 2019). Since receptor-interacting protein kinase 3 (RIPK3) is a key molecule for the necroptosis pathway, the degree of necroptosis execution could be quantified with an increased level of RIPK3 (Xu et al., 2019). Additionally, recent studies have shown that an increase of ROS induced by RIPK3 elevation could initiate necroptosis in the pathophysiological process of acute renal injury (Priante et al., 2019). Hyperglycemic conditions could activate various pathways that provoke cell death. One of the major impacts of a high glucose environment caused by diabetes is necroptosis in renal podocytes (LaRocca et al., 2016; Volpe et al., 2018).

Curcumin, a natural hydrophobic polyphenol compound responsible for the yellow color in *Curcuma longa*, has gathered attention from various research fields due to its natural antioxidant, anticancer, anti-inflammatory, antiangiogenic, and antiapoptotic effects (Gururaj et al., 2002; Majithiya and Balaraman, 2005; Koeberle et al., 2009; Perrone et al., 2015; Zhang et al., 2020). The effect of curcumin on high glucose-induced podocyte injury has been discussed in few studies, mainly focusing on curcumin's antioxidant and anti-inflammatory properties (Kanitkar et al., 2008; Meng et al., 2013; Den Hartogh et al., 2019). Curcumin has recently been reported to have a protective effect on hepatocyte or neuronal cells prone to necroptosis (Dai et al., 2013; Lu et al., 2016). There have been few studies using animal models to show improved renal function after curcumin treatment (Sharma et al., 2006; Kim et al., 2016). However, the role of curcumin in high glucose-induced podocyte necroptosis is to be clarified yet. Therefore, the objective of this study was to investigate the effect of curcumin treatment on high glucose-induced podocyte injury caused by oxidative stress or inflammatory responses.

MATERIALS AND METHODS

Chemicals

Dulbecco's modified Eagle's medium (DMEM), fetal bovine serum (FBS), and phosphate buffered saline (PBS) were purchased from Gibco (Grand Island, NY, United States). Trypsin/EDTA (#25-053-cl) and penicillin/streptomycin (#30-002-cl) were purchased from Corning (Corning, NY, United States). TNF-α (#AFL410) was purchased from R&D Systems (Minneapolis, Minnesota, United States). Curcumin (diferuloylmethane), DHZ [1,7-bis(4-hydroxy-3-methoxyphenyl)-1,6-heptadiene-3,5-dione], and reagents were purchased from Sigma (Paterson, NJ, United States). Curcumin dissolved in DMSO obtaining a concentration of 100 μg/ml was stored at −70°C. If necessary, it was diluted to various concentrations either in the cell culture medium or PBS for its use.

Cell Culture and Glucose Treatment

Conditionally immortalized mouse podocytes were kindly provided by Dr. Peter Mundel and cultured as described previously (Kang et al., 2019; Lee et al., 2019). Cell proliferation was retained in DMEM supplemented with 10% FBS with 10 U/mL IFN-γ and 1% penicillin/streptomycin at 33°C. Cell differentiation was induced in culture media without IFN-γ at 37°C for 14 days to develop podocyte foot processes similar to *in vivo*. Differentiated mouse podocytes were then challenged with either normal (5.6 mM) or high (30 mM) glucose medium for 24 h. For high glucose treatment, glucose powder [D-(+)-Glucose, #G7528, Sigma] was dissolved to obtain a 3 M stock. It was then used to treat the immortalized mouse podocytes. Mouse mesangial (MES-13) was purchased from the American Type Culture Collection (ATCC, Manassas, VA). MES-13 cells were cultured in DMEM containing 5.5 mM glucose, 1% antibiotics, and 10% FBS. The cultured cells were starved for 24 h and then stimulated with high glucose with or without 1 μM of curcumin and 1 μM of DHZ for 24 h.

Assessment of Cell Viability

To determine the toxicity of curcumin, the MTT [3-(4,5-dimethylthiazol-2-yl)-2,5-diphenyltetrazolium bromide] assay was performed. Using trypsin/EDTA, the cultured cells were detached from the culture plate and the cell suspension solution was put into a

96-well culture plate after measuring the optimum cell concentration (1×10^5/ml) *via* a hemocytometer. After the plate was incubated at 37°C for 24 h, different concentrations of curcumin were added to the serum-free culture medium and the plate was cultured for another 24 h. After removing the medium, 100 μL of the MTT solution was added to each well. Following incubation for 2 h, the solution was carefully removed and 100 μL DMSO was added to each well. The cells were extracted to measure the absorbance at a wavelength of 540 nm using a microplate reader.

Measurement of Intracellular ROS

To determine the effect of curcumin on intracellular ROS expression, after washing the 2-week incubated podocytes twice with PBS, 5M of oxidation-sensitive 2′-7′ dichlorofluorescein diacetate (DCF-DA, Invitrogen, Grand Island, NY, United States) fluorescent probe was added followed by incubation at 37°C for 10 min. To examine the effect of GSK′872 or N-acetyl-L-cysteine on ROS expression in the high glucose-treated podocytes, 10 μM stock of DCF-DA was dissolved in the culture media and added to cells. After incubating at 37°C for 30 min, excess dye was washed away. DCF-DA sensitive intracellular ROS (reactive oxygen species) was then observed and quantified using a Carl Zeiss LSM 710 confocal microscope.

Superoxide Anion Assay

To measure the superoxide anion, one of the ROS types, the superoxide anion assay kit (# CS1000, Sigma) was used. The mouse podocytes were transferred to a 96-well plate (3×10^5 cells/well) on the 10^{th} day after the start of the differentiation, and 2 days later, they were starved for 24 h. After treating the cells with GSK′872, curcumin or NAC in high glucose condition for 16 h, the medium was replaced with the assay medium (A5980) included in the superoxide assay kit and incubated at 37°C for 10 min. Then, luminol solution (L5043), xanthine oxidase from milk (X4878), superoxide dismutase (S6696), and enhancer solution (E4281) were added to the assay buffer (A5980) according to the conditions, and then reacted at 37°C for 30 min. The luminescence was measured using GloMax® Discover Microplate Reader (GM3000, Promega).

Enzyme-Linked Immunosorbent Assay

ELISA was performed using ELISA kits purchased from R&D Systems (Minneapolis, MN, United States) to analyze the supernatant CCL2 (C-C motif chemokine ligand 2) from the podocytes. After placing 100 μL of the sample into the well of a 95-well microplate, it reacted at room temperature for a given time. After washing the sample four times with a washing buffer, 200 μL conjugate was added to each well and reacted for 2 h. After washing with the washing buffer four times, 200 μL of the substrate solution was added and reacted without light for 20 min. After adding 50 μL of the stop solution to each well, the absorbance at 450 nm wavelength was measured using a microplate reader.

Quantitative Real-Time PCR

The total RNA was extracted using TRIzol purchased from Invitrogen (Carlsbad, CA, United States) following the manufacturer's protocol. cDNA was synthesized from 0.5 to 1 μg of the total RNA using a ReverTraAce® qPCR RT Master Mix (TOYOBO, Japan) according to the manufacturer's protocol. For PCR, 10 ng of cDNA, SYBR PCR master mix plus (TOYOBA, Osaka, Japan), and primer were mixed to make a total volume of 20 μL. PCR for CCL2, TGF (transforming growth factor)-β, and VEGF (vascular endothelial growth factor) used the gene-specific primers as follows: β-actin, 5′-cca tga aga tca aga tca ttg ctc c-3' (forward), and 5′-tc ttg t atc cac atc tgc t-3' (reverse); CCL2, 5′-ctg gat cg aac caa atg ag-3' (forward) and 5′-cgg gtc aac ttc aca ttc aa-3' (reverse); TGF-β, 5′-agc ccg aag cgg act act at-3' (forward), and 5′-ct tgt gag atg tct ttg gtt ttc-3' (reverse); and VEGF, 5′-gta cat ctt caa gcc gtc ctg tgt-3' (forward) and 5′-tcc gca tga tct gca tgg tg-3' (reverse). Real-time PCR was performed using CFX-96 (BIO-RAD). The condition of PCR used in this study was: 40 repeated cycles of 30 s at 95°C, 5 s at 95°C, 10 s at 58°C, and 15 s at 72°C. Expression analysis was performed using the $\Delta\Delta C_T$ method. Expression levels of all genes were normalized against the expression of β-actin in the same sample (Schefe et al., 2006).

Western Blot

Protein expression levels of RIPK3, TGF-β, and nephrin were measured by Western blot analysis using specific antibodies. After 24 h of treatment with different concentrations of glucose and curcumin, the media were removed and the plates were washed with cold PBS three times. These plates were stood upright and refrigerated at 4°C for 10 min to remove the remaining PBS/media with a micropipette. Then 90 μL of PRO-PREPTM protein extraction solution (iNtRON biotechnology, Seoul, Korea) was added to collect the podocytes and to extract the proteins. The protein extract was quantified by Lowry assay (BIO-RAD). SDS-PAGE was performed after adding the Laemmli buffer. The proteins were then transferred to the nitrocellulose membranes. The membranes were blocked with 1xPBS/T containing 5% skim milk (Merck, Rahway, NJ, United States) for an hour and then incubated with a primary antibody at 4°C overnight. The primary antibodies of β-actin (#sc-47778, 1:5,000, Santa Cruz), RIPK3 (#AHP1797, 1:1,000, Synaptic Systems), pRIPK3 (#ab195117, 1:1,000, Abcam), pMLKL (#ab196436, 1:1,000, Abcam), TGF-β (#sc-146, 1:500, Santa Cruz), and nephrin (#GP-N2, 1:500, Progen) were used.

The membranes were washed with 1xPBS/T three times for 10 min each and reacted with secondary antibodies, either mouses-HRP (#W4028, 1:5,000, Promega), rabbit-HRP (#31460, 1:2,000, Invitrogen), or guineapig-HRP (#sc-2438, Santa Cruz) for 3.5 h at 4°C. After washing again with 1xPBS/T three times for 10 min each, the membranes were developed with an ECL kit. Protein band images were obtained using Chemidoc (BIO-RAD). Intensities of obtained protein bands were quantified with ChemiDocTM XRS+ (Bio-RAD) imaging system using a Luminata Forte enhanced chemiluminescence solution (Millipore).

To further clarify the mechanism of curcumin's protective effect on RIPK3 production, Western blot analysis of RIPK3 and β-actin protein expressions was proceeded by abiding the same procedure as previously described except that the cell plate treatment was different. Cell plates were incubated in a serum-free condition for 24 h. They were then incubated for another

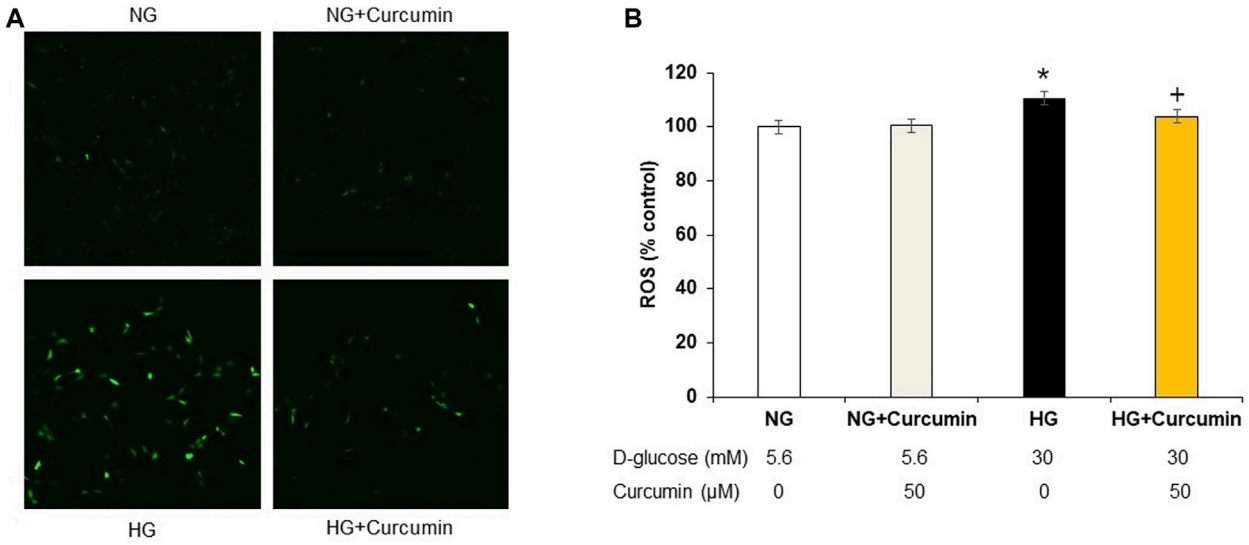

FIGURE 1 | Curcumin decreases ROS expression in high glucose-treated podocytes. DCF-DA-sensitive intracellular ROS was measured after incubating podocytes with NG (5.6 mM D-glucose), NG + Curcumin (5.6 mM D-glucose + curcumin), HG (30 mM D-glucose), and HG + Curcumin (30 mM D-glucose + curcumin) for 24 h. HG-induced intracellular ROS was markedly reduced by curcumin treatment **(A,B)**. 2′-7′ DCF-DA, dichlorofluorescein diacetate DCF-DA; NG, normal glucose; HG, high glucose. *, $p < 0.05$ *versus* NG; + $p < 0.05$ *versus* HG.

24 h with 0.2% FBS media containing normal or high glucose and 10 μM of GSK′872 (RIPK3 inhibitor, #5. 30389. 0001, EMD Millipore) or 50 μM of N-acetyl-L-cysteine (NAC) (antioxidant, #a7250, Sigma).

Statistical Analysis

Statistical comparisons were performed with Student's t-test. All analyses were performed with SPSS software. Experimental values are presented as mean ± SD using data obtained from at least three independent experiments. p-value < 0.05 was considered statistically significant.

RESULTS

MTT Assay

To establish the experimental conditions in which cellular toxicity would be minimized, the renal podocytes in a 96-well plate were treated with 0, 50, 100, 150, and 200 μM of curcumin for 24 h for the MTT assay. Curcumin concentration less than 50 uM did not show cytotoxicity, while cell viability was reduced to 77% at 100 uM and to 30% at 150 uM and 200 uM compared to the normal control (**Supplementary Figure S1**). Based on these results, 50 uM curcumin was used in this study.

Curcumin Treatment Alleviates ROS Generation in High Glucose-Treated Podocytes

Increased DCF-DA sensitive intracellular ROS generation under 30 mM high glucose condition was observed by using a confocal microscope (**Figure 1A**) and quantified by using a fluorometer (**Figure 1B**). The high glucose-treated podocytes showed significantly increased ROS expression. However, the curcumin treatment significantly reduced such changes.

Curcumin Treatment Decreases CCL2 Protein and mRNA Levels in High Glucose-Treated Podocytes

Supernatant CCL2 protein secreted by the high glucose-treated podocytes was analyzed. The results showed a 10-fold increase of the CCL2 protein expression compared to that of the normal glucose-treated podocyte group. Curcumin treatment significantly attenuated the elevated CCL2 expression to a certain extent, although not to the normal level (**Figure 2A**). The CCL2 mRNA expression was similarly increased more than 1.8 times greater in response to high-glucose (30 mM) stimulation. However, it was remarkably reduced back to the normal level after the curcumin treatment (**Figure 2B**). When the podocytes were stimulated with the inflammatory cytokine TNF-α (tumor necrosis factor α), they showed 1.8-fold increase in the supernatant CCL2 protein expression. However, the supernatant CCL2 protein expression was significantly recovered to normal level after the treatment with curcumin (**Figure 2C**).

Recovery of the VEGF Expression Level After Curcumin Treatment

The high-glucose-stimulated podocytes showed a 5.3-fold increase of the VEGF mRNA expression than the podocytes cultured in a normal glucose (5.6 mM) environment. However,

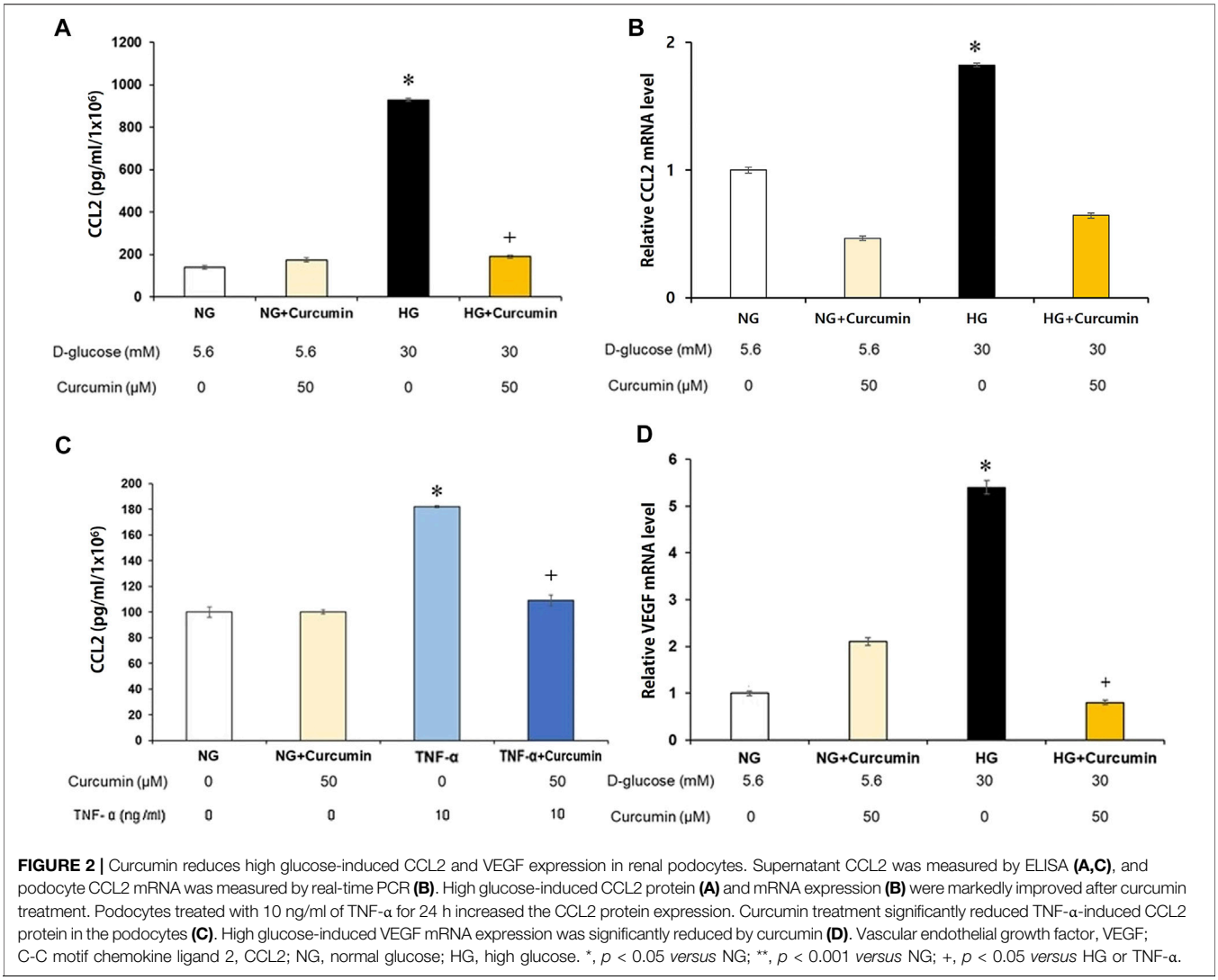

FIGURE 2 | Curcumin reduces high glucose-induced CCL2 and VEGF expression in renal podocytes. Supernatant CCL2 was measured by ELISA **(A,C)**, and podocyte CCL2 mRNA was measured by real-time PCR **(B)**. High glucose-induced CCL2 protein **(A)** and mRNA expression **(B)** were markedly improved after curcumin treatment. Podocytes treated with 10 ng/ml of TNF-α for 24 h increased the CCL2 protein expression. Curcumin treatment significantly reduced TNF-α-induced CCL2 protein in the podocytes **(C)**. High glucose-induced VEGF mRNA expression was significantly reduced by curcumin **(D)**. Vascular endothelial growth factor, VEGF; C-C motif chemokine ligand 2, CCL2; NG, normal glucose; HG, high glucose. *, $p < 0.05$ *versus* NG; **, $p < 0.001$ *versus* NG; +, $p < 0.05$ *versus* HG or TNF-α.

the VEGF mRNA expression was markedly decreased to a normal level after curcumin treatment (**Figure 2D**).

Curcumin Treatment Restores High Glucose-Mediated Reduction in the Expression of Nephrin

The podocytes stimulated with a high glucose showed nearly 0.4-fold decrease in the nephrin mRNA expression (**Figure 3A**) and approximately 0.6 times reduction in the nephrin protein expression (**Figure 3B**) than the differentiated podocytes treated with normal glucose. However, these changes were all significantly recovered by the curcumin treatment.

Reduced Expression of TGF-β at Protein and mRNA Levels After Curcumin Treatment

Compared with differentiated podocytes cultured in normal glucose, the podocytes stimulated with high glucose showed a 2-fold increase in TGF-β mRNA expression (**Figure 3C**) and a 3-fold increase in TGF-β protein expression (**Figure 3D**). However, these increases of the TGF-β mRNA and protein expression levels were significantly decreased after the curcumin treatment.

Increased RIPK3 Expression Is Recovered by Curcumin and Antioxidant NAC Treatment

As a result of the culturing podocytes exposed to high glucose for 24 h, the expression of RIPK3 was increased approximately 1.5-fold compared to that in the podocytes treated with normal glucose. When the high glucose-treated podocytes were cotreated with curcumin, however, the increased RIPK3 expression was significantly decreased similar to that in the normal control (**Figure 4A**). Mouse MES-13 cells, another renal cell line, were used to verify the increased expression of RIPK3 by high glucose. As shown in **Figure 4B**, RIPK3 expression was increased in the high glucose-treated mesangial cells but decreased by the treatment of curcumin and DHZ

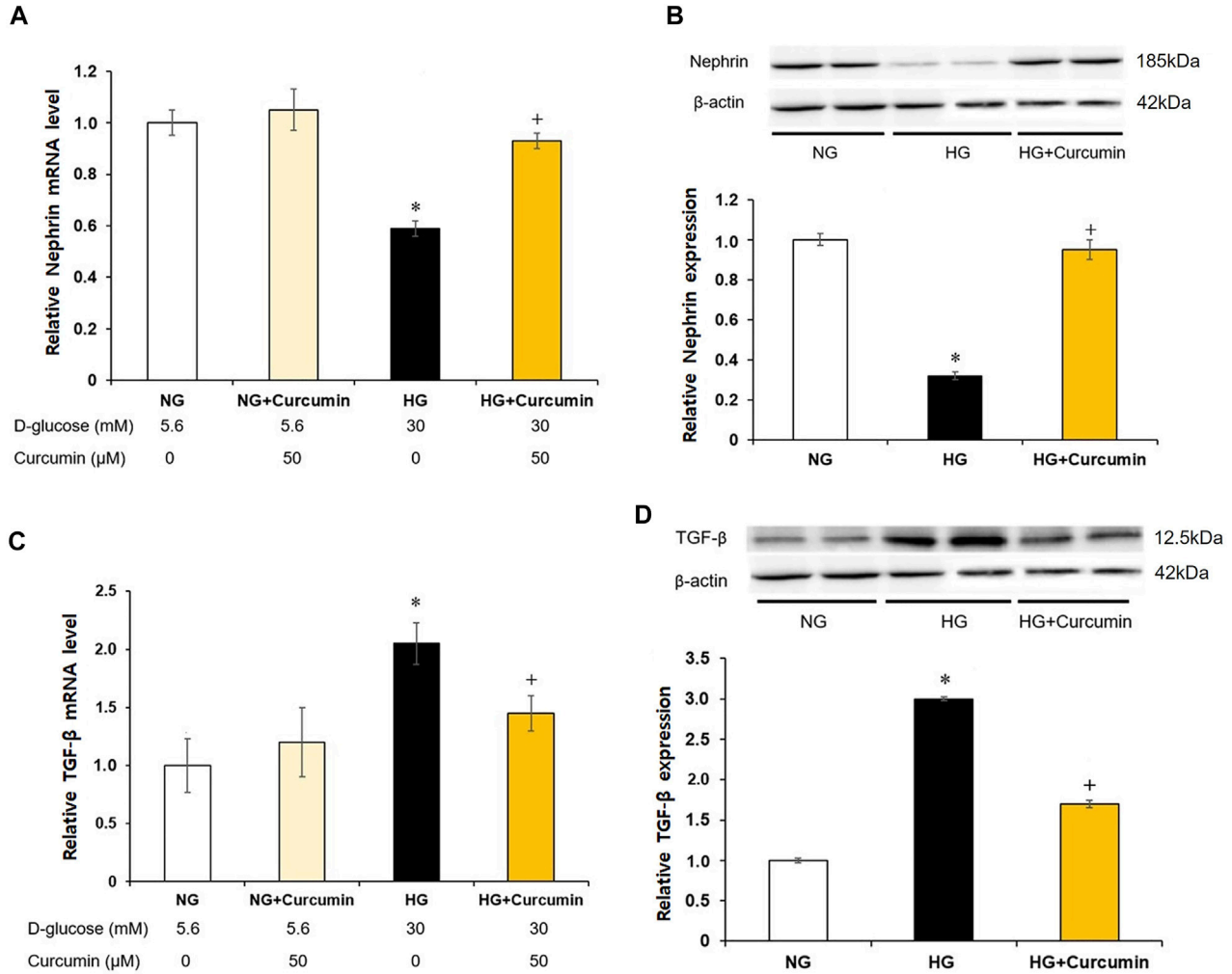

FIGURE 3 | Curcumin restores decreased nephrin and increases TGF-β expression in high glucose-treated podocytes. Podocytes were treated with high glucose with or without 50 μM of curcumin for 24 h. Decreased nephrin expression at mRNA **(A)** and protein **(B)** levels in high-glucose environment was significantly restored after curcumin treatment. High glucose-induced increases of TGF-β expression at mRNA **(C)** and protein **(D)** levels were markedly improved after curcumin treatment. NG, normal glucose; HG, high glucose. *, $p < 0.05$ *versus* NG; +, $p < 0.05$ *versus* HG.

(dehydrozingerone), a structural analog of curcumin. In addition, it was confirmed that the expression of pRIPK3 and pMLKL increased by the high glucose was also decreased by curcumin and DHZ treatment, like RIPK3. In addition, the high glucose-mediated RIPK3 overexpression was restored by an antioxidant NAC treatment as shown in the result for RIPK3 inhibitor GSK′872 (**Figure 5**). These results suggest that curcumin might protect podocyte injury by regulating the expression of RIPK3 increased by hyperglycemia in a diabetic environment.

Reciprocal Regulatory Relationship Between ROS and RIPK3

Next, to investigate the interaction between RIPK3 and ROS in podocyte injury, effects of RIPK3 inhibitor GSK′872 and NAC on ROS generation in the high glucose-treated podocytes were investigated. As shown in **Figures 6A,B**, while the intracellular ROS production was increased in the high glucose-treated podocytes compared to that in the control, ROS levels were decreased by the RIPK3 inhibitor GSK′872. Similarly, ROS was decreased by the NAC treatment. In addition, the podocytes stimulated with high glucose had higher level of intracellular superoxide anion production compared to the cells exposed to normal glucose. Treatment of curcumin, GSK′872, and NAC in podocytes exposed to high glucose can lower the levels of intracellular superoxide anion than in the podocytes exposed to high glucose (**Figure 6C**).

DISCUSSION

Previous studies about curcumin's protective effect on the renal podocytes were mainly focused on curcumin's anti-inflammatory

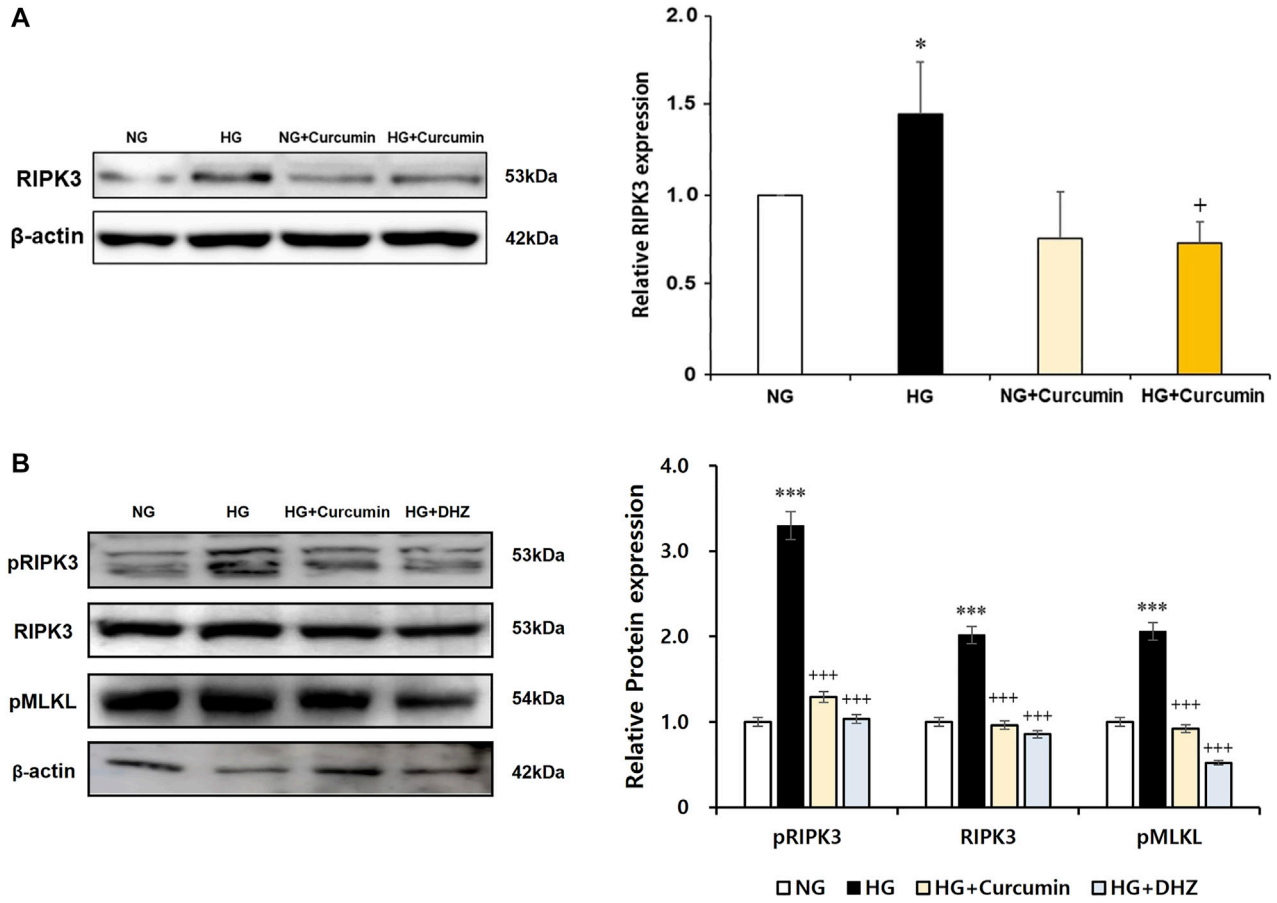

FIGURE 4 | Curcumin works as an inhibitor of RIPK3 to protect renal podocytes and MES-13 cells from high glucose-induced injury. High glucose-induced RIPK3 overexpression in podocytes was significantly reduced by curcumin treatment **(A)**. Representative immunoblot for RIPK3, pRIPK3, and pMLKL by Western blot in mouse mesangial (MES-13) cells treated with high glucose with or without 1 μM of curcumin and 1 μM of DHZ for 24 h **(B)**. NG, normal glucose; HG, high glucose. *, $p < 0.05$ *versus* NG; +, $p < 0.05$ *versus* HG.

and antioxidant effects and mechanisms (Sharma et al., 2006; Den Hartogh et al., 2019). Although some animal experiments have confirmed curcumin's protective effect on podocyte apoptosis or general renal damage (Sharma et al., 2006; Kim et al., 2016), the effect and mechanism of curcumin on podocytes necroptosis have not been clearly demonstrated yet. Thus, this study aimed to investigate curcumin's effects on high glucose-induced necroptosis of the renal podocytes by observing the alterations in RIPK3 level.

The major finding of this study was that high glucose exposure increased the RIPK3 expression in the renal podocytes and that this change was restored to normal levels by curcumin treatment. Western blot analysis of the RIPK3 expression after treatment with GSK′872 or NAC confirmed that curcumin functioned as an inhibitor of RIPK3 and an antioxidant. Our study is the first to demonstrate the potential role of curcumin as an inhibitor of RIPK3 in the renal podocytes. High glucose-induced RIPK3 overexpression was significantly reduced after curcumin treatment. Since the previous studies have shown that the RIPK1/RIPK3 pathway is a major regulator of podocyte necroptosis (Xu et al., 2019), the potential application of curcumin to minimize hyperglycemic damage to the kidney is compelling.

Our study showed that an increased intracellular ROS expression induced by high glucose exposure was recovered by the curcumin treatment, similar to other previous experiments confirming curcumin's antioxidant property (Balasubramanyam et al., 2003; Barzegar and Moosavi-Movahedi, 2011; Trujillo et al., 2013). ROS are the major components that can regulate necroptotic signaling. High glucose-induced intracellular ROS generation is the cause of podocytes death and loss in DN. Various types of ROS can be expressed in diabetic environment. NOX-derived ROS is known to be the most important one both numerically and functionally in the kidney cells (Jha et al., 2016). The recovery of intracellular ROS overexpression observed in this study consolidates curcumin's ability to suppress intracellular ROS generation in the renal podocytes prone to a high glucose environment.

CCL2 is an important inflammatory chemokine that regulates the recruitment and activation of monocytes and macrophages (Lee et al., 2009). CCL2 is also one of the downstream cytokines

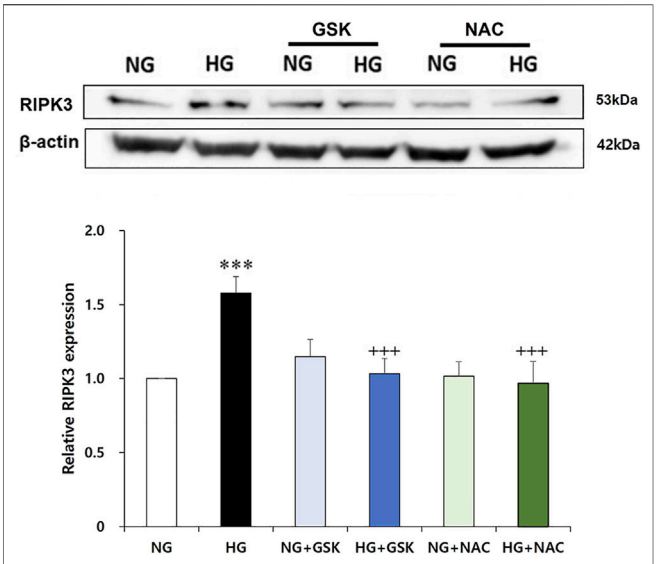

FIGURE 5 | GSK′872 and N-acetyl cysteine equally suppress RIPK3 expressions in high glucose-treated renal podocytes. A histogram shows RIPK3 expression in HG, GSK′872, or antioxidant-treated podocytes. Subsequent to 24-h starvation using serum-free media, each cell plate of podocytes was incubated with HG (30 mM), GSK′872 (RIPK3 inhibitor, 10 μM), or an antioxidant (NAC, 50 μM) for another 24 h. Plates were then suctioned and washed three times with PBS. Podocytes were harvested by adding 90 μL of PRO-PREP™ solution to each cell plate to perform Western blot analysis. The expression of RIPK3 was significantly lower in both GSK′872-treated and NAC-treated cell plates, which did not show any statistically significant difference from the negative control group. NG, normal glucose; HG, high glucose; GSK, GSK′872; NAC, N-acetyl cysteine. ***, $p < 0.001$ *versus* NG; +++, $p < 0.001$ *versus* HG.

produced by oxidative stress in diabetic conditions (Jha et al., 2016). Under diabetic conditions, CCL2 expression is upregulated in various kidney cell lines, leading to proliferation of mesangial cells, glomerulosclerosis, and kidney fibrosis (Lee et al., 2009). The mRNA expression of TNF-α, a potent cytokine, is believed to play a major role in diabetic nephropathy. It is increased in diabetic condition. As a consequence, inflammatory responses such as local generation of ROS and podocytes' CCL2 production can occur in the kidney (Lee et al., 2009). We showed that the CCL2 level was significantly decreased after the curcumin treatment in both the HG + curcumin and TNF-α + curcumin groups, suggesting that curcumin could prevent the development of an inflammatory response. In this study, as curcumin treatment reduced ROS and CCL2 expression levels, it was confirmed that curcumin had an anti-inflammatory effect on the podocytes in diabetic state. As previously mentioned, the activation of RIPK3 resulted in oxidative stress due to the progression of necroptosis and an elevation of CCL2 and TNF-α might appear. The decrease in the CCL2 expression after the curcumin treatment is likely because of curcumin's activity as an antioxidant and an inhibitor of RIPK3, leading to the reduced ROS expression and an anti-inflammatory response.

This study also revealed that curcumin treatment could suppress mRNA and protein overexpression levels of VEGF, a critical factor for angiogenesis, in the high glucose-induced podocytes. VEGF produced by the podocytes plays an important role in maintaining glomerular endothelial cells and the glomerular filtration barrier. The level of VEGF must be precisely controlled as both lower and higher than normal levels of VEGF may cause renal problems. Excessive VEGF level can lead to pathological microangiopathy, subsequently leading to neovascularization (Gil et al., 2021). Curcumin's role in inhibiting the VEGF expression is supported by the previous clinical trials and *in vivo* studies (Sawatpanich et al., 2010; Wang and Chen, 2019). The decrease in the VEGF level followed by curcumin and GSK′872 in this study reflected curcumin's role as an inhibitor of RIPK3 to suppress the vascular permeability promoted in necroptosis. As the increase of renal VEGF expression in DM patients' glomerulus is a well-known triggering factor of diabetic nephropathy (Tufro and Veron, 2012), therapeutic use of curcumin to reduce the VEGF expression is expected to help prevent diabetic kidney disease progression. However, further studies are needed.

Observing a high glucose-induced decrease in the mRNA and protein expression of nephrin was recovered after the curcumin treatment, suggesting curcumin's RIPK3 inhibitor activity to protect the renal podocytes against stress and inflammatory effects induced in hyperglycemic conditions. Since nephrin is a major protein secreted by the podocytes to form an integral part of primary renal function, nephrin's reduction is closely related to increased proteinuria, expansion of GBM, and decreased slit pore density (Cooper et al., 2002). The recovered expression of nephrin after curcumin treatment in this study shows curcumin's potential in preventing podocyte damage and maintaining its function.

Active TGF-β signaling can modify gene transcription *via* phosphorylation and translocation of Smad protein. This change can lead to podocyte apoptosis, foot effacement, and decreased VEGF production that can result in endothelial cell death (Gil et al., 2021). It has also been reported that an increased expression of CCL2 in the mesangial cells can stimulate collagen deposition, extend the mesangial matrix, and mediate collagen deposition and fibrosis in diabetic nephropathy (Lee et al., 2009; Epstein et al., 1994). As shown in **Figure 3**, high glucose-induced increases of the TGF-β mRNA and protein expression were significantly reduced after the curcumin treatment. As TNF-α and TGF-β coexist as downstream inflammatory cytokines in RIPK3 signaling, curcumin's function as an inhibitor RIPK3 can reduce the fibrotic response in the kidney due to the TGF-β and CCL2 overexpression stimulated by TNF-α (Jha et al., 2016; Bertheloot et al., 2021).

As previously mentioned, this study clarified that curcumin treatment could reduce high glucose-induced ROS and RIPK3 production in the podocytes and alleviated the increase of ROS generation after the treatment with RIPK3 inhibitor GSK′872. These findings suggest that ROS generation depends on RIPK3 pathway, which is supported by a recent study investigating lyso-Gb3-induced oxidative stress *via*

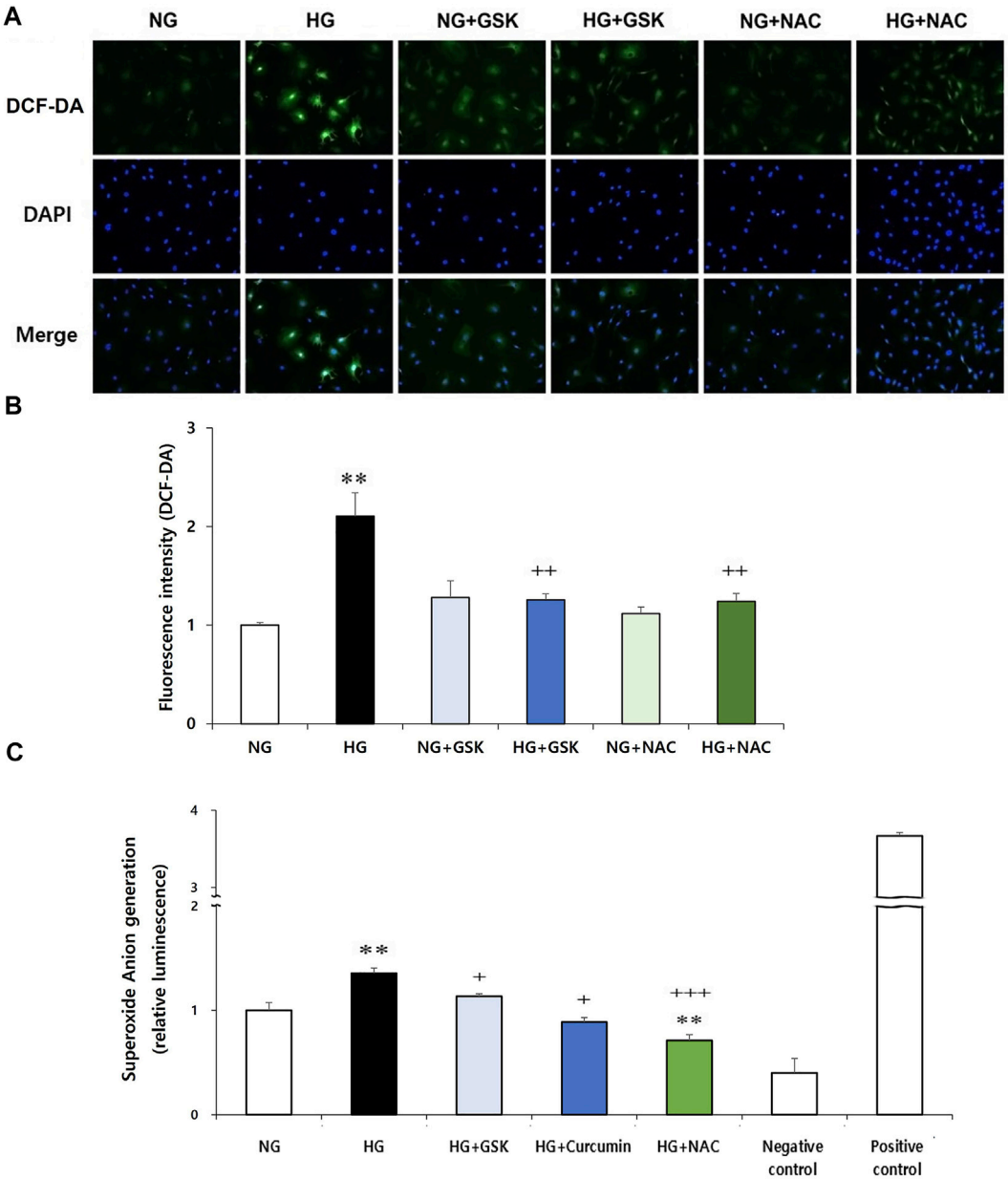

FIGURE 6 | GSK′872 or NAC treatment reduces intracellular ROS expression in high glucose-treated podocytes. DCF-DA-sensitive intracellular ROS was observed **(A)** and quantified **(B)** after treating the podocytes under six different conditions for 24 h: NG (5.6 mM D-glucose), HG (30 mM D-glucose), NG + GSK (5.6 mM D-glucose + 10 μM GSK′872), HG + GSK (30 mM D-glucose + 10 μM GSK′872), NG + NAC (5.6 mM D-glucose + 50 μM N-acetyl cysteine), and HG + NAC (30 mM D-glucose + 50 μM N-acetyl cysteine). In GSK- or NAC-treated groups, HG-induced intracellular ROS expression was significantly reduced **(A,B)**. NG, normal glucose; HG, high glucose; ROS, reactive oxygen species; GSK, GSK′872. **, $p < 0.01$ *versus* NG; ++, $p < 0.01$ *versus* HG. Superoxide anion was measured using a luminometer. After starvation for 24 h, drug treatment was performed for 16 h **(C)**. High glucose-induced superoxide anion production in podocytes was significantly reduced by curcumin, GSK′872, and NAC. Negative control, assay buffer + xanthine oxidase + SOD; positive control, assay buffer + xanthine oxidase. **, $p < 0.01$ *versus* NG; +, $p < 0.05$, ++, $p < 0.01$ *versus* HG.

RIPK3-dependent pathway and implicating that external stress factors can result in ROS generation *via* RIPK3-dependent pathway (Kim et al., 2021). In addition, observing a significant recovery of the abnormally increased intracellular ROS expression followed by GSK′872 or NAC treatment confirmed the interdependence between ROS and RIPK3. Our results collectively suggested that the antioxidant property of curcumin may inhibit RIPK3 overexpression, ultimately contributing to the normalization of the ROS expression.

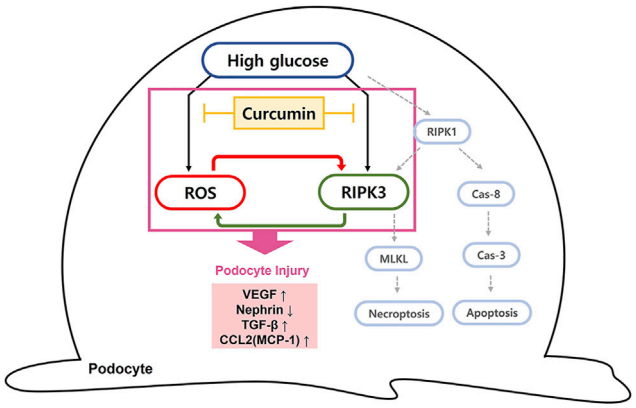

FIGURE 7 | Diagram of curcumin suppressing intracellular ROS and RIPK3 expression in high glucose-treated podocytes. Schematic representation of the possible signaling pathway leading to podocytopathy by high glucose. We suggest that the elevated hyperglycemia condition can induce the intracellular ROS generation and increase RIPK3 expression, resulting in podocytopathy through inflammatory response and fibrosis. Curcumin administration protects against podocyte injury by inhibiting ROS generation and downregulating RIPK3. Due to a cross-stimulating relationship between the two, the reduced level of each further contributes to the suppression effect of curcumin on intracellular ROS and RIPK3 expression. RIPK3 inhibition prevents necroptosis of podocytes since it prevents phosphorylation and aggregation of MLKL to proceed the final stage of necroptosis. Cas-8, caspase-8; Cas-3, caspase-3; MLKL, mixed lineage kinase domain-like protein.

Existing RIPK3 inhibitors such as GSK′872 are man-made synthetic materials that can specifically prevent cell necroptosis by blocking the RIPK3 domain. Multiple studies have emphasized curcumin's advantage over synthetic compounds, mainly due to its convenience and fewer side effects. In addition, revealing the novel properties of curcumin such as antiangiogenic effect, antiapoptotic effect, and anticancer effect is what makes curcumin a distinctive RIPK3 inhibitor (Gururaj et al., 2002; Perrone et al., 2015; Zhang et al., 2020). In the field of DM particularly, it has been confirmed that curcumin's antioxidative and anti-inflammatory properties can ameliorate the consequences of DM without any side effects (Meng et al., 2013; Den Hartogh et al., 2019). What differentiates curcumin from the existing RIPK3 inhibitors is that curcumin not only targets necroptosis, but also has a comprehensive role in improving the damages caused by DM. Using GSK′872, an inhibitor specific for RIPK3, may be more appropriate to use when studying necroptosis alone. However, to investigate a treatment target related to the overall improvement of the disease, it seems to be more useful to confirm curcumin's efficacy.

The ability of curcumin to regulate ROS and RIPK3 overexpression is expected to prevent podocytopathy by suspending the progression to necroptosis. A decreased ROS level is thought to reduce the incidence of necroptosis as ROS works as a stimulating factor for necroptosis. The inhibition of RIPK3 expression by curcumin can prevent the occurrence of necroptosis because without RIPK3 activation, MLKL, the terminal protein in necroptosis, cannot be phosphorylated or aggregated to proceed the final stage of necroptosis (**Figure 7**). In mesangial cells, high glucose-induced activation of RIPK3 and MLKL was inhibited by the treatment of curcumin and DHZ. Additional studies checking levels of necroptosis-related proteins (RIPK1, RIPK3, and MLKL) are needed to further verify the protective effect of curcumin on podocytes necroptosis.

CONCLUSION

In summary, our study showed that curcumin had protective effects against oxidative stress, inflammatory response, and fibrosis in high glucose-induced podocyte injury, eventually improving podocyte function. These renoprotective effects of curcumin might be associated with its ability to inhibit high glucose-induced RIPK3 expression by inhibiting oxidative stress. Our observations suggest that curcumin might be a potential therapeutic agent to minimize the progression of podocytopathy caused by diabetes as an inhibitor of RIPK3.

DATA AVAILABILITY STATEMENT

The raw data supporting the conclusion of this article will be made available by the authors, without undue reservation.

AUTHOR CONTRIBUTIONS

HC, MH, and EYL contributed to the conception and design of the study. MH and HGC performed formal analysis of the study. MH, HC, SWL, SYK, HGC, ESL, and JSK participated in the investigation of this study. MH, SWL, and ESL contributed to the methodology of the study. EYL supervised the study. HC wrote the original draft of the manuscript. HC, CHC, and EYL reviewedand edited the final version of the manuscript.

FUNDING

This work was supported by a grant (2020R1A2C2003438) of the National Research Foundation (NRF) funded by the Korea government (Ministry of Science and ICT). It was also supported by the Soonchunhyang University Research Fund.

SUPPLEMENTARY MATERIAL

The Supplementary Material for this article can be found online at: https://www.frontiersin.org/articles/10.3389/fcell.2022.800574/full#supplementary-material

REFERENCES

Anil Kumar, P., Welsh, G. I., Saleem, M. A., and Menon, R. K. (2014). Molecular and Cellular Events Mediating Glomerular Podocyte Dysfunction and Depletion in Diabetes Mellitus. *Front. Endocrinol.* 5, 151. doi:10.3389/fendo.2014.00151

Balasubramanyam, M., Koteswari, A. A., Kumar, R. S., Monickaraj, S. F., Maheswari, J. U., and Mohan, V. (2003). Curcumin-induced Inhibition of Cellular Reactive Oxygen Species Generation: Novel Therapeutic Implications. *J. Biosci.* 28 (6), 715–721. doi:10.1007/BF02708432

Barzegar, A., and Moosavi-Movahedi, A. A. (2011). Intracellular ROS protection Efficiency and Free Radical-Scavenging Activity of Curcumin. *PloS one* 6 (10), e26012. doi:10.1371/journal.pone.0026012

Bertheloot, D., Latz, E., and Franklin, B. S. (2021). Necroptosis, Pyroptosis and Apoptosis: an Intricate Game of Cell Death. *Cell Mol Immunol* 18, 1106–1121. doi:10.1038/s41423-020-00630-3

Cao, Z., and Cooper, M. E. (2011). Pathogenesis of Diabetic Nephropathy. *J. Diabetes Investig.* 2 (4), 243–247. doi:10.1111/j.2040-1124.2011.00131.x

Cooper, M. E., Mundel, P., and Boner, G. (2002). Role of Nephrin in Renal Disease Including Diabetic Nephropathy. *Semin. Nephrol.* 22 (5), 393–398. doi:10.1053/snep.2002.34724

Dabla, P. K. (2010). Renal Function in Diabetic Nephropathy. *World J. Diabetes* 1 (2), 48–56. doi:10.4239/wjd.v1.i2.48

Dai, M.-c., Zhong, Z.-h., Sun, Y.-h., Sun, Q.-f., Wang, Y.-t., Yang, G.-y., et al. (2013). Curcumin Protects against Iron Induced Neurotoxicity in Primary Cortical Neurons by Attenuating Necroptosis. *Neurosci. Lett.* 536, 41–46. doi:10.1016/j.neulet.2013.01.007

Den Hartogh, D. J., Gabriel, A., and Tsiani, E. (2019). Antidiabetic Properties of Curcumin II: Evidence from *In Vivo* Studies. *Nutrients* 12 (1), 58. doi:10.3390/nu12010058

Epstein, F. H., Border, W. A., and Noble, N. A. (1994). Transforming Growth Factor β in Tissue Fibrosis. *N. Engl. J. Med.* 331 (19), 1286–1292. doi:10.1056/NEJM199411103311907

Gil, C. L., Hooker, E., and Larrivée, B. (2021). Diabetic Kidney Disease, Endothelial Damage, and Podocyte-Endothelial Crosstalk. *Kidney Med.* 3 (1), 105–115. doi:10.1016/j.xkme.2020.10.005

Gururaj, A. E., Belakavadi, M., Venkatesh, D. A., Marmé, D., and Salimath, B. P. (2002). Molecular Mechanisms of Anti-angiogenic Effect of Curcumin. *Biochem. Biophysical Res. Commun.* 297 (4), 934–942. doi:10.1016/s0006-291x(02)02306-9

Jefferson, J. A., Alpers, C. E., and Shankland, S. J. (2011). Podocyte Biology for the Bedside. *Am. J. Kidney Dis.* 58 (5), 835–845. doi:10.1053/j.ajkd.2011.03.033

Jha, J. C., Banal, C., Chow, B. S. M., Cooper, M. E., and Jandeleit-Dahm, K. (2016). Diabetes and Kidney Disease: Role of Oxidative Stress. *Antioxid. Redox Signaling* 25 (12), 657–684. doi:10.1089/ars.2016.6664

Kang, J. S., Lee, S. J., Lee, J.-H., Kim, J.-H., Son, S. S., Cha, S.-K., et al. (2019). Angiotensin II-Mediated MYH9 Downregulation Causes Structural and Functional Podocyte Injury in Diabetic Kidney Disease. *Sci. Rep.* 9 (1), 7679. doi:10.1038/s41598-019-44194-3

Kanitkar, M., Gokhale, K., Galande, S., and Bhonde, R. R. (2008). Novel Role of Curcumin in the Prevention of Cytokine-Induced Islet Death *In Vitro* and Diabetogenesis *In Vivo*. *Br. J. Pharmacol.* 155 (5), 702–713. doi:10.1038/bjp.2008.311

Kim, B. H., Lee, E. S., Choi, R., Nawaboot, J., Lee, M. Y., Lee, E. Y., et al. (2016). Protective Effects of Curcumin on Renal Oxidative Stress and Lipid Metabolism in a Rat Model of Type 2 Diabetic Nephropathy. *Yonsei Med. J.* 57 (3), 664–673. doi:10.3349/ymj.2016.57.3.664

Kim, S.-Y., Park, S., Lee, S.-W., Lee, J.-H., Lee, E. S., Kim, M., et al. (2021). RIPK3 Contributes to Lyso-Gb3-Induced Podocyte Death. *Cells* 10 (2), 245. doi:10.3390/cells10020245

Koeberle, A., Northoff, H., and Werz, O. (2009). Curcumin Blocks Prostaglandin E2 Biosynthesis through Direct Inhibition of the Microsomal Prostaglandin E2 Synthase-1. *Mol. Cancer Ther.* 8 (8), 2348–2355. doi:10.1158/1535-7163.MCT-09-0290

LaRocca, T. J., Sosunov, S. A., Shakerley, N. L., Ten, V. S., and Ratner, A. J. (2016). Hyperglycemic Conditions Prime Cells for RIP1-dependent Necroptosis. *J. Biol. Chem.* 291 (26), 13753–13761. doi:10.1074/jbc.M116.716027

Lee, E. Y., Chung, C. H., Khoury, C. C., Yeo, T. K., Pyagay, P. E., Wang, A., et al. (2009). The Monocyte Chemoattractant protein-1/CCR2 Loop, Inducible by TGF-β, Increases Podocyte Motility and Albumin Permeability. *Am. J. Physiology-Renal Physiol.* 297 (1), F85–F94. doi:10.1152/ajprenal.90642.2008

Lee, S. J., Kang, J. S., Kim, H. M., Lee, E. S., Lee, J.-H., Chung, C. H., et al. (2019). CCR2 Knockout Ameliorates Obesity-Induced Kidney Injury through Inhibiting Oxidative Stress and ER Stress. *PloS one* 14 (9), e0222352. doi:10.1371/journal.pone.0222352

Lu, C., Xu, W., Zhang, F., Shao, J., and Zheng, S. (2016). Nrf2 Knockdown Disrupts the Protective Effect of Curcumin on Alcohol-Induced Hepatocyte Necroptosis. *Mol. Pharmaceutics* 13 (12), 4043–4053. doi:10.1021/acs.molpharmaceut.6b00562

Majithiya, J. B., and Balaraman, R. (2005). Time-dependent Changes in Antioxidant Enzymes and Vascular Reactivity of Aorta in Streptozotocin-Induced Diabetic Rats Treated with Curcumin. *J. Cardiovasc. Pharmacol.* 46 (5), 697–705. doi:10.1097/01.fjc.0000183720.85014.24

Meng, B., Li, J., and Cao, H. (2013). Antioxidant and Antiinflammatory Activities of Curcumin on Diabetes Mellitus and its Complications. *Curr. Pharm. Des.* 19 (11), 2101–2113. doi:10.2174/1381612811319110011

Perrone, D., Ardito, F., Giannatempo, G., Dioguardi, M., Troiano, G., Lo Russo, L., et al. (2015). Biological and Therapeutic Activities, and Anticancer Properties of Curcumin. *Exp. Ther. Med.* 10 (5), 1615–1623. doi:10.3892/etm.2015.2749

Priante, G., Gianesello, L., Ceol, M., Del Prete, D., and Anglani, F. (2019). Cell Death in the Kidney. *Ijms* 20 (14), 3598. doi:10.3390/ijms20143598

Sawatpanich, T., Petpiboolthai, H., Punyarachun, B., and Anupunpisit, V. (2010). Effect of Curcumin on Vascular Endothelial Growth Factor Expression in Diabetic Mice Kidney Induced by Streptozotocin. *J. Med. Assoc. Thai* 93 (Suppl. 2), S1–S8.

Schefe, J. H., Lehmann, K. E., Buschmann, I. R., Unger, T., and Funke-Kaiser, H. (2006). Quantitative Real-Time RT-PCR Data Analysis: Current Concepts and the Novel "gene Expression's C T Difference" Formula. *J. Mol. Med.* 84 (11), 901–910. doi:10.1007/s00109-006-0097-6

Sharma, S., Kulkarni, S. K., and Chopra, K. (2006). Curcumin, the Active Principle of Turmeric (Curcuma Longa), Ameliorates Diabetic Nephropathy in Rats. *Clin. Exp. Pharmacol. Physiol.* 33 (10), 940–945. doi:10.1111/j.1440-1681.2006.04468.x

Susztak, K., Raff, A. C., Schiffer, M., and Böttinger, E. P. (2006). Glucose-induced Reactive Oxygen Species Cause Apoptosis of Podocytes and Podocyte Depletion at the Onset of Diabetic Nephropathy. *Diabetes* 55 (1), 225–233. doi:10.2337/diabetes.55.01.06.db05-0894

Trujillo, J., Chirino, Y. I., Molina-Jijón, E., Andérica-Romero, A. C., Tapia, E., and Pedraza-Chaverrí, J. (2013). Renoprotective Effect of the Antioxidant Curcumin: Recent Findings. *Redox Biol.* 1 (1), 448–456. doi:10.1016/j.redox.2013.09.003

Tufro, A., and Veron, D. (2012). VEGF and Podocytes in Diabetic Nephropathy. *Semin. Nephrol.* 32 (4), 385–393. doi:10.1016/j.semnephrol.2012.06.010

Volpe, C. M. O., Villar-Delfino, P. H., Dos Anjos, P. M. F., and Nogueira-Machado, J. A. (2018). Cellular Death, Reactive Oxygen Species (ROS) and Diabetic Complications. *Cell Death Dis* 9 (2), 119. doi:10.1038/s41419-017-0135-z

Wang, T.-y., and Chen, J.-x. (2019). Effects of Curcumin on Vessel Formation Insight into the Pro- and Antiangiogenesis of Curcumin. *Evidence-Based Complement. Altern. Med.* 2019, 1–9. doi:10.1155/2019/1390795

Wolf, G., Chen, S., and Ziyadeh, F. N. (2005). From the Periphery of the Glomerular Capillary Wall toward the Center of Disease. *Diabetes* 54 (6), 1626–1634. doi:10.2337/diabetes.54.6.1626

Xu, Y., Gao, H., Hu, Y., Fang, Y., Qi, C., Huang, J., et al. (2019). High Glucose-Induced Apoptosis and Necroptosis in Podocytes Is Regulated by UCHL1 via RIPK1/RIPK3 Pathway. *Exp. Cel Res.* 382 (2), 111463. doi:10.1016/j.yexcr.2019.06.008

Zhang, P., Fang, J., Zhang, J., Ding, S., and Gan, D. (2020). Curcumin Inhibited Podocyte Cell Apoptosis and Accelerated Cell Autophagy in Diabetic Nephropathy via Regulating Beclin1/UVRAG/Bcl2. *Diabetes Metab. Syndr. Obes.* 13, 641–652. doi:10.2147/DMSO.S237451

Conflict of Interest: The authors declare that the research was conducted in the absence of any commercial or financial relationships that could be construed as a potential conflict of interest.

Publisher's Note: All claims expressed in this article are solely those of the authors and do not necessarily represent those of their affiliated organizations, or those of the publisher, the editors, and the reviewers. Any product that may be evaluated in this article, or claim that may be made by its manufacturer, is not guaranteed or endorsed by the publisher.

frontiers | Frontiers in Cell and Developmental Biology

BRIEF RESEARCH REPORT
published: 16 June 2022
doi: 10.3389/fcell.2022.924751

Adriamycin-Induced Nephropathy is Robust in N and Modest in J Substrain of C57BL/6

Claire Bryant[1], *Rachel Cianciolo*[2,3], *Rajgopal Govindarajan*[4,5] *and Shipra Agrawal*[1,6]*

[1]Center for Clinical and Translational Research, Abigail Wexner Research Institute at Nationwide Children's Hospital, Columbus, OH, United States, [2]Department of Veterinary Biosciences, The Ohio State University, Columbus, OH, United States, [3]Niche Diagnostics, LLC, Columbus, OH, United States, [4]Division of Pharmaceutics and Pharmacology, College of Pharmacy, The Ohio State University, Columbus, OH, United States, [5]Translational Therapeutics, The Ohio State University Comprehensive Cancer Center, Columbus, OH, United States, [6]Department of Pediatrics, College of Medicine, The Ohio State University, Columbus, OH, United States

Adriamycin (ADR)-induced nephropathy remains the leading model to study human primary focal segmental glomerulosclerosis (FSGS), a common pathway for podocyte damage and glomerular loss of function that leads to chronic kidney disease. However, the use of this model for reverse genetics is limited by historical categorization of C57BL/6 mice as an ADR-resistant strain, which is also the most common genetically modified strain. Additionally, conflicting reports exist utilizing C57BL/6 for ADR-nephrosis due to lack of understanding of substrain differences (J/N) and variability in ADR dosage, timing, and frequency to induce damage. We have undertaken a systematic approach to elucidate the specifics of ADR-nephrosis in C57BL/6 N and J substrains. We induced nephropathy with 2 doses of ADR, and measured albuminuria for 6 weeks and performed histological evaluations. Our findings revealed induction of robust and modest proteinuria in N and J substrains, respectively. The serum creatinine levels were elevated in N, but not J substrain. Both the substrains showed reduction in body weight with N greater than J, although mortality remained at 0% in both substrains. Histological analysis showed worse renal lesions in the N than the J substrain. Podocyte markers synaptopodin, nephrin, podocin, and WT1 were reduced to a greater extent in the N than the J substrain. In summary, we provide the nephrology community with a reproducible mouse model for FSGS, in a strain otherwise assumed to be ADR-resistant and highlight the differences between J and N substrains. This enables future studies, especially concerning genetically manipulated animal models in C57BL/6.

Keywords: glomerular disease, focal segment glomerulosclerosis, animal model, adriamycin (ADR), podocyte

OPEN ACCESS

Edited by:
Mario Ollero, INSERM U955 Institut Mondor de Recherche Biomédicale (IMRB), France

Reviewed by:
Shao-yu Zhang, INSERM U955 Institut Mondor de Recherche Biomédicale (IMRB), France
Yanggang Yuan, Nanjing Medical University, China

***Correspondence:**
Shipra Agrawal, Shipra.Agrawal@nationwidechildrens.org

Specialty section:
This article was submitted to Cell Death and Survival, a section of the journal Frontiers in Cell and Developmental Biology

Received: *20 April 2022*
Accepted: *30 May 2022*
Published: *16 June 2022*

Citation:
Bryant C, Cianciolo R, Govindarajan R and Agrawal S (2022) Adriamycin-Induced Nephropathy is Robust in N and Modest in J Substrain of C57BL/6. Front. Cell Dev. Biol. 10:924751. doi: 10.3389/fcell.2022.924751

INTRODUCTION

Various animal models have emerged to recapitulate the human forms of nephrotic syndrome to facilitate the discoveries to understand the mechanisms and therapeutic possibilities for glomerular disease (Pippin et al., 2009; Yang et al., 2018). Adriamycin (ADR)-induced nephropathy has been the leading model used to study human primary focal segmental glomerulosclerosis (FSGS), a common pathway for podocyte damage and glomerular loss of function that leads to kidney damage and failure (Wang et al., 2000; Pippin et al., 2009). Commonly used both in rats and mice, the ADR model

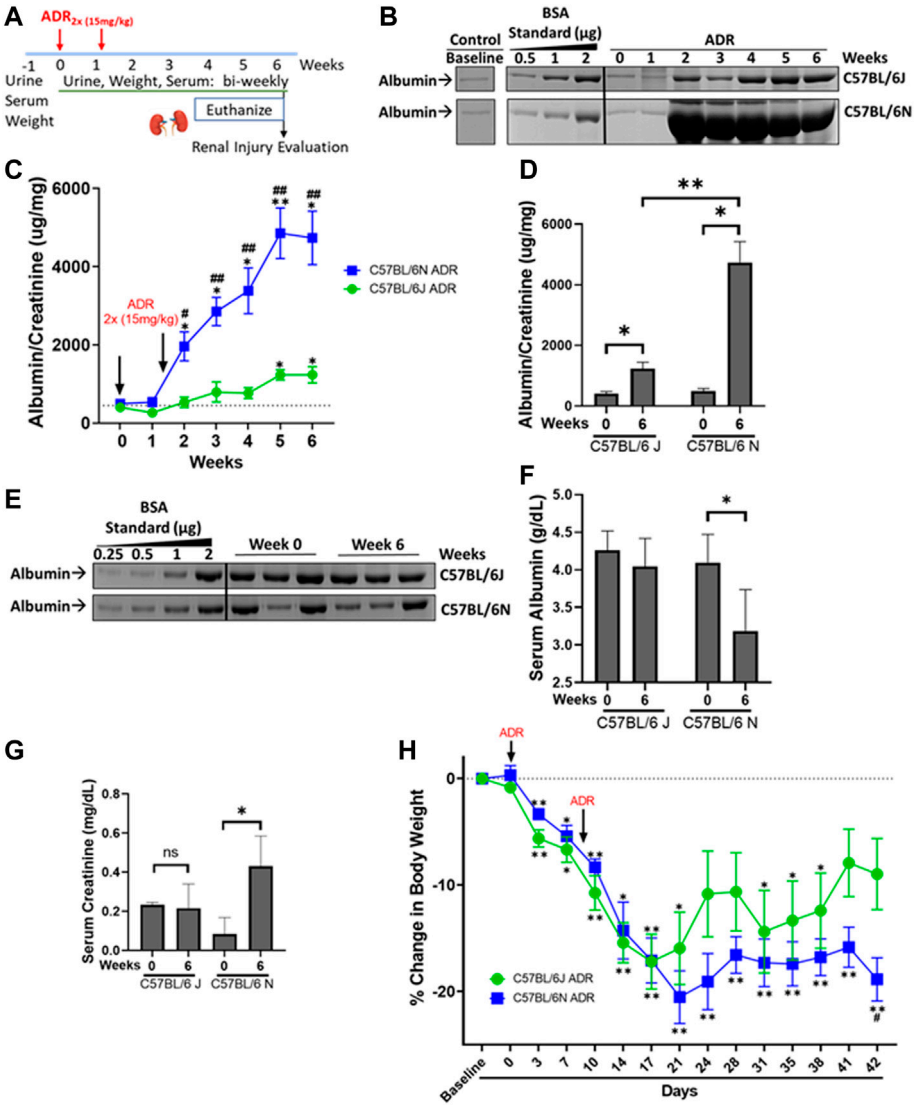

FIGURE 1 | ADR-Induced Proteinuria is Robust in the N and Modest in the J Substrain of C57BL/6 mice. **(A)** C57BL/6 J and N mice were injected with ADR (15 mg/kg/bw, i.v.) twice (Day 0 and Day 9). Urine, serum, and weight were collected throughout the study, and the mice were euthanized 6 weeks after the first injection, on Day 42, at which time the kidneys were harvested. **(B)** Representative urine gels with albumin bands are shown. Equal volumes of urine (5 µl) were analyzed by SDS-PAGE and Coomassie Blue staining. BSA (bovine serum albumin) standards were loaded at determined amounts and used to make a densitometry standard curve to determine albumin concentration. Urine from healthy un-injected mice were used as control. **(C)** Albumin/creatinine ratio was determined and plotted (*$p < 0.05$, **$p < 0.01$ vs. baseline of the same substrain, #$p < 0.05$, #$p < 0.01$ vs. J substrain at same week, Student *t*-test, $n = 4$/substrain). Dashed line parallel to *X* axis denotes the baseline albuminuria **(D)** Albumin/creatinine ratios plotted from urine samples from Week 0 and Week 6 for J and N substrains (*$p < 0.05$, **$p < 0.01$, Student *t*-test, $n = 4$/substrain). **(E)** Representative serum gels with albumin bands shown. Equal volumes of diluted serum (1 µl of 20X dilution) were analyzed by SDS-PAGE and Coomassie Blue staining. BSA (bovine serum albumin) standards were loaded at determined amounts and used to make a densitometry standard curve to determine albumin concentration. **(F)** Albumin values were determined and plotted (*$p < 0.05$ vs. baseline, Student one tailed *t*-test, $n = 4$/substrain). **(G)** Serum creatinine levels from Week 0 and Week 6 of both J and N substrains are plotted as measured by the enzymatic creatinine test kit (*$p < 0.05$). **(H)** Decrease in percentage body weight of both J and N substrains of mice at various time points compared to baseline, throughout the study are plotted. (*$p < 0.05$, **$p < 0.01$ vs. week 0 of same substrain, #$p < 0.05$ vs. J substrain of same week Student *t*-test, $n = 4$/substrain). Dashed line parallel to *X* axis denotes the baseline starting body weight.

has been used to study the mechanisms that develop in FSGS and chronic kidney disease (CKD) as it allows for a spatio-temporal evaluation of pathophysiological events. Unfortunately, this powerful model is highly strain-dependent in mice, as some strains are more resistant than others to ADR injections (Kimura et al., 1993; Pippin et al., 2009). Historically, the mouse strains BALB/cJ and 129/SvJ have been deemed to be highly susceptible and C57BL/6 to be resistant to ADR-induced nephrosis, attributed to the *Prmt7* (protein arginine methyltransferase 7) and *Prkdc* (protein kinase, DNA-

activated, catalytic polypeptide) gene defects conferring susceptibility to ADR (Zheng et al., 2005; Zheng et al., 2006; Papeta et al., 2010). This has been a major impediment in glomerular disease research as C57BL/6 is very commonly used when generating genetic glomerular disease models and a typical strain used for many knock-out and knock-in models. A recent editorial has briefly suggested that the N, but not the J substrain of C57BL/6 mice can be made modestly susceptible to ADR-induced nephropathy using a single ADR dose administration (Arif et al., 2016), while other reports point out the susceptibility of C57BL/6 without substrain specifications using high or multiple doses of ADR (Lee and Harris, 2011; Hakroush et al., 2014; Sonneveld et al., 2017; Yang et al., 2018). Overall, there are conflicting reports in literature reporting the use of this model of nephrosis in C57BL/6, and they are largely due to: 1) lack of a clear understanding of the substrain differences between J and N in C57BL/6, 2) variability of dosages of ADR administered, and 3) the variability in the timing and frequency of ADR administration. To minimize ambiguities, here, we sought to elucidate the specifics of ADR-induced nephropathy in N and J C57BL/6 substrains. Our findings highlight the differences in susceptibility magnitudes of N and J C57BL/6 substrains to ADR-induced nephropathy and provide the nephrology community with a reproducible mouse model for FSGS, in an otherwise assumed to be an ADR-resistant strain.

EXPERIMENTAL PROCEDURES

Animal Studies

The IACUC at Nationwide Children's Hospital approved this study. Male C57BL/6J and C57BL/6N mice were purchased at 8 weeks old from Jackson Laboratories (C57BL/6NJ, Strain # 005304, RRID: IMSR_JAX:005304, Common Name: B6N; C57BL/6J, Strain # 000664, RRID: IMSR_JAX:000664, Common Name: B6) and acclimated for 3 days. Both C57BL/6J and C57BL/6N mice were administered Adriamycin (ADR) (Sigma-Aldrich, St. Louis, MO) intravenously (IV) (15 mg/kg) on Day 0 and Day 9 (n = 4 each substrain) (**Figure 1A**). Control male J and N mice between the ages of 6–9 weeks did not receive ADR (n = 3/4 each substrain). Spot urine and serum were collected, and body weight recorded at baseline and regular biweekly points throughout the study. All ADR-injected mice experienced weight loss and a few mice (mostly N substrain) exhibited lethargy and dehydration. To minimize the symptoms of loss of appetite and body weight, lethargy, and dehydration, NutraGel (Bio-Serv, Flemington, NJ, United States) and wet chow were given on Days 9 and 29. The mice that exhibited wounds and swelling on their tails due to ADR injection were given buprenorphine and antibiotic ointment on Day 29 for pain alleviation. The mice were sacrificed by exposure to CO_2 on Day 42 and kidneys were harvested.

Urinalysis and Serum Chemistry

Urine collected bi-weekly throughout the study was resolved using sodium dodecyl sulfate-polyacrylamide gel electrophoresis (SDS-PAGE). Albumin standards [0.5, 1.0, and 2.0 μg bovine serum albumin (BSA)] were resolved alongside the urine samples on 8% gels, which was then stained with Coomassie Brilliant Blue G-250 (Alfa Aesar, Tewksbury, MA, United States) to visualize bands. Diluted serum was resolved on SDS-PAGE alongside albumin standards as well. The urinary and serum albumin was determined by densitometry from the BSA standard curves using Image J software (National Institutes of Health, Bethesda, MD, United States). Urinary (diluted 10X) and serum (undiluted) creatinine levels were determined using the Enzymatic Creatinine Test Kit (Diazyme, Poway, CA, United States), creatinine standards, and control. Albuminuria was determined and reported by normalizing the urinary albumin values to creatinine of the spot urine samples.

Histology

Kidney halves showing the cross sections of kidney containing cortex, medulla, and papilla were fixed in 10% buffered formalin for 48 h, followed by 3X PBS washes, and then placed in 70% ethanol for 24 h. They were then processed routinely and embedded in paraffin. The paraffin blocks were sectioned to 4 μm thickness, dried overnight, and baked at 60°C for 1 h. The slides were stained with periodic acid-Schiff method and reviewed by a pathologist blinded to the treatment method. For each animal, 100 glomeruli were assessed for segmental or global sclerosis and evidence of podocyte injury and the tubulointerstitium was semi-quantitively scored.

Immunofluorescence

Paraffin embedded kidneys were sectioned at 4 μm and deparaffinized with xylene and rehydrated in graded ethanol. Antigen retrieval was performed by boiling in 10 mM sodium citrate for 25 min, followed by washes in PBS-Tween (0.5% Tween-20). After blocking with SuperBlock (Scytek Labs Inc., Logan, UT, United States) for 60 min at 37°C followed by overnight at 4°C, the sections were incubated with primary antibodies [anti-synaptopodin (Santa Cruz Biotechnology, Dallas, TX, United States), anti-nephrin (Proteintech, Rosemont, IL, United States) and anti-WT1 (MilliporeSigma, Burlington, MA, United States)] overnight at 4°C at appropriate dilutions. Sections were washed with 2.5% SuperBlock in PBS-Tween three times, then incubated with secondary antibody (Alexa Fluor 488; Invitrogen, Carlsbad, CA, United States) in SuperBlock. The slides were mounted with Prolong Gold Antifade Mountant (Invitrogen, Carlsbad, CA, United States) and viewed and imaged with equal exposures for each primary antibody with BZ-X700 all-in-one fluorescence microscope (Keyence Inc., Itasca, IL, United States).

RNA Isolation and Real Time Reverse Transcriptase-Polymerase Chain Reaction

Kidney cortex was isolated and total RNA extracted using the RNeasy Kit (Qiagen, Germantown, MD, United States), according to manufacturer's instructions. Tissue in lysis buffer was lysed with a stainless-steel disruption bead in a Tissue Lyser (Qiagen, Germantown, MD, United States) for 1 min at 30.0 Hz, and RNA was isolated from the resulting lysate. Yield and purity was determined by measuring the absorbance on a spectrophotometer. 1 μg of RNA was DNase-digested (Invitrogen, Carlsbad, CA, United States), then inactivated with 25 mM EDTA at 65°C for 10 min cDNA was then

synthesized by reverse transcription with the iScript cDNA Synthesis Kit (Bio-Rad, Hercules, CA, United States), following manufacturer's instruction. cDNA was used for qualitative reverse transcription-polymerase chain reaction (qRT-PCR) using primers specific to *Nphs2* (F: ACCTTTCCATGAGGT GGTAAC, R: CTGGATGGCTTTGGACAC) normalized to *Rpl6* (F: CTGATCATCCTCACTGGGCG, R: GCGCAGAGG AACTCTGTTGA). PCR was performed using SYBR green (Bio-Rad, Hercules, CA, United States) on the Applied Biosystems 7500 Real-Time PCR System. PCR conditions were as follows: 95°C for 10 min, 40X (95°C for 15 s, 60°C for 1 min), followed by a melt curve to ensure specific products. The ΔΔCt method was used to analyze the results as described previously (Bryant et al., 2022).

Statistical Analysis

Statistical analysis was performed using unpaired Student's *t*-test and paired Student's *t*-test using the GraphPad Prism software version 8.2.0 for Windows (GraphPad Software, San Diego, CA, United States), as applicable to the dataset.

RESULTS

ADR-Induced Proteinuria is Robust in the N and Modest in the J Substrain of C57BL/6 Mice

To determine and compare the extent of susceptibility of C57BL/6 mouse substrains J and N to ADR-induced nephropathy, two doses of ADR injections (15 mg/kg) were administered 10 days apart (**Figure 1A**). Albuminuria appeared in both substrains during week 2 and continued to increase through week 6. While C57BL/6 J mice showed a modest induction of proteinuria, the N substrain showed massive proteinuria after the second dose of ADR (**Figures 1B,C**). The N substrain showed an increase in albuminuria starting at week 2 with a robust 9.5-fold increase from baseline at week 6 (4737 ± 682.9 mg/mg vs. 498.2 ± 84.71 mg/mg; $p = 0.0113$) (**Figures 1C,D**). The J substrain showed a modest increase starting at week 5, which was 3-fold from baseline at week 6 (1237 ± 208.2 mg/mg vs. 405.2 ± 74.23 mg/mg, $p = 0.0170$) (**Figures 1C,D**). Additionally, albuminuria was consistently higher in the N vs. J substrain for any week between weeks 2–6 (4737 ± 682.9 mg/mg vs. 1237 ± 208.2 mg/mg; 3.8-fold; $p = 0.0027$) (**Figure 1C**). Control mice, not injected with ADR had similar urine albumin/creatinine amounts as baseline or Day 0 samples from ADR-treated mice, for both J and N substrains (**Figure 1B**). Dehydration and lethargy experienced in some mice were minimized by providing them with wet chow and NutraGel on days 9 and 29, which likely led to the relatively diluted urine and apparently lowered albumin at week 6 compared to week 2 (**Figure 1B**). However, normalization of urinary albumin to urinary creatinine values still showed the continuous rise in albuminuria in these mice (**Figure 1C**). Furthermore, assessment of serum albumin levels showed a decrease in ADR-injected mice at week 6 as compared to baseline/week 0 in the N substrain (3.19 ± 0.5 g/dl vs. 4.1 ± 0.4 g/dl; $p = 0.05$). The decrease in the J substrain was milder, although a similar trend of decrease in serum albumin was observed with ADR-nephrosis at week 6 compared to baseline/week 0 (4.04 ± 0.4 g/dl vs. 4.26 ± 0.2 g/dl) (**Figures 1E,F**).

ADR-Induced Nephropathy Results in Elevated Serum Creatinine in the N Substrain Only and Decreased Body Weight in Both the Substrains

Serum creatinine level is an indicator of glomerular filtration rate and progression of nephropathy to chronic stage. Serum creatinine was elevated in the N substrain of C57BL/6 mice, where it increased ~5-fold at week 6 compared to baseline/week 0 (0.43 ± 0.15 mg/mg vs. 0.08 ± 0.08 mg/mg, $p = 0.0441$) (**Figure 1G**). However, serum creatinine did not change in the J substrain at the observed time points (**Figure 1G**). Weight loss was observed in both substrains, with N to a greater extent by week 6 (**Figure 1H**). Body weight decrease compared to baseline started during week 1 for both substrains, with the weights increasing a non-significant amount around week 4 when the mice were given pain medications and wet chow to reduce dehydration but decreasing again by the next week. Final day weights showed higher body weight decrease in the N than the J substrain (**Figure 1H**).

Glomerular and Tubular Histological Alterations Are More Prominent in N vs. J Substrain, and Are Correlative With Albuminuria

Histological evaluation and morphometric quantification showed that the N substrain mice injected with ADR displayed segmental sclerosis in some glomeruli, as well as hypertrophied podocytes and tubular degeneration with protein casts, interstitial fibrosis, and tubular atrophy (**Figure 2**; **Table 1**). The J substrain had fewer glomeruli with segmental glomerulosclerosis and podocyte injury compared to the N substrain (**Figure 2**). Segmental sclerosis was characterized by effacement of peripheral capillary lumens by extracellular matrix and these segments were often adhered to Bowman's capsules. Other lesions which have been reported in models of FSGS (e.g., mesangiolysis, crescents and hypercellularity) were not observed in either substrain. The tubulointerstitial scores were higher in the N substrain with larger portions of the renal parenchyma exhibiting tubular dilation and protein casts. Lesions of acute tubular necrosis and tubular epithelial cell cytoplasmic protein droplets were not observed in either substrain. Neither N nor J control groups had any of the aforementioned pathological lesions (**Figure 2**; **Table 1**).

Albuminuria is Associated With Podocyte Injury in N and J Substrains With Adriamycin-Induced Nephropathy

The structural and functional integrity of podocytes, specialized terminally differentiated epithelial cells in the glomeruli, is crucial for the optimum functioning of the glomerular filtration barrier (Benzing, 2020). Synaptopodin is one of the key determinants of

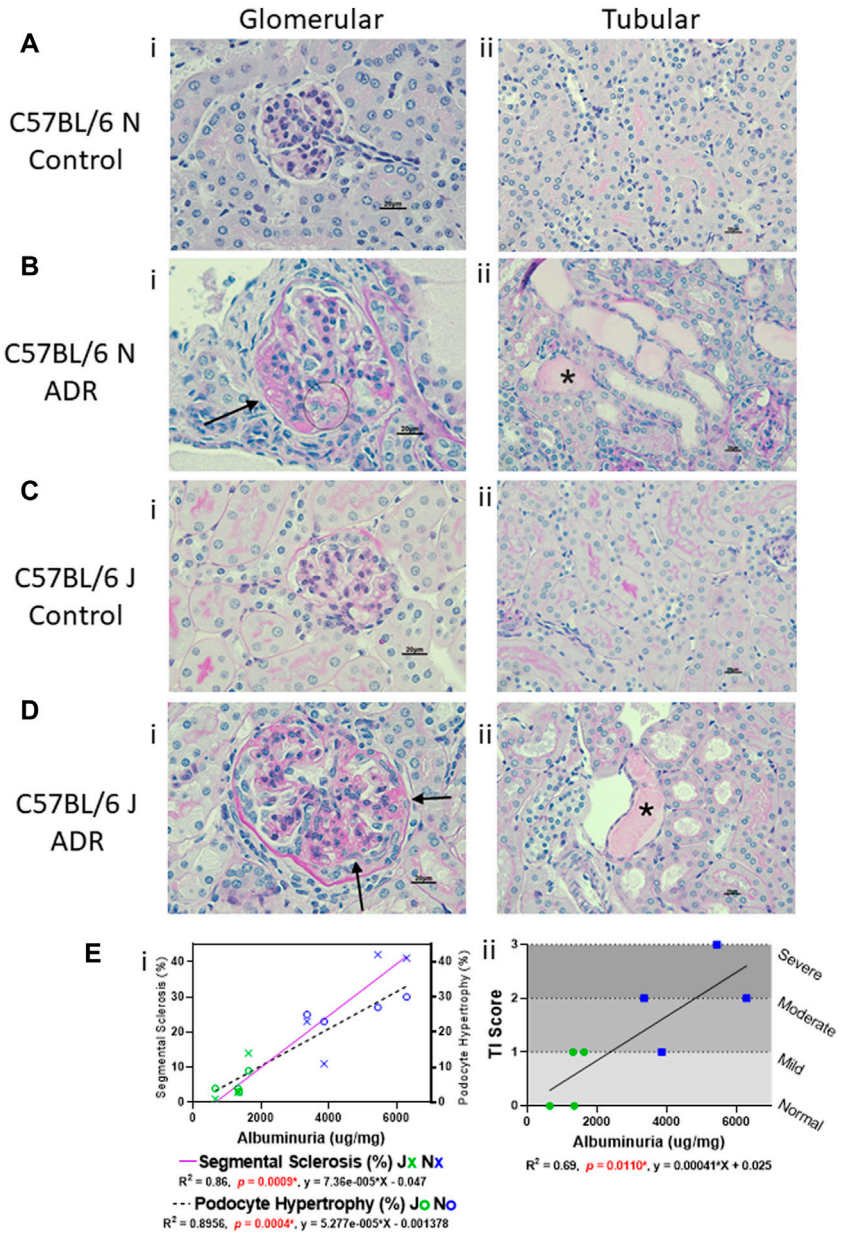

FIGURE 2 | Glomerular and Tubular Histological Alterations are more Prominent in N vs. J Substrain, and are Correlative with Albuminuria. **(A–D)** Histologic evaluation of kidneys stained with periodic acid-Schiff method (scale bar = 20 μm). Representative images showing **(i)** glomerular and **(ii)** tubular histology from **(A,B)** C57BL/6 N control and ADR-injected mice, and **(C,D)**, C57BL/6 J control and ADR-injected mice. **(Bi and Di)** Glomerular damage is indicated with an arrow for a sclerotic segment and circle for hypertrophied podocytes that contain protein reabsorption droplets. **(Bii and Dii)** Tubular protein casts are indicated with asterisks (*). **(E i)** Correlation of glomerular segmental sclerosis and podocyte hypertrophy with albuminuria in J and N ADR-injected mice. Segmental sclerosis is indicated with a purple solid line, and the data points are marked as X's (Blue = N, Green = J). Podocyte hypertrophy is indicated with a dashed line, and the data points are marked as circles (Blue = N, Green = J). **(E ii)** Correlation of tubular injury (TI) scores with albuminuria in J and N ADR-injected mice (Blue = N, Green = J). The tubular injury was scored subjectively with 0 = normal, 1 = mild, 2 = moderate, 3 = severe.

podocyte actin cytoskeletal integrity, nephrin and podocin form the crucial components of the slit diaphragm and WT-1 is an important transcriptional master regulator of podocyte function (Asanuma et al., 2005; Morrison et al., 2008; Benzing, 2020). We evaluated the expression of these critical podocyte markers in the kidneys of both N and J substrains of control and ADR-injured mice and found all these markers to be downregulated with ADR injury, and these effects were more pronounced in the N substrain than the J substrain (**Figures 3A–E**). Synpatopodin expression was diminished and disrupted in the injured glomeruli in both the substrains, with higher reduction observed in the N substrain than the J substrain. WT1 expression was found to be nuclear in healthy

TABLE 1 | Histological Scoring of ADR-Induced Nephropathy in both N and J Substrains.

ID	Glomerular					Tubular	
	% Segmental sclerosis	Score	% Global sclerosis	% Podocyte hypertrophy	% Histologically normal	Qualitative assessment of damage	Score
C57BL/6 N Control							
#15	0	0	0	1	99	Normal	0
#16	0	0	0	3	97	Normal	0
#17	0	0	0	2	98	Normal	0
C57BL/6 N ADR							
#5	42	3	1	27	30	Severe multifocal protein casts; some regions have tubular basophilia	3
#6	23	2	1	25	51	Moderate multifocal protein casts; some regions have tubular basophilia	2
#7	41	3	1	30	28	Moderate multifocal protein casts; some regions have tubular basophilia	2
#8	11	1	1	23	65	Mild multifocal protein casts; some regions have tubular basophilia	1
C57BL/6 J Control							
#9	0	0	0	8	92	Normal	0
#10	0	0	0	5	95	Normal	0
#11	1	0	0	6	93	Normal	0
#12	0	0	0	9	91	Normal	0
C57BL/6 J ADR							
#1	3	0	0	4	93	Mild multifocal tubular basophilia with protein casts	1
#2	3	0	0	3	94	Normal	0
#3	14	1	0	9	77	Mild multifocal protein casts	1
#4	1	0	0	4	95	Normal	0

Podocyte lesions included cytoplasmic vacuolation, protein reabsorption droplets and synechiae. The tubulointerstitium was semi-quantitively scored for tubular dilation, epithelial basophilia and tubular protein casts. The severity score was based on the portion of the tissue section that was affected. Normal samples received a score of 0. Mildly affected samples had approximately 1/3 of their parenchyma with lesions and they received a score of 1; moderate scores (2) were given when between 1/3 and 2/3 of the renal parenchyma had lesions; severely affected kidneys (3) had more than 2/3 of their parenchyma with lesions. Kidney scoring sheet of 100 glomeruli per sample. Scoring for sclerosis is based on <5% = 0, 5%–20% = 1, 20%–40% = 2, and >40% = 3 (Wharram et al., 2005). Tubular injury was assessed subjectively and the scoring system is 0 = normal, 1-mild, 2 = moderate, 3 = severe.

podocytes and the staining of nuclear WT1 in the podocytes was reduced in ADR-injured glomeruli in both N and J substrains. Although we observed some background non-specific staining with nephrin antibodies, its glomerular specific staining was also reduced in the ADR-injured glomeruli, more so in the N substrain than the J substrain. *Nphs2* encoding for podocin was found to be reduced in the N substrain mice after ADR injury and showed a trend towards reduction in the J substrain.

DISCUSSION

Mouse models are invaluable resources for reverse genetics to understand pathophysiology and to evaluate therapeutics. Most of the genetic glomerular disease models are generated in the C57BL/6 strain, however this strain has been historically categorized as a resistant strain to ADR-induced nephropathy (Zheng et al., 2005; Zheng et al., 2006; Papeta et al., 2010). A few recent reports have implicated the use of C57BL/6 strain for ADR-induced nephrosis, however the categorization of substrain susceptibilities is unavailable (Jeansson et al., 2009; Heikkila et al., 2010; Lee and Harris, 2011; Hakroush et al., 2014; Arif et al., 2016; Sonneveld et al., 2017; Yang et al., 2018). Furthermore, reports in the literature are somewhat confusing attributable to variability in dosage, timing and frequency of ADR administration. In order to address these and some of our own challenges of availability of genetically modified mice regarding genes of our interest in J and N substrains of C57BL/6 mice, we conducted regimented experimental studies to compare the extent of ADR-induced nephropathy in J and N substrains. We induced nephropathy with 2X ADR injections and measured albuminuria throughout the study for 6 weeks with terminal histological examinations and evaluation of glomerular and podocyte injury. A higher ADR dose and frequency were chosen than the conventional ADR-dosing schedule involving the susceptible BALB/cJ and 129/SvJ strains because of the notion that C57BL/6 mice are resistant strains and what we deduced as optimal for consistent nephropathy outcomes. We were able to successfully develop a robust nephrosis model in the N substrain and a mild nephrosis model in the J substrain.

In the mid-1990s, it became evident that ADR-induced FSGS was highly strain dependent in mice as the mouse strains BALB/cJ

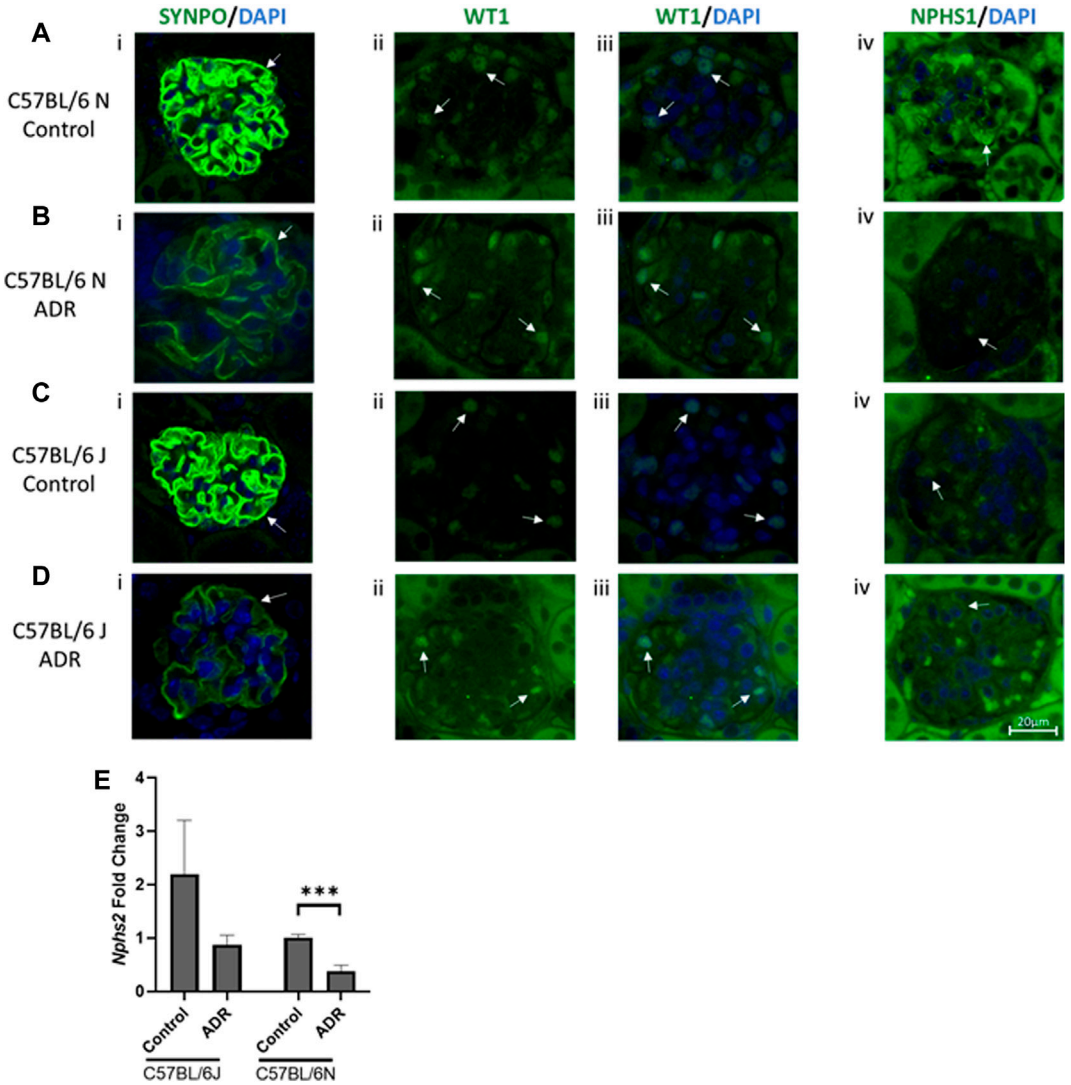

FIGURE 3 | Albuminuria is Associated with Podocyte Injury in N and J Substrains with Adriamycin-Induced Nephropathy. **(A–D)** Immunofluorescence staining and evaluation of glomeruli and podocytes with synaptopodin, WT1 and nephrin (scale bar = 20 μm). Representative images showing glomerular and podocyte **(i)** SYNPO (green)/DAPI (blue), **(ii)** WT1 (green), **(iii)** WT1 (green)/DAPI (blue), and **(iv)** NPHS1 (green)/DAPI (blue) staining from **(A,B)** C57BL/6 N control and ADR-injected mice, and **(C,D)**, C57BL/6 J control and ADR-injected mice. **(ii, iii)** WT1 colocalization with DAPI in the nucleus is indicated by a light blue color. Podocyte and glomerular specific staining is indicated with arrows. At least three glomeruli from three mice per group were examined. **(E)** RNA was isolated from the kidney cortex from C57BL/6 J and N substrains, control and ADR-injected mice. *Nphs2*/Podocin expression fold change is shown comparing control and ADR-treated mice. ***$p < 0.001$ by unpaired student *t*-test, $n = 3$/group.

and 129/SvJ were found to be highly susceptible, while C57BL/6 and FVB/NJ were deemed to be resistant (Kimura et al., 1993; Chen et al., 1995; Chen et al., 1998; Wang et al., 2000; Pippin et al., 2009). This has been a roadblock to utilize the C57BL/6 strain as a model of FSGS. In our own previously reported study (Nie et al., 2018), significant amount of time and resources were utilized in backcrossing the C57BL/6 mice harboring knock-out of our genes of interest (MK2 and MK3) to the 129/SvJ strain to render them susceptible to ADR-nephrosis. Such experiments can benefit from the knowledge of difference in substrain susceptibility between N and J and the ability to even make the J substrain modestly proteinuric with a modified protocol, as is described in this study. In some cases, it might be even preferable to utilize the C57BL/6 strain over the sensitive BALB/c mice, which respond poorly to kidney perfusion, thus not allowing for complete study of disease progression (Jeansson et al., 2009). With increasing complexities in mouse genetics and breeding experiments, monitoring of genetically engineered mice even within the C57BL/6 background remain to be challenging. The N substrain is a National Institute of Health (NIH) subline of C57BL/6, which was separated from C57BL/6J (Jackson Laboratories) in 1951, and it can be distinguished from C57BL/6J with at least 11 SNP differences, which likely results in phenotypic differences affecting a broad range of areas

including metabolism, immune function, and cardiovascular function (Simon et al., 2013; Fontaine and Davis, 2016). The current study highlights the usefulness of both C57BL/6 substrains for ADR-induced nephrosis by clarifying the susceptibility differences in the magnitude of ADR-induced nephropathy. A recent brief editorial highlighted the importance of discriminating between these two substrains in the context of ADR-induced nephrosis (Arif et al., 2016). Our study has further delved into this critical observation to demonstrate a robust vs. modest induction of ADR-induced nephropathy or FSGS in N vs. J mice, respectively, with a standardized protocol. Furthermore, our findings demonstrate a robust induction of proteinuria in N substrain as opposed to what was reported as just a mild proteinuria in the N substrain. Second, we also demonstrate a modest, but significant induction of proteinuria and glomerular lesions in J substrain, while many previous reports just dismissed this substrain to be completely resistant with absence of any proteinuria. Our study was also different in other aspects, such as utilization of 2 doses of ADR vs. one dose of ADR, serial albuminuria results shown until week 6 vs. only one time point 4 weeks albuminuria depiction, route of ADR administration (i.v. vs. retroorbital), and glomerular histology results vs. only foot process effacement (Arif et al., 2016), which is only an indicator of a less severe than FSGS form of NS (i.e., minimal change disease). Moreover, no detailed histological alterations were previously examined for ADR treated N and J substrains, It is important to note that we have observed glomerular and tubular histological lesions in N and mild alterations in J substrain, which were found to be correlative with proteinuria in the respective substrains. Furthermore, we have observed reduction in the expression of critical podocyte markers, synaptopodin, nephrin, WT1 and podocin, implicating podocyte damage and injury in both substrains with ADR-nephrosis, with more pronounced reduction in the N substrain compared to the J substrain. These changes in podocyte markers are consistent with the occurrence of proteinuria, which further underscores the importance of these models as relevant systems to evaluate podocyte-specific gene knock outs and podocyte-targeted therapies for FSGS.

We anticipate our findings to be valuable for the nephrology community in planning mouse studies to recapitulate FSGS. First, it is important to understand the substrain differences of J and N if the gene of interest is modified in the C57BL/6 background. This would be particularly beneficial in the N background before spending time and resources to backcross to a more susceptible strain such as BALB/cJ or 129/SvJ. This is also relevant as backcrossing into a different strain often leads to residual differences in the genetic background, if one compares the knock-out on the backcrossed strain with the wildtype of that strain (Hay et al., 2021). Second, the model of modest proteinuria and nephropathy in the J substrain could potentially be a favorable model for certain reverse genetics, where the expectation is the exacerbation of injury with a double hit or insult such as knock-out or knock-in of relevant genes critical for podocyte function. Consistently, a few studies have shown increase in nephrosis just after 3 weeks with e.g., podocyte-specific deletion of PPARγ when challenged with ADR in mice on C57BL/6J background (Jeansson et al., 2009; Heikkila et al., 2010; Hakroush et al., 2014; Sonneveld et al., 2017). Third, our studies suggest that it is critical to follow with a mandatory second dose of ADR at 15 mg/kg to induce nephropathy and persistent proteinuria. Fourth, it is important to relieve the distress caused by a strong drug such as ADR to the mice at multiple organ level by administering the minimal dose required and providing pain relief measures and hydration imparting nutragels during the experiment. Depending on the dosage and strain, mortality and severe weight loss are common problems associated with ADR-induced nephrosis even in susceptible strains such as 129/SvJ and BALB/cJ, which causes much distress to the animals and hinders the experiments and skews the results (Pippin et al., 2009; Hakroush et al., 2014; Nie et al., 2018). We have successfully induced nephrosis while observing 0% mortality with simple palliative measures, in both J and N substrains of C57BL/6. Only male mice were used in this study as the female mice are known to be more resistant to ADR-induced injury, especially in C57BL/6 J strain (Lee and Harris, 2011; Grant et al., 2019), although future studies may shed more light on the sex-dependent outcomes.

In summary, our studies demonstrate a reproducible method to induce robust and modest nephrosis in the N and J substrains of C57BL/6 mice, respectively, using ADR. This enables further studies, especially proper selection of C57BL/6 substrains for genetic manipulations to study ADR and relevant studies in established knockout or genetically manipulated animal models where the strain or substrain were predetermined. We also believe these results will persuade the scientific community to consider C57BL/6 mouse substrains J and N as distinctly useful models for the studies of kidney injuries.

DATA AVAILABILITY STATEMENT

The original contributions presented in the study are included in the article/Supplementary Material, further inquiries can be directed to the corresponding author.

ETHICS STATEMENT

The animal study was reviewed and approved by the Abigail Wexner Research Institute, Nationwide Children's Hospital (NCH) Institution Animal Care and Use Committee (IACUC).

AUTHOR CONTRIBUTIONS

CB performed animal experiments and downstream analyses of tissues and samples and immunofluorescence experiments. RC performed the histological analysis and prepared the scoring table. CB, RC, RG, and SA interpreted the data, prepared figures and drafted the results and manuscript. RG and SA edited the manuscript and SA conceived the project. All the authors approve of the final version of the manuscript.

FUNDING

This study was supported by the funds from Nationwide Children's Hospital (NCH) to SA and R01GM143217 awarded to RG.

ACKNOWLEDGMENTS

The authors thank members of the animal research core and the morphology core at NCH and the veterinary pathology core at OSU.

REFERENCES

Arif, E., Solanki, A. K., and Nihalani, D. (2016). Adriamycin Susceptibility Among C57BL/6 Substrains. *Kidney Int.* 89 (3), 721–723. doi:10.1016/j.kint.2015.10.019

Asanuma, K., Kim, K., Oh, J., Giardino, L., Chabanis, S., Faul, C., et al. (2005). Synaptopodin Regulates the Actin-Bundling Activity of α-actinin in an Isoform-specific Manner. *J. Clin. Invest.* 115 (5), 1188–1198. doi:10.1172/JCI2337110.1172/jci200523371

Benzing, T. (2020). Molecular Design of the Kidney Filtration Barrier. *Trans. Am. Clin. Climatol. Assoc.* 131, 125–139.

Bryant, C., Rask, G., Waller, A. P., Webb, A., Galdino-Pitta, M. R., Amato, A. A., et al. (2022). Selective Modulator of Nuclear Receptor PPARγ with Reduced Adipogenic Potential Ameliorates Experimental Nephrotic Syndrome. *iScience* 25 (4), 104001. doi:10.1016/j.isci.2022.104001

Chen, A., Sheu, L.-F., Ho, Y.-S., Lin, Y.-F., Chou, W.-Y., Chou, T.-C., et al. (1998). Experimental Focal Segmental Glomerulosclerosis in Mice. *Nephron* 78 (4), 440–452. doi:10.1159/000044974

Chen, A., Wei, C.-H., Sheu, L.-F., Ding, S.-L., and Lee, W.-H. (1995). Induction of Proteinuria by Adriamycin or Bovine Serum Albumin in the Mouse. *Nephron* 69 (3), 293–300. doi:10.1159/000188473

Fontaine, D. A., and Davis, D. B. (2016). Attention to Background Strain Is Essential for Metabolic Research: C57BL/6 and the International Knockout Mouse Consortium. *Diabetes* 65 (1), 25–33. doi:10.2337/db15-0982

Grant, M. K. O., Seelig, D. M., Sharkey, L. C., Choi, W. S. V., Abdelgawad, I. Y., and Zordoky, B. N. (2019). Sexual Dimorphism of Acute Doxorubicin-Induced Nephrotoxicity in C57Bl/6 Mice. *PLoS One* 14 (2), e0212486. doi:10.1371/journal.pone.0212486

Hakroush, S., Cebulla, A., Schaldecker, T., Behr, D., Mundel, P., and Weins, A. (2014). Extensive Podocyte Loss Triggers a Rapid Parietal Epithelial Cell Response. *J. Am. Soc. Nephrol.* 25 (5), 927–938. doi:10.1681/ASN.2013070687

Hay, A. M., Howie, H. L., Gorham, J. D., D'Alessandro, A., Spitalnik, S. L., Hudson, K. E., et al. (2021). Mouse Background Genetics in Biomedical Research: The Devil's in the Details. *Transfusion* 61 (10), 3017–3025. doi:10.1111/trf.16628

Heikkila, E., Juhila, J., Lassila, M., Messing, M., Perala, N., Lehtonen, E., et al. (2010). -Catenin Mediates Adriamycin-Induced Albuminuria and Podocyte Injury in Adult Mouse Kidneys. *Nephrol. Dial. Transplant.* 25 (8), 2437–2446. doi:10.1093/ndt/gfq076

Jeansson, M., Björck, K., Tenstad, O., and Haraldsson, B. (2009). Adriamycin Alters Glomerular Endothelium to Induce Proteinuria. *J. Am. Soc. Nephrol.* 20 (1), 114–122. doi:10.1681/ASN.2007111205

Kimura, M., Takahasi, H., Ohtake, T., Sato, T., Hishida, A., Nishimura, M., et al. (1993). Interstrain Differences in Murine Daunomycin-Induced Nephrosis. *Nephron* 63 (2), 193–198. doi:10.1159/000187182

Lee, V. W., and Harris, D. C. (2011). Adriamycin Nephropathy: a Model of Focal Segmental Glomerulosclerosis. *Nephrol. Carlt.* 16 (1), 30–38. doi:10.1111/j.1440-1797.2010.01383.x

Morrison, A. A., Viney, R. L., Saleem, M. A., and Ladomery, M. R. (2008). New Insights into the Function of the Wilms Tumor Suppressor geneWT1in Podocytes. *Am. J. Physiology-Renal Physiology* 295 (1), F12–F17. doi:10.1152/ajprenal.00597.2007

Nie, X., Chanley, M. A., Pengal, R., Thomas, D. B., Agrawal, S., and Smoyer, W. E. (2018). Pharmacological and Genetic Inhibition of Downstream Targets of P38 MAPK in Experimental Nephrotic Syndrome. *Am. J. Physiology-Renal Physiology* 314 (4), F602–F613. doi:10.1152/ajprenal.00207.2017

Papeta, N., Zheng, Z., Schon, E. A., Brosel, S., Altintas, M. M., Nasr, S. H., et al. (2010). Prkdc Participates in Mitochondrial Genome Maintenance and Prevents Adriamycin-Induced Nephropathy in Mice. *J. Clin. Invest.* 120 (11), 4055–4064. doi:10.1172/JCI43721

Pippin, J. W., Brinkkoetter, P. T., Cormack-Aboud, F. C., Durvasula, R. V., Hauser, P. V., Kowalewska, J., et al. (2009). Inducible Rodent Models of Acquired Podocyte Diseases. *Am. J. Physiology-Renal Physiology* 296 (2), F213–F229. doi:10.1152/ajprenal.90421.2008

Simon, M. M., Greenaway, S., White, J. K., Fuchs, H., Gailus-Durner, V., Wells, S., et al. (2013). A Comparative Phenotypic and Genomic Analysis of C57BL/6J and C57BL/6N Mouse Strains. *Genome Biol.* 14 (7), R82. doi:10.1186/gb-2013-14-7-r82

Sonneveld, R., Hoenderop, J. G., Isidori, A. M., Henique, C., Dijkman, H. B., Berden, J. H., et al. (2017). Sildenafil Prevents Podocyte Injury via PPAR-γ-Mediated TRPC6 Inhibition. *J. Am. Soc. Nephrol.* 28 (5), 1491–1505. doi:10.1681/ASN.2015080885

Wang, Y., Wang, Y. P., Tay, Y.-C., and Harris, D. C. H. (2000). Progressive Adriamycin Nephropathy in Mice: Sequence of Histologic and Immunohistochemical Events. *Kidney Int.* 58 (4), 1797–1804. doi:10.1046/j.1523-1755.2000.00342.x

Wharram, B. L., Goyal, M., Wiggins, J. E., Sanden, S. K., Hussain, S., Filipiak, W. E., et al. (2005). Podocyte Depletion Causes Glomerulosclerosis: Diphtheria Toxin-Induced Podocyte Depletion in Rats Expressing Human Diphtheria Toxin Receptor Transgene. *J. Am. Soc. Nephrol.* 16 (10), 2941–2952. doi:10.1681/ASN.2005010055

Yang, J. W., Dettmar, A. K., Kronbichler, A., Gee, H. Y., Saleem, M., Kim, S. H., et al. (2018). Recent Advances of Animal Model of Focal Segmental Glomerulosclerosis. *Clin. Exp. Nephrol.* 22 (4), 752–763. doi:10.1007/s10157-018-1552-8

Zheng, Z., Pavlidis, P., Chua, S., D'Agati, V. D., and Gharavi, A. G. (2006). An Ancestral Haplotype Defines Susceptibility to Doxorubicin Nephropathy in the Laboratory Mouse. *J. Am. Soc. Nephrol.* 17 (7), 1796–1800. doi:10.1681/ASN.2005121373

Zheng, Z., Schmidt-Ott, K. M., Chua, S., Foster, K. A., Frankel, R. Z., Pavlidis, P., et al. (2005). A Mendelian Locus on Chromosome 16 Determines Susceptibility to Doxorubicin Nephropathy in the Mouse. *Proc. Natl. Acad. Sci. U.S.A.* 102 (7), 2502–2507. doi:10.1073/pnas.0409786102

Conflict of Interest: Author RC was employed by Niche Diagnostics, LLC.

The remaining authors declare that the research was conducted in the absence of any commercial or financial relationships that could be construed as a potential conflict of interest.

Publisher's Note: All claims expressed in this article are solely those of the authors and do not necessarily represent those of their affiliated organizations, or those of the publisher, the editors and the reviewers. Any product that may be evaluated in this article, or claim that may be made by its manufacturer, is not guaranteed or endorsed by the publisher.

Advantages of publishing in Frontiers

OPEN ACCESS
Articles are free to read for greatest visibility and readership

FAST PUBLICATION
Around 90 days from submission to decision

HIGH QUALITY PEER-REVIEW
Rigorous, collaborative, and constructive peer-review

TRANSPARENT PEER-REVIEW
Editors and reviewers acknowledged by name on published articles

Frontiers
Avenue du Tribunal-Fédéral 34
1005 Lausanne | Switzerland

Visit us: www.frontiersin.org
Contact us: frontiersin.org/about/contact

REPRODUCIBILITY OF RESEARCH
Support open data and methods to enhance research reproducibility

DIGITAL PUBLISHING
Articles designed for optimal readership across devices

FOLLOW US
@frontiersin

IMPACT METRICS
Advanced article metrics track visibility across digital media

EXTENSIVE PROMOTION
Marketing and promotion of impactful research

LOOP RESEARCH NETWORK
Our network increases your article's readership